eCAM
Evidence-Based Complementary and Alternative Medicine

Marine Biotechnology

Guest Editors: Song Qin, W. E. G. Müller, and Edwin L. Cooper

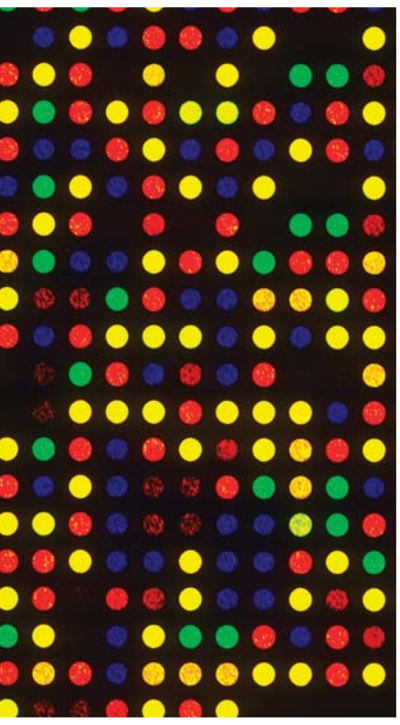

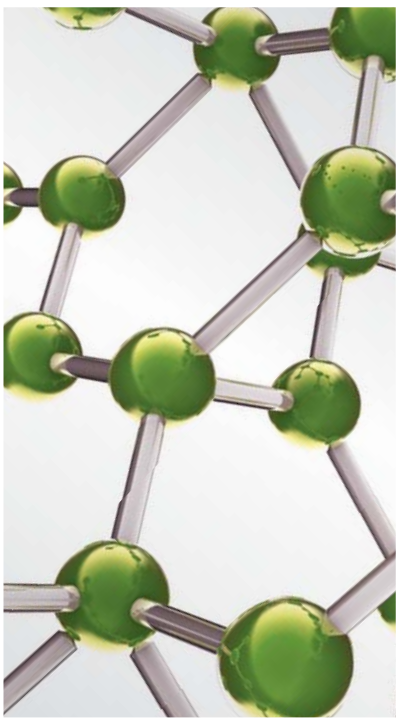


Marine Biotechnology

Evidence-Based Complementary
and Alternative Medicine

Marine Biotechnology

Guest Editors: Song Qin, W. E. G. Müller,
and Edwin L. Cooper

Editorial Board

Contents

Hindawi Publishing Corporation
Evidence-Based Complementary and Alternative Medicine
Volume 2011, Article ID 639140, 2 pages
doi:10.1155/2011/639140

Editorial
Marine Biotechnology

Song Qin,[1] W. E. G. Müller,[2] and Edwin L. Cooper[3]

[1] *Chinese Academy of Sciences, Beijing 100864, China*
[2] *Johannes Gutenberg University of Mainz, 55122 Mainz, Germany*
[3] *University of California, Los Angeles, Los Angeles, CA 90095, USA*

Correspondence should be addressed to Song Qin, sqin@yic.ac.cn

Received 4 September 2011; Accepted 4 September 2011

Modern marine biotechnology has been developing rapidly since the 1980s. There are promising and exciting achievements in biochemistry, genetics, genomics, aquaculture, bioenergy, and other related fields, beginning with genetic recombinant technology as applied to marine algae. Marine biotechnology clearly incorporates enormous social and economic benefits, thus providing a foundation for problems related to food as exemplified by ocean farming. Marine biotechnology is relatively young but reveals enormously vigorous and powerful applications. These include approaches of marine biotechnology from genomics to marine aquaculture and from genomic engineering to ocean farming.

For more specific health benefits to humans, applicable pharmaceuticals are likely to emerge as more natural products are shown to be effective. This special issue is devoted to marine biotechnology. This issue contains 33 papers that pertain to our original goals and include twelve topics: *algal biotechnology; marine microbiology; marine drugs; genomics, proteomics, and metabolomics in marine biotechnology; marine bioactive compounds; marine bioproducts; biomaterials and nanobiotechnology; biomineralization, biomineral, and biomarker; oceans and human health; drug discovery; biotechnology and development; pharmacologic mechanisms*.

For the convenience of the readers papers have generally been arranged according to the genus and species of the organism from which products have been derived. Briefly here are the descriptions: papers 1–6: bacteria; 7–13: algae; 14-15: fungi; 16–19: microbial libraries; 20–25: complex higher invertebrates; 26–27: sponges; 28: crabs; 29–31: fish; 32: humans. To round out the entire list, the final paper 33 focuses on metagenomic libraries.

The inspiration for this special issue has grown from early contributions to Evidence-Based Complementary and Alternative Medicine. The term bioprospecting was introduced by Müeller and later expanded by Cooper. The prefix bio signifies life while prospecting is defined as "an expectation, a possibility, a chance of success or advancement" to explore in search of something. When put together, they fit the kind of searches that have been explored in this issue. Compounds such as bioactive proteins (pore-forming protein and tachylectin) from sponges may be used for antibacterial activity while skeletal elements such as biosilica serve as blueprints for new biomaterials applicable to biomedicine. And since that time, other papers have emphasized the importance of the biosphere (both terrestrial and aquatic) as a vital store for expanding the repertoire of potential products that can ultimately be of use as sources of food and pharmaceuticals.

In addition to a search for marine natural products, clearly the symposium and now the resulting issue have underscored the need for international cooperation as we continue to search for products with valuable applications to human health. The aim of this issue was to present recent advances in the discovery and development of marine natural products, which has laid the foundation for the synthesis of proteins, drugs, and other bioproducts with special functions. Manuscripts in this special issue covered several aspects of recent developments in the vast field of marine biotechnology. Other manuscripts highlight previous investigations but are orientated towards the more practical concerns of application rather than simple analysis of exotic marine animals themselves. The firm grounding of biology and the resulting amalgam of molecules derived from invertebrate immune systems lies at the forefront of new scientific discovery and societal advancement.

Acknowledgments

We would like to warmly acknowledge the authors for their excellent contributions and the reviewers for their fundamental work and patience in assisting us during peer review. We express deep appreciation to Hanzhi Lin and Pu Yang for their extremely valuable assistance during the entire review process.

Song Qin
W. E. G. Müller
Edwin L. Cooper

Hindawi Publishing Corporation
Evidence-Based Complementary and Alternative Medicine
Volume 2011, Article ID 209406, 5 pages
doi:10.1155/2011/209406

Research Article

Isolation and Identification of *Acholeplasma* sp. from the Mud Crab, *Scylla serrata*

Ji-Gang Chen,[1,2] Dan Lou,[2] and Ji-Fang Yang[1,2,3]

[1] *Municipal Key Laboratory of Microorganism and Environmental Engineering, Ningbo, Zhejiang 315100, China*
[2] *College of Biological and Environmental Sciences, Zhejiang Wanli University, Ningbo, Zhejiang 315100, China*
[3] *College of Food Science and Technology, Huazhong Agricultural University, Wuhan, Hubei 430070, China*

Correspondence should be addressed to Ji-Fang Yang, jfkwlq@163.com

Received 5 January 2011; Accepted 3 June 2011

For the first time, a mollicute-like organism (MLO) was cultured from moribund mud crabs (*Scylla serrata*) during an outbreak of clearwater disease in Zhejiang Province, China. The MLO displayed a fried-egg colony morphology in culture, did not possess a cell wall, and was not retained by 0.45 μm and 0.2 μm filters. It was able to ferment glucose, sucrose, lactose, and maltose, but it did not utilize arginine and urea. The MLO grew in the absence of bovine serum and was not susceptible to digitonin. Sequence analysis of the 16S rRNA gene revealed that this MLO had 99% identity with *Acholeplasma laidlawii* PG-8A, which indicates that the organism isolated from mud crabs is a member of the genus *Acholeplasma*.

1. Introduction

The class Mollicutes represents a unique category of bacteria, the members of which are characterized by a small cell size, the absence of a cell wall, a reduced genome, and a simplified metabolic pathway [1]. They can be pathogenic or saprophytic and commensal [2]. To date, mollicutes have been observed and identified in many vertebrate, insect, and plant hosts [2]. Mollicutes also have been reported from several aquatic animals, such as fish [3], shrimp [4–8], crab [9], oyster [10], crayfish [11, 12], and bryozoan [13, 14]. However, mollicutes of aquatic animals, especially those of crustaceans, have not been studied extensively. Only a few mollicutes associated with crustaceans have been isolated, purified, and had their taxonomic status confirmed [4, 9].

The mud crab, *Scylla serrata* (Forska), traditionally called the green crab, is an economically important marine species cultured in the Chinese provinces of Zhejiang, Fujian, Guangdong, Guangxi, and Hainan. Since the 1990s, the *S. serrata* aquaculture industry has experienced rapid growth. However, the industry also is facing increasing economic losses caused by the outbreak of various diseases, such as sleeping disease (SD) [15] and milk disease [16]. In 2005, an epidemic of clearwater disease (CD) broke out in Zhejiang Province. The symptoms of this disease included debility, weak grip strength of pincers, hydroabdomen, white carapace, drying of gill filaments, and weak blood coagulation capacity. The estimated mortality at the affected farms was ~80%. Mollicute-like organisms (MLOs) together with reo-like viruses (unpublished data) have been implicated as causes of CD. However, the MLO has not been isolated and cultivated, thus the precise taxonomic status and pathogenesis of the MLO in *S. serrata* have been unclear.

In this study, the MLO from mud crabs showing signs of CD was isolated and cultivated. The taxonomic classification of this organism was determined by morphology, physiological properties, and DNA analysis, and its pathogenesis was investigated.

2. Materials and Methods

2.1. Mud Crab. Two male and three female moribund or dead mud crabs with CD were obtained from a pond of a mud crab farm during the CD outbreak in August 2005 in Sanmen County, Zhejiang Province. Using electron microscopy, two different organisms were detected in the five crabs: reo-like viruses and MLOs (unpublished data).

2.2. Culture. In a previous study, we found that the MLO was present mainly in the epithelium of gill cells (unpublished

data). Therefore, the gill was selected for isolation of the MLO. Excised gill tissue was placed in mycoplasma liquid medium (MLM); each 100 mL of medium contained 2.55 g of mycoplasma broth base (Frey), 0.5 mL of 0.4% phenol red, 0.2 mL of 10% thallium acetate (Sigma), 20 mL of mycoplasma-free FBS (Hangzhou Sijiqing Biological Engineering Materials Co., Ltd.), 1 mL of freshly prepared yeast extract solution, 1 mL of ampicillin solution (10 mg mL^{-1}), and 1 mL of 10% glucose solution, and the solution was adjusted to pH 7.8. MLO solid medium (MSM) was prepared in the same manner as described above, but it contained 1% medium technical agar (Oxoid). It was supplemented with mycoplasma broth base, yeast extract solution, FBS, thallium acetate, and ampicillin in the same concentrations as those used for MLM, but it did not contain phenol red and glucose.

The MLO culture procedure was designed as previously described by Ghadersohi and Owens [4] with slight modification. Briefly, gill and gut tissue from individual crabs was homogenized in 3 mL of MLM at 4°C using a glass tissue blender. Once a homogenous suspension was produced, 200 μL aliquots were used to prepare a series of 10-fold dilutions in MLM. Negative controls consisted of FBS and other medium constituents in MLM. Inoculated tubes were incubated at 37°C and examined daily for pH (color) changes. Whenever the color of the medium turned from red to yellow, 300 μL of the culture medium were transferred into a tube containing 3 mL fresh of MLM. After 6 to 7 days, 50 μL from each tube with the highest dilution indicating growth was spotted onto MSM plates. The plates were incubated in a humidified atmosphere with 5% CO_2 at 37°C for 14 days. Inoculated plates were examined for the presence of colonies using a stereomicroscope (Olympus). MLO colony growth differences in plates incubated aerobically and in 5% CO_2 were recorded. Cellular morphology of the organisms was examined by light microscopy after application of Gram and Giemsa stains.

2.3. Colony Staining. To observe MLO colonies and differentiate between *Mollicute* and bacterial L-form colonies, MLO colonies were stained with Dienes stain [17] as described by Ghadersohi and Owens [4]. The preparation was then examined with a microscope under low power.

2.4. Purification Experiment. Isolated MLOs were purified using the single colony technique [4]. A single colony was removed by cutting out a small block of agar using a sterile scalpel. The colony was transferred into a tube containing 3 mL of MLM and incubated for 48 h. The culture was diluted 1/10 and 1/100 in MLM, and 50 μL of each dilution were spotted onto MSM plates and incubated in a humidified atmosphere containing 5% CO_2 at 37°C for 7 days. This purification procedure was repeated three times.

2.5. Ultramicroscopy. For ultrathin sectioning, MLOs on MLM medium were pelleted by centrifugation (12 000 g for 10 min at 4°C), resuspended in 2.5% glutaraldehyde, embedded in 4% Noble agar, placed on Formvar-coated copper grids for solidification, and fixed again in 2.5% glutaraldehyde in phosphate buffered saline (PBS; 0.1 mol L^{-1}, pH 7.2) at 4°C for 2 h. After several rinses with PBS, the samples were post-fixed with 1% OsO_4 for 1 h. Subsequently, the tissues were dehydrated in an ethanol series and embedded in Spurr's resin. Ultrathin sections were stained with uranyl acetate and lead citrate and observed under a transmission electron microscope (TEM).

2.6. Biochemical Tests. The mud crab MLO's metabolism of glucose, sucrose, lactose, and maltose [18, 19] was examined, as was its hydrolysis of arginine and urea [20, 21] and its reduction of tetrazolium chloride and methylene blue [4]. All plates and tests were incubated at 37°C in a humidified atmosphere with 5% CO_2 for 7 days.

2.7. Sterol Requirement. The MLO's sterol requirement was established by testing the susceptibility of the isolates to digitonin and by placing the isolates in an MLM lacking serum [22].

2.8. Haemolysis and Hemadsorption. The isolated MLO was examined for hemolytic activity and hemadsorption using sheep, chicken, and rabbit erythrocytes using previously described methods [23].

2.9. Filtration Studies. MLO cultures were diluted 1 : 10 in a liquid medium and filtered through membrane filters (Millipore) with pore diameters of 0.22 μm and 0.45 μm. The numbers of colony-forming unit (CFU) per milliliter in the filtrates were determined by plating the filtrates onto agar and were compared with the numbers of CFU per milliliter in an unfiltered culture dilution [24].

2.10. Reversion Experiment. Isolated MLOs were subcultured eight consecutive times in liquid or solid growth medium lacking ampicillin or thallium acetate to determine whether the organisms reverted to bacterial L forms. Agar plates and fluid cultures of all passages were examined for alterations in the morphology of clones and cells, respectively. In addition, the agar colonies of each clone were stained with Dienes stain and examined with low power light microscopy.

2.11. Analysis of Partial 16S rRNA Gene Sequence. DNA for phylogenetic analysis was extracted from mid-log phase cultures after five passages of a clonal MLO isolate (strain ZJ2005) using the QIAamp DNA Mini kit (Qiagen). The 16S rRNA gene was amplified using M1 and M2 primers [24], cloned into the pMD18-T vector (TaKaRa), and then transformed into *E. coli* Top 10 competent cells. Plasmid DNA, which was purified using the QIAprep Spin Miniprep kit (Qiagen), was sequenced afterwards. The obtained 16S rRNA gene was compared to archived genetic sequences using BLAST searches within the GenBank database [25]. Highly similar sequences were selected for phylogenetic tree construction. The phylogenetic tree was constructed with the neighbor-joining method using MEGA 4.1 software [26].

2.12. Experimental Infection. The pathogenesis of ZJ2005 was tested in a mud crab bioassay. ZJ2005 cultures were grown in 5 mL of MLM at 37°C for 48 h, after which a

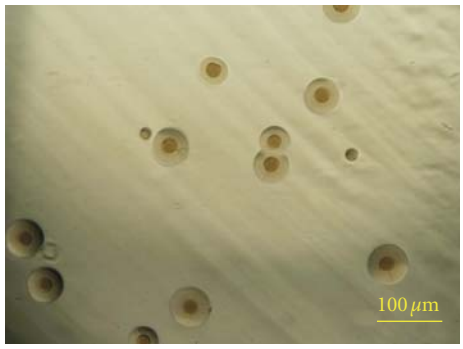

Figure 1: Typical fried-egg colony morphology of the mollicute-like organism from *Scylla serrata*. It was cultured on mycoplasma liquid medium under aerobic conditions for 5 days (bar = 100 μm).

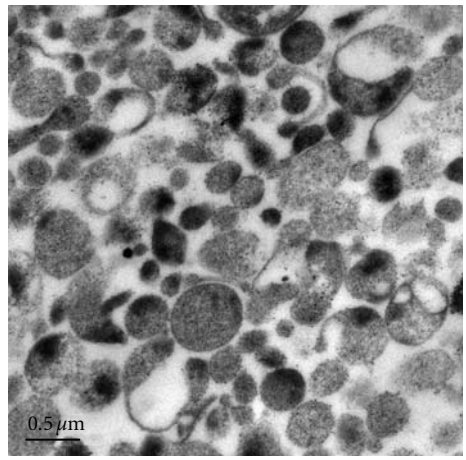

Figure 2: Electron micrograph of an ultrathin section of the mollicute-like organism from *Scylla serrata* (bar = 0.5 μm).

decimal dilution series was made in 1 mL MLM. An aliquot from each dilution was spotted onto MSM. The number of colonies on the agar was used to calculate the number of ZJ2005 organisms in the MLM culture.

A total of 30 clinically healthy mud crabs from a research breeding facility were used in the experimental infections and randomly placed into one of three groups. Members of Group 1 ($n = 10$) were injected with 200 μL of 0.75% saline water containing 1×10^6 CFU ZJ2005 into a leg joint of the fifth pair of pereiopods; the crabs then were placed in a 20‰ salinity, pathogen-free, 30 L aquarium and held at 25–28°C. Members of Group 2 ($n = 10$) were exposed to ZJ2005 by bathing them in 10 L of aerated sea water (20‰ salinity) in aquaria containing 1×10^6 CFU ZJ2005 at 28°C for 4 h. These passively exposed crabs were removed and placed in another 20‰ salinity, pathogen-free, 30 L aquarium at 25–28°C. Group 3 ($n = 10$) acted as the control group; crabs in this group were injected with 200 μL of sterile 0.75% saline water and then held in a 20‰ salinity, pathogen-free, 30 L aquarium at 25–28°C.

3. Results

3.1. Cultivation of Clinical Samples. MLOs were removed from all moribund mud crabs ($n = 5$). Isolated and cultured MLOs decreased the pH of the MLM and formed typical fried-egg shaped colonies (Figure 1). The colonies were readily stained with Dienes reagent, which confirmed that the isolate was a true member of the Mollicutes rather than a bacterial L form [4].

3.2. Morphology. Ultrathin sections showed two morphological types of cells: (i) markedly electron-dense filamentous lobulated cells of various shapes, but often they were curved (0.5–2 μm) and (ii) considerably larger cells (0.1–0.5 μm) of a more oval shape with a less compact and a less dense cytoplasm (Figure 2). The cells were bounded by a single unit membrane and contained densely packed ribosomes, between which were found fine strands of less dense material that were presumed to be portions of the cell's nuclear structure.

3.3. Biochemical Tests. The MLO of mud crabs was able to ferment glucose, sucrose, lactose, and maltose without utilizing arginine and urea. The MLO grew in the absence of bovine serum and was not susceptible to digitonin. It was haemolytic for all three types of erythrocytes tested, but it did not haemadsorb these cells. No dye reduction occurred when the MLO was grown in MSM containing tetrazolium chloride or methylene blue. It grew in MLM containing a NaCl concentration from 0.5 to 3%.

3.4. Filtration Studies. Cultures were diluted 1 : 10 in MLM and then sequentially passed through membrane filters with 0.45 μm and 0.22 μm pore diameters. Filtration reduced the colony number from 2.35×10^7 CFU mL^{-1} in the unfiltered culture to 9.00×10^6 CFU mL^{-1} in the 0.45 μm filtrate and to 6.59×10^4 CFU mL^{-1} in the 0.22 μm filtrate.

3.5. Reversion Experiments. The isolate was diluted 1 : 10 in an MLM medium without antibiotics and incubated at 37°C for a total of eight passages. Each passage was subcultured on agar without antibiotics, and the cultures were examined for differences in colony morphology. No reversion was observed.

3.6. 16S rRNA Gene Sequence Analysis. The 16S rRNA gene nucleotide sequence of ZJ2005 is 1425 nt in length (GenBank accession no. GU985440). Overall, the 16S rRNA gene nucleotide sequence similarity data placed strain ZJ2005 in the *Acholeplasma laidlawii* phylogenetic clade (Figure 3), where its closest relative (similarity score: 0.99) was an isolate provisionally named *A. laidlawii* PG-8A (GenBank accession no. FJ226559).

3.7. Experimental Infections. Cumulative mortality by 15 days was 4/10 for Group 1 (1 on day 4, 1 on day 6, and 2 on day 7). For Group 2, mortality by 15 days was 3/10 (1 on day 8 and 2 on day 12). Interestingly, no clinical signs were observed in any of the dead experimental crabs, but MLOs were isolated from the gut and gill of all of the dead

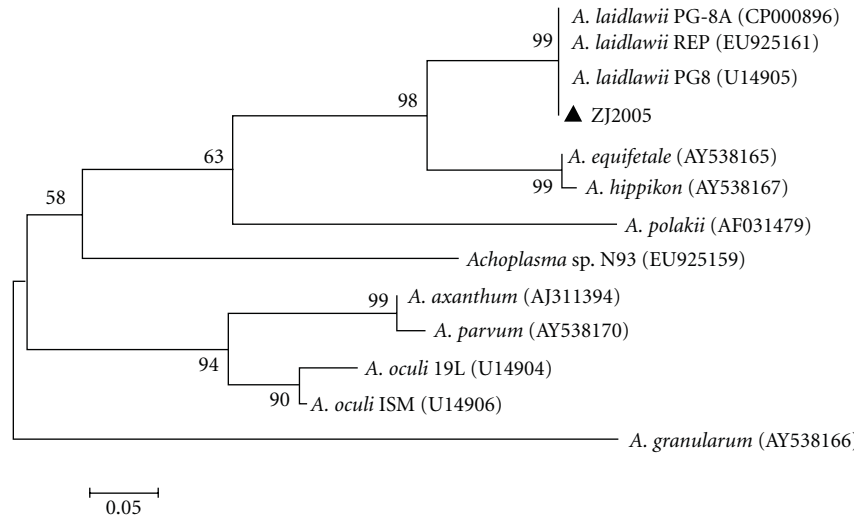

Figure 3: Phylogenetic tree based on 16S rRNA gene sequences showing the relationship of ZJ2005 and some members of the *Acholeplasma* group. Strain designations have been reported, and GenBank accession numbers are included. Bootstrap confidence level percentage values obtained from 1000 resamplings of the dataset are shown at the nodes. (bar, distance equivalent to 5 substitution per 100 nucleotides).

experimental crabs. No mortality, clinical signs, or MLOs were found in the unaffected experimental crabs and the crabs in control group.

4. Discussion

The properties of the MLO isolated from mud crabs fulfilled the essential criteria for *Mollicutes* as proposed by the International Committee Systematic Bacteriology Subcommittee on Taxonomy (1995): it had a typical fried-egg colony form in culture, a polymorphic cell form, absence of a cell wall, passage through 0.45 μm and 0.2 μm filters, lack of reversion to bacteria, and resistance to ampicillin [1]. The results of 16S rRNA gene analysis and the biological, biochemical, and morphological studies indicated that the isolated MLO is a member of the genus *Acholeplasma*. Taxonomically, *Acholeplasma* belongs to the kingdom *Bacteria*, division *Firmicutes*, class *Mollicutes*, order *Acholeplasmatales*, family *Acholeplasmataceae*, and genus *Acholeplasma.* There are 15 recognized species in this genus, including saprotrophic and pathogenic species [27–30]. Although *Acholeplasma* spp. are widely distributed in nature and can be detected and isolated from different plant, avian, and mammalian sources [31–33], they have not been reported previously in aquatic animals. Our detection of *Acholeplasma* in *S. serrata* increases our knowledge about the host ranges of these organisms and should lead to further investigation of other possible aquatic hosts and to studies of possible relationships between terrestrial and aquatic hosts.

The MLO in our study had 99% identity with *A. laidlawii* based on 16S rRNA genes. The three most useful criteria in *Acholeplasma* taxonomy are the 16S rRNA gene sequence, DNA-DNA hybridization analysis, and serology. The highest resolution is provided by 16S rRNA gene sequence analysis, which is useful for the discrimination of most species [9]. Our study has shown that the organism isolated from mud crabs is indeed a member of the genus *Acholeplasma*. However, further studies are needed to precisely identify the actual species. It is closely related to *A. laidlawii*, but it may represent a new species.

The MLO in the experimentally infected crabs did not cause high mortality or result in clinical signs of disease, which is not surprisingly because most *Acholeplasma* diseases are influenced by a variety of host and environmental factors. Moreover, a virulent strain can occur naturally, and some animals might carry *Acholeplasma* with no signs of disease until they are stressed [2]. However, the isolation of pure MLO from epithelium of gill and gut tissues of dead crabs suggests that the MLO might be only a cofactor for a reo-like virus, which was thought to be the main pathogen causing CD in mud crabs [34].

Acknowledgments

This work was supported by the National Natural Science Foundation of China (no. 30800856), the Major Scientific and Technical Project of the Ningbo Science and Technology Bureau in Zhejiang Province (no. 2007C11002), and a project of the Ningbo Science and Technology Bureau in Zhejiang Province (no. 2010C91035).

References

[1] International Committee on Systematic Bacteriology Subcommittee on the Taxonomy of Mollicutes, "Revised minimum standards for the description of new species of the class *Mollicutes* (division *Tenericutes*)," *International Journal of Systematic Bacteriology*, vol. 45, no. 3, pp. 605–612, 1995.

[2] J. W. Simecka, J. K. Davis, M. K. Davidson, S. E. Ross, C. T. Stadtlander, and G. H. Cassell, "*Mycoplasma* diseases of animals," in *Mycoplasmas: Molecular Biology and Pathogenesis*, J. Maniloff, R. McElhaney, L. Finch, and J. Baseman, Eds., pp. 91–394, American Society for Microbiology, Washington, DC, USA, 1992.

[3] H. Kirchhoff, P. Beyene, M. Fisher et al., "*Mycoplasma mobile* sp. nov., a new species from fish," *International Journal of Systematic Bacteriology*, vol. 37, no. 3, pp. 192–197, 1987.

[4] A. Ghadersohi and L. Owens, "Isolation, characterisation and DNA analysis of *Mycoplasma* spp. from moribund prawns *Penaeus monodon* cultured in Australia," *Diseases of Aquatic Organisms*, vol. 35, no. 1, pp. 53–61, 1999.

[5] R. M. Krol, W. E. Hawkins, and R. M. Overstreet, "Rickettsial and mollicute infections in hepatopancreatic cells of cultured Pacific white shrimp (*Penaeus vannamei*)," *Journal of Invertebrate Pathology*, vol. 57, no. 3, pp. 362–370, 1991.

[6] J. F. Yang and Y. L. Wu, "Electron microscope study on mycoplasma-like of penaeid shrimp (*Penaeus chinensis*)," *Donghai Marine Science*, vol. 10, no. 4, pp. 63–67, 1992.

[7] D. L. Choi, S. G. Sohn, M. A. Park, M. S. Heo, and T. Renault, "Detection of a mollicute-like organism in kuruma shrimp, *Penaeus japonicus*," *Journal of Fish Pathology*, vol. 9, no. 1, pp. 33–40, 1996.

[8] P. F. Frelier, R. F. Sis, T. A. Bell, and D. H. Lewis, "Microscopic and ultrastructural studies of necrotizing hepatopancreatitis in Pacific white shrimp (*Penaeus vannamei*) cultured in Texas," *Veterinary Pathology*, vol. 29, no. 4, pp. 269–277, 1992.

[9] W. Wang, B. Wen, G. E. Gasparich et al., "A spiroplasma associated with tremor disease in the Chinese mitten crab (*Eriocheir sinensis*)," *Microbiology*, vol. 150, no. 9, pp. 3035–3040, 2004.

[10] J. C. Harshbarger, S. C. Chang, and S. V. Otto, "Chlamydiae (with phages), mycoplasmas, and rickettsiae in Chesapeake Bay bivalves," *Science*, vol. 196, no. 4290, pp. 666–668, 1977.

[11] B. Edgerton, L. Owens, L. Harris, A. Thomas, and M. Wingfield, "A health survey of farmed redclaw crayfish, *Cherax quadricarinatus* (Von Martens), in tropical Australia," *Freshwater Crayfish*, vol. 10, pp. 322–337, 1995.

[12] R. Jiménez, R. Barniol, X. Romero, and M. Machuca, "A prokaryotic intracellular organism in the cuticular epithelium of cultured crayfish, *Cherax quadricarinatus (von Martens)*, in Ecuador," *Journal of Fish Diseases*, vol. 21, no. 5, pp. 387–390, 1998.

[13] R. L. Zimmer and R. M. Woollacott, "Mycoplasma-like organisms: occurrence with the larvae and adults of a marine bryozoan," *Science*, vol. 220, no. 4593, pp. 208–210, 1983.

[14] P. J. Boyle, J. S. Maki, and R. Mitchell, "Mollicute identified in novel association with aquatic invertebrate," *Current Microbiology*, vol. 15, no. 2, pp. 85–89, 1987.

[15] S. P. Weng, Z. X. Guo, J. J. Sun, S. M. Chan, and J. G. He, "A reovirus disease in cultured mud crab, *Scylla serrata*, in southern China," *Journal of Fish Diseases*, vol. 30, no. 3, pp. 133–139, 2007.

[16] Y. Y. Li, X. A. Xia, Q. Y. Wu, W. H. Liu, and Y. S. Lin, "Infection with *Hematodinium* sp. in mud crabs *Scylla serrata* cultured in low salinity water in southern China," *Diseases of Aquatic Organisms*, vol. 82, no. 2, pp. 145–150, 2008.

[17] L. Timms, "Isolation and identification of avian mycoplasma," *The Journal of Medical Laboratory Technology*, vol. 24, no. 2, pp. 79–89, 1967.

[18] B. Aluotto, R. G. Wittler, C. O. Willams, and J. E. Faber, "Standardized bacteriologic techniques for the characterization of Mycoplasma species," *International Journal of Systematic Bacteriology*, vol. 20, no. 1, pp. 35–38, 1970.

[19] S. Razin and V. P. Cirillo, "Sugar fermentation," in *Methods in Mycoplasmology*, S. Razin and J. G. Tully, Eds., pp. 337–343, Academic Press, New York, NY, USA, 1983.

[20] M. F. Barile, "Arginine hydrolysis," in *Methods in Mycoplasmology*, S. Razin and J. G. Tully, Eds., pp. 345–349, Academic Press, New York, NY, USA, 1983.

[21] S. Razin, "Urea hydrolysis," in *Methods in Mycoplasmology*, S. Razin and T. G. Tully, Eds., pp. 351–353, Academic Press, New York, NY, USA, 1983.

[22] J. G. Tully, "Tests for digitonin sensitivity and sterol requirement," in *Methods in Mycoplasmology*, S. Razin and J. G. Tully, Eds., pp. 355–362, Academic Press, New York, NY, USA, 1983.

[23] R. S. Gardelia and R. A. DelGiudice, "Hemagglutination, hemadsorption, and hemolysis," in *Methods in Mycoplasmology*, S. Razin and J. G. Tully, Eds., pp. 379–384, Academic Press, New York, NY, USA, 1983.

[24] H. Kirchhoff, K. Mohan, R. Schmidt et al., "*Mycoplasma crocodyli* sp. nov., a new species from crocodiles," *International Journal of Systematic Bacteriology*, vol. 47, no. 3, pp. 742–746, 1997.

[25] S. F. Altschul, W. Gish, W. Miller, E. W. Myers, and D. J. Lipman, "Basic local alignment search tool," *Journal of Molecular Biology*, vol. 215, no. 3, pp. 403–410, 1990.

[26] K. Tamura, J. Dudley, M. Nei, and S. Kumar, "MEGA4: molecular Evolutionary Genetics Analysis (MEGA) software version 4.0," *Molecular Biology and Evolution*, vol. 24, no. 8, pp. 1596–1599, 2007.

[27] C. R. Woese, J. Maniloff, and L. B. Zablen, "Phylogenetic analysis of the mycoplasmas," *Proceedings of the National Academy of Sciences of the United States of America*, vol. 77, no. 1, pp. 494–498, 1980.

[28] H. Neimark and J. London, "Origins of the mycoplasmas: sterol-nonrequiring mycoplasmas evolved from streptococci," *Journal of Bacteriology*, vol. 150, no. 3, pp. 1259–1265, 1982.

[29] J. D. Pollack, J. Banzon, K. Donelson et al., "Reduction of benzyl viologen distinguishes genera of the class *Mollicutes*," *International Journal of Systematic Bacteriology*, vol. 46, no. 4, pp. 881–884, 1996.

[30] A. F. Angulo, R. Reijgers, J. Brugman et al., "*Acholeplasma vituli* sp. nov., from bovine serum and cell cultures," *International Journal of Systematic and Evolutionary Microbiology*, vol. 50, no. 3, pp. 1125–1131, 2000.

[31] J. G. Tully, "Acholeplasmataceae," in *Bergey's Manual of Systematic Bacteriology*, N. R. Krieg and J. G. Holt, Eds., pp. 775–781, Williams & Wilkins, Baltimore, Md, USA, 1984.

[32] S. Razin, D. Yogev, and Y. Naot, "Molecular biology and pathogenicity of mycoplasmas," *Microbiology and Molecular Biology Reviews*, vol. 62, no. 4, pp. 1094–1156, 1998.

[33] R. D. Ayling, S. E. Bashiruddin, and R. A. J. Nicholas, "Mycoplasma species and related organisms isolated from ruminants in Britain between 1990 and 2000," *Veterinary Record*, vol. 155, no. 14, pp. 413–416, 2004.

[34] B. J. Wadher, C. L. Henderson, R. J. Miles, and H. Varsani, "A mutant of *Mycoplasma mycoides subsp. mycoides* lacking the H_2O_2-producing enzyme L-α-glycerophosphate oxidase," *FEMS Microbiology Letters*, vol. 72, no. 1-2, pp. 127–130, 1990.

Hindawi Publishing Corporation
Evidence-Based Complementary and Alternative Medicine
Volume 2011, Article ID 729216, 8 pages
doi:10.1155/2011/729216

Research Article

Immune Efficacy of a Genetically Engineered Vaccine against Lymphocystis Disease Virus: Analysis of Different Immunization Strategies

Fengrong Zheng,[1] Xiuqin Sun,[1] Xing'an Wu,[2] Hongzhan Liu,[3] Jiye Li,[1] Suqi Wu,[2] and Jinxing Zhang[2]

[1] *First Institute of Oceanography, State Oceanography Administration of China, 6 Xianxialing Road, Qingdao City, Shandong Province 266061, China*
[2] *Department of Microbiology, Fourth Military Medical University, 17 Changlexi Road, Xi'an City, Shanxi Province 710032, China*
[3] *Marine College, Shandong University, Weihai 264209, China*

Correspondence should be addressed to Xiuqin Sun, xiuqin_sun@fio.org.cn and Xing'an Wu, wuxingan@fmmu.edu.cn

Received 23 December 2010; Revised 24 March 2011; Accepted 16 May 2011

Here, we report the construction of a vaccine against lymphocystis disease virus (LCDV) using nucleic acid vaccination technology. A fragment of the major capsid protein encoding gene from an LCDV isolated from China (LCDV-cn) was cloned into an eukaryotic expression vector pEGFP-N2, yielding a recombinant plasmid pEGFP-N2-LCDV-cn0.6 kb. This plasmid was immediately expressed after liposomal transfer into the Japanese flounder embryo cell line. The recombinant plasmid was inoculated into Japanese flounder via two routes (intramuscular injection and hypodermic injection) at three doses (0.1, 5, and 15 μg), and then T-lymphopoiesis in different tissues and antibodies raised against LCDV were evaluated. The results indicated that this recombinant plasmid induced unique humoral or cell-mediated immune responses depending on the inoculation route and conferred immune protection. Furthermore, the humoral immune responses and protective effects were significantly increased at higher vaccine doses via the two injection routes. Plasmid pEGFP-N2-LCDV0.6 kb is therefore a promising vaccine candidate against LCDV in Japanese flounder.

1. Introduction

Nucleic acid immunization, based on the introduction of plasmid DNA encoding a protective antigen into animal tissue, can express the plasmid-encoded protein and induce subsequent immune responses [1]. Much effort has been invested in this technology since gene engineering vaccines possess multiple advantages over killed, attenuated, or subunit vaccines [2]. Indeed, gene engineering vaccines are known to stimulate both nonspecific and specific immune responses without the need for live organisms, replicating vectors or adjuvants [3]. Antigen synthesis induced by nucleic acid vaccination imitates natural infection by intracellular pathogens and leads to subsequent cell-mediated responses and ultimately, the generation of memory lymphocyte responses [4]. Additionally, gene engineering vaccines have already been shown to provide protection for fish to various intracellular pathogens, such as viral hemorrhagic septicemia and infectious hematopoietic necrosis virus [5, 6]. Anderson et al. (1996) reported the first application of gene engineering vaccine technology where a plasmid containing the glycoprotein (G) gene of IHNV was used to stimulate a protective immune response in rainbow trout fry [7]. Furthermore, several studies have shown that a nucleic acid vaccine against IHNV provides significant protection in rainbow trout against either waterborne or injection challenges in fish that range in size from 2 to 160 g [8–10]. Traxler et al. (1999) have reported significantly high levels of protection against IHNV also observed in vaccine efficacy studies in Atlantic salmon, other economically important species [11]. A Nucleic acid vaccine containing the G gene of other rhabdoviral pathogen of rainbow trout, viral hemorrhagic septicemia virus (VHSV), has also been shown to provide significant protection when administered alone or

in combination with a nucleic acid vaccine against IHNV [5, 6, 12].

Studies regarding nucleic acid vaccines for fish published in recent years have mainly focused on infectious hematopoietic necrosis virus (IHNV) [8, 9, 12–16], viral hemorrhagic septicemia virus (VHSV) [5, 6, 12, 17–19], hirame rhabdovirus (HIRRV) [20], herpesvirus (IHV-1) [21], infectious pancreatic necrosis [22], red sea bream iridovirus (RSIV), and spring viraemia of carp virus [23]. However, research regarding lymphocystis disease virus (LCDV), the causative agent of lymphocystis disease (LCD), a common chronic disease among many salt and fresh water fish species, remains limited. LCD occurs worldwide, and the rate of incidence appears to be increasing [24], severely affecting the fish farming industry.

We previously constructed two genetically engineered vaccines against LCDV for the prevention and control of LCD [25, 26] and investigated the distribution and expression of immune-related genes in Japanese flounder (*Paralichthys olivaceus*) after immunization with the vaccines [26, 27]. In this study, we investigated the optimal inoculation routes and doses for these vaccines in Japanese flounder.

2. Materials and Methods

The FG-9307 cell line from Japanese flounder gills and the flounder embryo cell (FEC) line from Japanese flounder were obtained from Dr. Shangliang Tong, Ocean University of China and Dr. Songlin Chen, Yellow Sea Fisheries Research Institute Chinese Academy of Fishery Sciences, respectively. The two cell lines were maintained in minimum essential medium (MEM) and Dulbecco's modified Eagle's medium (DMEM), respectively. Culture medium was supplemented with 15% heat-inactivated fetal bovine serum (FBS), 2 mM L-glutamine, 50 IU/mL penicillin, 50 mg/mL streptomycin (Cellgro, USA), and 1% nonessential amino acids (Cellgro, USA), buffered to pH 7.4 with 7.5% sodium bicarbonate. The fish FG-9307 and FEC lines were maintained at 22°C and 24°C, respectively.

Tumors obtained from infected fish were wiped to remove the connective tissue and then freeze-thawed three times and centrifuged at 3000 g for 15 min. The cell suspension was then loaded onto a 20–60% sucrose gradient and centrifuged at 20,000 g for 2 h. The virus was observed using a photomicroscope, and the virus concentration was determined using a spectrophotometer.

LCDV was propagated in the FG-9307 cell line [28, 29]. The culture medium was harvested when viral cytopathic effects were apparent, and the clarified crude virus was stored at −80°C until use.

2.1. Clone, Identification, and Sequence Analysis of 0.6 kb Fragment. Viral DNA was extracted from LCDV samples following the manufacturer's instructions (OMEGA, USA). DNA was precipitated with 100% ethanol, washed three times with 70% ethanol, air dried, and suspended in 40 μL sterile, distilled, and autoclaved water. DNA concentration was estimated using a spectrophotometer.

A fifty-microliter PCR reaction mixture consisting of 5 μL DNA, 0.05 nmol of each primer, 4 μL 2 mM $MgCl_2$, 2.5 units *Taq* DNA polymerase, 4 μL 2 nM dNTP, 5 μL PCR buffer, and ultrapure water 26 μL was prepared. A primer pair flanking the *Mcp* gene, the forward (5′-GAC GAA TTC ATG ATC GGT ATT AC-3′), and the reverse (5′-GAC GCG GCC GCG AAT AAT ATT CAC T-3′) primers were used. Amplification was performed at 94°C for 4 min, followed by 28 cycles of 1 min denaturation at 94°C, 45 s of annealing at 50°C, and 45 s of extension at 72°C, and a final extension at 72°C for 10 min.

2.2. Construction of Gene Engineering Vaccine against Lymphocystis Disease Virus. The gene encoding ORF 0147L of the major capsid protein (MCP), approximately 0.6 kb in length, and the eukaryotic expression vector pEGFP-N2 (Invitrogen) were verified by *Eco*RI and *Sal* I, respectively. The 0.6 bp fragment was cloned into the expression vector pEGFP-N2, behind the cytomegalovirus promoter and yielded EGFP-N2-LCDV0.6 kb.

2.3. Transfection of the Eukaryotic Expression Vector and Evaluation of Expression. Cell transfection was performed using Lipofectamine, in eukaryotic FEC, following the manufacturer's instructions (Gibco BRL). The cells were maintained at 24°C for 48 h after transfection. Fluorescent microscopy and RT-PCR were employed to evaluate the immediate expression of pEGFP-N2-LCDV-cn0.6 kb in the FEC line.

2.4. Preparation of Plasmid DNA. The recombinant plasmid pEGFP-N2-LCDV-cn0.6 kb was verified by digestion with restriction endonucleases *Xho*I and *Bam*HI and then transformed into *E. coli* DH5α. The recombinant plasmid (DNA vaccine) was prepared on a large-scale, distilled, and purified by resin using the Endo Free Plasmid Kit (Promega) according to the manufacturer's instructions. The DNA was then suspended in PBS and stored at −20°C. The quality and quantity of the DNA were determined by spectrophotometry.

2.5. Vaccination of Fish. LCDV free Japanese flounder fish, approximately 15–20 cm in body length and approximately 60–80 g in body weight, were used as fish to evaluate the vaccine function of plasmid DNA. The fish were obtained from a cultivation farm and kept in a tank with a flowthrough, filtered and virus free water system at approximately 18–22°C with water quality monitored daily. They were fed with commercially available dry feed pellets corresponding to 3–5% of total body weight, twice per day. Prior to vaccination, the fish were acclimatized for 2 weeks in the laboratory.

Fish (n = 600 per group) were randomly selected and anaesthetized using 0.02% tricaine methanesulfonate (MS-222). Fish were injected to a depth of 8 mm into the left epaxial muscle immediately anterior to the dorsal fin, using an insulin syringe and a 29 G needle. The experimental fish were divided into 11 groups: (1) control fish, (2) 100 μL phosphate-buffered saline (pH 7.4; PBS) via intramuscular injection (i.m.), (3) 5 μg pEGFP-N2 via i.m., (4) 0.1 μg

pEGFP-N2-LCDV-cn0.6 kb via i.m., (5) 5 μg pEGFP-N2-LCDV-cn0.6 kb via i.m., (6) 15 μg pEGFP-N2-LCDV-cn0.6 kb via i.m., (7) 100 μL PBS via hypodermic injection (i.h.), (8) 5 μg pEGFP-N2 via i.h., (9) 0.1 μg pEGFP-N2-LCDV-cn0.6 kb via i.h., (10) 5 μg pEGFP-N2-LCDV-cn0.6 kb via i.h., and (11) 15 μg pEGFP-N2-LCDV-cn0.6 kb via i.h. Plasmid DNA was dissolved in 100 μL of PBS. After vaccination, each group of 60 fish was kept in different tanks under the same experimental conditions.

2.6. Lymphoproliferative Assay

2.6.1. Preparation of Blood Lymphocytes from Fish. A 0.5 mL blood sample was isolated from the caudal sinus of fish in a sterile coequal anticoagulant in 2.5 mL of lymphoprep separation medium (Solarbio, Beijing, China). The coat layer was collected, washed twice in cold RPMI-1640 medium, and resuspended. The cells were then adjusted to 1×10^6 cells/mL with RPMI-1640 medium supplemented with 2 mM L-glutamine, 10% heat-inactivated FBS, 50 IU/mL penicillin, 50 mg/mL streptomycin, and 1% nonessential amino acids.

2.6.2. The Preparation of Anterior Kidney, Spleen, and Hind Intestines Lymphocytes from Fish. Anterior kidney, spleen, and hind intestines lymphocytes from fish in each control and vaccination group were collected aseptically by removing all tissues and placing the organ in a Petri dish containing 10 mL sterile RPMI-1640 medium (Hyclone, USA). Cells were released from all tissues by mechanical disruption using a curved forceps and a metallic sieve screen (200 μm). The resulting cell suspension was washed twice in RPMI-1640 medium and resuspended in 3 mL RPMI-1640 medium and centrifuged at 1500 g for 15 min. The coat layer was collected, washed twice in cold RPMI-1640 medium, and resuspended. The cells were then adjusted to 1×10^6 cells/mL with RPMI-1640 medium supplemented with 2 mM L-glutamine, 10% heat-inactivated FBS, 50 IU/mL penicillin and 50 mg/mL streptomycin (Cellgro), and 1% nonessential amino acids (Cellgro).

Lymphoproliferative Assay. Cells (500 μL) were cultured in triplicate in 24-well plates (Corning, NY) at 22°C in 5% CO_2 with 2 μL LCDV-cn (19.8 mg/mL), or no additives (negative control). The cells were cultured at 22°C in 5% CO_2 for 48 h. After 48 h, 200 μL Thiazolyl blue (Genview) was added to each well. The cells were incubated for a further 4 h, DMSO was then added to the wells at 500 μL/well, and the absorbance was measured at 570 and 600 nm using a kinetic microplate reader (Molecular Devices). The Thiazolyl blue assay was developed as a nonradioactive lymphocyte proliferation assay, which indirectly measures cell proliferation. The level of proliferation is indicated by the difference between the specific absorbance of the oxidized form (570 nm) and the reduced form (600 nm). The specific absorbance of the unstimulated cells (negative control) is subtracted from the specific absorbance of the cells to yield a delta-specific absorbance.

2.7. Determination of Serum Antibody Levels. Japanese flounder blood samples (1 mL) were collected on days 21, 35, 56, and 90 p.i. with a syringe from the caudal sinus of nine of the eleven groups and allowed to clot at 20°C for 20 min, then 4°C for 12 h. Serum was obtained after centrifugation at 500 g to remove cell particulate matter and stored at 80°C for further study.

The antibody responses of the fish from each group were evaluated for the presence of specific immunoglobulin against LCDV using an indirect ELISA. LCDV was diluted to a 100 μg/mL concentration in bicarbonate coating buffer (pH 9.6) and the solution was used to coat polystyrene plates with 100 μL/well. The plates were incubated at 4°C overnight, washed four times with wash buffer (Tris-buffered saline (TBS) at pH 7.4, 0.05% Tween 20), and blocked with 2% BSA in TBS for 2 h at room temperature. The blocking solution was then removed, and diluted fish serum samples (1 : 80 dilution in blocking solution) were added to individual triplicate wells at 100 μL/well. A positive control serum sample and a diluent only sample were tested in the same manner. The plates were incubated for 90 min at 37°C and then washed four times with wash buffer. The secondary antibody solution, a protein peroxidase conjugate (Sigma), was added at 100 μL/well at a 1 : 1500 dilution. After 90 min at 37°C, the plates were washed four times, and 100 μL of substrate solution (TMB Microwell peroxidase substrate; Kirkegaard & Perry Laboratories, Gaithersburg, MD) was added to each well. After 20 min of incubation at room temperature, 100 μL of stop solution (2 mol/L sulfuric acid) was added. The absorbance at 450 nm was then recorded using a microplate reader (Microplate reader Benchmark, Bio-Rad Laboratories, s.r.1. Milano, Italy). Each serum sample was compared with the control wells.

Challenge Experiment. The experimental fish were divided into four groups: (1) 100 μL PBS, (2) 5 μg pEGFP-N2, (3) 5 μg pEGFP-N2-LCDV-cn0.6 kb via i.m., and (4) 5 μg pEGFP-N2-LCDV-cn0.6 kb via i.h. After vaccination, each group was kept in a different tank under identical experimental conditions. Twenty-one days after vaccination, fish were placed in tanks and infected with LCDV. The fish were then observed, and the growth of tumors was noted after one and two months.

2.8. Statistical Analysis. Results from ELISA and lymphoproliferative assay data were subjected to a mixed model repeated analysis of variance, and SPSS software was employed to compare the various experimental groups each day. The data for each test was reported as the mean ± S.E.M. An overall level of significance with $P < 0.05$ was accepted.

3. Results

3.1. Construction and Identification of the Eukaryotic Expression Vector. The DNA vaccine pEGFP-N2-LCDV-cn0.6 kb was verified by *Xho*I and *Bam*HI endonuclease restriction analysis to contain the desired DNA fragment and associating

Table 1: The 0.6 kb MCP sequence of ORF0147 (71318–71696 amino acids).

ATGATCGGTAATACTATTGATATGACACAACCCGTTGATTCCAATGGTCAATT
ACCTGAAGAAGTGTTAATACTTCCTTTACCTTATTTCTTTTCTCGAGATAGCG
GTATGGCTTTACCCAGCGCTGCTTTGCCTTATAATGAAATAAGATTAACTTTT
CATCTGAGAGATTGGACTGAATTATTGATCTTTCAAAATAAAAACGACTCTA
CCATCATGCCTTTGACAGCAGGCGATTTAGACTGGGGTAAACCTGATTTAA
AGGATGTGCAAGTATGGATTACTAATGTAGTAGTAACCAATGAGGAACGTC
GTTTAATGGGTACAGTACCTAGAGACATCTTGGTGGAACAGGTACAAACAG
CACCTAAACATGTATTTCAACCTCTAACTATTCCAAGTCCTAATTTTGACATC
AGATTTTCTCATGCCATTAAAATCCTTTTTTTCGGTGTGCGTAATGTTACCTA
TCAAGCTATACAATCCAATTACACCAGTTCTTCTCCTGTAATCTTTGACGGT
GGAATTGCTAGCGATTTACCGGGTATTGCTGCTGATCCTATTTCAAATGTTAC
CTTGGTTTATGAAAATAGTGCTCGTCTTAATGAAATGGGTAGTGAATAT

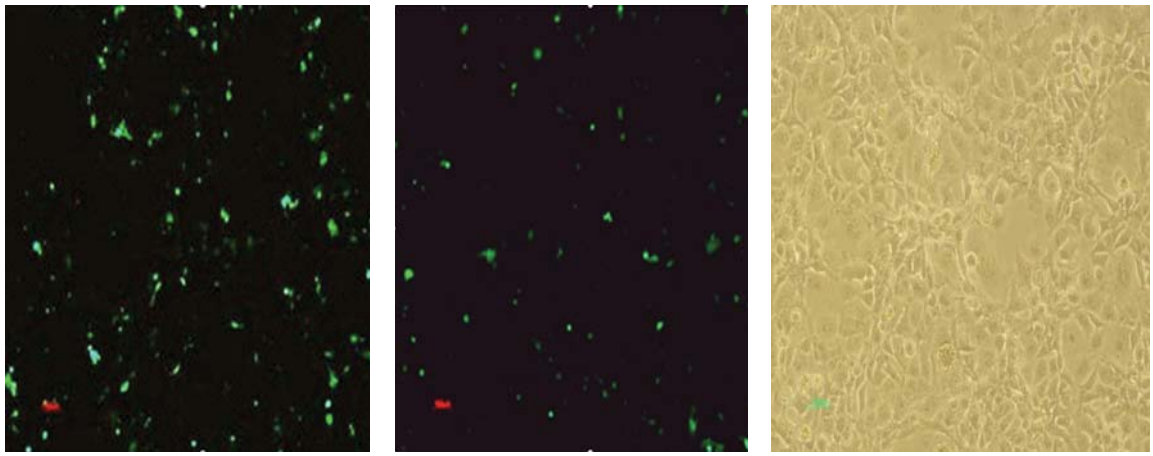

(a) (b) (c)

Figure 1: Fluorescent and optical microscopy images of cells transfected with pEGFP-N2-LCDV-cn0.6 kb and pEGFP-N2 plasmid DNA. (a) Fluorescent microscopy image of pEGFP-N2-LCDV-cn0.6 kb; (b) fluorescent microscopy image of pEGFP-N2; (c) optical microscopy image of pEGFP-N2-LCDV-cn0.6 kb.

elements. The plasmid was prepared, purified, and suspended in endotoxin-free water. The 0.6 kb MCP sequence is shown in Table 1.

3.2. The Detection of Immediate Expression of the Plasmid in the FEC Line by Fluorescent Microscopy. Fluorescent microscopic images of the expression of the FEC cell-transfected plasmid DNA, pEGFP-N2-LCDV-cn0.6 kb, are shown in Figure 1. The image clearly shows that the transfected cells emitted fluorescence, whereas the control untransfected cells did not. The RT-PCR results are shown in Figure 2.

3.3. Lymphoproliferative Detection Assay. Lymphocytes of tissues from all of the groups were cultured *in vitro*, following LCDV stimulation, and significant lymphoproliferative responses were detected on day 21 after vaccination in the peripheral blood, spleen, head, kidney, and hind intestine of all vaccination groups. The level of the response increased with the dose, but no significant difference was observed between the 5 μg and 15 μg doses. Lymphoproliferative responses were found to be particularly high in the peripheral blood and hind intestine samples (Figure 3). No antigen-specific lymphoproliferative responses were detected in

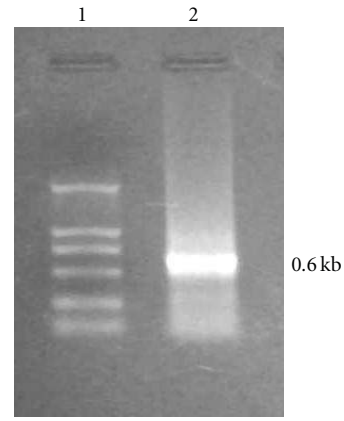

Figure 2: The detection of flounder embryo cells (FECs) transfected by pEGFP-N2-LCDV-cn0.6 kb by RT-PCR. (1) DL2000 DNA marker; (2) 0.6 kb fragment.

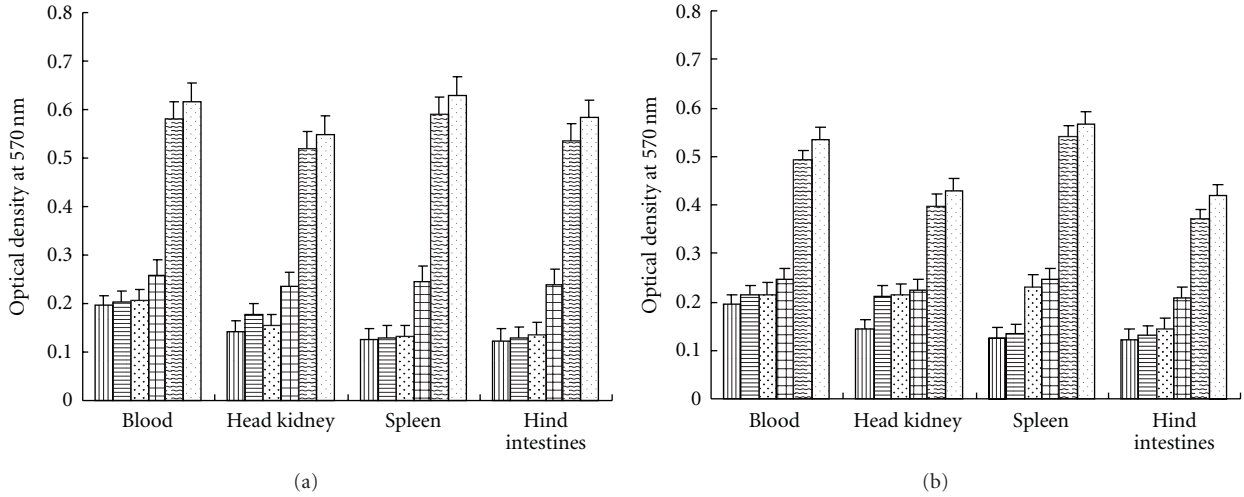

Figure 3: Proliferation of tissue lymphocytes from all groups after *in vitro* stimulation with LCDV. (a) Intramuscular injection; (b) hypodermic injection. Cells were harvested on day 21 and cultured for two days. Control group (vertical bar); PBS group (horizontal bar); 5 μg pEGFP-N2 group (triangular bracket); 0.1 μg pEGFP-N2-LCDV-cn0.6 kb group (pane); 5 μg pEGFP-N2-LCDV-cn0.6 kb group (wave bar); 15 μg pEGFP-N2-LCDV-cn0.6 kb group (dot). Results are shown as the mean ± S.E.M. of the OD_{450} values. Significant differences ($P < 0.05$) were observed between the pEGFP-N2-LCDV-cn0.6 kb group and the no-injection groups, and the PBS and pEGFP-N2 groups.

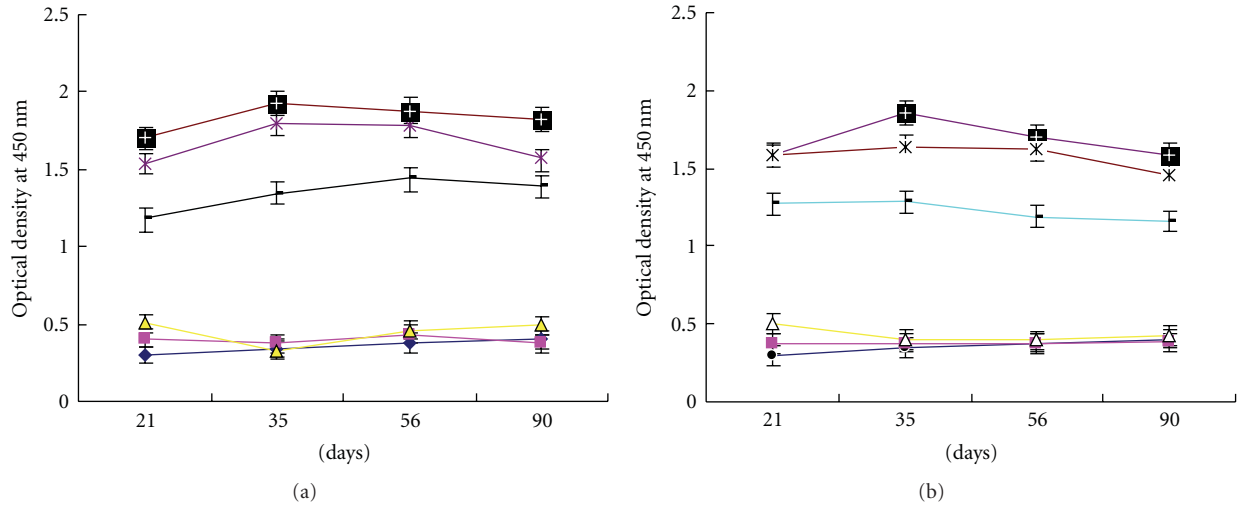

Figure 4: Detection of LCDV-specific antibodies from the sera of DNA-vaccinated Japanese flounder collected on days 21, 35, 56, and 90 after vaccination by ELISA. (a) Intramuscular injection; (b) hypodermic injection. 15 μg pEGFP-N2-LCDV-cn0.6 kb group (plus sign); 5 μg pEGFP-N2-LCDV-cn0.6 kb group (asterisk); 0.1 μg pEGFP-N2-LCDV-cn0.6 kb group (horizontal line); pEGFP-N2 group (triangle); PBS group (square); no injection (block dot). Results are shown as the mean ± S.E.M. of the OD_{450} values.

the pEGFP-N2 or saline groups. These results indicated that plasmid pEGFP-N2-LCDV-cn-MCP0.6 kb has the ability to enhance specific cellular responses, with significantly greater lymphocyte responses detected among the i.m. groups compared with the i.h. groups.

3.4. Antibody Production in the Vaccinated Fish. The antibody response of each group was evaluated for the presence of specific immunoglobulin against LCDV using an indirect ELISA (Figure 4). Low levels of LCDV-specific antibodies were detected in all of the pEGFP-N2-LCDV-cn0.6 kb-vaccinated fish after three weeks, and antibody levels increased along with the dose. Increasing concentrations of antibodies were generated up to 35 days after vaccination, with the greatest increase observed following a booster vaccination on day 21. Significantly greater responses were observed in the 5 and 15 μg groups than in the 0.1 μg group, and there were no significant differences between these former two groups. After day 56, the concentration of antibodies began to decline, though the fish maintained relatively high levels of antibodies until day 90. Slightly higher responses were seen

among the i.h. groups than the i.m. groups on day 21, but the antibody levels in the i.h. groups were lower than in the i.m. groups after 35 days, and this phenomenon persisted after 90 days.

3.5. Protection against LCDV. The protection yielded by recombinant plasmid pEGFP-N2-LCDV-cn0.6 kb is shown in Table 2. One month after challenge, the efficiency of tumor growth in the PBS group, the pEGFP-N2 group, and the pEGFP-N2-LCDV-cn0.6 kb-vaccinated groups was 22.4%, 19.6%, 2.6%, and 2.4%, respectively. The tumors were small and mainly grew in the mouth. Two months after challenge, the efficiency of tumor growth in the groups listed above was 32.6%, 32.1%, 3.17%, and 3.21%, respectively, and the tumors were large and existed throughout the whole body, spreading from the mouth and gills to the fins.

Table 2: The efficiency of tumor growth in the different groups of fish, one and two months after injection.

	PBS group	pEGFP-N2 group	Intramuscular injection 5 μg/fish group	Hypodermic injection 5 μg/fish group
The amount with tumour 1 month (fish)	112	98	26	24
The total amount 1 month (fish)	500	500	1000	1000
The efficiency of tumour growth	22.4%	19.6%	2.6%	2.4%
The amount with tumour 2 months (fish)	158	152	31	31
The total amount 2 months (fish)	484	473	978	967
The efficiency of tumour growth	32.6%	32.1%	3.17%	3.21%

4. Discussion

The development of genetically engineered vaccines for fish has been increasingly studied in recent years, and such vaccines have been shown to provide protection in fish against various intracellular pathogens, such as VHSV and IHNV [5, 6]. The fact that these vaccines successfully induced a protective immune response against intracellular pathogens suggested that a genetically engineered vaccine against LCDV infection was also feasible; however, until now, this possibility had not been widely studied. In the present study, we analyzed the MCP gene (01470.6-kb) of LCDV-cn, which encodes 71696–72318 amino acids, and revealed a 0.6 kb antigenic fragment. This fragment was cloned into the prokaryotic expression vector pCI-neo and was found to elicit specific responses to polyclonal antiserum against LCDV. The eukaryotic expression vector pEGFP-N2, containing the GFP gene, was used in our experiments under the control of the CMV promoter. We demonstrated that a genetically engineered vaccine encoding the LCDV MCP gene elicited significant levels of protective LCDV-specific immunity, the levels of which were dose dependent and roughly proportional to the amount of protection conferred.

We analyzed vaccination strategies based on two injection routes, intramuscular injection and hypodermic injection, and three injection doses, 0.1, 5, and 15 μg of naked circular plasmid DNA. These selected doses fall within the range of plasmid DNA (1–50 μg) routinely used to express foreign genes in fish muscle and were found to be adequate to induce antigen-specific immune responses in 60–80 g Japanese flounder. At this preliminary stage, no attempt was made to evaluate the effects of intramuscular injection using different doses of DNA, which has already been detailed for other fish species [1, 28–32]. Specific experiments based on Japanese flounder biology are required to address each of these points prior to potentially applying these vaccines to farmed fish.

In a previous study in goldfish, antibodies against β-galactosidase were detected as early as seven days after injection of LacZ-encoding DNA, and the antibody response lasted for at least 10 weeks although the number of antibody-producing cells appeared to decline rapidly [30]. In rainbow trout, antibodies to the VHSV G protein were detected 23 days after injection with a plasmid encoding the G gene, and serum antibodies to the G protein of IHNV were detected 3 to 15 weeks after inoculation [5, 7]. The results of the present study showed that injection of naked plasmid DNA containing the MCP gene induced an efficient, systemic, and antigen-specific immune response in Japanese flounder, with detectable anti-LCDV antibody levels in fish 21 days after injection.

Some differences were found in vaccine efficiency when comparing the three vaccine doses. Low levels of specific antibodies to LCDV were detected in all pEGFP-N2-LCDV-cn0.6 kb-vaccinated fish three weeks after inoculation, and the antibody level increased with the increasing dose. Significant protective immune responses were generated following administration of the 15 and 5 μg doses, but not the 0.1 μg dose on day 21, indicating that the 5 μg dose was more efficient than the 15 μg dose when considering overall protection. No specific antibody responses were detected in the PBS or pEGFP-N2 groups.

Although the specific immune responses varied according to dose, a different effect was exhibited when the nonspecific respiratory burst was evaluated. However, in the present study, the induction of a respiratory burst increased after vaccination, but no difference was observed between the control and vaccinated groups.

In conclusion, our results strongly suggested that both humoral and cellular responses were stimulated by the vaccine. These initial findings indicate the potential for the development of a protective vaccine against LCDV.

Acknowledgments

This study was supported by the State 863 project (2006AA100309). The authors wish to express their gratitude to Professor Songlin-Chen for donating the FEC cell line.

References

[1] J. Heppell, N. Lorenzen, N. K. Armstrong et al., "Development of DNA vaccines for fish: vector design, intramuscular injection and antigen expression using viral haemorrhagic septicaemia virus genes as model," *Fish and Shellfish Immunology*, vol. 8, no. 4, pp. 271–286, 1998.

[2] J. Heppell and H. L. Davis, "Application of DNA vaccine technology to aquaculture," *Advanced Drug Delivery Reviews*, vol. 43, no. 1, pp. 29–43, 2000.

[3] A. Tanghe, O. Denis, B. Lambrecht, V. Motte, T. Van Den Berg, and K. Huygen, "Tuberculosis DNA vaccine encoding Ag85A is immunogenic and protective when administered by intramuscular needle injection but not by epidermal gene gun bombardment," *Infection and Immunity*, vol. 68, no. 7, pp. 3854–3860, 2000.

[4] J. J. Donnelly, J. B. Ulmer, J. W. Shiver, and M. A. Liu, "DNA vaccines," *Annual Review of Immunology*, vol. 15, pp. 617–648, 1997.

[5] P. Boudinot, M. Blanco, P. De Kinkelin, and A. Benmansour, "Combined DNA immunization with the glycoprotein gene of viral hemorrhagic septicemia virus and infectious hematopoietic necrosis virus induces double-specific protective immunity and nonspecific response in rainbow trout," *Virology*, vol. 249, no. 2, pp. 297–306, 1998.

[6] N. Lorenzen, E. Lorenzen, K. Einer-Jensen, J. Heppell, T. Wu, and H. Davis, "Protective immunity to VHS in rainbow trout (Oncorhynchus mykiss, Walbaum) following DNA vaccination," *Fish and Shellfish Immunology*, vol. 8, no. 4, pp. 261–270, 1998.

[7] E. D. Anderson, D. V. Mourich, S. C. Fahrenkrug, S. LaPatra, J. Shepherd, and J. A. C. Leong, "Genetic immunization of rainbow trout (Oncorhynchus mykiss) against infectious hematopoietic necrosis virus," *Molecular Marine Biology and Biotechnology*, vol. 5, no. 2, pp. 114–122, 1996.

[8] S. Corbeil, S. E. LaPatra, E. D. Anderson et al., "Evaluation of the protective immunogenicity of the N, P, M, NV and G proteins of infectious hematopoietic necrosis virus in rainbow trout Oncorhynchus mykiss using DNA vaccines," *Diseases of Aquatic Organisms*, vol. 39, no. 1, pp. 29–36, 1999.

[9] S. Corbeil, S. E. Lapatra, E. D. Anderson, and G. Kurath, "Nanogram quantities of a DNA vaccine protect rainbow trout fry against heterologous strains of infectious hematopoietic necrosis virus," *Vaccine*, vol. 18, no. 25, pp. 2817–2824, 2000.

[10] S. E. LaPatra, S. Corbeil, G. R. Jones, W. D. Shewmaker, and G. Kurath, "The dose-dependent effect on protection and humoral response to a DNA vaccine against infectious hematopoietic necrosis (IHN) virus in subyearling rainbow trout," *Journal of Aquatic Animal Health*, vol. 12, no. 3, pp. 181–188, 2000.

[11] G. S. Traxler, E. Anderson, S. E. LaPatra, J. Richard, B. Shewmaker, and G. Kurath, "Naked DNA vaccination of Atlantic salmon Salmo salar against IHNV," *Diseases of Aquatic Organisms*, vol. 38, no. 3, pp. 183–190, 1999.

[12] N. Lorenzen, E. Lorenzen, K. Einer-Jensen, J. Heppell, and H. L. Davis, "Genetic vaccination of rainbow trout against viral haemorrhagic septicaemia virus: small amounts of plasmid DNA protect against a heterologous serotype," *Virus Research*, vol. 63, no. 1-2, pp. 19–25, 1999.

[13] E. D. Anderson, D. V. Mourich, and J. A. C. Leong, "Gene expression in rainbow trout (Oncorhynchus mykiss) following intramuscular injection of DNA," *Molecular Marine Biology and Biotechnology*, vol. 5, no. 2, pp. 105–113, 1996.

[14] S. E. LaPatra, S. Corbeil, G. R. Jones et al., "Protection of rainbow trout against infectious hematopoietic necrosis virus four days after specific or semi-specific DNA vaccination," *Vaccine*, vol. 19, no. 28-29, pp. 4011–4019, 2001.

[15] N. Lorenzen, E. Lorenzen, K. Einer-Jensen, and S. E. LaPatra, "Immunity induced shortly after DNA vaccination of rainbow trout against rhabdoviruses protects against heterologous virus but not against bacterial pathogens," *Developmental and Comparative Immunology*, vol. 26, no. 2, pp. 173–179, 2002.

[16] K. A. Garver, S. E. LaPatra, and G. Kurath, "Efficacy of an infectious hematopoietic necrosis (IHN) virus DNA vaccine in Chinook Oncorhynchus tshawytscha and sockeye O. nerka salmon," *Diseases of Aquatic Organisms*, vol. 64, no. 1, pp. 13–22, 2005.

[17] N. Lorenzen, E. Lorenzen, and K. Einer-Jensen, "Immunity to viral haemorrhagic septicaemia (VHS) following DNA vaccination of rainbow trout at an early life-stage," *Fish and Shellfish Immunology*, vol. 11, no. 7, pp. 585–591, 2001.

[18] P. E. McLauchlan, B. Collet, E. Ingerslev, C. J. Secombes, N. Lorenzen, and A. E. Ellis, "DNA vaccination against viral haemorrhagic septicaemia (VHS) in rainbow trout: size, dose, route of injection and duration of protection—early protection correlates with Mx expression," *Fish and Shellfish Immunology*, vol. 15, no. 1, pp. 39–50, 2003.

[19] B. Novoa, A. Romero, V. Mulero, I. Rodríguez, I. Fernández, and A. Figueras, "Zebrafish (Danio rerio) as a model for the study of vaccination against viral haemorrhagic septicemia virus (VHSV)," *Vaccine*, vol. 24, no. 31-32, pp. 5806–5816, 2006.

[20] J. Y. Seo, K. H. Kim, S. G. Kim et al., "Protection of flounder against hirame rhabdovirus (HIRRV) with a DNA vaccine containing the glycoprotein gene," *Vaccine*, vol. 24, no. 7, pp. 1009–1015, 2006.

[21] K. E. Nusbaum, B. F. Smith, P. DeInnocentes, and R. C. Bird, "Protective immunity induced by DNA vaccination of channel catfish with early and late transcripts of the channel catfish herpesvirus (IHV-1)," *Veterinary Immunology and Immunopathology*, vol. 84, no. 3-4, pp. 151–168, 2002.

[22] A. B. Mikalsen, J. Torgersen, P. Alestrom, A. L. Hellemann, E. O. Koppang, and E. Rimstad, "Protection of Atlantic salmon Salmo salar against infectious pancreatic necrosis after DNA vaccination," *Diseases of Aquatic Organisms*, vol. 60, no. 1, pp. 11–20, 2004.

[23] C. M. A. Caipang, T. Takano, I. Hirono, and T. Aoki, "Genetic vaccines protect red seabream, Pagrus major, upon challenge with red seabream iridovirus (RSIV)," *Fish and Shellfish Immunology*, vol. 21, no. 2, pp. 130–138, 2006.

[24] T. Kanellos, I. D. Sylvester, F. D'Mello et al., "DNA vaccination can protect Cyprinus Carpio against spring viraemia of carp virus," *Vaccine*, vol. 24, no. 23, pp. 4927–4933, 2006.

[25] F. R. Zheng, X. Q. Sun, H. Z. Liu, and J. X. Zhang, "Study on the distribution and expression of a DNA vaccine against lymphocystis disease virus in Japanese flounder (*Paralichthys olivaceus*)," *Aquaculture*, vol. 261, no. 4, pp. 1128–1134, 2006.

[26] F. R. Zheng, X. Q. Sun, H. Z. Liu et al., "Study on distribution and expression in vitro and in vivo of DNA vaccine against lymphocystis disease virus in Japanese flounder (*Paralichthys*

olivaceus)," *Chinese Journal of Oceanology and Limnology*, vol. 28, no. 1, pp. 67–74, 2010.

[27] F. R. Zheng, X. Q. Sun, M. Q. Xing, and H. Liu, "Immune response of DNA vaccine against lymphocystis disease virus and expression analysis of immune-related genes after vaccination," *Aquaculture Research*, vol. 41, no. 10, pp. 1444–1451, 2010.

[28] C. A. Tidona, P. Schnitzler, R. Kehm, and G. Darai, "Is the major capsid protein of iridoviruses a suitable target for the study of viral evolution?" *Virus Genes*, vol. 16, no. 1, pp. 59–66, 1998.

[29] E. Garcia-Rosado, D. Castro, S. Rodriguez, S. I. Perez-Prieto, and J. J. Borrego, "Isolation and characterization of lymphocystis virus (FLDV) from gilt-head sea bream (Sparus aurata, L.) using a new homologous cell line," *Bulletin of the European Association of Fish Pathologists*, vol. 19, no. 2, pp. 53–56, 1999.

[30] T. Kanellos, I. D. Sylvester, A. G. Ambali, C. R. Howard, and P. H. Russell, "The safety and longevity of DNA vaccines for fish," *Immunology*, vol. 96, no. 2, pp. 307–313, 1999.

[31] P. H. Russell, T. Kanellos, M. Negrou, and A. G. Ambali, "Antibody responses of goldfish (Carassius auratus L.) to DNA-immunisation at different temperatures and feeding levels," *Vaccine*, vol. 18, no. 22, pp. 2331–2336, 2000.

[32] P. H. Russell, T. Kanellos, I. D. Sylvester, K. C. Chang, and C. R. Howard, "Nucleic acid immunisation with a reporter gene results in antibody production in goldfish (Carassius auratus L.)," *Fish and Shellfish Immunology*, vol. 8, no. 2, pp. 121–128, 1998.

Hindawi Publishing Corporation
Evidence-Based Complementary and Alternative Medicine
Volume 2011, Article ID 393752, 6 pages
doi:10.1155/2011/393752

Research Article

Description of a *Sulfitobacter* Strain and Its Extracellular Cyclodipeptides

Cong Long,[1,2] Xiao-Ling Lu,[1] Yun Gao,[1] Bing-Hua Jiao,[1] and Xiao-Yu Liu[1]

[1] *Department of Biochemistry and Molecular Biology, College of Basic Medical Sciences, Second Military Medical University, Shanghai 200433, China*
[2] *Department of Clinical Laboratory, First Affiliated Hospital of Yangtze University, No. 8 Hangkong Road, Hubei Jingzhou 434100, China*

Correspondence should be addressed to Bing-Hua Jiao, jiaobh@uninet.com.cn and Xiao-Yu Liu, liuxiaoyu8888@msn.com

Received 14 January 2011; Accepted 16 May 2011

A marine bacterium M44 was separated from 30 m deep seawater in the East China Sea (26° 28.3′ N 122° 29.0′ E) in 2006. 16S rDNA gene sequence comparison showed that the strain M44 was a member of the genus *Sulfitobacter* and highly similar to KMM 3554^T. A series of experiments demonstrated that this strain M44 had many distinctive characteristics: its cells were gram-negative and mesophilic; its colonies were slightly yellowish, round, convex, and smooth; and it could grow at 10–28°C, pH 6.0–10.0, and in the presence of 0–12.5% (w/v) NaCl; the optimum growth conditions were 25°C and pH 7.0, and the optimum Na^+ concentration was 2.5%. In addition, strain M44 contained 18 : 1 ω7c, 11 methyl 18 : 1 ω7c and 16 : 0 fatty acids as major fatty acids, and the genomic DNA G+C content was 58.04 mol%. According to our results of the secondary metabolites, six cyclodipeptides were isolated from the strain M44, which were Cyclo (Val-Leu), Cyclo (Phe-Val), Cyclo (Phe-Leu), Cyclo (Leu-Ile), Cyclo (Phe-Ile), and Cyclo (Trp-Pro). It is the first study of secondary metabolites isolated from this genus.

1. Introduction

As marine bacteria live in hypothermic, hyperbaric, and oligotrophic environments that are significantly different from those of terrestrial ones, it is reasonable to suppose that they should have particular physiological and biochemical traits and metabolic pathways. In recent years, there has been more interest in isolation and identification of marine bacteria. Natural products of marine bacteria have been recognized as an important source of novel and biologically active substances [1].

The genus *Sulfitobacter* was first discovered by Sorokin [2] in 1995. In the next few years, bacteria of this genus were subsequently discovered in marine environments, such as seawater collected in the Mediterranean Sea [3], the East China Sea, Korea [4–6], sea grass collected at the Pacific, and starfish in the South China Sea [7]. Bacteria of this genus were also found in hypersaline Ekho Lake, East Antarctica [8]. Nine species have been identified so far.

By now, there are no more research reports on this genus and most of them focused on the physiological and biochemical properties of this genus. To our knowledge, there has been no report on the secondary metabolites of this genus. For the first time, we isolated the metabolites of M44 and elucidated the chemical structure of these compounds by spectral data and MS. The present paper summarized our work about multiphase taxonomic identification and extracellular products composition of a marine *Sulfitobacter* strain M44 from the East China Sea.

2. Materials and Methods

2.1. Sampling. The seawater was collected in 2006 at a depth of 30 m in the East China Sea (26° 28.3′ N 122° 29.0′ E). Strain M44 was obtained in pure culture after three successive transfers to fresh Zobell 2216E agar medium (peptone 0.5%, yeast powder 0.1%, ferric phosphate 0.01%, agar 1.5%), and preserved at −80°C and 4°C on Zobell 2216E agar.

2.2. Phenotype and Physiological Study. Cell morphology was examined under a light microscope (BH-2; Olympus). Colony morphology was observed on Zobell 2216E agar plates after incubation at 28°C for 2-3 days. The pH range for

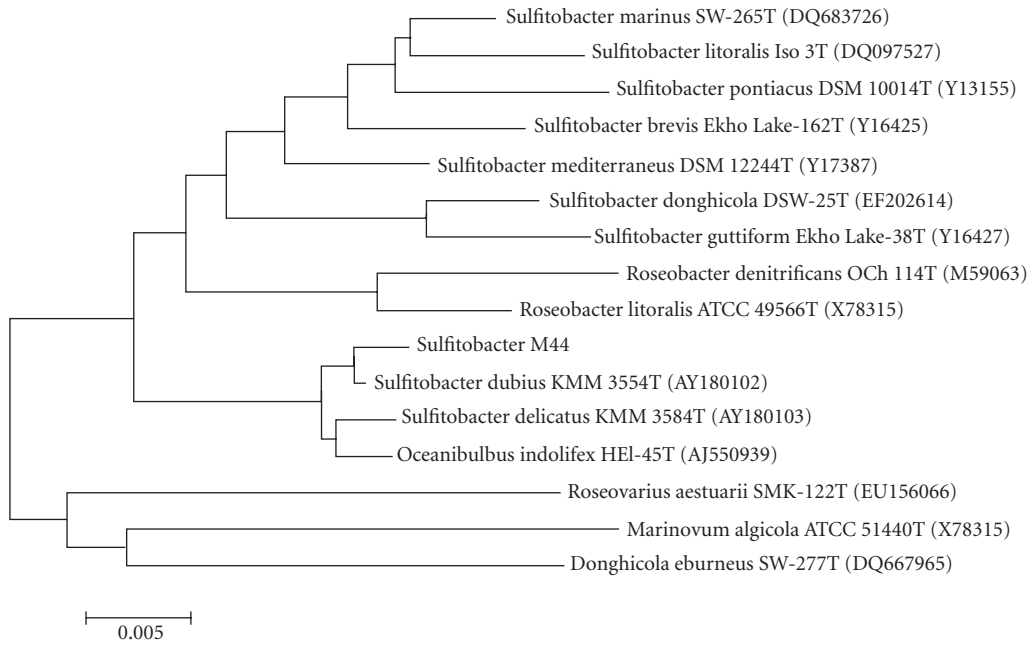

Figure 1: Phylogenetic tree showing the position of strain M44 and related species based on 16S rDNA gene sequence analysis. The tree was constructed by using the neighbour-joining method. Numbers at nodes represent percentage bootstrap support based on a neighbour-joining analysis of 1000 resampled datasets. GenBank accession numbers are given in parentheses. Bar, 0.5% sequence divergence.

growth was determined for the culture in Zobell 2216E broth (peptone 0.5%, yeast powder 0.1%, ferric phosphate 0.01%) at various pH values (4.0, 6.0, 7.0, 8.0, 9.0, and 10.0) adjusted with HCl or NaOH (1 mol/L). The temperature range for growth was examined on Zobell 2216E agar incubated at 8, 10, 20, 25, 28, 30, and 37°C. Sodium requirement [0, 2.5, 5, 7.5, 10.0, and 12.5% (w/v) NaCl] was also investigated. General physiological tests were performed using conventional methods. Biochemical traits were determined using API kits (API 20 E, API ZYMAPI 50CH; bioMérieux). The ability to oxidize sulfite was tested by the method of Pukall et al. [3]. The ability to oxidize thiosulfate and elemental sulfur was tested by the method of Sorokin [2].

2.3. Extraction and Analysis of Fatty Acids. Fatty acids were determined in cells grown on Zobell 2216E agar plates at 28°C for 2-3 days. Fatty acid methyl esters were obtained from a freeze-dried biomass (approx. 10 mg) by saponification, methylation, and extraction using the method of Svetashev et al. [9]. The fatty acid methyl ester mixtures were analyzed on an Agilent GC-6890N (FID), using an Agilent 19091B-102 gas chromatograph column, HP-ULTRA2 Capillary (25.0 m × 200 μm × 0.03 μm). The GC parameters were as follows: carrier gas, ultrahigh-purity hydrogen; carrier gas flow, 0.4 mL·min^{-1}; injection volume, 2 μL; column split ratio, 100 : 1; column temperature, 170–260°C at 5°C min^{-1}, 260–310°C at 40°C min^{-1} and keep 1.5 min (initial column temperature of 170°C); injection port temperature, 250°C; detector temperature, 310°C.

2.4. Molecular Identification. According to the method described by Rainey et al. [10], the genomic DNA of strain M44 was prepared by Genomic DNA Isolation kit (Watson). Then, gene encoding 16S rDNA was amplified by PCR with 16S rDNA Bacterial Identification PCR kit (TaKaRa). An ABI BigDye Terminator 3.1 cycle sequencing kit (Applied Biosystems) and an automated DNA sequencer (model ABI 3730; Applied Biosystems) were used to sequencing the 16S rDNA gene of M44.

2.5. Phylogenetic Analysis. The almost complete 16S rDNA gene sequence of strain M44 was submitted to GenBank to search for similar sequences by using the BLAST algorithm. A phylogenetic tree was constructed by using Kimura's two-parameter and pairwise-deletion model analysis in the program MEGA version 3.0 [11]. The resultant tree topologies were evaluated by bootstrap analysis based on 1000 replicates.

2.6. Determination of Base Composition of DNA. The G+C content of the DNA was determined by using the method of Mesbah et al. [12]. DNA of the strain M44 was enzymatically degraded into nucleosides. The obtained nucleoside mixtures were separated by HPLC, and the value of G+C mol% was calculated based on the result of G/G+T mol %.

2.7. Cultivation of Sulfitobacter Sp. M44. The bacterium was grown on Zobell 2216E agar medium and incubated at 25°C for a day. A loopful of bacterium was inoculated into a 500 mL Erlenmeyer flask containing 150 mL of marine Zobell 2216E broth and incubated on a rotatory shaker at 130 rpm, 25°C, for 7 days.

2.8. Isolation and Identification of Exocellular Cyclic Peptides. The entire culture broth (60 L) was centrifugated at 4000 rpm

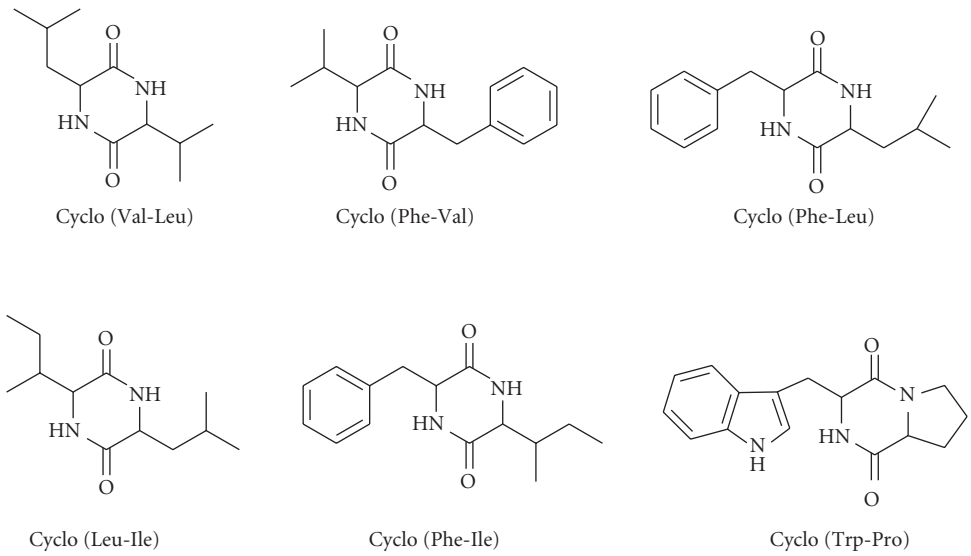

Figure 2: Structures of six diketopiperazines isolated from strain M44.

Table 1: Fatty acid compositions of strain M44 and related *Sulfitobacter* type strains.

Fatty acid	1	2	3	4	5
18 : 1 ω7c	67.01	73.7	63.9	59.9	79.1
11 methyl 18 : 1 ω7c	11.76	5	1.7	6.8	3.7
16 : 0	8.4	6.1	17.8	7	10.1
10 : 0 3 OH	5.42	6.3	3	5.7	3.4
12 : 1 3 OH	4.78	—	1.4	6.1	0

Strains: 1, M44; 2: *Sulfitobacter pontiacus* DSM 10014^T (date from [2]); 3: *Sulfitobacter dubius* ATCC BAA-320^T (date from [7]); 4: *Sulfitobacter delicatus* ATCC BAA-321^T (date from [7]); 5: *Sulfitobacter donghicola* DSW 25^T (date from [5]); values are percentages of total fatty acids; —: not detected.

for 5 min, and the supernatant extracted 3 times with an equal volume of ethyl acetate. The upper layer of liquid was evaporated in vacuum at 30°C to yield 5 g of the crude extract, which was subjected to Sephadex LH-20 gel column and eluted with CH_3OH to get five fractions, one of which was subsequently rechromatographed on C_{18} reversed-phase column with a gradient of water to methanol. The fractions obtained were further purified by reversed-phase high-performance liquid chromatography (RP-HPLC) (Agilent 1100 ZORBA × 80 Å, 4.6 mm × 250 mm) using CH_3CN-H_2O isocratic elution. ^1H and ^{13}C NMR spectra were recorded at 600 and 300 MHz, respectively, on a Bruker AMX-600 spectrometer. Mass spectra were recorded on a Fisons TRIO 2000 spectrometer.

3. Results

3.1. Physiological and Biochemical Properties. The colonies were slightly yellowish, regularly round, convex and smooth, and about 0.8–1.0 mm in diameter after incubation for 48 h on marine agar. No diffusible pigment was produced in the medium. Cells were gram-negative, chemoorganotroph with respiratory metabolism, mesophilic rod-shaped and single, about 0.6–0.8 μm in diameter, and did not form endospores.

The growth condition was determined at 10–28°C, pH 6.0–10.0, and the NaCl concentration was 0–12.5% (w/v), in which the optimum growth condition was 25°C, pH 7.0, and at a 2.5% NaCl concentration. The strain did not oxidize thiosulfate or elemental sulfur but oxidized sulfite. Oxidase, nitrate, indole, urease, H_2S production, lysine decarboxylase, and ornithine decarboxylase reactions were negative, while catalase, gelatin liquefaction, production of arginine dihydrolase, tryptophane desaminase, Voges-Proskauer reaction, and citric acid reactions were positive. Alkaline phosphatase, esterase (C4), esterase lipase (C8), lipase (C14), leucine arylamidase, valine arylamidase, acid phosphatase, and naphthol-AS-BI-phosphohydrolase were present, while cystine arylamidase, trypsin, α-chymotrypsin, α-galactosidase, β-galactosidase, β-glucuronidase, α-glucosidase, β-glucosidase, N-acetyl-β-glucosaminidase, α-mannosidase, and α-fucosidase were absent in assays with the API ZYM system. D-sucrose was utilized as the sole carbon source in assays with the API 50CH system. Acid was weakly produced from mannitol. The rest substrates were not utilized as sole carbon sources.

3.2. Fatty Acid Analysis. The main cellular fatty acids of the strain were 18 : 1 ω7c (67.01%), 11 methyl 18 : 1 ω7c (11.76%), 16 : 0 (8.40%), 10 : 0 3OH (5.42%), and 12 : 1 3OH (4.78%). Minor components included 12 : 0 3OH, 17 : 1 ω8c, 17 : 0, and 18 : 0 isomers.

Table 2: Characteristics that differentiate strain M44 from phylogenetically related *Sulfitobacter* type strains.

Characteristic	1	2	3	4	5
Motility	+	+	+	−	−
DNA G+C content (mol%)	58.04	61.7–62.5	60	63.7	56.9
NaCl range for growth (%, w/v)	0–12.5	0.5–8	1–12	1–8	1–6
Temperature range for growth (°C)	10–28	4–35	10–30	12–37	10–31
Oxidase	−	+	+	+	ND
Nitrate reduction	−	+	+	W	−
API/BIOLOG reactions:					
Citrate	+	W	+	−	−
Gluconate	−	+	+	+	−
Lipase (C14)	+	+	−	−	+
Melibiose	W	W	+	−	−
D-Sucrose	+	ND	−	−	−

Strains: 1: M44; 2: *Sulfitobacter pontiacus* DSM 10014^T (date from [2]); 3: *Sulfitobacter dubius* ATCC BAA-320^T (date from [7]); 4: *Sulfitobacter delicatus* ATCC BAA-321^T (date from [7]); 5: *Sulfitobacter donghicola* DSW 25^T (date from [5]); +: Positive; W: weakly positive; −: negative; ND: no data.

3.3. Molecular Identification of Sulfitobacter M44. Phylogenetic analysis (Figure 1) based on a consensus 1378-bp length of 16S rDNA gene sequences showed that strain M44 was grouped with members of the genus *Sulfitobacter* and formed a distinct cluster with KMM 3554^T (AY180102, 99% sequence similarity) in the neighbour-joining tree.

The G+C content of DNA was determined to be 58.04 mol% for strain M44.

3.4. Extracellular Cyclodipeptide Composition. Based on spectrum data (^{1}H-NMR, ^{13}C-NMR, ESI-MS), six extracellular cyclodipeptide constituents, which were Cyclo (Val-Leu) [13–15], Cyclo (Phe-Val) [16], Cyclo (Phe-Leu) [17], Cyclo (Leu-Ile) [18], Cyclo (Phe-Ile) [17], and Cyclo (Trp-Pro) [19], have been identified from *Sulfitobacter* sp. M44 (Figure 2).

4. Discussion

Based on the phenotypic properties and the results of physiological study and molecular identification, strain M44 has a great similarity to *Sulfitobacter dubius* and should be classified to the genus of *Sulfitobacter*, inwhich many different characteristics can be determined. The fatty acid profile of M44 and related strains gave patterns in which 18 : 1 ω7c ranging from 59.9% to 79.1% predominated, but different compositions could be distinguished on the basis of the remaining fatty acids. Firstly, although all these five strains could produce 11 methyl 18 : 1 ω7c, 16 : 0 and 3-OH 10 : 0 fatty acids, there were some differences in the distribution of them. For unsaturated fatty acid, M44 produced much more 11 methyl 18 : 1 ω7c than other related strains. For straight-chain 16 : 0 fatty acid, M44 showed a certain difference when compared with *Sulfitobacter dubius* ATCC BAA-320^T. The percentage of 16 : 0 fatty acid produced by M44 and *Sulfitobacter dubius* ATCC BAA-320^T was 8.4% and 17.8%, respectively. In addition, M44, *Sulfitobacter dubius* ATCC BAA-320^T, and *Sulfitobacter delicatus* ATCC BAA-321^T produced 3-OH 12 : 1 fatty acid, whereas *Sulfitobacter pontiacus* DSM 10014^T and *Sulfitobacter donghicola* DSW 25^T did not. The details of comparison of the fatty acid compositions were listed in Table 1.

The results of physiological and other characteristics of M44 are described in Table 2. Also included are some of the literature data for the phylogenetic relatives as judged by 16S rDNA gene sequence analysis. Most of these characteristics are the same, but M44 have some unique characteristics. For example, the result of oxidase test of M44 was negative, while the other related strains were positive; M44 used D-Sucrose as sole carbon source, while the other strains did not use it. Besides, M44 have also showed some different characteristics from other strains, which included motility, the ability of nitrate, citrate and lipase (C14) reduction, and the utilization of carbon resources, and so forth. In summary, although the results of 16S rDNA sequence analysis suggest that M44 belongs to the genus of *Sulfitobacter*, we cannot confirm the strain M44 belongs to a new *Sulfitobacter* species based on the current phenotype and physiological study.

According to recent studies, *Sulfitobacter* widely exists in coastal and open ocean environments. Several bioactivities associated with *Sulfitobacter* have been reported, including organic sulfur cycling in the ocean [7], production of sodium-channel blocking toxins [20], host chemical defense [21], and marine oil biodegradation [22]. Consequently, secondary metabolites of *Sulfitobacter* may play important roles in marine ecosystems. However, there has been no report on the elucidation of secondary metabolites of *Sulfitobacter*. Six cyclodipeptides were isolated from M44 according to our work. It is the first report on the secondary metabolites of this genus. A strain-termed *Oceanibulbus indolifex*, located in the same phylogenetic branch, has been reported to produce cyclodipeptides as well, but structurally different from M44 [23]. Published data have shown that cyclodipeptides are bioactive molecules showed a wide range of effects, such as antibacterial, antitumor, and antiviral [24]. In addition, cyclodipeptides can act as hormones and ion carrier molecules [25]. Recently, some cyclodipeptides have been identified as quorum-sensing bacterial sensors [26], which

are used by gram-negative bacteria for cell-cell communication and regulating gene expression in response to population density. That means cyclodipeptides may work through a complicated cross-talk rather than a direct action on other cells.

Generally, our work describes a *Sulfitobacter* strain M44 isolated from the East China Sea, which has some similarities and some differences to the known *Sulfitobacter* strains. And for the first time, we isolated and identified six cyclodipeptides from this genus. The further study should be focused on the molecular mechanism of cyclodipeptides, which may reveal why cyclodipeptides existed in microorganism widely.

Conflict of Interests

The authors declared that there is no conflict of interests.

Acknowledgment

The work was supported by the National Hi-tech R and D Program (2007AA091501), (2006AA09Z416), and (2006 AA09Z425).

References

[1] T. A. Gulder and B. S. Moore, "Chasing the treasures of the sea—bacterial marine natural products," *Current Opinion in Microbiology*, vol. 12, no. 3, pp. 252–260, 2009.

[2] D. Y. Sorokin, "*Sulfitobacter pontiacus* gen. nov., sp. nov. a new heterotrophic bacterium from the black sea, specialized on sulfite oxidation," *Microbiology*, vol. 64, pp. 354–364, 1995.

[3] R. Pukall, D. Buntefuss, A. Frühling et al., "*Sulfitobacter mediterraneus* sp. nov., a new sulfite-oxidizing member of the *α*-*Proteobacteria*," *International Journal of Systematic Bacteriology*, vol. 49, no. 2, pp. 513–519, 1999.

[4] J. A. R. Park, J. W. Bae, Y. D. Nam et al., "*Sulfitobacter litoralis* sp. nov., a marine bacterium isolated from the east sea, Korea," *International Journal of Systematic & Evolutionary Microbiology*, vol. 57, no. 4, pp. 692–695, 2007.

[5] J. H. Yoon, S. J. Kang, M. H. Lee, and T. K. Oh, "Description of *Sulfitobacter donghicola* sp. nov., isolated from seawater of the east sea in Korea, transfer of *staleya guttiformis* Labrenz et al. 2000 to the genus *Sulfitobacter* as *Sulfitobacter guttiformis* comb. nov. and emended description of the genus *Sulfitobacter*," *International Journal of Systematic & Evolutionary Microbiology*, vol. 57, no. 8, pp. 1788–1792, 2007.

[6] J. H. Yoon, SO. J. Kang, and T. K. Oh, "*Sulfitobacter marinus* sp. nov., isolated from seawater of the east sea in Korea," *International Journal of Systematic & Evolutionary Microbiology*, vol. 57, no. 2, pp. 302–305, 2007.

[7] E. P. Ivanova, N. M. Gorshkova, T. Sawabe et al., "*Sulfitobacter delicatus* sp. nov. and *Sulfitobacter dubius* sp. nov., respectively from a starfish *(Stellaster equestris)* and sea grass *(Zostera marina)*," *International Journal of Systematic & Evolutionary Microbiology*, vol. 54, no. 2, pp. 475–480, 2004.

[8] M. Labrenz, B. J. Tindall, P. A. Lawson, M. D. Collins, P. Schumann, and P. Hirsch, "*Staleya guttiformis* gen. nov., sp. nov. and *Sulfitobacter brevis* sp. nov., *α*-3-*proteobacteria* from hypersaline, heliothermal and meromictic antarctic Ekho Lake," *International Journal of Systematic & Evolutionary Microbiology*, vol. 50, no. 1, pp. 303–313, 2000.

[9] V. I. Svetashev, M. V. Vysotskii, E. P. Ivan ova, and V. V. Mikhailov, "Cellular fatty acids of *Alteromonas* species," *Systematic & Applied Microbiology*, vol. 18, no. 1, pp. 37–43, 1995.

[10] F. A. Rainey, N. Ward-Rainey, R. M. Kroppenstedt, and E. Stackebrandt, "The genus *Nocardiopsis* represents a phylogenetically coherent taxon and a distinct actinomycete lineage: proposal of *Nocardiopsaceae* fam. nov," *International Journal of Systematic Bacteriology*, vol. 46, no. 4, pp. 1088–1092, 1996.

[11] S. Kumar, K. Tamura, and M. Nei, "MEGA3: integrated software for molecular evolutionary genetics analysis and sequence alignment," *Briefings in Bioinformatics*, vol. 5, no. 2, pp. 150–163, 2004.

[12] M. Mesbah, U. Premachandran, and W. B. Whitman, "Precise measurement of the G+C content of deoxyribonucleic acid by high-performance liquid chromatography," *International Journal of Systematic Bacteriology*, vol. 39, pp. 159–167, 1989.

[13] D. E. Nitecki, B. Halpern, and J. W. Westley, "A simple route to sterically pure diketopiperazines," *Journal of Organic Chemistry*, vol. 33, no. 2, pp. 864–866, 1968.

[14] W. Pickenhagen and P. Dietrich, "Identification of the bitter principle of *Cocoa*," *Helvetica Chimica Acta*, vol. 58, no. 4, pp. 1078–1086, 1975.

[15] K. Suzuki, Y. Sasaki, N. Endo, and Y. Mihara, "Acetic acid-catalyzed diketopiperazine synthesis," *Chemical & Pharmaceutical Bulletin*, vol. 29, no. 1, pp. 233–237, 1981.

[16] T. Stark and T. Hofmann, "Structures, sensory activity, and dose/response functions of 2,5-diketopiperazines in roasted cocoa nibs *(Theobroma cacao)*," *Journal of Agricultural & Food Chemistry*, vol. 53, no. 18, pp. 7222–7231, 2005.

[17] M. Tullberg, M. Grøtli, and K. Luthman, "Efficient synthesis of 2,5-diketopiperazines using microwave assisted heating," *Tetrahedron*, vol. 62, no. 31, pp. 7484–7491, 2006.

[18] S. M. Wang, "Cyclodipeptides from the roots of *Pannax notoginseng*," *Natural Product Research & Development*, vol. 16, no. 5, pp. 383–386, 2004.

[19] V. Ivanova, U. Graefe, R. Schlegel et al., "Isolation and structure elucidation of tyramine and indole alkaloids from antarctic strain *Microbispora aerata* imbas-11A," *Biotechnology & Biotechnological Equipment*, vol. 17, no. 2, pp. 128–133, 2003.

[20] M. Vásquez, C. Grüttner, B. Möeller, and E. R. B. Moore, "Limited selection of sodium channel blocking toxin-producing bacteria from paralytic shellfish toxin-contaminated mussels *(Aulacomya ater)*," *Research in Microbiology*, vol. 153, no. 6, pp. 333–338, 2002.

[21] W. E. G. Müller, F. Brümmer, R. Batel, I. M. Müller, and H. C. Schrüder, "Molecular biodiversity case study: *Porifera* (sponges)," *Naturwissenschaften*, vol. 90, no. 3, pp. 103–120, 2003.

[22] O. G. Brakstad and A. G. G. L ødeng, "Microbial diversity during biodegradation of crude oil in seawater from the North Sea," *Microbial Ecology*, vol. 49, no. 1, pp. 94–103, 2005.

[23] I. Wagner-Döbler, H. Rheims, A. Felske et al., "*Oceanibulbus indolifex* gen. nov., sp. nov., a north sea alphaproteobacterium that produces bioactive metabolites," *International Journal of Systematic & Evolutionary Microbiology*, vol. 54, no. 4, pp. 1177–1184, 2004.

[24] M. B. Martins and I. Carvalho, "Diketopiperazines: biological activity and synthesis," *Tetrahedron*, vol. 63, no. 40, pp. 9923–9932, 2007.

[25] M. Adamczeski, E. Quinoa, and P. Crews, "Novel sponge-derived amino acids. 5. Structures, stereochemistry, and synthesis of several new heterocycles," *Journal of the American Chemical Society*, vol. 111, no. 2, pp. 647–654, 1989.

[26] G. Degrassi, C. Aguilar, M. Bosco, S. Zahariev, S. Pongor, and V. Venturi, "Plant growth-promoting *Pseudomonas putida* WCS358 produces and secretes four cyclic dipeptides: cross-talk with quorum sensing bacterial sensors," *Current Microbiology*, vol. 45, no. 4, pp. 250–254, 2002.

Hindawi Publishing Corporation
Evidence-Based Complementary and Alternative Medicine
Volume 2011, Article ID 615032, 6 pages
doi:10.1155/2011/615032

Research Article

Isolation and Characterization of a Phosphate-Solubilizing Halophilic Bacterium *Kushneria* sp. YCWA18 from Daqiao Saltern on the Coast of Yellow Sea of China

Fengling Zhu, Lingyun Qu, Xuguang Hong, and Xiuqin Sun

First Institute of Oceanography, State Oceanic Administration of China, No. 6 Xianxialing Road, High-Tech District, Qingdao 266061, China

Correspondence should be addressed to Lingyun Qu, qly@fio.org.cn

Received 15 January 2011; Accepted 16 April 2011

Phosphate-solubilizing bacteria (PSB) function in soil phosphorus cycle, increasing the bioavailability of soil phosphorus for plants. Isolation and application of salt-tolerant or halophilic PSB will facilitate the development of saline-alkali soil-based agriculture. A moderately halophilic bacterium was isolated from the sediment of Daqiao saltern on the eastern coast of China, which also performs phosphate-solubilizing ability. The bacterium was assigned to genus *Kushneria* according to its 16S rRNA gene sequence, and accordingly named as *Kushneria* sp. YCWA18. The fastest growth was observed when the culturing temperature was 28°C and the concentration of NaCl was 6% (w/v). It was founds that the bacterium can survive at a concentration of NaCl up to 20%. At the optimum condition, the bacterium solubilized 283.16 μg/mL phosphorus in 11 days after being inoculated in 200 mL $Ca_3(PO_4)_2$ containing liquid medium, and 47.52 μg/mL phosphorus in 8 days after being inoculated in 200 mL lecithin-containing liquid medium. The growth of the bacterium was concomitant with a significant decrease of acidity of the medium.

1. Introduction

Phosphorus (P) is one of the major essential macronutrients for plants, which is applied to the soil in the form of phosphatic manure. However, a large portion of the applied phosphorus is rapidly immobilized, being unavailable to plants [1]. In average, the content of phosphorus of soil is about 0.05% (w/w); however, only 0.1% of them are usable for plants [2]. Saline-alkali soil-based agriculture develops quickly in recent years. Similar to the fertile soil-based agriculture, the intensive culturing of salt-tolerant and even salt-resistant plants has dramatically decreased the availability of phosphorus in saline-alkali soil. The free phosphatic ion in soil plays a crucial role; the orthophosphatic ion is the only ion which can be assimilated in an appreciable amount by plants [3]. Soil microorganisms involve in a wide range of biological processes including the transformation of soil phosphorus. They solubilize soil phosphorus for the growth of plants [4].

The growth of phosphate-solubilizing bacteria (PSB) often causes soil acidification, playing a key role in phosphorus solubilization [5]. Therefore, PSB are considered the important solubilizers of insoluble inorganic phosphate. In turn, plants reimburse PSB with carbohydrates [6]. Since the beginning of last century, many PSB have been isolated including, for example, those in *Bacillus*, *Pseudomonas*, *Erwinia*, *Agrobacterium, Serratia*, *Flavobacterium*, *Enterobacter*, *Micrococcus*, *Azotobacter*, *Bradyrhizobium*, *Salmonella*, *Alcaligenes*, *Chromobacterium*, *Arthrobacter*, *Streptomyces*, *Thiobacillus,* and *Escherichia* [7]. The microorganisms functioning similarly also include some fungi in genus *Penicillium*, *Aspergillus*, *Rhizopus*, *Fusarium,* and *Sclerotium* [7]. Unfortunately, most PSB isolated previously performed relatively low salinity tolerance, being less appropriate for saline-alkali soil-based agriculture. It is urgently needed to isolate highly halophilic PSB for the development of saline-alkali soil-based agriculture. In this study, a moderately halophilic, phosphate-solubilizing bacterium YCWA18 was isolated and characterized.

2. Materials and Methods

2.1. Bacterial Isolation. The sediment was sampled at Daqiao saltern, Jimo, Qingdao, on the eastern coast of China

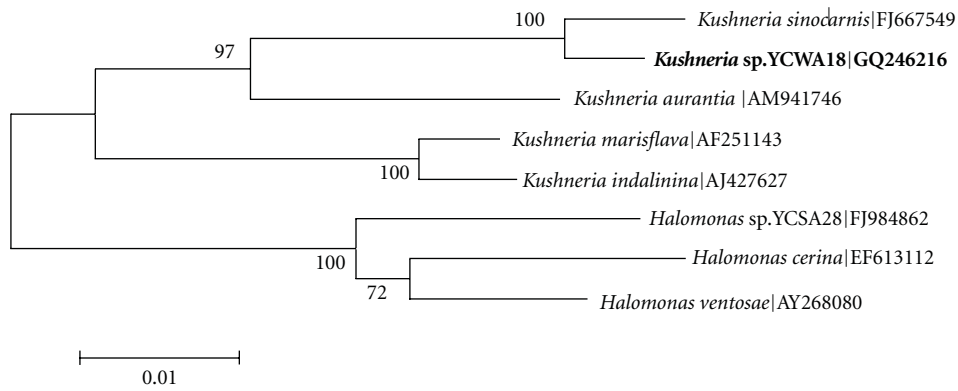

Figure 1: Neighbor-joining phylogenetic tree based on 16S rRNA gene sequences, showing the position of strain YCWA18 with respect to related species.

(E 120°49′12″, N 36°30′00″). Approximately 1 g sediment was suspended in 100 mL sterilized seawater and vortexed for 10 min. The isolates were obtained by plating a serial of 10-fold dilutions of sediment suspension onto a modified marine agar medium (2216E, one liter of seawater contains 5 g tryptone, 1 g yeast extract and 15 g agar, pH 7.5) [8] and incubating at 28°C for 7 days. The isolates were purified by restreaking on 2216E agar plate and microscopic confirmation.

The isolates were screened for their phosphorus-solubilizing ability by culturing at 28°C on the media supplemented either lecithin or $Ca_3(PO_4)_2$. When the colonies appeared in one week, those causing a clear phosphate-solubilizing zone were selected out for further characterization. The size of phosphate-solubilizing zone was determined for each colony.

The modified $Ca_3(PO_4)_2$ culture medium contained with the following ingredients (l^{-1}) [9]: glucose 10 g, $(NH_4)_2SO_4$ 0.5 g, NaCl 30 g, KCl 0.3 g, $FeSO_4 \cdot 7H_2O$ 0.03 g, $MnSO_4 \cdot 4H_2O$ 0.03 g, $MgSO_4 \cdot 7H_2O$ 0.3 g, $Ca_3(PO_4)_2$ 10 g, agar 20 g, H_20 1000 mL, pH 7.0–7.5. The lecithin culture medium was composed of (l^{-1}) [10]: glucose 10 g, $(NH_4)_2SO_4$ 0.5 g, NaCl 30 g, KCl 0.3 g, $FeSO_4 \cdot 7H_2O$ 0.03 g, $MnSO_4 \cdot 4H_2O$ 0.03 g, $MgSO_4 \cdot 7H_2O$ 0.3 g, lecithin 0.2 g, $CaCO_3$ 5 g, yeast extract 0.4 g, agar 20 g, H_20 1000 mL, pH 7.0–7.5.

The ingredients were prepared and sterilized by an autoclave for 20 min at 115°C without lecithin. Lecithin was prepared by diluting in sterile water and was added to the medium before inoculation.

Bacterial isolate was freeze-stored in 2216E medium supplemented with 30% (v/v) glycerol at −80°C.

2.2. Bacterial Characterization. The isolate was phenotypically characterized following the minimal standards for describing the new taxa of family *Halomonadaceae* recommended previously [11]. Gram-staining was carried out with the method described by Dussault [12]. Anaerobic growth performance was determined by inoculating the semisolid 2216E (0.6% agar, w/v) at the bottom of tube and sealing with 2 mL agar (2%, w/v) and 2 mL paraffin. Acidification in liquid medium was observed using bromocresol purple supplemented with 1% of carbohydrate. Other morphological, physiological, and biochemical characterizations were done as described by Mata et al. [13].

2.3. Tests of Salt, pH, and Temperature Tolerance. NaCl tolerance was determined in 2216E medium containing 0, 0.5, 1, 2, 3, 4, 5, 6, 7, 8, 9, 10, 12.5, 15, 20, 25, and 28% (w/v) total salts. The pH range for growth was tested at pH 2.0–11.0 in increments of pH 1.0. Growth was determined at A_{600}. Growth at 0, 6, 10, 15, 20, 24, 28, 32, 37, 42, and 45°C was also determined.

2.4. Taxonomical Assignment. DNA was extracted with the method of Hiraishi [14] and used as the template for the amplification of 16S rRNA gene with universal primers 27F and 1492R [15]. The sequence obtained was aligned with its orthologs retrieved from both GenBank and TYP16S databases. The phylogenetic assignment was performed using MEGA software with bootstrap percentages calculated with 1000 replications.

2.5. Determination of Phosphorus-Solubilizing Ability. The bacterium was inoculated into 200 mL liquid media supplemented with either $Ca_3(PO_4)_2$ or lecithin and cultured at 28°C for 12 days with continuous agitation (150 r/min). 10 ml culture was sampled aseptically every 24 hours for the determination of acidity and available phosphorus. The acidity was assayed simply by reading on a pH meter, and the phosphorus availability was determined with Mo-blue method [16]. Optimum pH and temperature for P-solubilization in liquid $Ca_3(PO_4)_2$ medium were determined following the above method.

3. Results

3.1. Characterization of the Isolate. The closest species of the isolate was *Kushneria sinocarnis*; the similarity between their 16S rRNA genes is 98.57%. As shown in Figure 1, the isolate was assigned to the clade of *K. sinocarnis* with 100% bootstrap support. The isolate was named *Kushneria* sp. YCWA18.

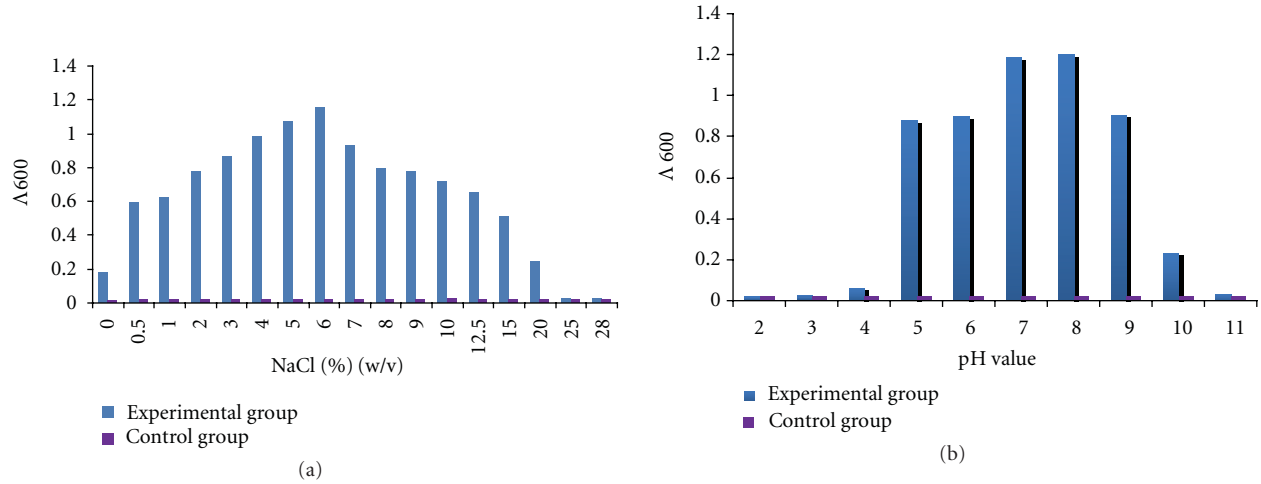

Figure 2: Test of NaCl and pH tolerance of the isolate ((a): NaCl; (b): pH).

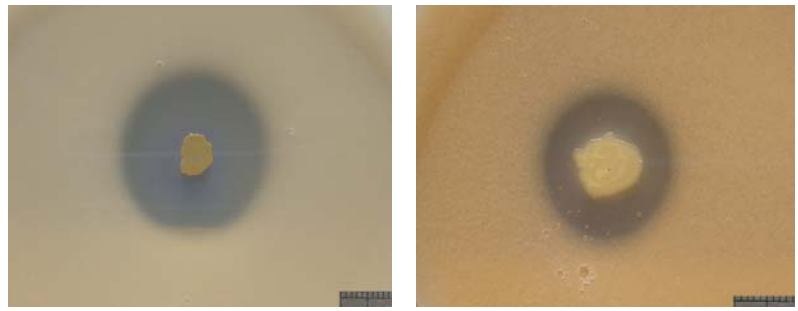

(a) (b)

Figure 3: The phosphate-solubilizing zone formed on medium containing $Ca_3(PO_4)_2$ (a) and lecithin (b). Bar: 1 cm.

It is a Gram-negative bacterium and grows aerobically. Its colony is yellow and round with a diameter between 1.2–2.5 mm after growing on 2216E for 48 hours. The fastest growth is observed at 6% NaCl (w/v), 28°C and pH 7.0–8.0 (Figure 2). The isolate can survive at high concentrations of NaCl (up to 20%) and pH range of 4.0–10.0 (Figure 2). It reduces nitrate and hydrolyzes aesculin but not urea, Tween20 and Tween80. The isolate produces acid from carbohydrates including D-fructose, α-D-glucose, D-mannose, maltose, D-sorbitol, succinamic acid, adonitol and L-alanylglycine but not D-psicose, D- glucosaminic acid, and inosine.

3.2. Growth on $Ca_3(PO_4)_2$ and Lecithin Containing Solid Media. The isolate grows well at 28°C on lecithin and $Ca_3(PO_4)_2$ containing solid media. In 3 days (lecithin containing medium) or 5 days ($Ca_3(PO_4)_2$ containing medium), clear phosphate-solubilizing zone forms. In 10 days, the phosphate-solubilizing zone expanded to the biggest (about 2.5–3.0 cm on $Ca_3(PO_4)_2$ containing plate, Figure 3(a) and about 1.7–2.0 cm on lecithin containing medium, Figure 3(b)).

3.3. Growth in $Ca_3(PO_4)_2$ and Lecithin-Containing Liquid Media. As showed in Figure 4, $Ca_3(PO_4)_2$ solubilization is slow in the first two days and then becomes fast, reaching the highest (283.16 μg/mL) in about 11 days. Lecithin solubilization starts to increases in 1 day, reaching the highest 47.52 μg/mL in 8 days. It was found that the growth of the isolate caused a significant increase of acidity in $Ca_3(PO_4)_2$ containing medium. In about 4 days, the acidity increased from pH 7.21 to pH 4.24. In contrast, the acidity decreased from pH 7.1 to pH 7.46 in lecithin-containing medium.

3.4. The Influence of Temperature and Acidity on Phosphorus Solubilization in $Ca_3(PO_4)_2$-Containing Medium. As showed in Figure 5, the concentration of soluble phosphorus in $Ca_3(PO_4)_2$ containing medium starts to increases in 2 days when the isolate was cultured at 28°C and 32°C, reaching the highest in 7-8 days, faster than the increment achieved at 24°C. At 28°C, the bacterium obtained the highest solubilizing ability of $Ca_3(PO_4)_2$, about 283.16 μg/mL in 200 mL $Ca_3(PO_4)_2$ containing medium at 28°C, while at 32°C and 24°C, it obtained the ability of 217.58 μg/mL, and 187 μg/mL, respectively, and it was found that phosphorus solubilization reached the maximum when the pH value of $Ca_3(PO_4)_2$ containing medium is 7.0.

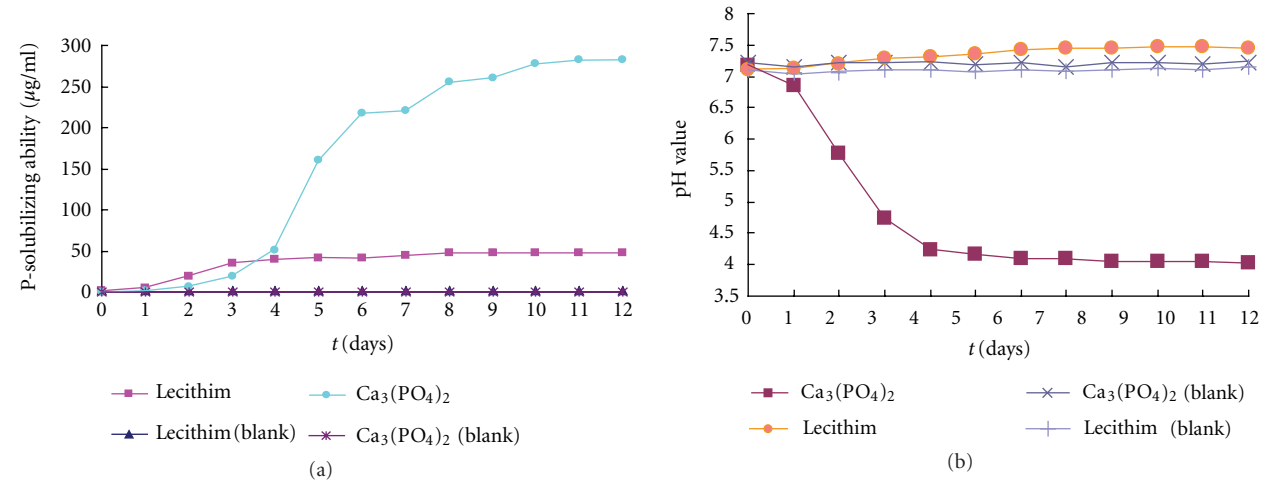

Figure 4: Phosphorus-solubilizing performance of the isolate ((a) P-solubilizing ability; (b) pH value of the medium).

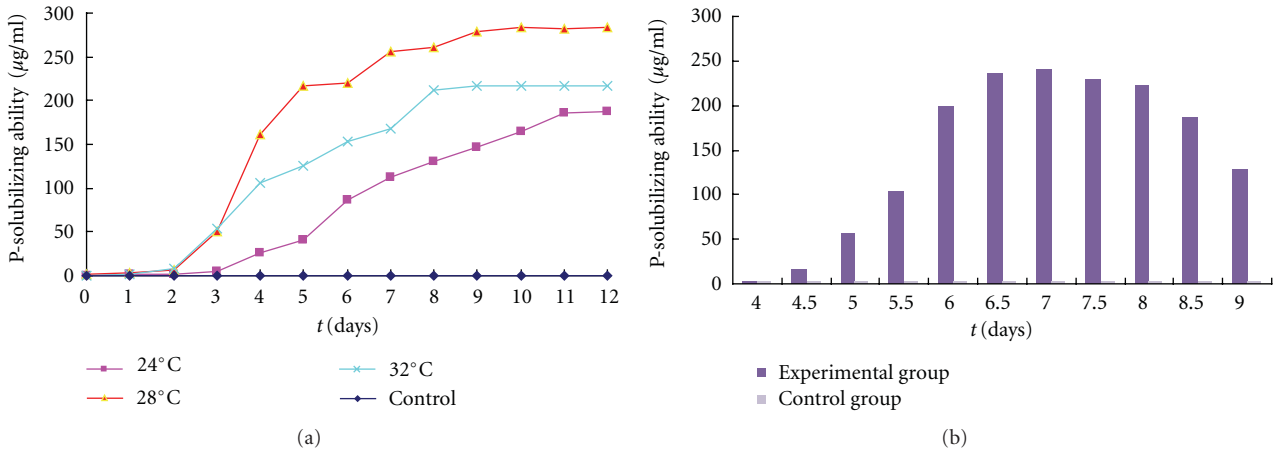

Figure 5: The influence of temperature (a) and acidity (b) on the phosphorus solubilization in $Ca_3(PO_4)_2$ containing medium.

4. Discussions

Phosphorus is an important limiting factor in agriculture production, and microbial activation seems to be an effective way to solve the solidified phosphorus in soil. Many bacterial strains with P-solubilizing abilities have been examined in previous studies, but few of them can function well at high NaCl concentration, and reports on isolation of halophilic PSB strain have not been found yet. The result obtained in this study shows that the isolate YCWA18 has a broad growth range: it can survive at high concentrations of NaCl (up to 20%) and pH range of 4.0–10.0, and it can solubilize both inorganic phosphorus and organophosphorus, and result also shows that its P-solubility for $Ca_3(PO_4)_2$ is higher than for lecithin (Figure 3).

The formation of the clear zones is concerned with the P-solubilization of the strain (Figure 3). It may secrete some substances into surroundings in the course of growing, which can solubilize phosphate or organophosphate. P-solubilization result may vary depending on kinds of the metabolin, how quickly it releases, and also its spread degree on the medium. Therefore, observational method of P-solubilizing zone can only be used to qualitative assays [17].

Phosphorus solubilization is a complex process, which is influenced by diverse factors such as nutritional richness and physiological and growing status of the bacterium [18]. A number of theories have been proposed to explain the mechanism of phosphate solubilization, and the most important among them are acid production theory and enzyme theory. According to the acid production, the process of phosphate solubilization by PSB is due to the production of low molecular weight organic acids that was accompanied by the acidification of the medium [6, 19, 20], and those organic acids can chelate the cation with their hydroxyl and carboxyl groups [21]. The analysis of culture filtrates of PSBs has shown the presence of number of organic acids such as malic, glyoxalic, succinic, fumaric, tartaric, alpha keto butyric, oxalic, citric, 2-ketogluconic, and gluconic acid [22–24]. A decrease in the pH of the medium from the initial value of 7.0 to a final value of 2.0 was recorded by many

workers [25, 26], and in our study, the decrease of the pH of $Ca_3(PO_4)_2$-containing medium from pH 7.21 to pH 4.24 also supported this theory.

Enzymolysis is the possible mechanism of lecithin solubilization [27]. The acidity of lecithin-containing medium during culturing is a little higher than that of the control (Figure 4(b)). We believe that phosphorus solubilization from lecithin is not through acidification. It is possible that the increase of lecithin-containing medium during culturing is caused by enzymes which act on lecithin and produce choline.

The association among bacterial growth, supernatant acidity, and the concentration of solubilized phosphorus has been found [28]. As a well-developed strategy, microorganisms have been recruited to transform insoluble phosphorus of mineral sources into the soluble one [29]. As a particular case, Gram-negative bacteria mobilize insoluble phosphate very efficiently; they produce gluconic acid during the extracellular oxidation of glucose catalyzed by quinoprotein glucose dehydrogenase [30]. Microbial phosphorus mobilization should be the only way of increasing plant-available phosphorus in soil [31].

Diverse microorganisms are able to change phosphorus forms; however, their transforming ability may associate with the ecological conditions including soil characteristics and vegetation. It has been found that the performance of phosphorus-solubilizing microorganisms is severely affected by environmental factor, especially stress ones [32, 33]. In order to obtain the bacteria with high phosphorus-solubilizing ability, it is important to use samples of environmental extremes, for example, saline-alkali soil. In this work, a high phosphorus-solubilizing bacterium was isolated from the sediment if a saltern. It can grow on the solid media containing 20% (w/v) of sodium chloride, being halotolerant according to the suggested standards [34]. The biological characteristics and factors influencing its phosphate-solubilizing ability need to be studied further. Our trials paved an effective avenue of isolating halophilic and phosphorus-solubilizing bacteria from marine environment in order to promote saline-alkali soil-based agriculture.

Acknowledgment

This work was supported financially by National Natural Science Foundation of China (41006103), Public science and technology research funds projects of ocean (201105007-01), the National Infrastructure of Natural Resources for Science and Technology Program of China (2004DKA30640), and the Scientific Research Foundation of the First Institute of Oceanography, SOA (2011G24).

References

[1] A. H. Goldstein, "Bacterial solubilization of mineral phosphates: historical perspectives and future prospects," *American Journal of Alternative Agriculture*, vol. 1, pp. 57–65, 1986.

[2] F. Scheffer and P. Schachtschabel, *Lehrbuch der Bodenkunde*, Ferdinand Enke Verlag, Stuttgart, Germany, 1992.

[3] R. E. Beever and D. J. W. Burns, "Phosphorus uptake, storage and utilization by fungi," *Advances in Botanical Research*, vol. 8, pp. 121–219, 1980.

[4] H. Rodríguez and R. Fraga, "Phosphate solubilizing bacteria and their role in plant growth promotion," *Biotechnology Advances*, vol. 17, no. 4–5, pp. 319–359, 1999.

[5] M. H. Abd-Alla, "Phosphatases and the utilization of organic phosphorus by *Rhizobium leguminosarum* biovar viceae," *Letters in Applied Microbiology*, vol. 18, no. 5, pp. 294–296, 1994.

[6] A. H. Goldstein, "Recent progress in understanding the molecular genetics and biochemistry of calcium phosphate solubilization by Gram negative bacteria," *Biological Agriculture and Horticulture*, vol. 12, no. 2, pp. 185–193, 1995.

[7] X. R. Zhao and Q. M. Lin, "A review of phosphate—dissolving microorganisms," *Soil Fertilizer*, vol. 3, pp. 7–11, 2001.

[8] Y. H. Hou, Q. F. Wang, J. H. Shen, J. L. Miao, and G. Y. Li, "Molecular identification of a halotolerant bacterium NJ82 from Antarctic Sea ice and preliminary study on its salt tolerance," *Microbiology*, vol. 35, no. 4, pp. 486–490, 2008.

[9] C. S. Nautiyal, "An efficient microbiological growth medium for screening phosphate solubilizing microorganisms," *FEMS Microbiology Letters*, vol. 170, no. 1, pp. 265–270, 1999.

[10] S. Niewolak, "Occurrence of microorganisms in fertilized lakes. II. Lecithin- mineralizing microorganisms," *Polskie Archiwum Hydrobiologii*, vol. 27, pp. 53–71, 1980.

[11] D. R. Arahal, R. H. Vreeland, C. D. Litchfield et al., "Recommended minimal standards for describing new taxa of the family Halomonadaceae," *International Journal of Systematic and Evolutionary Microbiology*, vol. 57, no. 10, pp. 2436–2446, 2007.

[12] H. P. Dussault, "An improved technique for staining red halophilic bacteria," *Journal of bacteriology*, vol. 70, no. 4, pp. 484–485, 1955.

[13] J. A. Mata, J. Martínez-Cánovas, E. Quesada, and V. Béjar, "A detailed phenotypic characterisation of the type strains of *Halomonas* species," *Systematic and Applied Microbiology*, vol. 25, no. 3, pp. 360–375, 2002.

[14] A. Hiraishi, "Direct automated sequencing of 16S rDNA amplified by polymerase chain reaction from bacterial cultures without DNA purification," *Letters in Applied Microbiology*, vol. 15, no. 5, pp. 210–213, 1992.

[15] D. J. Lane, "16S/23S rRNA sequencing," in *Nucleic Acid Techniques in Bacterial Systematics*, pp. 115–175, John Wiley and Sons, New York, NY, USA, 1991.

[16] F. S. Watanabe and S. R. Olsen, "Test of an ascorbic acid method for determining phosphorous in water and $NaHCO_3$ extracts from soil," *Soil Science Society of America Proceedings*, vol. 29, pp. 677–678, 1965.

[17] D. Piccini and R. Azcon, "Effect of phosphate-solubilizing bacteria and vesicular-arbuscular mycorrhizal fungi on the utilization of Bayovar rock phosphate by alfalfa plants using a sand-vermiculite medium," *Plant and Soil*, vol. 101, no. 1, pp. 45–50, 1987.

[18] I. Reyes, L. Bernier, R. R. Simard, and H. Antoun, "Effect of nitrogen source on the solubilization of different inorganic phosphates by an isolate of *Penicillium rugulosum* and two UV-induced mutants," *FEMS Microbiology Ecology*, vol. 28, no. 3, pp. 281–290, 1999.

[19] M. E. Puente, Y. Bashan, C. Y. Li, and V. K. Lebsky, "Microbial populations and activities in the rhizoplane of rock-weathering desert plants. I. Root colonization and weathering of igneous rocks," *Plant Biology*, vol. 6, no. 5, pp. 629–642, 2004.

[20] K. Y. Kim, D. Jordan, and H. B. Krishnan, "Rahnella aquatilis, a bacterium isolated from soybean rhizosphere, can solubilize hydroxyapatite," *FEMS Microbiology Letters*, vol. 153, no. 2, pp. 273–277, 1997.

[21] K. Kpomblekou and M. A. Tabatabai, "Effect of organic acids on release of phosphorus from phosphate rocks," *Soil Science*, vol. 158, no. 6, pp. 442–453, 1994.

[22] F. Lapeyrie, J. Ranger, and D. Vairelles, "Phosphate-solubilizing activity of ectomycorrhizal fungi in vitro," *Canadian Journal of Botany*, vol. 69, no. 2, pp. 342–346, 1991.

[23] J. E. Cuningham and C. Kuiak, "Production of citric and oxalic acid and solubilization of calcium phosphate by *Penicillium billai*," *Applied and Environmental Microbiology*, vol. 58, pp. 1451–1458, 1992.

[24] F. Fasim, N. Ahmed, R. Parsons, and G. M. Gadd, "Solubilization of zinc salts by a bacterium isolated from the air environment of a tannery," *FEMS Microbiology Letters*, vol. 213, no. 1, pp. 1–6, 2002.

[25] A. C. Gaur and S. Sachar, "Effect of rock phosphate and glucose concentration on phosphate solubilization by *Aspergillus awamori*," *Current Science*, vol. 49, pp. 553–554, 1980.

[26] P. Illmer and F. Schineer, "Solubilization of insoluble phosphates by micro- organisms isolated from forest soils," *Soil Biology and Biochemistry*, vol. 24, pp. 389–395, 1992.

[27] D. M. Karl, "Cellular nucleotide measurements and applications in microbial ecology," *Microbiological Reviews*, vol. 44, no. 4, pp. 758–760, 1980.

[28] H. Rodríguez and R. Fraga, "Phosphate solubilizing bacteria and their role in plant growth promotion," *Biotechnology Advances*, vol. 17, no. 4–5, pp. 319–339, 1999.

[29] A. K. Halder, A. K. Mishra, P. Bhattacharyya, and P. K. Chakrabartty, "Solubilization of rock phosphate by Rhizobium and Bradyrhizobium," *Journal of General and Applied Microbiology*, vol. 36, no. 2, pp. 81–92, 1990.

[30] A. H. Goldstein, "Involvement of the quinoprotein glucose dehydrogenase in the solubilization of exogenous phosphates by Gram-negative bacteria," in *Phosphate in Microorganisms: Cellular and Molecular Biology*, A. Torriani-Gorini, E. Yagil, and S. Silver, Eds., pp. 197–203, ASM Press, Washington, DC, USA, 1996.

[31] P. Illmer and F. Schinner, "Solubilization of inorganic calcium phosphates—solubilization mechanisms," *Soil Biology and Biochemistry*, vol. 27, no. 3, pp. 257–263, 1995.

[32] C. Sánchez-Porro, R. R. de la Haba, N. Soto-Ramírez, M. C. Márquez, R. Montalvo-Rodríguez, and A. Ventosa, "Description of *Kushneria aurantia* gen. nov., sp. nov., a novel member of the family *Halomonadaceae*, and a proposal for reclassification of *Halomonas marisflavi* as *Kushneria marisflavi* comb. nov., of *Halomonas indalinina* as *Kushneria indalinina* comb. nov. and of *Halomonas avicenniae* as *Kushneria avicenniae* comb. nov," *International Journal of Systematic and Evolutionary Microbiology*, vol. 59, no. 2, pp. 397–405, 2009.

[33] J. H. Yoon, S. H. Choi, K. C. Lee, Y. H. Kho, K. H. Kang, and Y. H. Park, "*Halomonas marisflavae* sp. nov., a halophilic bacterium isolated from the Yellow Sea in Korea," *International Journal of Systematic and Evolutionary Microbiology*, vol. 51, no. 3, pp. 1171–1177, 2001.

[34] A. Cabrera, M. Aguilera, S. Fuentes, C. Incerti, N. J. Russell, and A. Ramos-Cormenzana, "*Halomonas indalinina* sp. nov., a moderately halophilic bacterium isolated from a solar saltern in Cabo de Gata, Almería, southern Spain," *International Journal of Systematic and Evolutionary Microbiology*, vol. 57, no. 2, pp. 376–380, 2007.

Hindawi Publishing Corporation
Evidence-Based Complementary and Alternative Medicine
Volume 2011, Article ID 670349, 17 pages
doi:10.1155/2011/670349

Review Article

Bioactive Pigments from Marine Bacteria: Applications and Physiological Roles

Azamjon B. Soliev, Kakushi Hosokawa, and Keiichi Enomoto

Department of Environmental Systems Engineering, Kochi University of Technology, 185 Miyanokuchi, Tosayamada, Kami, Kochi 782-8502, Japan

Correspondence should be addressed to Keiichi Enomoto, enomoto.keiichi@kochi-tech.ac.jp

Received 15 January 2011; Accepted 28 June 2011

Research into natural products from the marine environment, including microorganisms, has rapidly increased over the past two decades. Despite the enormous difficulty in isolating and harvesting marine bacteria, microbial metabolites are increasingly attractive to science because of their broad-ranging pharmacological activities, especially those with unique color pigments. This current review paper gives an overview of the pigmented natural compounds isolated from bacteria of marine origin, based on accumulated data in the literature. We review the biological activities of marine compounds, including recent advances in the study of pharmacological effects and other commercial applications, in addition to the biosynthesis and physiological roles of associated pigments. Chemical structures of the bioactive compounds discussed are also presented.

1. Introduction

1.1. Marine Bacteria and Its Role in Life Sciences. A wide variety of diseases and medical problems represent a challenging threat to humans, who since ancient times have searched for natural compounds from plants, animals, and other sources to treat them. Although the process of finding effective treatments against fatal diseases is difficult, extensive searches for natural bioactive compounds have previously yielded some successful results. The isolation and identification of specific natural compounds led to the development of folk medicine, and humans learned to separate the isolates into medicinal drugs, which could be used to treat different diseases, and poisonous substances, which could be used for nonmedicinal purposes (i.e., during tribal wars, hunting, etc.). Statistically, at least 50% of the existing drugs that are used to treat human illnesses are derived from natural products, most of which are obtained from terrestrial organisms [1]. However, due to continuous and exhaustive research, land-based natural bioactive compounds have become increasingly difficult to find. Instead, water-based natural compounds have become a more promising source, not only from a pharmacological view, but also for industrial and commercial applications.

Theoretically, life is considered to have originated in the sea and, as a result of evolutionary changes, developed into a wide variety of diverse biological systems. The Earth's surface consists of 70% water, which is inhabited by 80% of all life forms [1], and consequently aquatic organisms have a greater diversity than their terrestrial counterparts. As research into the marine environment is still in its early phases, many mysteries associated with aquatic fauna and flora have yet to be discovered. Therefore, the marine environment has recently become an attractive research subject for many investigations, because of its rich biodiversity. Despite being comprised of a diverse ecosystem, the search for marine metabolites is difficult because of the inaccessibility and nonculturability of the majority of organisms [2]. Nevertheless, the existing technologies like deep seawater pumping facilities, scuba diving, and other available equipments, have facilitated investigation of the sea environment. As a result, scientific research has increasingly focused on marine biochemistry, microbiology, and biotechnology.

Microorganisms and their isolates represent a major source of undiscovered scientific potential. It should be noted that the number of microbial organisms isolated from the vast ocean territories continues to increase each year. Consequently, natural products isolated from microorganisms inhabiting environments other than soil are an attractive research tool, not only for biochemists and microbiologists,

but also for pharmacologists and clinicians. Laatsch [3] described the isolation and description of nearly 250 marine bacterial metabolites versus 150 isolated from terrestrial bacteria between 2000 and 2005. Research into marine microorganisms and their metabolites has therefore become a major task in the search for novel pharmaceuticals.

Although many compounds show promising biological activities, it is difficult to point out any particular bioactive agent that has readily been commercialized as a medicine. Currently, 13 natural products isolated from marine microorganisms are being tested in different phases of clinical trials, and a large number of others are in preclinical investigations [4], thus highlighting the potential of marine natural compounds.

Despite thousands of marine bioactive compounds having been isolated and identified, in this paper, we will focus on the pharmacologically active pigmented compounds produced by marine microorganisms exhibiting *in vitro* or *in vivo* biological activities. Although pigmented compounds produced by terrestrial bacteria are beyond the scope of this review, specific examples will still be mentioned for comparative purposes, to outline common biological activities or because identical pigments were isolated from both types of microorganisms.

1.2. Marine Microorganisms and Their Bioactive Isolates. Marine and terrestrial microfloras differ from each other due to the influence of their respective environmental conditions. Microorganisms living in the sea must be able to survive and grow in the water environment with low nutrition, high salinity, and high pressure. That is why most bacteria isolated from seawater are Gram-negative rods, as it is postulated that their outer membrane structure is evolutionarily adapted to aquatic environmental factors. Marine microorganisms can be divided on the basis of habitat into psychrophiles (living at low temperatures), halophiles (living at high salinity), and barophiles (living under high pressure). Although these characteristics highlight the differences between marine and terrestrial microorganisms, it remains difficult to separate bacterial genera on the basis of habitat due to the ubiquitous presence of similar species in both environments. As such, most bioactive compounds have been isolated from bacteria in both environments.

Marine bacteria, however, are attractive to researchers because they can potentially produce compounds with unique biological properties [5]. Until now, marine *Streptomyces, Pseudomonas, Pseudoalteromonas, Bacillus, Vibrio*, and *Cytophaga* isolated from seawater, sediments, algae, and marine invertebrates are known to produce bioactive agents. They are able to produce indole derivatives (quinones and violacein), alkaloids (prodiginines and tambjamines), polyenes, macrolides, peptides, and terpenoids. Examples of bioactive-pigmented compounds isolated from marine (and some terrestrial) bacteria are discussed below.

2. Pigments from Marine Bacteria

Bioactive pigments from marine bacteria are summarized in Table 1.

2.1. Prodiginines. Red-pigmented prodigiosin compounds were first isolated from the ubiquitous bacterium *Serratia marcescens* and identified as secondary metabolites. The common aromatic chemical structure of these pigmented compounds was first named prodiginine by Gerber [6] (Figure 1). Prodigiosin was the first prodiginine for which the chemical structure was determined [7]. The name "prodigiosin" has been attributed to the isolation of prodigiosin from *Bacillus prodigiosus* bacterium (later renamed *Serratia marcescens*) [8], which was historically famed for the mysterious "bleeding bread" report [9, 10]. Prodiginines share a common pyrrolyldipyrromethene core structure and have a wide variety of biological properties, including antibacterial, antifungal, antimalarial, antibiotic, immunosuppressive, and anticancer activities [9, 11]. Such properties potentially make them one of the most powerful research tools in the past decade.

There are many research reports and reviews regarding prodiginines and their biological activity investigations. In addition to the *Serratia*, several species of marine bacteria of the genera *Streptomyces* [8], *Actinomadura* [8], *Pseudomonas* [12], *Pseudoalteromonas* [13–18], and others [19] have also been reported to produce prodigiosin and related compounds. In particular, *Alteromonas denitrificans,* which was isolated from the fjord systems off the west coast of Norway [16] and later reclassified as *Pseudoalteromonas denitrificans* [20], has been reported to produce cycloprodigiosin. This compound has immunosuppressive, antimalarial, and apoptosis-inducing activities [18, 21, 22]. *Pseudoalteromonas rubra*, found in the Mediterranean coastal waters [13], also produces cycloprodigiosin, in addition to prodigiosins [14, 15]. *α-Proteobacteria* isolated from a marine tunicate collected in Zamboanga, Philippines, was reported to produce heptyl prodigiosin. *In vitro* antimalarial activity against *Plasmodium falciparum* 3D7 (IC_{50} = 0.068 mM and SI = 20) was about 20 times the *in vitro* cytotoxic activity against L5178Y mouse lymphocytes [23]. *In vivo* experiments using *Plasmodium berghei*-infected mice, at concentrations of 5 mg/kg and 20 mg/kg, significantly increased their survival, while also causing sclerotic lesions at the site of injection.

Other bacteria reported to produce red pigments include *Hahella* [24], *Vibrio* [25], *Zooshikella* [26], and *Pseudoalteromonas* [17], isolated from the coasts of Korea, Taiwan, and Japan. Kim et al. [27] identified red-pigmented prodiginines from *Hahella chejuensis*. Nakashima et al. also evaluated the biological activity of similar prodiginines from a bacterium assumed to belong to the genus *Hahella* [28]. Red pigment-producing bacterial species have further been isolated from river water [29, 30] and even from a swimming pool [31]. The most active prodiginine derivatives have already entered clinical trials as potential drugs against different cancer types [9].

Japan is surrounded by sea and has a bordering coastline of the Pacific Ocean in the South and the Sea of Japan in the North and West, and is consequently rich in marine re-sources. Therefore, one of the main tasks of our research group is to investigate the marine environment and its biodiversity, especially marine microorganisms and their respective metabolites.

Table 1: Biologically active pigmented compounds isolated from marine bacteria.

Pigment	Activity	Bacterial strains	References
(1) Undecylprodigiosin	Anticancer	*Streptomyces rubber*	[8]
(2) Cycloprodigiosin	Immunosuppressant; Anticancer; Antimalarial	*Pseudoalteromonas denitrificans*	[18, 21, 22]
(3) Heptyl prodigiosin	Antiplasmodial	*α-Proteobacteria*	[23]
(4) Prodigiosin	Antibacterial; Anticancer; Algicidal	*Pseudoalteromonas rubra* *Hahella chejuensis*	[14] [27]
(5) Astaxanthin (carotene)	Antioxidation	*Agrobacterium aurantiacum*	[34]
(6) Violacein	Antibiotic; Antiprotozoan; Anticancer	*Pseudoalteromonas luteoviolacea* *Pseudoalteromonas tunicata* *Pseudoalteromonas* sp. 520P1 *Collimonas* CT	[48, 52, 53] [43] [50] [51]
(7) Methyl saphenate (phenazine derivative)	Antibiotic	*Pseudonocardia* sp. B6273	[63]
(8) Phenazine derivatives	Cytotoxic	*Bacillus* sp.	[64]
(9) Pyocyanin and pyorubrin	Antibacterial	*Pseudomonas aeruginosa*	[58]
(10) Phenazine-1-carboxylic acid	Antibiotic	*Pseudomonas aeruginosa*	[59]
(11) 5,10-dihydrophencomycin methyl ester	Antibiotic	*Streptomycete* sp.	[65]
(12) Fridamycin D, Himalomycin A, Himalomycin B	Antibacterial	*Streptomycete* sp. B6921	[68]
(13) Chinikomycin A and Chinikomycin B, Manumycin A	Anticancer	*Streptomycete* sp. M045	[71]
(14) Tambjamines (BE-18591, pyrrole and their synthetic analogs)	Antibiotic, Anticancer	*Pseudoalteromonas tunicata*	[76, 80]
(15) Melanins	Protection from UV irradiation	*Vibrio cholerae* *Shewanella colwelliana* *Alteromonas nigrifaciens* *Cellulophaga tyrosinoxydans*	[83, 84] [83, 86] [85] [88]
(16) Scytonemin	Protection from UV irradiation Anti-inflammatory, Antiproliferative	Cyanobacteria	[93]
(17) Tryptanthrin	Antibiotic	*Cytophaga/Flexibacteria* AM13,1 strain	[95]

Previously, a total of 85 strains of bacteria were isolated by our research group from the Pacific Ocean at a depth of 320 m off Cape Muroto in the Kochi Prefecture of Japan. Among them, 13 strains were found to produce a purple pigment and one a red pigment. The red pigment-producing bacterium was later named strain 1020R [32]. Detailed investigations have revealed that this strain is closely related to the prodigiosin-producing bacterium *Pseudoalteromonas rubra* and is Gram-negative with rod-shaped morphology. Physicochemical investigations have revealed that the pigment produced by this strain contains at least seven structurally similar prodiginine compounds. Chemical structures for four of these were successfully determined, and each only differed by the length of the alkyl chain attached to the C-3 position of the C-ring. These compounds were further identified as prodigiosin and its analogues 2-methyl-3-butyl-prodiginine, 2-methyl-3-pentyl-prodiginine (prodigiosin), 2-methyl-3-hexyl-prodiginine, and 2-methyl-3-heptyl-prodiginine. Compound cytotoxicity to U937 leukemia cells was strongly dependent on the length of these alkyl side chains, which decreased with an increase in chain length. 2-methyl-3-butyl-prodiginine was the most potent cytotoxic pigment among them. Molecular investigations into the cytotoxic mechanisms of these prodiginine derivatives demonstrated effects on caspase-3 activation and DNA fragmentation, indicating the potential to induce apoptosis in leukemia cells.

2.2. Carotenes. Carotenes are polyunsaturated hydrocarbons that contain 40 carbon atoms per molecule and are exclusively synthesized by plants. They are orange photosynthetic pigments important for plant photosynthesis. Recently, an unusual halophilic bacterium, which requires 15–25% salt for its normal growth, was found in Santa Pola near Alicante and on the Balearic island of Mallorca, Spain. It appeared to be red or pink due to a wide variety of isoprenoid compounds (phytoene, phytofluene, lycopene, and β-carotene) produced by this prokaryote. Oren and Rodríguez-Valera [33] investigated red-pigmented saltern crystallizer ponds in these areas of Spain and demonstrated that the pigments were carotenoid or carotenoid-like compounds produced by halophilic bacteria related to the *Cytophaga-Flavobacterium-Bacteroides* group. Thus, it has been shown that *Salinibacter* is an important component of the microbial community

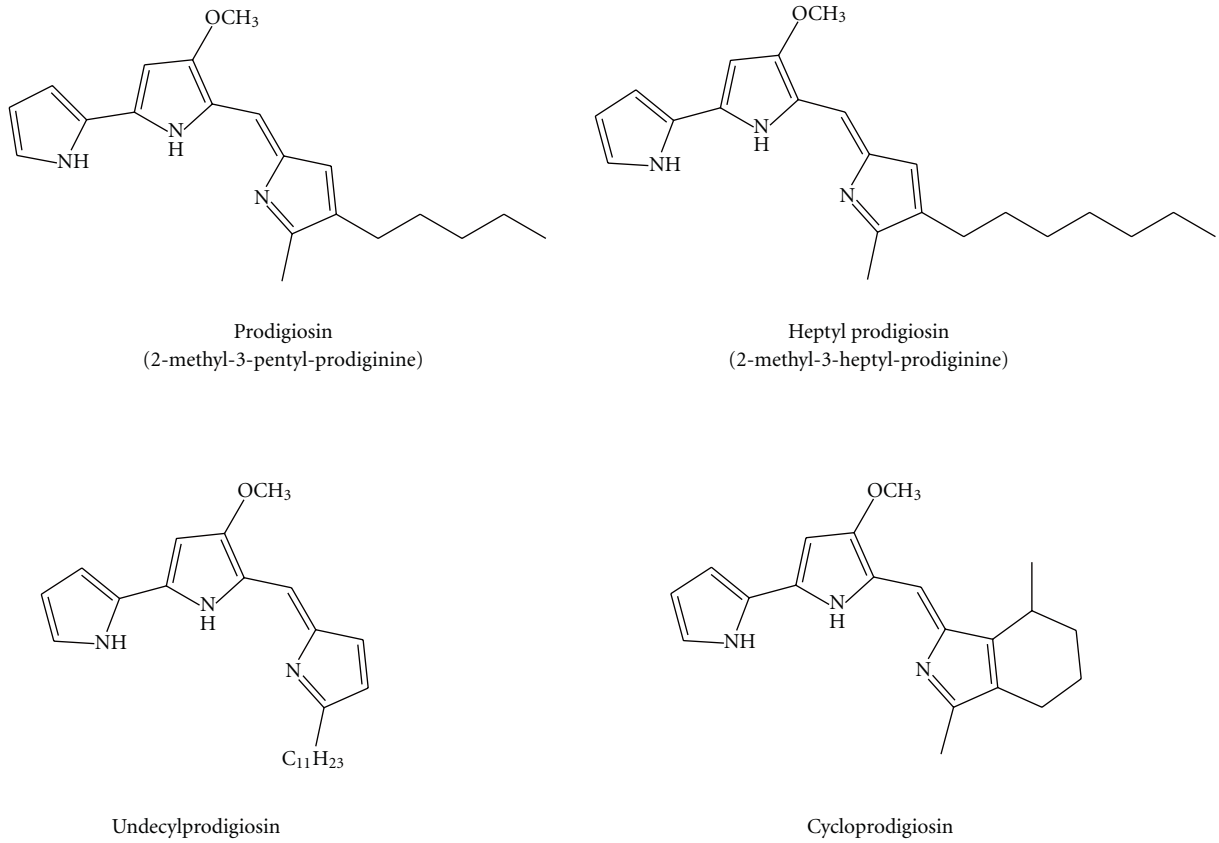

Figure 1: Prodiginine derivatives.

that contributes to the red coloration of Spanish saltern ponds.

Astaxanthin is one of the carotenoids that have commercial value as a food supplement for humans and as food additives for animals and fish (Figure 2). A carotenoid biosynthesis gene cluster for the production of astaxanthin has been isolated from the marine bacterium *Agrobacterium aurantiacum* [34]. Recently, another astaxanthin-producing marine bacterium was isolated and identified as *Paracoccus haeundaensis* [35].

2.3. Violacein. The violet pigment violacein is an indole derivative, predominantly isolated from bacteria of the genus *Chromobacterium* that inhabit the soil and water of tropical and subtropical areas [36]. Over the past decade, the biosynthesis and biological activities of violacein have been extensively studied, and many scientific papers and reviews have been published [37–41]. Violacein has a variety of biological activities, including antiviral, antibacterial, antiulcerogenic, antileishmanial, and anticancer properties [36, 37, 41, 42] (Figure 3). Use of violacein as a chemical defense against eukaryotic predators has also been investigated [43–46].

One of the first published reports on violacein production by marine bacteria was by Hamilton and Austin [47]. This bacterial strain, *Chromobacterium marinum,* was isolated from open ocean waters and produced a blue pigment that was identified as violacein on the basis of physicochemical characteristics [47]. Later, Gauthier [48] described 16 violet-pigmented heterotrophic bacilli isolated from Mediterranean coastal waters and proposed the name *Alteromonas luteo-violaceus* for these strains. Another six bacterial species were also isolated by Gauthier et al. [49] from neritic waters on the French Mediterranean coast and were very similar to *Alteromonas* species. These species produced characteristic pigmentations ranging from pinkish-beige with reddish-brown diffusible pigment**,** lemon yellow**,** bright red turning carmine in old cultures, and orange to greenish-brown. Light violet, dark violet, or almost black pigments were also produced and later identified as violacein. The strains showed antibiotic activity against *Staphylococcus aureus* [49]. Subsequently, many other reports on violacein production have been published [50, 51].

Several purple pigment-producing *Alteromonas* species were also isolated from Kinko Bay in Kagoshima Prefecture, Japan. One of these, *Alteromonas luteoviolacea* (reclassified as *Pseudoalteromonas luteoviolacea*), is the only extensively characterized marine bacterium ever reported that produces violacein [48, 52, 53]. Previously, we have also reported 13 strains of Gram-negative, rod-shaped bacteria that produce a violacein-like purple pigment, which were isolated from the Pacific Ocean at a depth of 320 m off the coast of Cape Muroto, Kochi Prefecture, Japan [32]. Among them, two groups of novel violacein and deoxyviolacein producing marine bacteria were isolated and characterized in detail

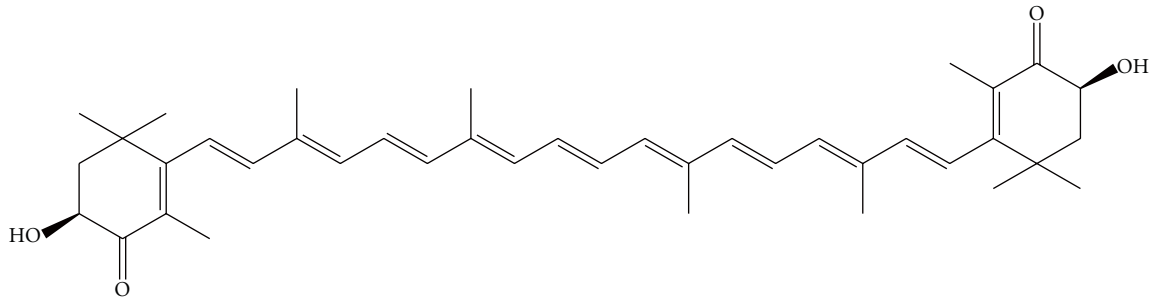

Astaxanthin

Figure 2: Astaxanthin.

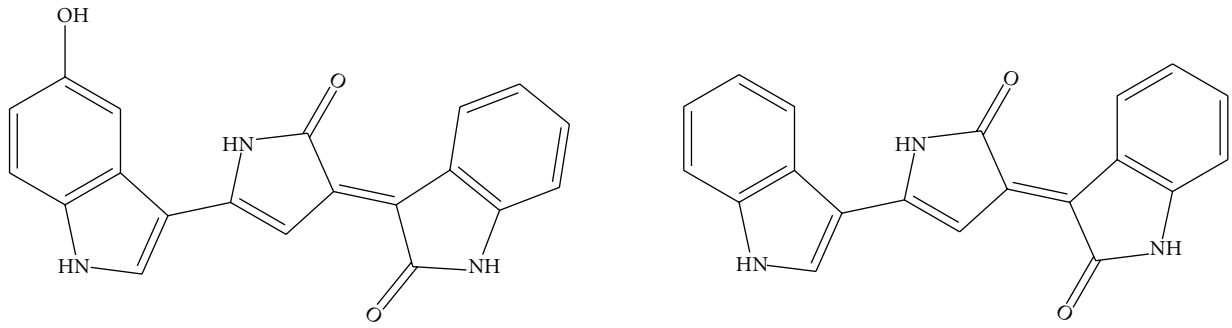

Violacein Deoxyviolacein

Figure 3: Violacein and deoxyviolacein.

[50]. Biological investigations of violacein produced by these strains revealed potent cytotoxic effects against U937 and HL60 leukemia cell lines, with an IC_{50} value of 0.5–1 μM. The molecular mechanisms currently known to be involved in violacein cytotoxicity include caspases activation, chromatin condensation, and DNA fragmentation, which all contribute to cell apoptosis. Recently, we also demonstrated that the protein kinases actively involved in the signal transduction pathway are also targeted by violacein.

2.4. Phenazine Compounds. Phenazines are redox-active, small nitrogen-containing aromatic compounds produced by a diverse range of bacterial genera, including *Streptomyces* (terrestrial), *Pseudomonas* (ubiquitous), *Actinomycetes* (terrestrial and aquatic), *Pelagibacter* (aquatic), and *Vibrio* (aquatic), under the control of quorum sensing [54, 55] (Figure 4). These compounds were subjected to extensive studies due to their broad spectrum of antibiotic activities against other bacteria, fungi, or plant/animal tissues [56–62]. Phenazine color intensity may vary among the derivatives and range from blue, green, purple, yellow, red to even brown [58, 63]. More than 6,000 phenazine derivatives have been identified and described during the last two centuries [59].

Maskey et al. [63] reported the isolation of two yellow pigments from the marine *Pseudonocardia* sp. B6273, a member of the *Actinomycetes.* Structural investigations identified the two pigments as novel phenazostatin D, inactive against the tested microorganisms, and methyl saphenate, a known phenazine antibiotic. Li et al. [64] also reported the isolation of a novel phenazine derivative with cytotoxic effects against P388 cells, together with six previously identified compounds from the marine *Bacillus* sp., collected from a Pacific deep-sea sediment sample at a depth of 5059 m. A novel phenazine derivative with antibiotic activity, identified as 5,10-dihydrophencomycin methyl ester, along with (2-hydroxyphenyl)-acetamide, menaquinone MK9 (II, III, VIII, IX-H8), and phencomycin, was isolated from an unidentified marine *Streptomyces* sp. by Pusecker et al. [65].

Pyocyanin and 1-hydroxyphenazine also downregulate the ciliary beat frequency of respiratory epithelial cells by reducing cAMP and ATP, alter the calcium concentration by inhibition of plasma membrane Ca^{2+}-ATPase, and induce death in human neutrophils [60, 61, 66]. Due to the abundance and biotechnological application of *Pseudomonas aeruginosa* phenazines, pyocyanin and pyorubrin have also been suggested as food colorant pigments [58].

2.5. Quinones. Quinones are additional colored compounds with an aromatic ring structure that have been isolated from marine environment [67, 68] (Figure 5). Quinone derivatives range in color from yellow to red, exhibit antiviral, antiinfective, antimicrobial, insecticidal, and anticancer activities, and have many commercial applications as natural and artificial dyes and pigments [69, 70].

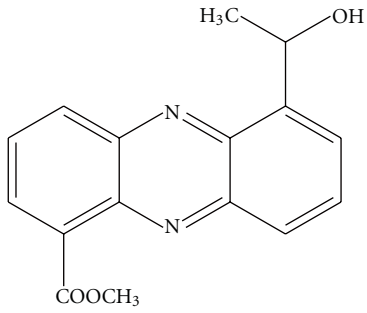

Methyl saphenate

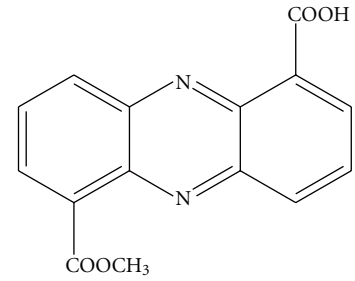

Phencomycin

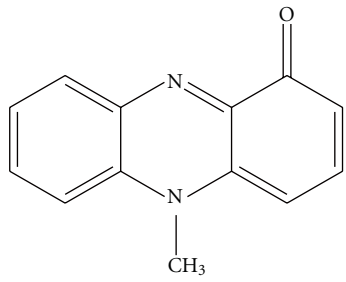

Pyocyanin

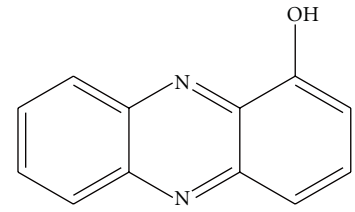

1-hydroxyphenazine

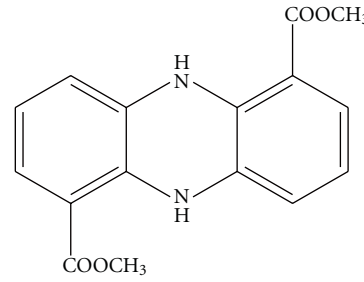

5,10-dihydrophencomycin methyl ester

Figure 4: Phenazine derivatives.

Streptomyces sp. B6921 strain produced glycosylated pigmented anthracycline antibiotics, including fridamycin D and two new compounds, named himalomycin A and B, each of which displayed similar levels of strong antibacterial activity against *Bacillus subtilis*, *Streptomyces viridochromogenes* (Tü 57), *S. aureus*, and *Escherichia coli*. This strain also produced rabelomycin, *N*-benzylacetamide, and *N*-(2′-phenylethyl) acetamide [68]. Two novel pigmented antitumor antibiotics, chinikomycin A and B, together with manumycin A, were isolated from a marine *Streptomyces* sp. strain M045 [71]. The two chlorine containing quinone derivatives were shown not to have antiviral, antimicrobial, and phytotoxic activities; however, they exhibited antitumor activity against different human cancer cell lines. Chinikomycin A selectively inhibited the proliferation of mammary cancer, melanoma, and renal cancer cell lines, while chinikomycin B showed selective antitumor activity against a mammary cancer cell line [71].

Other bacteria, including a marine isolate *Pseudomonas nigrifaciens* (later reclassified as *Alteromonas nigrifaciens*),

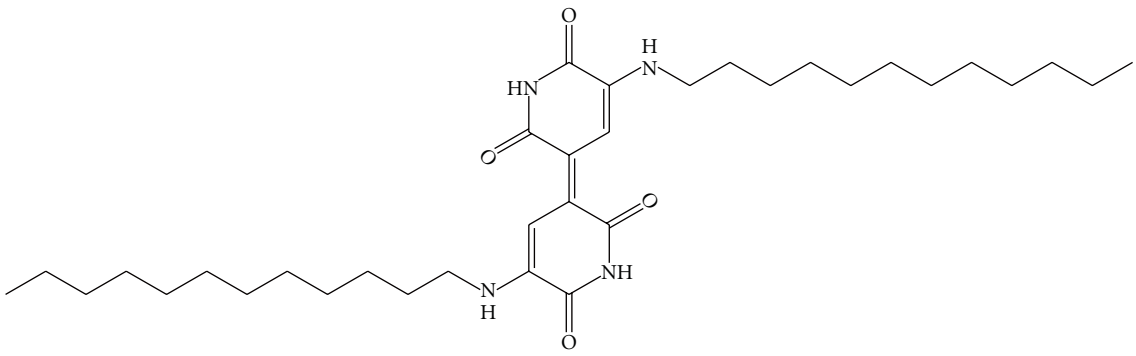

5,5′-didodecylamino-4,4′-dihydroxy-3,3′-diazodiphenoquinone-(2,2′)

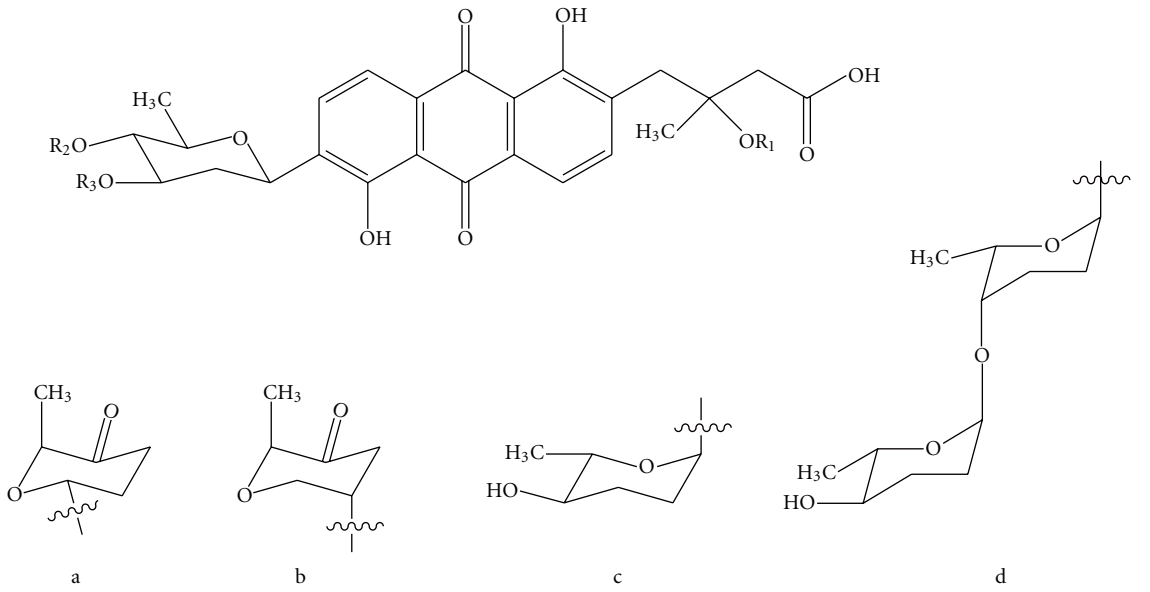

Fridamycin D: R1 = H, R2 = a, R3 = b;

Hymalomycin A: R1 = d, R2 = a, R3 = b;

Hymalomycin B: R1 = d, R2 = c, R3 = H

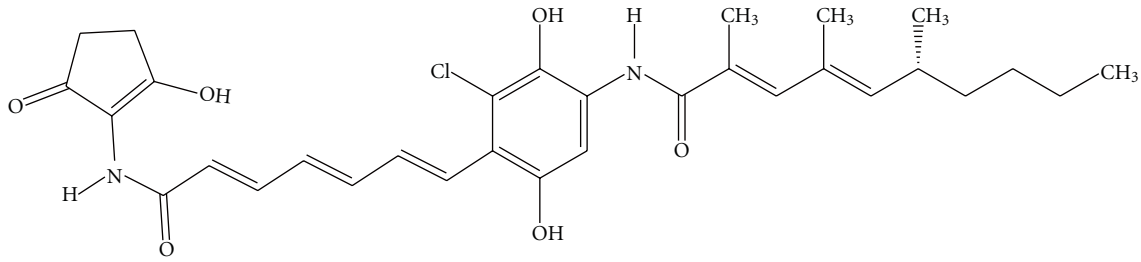

Chinikomycin A

Figure 5: Quinones.

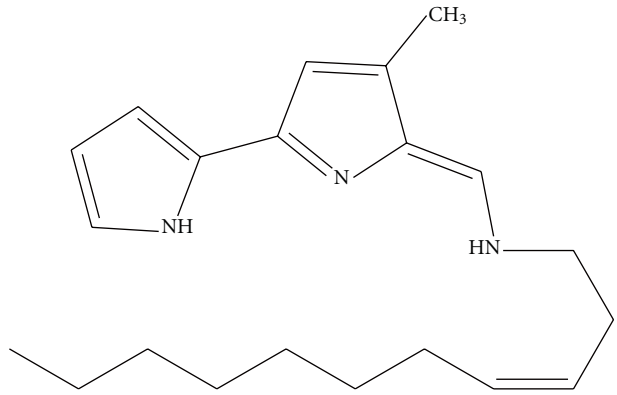

YP1 (Tambjamine)

Figure 6: Tambjamine.

produce the blue pigment indigoidine [72]. Kobayashi et al. [73] isolated a new violet pigment with an alkylated indigoidine structure from *Shewanella violacea,* a deep-sea bacterium from sediments of Ryukyu Trench at a depth of 5110 m. This pigment was established as 5,5′-didodecylamino-4,4′-dihydroxy-3,3′-diazodiphenoquinone-(2,2′) based on X-ray diffraction analysis of single crystals. It does not have antibiotic activity against *E. coli*; however, it could potentially be used as a dye because of its high stability and low solubility. Thus, it could be suitable for industrial applications.

2.6. Tambjamines. It has long been noticed that marine bacteria have the ability to prevent biofouling. Holmström et al. [74] found that, amongst the marine *Pseudoalteromonas* species, *P. tunicata* has the widest range of antibiofouling activities against microorganisms, including bacteria, invertebrate larvae, algal spores, protozoan, and fungi, and provides protection for host marine organisms. These activities were linked to the production of unidentified yellow and purple pigments [75]. Recently, this yellow pigment was isolated from *P. tunicata* and was identified as a new member of the tambjamine class of compounds [76].

Tambjamines (Figure 6) are alkaloids isolated from various marine organisms like bryozoans, nudibranchs, and ascidians [77–79]. This yellow pigment has also been isolated from marine bacteria [76]. The tambjamines also exhibit antibiotic activity against *E. coli*, *Staphylococcus*, *Vibrio anguillarum* [77], *B. subtilis*, and *Candida albicans* [80, 81] and displayed cytotoxic activity against several tumor cell lines [80]. Recently, Pinkerton et al. [80, 82] reported the first total synthesis of nine tambjamines and their antimicrobial and cytotoxic activities. All of the tested tambjamines showed antibacterial, antifungal, and cytotoxic effects that contributed to cell death through apoptosis, but not necrosis. These activities were, however, lesser than the positive control (doxorubicin) [80].

2.7. Melanins. Vibrio cholerae, Shewanella colwelliana, and *Alteromonas nigrifaciens* were some of the first marine bacterial strains described to produce melanin or melanin-like pigments [83–86]. The pigment synthesized by *Vibrio cholerae* was reported to be a type of allomelanin derived from homogentisic acid [87]. Melanin formation in *V. cholerae* is a consequence of alterations in tyrosine catabolism and not from the tyrosinase-catalyzed melanin synthetic pathway. *Cellulophaga tyrosinoxydans* was reported to have tyrosinase activity and produce a yellow pigment suggested to be a pheomelanin [88].

The most illustrative example of melanin-producing marine bacteria is the actinomycetes. This is particularly the case for the genus *Streptomyces,* from which most compounds with known biological activity have been isolated [89]. All *Streptomyces* strains are reported to use tyrosinases in the synthesis of melanin pigments [90]. Another important melanin-synthesizing bacterium is *Marinomonas mediterranea*, which produces black eumelanin from L-tyrosine [91].

2.8. Other Pigmented Compounds. Scytonemin, a yellow-green pigment isolated from aquatic cyanobacteria, forms when the bacteria are exposed to sunlight (Figure 7). It protects bacteria by preventing about 85–90% of all UV-light from entering through the cell membrane [92]. High UV-A irradiation inhibited photosynthesis and delayed cellular growth until sufficient amounts of scytonemin had been produced by the cyanobacteria. Scytonemin may also have anti-inflammatory and antiproliferative activities by inhibiting protein kinase Cβ (PKCβ), a well-known mediator of the inflammatory process, and polo-like protein kinase 1 (PLK1), a regulator of cell cycle progression [93]. In addition, scytonemin inhibited phorbol-induced mouse ear edema and the proliferation of human umbilical vein endothelial cells.

Recently, two *γ-Proteobacteria* strains of the genus *Rheinheimera* were isolated from the German Wadden Sea and from Øresund, Denmark that produced a deep blue pigment [94]. Structural analysis of the pigment revealed that this new compound has no similarity with any known blue pigments, like violacein and its derivatives. Due to its blue

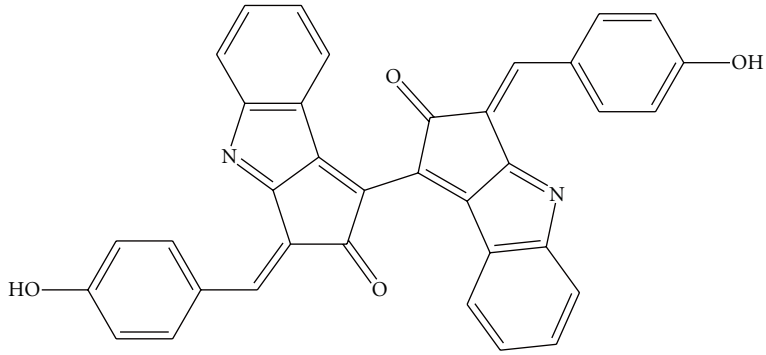

Scytonemin

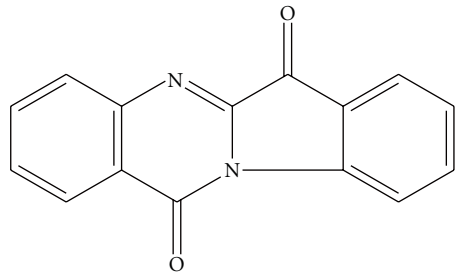

Tryptanthrin

Figure 7: Other pigmented compounds.

color and marine origin, the new pigment was named glaukothalin (from Greek *glaukos* "blue" and *thalatta* "sea"). The ecological role and biological activities of glaukothalin are currently under investigation.

AM13,1 strain, which was identified to belong to the *Cytophaga/Flexibacteria* cluster of North Sea bacteria, was found to produce yellow tryptanthrin, a rare compound that had never before been found in bacteria [95]. This compound was suggested to be a biocondensation product of anthranilic acid and isatin and exhibited a broad yet moderate antibiotic activity. Thus, the yellow color of the AM13,1 colonies was potentially due to their tryptanthrin content. In another yellow cultured Hel21 strain, pigment color may be a consequence of carotenoid zeaxanthin or one of the many vitamin K derivatives (e.g., menaquinone MK6) [95].

3. Biosynthesis of Pigments

Numerous reports detail the regulation and biosynthesis of bacterial secondary metabolites. Increased research and verification of specific bacterial pathways has predominantly been due to the antibiotic, immunosuppressive, and anticancer potential of these compounds. A brief discussion of this topic is given next, as detailed information is further provided in the cited references.

Biosynthesis of bacterial prodiginines has extensively been studied and reviewed [96, 97]. Prodigiosin biosynthesis was proposed to originate during the enzymatic condensation of 2-methyl-3-n-amyl-pyrrole (MAP) and 4-methoxy-2,2′-bipyrrole-5-carbaldehyde (MBC) precursors. Prodiginine biosynthetic gene clusters for *Serratia* sp. ATCC 39006 [98], *Serratia marcescens* ATCC 274 [98], *Hahella chejuensis* KCTC 2396 [27, 99], and *Streptomyces coelicolor* A3(2) [100] have been identified, sequenced, and expressed. Several gene clusters are involved in the biosynthetic pathway, depicted as *pig* in *Serratia* strains, *red* in *S. coelicolor* A3(2), and *hap* (numbered) in *H. chejuensis* KCTC 2396, with each encoding several proteins responsible for synthesis. The largest gene cluster found in *S. coelicolor* A3(2) consists of four transcriptional units, whereas the other three clusters

are strongly homologous to each other and are arranged unidirectionally.

In *Serratia* strains, *pig*B–*pig*E genes were identified to encode proteins responsible for the biosynthesis of MAP and condensation with MBC to form prodigiosin [96, 97]. A common pathway of MBC biosynthesis is proposed for all strains, in which proline, acetate, serine, and S-adenosylmethionine are incorporated into the bipyrrole at the initial stage [97]. PigA, PigF, PigG, PigH, PigI, PigJ, PigM, and PigN in *Serratia* strains and RedE, RedI, RedM, RedN, RedO, RedW, RedV, and RedX proteins in *S. coelicolor* A3(2) have been determined to participate in MBC biosynthesis [97]. PigB, PigD, and PigE enzymes in *Serratia* strains were proposed to be involved in the MAP biosynthesis, which requires 2-octenal as the initial precursor [97]. Monopyrroles condense with MBC during the final step of prodigiosin and/or undecylprodigiosin biosynthesis. PigC and its homologues catalyze this condensation in bacteria.

Some prodiginines can also be produced when monopyrroles are supplied to colorless *S. marcescens* mutants [8]. Addition of monopyrroles directly to a culture medium or as a vapor across the culture surface of a colorless mutant of *S. marcescens* resulted in the strain becoming initially pink and later red, indicating prodiginine formation [8]. Similar prodiginine biosynthesis produced by exogenously adding MAP and MBC was observed in white strains of *Serratia marcescens* isolated from patients [101].

The violacein biosynthesis pathway and associated biosynthetic enzymes have been extensively studied [38, 40, 102], although certain reactions and intermediates are yet to be elucidated. Currently, this proposed system involves an operon of five genes, *vioA–vioE*, which are transcriptionally regulated by a quorum-sensing mechanism that uses acylhomoserine lactones as autoinducers. At the early stationary phase of bacterial growth, acylhomoserine lactones accumulate in the culture medium, inducing the transcription of the *vio* genes. Therefore, violacein is considered a typical secondary metabolite in bacteria. The first enzyme encoded by the *vio* gene operon, VioA, converts L-tryptophan to indole-3-pyruvic acid imine (IPA imine), and the second enzyme, VioB, catalyzes the reaction to convert IPA imine into an unidentified compound X (possibly an IPA imine dimer) [103, 104]. Compound X then undergoes successive reactions, catalyzed by the enzymes VioE, VioD, and VioC, to produce violacein.

Phenazine pigment biosynthesis reportedly involves shikimic acid as a precursor and forms chorismic acid as an intermediate product. Two molecules of chorismic acid then form phenazine-1,6-dicarboxylic acid, which is sequentially modified to create a variety of phenazine derivatives with different biological activities [105]. *Pseudomonas aeruginosa* PAO1 has two gene clusters (*phzA1B1C1D1E1F1G1* and *phzA2B2C2D2E2F2G2*), with each cluster capable of producing phenazine-1-carboxylic acid (PCA) from chorismic acid [106]. It is proposed that PhzM and PhzS catalyze the subsequent conversion of PCA to pyocyanin. In addition, PhzH is responsible for producing phenazine-1-carboxamide from PCA.

Fridamycin, hymalomycin, and chinikomycin are typical bacterial compounds that share a quinone skeleton. However, little information regarding the biosynthesis of these compounds has been accumulated.

Detection and identification of the entire *P. tunicata* gene cluster involved in the biosynthetic pathway production of the tambjamine YP1 using recombinant *E. coli* was conducted by Australian researchers Burke et al. [107]. In total, 19 proteins encoded the Tam cluster participate in the postulated biosynthetic pathway. Among them, 12 were found to have high sequence similarity to the red proteins responsible for undecylprodigiosin synthesis in *S. coelicolor* A3(2) and the pig proteins involved in prodigiosin biosynthesis in *Serratia* sp. [107]. Such similarity in the chemical structures of these two classes of compounds results in tambjamines having two pyrrole rings while the prodiginines have three. As is the case for the prodiginines, 4-methoxy-2,2-bipyrrole-5-carbaldehyde (MBC) is initially formed from proline, serine, and malonyl CoA in the tambjamine biosynthetic pathway. A double bond is inserted by TamT and an amino group is transferred by TamH to dodecenoic acid activated by AfaA, which is predicted to be an acyl-CoA synthase. The resulting dodec-3-en-1-amine is condensed with MBC by TamQ to form tambjamine YP1 [107].

In addition to *V. cholera*, *S. colwelliana*, *A. nigrifaciens*, and *C. tyrosinoxydans*, melanin syntheses have also been reported in *M. mediterranea*, which contains the tyrosinase gene operon [108], and in an epiphytic *Saccharophagus degradans* 2-40 bacterium [109]. While the specific details of melanin formation continue to be debated, well-defined biosynthetic schemes have now been proposed. Two different biosynthetic pathways synthesize the eumelanins and pheomelanins. Both pathways are initiated by the oxidation of L-tyrosine to 3,4-dihydroxyphenylalanine (DOPA) and the subsequent creation of dopaquinone by tyrosinase. The latter product is transformed either to pheomelanin by combining with cystein and forming an intermediate S-cysteinyldopa and benzothiazine or to eumelanin with intermediate leucodopachrome, dopachrome (red), 5,6-dihydroxyindole, 5,6-indolequinone (yellow) formation [69].

Nostoc punctiforme ATCC 29133 is the only scytonemin-producing organism whose genome has been fully sequenced [110]. This scytonemin biosynthesis potentially involves a gene cluster consisting of 18 open reading frames (ORFs) (NpR1276 to NpR1259). Although, the functional roles of all these ORFs are not yet fully determined, some intriguing hypotheses have been proposed. In particular, both tyrosine and tryptophan are implicated as biosynthetic precursors for scytonemin in the pigment formation pathway. NpR1275, which functionally resembles leucine dehydrogenase, is utilized in the early stages of scytonemin synthesis in *N. punctiforme*, thereby oxidizing tryptophan and/or tyrosine to their corresponding pyruvic acid derivative.

Alternatively, it is suggested that NpR1269, a putative prephenate dehydrogenase, generates *p*-hydroxyphenylpyruvic acid, which is a derivative of tyrosine in the early pathway stages. NpR1276 uses two pyruvic acid derivatives from tryptophan and tyrosine for the synthesis of a labile β-ketoacid product, which is homologous to the thiamin

diphosphate- (ThDP-) dependent enzyme acetolactate synthase. NpR1274 possibly catalyzes the intermediate cyclization and decarboxylation of the β-ketoacid product to form the indole-fused cyclopentane moiety of the pigment [111]. Monomer precursors that are formed then undergo dimerization to produce scytonemin. NpR1263, which was found to be similar to a tyrosinase in melanin biosynthesis, participates in these later oxidative dimerization steps, thereby forming scytonemin [112]. Functional roles of other ORFs and their putative intermediate products for the pigment production are still under investigation.

4. Concerns regarding the Physiological Role of Pigmented Compounds

A number of bacterial species, including those inhabiting the vast marine environment, produce a wide variety of pigments that are important to cellular physiology and survival. Many of these natural metabolites were found to have antibiotic, anticancer, and immunosuppressive activities. These secondary metabolites, produced by microorganisms mostly via the quorum sensing mechanism, have the ability to inhibit the growth of or even kill bacteria and other microorganisms at very low concentrations. Due to such diverse and promising activities against different kinds of diseases, these compounds can play an important role in both pharmaceutical and agricultural research.

It still remains uncertain why these pigmented secondary metabolites from bacteria have antibiotic and/or cytotoxic activities. Although, their true physiological role is yet to be fully discovered, there are a few reports that provide reasonable explanations by making comparisons with nonpigmented bacteria. In particular, the relationships between pigment production and toxicity have been studied by Holmström et al. [113], who found that 90% of all dark-pigmented compounds taken from marine living surfaces showed inhibitory activity towards invertebrate larvae. Two fractions isolated after column chromatography, one colorless and the other a yellowish-green color, were identified as phenazine derivatives from unidentified marine *Streptomycete* sp. by Pusecker et al. [65]. The colorless fraction was biologically inactive, while the pigmented phenazine derivative showed highly active antibiotic properties. Previous studies have also demonstrated that marine bacterial metabolites with antibiotic properties were always pigmented [114]. Screening of 38 antibiotic-producing bacterial strains revealed that all pigmented bacteria belonging to the *Pseudomonas-Alteromonas* group displayed antibiotic activity, while nonpigmented bacteria were inactive.

Considering data from all reported literature, a number of reasonable biological functions for pigment production in bacteria have been established. In general, the pigmented marine isolates seem to play two important roles: firstly, they provide an adaption to environmental conditions, and, secondly, they provide defense against predators [115]. For instance, it has been shown that the brown colored melanin pigments produced by a variety of species, as well as a yellow-green colored scytonemin pigment isolated from cyanobacteria, protect cells from UV irradiation and desiccation [69, 93]. Therefore, in order to adapt to the excessive sunlight and survive under harmful UV irradiation, bacteria must produce these indispensable compounds. Griffiths et al. [116] found that carotenoids, which were later suggested to be a substitute for sterols, are an important structural component of microbial membranes [117] and may protect bacterial cells from photooxidation or damage caused by visible light irradiation.

Several bacterial pigments that act as antagonists by exhibiting antibiotic activity against other organisms can be considered as potent weapons for survival and effective chemical defenses against eukaryotic predators. This class of bioactive agents includes almost all pigmented compounds commonly produced by *Pseudoalteromonas, Pseudomonas*, and *Streptomyces* species. These compounds inhibit the settlement of marine invertebrate larvae [118], the germination of algal spores [119] and protect the host surface by interfering with bacterial colonization and biofilm formation [74]. They may also inhibit other organisms that compete for space and nutrients.

Such hypotheses are also supported by a number of studies that found that these bacterial compounds were active against other prokaryotes and even eukaryotes [120–128]. In many studies, pigmented bacterial strains demonstrated a strong and broad range of antibiotic activities against other organisms, while nonpigmented strains did not [74, 129]. A clear correlation between pigment production and antibacterial activities of the two *Silicibacter* sp. strain TM1040 and *Phaeobacter* strain 27-4 grown under static conditions was further reported by Bruhn et al. [129]. Mutant strains, which lacked pigment production, also lost their biological activities. Holmström et al. have also shown a close relationship between pigmentation and inhibitory activity, whereby 20 out of 22 dark pigmented bacterial strains tested displayed inhibitory activity against the settlement of two invertebrate larvae and algal spores [113].

Amongst other bacterial strains, *Pseudoalteromonas* has the most diverse antibiotic activities against alga biofouling, and the dark green pigmented *P. tunicata* exhibits the most active and broadest range of inhibitory activity when compared to other strains from this genus [74]. Two nonpigmented *P. nigrifaciens* and *P. haloplanktis* strains were also found not to display any antibiotic activities using various bioassays [74].

Blue-pigmented pyocyanin production in *P. aeruginosa* (Pup14B) was observed by Angell et al. to be induced by *Enterobacter* species (Pup14A and KM1), and this pyocyanin displayed moderate antibiotic activity against *E. coli* and yeast [130]. It was experimentally demonstrated that metabolites produced by Pup14A strain are necessary for the production of this pigment in Pup14B strain [130]. Many other reports describe synergism between bacteria and higher organisms; however, this is a rare example between two bacterial species [131]. Such an unusual case contrasts with the hypothesis of the regulated biodiversity of marine bacteria, in which surface-associated microorganisms produce antimicrobial agents [74] to prevent competing microorganisms. The symbiosis of the two bacterial species is not yet

fully understood, although both species appear to benefit from the pigment production.

One of the promising biological activities of marine bacteria isolates is their cytotoxic effect against cancer cells. Despite many investigations, the exact molecular mechanism of this pigmented compound cytotoxicity remains undetermined and requires further study. For example, violacein is known to cause apoptosis in tumorous cells [41]. However, the pathways leading to cell death have not yet been linked to the possible effects of the pigment, which was also shown to affect signal transduction agents, such as protein kinase and protein phosphatase family enzymes that play crucial role in cell differentiation and proliferation.

In a study by Bromberg et al., violacein showed inhibitory activity against protein phosphatases isolated from human lymphocytes [132]. A similar study was also conducted by Fürstner et al. to assess the inhibitory activity of prodigiosin derivatives [133]. Other targets of these compounds, including ion channels, are further being investigated [134–137].

Unexpected problems have also arisen when investigating marine environments. While the marine environment is a promising source for identifying microorganisms that can produce important biologically active pigments, yields of these compounds remain variable and are sometimes too low to provide enough material for drug development [138] or commercial applications. The main reason for such low yields is that these compounds are secondary metabolites and production depends on the quorum sensing mechanism.

Despite marine bacteria being capable of growing in the extremely low concentrations of nutrients that often exist in seawater, most species still require seawater or its equivalent as a growth medium for artificial culturing. Seawater is therefore used for the growth of marine bacteria, or similar levels of sodium, potassium, and magnesium chloride are supplemented in cultures. Optimal growth and the production of pigments are only sustained for most bacteria when appropriate salt mixtures are used for culturing, as is the case for the prodigiosin-producing marine *Pseudomonas magnesiorubra* and *Vibrio psychroerythrus*, among other marine species. These bacteria grew optimally and produced red pigment when cultured in seawater or its equivalent, while pigment production by the terrestrial *Serratia marcescens* was inhibited in 3% sea salts [8].

Enhancing low pigment productivity is one of the main issues facing researchers, and some solutions have already been reported. It is well established that antibiotic production by bacteria might be regulated both qualitatively and quantitatively by the nature of the culture medium. In particular, the addition of individual natural compounds to nutrient media or the use of gene expression methods was found to increase the pigment production far beyond expectations. For example, saturated fatty acids, especially peanut broth, was found to be a better choice in increasing prodigiosin production by 40-fold (approximately ~39 mg/mL) in *S. marcescens* [139].

Undecylprodigiosin synthesis by *S. marcescens* was also markedly enhanced by the addition of vegetable (soybean, olive, and sunflower) oils (2–6% [v/v]) and amino acids to the fermentation broth [140, 141]. Violacein production by the recombinant *Citrobacter freundii* strain, the genes of which were reconstructed from *Duganella* sp. B2, reached up to 1.68 g/L, making it fourfold higher than the highest production previously reported [142]. It is anticipated that these methods will facilitate the production of sufficient quantities of many bioactive and pharmacologically important compounds obtained from bacteria of marine origin. These compounds, including prodiginine and violacein, are now considered as potential drug candidates for potentially fatal diseases such as cancer and malaria. Although further improvement of culture methods and technologies for pigment production including recombinant technology is necessary, bioactive compounds from marine bacteria may potentially replace the existing drugs that have lower therapeutic actions.

5. Conclusions

Recently, a number of review papers have appeared in the literature, and they give an overview of all investigations of the marine environment and its isolates. While previous reviews have covered the biological activities of natural products isolated from marine microorganisms [115, 143] and other living organisms [144, 145], our paper is the first to review the importance of pigmented compounds from marine origin and their potential pharmacological applications.

Most studies investigating marine microorganisms have shown the efficacy and the potential clinical applications of pigmented secondary metabolites in treating several diseases. These studies have also emphasized the effects of microbial metabolites as antibiotic, anticancer, and immunosuppressive compounds. Despite the enormous difficulty in isolating and harvesting marine bacteria, significant progress has been achieved in this field, and investigations of bioactive compounds produced by these species are rapidly increasing. As such, the number of compounds isolated from marine microorganisms is increasing faster when compared with terrestrial species [95].

Overall, this review of pigmented marine bioactive compounds and their pharmacological applications highlights the importance of discovering novel marine bacterial metabolites. Such compounds have a wide variety of biologically active properties and continue to provide promising avenues for both fundamental sciences and applied biomedical research.

References

[1] A. W. Bruckner, "Life-saving products from coral reefs," *Issues in Science and Technology*, vol. 18, no. 3, p. 35, 2002.

[2] P. Hugenholtz and N. R. Pace, "Identifying microbial diversity in the natural environment: a molecular phylogenetic approach," *Trends in Biotechnology*, vol. 14, no. 6, pp. 190–197, 1996.

[3] H. Laatsch, "Marine bacterial metabolites," 2005, http://wwwuser.gwdg.de/~ucoc/laatsch/Reviews__Books__Patents/R30_Marine_BacterialMetabolites.pdf.

[4] A. M. S. Mayer, K. B. Glaser, C. Cuevas et al., "The odyssey of marine pharmaceuticals: a current pipeline perspective,"

Trends in Pharmacological Sciences, vol. 31, no. 6, pp. 255–265, 2010.

[5] W. Fenical, "Chemical studies of marine bacteria: developing a new resource," *Chemical Reviews*, vol. 93, no. 5, pp. 1673–1683, 1993.

[6] N. N. Gerber, "Prodigiosin-like pigments from *Actinomadura (Nocardia) pelletieri* and *Actinomadura madurae*," *Applied Microbiology*, vol. 18, no. 1, pp. 1–3, 1969.

[7] H. Rapoport and K. G. Holden, "The synthesis of prodigiosin," *Journal of the American Chemical Society*, vol. 84, no. 4, pp. 635–642, 1962.

[8] N. N. Gerber, "Prodigiosin-like pigments," *CRC Critical Reviews in Microbiology*, vol. 3, no. 4, pp. 469–485, 1975.

[9] N. R. Williamson, P. C. Fineran, T. Gristwood, S. R. Chawrai, F. J. Leeper, and G. P. C. Salmond, "Anticancer and immunosuppressive properties of bacterial prodiginines," *Future Microbiology*, vol. 2, no. 6, pp. 605–618, 2007.

[10] J. W. Bennett and R. Bentley, "Seeing red: the story of prodigiosin," *Advances in Applied Microbiology*, vol. 47, pp. 1–32, 2000.

[11] B. Montaner and R. Pérez-Tomás, "The prodigiosins: a new family of anticancer drugs," *Current Cancer Drug Targets*, vol. 3, no. 1, pp. 57–65, 2003.

[12] N. M. Gandhi, J. R. Patell, J. Gandhi, N. J. De Souza, and H. Kohl, "Prodigiosin metabolites of a marine *Pseudomonas* species," *Marine Biology*, vol. 34, no. 3, pp. 223–227, 1976.

[13] M. J. Gauthier, "*Alteromonas rubra* sp. nov., a new marine antibiotic producing bacterium," *International Journal of Systematic Bacteriology*, vol. 26, no. 4, pp. 459–466, 1976.

[14] N. N. Gerber and M. J. Gauthier, "New prodigiosin-like pigment from *Alteromonas rubra*," *Applied and Environmental Microbiology*, vol. 37, no. 6, pp. 1176–1179, 1979.

[15] D. Fehér, R. S. Barlow, P. S. Lorenzo, and T. K. Hemscheidt, "A 2-substituted prodiginine, 2-(*p*-hydroxybenzyl)prodigiosin, from *Pseudoalteromonas rubra*," *Journal of Natural Products*, vol. 71, no. 11, pp. 1970–1972, 2008.

[16] Ø. Enger, H. Nygaard, M. Solberg, G. Schei, J. Nielsen, and I. Dundas, "Characterization of *Alteromonas denitrificans* sp. nov.," *International Journal of Systematic Bacteriology*, vol. 37, no. 4, pp. 416–421, 1987.

[17] T. Sawabe, H. Makino, M. Tatsumi et al., "*Pseudoalteromonas bacteriolytica* sp. nov., a marine bacterium that is the causative agent of red spot disease of *Laminaria japonica*," *International Journal of Systematic Bacteriology*, vol. 48, no. 3, pp. 769–774, 1998.

[18] C. Yamamoto, H. Takemoto, K. Kuno et al., "Cycloprodigiosin hydrochloride, a new H^+/Cl^- symporter, induces apoptosis in human and rat hepatocellular cancer cell lines *in vitro* and inhibits the growth of hepatocellular carcinoma xenografts in nude mice," *Hepatology*, vol. 30, no. 4, pp. 894–902, 1999.

[19] S. M. Lewis and W. A. Corpe, "Prodigiosin-producing bacteria from marine sources," *Applied Microbiology*, vol. 12, no. 1, pp. 13–17, 1964.

[20] G. Gauthier, M. Gauthier, and R. Christen, "Phylogenetic analysis of the genera *Alteromonas, Shewanella*, and *Moritella* using genes coding for small-subunit rRNA sequences and division of the genus *Alteromonas* into two genera, *Alteromonas* (emended) and *Pseudoalteromonas* gen. nov., and proposal of twelve new species combinations," *International Journal of Systematic Bacteriology*, vol. 45, no. 4, pp. 755–761, 1995.

[21] K. Kawauchi, K. Shibutani, H. Yagisawa et al., "A possible immunosuppressant, cycloprodigiosin hydrochloride, obtained from *Pseudoalteromonas denitrificans*," *Biochemical and Biophysical Research Communications*, vol. 237, no. 3, pp. 543–547, 1997.

[22] H. S. Kim, M. Hayashi, Y. Shibata et al., "Cycloprodigiosin hydrochloride obtained from *Pseudoalteromonas denitrificans* is a potent antimalarial agent," *Biological and Pharmaceutical Bulletin*, vol. 22, no. 5, pp. 532–534, 1999.

[23] J. E. Lazaro, J. Nitcheu, R. Z. Predicala et al., "Heptyl prodigiosin, a bacterial metabolite, is antimalarial in vivo and non-mutagenic in vitro," *Journal of Natural Toxins*, vol. 11, no. 4, pp. 367–377, 2002.

[24] H. K. Lee, J. Chun, E. Y. Moon et al., "*Hahella chejuensis* gen. nov., sp. nov., an extracellular- polysaccharide-producing marine bacterium," *International Journal of Systematic and Evolutionary Microbiology*, vol. 51, no. 2, pp. 661–666, 2001.

[25] W. Y. Shieh, Y. W. Chen, S. M. Chaw, and H. H. Chiu, "*Vibrio ruber* sp. nov., a red, facultatively anaerobic, marine bacterium isolated from sea water," *International Journal of Systematic and Evolutionary Microbiology*, vol. 53, no. 2, pp. 479–484, 2003.

[26] H. Yi, Y. H. Chang, H. W. Oh, K. S. Bae, and J. Chun, "*Zooshikella ganghwensis* gen. nov., sp. nov., isolated from tidal flat sediments," *International Journal of Systematic and Evolutionary Microbiology*, vol. 53, no. 4, pp. 1013–1018, 2003.

[27] D. Kim, J. S. Lee, Y. K. Park et al., "Biosynthesis of antibiotic prodiginines in the marine bacterium *Hahella chejuensis* KCTC 2396," *Journal of Applied Microbiology*, vol. 102, no. 4, pp. 937–944, 2007.

[28] T. Nakashima, M. Kurachi, Y. Kato, K. Yamaguchi, and T. Oda, "Characterization of bacterium isolated from the sediment at coastal area of Omura bay in Japan and several biological activities of pigment produced by this isolate," *Microbiology and Immunology*, vol. 49, no. 5, pp. 407–415, 2005.

[29] D. A. Austin and M. O. Moss, "Numerical taxonomy of red-pigmented bacteria isolated from a lowland river, with the description of a new taxon, *Rugamonas rubra* gen. nov., sp. nov.," *Journal of General Microbiology*, vol. 132, no. 7, pp. 1899–1909, 1986.

[30] M. O. Moss, "A note on a prodigiosin-producing *pseudomonad* isolated from a lowland river," *Journal of Applied Bacteriology*, vol. 55, no. 2, pp. 373–375, 1983.

[31] L. I. Sly and M. H. Hargreaves, "Two unusual budding bacteria isolated from a swimming pool," *Journal of Applied Bacteriology*, vol. 56, no. 3, pp. 479–486, 1984.

[32] S. Yada, M. Ohba, K. Enomoto et al., "Analysis of bacterial species in the Muroto deep seawater," *Deep Ocean Water Resources*, vol. 4, no. 2, pp. 47–56, 2003 (Japanese).

[33] A. Oren and F. Rodríguez-Valera, "The contribution of halophilic Bacteria to the red coloration of saltern crystallizer ponds," *Federation of European Materials Societies Microbiology Ecology*, vol. 36, no. 2-3, pp. 123–130, 2001.

[34] N. Misawa, Y. Satomi, K. Kondo et al., "Structure and functional analysis of a marine bacterial carotenoid biosynthesis gene cluster and astaxanthin biosynthetic pathway proposed at the gene level," *Journal of Bacteriology*, vol. 177, no. 22, pp. 6575–6584, 1995.

[35] J. H. Lee, Y. S. Kim, T. J. Choi, W. J. Lee, and Y. T. Kim, "*Paracoccus haeundaensis* sp. nov., a Gram-negative, halophilic, astaxanthin-producing bacterium," *International Journal of Systematic and Evolutionary Microbiology*, vol. 54, no. 5, pp. 1699–1702, 2004.

[36] D. Rettori and N. Durán, "Production, extraction and purification of violacein: an antibiotic pigment produced by

Chromobacterium violaceum," *World Journal of Microbiology and Biotechnology*, vol. 14, no. 5, pp. 685–688, 1998.

[37] N. Durán and C. F. M. Menck, "*Chromobacterium violaceum*: a review of pharmacological and industiral perspectives," *Critical Reviews in Microbiology*, vol. 27, no. 3, pp. 201–222, 2001.

[38] C. Sánchez, A. F. Braña, C. Méndez, and J. A. Salas, "Reevaluation of the violacein biosynthetic pathway and its relationship to indolocarbazole biosynthesis," *ChemBioChem*, vol. 7, no. 8, pp. 1231–1240, 2006.

[39] S. Asamizu, Y. Kato, Y. Igarashi, and H. Onaka, "VioE, a prodeoxyviolacein synthase involved in violacein biosynthesis, is responsible for intramolecular indole rearrangement," *Tetrahedron Letters*, vol. 48, no. 16, pp. 2923–2926, 2007.

[40] C. J. Balibar and C. T. Walsh, "In vitro biosynthesis of violacein from L-tryptophan by the enzymes VioA-E from *Chromobacterium violaceum*," *Biochemistry*, vol. 45, no. 51, pp. 15444–15457, 2006.

[41] N. Durán, G. Z. Justo, C. V. Ferreira, P. S. Melo, L. Cordi, and D. Martins, "Violacein: properties and biological activities," *Biotechnology and Applied Biochemistry*, vol. 48, no. 3-4, pp. 127–133, 2007.

[42] C. R. Andrighetti-Fröhner, R. V. Antonio, T. B. Creczynski-Pasa, C. R. M. Barardi, and C. M. O. Simões, "Cytotoxicity and potential antiviral evaluation of violacein produced by *Chromobacterium violaceum*," *Memórias do Instituto Oswaldo Cruz*, vol. 98, no. 6, pp. 843–848, 2003.

[43] C. Matz, P. Deines, J. Boenigk et al., "Impact of violacein-producing bacteria on survival and feeding of bacterivorous nanoflagellates," *Applied and Environmental Microbiology*, vol. 70, no. 3, pp. 1593–1599, 2004.

[44] R. M. Brucker, R. N. Harris, C. R. Schwantes et al., "Amphibian Chemical defense: antifungal metabolites of the microsymbiont *Janthinobacterium lividum* on the salamander *Plethodon cinereus*," *Journal of Chemical Ecology*, vol. 34, no. 11, pp. 1422–1429, 2008.

[45] M. H. Becker, R. M. Brucker, C. R. Schwantes, R. N. Harris, and K. P. C. Minbiole, "The bacterially produced metabolite violacein is associated with survival of amphibians infected with a lethal fungus," *Applied and Environmental Microbiology*, vol. 75, no. 21, pp. 6635–6638, 2009.

[46] R. N. Harris, R. M. Brucker, J. B. Walke et al., "Skin microbes on frogs prevent morbidity and mortality caused by a lethal skin fungus," *International Society for Microbial Ecology Journal*, vol. 3, no. 7, pp. 818–824, 2009.

[47] R. D. Hamilton and K. E. Austin, "Physiological and cultural characteristics of *Chromobacterium marinum* sp. n.," *Antonie van Leeuwenhoek*, vol. 33, no. 3, pp. 257–264, 1967.

[48] M. J. Gauthier, "Morphological, physiological, and biochemical characteristics of some violet-pigmented bacteria isolated from seawater," *Canadian Journal of Microbiology*, vol. 22, no. 2, pp. 138–149, 1976.

[49] M. J. Gauthier, J. M. Shewan, D. M. Gibson, and J. V. Lee, "Taxonomic position and seasonal variations in marine neritic environment of some gram-negative antibiotic-producing bacteria," *Journal of General Microbiology*, vol. 87, no. 2, pp. 211–218, 1975.

[50] S. Yada, Y. Wang, Y. Zou et al., "Isolation and characterization of two groups of novel marine bacteria producing violacein," *Marine Biotechnology*, vol. 10, no. 2, pp. 128–132, 2008.

[51] S. Hakvåg, E. Fjærvik, G. Klinkenberg et al., "Violacein-producing *Collimonas* sp. from the sea surface microlayer of costal waters in Trøndelag, Norway," *Marine Drugs*, vol. 7, no. 4, pp. 576–588, 2009.

[52] S. A. MacCarthy, T. Sakata, D. Kakimoto, and R. M. Johnson, "Production and isolation of purple pigment by *Alteromonas luteoviolacea*," *Bulletin of the Japanese Society of Scientific Fisheries*, vol. 51, no. 3, pp. 479–484, 185.

[53] N. J. Novick and M. E. Tyler, "Isolation and characterization of *Pseudoalteromonas luteoviolacea* strains with sheathed flagella," *International Journal of Systematic Bacteriology*, vol. 35, no. 1, pp. 111–113, 1985.

[54] J. M. Turner and A. J. Messenger, "Occurrence, biochemistry and physiology of phenazine pigment production," *Advances in Microbial Physiology*, vol. 27, no. C, pp. 211–275, 1986.

[55] L. S. Pierson and E. A. Pierson, "Metabolism and function of phenazines in bacteria: impact on the behavior of bacteria in the environment and biotechnological process," *Applied Microbiology and Biotechnology*, vol. 86, no. 6, pp. 1659–1670, 2010.

[56] J. Gibson, A. Sood, and D. A. Hogan, "*Pseudomonas aeruginosa-Candida albicans* interactions: localization and fungal toxicity of a phenazine derivative," *Applied and Environmental Microbiology*, vol. 75, no. 2, pp. 504–513, 2009.

[57] J. B. Laursen and J. Nielsen, "Phenazine natural products: biosynthesis, synthetic analogues, and biological activity," *Chemical Reviews*, vol. 104, no. 3, pp. 1663–1685, 2004.

[58] S. Saha, R. Thavasi, and S. Jayalakshmi, "Phenazine pigments from *Pseudomonas aeruginosa* and their application as antibacterial agent and food colourants," *Research Journal of Microbiology*, vol. 3, no. 3, pp. 122–128, 2008.

[59] A. Nansathit, S. Apipattarakul, C. Phaosiri, P. Pongdontri, S. Chanthai, and C. Ruangviriyachai, "Synthesis, isolation of phenazine derivatives and their antimicrobial activities," *Walailak Journal of Science and Techology*, vol. 6, no. 1, pp. 79–91, 2009.

[60] H. Ran, D. J. Hassett, and G. W. Lau, "Human targets of *Pseudomonas aeruginosa* pyocyanin," *Proceedings of the National Academy of Sciences of the United States of America*, vol. 100, no. 2, pp. 14315–14320, 2003.

[61] G. W. Lau, H. Ran, F. Kong, D. J. Hassett, and D. Mavrodi, "*Pseudomonas aeruginosa* pyocyanin is critical for lung infection in mice," *Infection and Immunity*, vol. 72, no. 7, pp. 4275–4278, 2004.

[62] M. W. Tan, S. Mahajan-Miklos, and F. M. Ausubel, "Killing of *Caenorhabditis elegans* by *Pseudomonas aeruginosa* used to model mammalian bacterial pathogenesis," *Proceedings of the National Academy of Sciences of the United States of America*, vol. 96, no. 2, pp. 715–720, 1999.

[63] R. P. Maskey, I. Kock, E. Helmke, and H. Laatsch, "Isolation and structure determination of phenazostatin D, a new phenazine from a marine actinomycete isolate *Pseudonocardia* sp. B6273," *Zeitschrift für Naturforschung*, vol. 58b, no. 7, pp. 692–694, 2003.

[64] D. Li, F. Wang, X. Xiao, X. Zeng, Q. Q. Gu, and W. Zhu, "A new cytotoxic phenazine derivative from a deep sea bacterium *Bacillus* sp.," *Archives of Pharmacal Research*, vol. 30, no. 5, pp. 552–555, 2007.

[65] K. Pusecker, H. Laatsch, E. Helmke, and H. Weyland, "Dihydrophencomycin methyl ester, a new phenazine derivative from a marine streptomycete," *Journal of Antibiotics*, vol. 50, no. 6, pp. 479–483, 1997.

[66] R. Wilson, T. Pitt, G. Taylor et al., "Pyocyanin and 1-hydroxyphenazine produced by *Pseudomonas aeruginosa* inhibit the beating of human respiratory cilia in vitro," *Journal of Clinical Investigation*, vol. 79, no. 1, pp. 221–229, 1987.

[67] M. Akagawa-Matsushita, T. Itoh, Y. Katayama, H. Kuraishi, and K. Yamasato, "Isoprenoid quinone composition of some

marine *Alteromonas, Marinomonas, Deleya, Pseudomonas* and *Shewanella* species," *Journal of General Microbiology*, vol. 138, no. 11, pp. 2275–2281, 1992.

[68] R. P. Maskey, E. Helmke, and H. Laatsch, "Himalomycin A and B: isolation and structure elucidation of new fridamycin type antibiotics from a marine *Streptomyces* isolate," *Journal of Antibiotics*, vol. 56, no. 11, pp. 942–949, 2003.

[69] P. Z. Margalith, *Pigment Microbiology*, Chapman & Hall, London, UK, 1992.

[70] J. Koyama, "Anti-infective quinone derivatives of recent patents," *Recent Patents on Anti-Infective Drug Discovery*, vol. 1, no. 1, pp. 113–125, 2006.

[71] F. Li, R. P. Maskey, S. Qin et al., "Chinikomycin A and B: isolation, structure elucidation and biological activity of novel antibiotics from a marine *Streptomyces* sp. isolate M045," *Journal of Natural Products*, vol. 68, no. 3, pp. 349–353, 2005.

[72] C. F. Norton and G. E. Jones, "A marine isolate of *Pseudomonas nigrifacience*. II. Characterization of its blue pigment," *Archiv für Mikrobiologie*, vol. 64, no. 4, pp. 369–376, 1969.

[73] H. Kobayashi, Y. Nogi, and K. Horikoshi, "New violet 3,3′-bipyridyl pigment purified from deep-sea microorganism *Shewanella violacea* DSS12," *Extremophiles*, vol. 11, no. 2, pp. 245–250, 2007.

[74] C. Holmström, S. Egan, A. Franks, S. McCloy, and S. Kjelleberg, "Antifouling activities expressed by marine surface associated *Pseudoalteromonas* species," *Federation of European Materials Societies Microbiology Ecology*, vol. 41, no. 1, pp. 47–58, 2002.

[75] S. Egan, S. James, C. Holmström, and S. Kjelleberg, "Correlation between pigmentation and antifouling compounds produced by *Pseudoalteromonas tunicate*," *Environmental Microbiology*, vol. 4, no. 8, pp. 433–442, 2002.

[76] A. Franks, P. Haywood, C. Holmström, S. Egan, S. Kjelleberg, and N. Kumar, "Isolation and structure elucidation of a novel yellow pigment from the marine bacterium *Pseudoalteromonas tunicata*," *Molecules*, vol. 10, no. 10, pp. 1286–1291, 2005.

[77] B. Carté and D. J. Faulkner, "Defensive metabolites from three nembrothid nudibranchs," *Journal of Organic Chemistry*, vol. 48, no. 14, pp. 2314–2318, 1983.

[78] N. Lindquist and W. Fenical, "New tambjamines class alkaloids from the marine ascidian *Atapozoa* sp. and its nudibranch predators. Origin of the tambjamines in *Atapozoa*," *Experientia*, vol. 47, no. 5, pp. 504–506, 1991.

[79] A. J. Blackman and C. P. Li, "New tambjamine alkaloids from the marine bryozoan *Bugula dentate*," *Australian Journal of Chemistry*, vol. 47, no. 8, pp. 1625–1629, 1994.

[80] D. M. Pinkerton, M. G. Banwell, M. J. Garson et al., "Antimicrobial and cytotoxic activities of synthetically derived tambjamines C and E-J, BE-18591, and a related alkaloid from the marine bacterium *Pseudoalteromonas tunicata*," *Chemistry & Biodiversity*, vol. 7, no. 5, pp. 1311–1324, 2010.

[81] A. C. Granato, J. H. H. L. de Oliveira, M. H. R. Seleghim et al., "Produtos naturais da ascidia *Botrylloides giganteum*, das esponjas *Verongula gigantea, Ircinia felix, Cliona delitrix* e do *nudibrânquio Tambja eliora*, da costa do Brasil," *Quimica Nova*, vol. 28, no. 2, pp. 192–198, 2005.

[82] D. M. Pinkerton, M. G. Banwell, and A. C. Willis, "Total syntheses of tambjamines C, E, F, G, H, I and J, BE-18591, and a related alkaloid from the marine bacterium *Pseudoalteromonas tunicata*," *Organic Letters*, vol. 9, no. 24, pp. 5127–5130, 2007.

[83] S. I. Kotob, S. L. Coon, E. J. Quintero, and R. M. Weiner, "Homogentisic acid is the primary precursor of melanin synthesis in *Vibrio cholerae*, a *Hyphomonas* strain, and *Shewanella colwelliana*," *Applied and Environmental Microbiology*, vol. 61, no. 4, pp. 1620–1622, 1995.

[84] C. Ruzafa, A. Sanchez-Amat, and F. Solano, "Characterization of the melanogenic system in *Vibrio cholerae*, ATCC 14035," *Pigment Cell Research*, vol. 8, no. 3, pp. 147–152, 1995.

[85] E. P. Ivanova, E. A. Kiprianova, V. V. Mikhailov et al., "Characterization and identification of marine *Alteromonas nigrifaciens* strains and emendation of the description," *International Journal of Systematic Bacteriology*, vol. 46, no. 1, pp. 223–228, 1996.

[86] W. C. Fuqua and R. M. Weiner, "The *melA* gene is essential for melanin biosynthesis in the marine bacterium *Shewanella colwelliana*," *Journal of General Microbiology*, vol. 139, no. 5, pp. 1105–1114, 1993.

[87] A. Sanchez-Amat, C. Ruzafa, and F. Solano, "Comparative tyrosine degradation in *Vibrio cholerae* strains. The strain ATCC 14035 as a prokaryotic melanogenic model of homogentisate-releasing cell," *Comparative Biochemistry and Physiology—Part B*, vol. 119, no. 3, pp. 557–562, 1998.

[88] H. Y. Kahng, B. S. Chung, D. H. Lee, J. S. Jung, J. H. Park, and C. O. Jeon, "*Cellulophaga tyrosinoxydans* sp. nov., a tyrosinase-producing bacterium isolated from seawater," *International Journal of Systematic and Evolutionary Microbiology*, vol. 59, no. 4, pp. 654–657, 2009.

[89] W. Fenical and P. R. Jensen, "Marine microorganisms: a new biomedical resource," in *Marine Biotechnology*, D. H. Attaway and O. R. Zaborsky, Eds., pp. 419–457, Plenum Press, New York, NY, USA, 1993.

[90] H. Claus and H. Decker, "Bacterial tyrosinases," *Systematic and Applied Microbiology*, vol. 29, no. 1, pp. 3–14, 2006.

[91] F. Solano, E. García, E. P. de Egea, and A. Sanchez-Amat, "Isolation and characterization of strain MMB-1 (CECT 4803), a novel melanogenic marine bacterium," *Applied and Environmental Microbiology*, vol. 63, no. 9, pp. 3499–3506, 1997.

[92] P. J. Proteau, W. H. Gerwick, F. Garcia-Pichel, and R. Castenholz, "The structure of scytonemin, an ultraviolet sunscreen pigment from the sheaths of cyanobacteria," *Experientia*, vol. 49, no. 9, pp. 825–829, 1993.

[93] C. S. Stevenson, E. A. Capper, A. K. Roshak et al., "Scytonemin—a marine natural product inhibitor of kinases key in hyperproliferative inflammatory diseases," *Inflammation Research*, vol. 51, no. 2, pp. 112–114, 2002.

[94] H.-P. Grossart, M. Thorwest, I. Plitzko, T. Brinkhoff, M. Simon, and A. Zeeck, "Production of a blue pigment (glaukothalin) by marine *Rheinheimera* spp.," *International Journal of Microbiology*, vol. 2009, Article ID 701735, 7 pages, 2009.

[95] I. Wagner-Döbler, W. Beil, S. Lang, M. Meiners, and H. Laatsch, "Integrated approach to explore the potential of marine microorganisms for the production of bioactive metabolites," *Advances in Biochemical Engineering/Biotechnology*, vol. 74, pp. 207–238, 2002.

[96] N. R. Williamson, H. T. Simonsen, R. A. A. Ahmed et al., "Biosynthesis of the red antibiotic, prodigiosin, in *Serratia*: identification of a novel 2-methyl-3-n-amylpyrrole (MAP) assembly pathway, definition of the terminal condensing enzyme, and implications for undecylprodigiosin biosynthesis in *Streptomyces*," *Molecular Microbiology*, vol. 56, no. 4, pp. 971–989, 2005.

[97] N. R. Williamson, P. C. Fineran, F. J. Leeper, and G. P. C. Salmond, "The biosynthesis and regulation of bacterial

prodiginines," *Nature Reviews Microbiology*, vol. 4, no. 12, pp. 887–899, 2006.

[98] A. K. P. Harris, N. R. Williamson, H. Slater et al., "The *Serratia* gene cluster encoding biosynthesis of the red antibiotic, prodigiosin, shows species- and strain-dependent genome context variation," *Microbiology*, vol. 150, no. 11, pp. 3547–3560, 2004.

[99] H. Jeong, J. H. Yim, C. Lee et al., "Genomic blueprint of *Hahella chejuensis*, a marine microbe producing an algicidal agent," *Nucleic Acids Research*, vol. 33, no. 22, pp. 7066–7073, 2005.

[100] A. M. Cerdeño, M. J. Bibb, and G. L. Challis, "Analysis of the prodiginine biosynthesis gene cluster of *Streptomyces coelicolor* A3(2): new mechanisms for chain initiation and termination in modular multienzymes," *Chemistry and Biology*, vol. 8, no. 8, pp. 817–829, 2001.

[101] M.-J. Ding and R. P. Williams, "Biosynthesis of prodigiosin by white strains of *Serratia marcescens* isolated from patients," *Journal of Clinical Microbiology*, vol. 17, no. 3, pp. 476–480, 1983.

[102] K. Shinoda, T. Hasegawa, H. Sato et al., "Biosynthesis of violacein: a genuine intermediate, protoviolaceinic acid, produced by VioABDE, and insight into VioC function," *Chemical Communications*, no. 40, pp. 4140–4142, 2007.

[103] S. Hirano, S. Asamizu, H. Onaka, Y. Shiro, and S. Nagano, "Crystal structure of VioE, a key player in the construction of the molecular skeleton of violacein," *Journal of Biological Chemistry*, vol. 283, no. 10, pp. 6459–6466, 2008.

[104] K. S. Ryan, C. J. Balibar, K. E. Turo, C. T. Walsh, and C. L. Drennan, "The violacein biosynthetic enzyme VioE shares a fold with lipoprotein transporter proteins," *Journal of Biological Chemistry*, vol. 283, no. 10, pp. 6467–6475, 2008.

[105] G. S. Byng, D. C. Eustice, and R. A. Jensen, "Biosynthesis of phenazine pigments in mutant and wild-type cultures of *Pseudomonas aeruginosa*," *Journal of Bacteriology*, vol. 138, no. 3, pp. 846–852, 1979.

[106] D. V. Mavrodi, R. F. Bonsall, S. M. Delaney, M. J. Soule, G. Phillips, and L. S. Thomashow, "Functional analysis of genes for biosynthesis of pyocyanin and phenazine-1-carboxamide from *Pseudomonas aeruginosa* PAO1," *Journal of Bacteriology*, vol. 183, no. 21, pp. 6454–6465, 2001.

[107] C. Burke, T. Thomas, S. Egan, and S. Kjelleberg, "The use of functional genomics for the identification of a gene cluster encoding for the biosynthesis of an antifungal tambjamine in the marine bacterium *Pseudoalteromonas tunicate*," *Environmental Microbiology*, vol. 9, no. 3, pp. 814–818, 2007.

[108] D. López-Serrano, F. Solano, and A. Sanchez-Amat, "Identification of an operon involved in tyrosinase activity and melanin synthesis in *Marinomonas mediterranea*," *Gene*, vol. 342, no. 1, pp. 179–187, 2004.

[109] S. K. Kelley, V. E. Coyne, D. D. Sledjeski, W. C. Fuqua, and R. M. Weiner, "Identification of a tyrosinase from a periphytic marine bacterium," *Federation of European Materials Societies Microbiology Letters*, vol. 67, no. 3, pp. 275–279, 1990.

[110] T. Soule, V. Stout, W. D. Swingley, J. C. Meeks, and F. Garcia-Pichel, "Molecular genetics and genomic analysis of scytonemin biosynthesis in *Nostoc punctiforme* ATCC 29133," *Journal of Bacteriology*, vol. 189, no. 12, pp. 4465–4472, 2007.

[111] E. P. Balskus and C. T. Walsh, "An enzymatic cyclopentyl[*b*]indole formation involved in scytonemin biosynthesis," *Journal of the American Chemical Society*, vol. 131, no. 41, pp. 14648–14649, 2009.

[112] E. P. Balskus and C. T. Walsh, "Investigating the initial steps in the biosynthesis of cyanobacterial sunscreen scytonemin," *Journal of the American Chemical Society*, vol. 130, no. 46, pp. 15260–15261, 2008.

[113] C. Holmström, S. James, S. Egan, and S. Kjelleberg, "Inhibition of common fouling organisms by pigmented marine bacterial isolates with special reference to the role of pigmented bacteria," *Biofouling*, vol. 10, no. 1–3, pp. 251–259, 1996.

[114] M. L. Lemos, A. E. Toranzo, and J. L. Barja, "Antibiotic activity of epiphytic bacteria isolated from intertidal seaweeds," *Microbial Ecology*, vol. 11, no. 2, pp. 149–163, 1985.

[115] I. Bhatnagar and S. K. Kim, "Immense essence of excellence: marine microbial bioactive compounds," *Marine Drugs*, vol. 8, no. 10, pp. 2673–2701, 2010.

[116] M. Griffiths, W. R. Sistrom, G. Cohen-Bazire, and R. Y. Stanier, "Function of carotenoids in photosynthesis," *Nature*, vol. 176, no. 4495, pp. 1211–1214, 1955.

[117] S. Rottem and O. Markowitz, "Carotenoids act as reinforcers of the *Acholeplasma laidlawii* lipid bilayer," *Journal of Bacteriology*, vol. 140, no. 3, pp. 944–948, 1979.

[118] C. Holmström, D. Rittschof, and S. Kjelleberg, "Inhibition of settlement by larvae of *Balanus amphitrite* and *Ciona intestinalis* by a surface-colonizing marine bacterium," *Applied and Environmental Microbiology*, vol. 58, no. 7, pp. 2111–2115, 1992.

[119] S. Egan, S. James, C. Holmström, and S. Kjelleberg, "Inhibition of algal spore germination by the marine bacterium *Pseudoalteromonas tunicata*," *Federation of European Microbiological Societies Microbiology Ecology*, vol. 35, no. 1, pp. 67–73, 2001.

[120] S. Egan, T. Thomas, C. Holmström, and S. Kjelleberg, "Phylogenetic relationship and antifouling activity of bacterial epiphytes from the marine alga *Ulva lactuca*," *Environmental Microbiology*, vol. 2, no. 3, pp. 343–347, 2000.

[121] R. J. Andersen, M. S. Wolfe, and D. J. Faulkner, "Autotoxic antibiotic production by a marine *Chromobacterium*," *Marine Biology*, vol. 27, no. 4, pp. 281–285, 1974.

[122] M. J. Gauthier and G. N. Flatau, "Antibacterial activity of marine violet-pigmented *Alteromonas* with special reference to the production of brominated compounds," *Canadian Journal of Microbiology*, vol. 22, no. 11, pp. 1612–1619, 1976.

[123] C. Holmström and S. Kjelleberg, "The effect of external biological factors on settlement of marine invertebrates and new antifouling technology," *Biofouling*, vol. 8, no. 2, pp. 147–160, 1994.

[124] C. Holmström, P. Steinberg, V. Christov, G. Christie, and S. Kjelleberg, "Bacteria immobilised in gels: improved methodologies for antifouling and biocontrol applications," *Biofouling*, vol. 15, no. 1–3, pp. 109–117, 2000.

[125] I. Imai, Y. Ishida, K. Sakaguchi, and Y. Hata, "Algicidal marine bacteria isolated from northern Hiroshima Bay, Japan," *Fisheries Science*, vol. 61, no. 4, pp. 628–636, 1995.

[126] C. Lovejoy, J. P. Bowman, and G. M. Hallegraeff, "Algicidal effects of a novel marine *Pseudoalteromonas* isolate (class *Proteobacteria*, gamma subdivision) on harmful algal bloom species of the genera *Chattonella*, *Gymnodinium*, and *Heterosigma*," *Applied and Environmental Microbiology*, vol. 64, no. 8, pp. 2806–2813, 1998.

[127] J. S. Maki, D. Rittschof, and R. Mitchell, "Inhibition of larval barnacle attachment to bacterial films: an investigation of physical properties," *Microbial Ecology*, vol. 23, no. 1, pp. 97–106, 1992.

[128] S. A. Mary, S. V. Mary, D. Rittschof, and R. Nagabhushanam, "Bacterial-barnacle interaction: potential of using juncellins and antibiotics to alter structure of bacterial communities,"

Journal of Chemical Ecology, vol. 19, no. 10, pp. 2155–2167, 1993.

[129] J. B. Bruhn, L. Gram, and R. Belas, "Production of antibacterial compounds and biofilm formation by *Roseobacter* species are influenced by culture conditions," *Applied and Environmental Microbiology*, vol. 73, no. 2, pp. 442–450, 2007.

[130] S. Angell, B. J. Bench, H. Williams, and C. M. H. Watanabe, "Pyocyanin isolated from a marine microbial population: synergistic production between two distinct bacterial species and mode of action," *Chemistry & Biology*, vol. 13, no. 12, pp. 1349–1359, 2006.

[131] H. B. Bode, "No need to be pure: mix the cultures!," *Chemistry and Biology*, vol. 13, no. 12, pp. 1245–1246, 2006.

[132] N. Bromberg, G. Z. Justo, M. Haun, N. Durán, and C. V. Ferreira, "Violacein cytotoxicity on human blood lymphocytes and effect on phosphatases," *Journal of Enzyme Inhibition and Medicinal Chemistry*, vol. 20, no. 5, pp. 449–454, 2005.

[133] A. Fürstner, K. Reinecke, H. Prinz, and H. Waldmann, "The core structures of roseophilin and the prodigiosin alkaloids define a new class of protein tyrosine phosphatase inhibitors," *ChemBioChem*, vol. 5, no. 11, pp. 1575–1579, 2004.

[134] T. Sato, H. Konno, Y. Tanaka et al., "Prodigiosins as a new group of H^+/Cl^- symporters that uncouple proton translocators," *Journal of Biological Chemistry*, vol. 273, no. 34, pp. 21455–21462, 1998.

[135] S. Ohkuma, T. Sato, M. Okamoto et al., "Prodigiosins uncouple lysosomal vacuolar-type ATPase through promotion of H^+/Cl^- symport," *Biochemical Journal*, vol. 334, no. 3, pp. 731–741, 1998.

[136] J. L. Seganish and J. T. Davis, "Prodigiosin is a chloride carrier that can function as an anion exchanger," *Chemical Communications*, no. 46, pp. 5781–5783, 2005.

[137] K. Kawauchi, K. Tobiume, K. Iwashita et al., "Cycloprodigiosin hydrochloride activates the Ras-PI3K-Akt pathway and suppresses protein synthesis inhibition-induced apoptosis in PC12 cells," *Bioscience, Biotechnology and Biochemistry*, vol. 72, no. 6, pp. 1564–1570, 2008.

[138] D. S. Bhakuni and D. S. Rawat, *Bioactive Marine Natural Products*, Springer, New York, NY, USA, 2005.

[139] A. V. Giri, N. Anandkumar, G. Muthukumaran, and G. Pennathur, "A novel medium for the enhanced cell growth and production of prodigiosin from *Serratia marcescens* isolated from soil," *BMC Microbiology*, vol. 4, no. 11, pp. 1–10, 2004.

[140] Y.-H. Wei and W. C. Chen, "Enhanced production of prodigiosin-like pigment from *Serratia marcescens* SMΔR by medium improvement and oil-supplementation strategies," *Journal of Bioscience and Bioengineering*, vol. 99, no. 6, pp. 616–622, 2005.

[141] Y.-H. Wei, W.-J. Yu, and W.-C. Chen, "Enhanced undecylprodigiosin production from *Serratia marcescens* SS-1 by medium formulation and amino-acid supplementation," *Journal of Bioscience and Bioengineering*, vol. 100, no. 4, pp. 466–471, 2005.

[142] P. X. Jiang, H. S. Wang, C. Zhang, K. Lou, and X. H. Xing, "Reconstruction of the violacein biosynthetic pathway from *Duganella* sp. B2 in different heterologous hosts," *Applied Microbiology and Biotechnology*, vol. 86, no. 4, pp. 1077–1088, 2010.

[143] A. Debbab, A. H. Aly, W. H. Lin, and P. Proksch, "Bioactive compounds from marine bacteria and fungi," *Microbial Biotechnology*, vol. 3, no. 5, pp. 544–563, 2010.

[144] J. W. Blunt, B.-R. Copp, W. P. Hu, M. H. G. Munro, P. T. Northcote, and M. R. Prinsep, "Marine natural products," *Natural Product Reports*, vol. 26, no. 2, pp. 170–244, 2009.

[145] R. K. Jha and X. Zi-Rong, "Biomedical compounds from marine organisms," *Marine Drugs*, vol. 2, no. 3, pp. 123–146, 2004.

Hindawi Publishing Corporation
Evidence-Based Complementary and Alternative Medicine
Volume 2011, Article ID 824104, 7 pages
doi:10.1155/2011/824104

Research Article

Bacillus amyloliquefaciens G1: A Potential Antagonistic Bacterium against Eel-Pathogenic *Aeromonas hydrophila*

Haipeng Cao,[1] Shan He,[2] Ruopeng Wei,[3] Marek Diong,[1] and Liqun Lu[1]

[1] *Key Laboratory of Exploration and Utilization of Aquatic Genetic Resources of Ministry of Education, Aquatic Pathogen Collection Center of Ministry of Agriculture, Shanghai Ocean University, Shanghai 201306, China*
[2] *Education Department, Shanghai Normal University, Shanghai 200235, China*
[3] *Technology Department, Shanxi Veterinary Drug and Feed Engineering Technology Research Center, Yuncheng 044000, China*

Correspondence should be addressed to Liqun Lu, caohaipeng19810818@yahoo.com.cn

Received 24 December 2010; Accepted 16 May 2011

Recent studies have revealed that the use of probiotics is an alternative to control marine aeromonas. However, few probiotics are available against *Aeromonas hydrophila* infections in eels. In the present study, a potential antagonistic strain G1 against the eel-pathogenic *A. hydrophila* was isolated from sediment underlying brackish water. Its extracellular products with antibacterial activities were shown to be stable under wide range of pH, temperature, and proteinase K. It was initially identified as *Bacillus amyloliquefaciens* using API identification kits and confirmed to be *B. amyloliquefaciens* strain (GenBank accession number DQ422953) by phylogenetic analysis. In addition, it was shown to be safe for mammalians, had a wide anti-*A. hydrophila* spectrum, and exhibited significant effects on inhibiting the growth of the eel-pathogenic *A. hydrophila* both *in vitro* and *in vivo*. To the best of our knowledge, this is the first report on a promising antagonistic *Bacillus amyloliquefaciens* strain from brackish water sediment against eel-pathogenic *A. hydrophila*.

1. Introduction

Eels are important warm water fish species cultured in several European countries including Italy, Spain, Germany, Denmark, and the Netherlands, as well as in Japan, Taiwan, Malaysia, and China [1]. Among the cultured eels, *Anguilla anguilla* (L.) is one of the most important commercial fish species, especially in the brackish Comacchio lagoons of the northern Adriatic Sea [2]. For decades, outbreaks of infectious diseases caused by *Aeromonas hydrophila* are considered to be a major economic problem to the aquaculture and quality of *Anguilla anguilla* (L.), leading to severe losses in the production and marketing of *A. anguilla* (L.) [3, 4]. At present, aeromonas can be partially controlled by fish farmers with crude application of antibiotics such as terramycin and florfenicol. However, antibiotic treatment is cost-prohibitive to farmers in many undeveloped and developing countries, and antibiotic use may be detrimental to the environment and human health, involving the development and transfer of antibiotic resistance to other aquatic bacteria, fish pathogens, human pathogens, and the accumulation of antibiotic residuals in the products [5]. Thus, besides the alternative control strategies such as improved husbandry and water quality, better nutrition, lower stocking densities, the use of beneficial microorganisms is also widely expected to become an alternative method for the prevention and control of aeromonas.

Microbial antagonism is a common phenomenon in nature [6] and plays a major role in reducing or eliminating the incidence of opportunistic pathogens in the gastrointestinal tract of aquatic animals [7]. Recently, the application of *Bacillus* sp. as a probiotic species for controlling aquatic pathogens shows promise [8]. For example, Sugita et al. isolated a *Bacillus* strain that was antagonistic to 63% of the isolates from fish intestine [9]. Sun et al. obtained two dominant gut *Bacillus* strains with antagonistic activity that could improve growth performance and immune responses of grouper *Epinephelus coioides* [10]. However, no information is available about *B. amyloliquefaciens* as a biocontrol agent for aquatic pathogens.

In this study, we isolated a *B. amyloliquefaciens* strain G1 antagonistic to the eel-pathogenic *A. hydrophila*, determined its taxonomic position, observed the physicochemical properties of its extracellular products, and assayed its *in vitro*

and *in vivo* growth inhibition effects on *A. hydrophila*, and its antagonistic spectrum and pathogenicity. The data could establish its potential as an environmentally friendly probiotic for eel aquaculture.

2. Materials and Methods

2.1. Sample Collection and Isolation of Marine Bacteria. Brackish water sediment samples were collected from perch and white shrimp farms located at Qingpu District, Shanghai China. The samples were kept in a refrigerator until use. One gram of the sediment was suspended in 100 mL of autoclaved filtered brackish water, heated for 10 min at 80°C to destroy vegetative bacteria and fungi to facilitate isolation of bacilli with spores that survived the heat pretreatment. Sediment samples were then incubated in a shaker incubator (Thermo Forma Co. Ltd., USA) at 30°C with shaking at 200 rpm for 30 min. Mixtures were allowed to settle, serial dilutions up to 10^{-4} were prepared using sterile distilled water and agitated with a vortex (Hushi Laboratory Equipment Co. Ltd., Shanghai) at 200 rpm. Isolation of bacteria from this mixture was done with serial dilution technique on brackish water nutrient agar (NA) (Sinopharm Chemical Reagent Co. Ltd., Shanghai) medium. Purification of bacteria was done using repeated streaking and single colony culture at 30°C. Bacterial isolates were subcultured and transferred to brackish water NA slants. Until further use, the slants were kept at 4°C as described by Das et al. [11].

2.2. Screening of Antagonistic Bacteria

2.2.1. Indicator Bacterium. *A. hydrophila* strain ZN1, the pathogen of septicemia in European eel *Anguilla Anguilla* (L.) [12], was obtained from Fujian Institute of Aquatic Product in Freshwater.

2.2.2. Antibacterial Activity Assay. The antibacterial activities of all the bacterial isolates were examined against the eel-pathogenic *A. hydrophila* strain ZN1 by the paper disc method [13]. Briefly, a culture of *A. hydrophila* was independently spread on brackish water NA plates, then the 5 mm sterile paper discs containing the bacterial isolate with a cell density of 10^6 cfu/disc were placed on the brackish water NA plates. Control plates consisted of *A. hydrophila* only. Zones of inhibition around the paper discs were observed and recorded on *A. hydrophila* lawn culture plates after two days of incubation at 30°C.

2.3. Phenotypic Characterization and Identification. The isolate was grown on brackish water NA plates (Sinopharm Chemical Reagent Co., Ltd.) at 30°C for 24 h, and then the bacterial suspension was used to inoculate the 50 CHB/E API strip (Bio-Merieux, SA) following the manufacturer's instruction. The strip was incubated at 30°C and observed after 48 h for checking against the API identification index and database.

2.4. Molecular Identification

2.4.1. DNA Extract, PCR, and Sequencing. The Genomic DNA was extracted from a pure culture of the isolate using a genomic DNA extraction kit following instructions of the manufacturer (Shanghai Sangon Biological Engineering Technology & Services Co., Ltd.). The 16S rRNA gene fragments (ca. 1.5 kb) were amplified by PCR using a pair of universal bacterial 16S rRNA gene primers (27f): 5′-AGAGTTTGATCCTGGCTCAG-3′ and (1492r): 5′-TACGGCTACCTTGTTACGACTT-3′. The PCR was carried out according to Nduhiu et al. [14]. Briefly, 1 μL of the DNA extract was amplified in a 25 μL reaction mix containing 16.75 μL sterilized distilled water, 2.5 μL deoxyribonucleoside triphosphate (dNTP 10 mM), 2.5 μL 10x buffer, 1 μL $MgCl_2$ (50 mM), 0.5 μL of each primer (10 mM), and 0.25 μL (1 U) ExTaq DNA polymerase. Amplification was done using 35 cycles of denaturation at 95°C for 1 min, annealing at 60°C for 1 min, and extension at 72°C for 1.5 min followed by a final extension 72°C for 7 min using a PCR minicycler (Eppendorf Ltd., Germany). The PCR product was electrophoresed on 1% agarose gel and visualized via ultraviolet transillumination. Sequencing was performed by a fluorescent labeled dideoxynucleotide termination method (with BigDye terminator) on ABI 3730 automated DNA Sequencer.

2.4.2. Phylogenetic Analysis. The partial 16S rRNA sequence was assembled using MegAlign, Editseq, and Seqman software with a Macintosh computer. Searches were done against the National Centre for Biotechnology Information (NCBI) database using the Basic Local Alignment Search Tool (BLAST) program. The phylogenetic tree based on the 16S rRNA gene sequence of the isolate was constructed using the neighbor-joining method.

2.5. Physicochemical Analysis of Extracellular Products

2.5.1. Preparation of the Extracellular Products. The isolate was incubated in 400 mL of brackish water nutrient broth (NB) (Sinopharm Chemical Reagent Co. Ltd., Shanghai) medium at 30°C with shaking at 200 rpm until the cell density reached 10^9 cfu/mL. Then the cultured medium was centrifuged at 8000 rpm at 4°C for 20 min, the supernatant containing the antagonistic substance was extracted, and the extracellular products (ECPs) were obtained as described by Bordoloi et al. [15]. Briefly, the supernatant was extracted twice with equal volumes of ethyl acetate (1 : 1). The crude extract was dried over sodium sulfate and then evaporated under vacuum.

2.5.2. PH Stability Assay. The influence of pH on the stability of ECPs was measured in the pH range of 5.0 to 9.0 as described by Lee et al. [16]. Briefly, the 10 mg of ECPs was added to 50 μL of 50 mM citric acid buffer (pH 5), potassium phosphate buffer (pH 6–8), and carbohydrate buffer (pH 9) (Sinopharm Chemical Reagent Co. Ltd., Shanghai), then each mixture was applied to *A. hydrophila* strain ZN1

lawn cell plates. Zones of inhibition were recorded on *A. hydrophila* lawn culture plates.

2.5.3. Thermal Stability Assay. The analysis on the thermal stability of ECPs was examined as described by Lee et al. [16]. Briefly, the 10 mg of ECPs was treated independently at 20, 40, 60, 80, and 100°C for 30 min. Then each treatment sample was applied to *A. hydrophila* strain ZN1 lawn cell plates. Zones of inhibition were recorded on *A. hydrophila* lawn culture plates.

2.5.4. Enzyme Stability Assay. The 10 mg of ECPs was digested with 15 μL of proteinase K (974 U/mL) (Shanghai Sangon Biological Engineering Technology and Services Co. Ltd.) at 30°C for 2 h. Then the processed sample was applied to *A. hydrophila* strain ZN1 lawn cell plates. Zones of inhibition were recorded on *A. hydrophila* lawn culture plates.

2.6. In Vitro Pathogen Growth Inhibition Assay. The assay was carried out in twelve 250 mL glass flask supplied with 98 mL of brackish water NB medium, and each treatment consisted of three flasks. In each flask, 1 mL of the isolate's suspension with a final cell density of 10^3 cfu/mL, 10^4 cfu/mL, 10^5 cfu/mL, and 1 mL of the *A. hydrophila* suspension with a final cell density of 10^3 cfu/mL were independently inoculated in 98 mL of brackish water NB medium, then the mixtures were incubated at 30°C with shaking at 200 rpm. The control group consisted of *A. hydrophila* strain only. Cell growth of *A. hydrophila* was measured using brackish water RS medium (Beijing Land Bridge Technology Co. Ltd.) at 24 h intervals.

2.7. Antagonistic Spectrum Assay. Eight pathogenic strains of *A. hydrophila* (ATCC7966, X1, S1, T3, R402L, RK1119, 706C, and 40142G) were obtained from National Collection Centre for Aquatic Pathogens, China. The antagonistic spectrum of the isolate was checked against the eight pathogenic *A. hydrophila* strains by the paper disc method [13]. The antagonistic activity against *A. hydrophila* strain ZN1 was served as the control. Zones of inhibition were observed and recorded on *A. hydrophila* lawn culture plates after two days of incubation at 30°C.

2.8. Virulence Assay. Hemolytic activity assay was carried out with brackish water rabbit blood agar (RBA) plates (Sinopharm Chemical Reagent Co., Ltd.) at 30°C for 2 days. Virulence was further assayed in mice. Briefly, four-week-old female BALB/c mice, weighing 20 g each, were obtained from Laboratory Animal Centre of Second Military Medical University, Shanghai. Mice were lightly anesthetized with Halothane (Sinopharm Chemical Reagent Co., Ltd.) in a glass desiccator and challenged with the isolate's suspension prepared as mentioned above. The isolate's suspension was orally administered at the final cell density of 10^5, 10^6, 10^7, 10^8, and 10^9 cfu/g through a micropipette fitted with a fine micropipette tip and thin flexible tube. The control mice were orally administered with the autoclaved brackish water NB medium. Ten mice were tested in each dilution. The mice were housed in cages at 20–25°C, fed with the pellet feed and purified water. Mice were examined daily and any signs of disease and mortality were recorded up to 14 days. The 50% lethal dose (LD_{50}) was determined according to Mittal et al. [17].

2.9. In Vivo Protection Test. Ninety *Anguilla anguilla* (L.), weighing 90–100 g each, were allowed to acclimatize for 7 days and were randomly placed in three 200 L tanks (10 fish per tank, three tank per group) for the three treatments (the control, low cell density, and high cell density groups) described below. The tanks used recycled brackish water that was kept at 28°C throughout the experiment. The isolate's suspension was prepared as mentioned above and its cell densities were determined. Under sterile conditions, the isolate was manually incorporated into commercial dry pellets at rates of 3×10^7 and 3×10^9 cfu/g in feed for low and high cell densities of the isolate diets, respectively. Fish fed only commercial dry pellets served as a control. Fish were fed approximately 1% of body weight once a day. Two weeks after feeding, all the fish were bath-challenged with skin scarification through exposure to *A. hydrophila* strain ZN1 with a final cell density of 10^9 cfu/mL as recommended by Schadich and Cole [18]. Briefly, all the fish were skin scarified, the skin scarified fish in the low cell density and high cell density groups were exposed to the suspension of *A. hydrophila* strain ZN1 overnight, while the skin scarified fish were exposed individually to brackish water only. After the bacterial exposure, the fish were returned to their living containers. Dead fish were immediately removed for pathogen isolation as described by Bucke [19], and mortalities were recorded each day for 14 days following the immersion challenge.

2.10. Statistical Analysis. Data were presented as the mean ± standard deviation (SD) for the indicated number of independently performed experiments. $P < 0.05$ was considered statistically significant using one-way analysis of variance.

3. Results

3.1. Isolation of Marine Antagonistic Strains. A total of 45 bacteria were isolated from the brackish water sediment samples. Only one isolate, named G1, was found to exhibit strong antagonistic activity to the eel-pathogenic *A. hydrophila* strain ZN1, displaying inhibition zones of 15 mm (data not shown). According to Lategan et al. [20], zones of inhibition >12 mm against *A. hydrophila* were considered as susceptibility to the isolates. Thus, isolate G1 was chosen for further study.

3.2. Characterization and Identification. The API identification kits identified isolate G1 as *Bacillus amyloliquefaciens* (data not shown), and it showed an identity of 94% with the type strain ATCC23350 in phenotypic characterization. Isolate G1 and the type strain ATCC23350 were found both positive for glycerin, L-Arabinose, D-Ribose, D-Xylose, D-Galactose, D-Glukose, D-Fructose, D-Mannose, inositol, D-Mannitol, D-Sorbitol, Methyl-αD-Glucopyranoside,

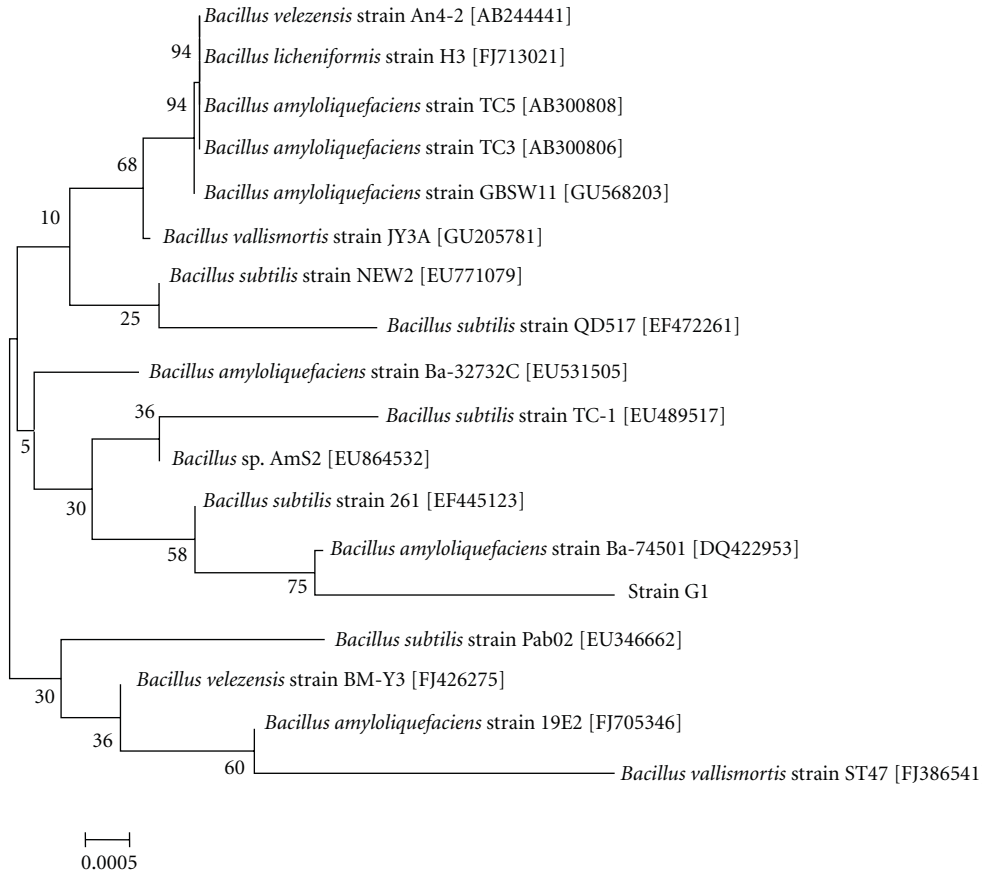

Figure 1: Phylogenetic tree constructed using neighbor-joining method.

amygdalin, arbutin, esculin, salicin, D-Cellobiose, D-Maltose, D-Lactose, D-Melibiose, D-Saccharose, D-Trehalose, D-Melezitose, D-Raffinose, amidon, glycogen, and gentiobiose. However, there were some differences between isolate G1 and the type strain ATCC23350. For example, in contrast to the type strain ATCC23350, isolate G1 was unable to ferment inulin.

The 1.5 kb 16S rRNA sequence of isolate G1 was submitted to GenBank database with the accession number HM245965. Similarities between the 16S rRNA sequence of isolate G1 and those of *B. amyloliquefaciens* strains in the GenBank database were 99.0%, which proved the initial identification. The constructed phylogenetic tree using neighbor-joining method further demonstrated that isolate G1 was closely related to the *B. amyloliquefaciens* strain (GenBank accession number DQ422953) (Figure 1). The identification result from phylogenetic analysis was consistent with that found through API identification kits.

3.3. Physicochemical Properties of the Extracellular Products. The ECPs were obtained from the supernatant (pH 8.5) of isolate G1 with ethyl acetate. The ECPs could inhibit the growth of the eel-pathogenic *A. hydrophila*, creating the clear inhibition zone on the *A. hydrophila* lawn culture plate (data not shown). The antagonistic activity of the ECPs was retained over the wide pH range of 5.0 to 9.0 against *A. hydrophila* strain ZN1, and it was also thermally stable at up to 100°C for 30 min, both showing no significant difference between the inhibition zones (data not shown). In addition, the antagonistic activity of the ECPs was still retained with proteinase K treatment, forming a clear zone on the *A. hydrophila* lawn culture plate (data not shown). The results indicated that the antagonistic substance in the ECPs was stable under wide range of pH, temperature, and proteinase K.

3.4. In Vitro Growth Inhibition Effect. The *in vitro* effect of isolate G1 on the growth inhibition of *A. hydrophila* strain ZN1 was shown in Figure 2. The cell density of *A. hydrophila* was significantly lower than that in the control when isolate G1 was inoculated at the final cell density of 10^3 to 10^5 cfu/mL, and the logarithms of the cell density of *A. hydrophila* were, respectively, reduced by 32.65%, 47.28%, and 59.49% after the incubation of 96 h, compared with the control group. The result indicated that isolate G1 could be used for exclusion of *A. hydrophila.*

3.5. Antagonistic Activity against Aeromonas hydrophila Strains. The antagonistic activity against the eight pathogenic *A. hydrophila* strains was shown in Figure 3. The result indicated that isolate G1 had highly antagonistic activity

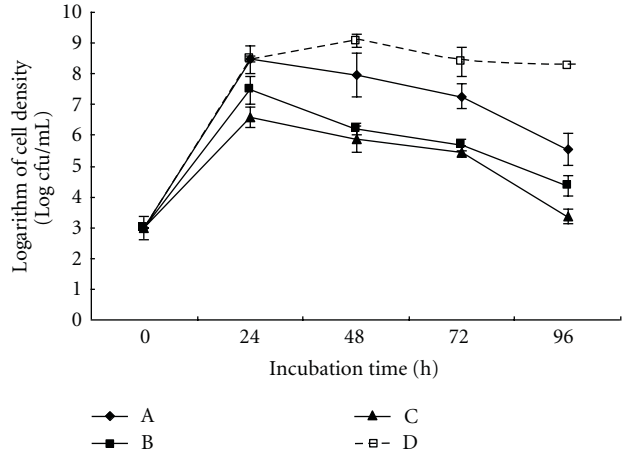

Figure 2: Inhibitory effect of srain G1 at the final cell density of 10^3 cfu/mL (A), 10^4 cfu/mL (B), 10^5 cfu/mL (C), and 0 cfu/mL (D) on the growth of the eel-pathogenic *A. hydrophila*.

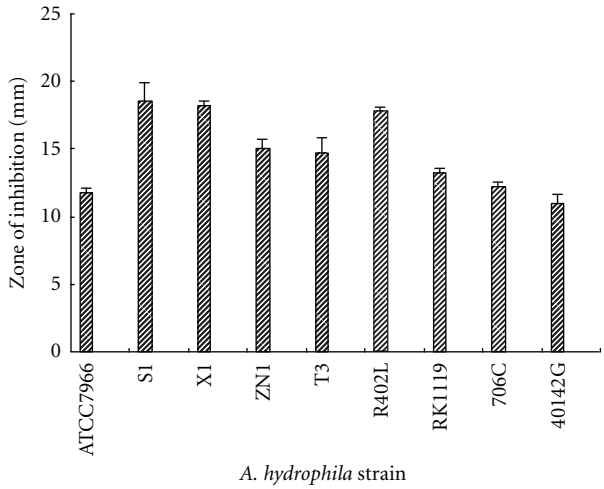

Figure 3: Antagonistic spectrum of srain G1 against pathogenic *A. hydrophila* strains.

against the other pathogenic *A. hydrophila* strains besides *A. hydrophila* strain ZN1. The maximum zone of inhibition (18.5 mm) was recorded in strain S1, and followed by strain X1 (18.25 mm), strain R402L (17.75 mm), strain ZN1 (15 mm), strain T3 (14.75 mm), strain RK1119 (13.25 mm), and strain 706C (12.25 mm). According to Lategan et al. [20], zones of inhibition >12 mm against *A. hydrophila* were considered as susceptibility to the isolate. Therefore, isolate G1 had a wide antagonistic spectrum against pathogenic *A. hydrophila* strains.

3.6. Safety. No hemolytic activity was detected with isolate G1, with no zones of hemolysis being formed on the RBA plates (data not shown). In addition, no acute mortality or any visible disease signs were observed in the test mice treated with 10^5 to 10^9 cfu/g of isolate G1's suspension (data not shown). It is concluded that the LD_{50} value of isolate G1 was estimated to exceed 10^9 cfu/g according to Mittal et al. [17].

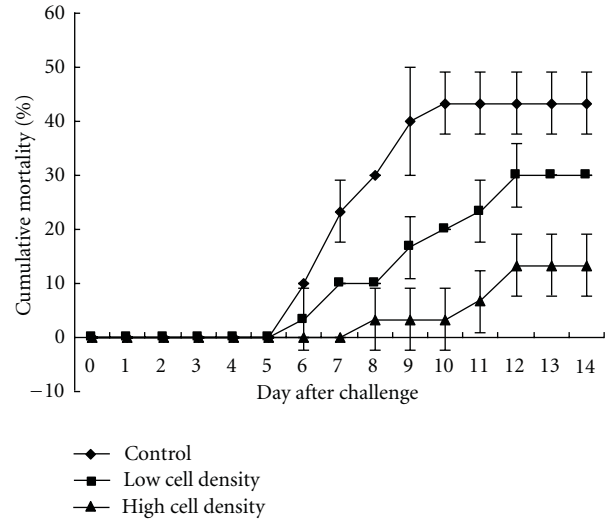

Figure 4: Protective effect of srain G1 on *Anguilla anguilla* (L.) under the eel-pathogenic *A. hydrophila* challenge trial.

3.7. In Vivo Protective Effect. The *in vivo* protective effect of isolate G1 on *Anguilla anguilla* (L.) under the eel-pathogenic *A. hydrophila* challenge trial was shown in Figure 4. After 14 days following the immersion challenge, the cumulative mortality was 69.24% lower in the high cell density group than in the control group, and the cumulative mortality was also 30.76% lower in the low cell density group than in the control group. The death of all the test fish observed in the challenge trials was caused by *A. hydrophila*, as determined by bacterial isolation and API identification kits (data not shown). The result indicated the protective effect of isolate G1 against *A. hydrophila* infection in *Anguilla anguilla* (L.).

4. Discussion

The use of antagonistic bacteria is widely expected to become an alternative method for the prevention and control of bacterial disease in fish. Numerous studies have shown that bacteria can produce inhibitory substances that had the effect of inhibiting the bacterial pathogens in aquaculture systems [13]. The use of such bacteria to inhibit pathogens by release of antimicrobial substances is now gaining importance in the eel farming as a better and more effective alternative than administering antibiotics to manage the health of eels [18]. The present study reported a promising antagonistic *B. amyloliquefaciens* isolate G1 from the brackish water sediment samples, which showed antagonistic property towards the eel-pathogenic *A. hydrophila* and other pathogenic *A. hydrophila* strains. Our data indicated that the isolate could be a suitable candidate probiotic for eel farming: (1) a significant *in vitro* inhibitory effect on the growth of eel-pathogenic *A. hydrophila*; (2) a significant *in vivo* protective effect against *A. hydrophila* infection in *Anguilla anguilla* (L.); (3) stability of the antagonistic action of its extracellular products over a wide range of pH, temperatures, and proteinase K.

In the present study, the extracellular products (ECPs) of isolate G1 showed inhibitory activity on the eel-pathogenic

A. hydrophila strain ZN1 (data not shown), and the inhibitory activity of the ECPs was not significantly affected under wide range of pH, temperature, and proteinase K. Relevant studies indicated that the antagonistic action responsible for the inhibition of bacterial pathogens such as *Erwinia amylovora*, *Ralstonia solanacearum* was due to difficidin, bacilysin, or a 29 kDa fusion protein of the *LCI* gene [21, 22]. The production of antibiotic substance by isolate G1 might be one of these important inhibiting agents. To clarify this, further characterization of the inhibitory component of isolate G1 would be necessary. In addition, the inhibitory activity of the ECPs of isolate G1 even after treatment at high temperatures (data not shown) and proteinase K (data not shown) suggested the stability of the antagonistic component. Similar observations were also recorded by Hu et al. [22], who reported that the antibacterial activity of the active fractions of *B. amyloliquefaciens* isolate Bg-C31 was not affected at 100°C and proteinase K. The property of thermal stability would be useful during industrial level production.

For application of isolate G1 as a probiotic during routine hatchery operations and natural *A. hydrophila* infections, the data on the effect of inhibiting the growth of *A. hydrophila* were essential. The present study indicated that isolate G1 could significantly reduce the cell density of *A. hydrophila* by 32.65%, 47.28%, and 59.49% after the inoculation at the final cell density of 10^3 to 10^5 cfu/mL, respectively (Figure 2), and produced a maximum inhibition zone with 18.5 mm on *A. hydrophila* lawn culture plates (Figure 3). In a related study on the antibacterial activity of *Bacillus* sp., *Bacillus subtilis* strain P73 and strain P72 only exhibited a maximum inhibition zone with 14.5 mm on *A. hydrophila* lawn culture plates [23]. Therefore, isolate G1 might be considered as a stronger antagonistic bacterium.

In order to be considered as a probiotic for application, the candidate strain had to be evaluated for its pathogenicity to a mammalian system and protective effect [24]. The present study showed that isolate G1 could not form any hemolytic rings on the RBA plates (data not shown), and the LD_{50} value to BALB/c mice exceeded 10^9 cfu/g. As described by Cutting [25], the *Bacillus* strain was regarded as no infectivity or toxicity when its oral LD_{50} value to mice is above 4.7×10^8 cfu/g. Thus, isolate G1 was evaluated as a safe strain. Supplementation of *Saccharomyces cerevisiae* has been used to control *Aeromonas hydrophila* infection in *Oreochromis niloticus* (L.) [26], but no relevant data are available about antagonistic bacteria against *A. hydrophila* infection in eels. The present study indicated that supplementation of isolate G1 could significantly reduce the cumulative mortality of *Anguilla anguilla* (L.) challenged with *A. hydrophila* (Figure 4), confirming the protective effect of isolate G1 against *A. hydrophila* infection in eels.

In conclusion, the unique characteristics of *B. amyloliquefaciens* G1, such as the antibacterial property towards a wide spectrum of pathogenic *A. hydrophila* strains, the significant growth inhibition effect on the eel-pathogenic *A. hydrophila*, the protective effect against *A. hydrophila* infection in *Anguilla anguilla* (L.), resistance of its extracellular products to a wide range of pH, temperatures, and proteinase K, and its safety to the mammalian system, supported this strain as a promising probiotic for the biocontrol of *A. hydrophila* infections in *A. anguilla* (L.).

Acknowledgments

This work has been financially supported by Key Laboratory of Aquatic Genetic Resources and Utilization of Ministry of Agriculture, China, the earmarked fund for Modern Agro-industry Technology Research System and the Program for Professor of Special Appointment (Eastern Scholar) at Shanghai Institutions of Higher Learning.

References

[1] W. C. Lee, Y. H. Chen, and I. C. Liao, "The competitiveness of the eel aquaculture in Taiwan, Japan, and China," *Aquaculture*, vol. 221, no. 1–4, pp. 115–124, 2003.

[2] B. S. Dezfuli, C. Szekely, G. Giovinazzo, K. Hills, and L. Giari, "Inflammatory response to parasitic helminths in the digestive tract of *Anguilla anguilla* (L.)," *Aquaculture*, vol. 296, no. 1-2, pp. 1–6, 2009.

[3] H. Daskalov, "The importance of *Aeromonas hydrophila* in food safety," *Food Control*, vol. 17, no. 6, pp. 474–483, 2006.

[4] H. P. Fan, "New diseases and control techniques in the eel farming," *Scientific Fish Farming*, vol. 7, pp. 49–50, 2007.

[5] R. Harikrishnan, C. Balasundaram, and M. Heo, "Effect of probiotics enriched diet on Paralichthys olivaceus infected with lymphocystis disease virus (LCDV)," *Fish & Shellfish Immunology*, vol. 29, pp. 868–874, 2010.

[6] M. A. A. Al-Fatimi, W. D. Jülich, R. Jansen, and U. Lindequist, "Bioactive components of the traditionally used mushroom *Podaxis pistillaris*," *Evidence-Based Complementary and Alternative Medicine*, vol. 3, no. 1, pp. 87–92, 2006.

[7] J. L. Balcázar, I. Blas, I. R. Ruiz-Zarzuela, D. Cunningham, D. Vendrell, and J. L. Múzquiz, "The role of probiotics in aquaculture," *Veterinary Microbiology*, vol. 114, no. 3-4, pp. 173–186, 2006.

[8] S. Das, L. R. Ward, and C. Burke, "Prospects of using marine actinobacteria as probiotics in aquaculture," *Applied Microbiology and Biotechnology*, vol. 81, no. 3, pp. 419–429, 2008.

[9] H. Sugita, Y. Hirose, N. Matsuo, and Y. Deguchi, "Production of the antibacterial substance by *Bacillus* sp. strain NM 12, an intestinal bacterium of Japanese coastal fish," *Aquaculture*, vol. 165, no. 3-4, pp. 269–280, 1998.

[10] Y. Sun, H. Yang, R. Ma, and W. Lin, "Probiotic applications of two dominant gut Bacillus strains with antagonistic activity improved the growth performance and immune responses of grouper epinephelus coioides," *Fish and Shellfish Immunology*, vol. 29, pp. 803–809, 2010.

[11] B. K. Das, S. K. Samal, B. R. Samantaray, S. Sethi, P. Pattnaik, and B. K. Mishra, "Antagonistic activity of cellular components of *Pseudomonas* species against *Aeromonas hydrophila*," *Aquaculture*, vol. 253, pp. 17–24, 2006.

[12] H. Gong, T. L. Lin, C. A. Xu, X. P. Zhang, and X. L. Yang, "Purification of aerolysin of *Aeromonas hydrophila* by affinity chromatography and analysis of its hemolytic activity," *Chinese Journal of Zoonoses* , vol. 25, no. 5, pp. 422–426, 2009.

[13] K. K. Vijayan, I. S. Bright Singh, N. S. Jayaprakash et al., "A brackishwater isolate of pseudomonas PS-102, a potential antagonistic bacterium against pathogenic vibrios in penaeid and non-penaeid rearing systems," *Aquaculture*, vol. 251, no. 2–4, pp. 192–200, 2006.

[14] G. J. Nduhiu, J. N. Ombui, and D. W. Nduati, "Genetic characterisation of food borne *Bacillus cereus* strains from milk, cheese and rice by multiplex PCR assay," *International Journal of Integrative Biology*, vol. 2, pp. 82–86, 2009.

[15] G. N. Bordoloi, B. Kumari, A. Guha et al., "Isolation and structure elucidation of a new antifungal and antibacterial antibiotics produced by *Streptomyces* sp. 201," *Bioscience, Biotechnology, and Biochemistry*, vol. 65, no. 8, pp. 1856–1858, 2001.

[16] N. K. Lee, I. C. Yeo, J. W. Park, B. S. Kang, and Y. T. Hahm, "Isolation and characterization of a novel analyte from *Bacillus subtilis* SC-8 antagonistic to *Bacillus cereus*," *Journal of Bioscience and Bioengineering*, vol. 110, no. 3, pp. 298–303, 2010.

[17] K. R. Mittal, G. Lalornde, and D. Leblarc, "*Aeromonas hydrophila* in rainbow trout: relation between virulence and surface characterisitics," *Canadian Journal of Microbiology*, vol. 26, pp. 1501–1503, 1980.

[18] E. Schadich and A. L. J. Cole, "Pathogenicity of *Aeromonas hydrophila*, *Klebsiella pneumoniae*, and *Proteus mirabilis* to brown tree frogs (*Litoria ewingii*)," *Comparative Medicine*, vol. 60, no. 2, pp. 114–117, 2010.

[19] D. Bucke, "Histology," in *Methods for the Microbiological Examination of Fish and Shellfish*, B. Austin and D. A . Austin, Eds., pp. 69–97, John Wiley & Sons, New York, NY, USA, 1989.

[20] M. J. Lategan, F. R. Torpy, and L. F. Gibson, "Control of saprolegniosis in the eel *Anguilla australis* Richardson, by *Aeromonas* media strain A199," *Aquaculture*, vol. 240, no. 1–4, pp. 19–27, 2004.

[21] X. H. Chen, R. Scholz, M. Borriss et al., "Difficidin and bacilysin produced by plant-associated *Bacillus amyloliquefaciens* are efficient in controlling fire blight disease," *Journal of Biotechnology*, vol. 140, no. 1-2, pp. 38–44, 2009.

[22] H. Q. Hu, X. S. Li, and H. He, "Characterization of an antimicrobial material from a newly isolated *Bacillus amyloliquefaciens* from mangrove for biocontrol of capsicum bacterial wilt," *Biological Control*, vol. 54, no. 3, pp. 359–365, 2010.

[23] A. Sansawat and M. Thirabunyanon, "Anti-*Aaeromonas hydrophila* activity and characterisation of novel probiotic strains of Bacillus subtilis isolated from the gastrointestinal tract of giant freshwater prawns," *Maejo International Journal of Science and Technology*, vol. 3, no. 1, pp. 77–87, 2009.

[24] L. Verschuere, G. Rombaut, P. Sorgeloos, and W. Verstraete, "Probiotic bacteria as biological control agents in aquaculture," *Microbiology and Molecular Biology Reviews*, vol. 64, no. 4, pp. 655–671, 2000.

[25] S. M. Cutting, "*Bacillus* probiotics," *Food Microbiology*, vol. 28, no. 2, pp. 214–220, 2010.

[26] M. Abdel-Tawwab, A. M. Abdel-Rahman, and N. E. M. Ismael, "Evaluation of commercial live bakers'yeast, *Saccharomyces cerevisiae* as a growth and immunity promoter for Fry Nile tilapia, *Oreochromis niloticus* (L.) challenged *in situ* with *Aeromonas hydrophila*," *Aquaculture*, vol. 280, pp. 185–189, 2008.

Hindawi Publishing Corporation
Evidence-Based Complementary and Alternative Medicine
Volume 2011, Article ID 969275, 7 pages
doi:10.1155/2011/969275

Research Article

Enhanced Antitumoral Activity of Extracts Derived from Cultured *Udotea flabellum* (Chlorophyta)

Rosa Moo-Puc,[1,2] Daniel Robledo,[1] and Yolanda Freile-Pelegrin[1]

[1] *Department of Marine Resources, Cinvestav, Km 6 Carretera Antigua a Progreso, Cordemex, A.P. 73, 97310 Mérida, YUC, Mexico*
[2] *Unidad de Investigación Médica Yucatán, Unidad Médica de Alta Especialidad, Centro Médico Ignacio García Téllez, Instituto Mexicano del Seguro Social; 41 No 439 x 32 y 34, Colonia Industrial CP, 97150 Mérida, YUC, Mexico*

Correspondence should be addressed to Daniel Robledo, robledo@mda.cinvestav.mx

Received 16 January 2011; Accepted 3 June 2011

Very few studies have been performed to evaluate the effect of culture conditions on the production or activity of active metabolites in algae. Previous studies suggest that the synthesis of bioactive compounds is strongly influenced by irradiance level. To investigate whether the antiproliferative activity of *Udotea flabellum* extracts is modified after cultivation, this green alga was cultured under four photon flux densities (PFD) for 30 days. After 10, 20, and 30 days, algae were extracted with dichloromethane: methanol and screened for antiproliferative activity against four human cancer cell lines (laryngeal—Hep-2, cervix—HeLa, cervix squamous—SiHa and nasopharynx—KB) by SRB assay. Lipid and phenol content were evaluated by standardized methods on algae organic extracts. After 10 days of cultivation, organic *U. flabellum* extracts showed a significant increase in antiproliferative activity on Hela and SiHa cells when compared to noncultured algae extracts. Extracts obtained after 10 and 20 days of culture were active on KB and Hep-2 cells. Total phenol and polyunsaturated fatty acid content in organic extracts changed with cultivation time but not by irradiance treatment. Extracts from *U. flabellum* obtained after 10 and 20 days of culture have been selected for fractionation and isolation of active compounds.

1. Introduction

Natural products and related drugs are used to treat 87% of all categorized human diseases including bacterial infection, cancer, and immunological disorders [1]. Approximately 25% of prescribed drugs in the world originate from plants [2] and over 3000 species of plants have been reported to have anticancer properties [3]. Recent trends in drug research on natural sources suggest that algae are a promising source of novel biochemical active substances [4]. To survive in a competitive environment, marine algae have developed defense strategies that result in a significant level of structural chemical diversity that is derived from different metabolic pathways [5]. The effect of culture conditions on the production or activity of active metabolites in algae has scarcely been studied and consequently remains poorly understood. In other alga models, such as the cyanophyte *Scytonema*, increasing irradiance gradually increased antibiotic production [6]. Similarly, *Spyridia filamentosa*, a red alga cultured at different light irradiances, had contrasting antibiotic activities that were strongly influenced by irradiance level [7]. Most recently, extracts obtained from *Penicillus dumetosus* cultured at different light irradiances displayed varying antiproliferative activity against diverse cancer cell lines [8]. The feasibility of algal cultivation can help to induce adaptations that can be measured through metabolite synthesis or biological activity. Fully controlled greenhouse-based cultivation systems have been developed for high-quality year-round vegetable production for the botanical drug market [9]. Therefore, a better understanding of the potential manipulation of algal culture conditions to modify metabolite synthesis and activity is required.

Tropical green algae in the order Bryopsidales, including those of the genera *Avranvillaea*, *Caulerpa*, *Halimeda*, *Penicillus*, and *Udotea*, are noted for the production of sesqui and diterpenoids, compounds that have also shown antifungal and antiproliferative activity [5, 10]. Recent studies have shown that both aqueous and organic extracts of *Udotea flabellum* exhibit in vitro antiprotozoal [11, 12] as well as cytotoxic and antiproliferative activities on cancer cell lines [13]. In some cases, the antiproliferative activity of marine algae extracts has been positively correlated with

total polyphenol content, suggesting a causal link between the extract content of polyphenols and phenolic acids [14], while other authors have reported a variety of fatty acids and derivatives with antiproliferative effects in different cancer cell models [15]. Despite the observations of antiproliferative activity in marine algae, there is limited information on how this activity may change under contrasting environmental conditions. Therefore, the objective of this study was to investigate the antiproliferative activity of crude organic extracts of cultured *Udotea flabellum* on four human malignant cell lines (HeLa, Hep-2, SiHa, and KB) and their change over time under four light treatments. Furthermore, the study evaluated whether phenol content and lipid composition were related to its antiproliferative activity.

2. Materials and Methods

2.1. Alga Collection and Culture Conditions. *Udotea flabellum* (J. Ellis and Solander) M. A. Howe were collected along the YUC Peninsula coast, Mexico, stored in plastic bags and chilled in ice during transport to the Cinvestav Marine Station at Telchac, Yucatan, Mexico. Algae were cultivated under four light treatments: full (100%) sunlight, 75% sunlight, 50% sunlight, and 0% sunlight, designated treatment A, B, C, and D, respectively. Agricultural greenhouse shade net was used in order to obtain variable light intensities in the culture system. Light intensity varied over cultivation time: during the first 10 days, the photon flux density (PFD) in full sunlight and 75% sunlight treatments were not significantly different (one-way ANOVA, $F[3, 36] = 68.21$, $P < 0.0001$; post hoc Tukey's test $P < 0.0001$) at 55 ± 12.9 and $65 \pm 12.5\,\mu$mol photon $m^{-2}s^{-1}$, respectively, while 50, and 0% treatments received 60, and 3% of incident PFD, respectively (42 ± 12.0 and $2 \pm 0.7\,\mu$mol photon $m^{-2}s^{-1}$). After 20 and 30 days of cultivation, a similar trend was registered, with the 75% treatment receiving 75–100% of incident PFD and the 50% treatment receiving 42–52%; the 0% treatment only received 2% of incident PFD (Figure 1).

2.2. Preparation of Extracts. Freshly collected samples of the wild material were lyophilized and ground into powder to perform plant extraction protocols and analytical methods; this material was considered as a control before cultivation (time 0). Entire plants ($n = 15$) were taken from each culture treatment—A, B, C, and D—at 10, 20, and 30 days into the experimental period to perform organic extraction and analysis. Lyophilized samples (20 g) were exhaustively extracted with 200 mL of dichloromethane: methanol (7 : 3) by maceration for 24 h at room temperature. These extracts were filtered and concentrated to dryness in vacuum at 40°C and stored at −20°C until required. Every extract was labeled according to culture conditions: light intensity (A, B, C, or D) and time (10, 20, and 30 days).

2.3. Chemicals. Dulbecco's Modified Eagle's Medium (DMEM), heat-inactivated fetal bovine serum (FBS) and penicillin and streptomycin (PS) were purchased from Gibco, USA. 3-(4,5-dimethylthiazol-2-yl)-2,5-diphenyl tetrazolium bromide (MTT), Dimethyl sulfoxide (DMSO), sulforhodamine B (SRB) and trichloroacetic acid (TCA) were obtained from Sigma.

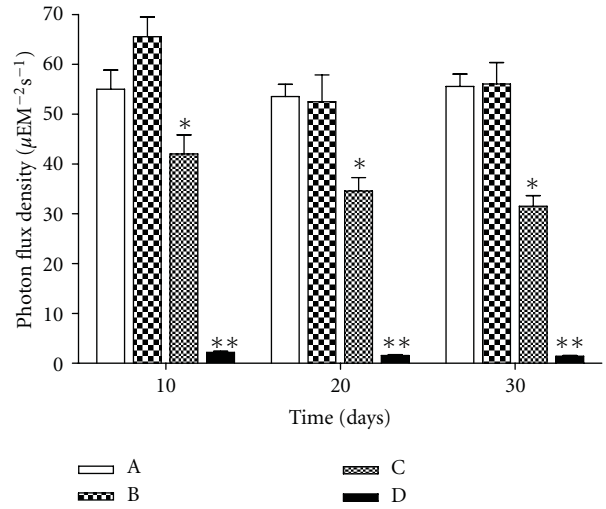

Figure 1: Photon flux density during cultivation of *U. flabellum*. (A) full sunlight (100 %), (B) 75 % sunlight, (C) 50 % sunlight, and (D) 0 % sunlight. Asterisk indicates significant differences.

2.4. Cell Culture. The following cell lines were used for the antiproliferative assays: normal Mardin-Darbin cell kidney (MDCK), and four human carcinoma cells, namely, laryngeal (Hep-2), cervix (HeLa), cervix squamous (SiHa) and nasopharynx (KB). The cells were grown in DMEM media supplemented with 10% v/v fetal bovine serum (FBS) with 100 U mg mL^{-1} of PS. Cell lines were maintained at 37°C in a 5% CO_2 atmosphere with 95% humidity, and the culture medium was changed once every 5 days.

2.5. Cytotoxicity Assay. The cytotoxicity assay was performed according to Rahman et al. [16], where 1.5×10^4 viable cells from each cell line were seeded in a 96-well plate and incubated for 24 to 48 h. When cells reached >80 % confluence, the medium was replaced and the cells were treated with the organic extracts dissolved in dimethyl sulfoxide (DMSO at a maximum concentration of 0.05%) at 6.25, 12.5, 25, and 50 μg mL^{-1}. After 72 h of incubation, 10 μL of MTT solution (5 mg mL^{-1}) was added to each well and incubated at 37°C for 4 h. The medium was removed and formazan, generated by the activity of dehydrogenases, was dissolved in acidified isopropanol (0.4 N HCl). The amount of MTT-formazan generated is directly proportional to the number of living cells and was determined by measuring the optical density (OD) at 540 nm using a Bio-assay reader (BioRad, USA). Untreated cells were used as a negative control. The concentration of the organic extract that killed 50% of the cells (CC_{50}) was calculated with GraphPad-PRISM 4.00 software. All determinations were performed in triplicate.

2.6. Antiproliferative Assay. For the antiproliferative assay, we used sulforhodamine B (SRB), a colorimetric assay which estimates cell number by staining total cellular protein with

the SRB dye, in order to assess cell growth inhibition [16]. This method used the same conditions as the cytotoxic assay except that the medium was replaced with DMEM 10% FBS to induce cellular proliferation during extract treatments. After 48 h incubation, the medium was discarded and cells were fixed with 100 μL of ice-cold 40% TCA. Thereafter, the cells were incubated at 4°C for 1 h and the plates were washed five times with cold water. The excess water was drained off and the plates were left to dry; 50 μL of SRB stain (10 mg w/v in 1% acetic acid) was added to each well for 30 min. Finally, the plates were washed with 50 mL of 1% acetic acid and rinsed four times until dye adhering to the cells was observed. The OD was measured at 540 nm using a microplate reader (model 450, Bio-Rad, USA). Untreated cells were used as a negative control. Docetaxel, a clinically well-established antimitotic chemotherapy medication was used as a positive control of antiproliferative activity. The IC_{50} value, that is, the concentration of organic extract that produced a 50% reduction in the surviving fraction, was calculated using GraphPad-PRISM 4.00 software. MDCK cell line was used to evaluate the selective index (SI) of *U. flabellum* extracts. SI is defined as the ratio of cytotoxic to antiproliferative activity. All determinations were performed in triplicate.

2.7. Phenolic Content. Total phenolic content of the algal extracts was determined spectrophotometrically using Folin-Ciocalteu reagent [17]. First, 20 mg of the dry extract was diluted with methanol (3 mL). Aliquots of the diluted extracts (0.1 mL) were transferred into the test tubes; 2.9 mL of distilled water and 0.5 mL of Folin-Ciocalteu reagent were added. After 10 min, 1.5 mL of 20% sodium carbonate solution was added, mixed thoroughly and allowed to stand at room temperature in the dark for 1 h. Absorbance was measured at 725 nm and total phenolic content (expressed as % of dry weight) was calculated based on a standard curve of phloroglucinol.

2.8. Lipid Content. Total lipids were determined according to a previously reported method [18]. The algae extract (20 mg) was homogenized with a mixture of H_2O, methanol and chloroform (1 : 1 : 9 v/v). The chloroform layer containing dissolved lipids was collected, dried with nitrogen, and saponified with 1.2 M NaOH. Fatty acids were converted to methyl esters with 0.6 mL of 10 M HCl and 1 mL of 12% boron trichloride in methanol at 80°C for 60 min. After methylation, 1 mL of hexane: diethylether (1 : 1) and 3 mL of 0.3 M NaOH were added, and the resultant mixture was dried with nitrogen and recovered with hexane. The total content of fatty acid methyl esters was analyzed by gas chromatography (Hewlett Packard 6890 Plus with Supelco SP2560 bis-cyanopropyl polysiloxane capillary column 100 m $\times$ 0.25 mm $\times$ 0.25 μm internal diameter). The column temperature programming was set from 140 (5 min) to 240°C (20 min) at a rate of 4°C min^{-1}. Injector and detector temperature was 260°C. Helium was used as the carrier gas at a flow rate of 1.1 mL min^{-1}. Fatty acid methyl esters were identified by comparing their retention times with those of standard samples. The lipid analyses were carried out in duplicate, and the results expressed as percentages of algae extract dry weight (% dry wt).

2.9. Statistical Analysis. Data were analyzed with GraphPad 4.0 Software Inc. (San Diego, Calif, USA). The dose-response curves (variable slope) were fitted with the algorithm: $Y = E_{min} + [(E_{max} - E_{min})/(1 + 10(\text{Log ED50} - \text{Log D})\ \text{Hill slope})]$. Statistical analysis was performed with parametric tests because variances were homogeneous between groups. An unpaired Student's *t*-test (two-tailed) was applied when only two groups were compared. A one-way ANOVA followed by post hoc Dunnett's test was used to assess the differences when three or more groups were simultaneously compared. Values in text and figures are expressed as means ± SD.

3. Results

3.1. Antiproliferative Activity. The antiproliferative activity of *U. flabellum* extracts on the growth of four cancer cells *in vitro* are summarized in Table 1. The organic extract of wild *U. flabellum* collected (time 0) showed antiproliferative activity (IC_{50}) on SiHa (276.2 ± 1.9 μg mL^{-1}), HeLa (296.6 ± 0.9 μg mL^{-1}), Hep-2 (52.9 ± 1.0 μg mL^{-1}), and KB (47.8 ± 1.2 μg mL^{-1}). After10 and 20 days of cultivation, the antiproliferative activity of the *U. flabellum* extracts on the SiHa cell line significantly improved when compared with non cultured *U. flabellum* extracts (IC_{50} 276.2 μg mL^{-1}), with a reduction of 85–95% after 10 days and 63–77% after 20 days of cultivation. The antiproliferative activity of extracts on the HeLa cell line had the same tendency, with a 70–90% reduction of the non cultured *U. flabellum* extracts IC_{50}; whereas extracts obtained after 30 days of culture increased IC_{50} by approximately 78–185% and 40–95% on the SiHa and HeLa cell lines, respectively. For the Hep-2 and KB cell lines *U. flabellum* extracts only showed a 36–69% and 40–51% reduction of IC_{50} after 10 days of cultivation.

In general, *U. flabellum* extracts obtained after cultivation showed improved SI on cancer cells, particularly the extracts from culture treatment A (10 days), which showed the highest selectivity index ranging from 6–28 and 8–20 on the SiHa and Hep-2 cell lines, respectively (Table 2).

3.2. Phenol and Lipid Content. *U. flabellum* extracts before cultivation (time 0) showed a total phenol content of 1.7 ± 0.2% dry wt. *U. flabellum* extracts increased phenolic content by 100% for all treatments after 10 and 20 days of cultivation (Figure 2(a)). Lipid and fatty acid content in *U. flabellum* extracts varied in relation to time and light availability (Figure 2(b)). *U. flabellum* extracts before cultivation (time 0) showed a total lipid content of 46.4 ± 1.5%, increasing by 60 and 70% after 20 and 30 days of cultivation without light. GC analysis revealed that saturated fatty acids (SAFA) were dominant (58.6%) while monounsaturated fatty acid (MUFA) and polyunsaturated fatty acid (PUFA) were present at 14.2% and 27.1%, respectively (Figure 2(c)). In general, after cultivation SAFA content decreased by 6–19% in relation to the control while MUFA content remained similar throughout time and cultivation treatment.

Table 1: Growth inhibition (IC_{50}) of *U. flabellum* extracts on cancer cell lines ($P \leq 0.001$).

Cancer cells	$IC_{50\pm}$SD ($\mu g\,mL^{-1}$)			
	Time = 0	Day = 10	Day = 20	Day = 30
SiHa	276.2 ± 1.91			
A		30.4 ± 3.9	100.6 ± 2.65	493.1 ± 2.1
B		42.7 ± 0.9	75.8 ± 1.1	623.3 ± 2.7
C		10.2 ± 1.2	64.5 ± 1.5	788.9 ± 1.2
D		13.1 ± 2.7	62.4 ± 1.2	547.8 ± 2.1
		$F(4, 10) = 6814$	$F(4, 10) = 8113$	$F(4, 10) = 24910$
Docetaxel	0.32 ± 0.01			
HeLa	296.6 ± 0.9			
A		49.7 ± 2.1	45.3 ± 1.3	413.6 ± 0.9
B		39.2 ± 3.1	34.8 ± 1.9	580.4 ± 1.9
C		53.8 ± 2.7	67.4 ± 2.8	568.2 ± 1.2
D		63.8 ± 1.8	76.6 ± 1.8	482.6 ± 0.9
		$F(4, 10) = 7143$	$F(4, 10) = 10350$	$F(4, 10) = 27690$
Docetaxel	0.20 ± 0.04			
Hep-2	52.9 ± 1			
A		16.6 ± 1.3	71.7 ± 2.1	98.4 ± 1.2
B		19.1 ± 1.8	60.3 ± 1.8	100.7 ± 1.8
C		16.7 ± 0.9	75.2 ± 1.9	91.5 ± 2.3
D		33.5 ± 1.4	91.1 ± 1.9	106.1 ± 1.6
		$F(4, 10) = 424.1$	$F(4, 10) = 203.4$	$F(4, 10) = 521.7$
Docetaxel	0.08 ± 0.03			
KB	47.8 ± 1.2			
A		23.4 ± 1.9	134.6 ± 1.9	106.4 ± 1.5
B		29.8 ± 2.1	138.1 ± 1.5	109.7 ± 1.5
C		32.4 ± 1.7	117.3 ± 1.2	123.4 ± 0 .9
D		28.9 ± 1.2	112.7 ± 1.4	126.7 ± 2.3
		$F(4, 10) = 113.9$	$F(4, 10) = 1854$	$F(4, 10) = 1269$
Docetaxel	0.23 ± 0.07			

IC_{50}: half maximal (50%) inhibitory concentration (IC) of organic extracts.

Table 2: Cytotoxicity (CC_{50}) of *U. flabellum* extracts on normal cell line and selective index (SI) for each cancer cell line.

Time (Irradiance treatment)	CC_{50} MDCK Cells	SI			
		SiHa	HeLa	Hep-2	KB
Time = 0	297.9±11.2				
Day = 10					
A	322.3 ± 8.9	10	6.5	19.4	13.7
B	272.6 ± 4.1	6.4	7.0	14.5	9.3
C	286.6 ± 5.1	28	5.3	17.1	8.8
D	276.9 ± 5.8	21	4.3	8.2	9.6
Day = 20					
A	358.2 ± 2.9	3.6	7.9	5.0	2.6
B	323.3 ± 4.6	4.3	9.2	5.4	2.3
C	375.9 ± 6.7	5.8	5.5	5.0	3.2
D	386.1 ± 7.1	6.0	5.0	4.2	3.4
Day = 30					
A	528.4 ± 10.2	1.0	1.0	5.4	5.0
B	436.3 ± 9.6	0.5	6.7	4.3	4.0
C	524.8 ± 8.6	0.6	0.9	5.7	4.2
D	424.4 ± 7.8	0.7	0.8	4.0	3.3

CC_{50}: mean concentration that killed 50% of cells; SI = ratio of cytotoxic to antiproliferative activity.

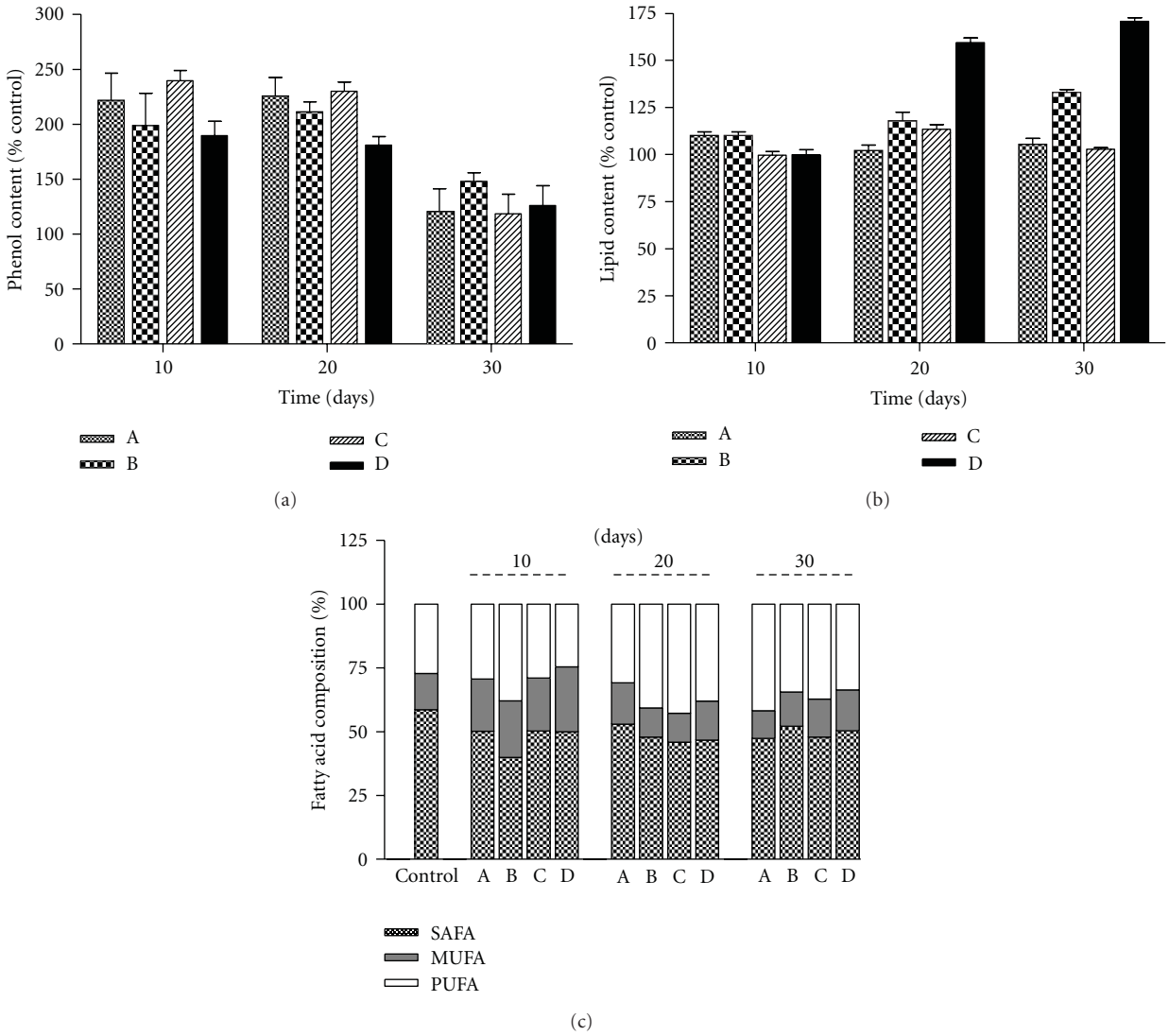

Figure 2: Phenol and lipid content of *Udotea flabellum* extracts. (a) Total phenol content expressed as a percentage of the control (%), (b) lipid content in organic extracts expressed as a percentage of the control (%), (c) fatty acid composition in organic extracts expressed in % dry weight (d wt) over the culture period. Each symbol is the mean±SD of three assays, normalized with the control extract collected at the same time and place without culture treatment. Time when the samples were collected from the culture tank: 10, 20, and 30 days.

On the other hand, PUFA content increased 3–15% in plants subjected to culture treatments when compared to the control. The predominant SAFA was palmitic acid (16 : 0), while in the MUFA fraction palmitoleic acid (C16 : 1) and oleic acid (C18 : 1) predominated.

4. Discussion

Under experimental culture conditions the biological activity of the *U. flabellum* organic extracts improved, showing an increased inhibitory effect with a reduction in the initial IC_{50}, thus improving the effect of culture conditions on biological activity (Figure 3). *U. flabellum* extracts obtained after cultivation also improved SI on cancer cells, particularly on the SiHa and Hep-2 cell lines. According to the American National Cancer Institute, the IC_{50} limit in order to consider a crude extract promising for further purification is $<30\,\mu g\,mL^{-1}$ [19]. Considering the above-mentioned criterion, after 10 days of cultivation all *U. flabellum* extracts increased their activity against SiHa, Hep-2 and KB cells.

U. flabellum extracts increased phenolic content by 100% for all treatments after 10 and 20 days of cultivation. In this study, the inhibition of cancer cell proliferation by *U. flabellum* extracts could not be explained solely by the concentration of polyphenolic compounds. This suggests that other phytochemicals may play a major role in the antiproliferative activity of *U. flabellum* extracts. Previous studies on tropical green algae of the family Udoteaceae have isolated sesquiterpenoids and diterpenoids with biological activity [20] and udoteatrial hydrate with moderate antimicrobial activity against *Staphylococcus aureus* [21].

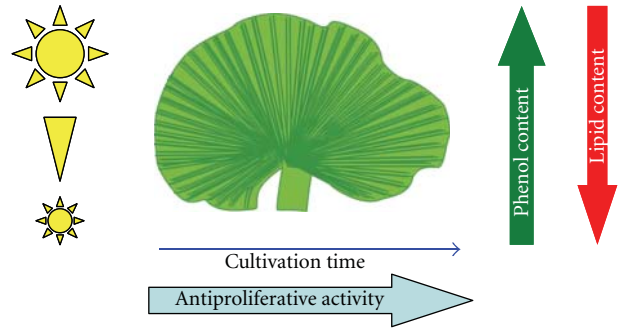

Figure 3: Effects of culture conditions and light on *Udotea flabellum* chemical composition and their role in the antiproliferative activity in cancerous cell lines *in vitro*. Increasing light promotes an increase in phenolic compounds, whereas, lipid content decreases. Therefore, algae extracts increases antiproliferative activity for SiHa, HeLa, Hep-2 and KB cells with time under controlled culture conditions.

Phenolic compounds have been under study as potential therapeutic agents against a wide range of diseases including neurodegenerative diseases, cancer, diabetes, cardiovascular dysfunction, inflammatory diseases, and aging [22]. In some cases the antiproliferative activity of alga extracts has been positively correlated with total polyphenol content, suggesting a causal link between extract content of polyphenols and phenolic acids [14]. This causal link has also been found with the cytotoxicity *in vitro* of some red and brown algae extracts [23, 24]. Moreover, phenolic compounds including phlorotannins can induce oxidative stress in cancer cells [25]. The above could explain the ability of some algae extracts, such as those from *Lithothamnion calcareum*, to suppress colon polyp formation in mice [26].

In general, *U. flabellum* extracts had high levels of PUFA (linoleic acid and alpha linoleic acid). A variety of fatty acids and derivatives have antiproliferative effects in different cancer cell models [15]. Despite the amount of useful information derived from lipid class analyses in algal physiology, most of the studies available are restricted to microalgae, and little is known about lipid class changes in macroalgae during cultivation.

5. Conclusions

The results of this study indicate that the metabolism of a number of active compounds of *U. flabellum* are substantially influenced by culture time but not light treatments, and hence have an influence on the production of metabolites that render them biologically active. Extracts obtained from *U. flabellum* after 10 and 20 days of culture under conditions described in this study showed increased antiproliferative activity on SiHa, HeLa, Hep-2 and KB cells. Although we observed that culture time influenced phenol and lipid content, the compound responsible for the antiproliferative activity of *U. flabellum* extracts remains to be identified.

Acknowledgments

This work was supported by SEP-CONACYT 53687. Cinvestav financed a postdoctoral fellowship for R. Moo-Puc. The authors thank C. Chávez Quintal and M. L. Zaldivar Romero for technical assistance during analysis.

References

[1] D. J. Newman and G. M. Cragg, "Natural products as sources of new drugs over the last 25 years," *Journal of Natural Products*, vol. 70, no. 3, pp. 461–477, 2007.

[2] S. M. K. Rates, "Plants as source of drugs," *Toxicon*, vol. 39, no. 5, pp. 603–613, 2001.

[3] J. G. Graham, M. L. Quinn, D. S. Fabricant, and N. R. Farnsworth, "Plants used against cancer—an extension of the work of Jonathan Hartwell," *Journal of Ethnopharmacology*, vol. 73, no. 3, pp. 347–377, 2000.

[4] J. W. Blunt, B. R. Copp, W. P. Hu, M. H. G. Munro, P. T. Northcote, and M. R. Prinsep, "Marine natural products," *Natural Product Reports*, vol. 24, no. 1, pp. 31–86, 2007.

[5] M. P. Puglisi, L. T. Tan, P. R. Jensen, and W. Fenical, "Capisterones A and B from the tropical green alga *Penicillus capitatus*: unexpected anti-fungal defenses targeting the marine pathogen *Lindra thallasiae*," *Tetrahedron*, vol. 60, no. 33, pp. 7035–7039, 2004.

[6] A. Chetsumon, F. Umeda, I. Maeda, K. Yagi, T. Mizoguchi, and Y. Miura, "Broad spectrum and mode of action of an antibiotic produced by *Scytonema* sp. TISTR 8208 in a seaweed-type bioreactor," *Applied Biochemistry and Biotechnology*, vol. 70–72, pp. 249–256, 1998.

[7] P. O. Robles Centeno and D. L. Ballantine, "Effects of culture conditions on production of antibiotically active metabolites by the marine alga *Spyridia filamentosa* (Ceramiaceae, Rhodophyta). I. Light," *Journal of Applied Phycology*, vol. 11, no. 2, pp. 217–224, 1999.

[8] R. Moo-Puc, D. Robledo, and Y. Freile-Pelegrin, "Improved antitumoral activity of extracts derived from cultured *Penicillus dumetosus*," *Tropical Journal of Pharmaceutical Research*, vol. 10, no. 2, pp. 177–185, 2011.

[9] K. H. Lee, "Research and discovery trends of Chinese medicine in the new century," *Journal of Chinese Medicine*, vol. 15, no. 3, pp. 151–160, 2004.

[10] X. C. Li, M. R. Jacob, Y. Ding et al., "Capisterones A and B, which enhance fluconazole activity in *Saccharomyces cerevisiae*, from the marine green alga *Penicillus capitatus*," *Journal of Natural Products*, vol. 69, no. 4, pp. 542–546, 2006.

[11] R. Moo-Puc, D. Robledo, and Y. Freile-Pelegrin, "Evaluation of selected tropical seaweeds for in vitro anti-trichomonal activity," *Journal of Ethnopharmacology*, vol. 120, no. 1, pp. 92–97, 2008.

[12] Y. Freile-Pelegrin, D. Robledo, M. J. Chan-Bacab, and B. O. Ortega-Morales, "Antileishmanial properties of tropical marine algae extracts," *Fitoterapia*, vol. 79, no. 5, pp. 374–377, 2008.

[13] R. Moo-Puc, D. Robledo, and Y. Freile-Pelegrín, "In vitro cytotoxic and antiproliferative activities of marine macroalgae from Yucatán, Mexico," *Ciencias Marinas*, vol. 35, no. 4, pp. 345–358, 2009.

[14] Y. V. Yuan and N. Walsh, "Antioxidant and antiproliferative activities of extracts from a variety of edible seaweeds," *Food and Chemical Toxicology*, vol. 44, no. 7, pp. 1144–1150, 2006.

[15] K. J. Tronstad, O. Bruserud, K. Berge, and R. K. Berge, "Antiproliferative effects of a non-β-oxidizable fatty acid, tetradecylthioacetic acid, in native human acute myelogenous leukemia blast cultures," *Leukemia*, vol. 16, no. 11, pp. 2292–2301, 2002.

[16] A. Rahman, M. Iqbal Choudhary, and W. J. Thomsen, "Bioassay techniques for drug development," in *Manual of Bioassay Techniques for Natural Products Research*, W. J. Thomsen, Ed., pp. 34–35, Harwood Academic Publishers, The Netherlands, 1st edition, 2001.

[17] S. N. Lim, P. C. K. Cheung, V. E. C. Ooi, and P. O. Ang, "Evaluation of antioxidative activity of extracts from a brown seaweed, *Sargassum siliquastrum*," *Journal of Agricultural and Food Chemistry*, vol. 50, no. 13, pp. 3862–3866, 2002.

[18] E. G. Bligh and W. J. Dyer, "A rapid method of total lipid extraction and purification," *Canadian Journal of Biochemistry and Physiology*, vol. 37, no. 8, pp. 911–917, 1959.

[19] M. Suffness and J. M. Pezzuto, "Assays related to cancer drug discovery," in *Methods in Plant Biochemistry: Assays for Bioactivity*, K. Hostettmann, Ed., vol. 6, pp. 71–133, Academic Press, London, UK, 1990.

[20] W. Fenical and V. J. Paul, "Antimicrobial and cytotoxic terpenoids from tropical green algae of the family Udoteaceae," *Hydrobiologia*, vol. 116-117, no. 1, pp. 135–140, 1984.

[21] T. Nakatsu, B. N. Ravi, and D. J. Faulkner, "Antimicrobial constituents of *udotea Flabellum*," *Journal of Organic Chemistry*, vol. 46, no. 12, pp. 2435–2438, 1981.

[22] M. A. Soobrattee, V. S. Neergheen, A. Luximon-Ramma, O. I. Aruoma, and T. Bahorun, "Phenolics as potential antioxidant therapeutic agents: mechanism and actions," *Mutation Research*, vol. 579, no. 1-2, pp. 200–213, 2005.

[23] R. C. Vinayak, A. S. Sabu, and A. Chatterji, "Bio-evaluation of two red seaweeds for their cytotoxic and antioxidant activities in vitro," *Journal of Complementary and Integrative Medicine*, vol. 7, no. 1, article number 42, 2010.

[24] V. Rashmi, A. S. Sabu, and A. Chatterji, "Bio-prospecting of a few brown seaweeds for their cytotoxic and antioxidant activities," *Evidence-Based Complementary and Alternative Medicine*, vol. 2011, Article ID 673083, 9 pages, 2011.

[25] L. Reddy, B. Odhav, and K. D. Bhoola, "Natural products for cancer prevention: a global perspective," *Pharmacology and Therapeutics*, vol. 99, no. 1, pp. 1–13, 2003.

[26] M. N. Aslam, T. Paruchuri, N. Bhagavathula, and J. Varani, "A mineral-rich red algae extract inhibits polyp formation and inflammation in the gastrointestinal tract of mice on a high-fat diet," *Integrative Cancer Therapies*, vol. 9, no. 1, pp. 93–99, 2010.

Hindawi Publishing Corporation
Evidence-Based Complementary and Alternative Medicine
Volume 2011, Article ID 751452, 6 pages
doi:10.1155/2011/751452

Research Article

Biosynthesis and Immobilization of Biofunctional Allophycocyanin

Yingjie Chen,[1,2] Shaofang Liu,[1,2] Yulin Cui,[1,2] Peng Jiang,[1] Huaxin Chen,[1] Fuchao Li,[1] and Song Qin[1]

[1] *Key Laboratory of Experimental Marine Biology, Institute of Oceanology, Chinese Academy of Sciences, Qingdao 266071, China*
[2] *Graduate University of Chinese Academy of Sciences, Beijing 100049, China*

Correspondence should be addressed to Peng Jiang, jiangpeng@ms.qdio.ac.cn and Song Qin, sqin@yic.ac.cn

Received 14 January 2011; Revised 27 April 2011; Accepted 20 June 2011

The holo-allophycocyanin-α subunit, which has various reported pharmacological uses, was biosynthesized with both Strep-II-tag and His-tag at the N-terminal in *Escherichia coli*. The streptavidin-binding ability resulting from the Strep II-tag was confirmed by Western blot. Additionally, the metal-chelating ability deriving from the His-tag not only facilitated its purification by immobilized metal-ion affinity chromatography but also promoted its immobilization on Zn (II)-decorated silica-coated magnetic nanoparticles. The holo-allophycocyanin-α subunit with streptavidin-binding ability was thereby immobilized on magnetic nanoparticles. Magnetic nanoparticles are promising as drug delivery vehicles for targeting and locating at tumors. Thus, based on genetic engineering and nanotechnology, we provide a potential strategy to facilitate the biomodification and targeted delivery of pharmacological proteins.

1. Introduction

Allophycocyanin (APC) is a biliprotein located in the core of the phycobilisome found in blue-green and red algae [1–4]. This biliprotein is composed of two different subunits, α and β, each subunit having one phycobilin (PCB; [5, 6]). As a bioactive protein, the pharmaceutical properties of APC have been demonstrated [7]. Primarily, the chromophore, a potent peroxyl radical scavenger, was thought to be mainly responsible for its antitumor activity [8, 9]. However, recent studies on the precise activity of apoprotein confirmed its important role in the bioactivities of APC [10, 11]. Through the development of recombinant DNA technology, holo-allophycocyanin subunits have been engineered and produced in large quantities [12, 13]. These subunits have shown even stronger radical scavenging abilities than apoprotein and native APC [13], suggesting the feasibility of biosynthesis for producing medical proteins.

During the genetic engineering process, a number of antibody epitope tags have been exploited to confer target identification capability to recombinant proteins. Recently, Strep-II-tag, a short peptide sequence that provides proteins with streptavidin-binding ability, has received increasing attention with respect to the possibility that it might avoid chemical manipulation for the conjugation of antibodies to bioactive proteins [14–16]. In addition, a short His-tag, which is the most commonly used tag, can be easily fused to proteins without impairing their function and confer metal chelating ability [17]. His-tagged proteins can thus be readily purified in a single step by immobilized metal-ion affinity chromatography (IMAC; [18–20]). In addition, there is potential to specifically immobilize His-tagged proteins on a solid surface modified with metal cations [21–23]. Therefore, recombinant DNA technology has made it feasible to engineer and produce pharmaceutical proteins with bioaffinity and target identification capabilities.

Meanwhile, modern development of nanotechnology has produced novel carriers for the targeted delivery of drugs [24, 25], especially magnetic nanoparticles, which can be manipulated simply with an external magnetic field [25]. In these magnetic drug-delivery platforms, a silica coating is always used to reduce random fluctuations and biodegradations of the magnetic core, partly because of its heat resistance and biomolecule-binding abilities. Furthermore, exploitation of new materials has led to the creation of silica-coated magnetic nanoparticles modified with metal cations

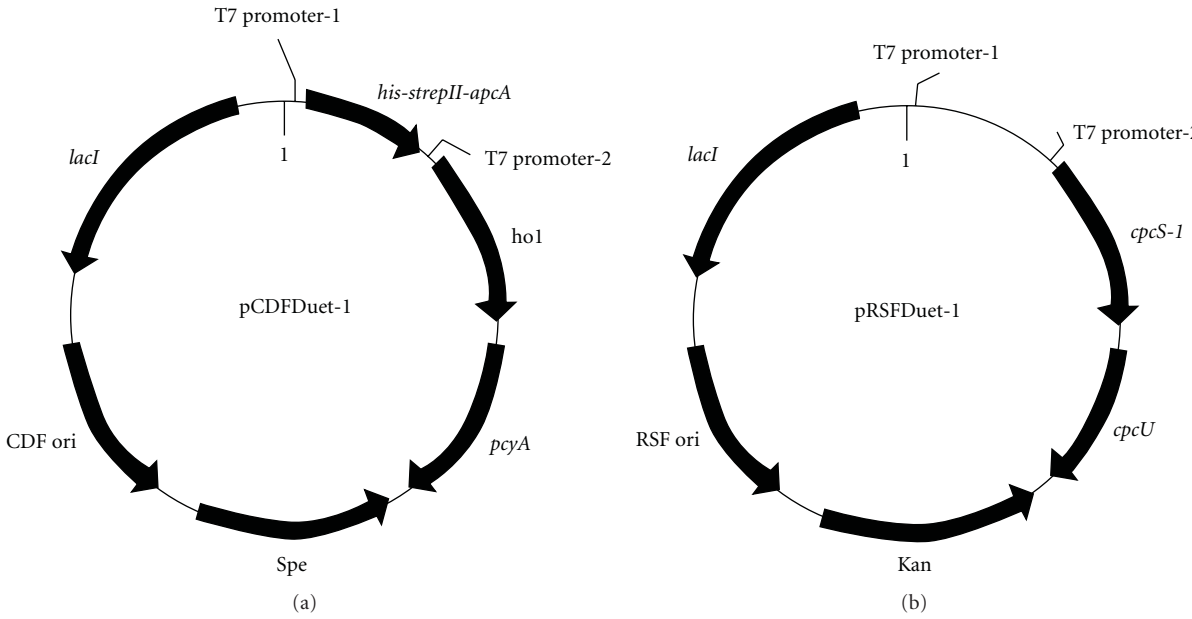

Figure 1: The pCDFDuet-*his-strepII-apcA-ho1-pcyA* and pRSFDuet-*cpcS-cpcU* expression vectors.

[26–29]. Thus, it is possible for magnetic nanoparticles to be utilized in the immobilization and delivery of His-tagged proteins.

In this work, based on both genetic engineering and nanotechnology, we developed a potential strategy to facilitate the biomodification and targeted delivery of pharmacological proteins. Zn (II)-decorated silica-coated magnetic nanoparticles (ZnSiMNPs) were prepared and characterized as protein carriers, while cyanobacterial allophycocyanin (APC), a unique and inexpensive pigment protein with various pharmacological uses, was chosen as a model protein. This biliprotein was biosynthesized with both His-tag and Strep-II-tag at the N-terminal in *Escherichia coli*. Finally, the protein was immobilized via the His-tag on ZnSiMNPs and its streptavidin-binding ability was confirmed.

2. Materials and Methods

2.1. Construction of Expression Vectors. In general, standard procedures were used for DNA manipulation. All genes for biosynthesis of holo-APC-α subunit were PCR-amplified from *Synechocystis* sp. PCC6803 with specific primers. The primers used to amplify the *strepII-apcA* gene were 5′AAGGATCCGAGTAACTGGTCACACCCACAATTCGAGAAAATGAGTATCGTCACGAA3′ and 5′GCGAGCTCCTAGCTCATTTTTCCGAT3′. The other primers were similar to those described previously [3]. As shown by the schemes in Figure 1, the s*trepII-apcA* gene was fused to a His-tag and denoted as *his-strepII-apcA* for apo-APC-α with a His-Strep-II-tag at the N-terminal. The *ho1* and *pcyA* genes for the biosynthesis of PCB were ligated into the pCDFDeut-1 vector (Novagen), and the *cpcS* and *cpcU* genes for PCB attachment to apoproteins were ligated into the pRSFDeut-1 vector (Novagen). The final plasmid constructs were sequenced to check their veracity.

2.2. Expression and Purification of the Recombinant Proteins. The pCDFDuet-*his-strepII-apcA-ho1-pcyA* and pRSFDeut-*cpcS-cpcU* expression vectors were cotransformed into *Escherichia coli* BL21. The transformants were selected by 50 μg/mL spectinomycin and 50 μg/mL kanamycin. A single colony of the transformed *Escherichia coli* BL21 was cultured in 5 mL of LB medium at 37°C overnight. The bacterial culture was then transferred into 400 mL of LB and cultured at 37°C. When the OD_{600} reached 0.6~0.8, the culture was induced with 0.5 mM isopropyl β-D-thiogalactoside at 28°C. Bacteria were harvested after 8 h induction and stored at −20°C before use.

To obtain the recombinant proteins, ultrasonicated bacteria supernatant was passed through a Ni^{2+}-NTA affinity column (GE Healthcare Bio-Sciences). The retained protein on the column was eluted by 50 mM sodium phosphate and 300 mM imidazole, pH 7.4. The pooled elution was loaded onto a Sephadex G-25 size-exclusion column to eliminate imidazole. The protein fraction was collected and concentrated and analyzed by UV-visible and fluorescence spectroscopy.

2.3. Western Blotting Analysis. Western hybridization was performed with streptavidin-derivatized horseradish peroxidase to detect the bioaffinity of the holo-APC-α with tags. A molecular weight marker, a whole bacterial culture extract, and the protein solution purified above were run side by side on the gel in duplicate. After running, the gel was cut in half. One half was stained with Coomassie brilliant blue and the other was transferred to nitrocellulose following the kit manufacturer's instructions. This nitrocellulose was then incubated in TBS (25 mM Tris-HCl, 138 mM NaCl, and 2.68 mM KCl, pH 7.4) plus 0.05% polyoxyethylenesorbitan monolaurate (Tween 20) and 3% BSA for 1 h at room temperature. After a brief rinse with the same buffer without

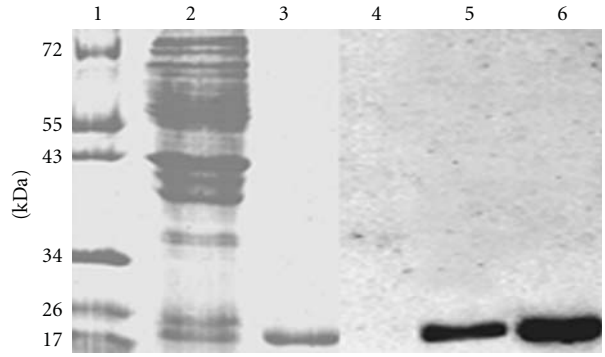

Figure 2: SDS-PAGE analyses indicate the expression of His-Strep-II-holo-APC-α and its bioaffinity. Lanes from 1 to 3 were stained by Coomassie brilliant blue: 1: marker; 2: whole protein in bacteria extract; 3: purified protein. Lanes 4 to 6 show the results for western blotting: 4: marker; 5: whole protein in bacteria extract; 6: purified protein.

BSA, the blot was incubated with a streptavidin-derivatized horseradish peroxidase conjugate in TBS/0.05% Tween-20/3% BSA for 1 h at room temperature. It was then washed three times with TBS/0.05% Tween 20 and once with TBS. Finally, the HRP substrate was added and the blot was developed for approximately 3 min.

2.4. Preparation and Characterization of ZnSiMNPs. Silica-coated magnetic nanoparticles (SiMNPs) were first prepared with a water-in-oil microemulsion method described previously [30, 31]. Then, 1.0 wt.% SiMNPs were suspended in 5.0 mM $ZnSO_4$ solution. After 10 min ultrasonic homogenization, the suspension was left to stir overnight at 25°C. The magnetic nanoparticles (ZnSiMNPs) were magnetically harvested and washed several times. The ZnSiMNPs were then suspended in water prior to use. The morphology of the nanoparticles was analyzed by transmission electron microscopy (TEM).

2.5. Immobilization and Imaging of Holo-APC-α on Magnetic Nanoparticles. The ZnSiMNPs or SiMNPs were added to a 0.5 mL holo-APC-α solution prepared as described above. The mixture was gently agitated at room temperature for 30 min. Nanoparticles were separated from the remaining solution with a magnetic rack. The nanoparticles were washed and suspended in 50 mM sodium phosphate, pH 7.4. In order to test the retentive bioaffinity of proteins loaded onto the nanoparticles, 10 μL of 1 mg/mL streptavidin-FITC was added to the suspension. After incubation for 30 min, the loaded nanoparticles were collected, washed, and suspended in 50 mM sodium phosphate, pH 7.4, then analyzed with fluorescence microscopy.

3. Results

3.1. Bioaffinity of Recombinant Protein. After 8 h induction, the color of the bacteria in the fermentation solution changed to cyan. The cells were collected and ultrasonically disrupted, and the cyanosupernatant was purified with a Ni^{2+}-NTA affinity column. The eluted solution from this column was clearly blue. Results of SDS-PAGE and Western blotting analyses for the whole bacteria cell extract and purified proteins are shown in Figure 2, showing many protein bands in the whole bacteria extract. A single-protein-band protein near 22 kDa, corresponding to the calculated molecular masses of holo-APC-α with His-tag and Strep-II-tag, resulted from the protein sample purified by the Ni^{2+}-NTA affinity column. The selective purification of this recombinant protein by the Ni^{2+}-NTA affinity column confirmed the inclusion of an active His-tag. Western blot analysis showed a single band at a similar location to the SDS-PAGE results for the whole bacterial cell extract and purified protein, indicating the presence of the Strep-II-tag and confirming its bioaffinity.

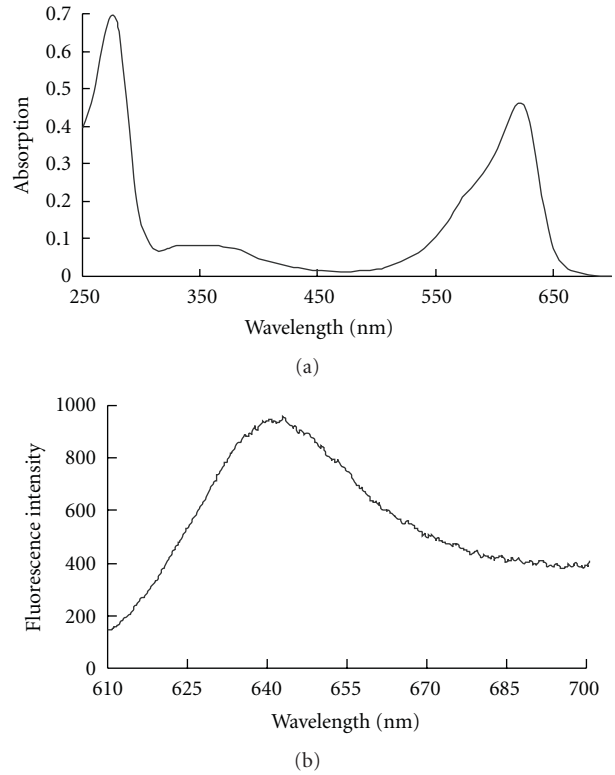

Figure 3: UV-vis absorption (a) and fluorescence emission spectra (b) for the purified His-Strep-II-holo-APC-α indicate the correct attachment of PCB on the apoprotein.

3.2. Spectra of Recombinant Protein. The purified protein solution had an adsorption maximum at 615 nm and a fluorescence emission maximum at 643 nm (Figure 3). The absorption and fluorescence spectra of the holo-APC-α recombinant with His-tag and Strep-II-tag were consistent with those reported for the native protein [12], indicating the correct attachment of PCB on the apoprotein.

3.3. Characterization of ZnSiMNPs. TEM images of the SiMNPs and ZnSiMNPs are shown in Figure 4. These two types of spherical nanoparticles had a similar size, close to 100 nm. However, the surface of SiMNPs appeared somewhat

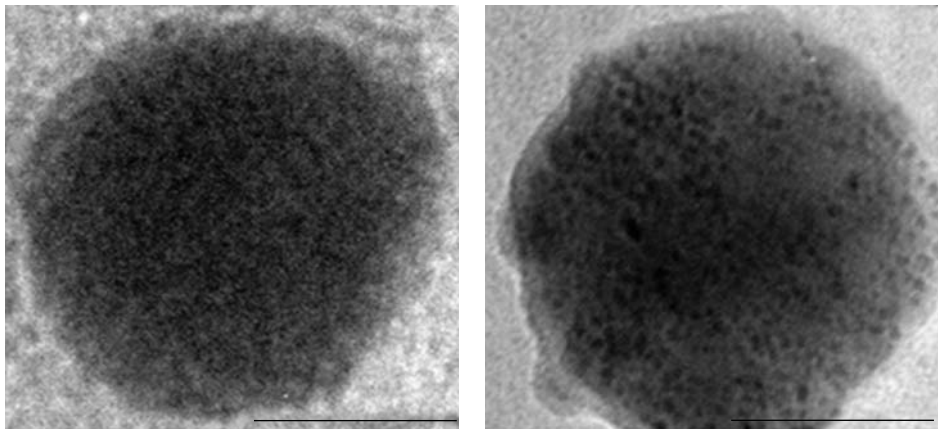

(a) (b)

Figure 4: TEM images of the smooth surface of SiMNPs (a) and the semishell of ZnSiMNPs (b). Bars: 50 nm.

(a)

(b)

Figure 5: Fluorescence microscopy images of His-Strep-II-holo-APC-α laden ZnSiMNPs after hybridization with streptavidin-FITC: excited by green (a) or blue (b) light, confirming the surface immobilization of holo-APC-α and the retentive streptavidin-binding ability of proteins loaded onto the nanoparticles. Bars: 1 μm.

smooth, while ZnSiMNPs were evidently decorated with 3–5 nm nanoparticles, which had the appearance of a semishell. This semishell appearance was similar to the decoration of nanophasic nickel on silica microspheres [27], so it is likely that the coating was caused by the deposition of zinc on silica.

3.4. Immobilization and Bioaffinity of Protein on ZnSiMNPs. After incubation with His-Strep-II-holo-APC-α, nanoparticles were separated with a magnet. ZnSiMNPs changed color from brown to blue, while the SiMNPs remained brown. This visible difference indicates the key role of zinc decoration on the surface immobilization of His-Strep-II-holo-APC-α on the nanoparticles. In order to further verify the bioaffinity of the protein immobilized on the ZnSiMNPs, streptavidin-FITC was used. As shown in Figure 5, ZnSiMNPs showed a fluorescent signal, representative of holo-APC-α or FITC with the excitation of green or blue light, respectively, suggesting the surface immobilization of holo-APC-α and the retentive streptavidin-binding ability of proteins loaded onto the nanoparticles. As a control, SiMNPs showed no fluorescence upon excitation by either green or blue light.

4. Discussion

Based on genetic engineering and nanotechnology, this study demonstrated a potential strategy to facilitate the biomodification and targeted delivery of pharmacological proteins. This strategy is represented schematically in Figure 6. Cyanobacterial allophycocyanin, a unique and inexpensive pigment protein with various pharmacological uses, was chosen as a model protein. This research reports, for the first time, the recombinant construction of holo-APC-α with both a His-tag and a Strep-II-tag. This recombinant protein had similar spectral properties to native holo-APC-α and showed streptavidin-binding capability due to the fusion of the Strep-II-tag. In addition, the metal-chelating ability derived from the His-tag not only facilitated its purification but also promoted its immobilization on ZnSiMNPs. Together with the results of electrophoresis, Western blotting, and spectral analysis, we concluded that holo-APC-α engineered with a His-tag and a Strep-II-tag was successfully biosynthesized. This recombinant protein could be immobilized on ZnSiMNPs and modified with

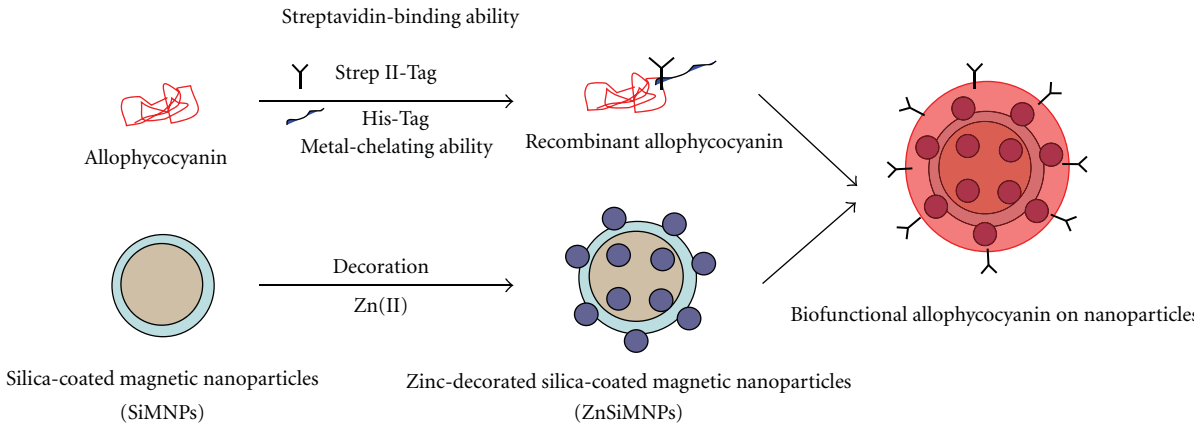

Figure 6: Schemes for potential strategies to facilitate biomodification of nanoparticles and targeted delivery of pharmacological proteins.

streptavidin without chemical manipulation. Furthermore, the utilization of magnetic nanoparticles as drug delivery carriers is promising for targeting delivery to tumor sites.

Acknowledgments

This work was supported by the National High Technology Research and Development Program of China (2009AA10Z106), Promotive Research Fund for Excellent Young and Middle-aged Scientists of Shandong Province (2010BSB02009), Major State Basic Research Development Program (2011CB200902), and the Public Science and Technology Research Funds Projects of Ocean (200905021-3).

References

[1] R. MacColl, "Cyanobacterial phycobilisomes," *Journal of Structural Biology*, vol. 124, no. 2-3, pp. 311–334, 1998.

[2] W. A. Samsonoff and R. MacColl, "Biliproteins and phycobilisomes from cyanobacteria and red algae at the extremes of habitat," *Archives of Microbiology*, vol. 176, no. 6, pp. 400–405, 2001.

[3] L. N. Liu, X. L. Chen, Y. Z. Zhang, and B. C. Zhou, "Characterization, structure and function of linker polypeptides in phycobilisomes of cyanobacteria and red algae: an overview," *Biochimica et Biophysica Acta*, vol. 1708, no. 2, pp. 133–142, 2005.

[4] N. Tandeau de Marsac, "Phycobiliproteins and phycobilisomes: the early observations," *Photosynthesis Research*, vol. 76, no. 1-3, pp. 197–205, 2003.

[5] A. McGregor, M. Klartag, L. David, and N. Adir, "Allophycocyanin trimer stability and functionality are primarily due to polar enhanced hydrophobicity of the phycocyanobilin binding pocket," *Journal of Molecular Biology*, vol. 384, no. 2, pp. 406–421, 2008.

[6] R. MacColl, "Allophycocyanin and energy transfer," *Biochimica et Biophysica Acta*, vol. 1657, no. 2-3, pp. 73–81, 2004.

[7] S. R. Shih, K. N. Tsai, Y. S. Li, C. C. Chueh, and E. C. Chan, "Inhibition of enterovirus 71-induced apoptosis by allophycocyanin isolated from a blue-green alga *Spirulina platensis*," *Journal of Medical Virology*, vol. 70, no. 1, pp. 119–125, 2003.

[8] E. A. Lissi, M. Pizarro, A. Aspee, and C. Romay, "Kinetics of phycocyanine bilin groups destruction by peroxyl radicals," *Free Radical Biology and Medicine*, vol. 28, no. 7, pp. 1051–1055, 2000.

[9] V. B. Bhat and K. M. Madyastha, "Scavenging of peroxynitrite by phycocyanin and phycocyanobilin from *Spirulina platensis*: protection against oxidative damage to DNA," *Biochemical and Biophysical Research Communications*, vol. 285, no. 2, pp. 262–266, 2001.

[10] B. Ge, Z. Tang, F. Zhao, Y. Ren, Y. Yang, and S. Qin, "Scale-up of fermentation and purification of recombinant allophycocyanin over-expressed in *Escherichia coli*," *Process Biochemistry*, vol. 40, no. 10, pp. 3190–3195, 2005.

[11] X. Y. Guan, W. J. Zhang, X. W. Zhang et al., "A potent antioxidant property: fluorescent recombinant α-phycocyanin of Spirulina," *Journal of Applied Microbiology*, vol. 106, no. 4, pp. 1093–1100, 2009.

[12] I. C. Hu, T. R. Lee, H. F. Lin, C. C. Chiueh, and P. C. Lyu, "Biosynthesis of fluorescent allophycocyanin α-subunits by autocatalytic bilin attachment," *Biochemistry*, vol. 45, no. 23, pp. 7092–7099, 2006.

[13] W. Zhang, X. Guan, Y. Yang et al., "Biosynthesis of fluorescent allophycocyanin α-subunits by autocatalysis in *Escherichia coli*," *Biotechnology and Applied Biochemistry*, vol. 52, no. 2, pp. 135–140, 2009.

[14] T. G. M. Schmidt, J. Koepke, R. Frank, and A. Skerra, "Molecular interaction between the strep-lag affinity peptide and its cognate target, streptavidin," *Journal of Molecular Biology*, vol. 255, no. 5, pp. 753–766, 1996.

[15] A. D. Keefe, D. S. Wilson, B. Seelig, and J. W. Szostak, "One-step purification of recombinant proteins using a nanomolar-affinity streptavidin-binding peptide, the SBP-tag," *Protein Expression and Purification*, vol. 23, no. 3, pp. 440–446, 2001.

[16] Y. A. Cai, J. T. Murphy, G. J. Wedemayer, and A. N. Glazer, "Recombinant phycobiliprotiens: recombinant C-phycocyanins equipped with affinity tags, oligomerization, and biospecific recognition domains," *Analytical Biochemistry*, vol. 290, no. 2, pp. 186–204, 2001.

[17] R. Janknecht, G. de Martynoff, J. Lou, R. A. Hipskind, A. Nordheim, and H. G. Stunnenberg, "Rapid and efficient purification of native histidine-tagged protein expressed by recombinant vaccinia virus," *Proceedings of the National Academy of Sciences of the United States of America*, vol. 88, no. 20, pp. 8972–8976, 1991.

[18] K. L. M. C. Franken, H. S. Hiemstra, K. E. van Meijgaarden et al., "Purification of His-tagged proteins by immobilized chelate affinity chromatography: the benefits from the use of organic solvent," *Protein Expression and Purification*, vol. 18, no. 1, pp. 95–99, 2000.

[19] K. Ye, S. Jin, M. M. Ataai, J. S. Schultz, and J. Ibeh, "Tagging retrovirus vectors with a metal binding peptide and one-step purification by immobilized metal affinity chromatography," *Journal of Virology*, vol. 78, no. 18, pp. 9820–9827, 2004.

[20] E. K. M. Ueda, P. W. Gout, and L. Morganti, "Current and prospective applications of metal ion-protein binding," *Journal of Chromatography A*, vol. 988, no. 1, pp. 1–23, 2003.

[21] D. Kröger, M. Liley, W. Schiweck, A. Skerra, and H. Vogel, "Immobilization of histidine-tagged proteins on gold surfaces using chelator thioalkanes," *Biosensors and Bioelectronics*, vol. 14, no. 2, pp. 155–161, 1999.

[22] C. H. Ho, L. Limberis, K. D. Caldwell, and R. J. Stewart, "A metal-chelating pluronic for immobilization of histidine-tagged proteins at interfaces: immobilization of firefly luciferase on polystyrene beads," *Langmuir*, vol. 14, no. 14, pp. 3889–3894, 1998.

[23] C. Mateo, G. Fernández-Lorente, E. Cortés, J. L. Garcia, R. Fernández-Lafuente, and J. M. Guisan, "One-step purification, covalent immobilization, and additional stabilization of poly-his-tagged proteins using novel heterofunctional chelate-epoxy supports," *Biotechnology and Bioengineering*, vol. 76, no. 3, pp. 269–276, 2001.

[24] S. Paul, S. S. Bhattacharyya, N. Boujedaini, and A. R. Khuda-Bukhsh, "Anticancer potentials of root extract of Polygala senega and its PLGA nanoparticles-encapsulated form," *Evidence-Based Complementary and Alternative Medicine*, vol. 2011, Article ID 517204, 13 pages, 2011.

[25] M. Arruebo, R. Fernández-Pacheco, M. R. Ibarra, and J. Santamaría, "Magnetic nanoparticles for drug delivery," *Nano Today*, vol. 2, no. 3, pp. 22–32, 2007.

[26] Y. Liao, Y. Cheng, and Q. Li, "Preparation of nitrilotriacetic acid/Co^{2+}-linked, silica/boron-coated magnetite nanoparticles for purification of 6 × histidine-tagged proteins," *Journal of Chromatography A*, vol. 1143, no. 1-2, pp. 65–71, 2007.

[27] S. Ramesh, Y. Koltypin, R. Prozorov, and A. Gedanken, "Sonochemical deposition and characterization of nanophasic amorphous nickel on silica microspheres," *Chemistry of Materials*, vol. 9, no. 2, pp. 546–551, 1997.

[28] M. Bele, G. Hribar, S. Čampelj et al., "Zinc-decorated silica-coated magnetic nanoparticles for protein binding and controlled release," *Journal of Chromatography B*, vol. 867, no. 1, pp. 160–164, 2008.

[29] Z. Ma, Y. Guan, and H. Liu, "Superparamagnetic silica nanoparticles with immobilized metal affinity ligands for protein adsorption," *Journal of Magnetism and Magnetic Materials*, vol. 301, no. 2, pp. 469–477, 2006.

[30] X. He, H. Huo, K. Wang, W. Tan, P. Gong, and J. Ge, "Plasmid DNA isolation using amino-silica coated magnetic nanoparticles (ASMNPs)," *Talanta*, vol. 73, no. 4, pp. 764–769, 2007.

[31] X. He, Y. Chen, K. Wang, P. Wu, P. Gong, and H. Huo, "Selective separation of proteins with pH-dependent magnetic nanoadsorbents," *Nanotechnology*, vol. 18, no. 36, Article ID 365604, 2007.

Hindawi Publishing Corporation
Evidence-Based Complementary and Alternative Medicine
Volume 2011, Article ID 691067, 7 pages
doi:10.1155/2011/691067

Research Article

Hypoglycemic Properties of Oxovanadium (IV) Coordination Compounds with Carboxymethyl-Carrageenan and Carboxymethyl-Chitosan in Alloxan-Induced Diabetic Mice

Hongyu Zhang,[1,2] Yuetao Yi,[1,3] Dawei Feng,[1] Yipeng Wang,[1] and Song Qin[1,3]

[1] *Yantai Institute of Coastal Zone Research, Chinese Academy of Sciences, Yantai 264003, China*
[2] *Graduate School of Chinese Academy of Sciences, Beijing 100049, China*
[3] *Biological Resources Laboratory, Yantai Institute of Coastal Zone Research, Chinese Academy of Sciences, Yantai, 264003, China*

Correspondence should be addressed to Yuetao Yi, ytyi@yic.ac.cn and Song Qin, sqin@yic.ac.cn

Received 12 January 2011; Accepted 1 June 2011

In order to avoid low absorption, incorporation, and undesirable side effects of inorganic oxovanadium compounds, the antidiabetic activities of organic oxovanadium (IV) compounds in alloxan-induced diabetic mice were investigated. Vanadyl carboxymethyl carrageenan (VOCCA) and vanadyl carboxymethyl chitosan (VOCCH) were synthesized and administrated through intragastric administration in different doses for 20 days in alloxan-induced diabetic mice. Glibenclamide was administrated as the positive control. Our results showed that low-dose group, middle-dose group, and high-dose group of VOCCA and VOCCH could significantly reduce the levels of blood glucose ($P < 0.05$) compared with untreated group, but not in normal mice. Besides, high-dose groups of VOCCA and VOCCH exhibited more significant hypoglycemic activities ($P < 0.01$). After treated with VOCCH, the oral glucose tolerance of high-dose group of VOCCH was improved compared with model control group ($P < 0.05$).

1. Introduction

Diabetes mellitus (DM), which results from insulin deficiency or insulin resistance, is a serious chronic metabolic disease [1]. The DM includes insulin-dependent type 1 DM and non-insulin-dependent type 2 DM. Until now, type 1 DM can only be controlled by subcutaneous injections of insulin, which causes many problems to the patients. In order to treat type 2 DM, some drugs have also been synthesized [2], for example, sulfonylureas, sulfonamides, biguanides, thiozolidinediones, and so on. Orally active therapeutic agents instead of painful insulin injections for type 1 DM and synthetic drugs without side effects for type 2 DM have become an urgent and important requirement.

Vanadium is not only an important trace element for organisms, but also the necessary element for human body [3]. It has been demonstrated that many vanadium compounds possess therapeutic effects as insulin mimetics [4, 5]. Heyliger et al. first reported the insulin mimetic activity of oral vanadate *in vivo* in 1985 [6]. Since then, extensive studies have been carried out to explore vanadium chemistry, including the synthesis of novel complexes and their antidiabetic activities both *in vitro* and *in vivo* [7–16]. Furthermore, many clinical trials of vanadium compounds have also been reported [17–20], in which vanadium salts such as $VOSO_4$ and $NaVO_3$ were administered to diabetic patients. In order to enhance both lipophilicity and bioavailability of vanadium compound, overcome the disadvantage of side effects, increase the half-life of the compound, decrease systemic drug toxicity, improve treatment absorption rates, and provide protection for pharmaceuticals against biochemical degradation, two types of less toxic vanadyl (+4 oxidation state of vanadium) complexes with different coordination structures were synthesized and examined.

In addition, the polysaccharide polymer is biodegradable and biocompatible and would be effective in enhancing drug bioavailability through the mechanism of delaying release. In order to investigate the impact of different organic ligands on vanadyl complexes, vanadyl carboxymethyl k-carrageenin and vanadyl carboxymethyl chitosan were synthesized. The

present study was performed to investigate the antidiabetic properties of these two new vanadyl complexes in alloxan-induced diabetic mice.

2. Materials and Methods

2.1. Materials and Equipments. K-carrageenin and chitosan with a deacetylation degree of 95.3% were purchased from Qingdao Baicheng Biochemical Corp (China), their viscosity-average molecular weights were 3.77×10^5 and 2.0×10^5, respectively. Isopropanol, glucose, alloxan, and vanadyl sulfate hydrate ($VOSO_4 \cdot xH_2O$, $x = 3$ to 5) were purchased from the Sigma-Aldrich Chemical Co. Glibenclamide was purchased from Pacific pharmaceutical technology group. Ethanol, sodium hydroxide, and other reagents were purchased from Sinopharm Co. Kunming mice were provided by experimental animal center, Kunming. The IR spectra were measured on a JASCO-4100FT-IR spectrometer with KBr disks. The content of vanadium is measured on 7AS-986 (G) Atomic Absorption Spectrometer. Chemicals and solvents were reagent grade.

2.2. Synthesis of VOCCA and VOCCH. K-carrageenin (chitosan) (50 g) was added into 750 mL isopropanol and stirred for 30 min. 40 mL sodium hydroxide solution (mass fraction is 50%) was slowly dropped into the mixture (25 min) and stirred for 3 h. Then 60 g monochloroacetic acid was added into the mixture for 5 times in 30 min, and the system temperature was kept at 60°C for 4 h. After incubating for 4 h, the temperature was lowered to 25°C and the pH was adjusted to 7.0. The mixture was then concentrated with ethanol three times in volume of the mother liquid. After filtration, washing, drying, and smashing, the carboxymethyl carrageenin and carboxymethyl chitosan were obtained.

Ashing method [21] was applied to calculate the SD of carboxymethyl groups of carboxymethyl carrageenin and carboxymethyl chitosan. Carboxymethyl carrageenin and carboxymethyl chitosan were vacuum dried at 60°C to constant mass; carboxymethyl carrageenin and carboxymethyl chitosan were heated and scorched at 700°C for 15–20 min. The residues were Na_2O, leached with 50 mL HCl solution (0.1 moI/L), heated, and followed by residual titration with 0.1 mol/L standard NaOH. The SD of carboxymethyl groups of carboxymethyl carrageenin and carboxymethyl chitosan were calculated as the formula discussed by Wang and Ye.

Vanadyl carboxymethyl carrageenin (chitosan) (the SD of carboxymethyl carrageenin and carboxymethyl chitosan were 47.3% and 84.9%, resp.) was prepared by mixing various amounts of $VOSO_4$ with carboxymethyl carrageenin (the mass ratio of V to carboxymethyl carrageenin (chitosan) was 1%) solutions under magnetic stirring for 24 h at room temperature. Ethanol four times in volume of the mother liquid was added to the solution to complete precipitation of vanadyl carboxymethyl carrageenin (chitosan) complex. The resulting precipitate was washed with ethanol and dried under a vacuum condition at room temperature, and white solid vanadyl carboxymethyl carrageenin and carboxymethyl chitosan were obtained. VOCCA and VOCCH were dissolved in tap water to the concentration of 5% (w/v) every day and kept at 4°C.

2.3. Vanadium Content Determination. 7AS-986 (G) Atomic Absorption Spectrometry was applied to determine the content of vanadium of the complex according to the standard method of the instruction.

2.4. Maximal Tolerant Dose (MTD) Determination of VOCCA. The result of preliminary acute toxicity test showed no death of mouse. Afterwards, the Maximal Tolerant Dose (MTD) test was carried out. Twenty normal mice weighing 20 ± 2 g were fasted for 24 h, then VOCCA (5%, 0.8 mL) was administered intragastrically three times a day for two weeks. After two weeks, the maximum tolerated dose was calculated according to the formula:

$$\text{MTD} = \frac{\text{the dose of intragastric administration} \times 3}{\text{body weight of rat}}. \quad (1)$$

2.5. Construction of Diabetic Mouse Model. Male mice weighing 20–24 g were used for animal model construction. Mice were fasted for 24 h and then intraperitoneally injected alloxan (160 mg/kg). Five days after alloxan injection, the mice were fasted for 6 h and blood samples were obtained from tail vein of the mice. The blood glucose levels were measured by the glucose oxidase method. The alloxan-injected mice with the blood glucose level between 10 and 20 mmol/L were considered as diabetic mice.

2.6. Glucose-Lowering Test. Normal mice and diabetic mice were randomly divided into 6 groups (10 mice per group). Normal control group: normal mice; model control group: diabetic mice treated with tap water; glibenclamide control group: diabetic mice treated with 0.2 g/kg glibenclamide; low-dose group: diabetic mice treated with 0.3125 g/kg VOCCH and 0.6250 g/kg VOCCA; middle-dose group: diabetic mice treated with 0.6250 g/kg VOCCH and 1.250 g/kg VOCCA; high-dose group: diabetic mice treated with 1.2500 g/kg VOCCH and 2.500 g/kg VOCCA. The samples above were administered intragastrically for 20 days.

2.7. Oral Glucose Tolerance Test (OGTT) of VOCCH. After the VOCCH was administered intragastrically in both normal and alloxan-induced diabetic mice for 20 days, oral glucose tolerance test was executed. Glucose loaded with the single dose of 2.5 g/kg was intragastrically administered to mice fasted for 6 h, and the blood glucose level was checked at 0, 0.5, 2 h.

2.8. Blood Sample Collection. The blood samples were obtained from tail vein of mice. Firstly, the tail of mouse was put into hot water (50°C) for several minutes and cleaned, then the tail tip was cut for 1-2 mm long and blood sample was obtained.

2.9. Statistical Analysis. All data were expressed as the mean ± SD. Statistical analysis was performed by one-way analysis

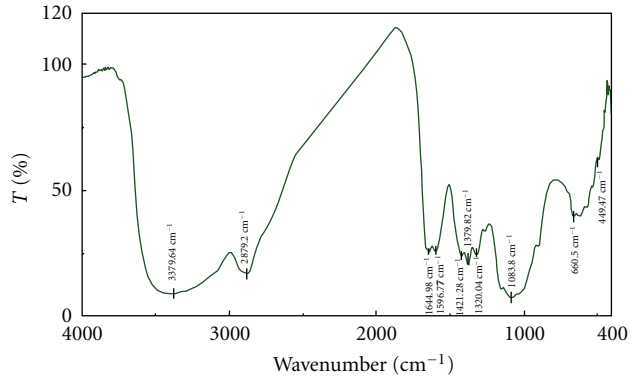

Figure 1: FT-IR spectra of chitosan.

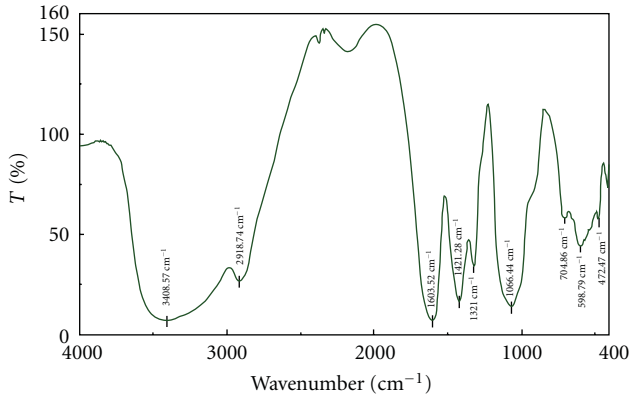

Figure 2: FT-IR spectra of carboxymethyl chitosan.

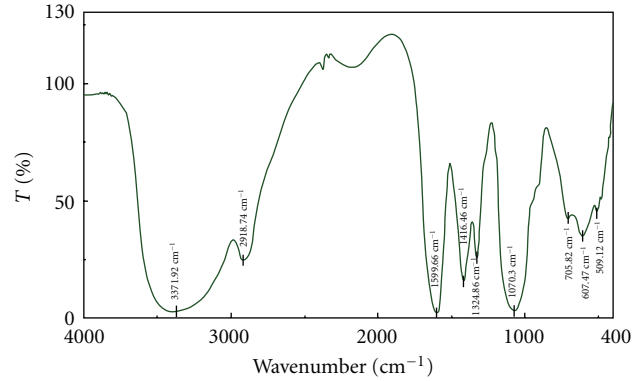

Figure 3: FT-IR spectra of vanadyl carboxymethyl chitosan.

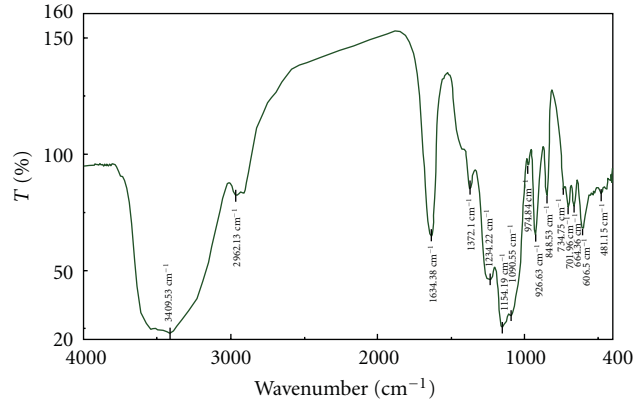

Figure 4: FT-IR spectra of carrageenan.

of variance (ANOVA) followed by the least significant difference (LSD) test for the multiple comparisons among the groups. Values for $P < 0.05$ were considered statistically significant.

3. Result

3.1. Character of VOCCA and VOCCH. Figures 1, 2, and 3 are infrared spectra of chitosan, carboxymethyl chitosan, and vanadyl carboxymethyl chitosan. Infrared spectrum (Figure 2) showed that C–OH stretching vibration absorption peak of carboxymethyl chitosan was located at 1066.44 cm^{-1}, N–H and O–H at 3408.57 cm^{-1}, –OH antisymmetrical stretching vibration absorption peak (COO) was located at 1603.52 cm^{-1}, and its symmetrical stretching vibration (COO) absorption peak was at 1421.28 cm^{-1}.

Infrared spectrum of VOCCH (Figure 3) showed that C–OH absorption peak was displaced to 1070.30 cm^{-1}, N–H and O–H absorption peaks were displaced to 3371.92 cm^{-1}, OH antisymmetrical stretching vibration absorption peak and its symmetrical stretching vibration (COO) absorption peak were displaced to 1599.66 cm^{-1} and 1416.46 cm^{-1}. This indicated that carboxyl, amino-group, and hydroxyl participated in the interaction of carboxymethyl chitosan and VO^{2+}. The content of V in VOCCH was 0.36%.

Figures 4, 5, and 6 are the IR spectra of carrageenan, carboxymethyl carrageenan, and vanadyl carboxymethyl carrageenan. Compared to the carrageenan, carboxymethyl carrageenan showed characteristic peak 1610 cm^{-1} of C=O group. Further, the peak of C=O in carboxymethyl carrageenan at 1610 cm^{-1} shift to 1604 cm^{-1} of vanadyl carboxymethyl carrageenan, also the shifts of absorption peaks of S=O and OH were observed (Figure 6). These results clearly indicated the incorporation of carboxymethyl group and VO^{2+} into carrageenan and carboxymethyl carrageenan, respectively. The content of V of VOCCA measurement on Atomic Absorption Spectrometry was 0.18%.

3.2. MTD of VOCCA. In the test of maximal tolerant dose, there were no convulsions, vomiting, or other negative symptoms.

$$\text{MTD} = 0.8\,\text{mL} \times 5\,\text{g/mL} \times \frac{3}{20}\,\text{g} = 6.0\,\text{g/Kg}. \quad (2)$$

3.3. Glucose-Lowering Studies and OGTT. In Figures 7 and 8, the body weights of each group before and after treatment with VOCCA and VOCCH are shown. In this study, the body weights of diabetic mice were lowered compared with those of normal control mice throughout the experimental period of 20 days. At the end of the experiment, the body weights of vanadium-treated groups exhibited no significant deviation with model control group and glibenclamide control group.

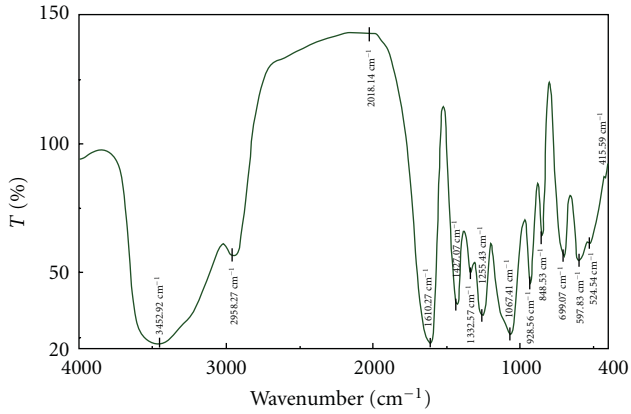

Figure 5: FT-IR spectra of carboxymethyl carrageenan.

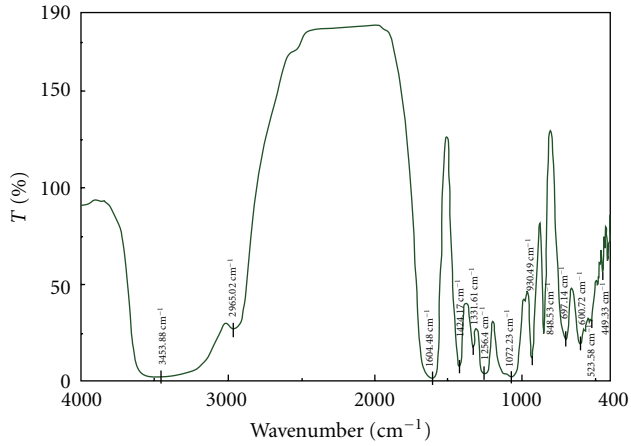

Figure 6: FT-IR spectra of vanadyl carboxymethyl carrageenan.

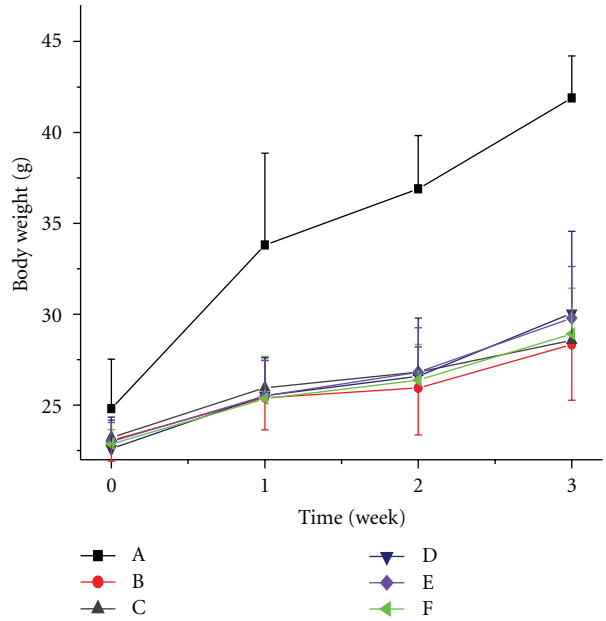

Figure 7: Impacts of intragastric VOCCA administration on body weight in both normal and alloxan-diabetic mice; (A): normal control group, (B): model control group, (C): glibenclamide control group, (D): low dose group, (E): middle dose group, (F): high dose group.

Table 1: Impacts of intragastric VOCCA on blood glucose levels in both normal and alloxan-diabetic mice.

Group	Dose ($g \cdot Kg^{-1}$)	0 week	3 week
Normal control group	0	5.7 ± 0.6	6.0 ± 0.16
Model control group	0	17.8 ± 4.6	32.2 ± 3.3
Glibenclamide control group	0.2000	17.9 ± 4.3	26.7 ± 2.6
Low-dose group	0.6250	18.0 ± 4.3	28.9 ±4.5[ad]
Middle-dose group	1.2500	17.8 ± 4.4	28.1 ±5.0[ad]
High-dose group	2.500	17.6 ± 4.3	25.9 ±4.7[ac]

[a]$P < 0.01$, [b]$P < 0.05$, versus normal control group; [c]$P < 0.01$, [d]$P < 0.05$, versus model control group.

The body weight profile indicated that there was no negative impact on body weight of the mice after treated with both VOCCA and VOCCH. These complexes showed comparable results with other vanadyl coordination compounds [22].

The changes of blood glucose levels are shown in Tables 1 and 2. The initial blood glucose levels of the diabetic mice were similar. Low-dose group, middle-dose group, and high-dose group of VOCCA could statistically significantly reduce the levels of blood glucose ($P < 0.05$) compared with model control group, and high-dose group of VOCCA had more significant hypoglycemic activity ($P < 0.01$) (Table 1). There was no obvious difference among low-dose group, middle-dose group, and high-dose group compared with glibenclamide control group ($P > 0.05$). Low-dose group, middle-dose group, and high-dose group of VOCCH could statistically significantly reduce the levels of blood glucose ($P < 0.05$) compared to model control group. However, high-dose group showed more apparent effect than glibenclamide control group ($P < 0.01$) (Table 2). Furthermore, the oral glucose tolerance was improved in diabetic animals after treated with VOCCH ($P < 0.05$) (Figure 9). Meanwhile, low-dose group, middle-dose group, and high-dose group of VOCCA and VOCCH showed no negative influence on blood glucose levels of normal mice (Tables 1 and 2).

Among low-dose group, middle-dose group and high-dose group of VOCCA and VOCCH at the same concentration of vanadium, the blood glucose levels of VOCCH groups reduced from 29.8 (model control group) to 24.2, 22.4, 17.1, respectively, while VOCCA groups reduced from 32.2 (model control group) to 28.9, 28.1, and 25.9, respectively, which indicated that VOCCH would be better candidate as insulin enhancer than VOCCA.

As shown in Figure 9, the blood glucose concentrations of mice increased greatly after loading with D-glucose and then reduced smoothly. In the OGTT test, the blood glucose concentrations of normal mice remained less than 8 mM, while the model control group was consistently higher than that of the vanadium-treated groups. The blood glucose

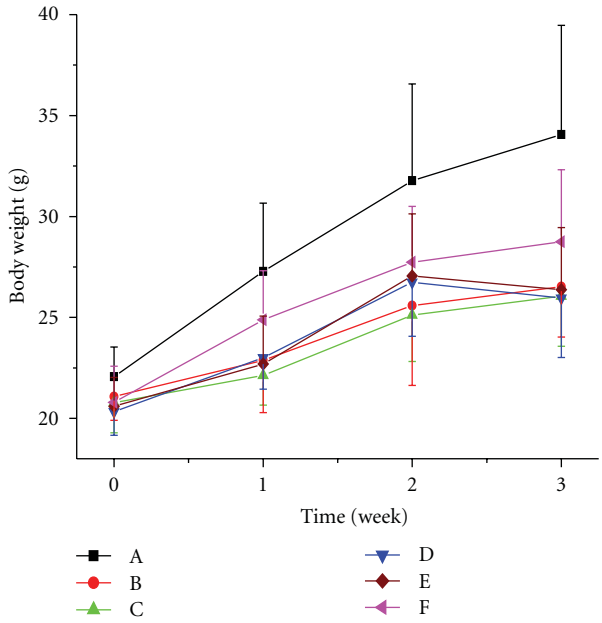

Figure 8: Impacts of intragastric VOCCH administration on body weight in both normal and alloxan-diabetic mice; (A): normal control group, (B): model control group, (C): glibenclamide control group, (D): low-dose group, (E): middle-dose group, (F): high-dose group.

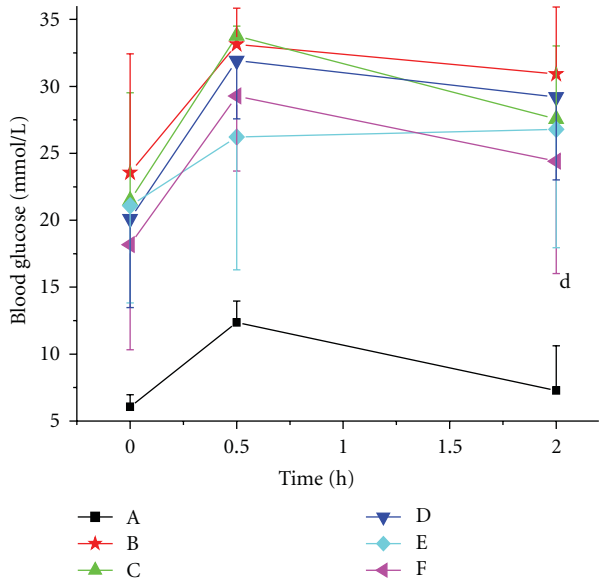

Figure 9: Impacts of VOCCH on glucose tolerance in normal mice and alloxan-diabetic mice. (A): normal control group, (B): model control group, (C): glibenclamide control group, (D): low dose group, (E): middle dose group, (F): high dose group. $d^P < 0.05$, versus model control group.

levels of diabetic mice remained above the basal levels at the end of the test. However, the blood glucose concentrations of vanadium treated groups were significantly lower than model control groups. Furthermore, the results of the OGTT indicated that impaired glucose tolerance was improved after treatment with VOCCH.

Table 2: Impacts of intragastric VOCCH on blood glucose levels in both normal and alloxan-diabetic mice.

Group	Dose ($g \cdot Kg^{-1}$)	0 week	3 week
Normal control group	0	5.7 ± 0.6	5.1 ± 0.5
Model control group	0	17.0 ± 4.7	29.8 ± 5.4
Glibenclamide control group	0.200	17.1 ± 4.5	21.4 ± 4.5
Low-dose group	0.3125	17.6 ± 4.7	24.2 ±3.4[ad]
Middle-dose group	0.6250	17.5 ± 4.4	22.4 ±5.6[ac]
High-dose group	1.2500	17.2 ± 4.3	17.1 ±6.9[acf]

[a]$P < 0.01$, versus normal control group; [c]$P < 0.01$, [d]$P < 0.05$, versus model control group; [f]$P < 0.01$, versus glibenclamide control group.

4. Discussion

Insulin-mimetic properties of vanadium salts and vanadium compounds have been widely reported in both type 1 and type 2 diabetic animal models [23–25]. Inorganic vanadium compounds have already been known to be effective in treatment of diabetic hyperglycemia, but the side effects, such as vomiting, diarrhea, hepatic, and renal toxicity limit their application [26, 27]. Organic vanadium coordination compounds have been proved with better absorption efficiency in gastrointestinal tract [28]. In this study, high doses of VOCCH and VOCCA exhibited antidiabetic activity at significantly lower intake levels of elemental vanadium compared to glibenclamide. Vomiting and diarrhea, the major side effects of vanadium compounds, were not observed. For example, BMOV and similar compounds like bis (ethylmaltolato) oxovanadium (IV) (BEOV) have already been in clinical trials [29]. However, the toxicity, lower bioavailability and nonlinear pharmacokinetics of these compounds compromise their pharmacological success [30]. These results indicated that the corporation of essential trace element vanadium and polysaccharide could enhance their biological activity, intercoordination, and bioavailability. The insulin-enhancing properties of organic vanadium complexes have previously been compared with those of inorganic vanadium salts [31, 32]. It was reported that vanadium-enriched *Cordyceps sinensis* was beneficial for contemporary treatment of depression and diabetes through the coeffect [33]. VOCCA and VOCCH also may be potential strategies for lowering the blood sugar level through the coeffect of vanadium and carboxymethyl-carrageenan and carboxymethyl-chitosan. In the present study, VOCCH, VOCCA, and $VOSO_4$ showed similar hypoglycemic functions. However, the vanadium intake amount in the form of VOCCH and VOCCA was significantly lower than that of $VOSO_4$ [22]. These results indicated that the anti-diabetic abilities of VOCCH and VOCCA were more effective than $VOSO_4$.

5. Conclusion

A beneficial role of enhancing anti-diabetic actions of VOCCH and VOCCA was found in this study. VOCCH

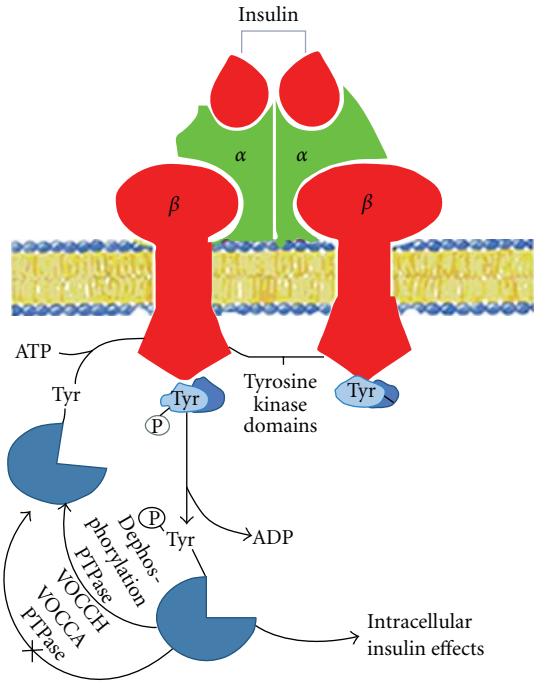

Figure 10: Schematic presentation of insulin signal transduction and possible action mechanisms of VOCCH and VOCCA.

and VOCCA would be good candidates of insulin enhancers to effectively activate glucose metabolism *in vivo* and regulate glucose metabolism by influencing insulin levels. The ligands of carboxymethyl carrageenin and carboxymethyl chitosan allowed vanadium to supply at the minimal doses, prolonged the duration of drug activity, and reduced the toxicity of vanadium. This implied that carboxymethyl carrageenin and carboxymethyl chitosan would be promising biocompatible and biodegradable vehicles for the delivery of VO^{2+} ions.

Insulin receptor which is a kind of transmembrane glycoprotein complex molecules consists of two alpha subunits (135 kd) and two beta subunits (95 kd); they linked by three disulfide bonds. Alpha subunits are outside of cell; beta subunits are embedded in membranes. The combination of insulin and alpha subunits caused phosphorylation of multiple tyrosine residues of beta subunits, which activated protein tyrosine kinase (PTK) and triggered a series of cascade amplification reaction of phosphorylation and dephosphorylation to adjust the metabolism. PTPase (protein tyrosine phosphatase) is the main negative regulatory factor in insulin signaling pathways; it caused dephosphorylation of insulin receptor and its substrate and weakened insulin signals.

Possible mechanisms for hypoglycemic properties of VOCCA and VOCCH are as follows: VOCCA and VOCCH could inhibit the dephosphorylation activity of PTPase, so dephosphorylation of tyrosine kinase and downstream signal substrate will be inhibited. In this way, the action time of insulin signal was prolonged, so VOCCA and VOCCH could lower the blood sugar level (Figure 10).

Acknowledgments

This work was supported by the Knowledge Innovation Program of the Chinese Academy of Sciences (KZCX2-YW-225), the Science & Technology Development Plan of Shandong Province (2010GSF10208), and the CAS/SAFEA International Partnership Program for Creative Research Teams.

References

[1] H. Sakurai, "A new concept: the use of vanadium complexes in the treatment of diabetes mellitus," *Chemical Record*, vol. 2, no. 4, pp. 237–248, 2002.

[2] H. Sakurai and H. Yasui, "Structure-activity relationship of insulinomimetic vanadyl-picolinate complexes in ciew of their clinical use," *Journal of Trace Elements in Experimental Medicine*, vol. 16, no. 4, pp. 269–280, 2003.

[3] B. Mukherjee, B. Patra, S. Mahapatra, P. Banerjee, A. Tiwari, and M. Chatterjee, "Vanadium—an element of a typical biological significance," *Toxicology Letters*, vol. 150, no. 2, pp. 135–143, 2004.

[4] Y. Shechter and S. J. D. Karlish, "Insulin-like stimulation of glucose oxidation in rat adipocytes by vanadyl (IV) ions," *Nature*, vol. 284, no. 5756, pp. 556–558, 1980.

[5] J. Meyerovitch, Z. Farfel, J. Sack, and Y. J. Shechter, "Oral administration of vanadate normalizes blood glucose levels in streptozotocin-treated rats: characterization and mode of action," *The Journal of Biological Chemistry*, vol. 262, no. 14, pp. 6658–6662, 1987.

[6] C. E. Heyliger, A. G. Tahiliani, and J. H. McNeill, "Effect of vanadate on elevated blood glucose and depressed cardiac performance of diabetic rats," *Science*, vol. 227, no. 4693, pp. 1474–1477, 1985.

[7] S. M. Brichard and J. C. Henquin, "The role of vanadium in the management of diabetes," *Trends in Pharmacological Sciences*, vol. 16, no. 8, pp. 265–270, 1995.

[8] N. Sekar, J. Li, and Y. Shechter, "Vanadium salts as insulin substitutes: mechanisms of action, a scientific and therapeutic tool in diabetes mellitus research," *Critical Reviews in Biochemistry and Molecular Biology*, vol. 31, no. 5, pp. 339–359, 1996.

[9] V. Badmaev, S. Prakash, M. Majeed, and J. Altern, "Vanadium: a review of its potential role in the fight against diabetes," *Journal of Alternative and Complementary Medicine*, vol. 5, no. 3, pp. 273–291, 1999.

[10] S. M. Brichard, C. J. Bailey, and J. C. Henquin, "Marked improvement of glucose homeostasis in diabetic ob/ob mice given oral vanadate," *Diabetes*, vol. 39, no. 11, pp. 1326–1332, 1990.

[11] K. H. Thompson and C. Orvig, "Design of vanadium compounds as insulin enhancing agents," *Journal of the Chemical Society, Dalton Transactions*, no. 17, pp. 2885–2892, 2000.

[12] H. Sakurai, Y. Kojima, Y. Yoshikawa, K. Kawabe, and H. Yasui, "Antidiabetic vanadium(IV) and zinc(II) complexes," *Coordination Chemistry Reviews*, vol. 226, no. 1-2, pp. 187–198, 2002.

[13] S. Karmaker, T. K. Saha, Y. Yoshikawa, H. Yasui, and H. Sakurai, "A novel drug delivery system for type 1 diabetes: insulin-mimetic vanadyl-poly(γ-glutamic acid) complex," *Journal of Inorganic Biochemistry*, vol. 100, no. 9, pp. 1535–1546, 2006.

[14] S. Tas, E. Sarandol, S. Z. Ayvalik, Z. Serdar, and M. Dirican, "Vanadyl sulfate, taurine, and combined vanadyl sulfate and taurine treatments in diabetic rats: effects on the oxidative and

antioxidative systems," *Archives of Medical Research*, vol. 38, no. 3, pp. 276–283, 2007.

[15] R. Shukla and R. R. Bhonde, "Adipogenic action of vanadium: a new dimension in treating diabetes," *BioMetals*, vol. 21, no. 2, pp. 205–210, 2008.

[16] J. J. Smee, J. A. Epps, K. Ooms et al., "Chloro-substituted dipicolinate vanadium complexes: synthesis, solution, solid-state, and insulin-enhancing properties," *Journal of Inorganic Biochemistry*, vol. 103, no. 4, pp. 575–584, 2009.

[17] A. B. Goldfine, D. C. Simonson, F. Folli, M. E. Patti, and C. R. Kahn, "Metabolic effects of sodium metavanadate in humans with insulin-dependent and noninsulin-dependent diabetes mellitus in vivo and in vitro studies," *Journal of Clinical Endocrinology and Metabolism*, vol. 80, no. 11, pp. 3311–3320, 1995.

[18] N. Cohen, M. Halberstam, P. Shlimovich et al., "Oral vanadyl sulfate improves hepatic and peripheral insulin sensitivity in patients with non-insulin-dependent diabetes mellitus," *Journal of Clinical Investigation*, vol. 95, no. 6, pp. 2501–2509, 1995.

[19] M. Halberstam, N. Cohen, P. Shlimovich, L. Rossetti, and H. Shamoon, "Oral vanadyl sulfate improves insulin sensitivity in NIDDM but not in obese nondiabetic subjects," *Diabetes*, vol. 45, no. 5, pp. 659–666, 1996.

[20] K. Cusi, S. Cukier, R. A. DeFronzo, M. Torres, F. M. Puchulu, and J. C. Redondo, "Vanadyl sulfate improves hepatic and muscle insulin sensitivity in type 2 diabetes," *Journal of Clinical Endocrinology and Metabolism*, vol. 86, no. 3, pp. 1410–1417, 2001.

[21] Z. M. Wang and X. Y. Ye, "Ashing method to determine the degree of carboxymethyl subsititution degrees of carboxymethyl chitosan," *Fenxihuaxue*, vol. 22, pp. 1121–1124, 1994.

[22] M. Li, J. J. Smee, W. J. Ding, and D. C. Crans, "Anti-diabetic effects of sodium 4-amino-2,6-dipicolinatodioxovanadium(V) dihydrate in streptozotocin-induced diabetic rats," *Journal of Inorganic Biochemistry*, vol. 103, no. 4, pp. 585–589, 2009.

[23] S. Mohammad, A. Taha, R. N. K. Bamezai, and N. Z. Baquer, "Modulation of glucose transporter (GLUT4) by vanadate and *Trigonella* in alloxan-diabetic rats," *Life Sciences*, vol. 78, no. 8, pp. 820–824, 2006.

[24] W. J. Ding, T. Hasegawa, H. Hosaka, D. Peng, K. Takahashi, and Y. Seko, "Effect of long-term treatment with vanadate in drinking water on KK mice with genetic non-insulin-dependent diabetes mellitus," *Biological Trace Element Research*, vol. 80, no. 2, pp. 159–174, 2001.

[25] L. H. Gao, W. P. Liu, B. L. Wang et al., "Effects of bis(α-furancarboxylato)oxovanadium(IV) on non-diabetic and streptozotocin-diabetic rats," *Clinica Chimica Acta*, vol. 368, no. 1-2, pp. 173–178, 2006.

[26] P. Leopardi, P. Villani, E. Cordelli, E. Siniscalchi, E. Veschetti, and R. Crebelli, "Assessment of the in vivo genotoxicity of vanadate: analysis of micronuclei and DNA damage induced in mice by oral exposure," *Toxicology Letters*, vol. 158, no. 1, pp. 39–49, 2005.

[27] G. B. Garcia, M. E. Biancardi, and A. D. Quiroga, "Vanadium (V)-induced neurotoxicity in the rat central nervous system: a histo-immunohistochemical study," *Drug and Chemical Toxicology*, vol. 28, no. 3, pp. 329–344, 2005.

[28] A. K. Srivastava, "Anti-diabetic and toxic effects of vanadium compounds," *Molecular and Cellular Biochemistry*, vol. 206, no. 1-2, pp. 177–182, 2000.

[29] K. H. Thompson, J. Lichter, C. LeBel, M. C. Scaife, J. H. McNeill, and C. Orvig, "Vanadium treatment of type 2 diabetes: a view to the future," *Journal of Inorganic Biochemistry*, vol. 103, no. 4, pp. 554–558, 2009.

[30] H. Sakurai, Y. Yoshikawa, and H. Yasui, "Current state for the development of metallopharmaceutics and anti-diabetic metal complexes," *Chemical Society Reviews*, vol. 37, no. 11, pp. 2383–2392, 2008.

[31] B. A. Reul, S. S. Amin, J. P. Buchet, L. N. Ongemba, D. C. Crans, and S. M. Brichard, "Effects of vanadium complexes with organic ligands on glucose metabolism: a comparison study in diabetic rats," *British Journal of Pharmacology*, vol. 126, no. 2, pp. 467–477, 1999.

[32] P. Buglyo, D. C. Crans, E. M. Nagy et al., "Aqueous chemistry of the vanadium^{III} (V^{III}) and the V^{III}–dipicolinate systems and a comparison of the effect of three oxidation states of vanadium compounds on diabetic hyperglycemia in rats," *Inorganic Chemistry*, vol. 44, no. 15, pp. 5416–542, 2005.

[33] J. Y. Guo, C. C. Han, and Y. M. Liu, "A contemporary treatment approach to both diabetes and depression by cordyceps sinensis: rich in vanadium," *Evidence-Based Complementary and Alternative Medicine*, vol. 7, no. 3, pp. 387–389, 2010.

Hindawi Publishing Corporation
Evidence-Based Complementary and Alternative Medicine
Volume 2011, Article ID 658906, 7 pages
doi:10.1155/2011/658906

Research Article

Changes of Photosynthetic Behaviors in *Kappaphycus alvarezii* Infected by Epiphyte

Tong Pang,[1,2] Jianguo Liu,[1] Qian Liu,[1] and Wei Lin[1]

[1] *Institute of Oceanology, Chinese Academy of Sciences, Qingdao, Shandong 266071, China*
[2] *Graduate University of Chinese Academy of Sciences, Beijing 10049, China*

Correspondence should be addressed to Jianguo Liu, jgliu@qdio.ac.cn

Received 18 January 2011; Accepted 25 May 2011

Epiphytic filamentous algae (EFA) were noted as a serious problem to reduce the production and quality of *K. alvarezii*. The morphological studies revealed that the main epiphyte on *K. alvarezii* was *Neosiphonia savatieri* in China. Though the harmful effects of EFA on the production of *K. alvarezii* have been reported, the detailed mechanism of the *N. savatieri* in limiting the production of *K. alvarezii* has not been studied yet. The present paper studied the effects of *N. savatieri* infection on photosynthetic behaviors in *K. alvarezii* by detecting chlorophyll fluorescence transient in vivo. The results revealed that damage of oxygen-evolving complex (OEC), decrease of active reaction centers (RCs), and the plastoquinone (PQ) pool as well as significant reduction in the performance indexes (PI) of PSII were caused by the infection of *N. savatieri*. The influence of *N. savatieri* on photosynthetic activity of *K. alvarezii* should be one of the important reasons to reduce the production of *K. alvarezii* infected by *N. savatieri*.

1. Introduction

Kappaphycus alvarezii (Solieriaceae, Rhodophyta) have been farmed as raw materials for carrageenan production in many countries since 1970s [1]. However, the carrageenan industry was faced with raw material problems relating to quality and quantity [2]. Epiphyte infection was one of the main reasons causing the decrease of quality and quantity of raw materials.

Epiphytic filamentous algae (EFA) were noted as a serious problem since early *K. alvarezii* cultivation [3]. The outbreaks of EFA (*Polysiphonia* sp., *Neosiphonia savatieri*) in Philippines and Malaysia, which caused a decrease of *K. alvarezii* production, were reported by Hurtado et al. [4] and Vairappan [5], respectively. Vairappan [5] noted that the outbreak of EFA correlated with drastic changes in seawater temperature and salinity from March to June and September to November. For further information, the infected *K. alvarezii* from carrageenophyte farms in the Philippines, Indonesia, Malaysia, and Tanzania were collected and studied to establish baseline information on the epiphyte's identity, density, symptoms, and secondary infection on the host seaweed [6]. Vairappan et al. [6] found out that the dominant epiphyte in these four culture areas was *N. apiculata*.

EFA comprise numerous species of filamentous algae that attach to the cortical layer of the host thalli. They leave the *K. alvarezii* stunted, rough, and poorly branched [7]. However, more detailed physiological mechanism of EFA on *K. alvarezii* has not been thoroughly studied yet. Anyway, EFA cannot do harm to host thalli without two channels: exchange of materials and energy metabolism. Photosynthesis is the basic anabolism and the only way light energy transfers into electric then chemical energy in plants. Thus, the process is vital for algal growth and survival. Chlorophyll a (Chl a) fluorescence analysis has been proved to be a very useful, noninvasive tool for plant study and more specifically the behavior of photosystem II [8–11]. Recent improvements in detecting the fluorescence signal through direct and time-resolved measurements could provide detailed information on the fast fluorescence rise. All oxygenic photosynthetic materials investigated so far show a polyphasic rise consisting of the basic steps from the "origin" (O) through two "inflections" (I_1, designated as J, and I_2, termed I) to a "peak" fluorescence [12]. The O-J-I-P polyphasic transient was found to change its shape according to changes in the environment conditions [11, 13, 14]. The analysis of the fast fluorescence rise according to the JIP test allows the derivation of several expressions leading to the actual description of a photosynthetic sample in a current physiological state [8]. Here, we presented the dominant EFA in China and its impacts on photosynthetic behaviors in

K. alvarezii by using continuously Chl a fluorescence, which were recorded in vivo with high time resolution and analyzed according to JIP-test.

2. Materials and Methods

2.1. Materials. Both infected and healthy green *K. alvarezii* were collected from Lian Bay, Hainan province, China (18°27′N, 110°5′E). Detritus on the materials were cleaned by seawater. Sections and dominant epiphytes was removed by a razor blade and then transferred to microscope slides. Slides were viewed at 100x magnification under optical microscope. Images were taken using an attached Cannon digital camera to investigate the morphological characters of epiphyte.

EFA-infected green *K. alvarezii* were precleaned with a soft brush to remove all the epiphytes and contaminants and then were brought to our laboratory beside the bay accompanied with the healthy ones to carry out the physiological studies.

2.2. Chl a Fluorescence Measurement. Algal thalli, about 3-4 mm in diameter and 3 cm in length, were selected, respectively, from infected and healthy green *K. alvarezii*. Each thallus was transferred into one capped transparent glass vial filled with seawater, and subsequently the vial was incubated at room temperature in darkness for 15 min. Chl a fluorescence of dark-adapted sample was measured by a plant efficiency analyzer (Handy PEA, Hansatech UK) and a single vial adapter for liquid-phase samples (HPEA/LPA2 Hansatech, UK). Red light of 650 nm wavelength (1500 μmol m^{-2} s^{-1}) was continuously provided for 1 s. The fluorescence transients were recorded in a time span from 10 μs to 1 s. For the first 300 μs, fluorescence was sampled at 10 μs intervals. The time resolution of digitization was then switched to slower acquisition rates as the kinetics of the fluorescence signal slow. Each group of experiments was done for four times.

2.3. Analysis of OJIP Chl a Fluorescence Induction Transient. Each transient was analyzed according to JIP-test [15–18] by utilizing the following data: the minimal fluorescence intensity (F_O) when all RCs are open, the maximal fluorescence intensity (F_m), assuming that excitation intensity is high enough to close all the RCs of PSII, and the fluorescence intensities at times 300 μs (F_K), 2 ms (F_J), and 30 ms (F_I). Based on the above data, the following parameters were then calculated: the relative variable fluorescence intensity at the J-step, $V_J \equiv (F_J - F_O)/(F_m - F_O)$; the relative variable fluorescence intensity at the K-step, $V_K \equiv (F_K - F_O)/(F_m - F_O)$; the approximated initial slope of the fluorescence transient, $M_O \equiv 4(F_K - F_O)/(F_m - F_O)$; the total complementary area above the O-J-I-P transient, Area $= \int_0^{tF_m} (F_m - F_t)dt$.

The normalized total complementary area above the O-J-I-P transient (reflecting single-turnover Q_A reduction events) is $S_m \equiv$ (Area)$/(F_m - F_O)$; the times of Q_A have been reduced to $Q_A{}^-$ in the time span from t_0 to t_{F_m}, $N \equiv S_m \times M_O \times (1/V_J)$.

The maximum quantum yield of primary photochemistry is $\varphi_{P_O} \equiv \mathrm{TR}_O/\mathrm{ABS} = [1 - (F_O/F_m)]$; the probability that a trapped exciton moves an electron into the electron transport chain beyond $Q_A{}^-$ is $\psi_O \equiv \mathrm{ET}_O/\mathrm{TR}_O = (1 - V_J)$; the quantum yield for electron transport is $\varphi_{E_O} \equiv \mathrm{ET}_O/\mathrm{ABS} = [1 - (F_O/F_m)] \times \psi_O$.

The specific energy fluxes (per Q_A-reducing PSII reaction center (RC)) for the energy absorbed is $\mathrm{ABS/RC} = M_O \times (1/V_J) \times (1/\varphi_{P_O})$; the energy trapped is $\mathrm{TR}_O/\mathrm{RC} = M_O \times (1/V_J)$; the electron transported is $\mathrm{ET}_O/\mathrm{RC} = M_O \times (1/V_J) \times \psi_O$; and the energy dissipated is $\mathrm{DI}_O/\mathrm{RC} = (\mathrm{ABS/RC}) - (\mathrm{TR}_O/\mathrm{RC})$.

Phenomenological energy fluxes (per excited cross-section (CS)) for absorption (ABS/CS), trapping (TR_O/CS), electron transport (ET_O/CS), and dissipation (DI_O/CS) were calculated by the following equations: $\mathrm{ABS/CS}_O \approx F_O$ (at $t = t_0$); $\mathrm{ABS/CS}_m \approx F_m$ (at $t = t_{F_m}$); $\mathrm{TR}_O/\mathrm{CS}_O = \varphi_{P_O} \times (\mathrm{ABS/CS}_O)$ (at $t = t_0$); $\mathrm{TR}_O/\mathrm{CS}_m = \varphi_{P_O} \times (\mathrm{ABS/CS}_m)$ (at $t = t_{F_m}$); $\mathrm{ET}_O/\mathrm{CS}_O = \varphi_{E_O} \times (\mathrm{ABS/CS}_O)$ (at $t = t_0$); $\mathrm{ET}_O/\mathrm{CS}_m = \varphi_{E_O} \times (\mathrm{ABS/CS}_m)$ (at $t = t_{F_m}$); $\mathrm{DI}_O/\mathrm{CS}_O = (\mathrm{ABS/CS}_O) - (\mathrm{TR}_O/\mathrm{CS}_O)$ (at $t = 0$); $\mathrm{DI}_O/\mathrm{CS}_m = (\mathrm{ABS/CS}_m) - (\mathrm{TR}_O/\mathrm{CS}_m)$ (at $t = t_{F_m}$).

The density of reaction centers per exited cross-section was computed by the equations below: $\mathrm{RC/CS}_O = \varphi_{P_O} \times (V_J/M_O) \times (\mathrm{ABS/CS}_O)$ (at $t = 0$); $\mathrm{RC/CS}_m = \varphi_{P_O} \times (V_J/M_O) \times (\mathrm{ABS/CS}_m)$ (at $t = t_{F_m}$).

The performance indexes for absorption ($\mathrm{PI}_{\mathrm{ABS}}$) and per excited cross-section ($\mathrm{PI}_{\mathrm{CS}}$) were calculated as follows: $\mathrm{PI}_{\mathrm{ABS}} \equiv (\mathrm{RC/ABS}) \times [\varphi_{P_O}/(1 - \varphi_{P_O})] \times [\psi_O/(1 - \psi_O)]$; $\mathrm{PI}_{\mathrm{CS}_O} \equiv (\mathrm{RC/CS}_O) \times [\varphi_{P_O}/(1 - \varphi_{P_O})] \times [\psi_O/(1 - \psi_O)]$ (at $t = t_0$); $\mathrm{PI}_{\mathrm{CS}_m} \equiv (\mathrm{RC/CS}_m) \times [\varphi_{P_O}/(1 - \varphi_{P_O})] \times [\psi_O/(1 - \psi_O)]$ (at $t = t_{F_m}$).

2.4. Chlorophyll a Measurement. Cleaned algal thalli, 3-4 mm in diameter and 0.5 g fresh weight, were selected, respectively, from infected and healthy green *K. alvarezii*. The thalli were homogenized in 5 mL of 95% ethanol for 15 min then were centrifuged at 1000 rpm for 5 min. After centrifugation, 4 mL supernatant was transferred into a colorimetric tube and diluted to 25 mL with 95% ethanol. Absorbance was measured by 722 s spectrophotometer (Shanghai precision & scientific instrument CO., LTD) at 665 nm and 649 nm. Each group of experiments was done for 3 times. Pigment concentration was calculated according to Wintermans and de Mots [19],

$$\text{Chl a } (\mu\text{g/g}) = (13.7\mathrm{OD}_{665\,\mathrm{nm}} - 5.76\mathrm{OD}_{649\,\mathrm{nm}}) \times \frac{\text{dilution rate}}{0.5\,\mathrm{g}}. \quad (1)$$

2.5. Phycobiliprotein Measurement. Cleaned algal thalli, 3-4 mm in diameter and 0.5 g fresh weight, were selected, respectively, from infected and healthy green *K. alvarezii*. The thalli were chopped into 3 mm^3 and then homogenized in 3 mL of 10 mM $CaCl_2$ solution, which was stocked in 4°C for 12 hours prior to the experiment, for 15 min. Subsequently,

the homogenized solution was transferred into a colorimetric tube then diluted to 25 mL with 10 mM $CaCl_2$. After that, the colorimetric tubes were incubated at 4°C in dark for 48 hours. Absorbance of the supernatant at 562 nm, 615 nm, and 652 nm was measured by 722 s spectrophotometer. Each group of experiments was done for 3 times. Phycobiliproteins were calculated according to Venkataraman [20] as below:

$$\text{Phycocyanin (PC)(mg/g)} = \frac{(\text{OD}_{615\,\text{nm}} - 0.474\text{OD}_{652\,\text{nm}})}{5.34} \times \frac{\text{dilution rate}}{0.5\,\text{g}}, \quad (2)$$

$$\text{Phycoerythrin (PE)(mg/g)} = \frac{(\text{OD}_{562\,\text{nm}} - 2.41\text{PC} - 0.849\text{APC})}{9.62} \times \frac{\text{dilution rate}}{0.5\,\text{g}}, \quad (3)$$

$$\text{Allophycocyanin (APC)(mg/g)} = \frac{(\text{OD}_{562\,\text{nm}} - 0.208\text{OD}_{615\,\text{nm}})}{5.09} \times \frac{\text{dilution rate}}{0.5\,\text{g}}, \quad (4)$$

$$\text{Phycobiliprotein (PEP)(mg/g)} = \text{PC} + \text{APC} + \text{PE}. \quad (5)$$

2.6. Statistics. Statistical analyses were performed using SPSS 13.0 software (SPSS Inc., Chicago, USA). Independent sample t-test at $P < 0.05$ was used to test the significant differences between the infected and the healthy controls.

3. Results

3.1. Dominant Epiphytes on the K. alvarezii. The dominant epiphytes are brownish red and rigid and have percurrent main axes that reach 2–15 mm. The epiphyte thalli grow on the surface of *K. alvarezii* solitarily and close to each other in the peak season (Figure 1(a)). A basal attachment system of the axis is at first composed of a primary rhizoid only (Figure 1(b)), and later forms a tuft of rhizoids by the production of secondary rhizoids that cut off from the pericentral cells of lower segments (Figure 1(c)). The primary rhizoid often penetrates through the outer cortical cells of *K. alvarezii* to medullary layer (Figure 1(b)). The main axes are 60–250 μm in diameter, with segment length 0.5–1.0-fold of diameters. The axes abruptly taper at the apices. Each vegetative segment consists of 4 pericentral cells and lacks cortical cells. The axis produces vegetative trichoblasts or first-order branches from each segment in a spiral manner. Tetrasporangia are formed in the distal segments, one per segment, in a spiral manner. Mature tetrasporangia are 90–110 μm in diameter and protuberant (Figure 1(d)). Procarpial trichoblasts replace vegetative trichoblasts or lateral branches and appear on the distal portion of branches. Each procarpial trichoblast produces a single procarp on the suprabasal segment. The procarp consists of a three-celled carpogonial branch and initials of two sterile groups, one two-celled and lateral, and the other one-celled and basal (Figure 1(e)). Mature cystocarps are broadly ovoid or napiform with 200–350 μm × 200–300 μm in size. Spermatangia are produced on a lateral of fertile trichoblasts that issues from the suprabasal segment. Mature spermatangial branches are conical with 130–200 μm × 45–60 μm in size. They have a one-celled sterile suprabasal segment and the basal segment embedded in the parental branch (Figure 1(f)).

Rhizoids cut off from the pericentral cells of the lower segments, the production of lateral branch in a spiral arrangement, three-celled carpogonial branches, spermatangial trichoblasts with a sterile lateral, and spiralled tetrasporangia found in the epiphyte ally it with *Neosiphonia* than *Polysiphonia* [21]. In addition to these features, the morphology and size of the main axes, tetrasporangia, carpogonial, and spermatangial all ally it with *N. savatieri* than *N. apiculata* [22, 23]. Therefore, based on the results above the dominant EFA in Lian Bay, Hainan province, China are *N. savatieri*.

3.2. Fast Chl a Fluorescence Kinetics, O-JIP. Figure 2 showed the fast Chl a fluorescence induction kinetics of both the healthy and the infected *K. alvarezii*. When the thalli of *K. alvarezii* are exposed to saturating actinic light, the Chl a fluorescence curves start from the initial F_O intensity and increase to a peak (P or F_m). When the curves were plotted on logarithmic scale, two intermediate steps F_J (about 2 ms) and F_I (about 30 ms) can be found between F_O and F_m. To visualize the comparative effects of *N. savatieri* infection on each step, the curves were replotted as relative variable fluorescence, $V_t = (F_t - F_O)/(F_m - F_O)$ in the insert chart of Figure 2. Based on the insert chart in Figure 2, certain increases in the peaks at K-, J-, and I-steps were found in the *N. savatieri*-infected *K. alvarezii* compared with the healthy seaweed.

3.3. Donor and Acceptor Side of PSII Reaction Center. Increase amplitude in K-step was used as a specific indicator of damage to the oxygen-evolving complex (OEC) [12, 17, 24, 25]. The amplitude in the K-step of *K. alvarezii*, expressed as the ratio V_K, was shown in Table 1. An obvious increase in V_K was observed in *N. savatieri*-infected *K. alvarezii*, which reflected that the OEC of host was at least partly damaged. Meanwhile, the number of RCs per excited cross-section (RC/CS_O or RC/CS_m) was reduced in *K. alvarezii* after *N. savatieri* infection. V_J was used as an indicator of the proportion of active reaction centers (RCs) [12, 15, 17]. The increase of V_J (Table 1) further indicated that the number of active RCs in the *N. savatieri*-infected seaweed obviously decreased.

The approximated initial slope of the fluorescence transient (M_O), a profile of the maximal reduction rate of Q_A, increased by 89.5% in *N. savatieri*-infected *K. alvarezii* (Table 1). However, the normalized total complementary area above the O-J-I-P transient (S_m), the energy needed to reduce all the Q_A, decreased by 29.5% (Table 1). The increase in M_O and decrease in S_m was one indicator of the decrease in the plastoquinone (PQ) pool [12, 15, 17, 25]. Therefore, the changes of the M_O and S_m in *K. alvarezzi,* after *N. savatieri*

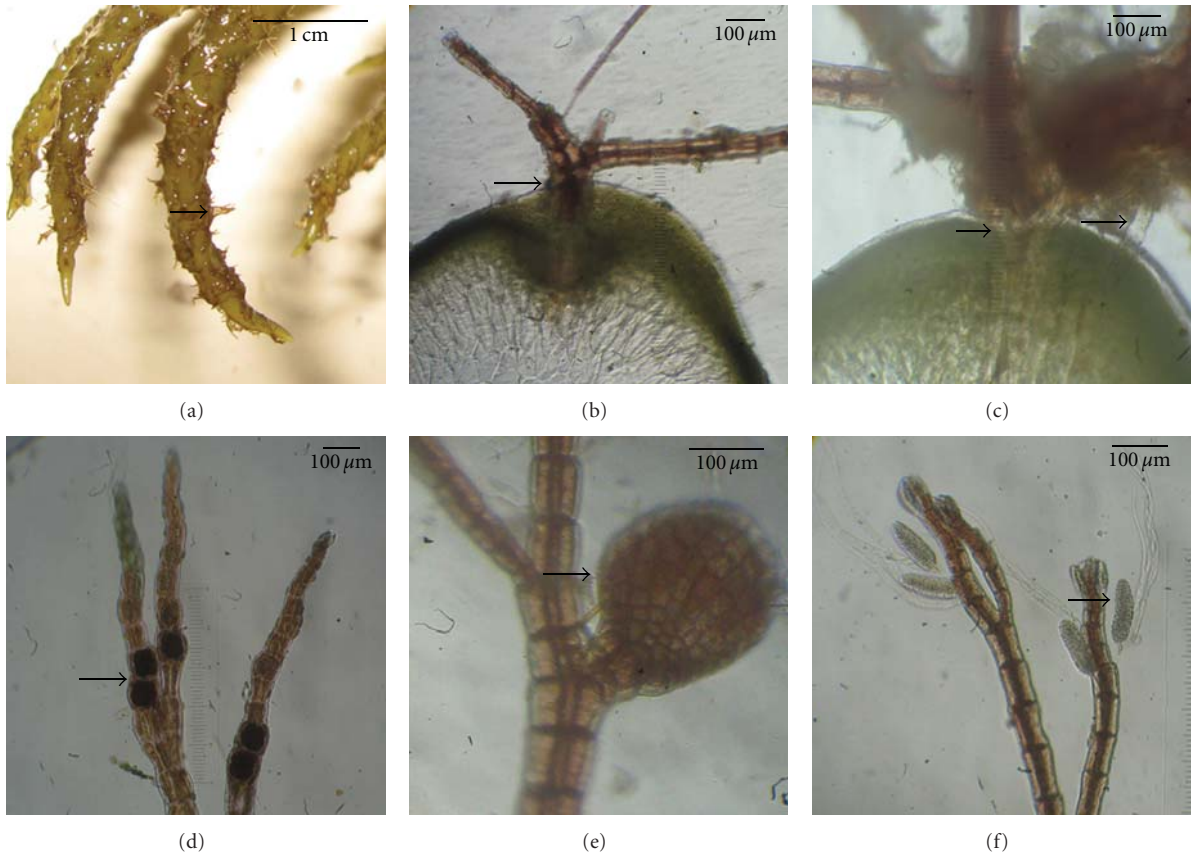

Figure 1: Epiphytes on the *K. alvarezii.* (a) Epiphytes on the surface of *K. alvarezii*. (b) Epiphyte on the transverse section of *K. alvarezii* and a single primary rhizoid penetrate through the outer cortical cells to inner cortical cells. (c) Epiphyte on the transverse section of *K. alvarezii* and a tuft of secondary rhizoids that are cut off from the pericentral cells of lower segments, (d) tetrasporangial branches of epiphyte, (e) broadly ovoid cystocarp of epiphyte, and (f) spermatangial branches of epiphyte.

Table 1: Profiles reflecting the donor and acceptor side of PSII in the healthy and infected *K. alvarezii.*

	V_K*	RC/CS$_O$	RC/CS$_m$	V_J*	M_O*	S_m*	N
Healthy	0.14 ± 0.03	299 ± 61	695 ± 150	0.49 ± 0.08	0.57 ± 0.11	23.73 ± 2.29	27.52 ± 2.08
Infected	0.27 ± 0.06	259 ± 30	606 ± 70	0.61 ± 0.07	1.08 ± 0.26	16.73 ± 4.54	28.25 ± 3.59
RV	1.929	0.866	0.872	1.245	1.895	0.705	1.027

Values present mean ± SE of four replicates, *indicates significant differences at $P < 0.05$ between the healthy and infected *K. alvarezii*, and RV indicates the relative value of infected sample to the healthy sample.

infection showed the plastoquinone (PQ) pool of the host decreased. What is more, $N \equiv S_m \times M_O \times (1/V_J)$, the negligible change (2.7%) in the turnover number of $Q_A(N)$ were induced by the integrated effects of changes in M_O, V_J, and S_m.

3.4. Energy Distribution via PSII Reaction Center. After *N. savatieri* infection, the energy fluxes via PSII reaction centers (RCs) in *K. alvarezii* significantly changed. The light energy for absorption (ABS/RC) and trapping (TR$_O$/RC) in *N. savatieri* infected *K. alvarezii*-increased by 49.5% and 50% (Table 2). However, the specific energy fluxes (per Q_A-reducing PSII reaction center (RC)) for the energy dissipated (DI$_O$/RC) increased significantly (Table 2), and the energy for electron transported per reaction center (ET$_O$/RC) in the *N. savatieri*-infected *K. alvarezii* did not change so significantly. Therefore, most of the energy trapped was not used for photosynthesis but dissipated by the reaction centers.

Similarly, the energy distribution was further expressed via excited cross-section. Regardless of Chl a fluorescence at t_{F_O} or t_{F_m}, the phenomenological energy fluxes per excited cross section (CS) for absorption (ABS/CS), trapping (TR$_O$/CS), and dissipation (DI$_O$/CS) in *K. alvarezii* increased by 27% (Table 3) after *N. savatieri* infection. The increase in the DI$_O$/CS acted as a counterbalance to the increase of TR$_O$/CS. Therefore, the change of electron transport per excited cross section (ET$_O$/CS) in *K. alvarezzii* after *N. savatieri* infection was negligible (Table 3).

Table 2: Profiles reflecting energy flux per reaction center in the healthy and infected *K. alvarezii.*

	ABS/RC*	TR_O/RC*	DI_O/RC*	ET_O/RC
Healthy	2.04 ± 0.08	1.16 ± 0.05	0.88 ± 0.04	0.59 ± 0.07
Infected	3.05 ± 0.50	1.74 ± 0.29	1.30 ± 0.24	0.66 ± 0.13
RV	1.495	1.500	1.477	1.119

Values present mean ± SE of four replicates, *indicates significant differences at $P < 0.05$ between the healthy and infected *K. alvarezii*, and RV indicates the relative value of infected sample to the healthy sample.

Table 3: Profiles reflecting energy flux per excited cross section in the healthy and infected *K. alvarezii.*

		ABS/CS	TR_O/CS	DI_O/CS	ET_O/CS
Heathy	$t = 0$	614 ± 147	349 ± 86	264 ± 61	174 ± 17
Infected	$t = 0$	778 ± 68	445 ± 33	333 ± 41	170 ± 27
RV	$t = 0$	1.267	1.275	1.261	0.977
Healthy	$t = t_{F_m}$	1427 ± 354	812 ± 207	614 ± 147	405 ± 44
Infected	$t = t_{F_m}$	1821 ± 140	1042 ± 94	778 ± 68	401 ± 84
RV	$t = t_{F_m}$	1.276	1.283	1.267	0.999

Values present mean ± SE of four replicates and RV indicates the relative value of infected sample to the healthy sample.

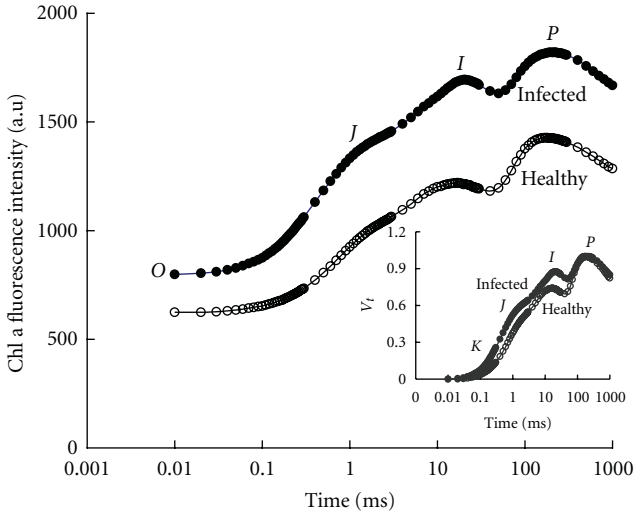

Figure 2: Changes of the fluorescence kinetics, O-J-I-P, plotted on logarithmic time scale from 10 μs to 1 s of *N. savatieri*-infected *K. alvarezii* (the original data without any normalization). In the insert chart, a relative variable fluorescence, $V_t = (F_t - F_O)/(F_m - F_O)$ from 10 μs to 1 s, is shown. Values present mean of four replicates.

3.5. Performance Indexes (PI) and Quantum Yields. The probability that trapped exciton moves an electron into the electron transport chain beyond $Q_A^-(\psi_O)$, and the quantum yield for electron transport (φ_{E_O}) decreased by 23.5% and 24.1% in *N. savatieri*-infected *K. alvarezii* comparing with the healthy control (Table 4). No significant changes in the maximum quantum yield of primary photochemistry (φ_{P_O}) were found in the infected *K. alvarezii* compared with the control. However, the comprehensive performance indexes (PI) significantly decreased (Table 4). The average PI_{ABS}, PI_{CS_O}, and PI_{CS_m} in *N. savatieri*-infected *K. alvarezii* decreased by 57.7%, 44%, and 42.9%, respectively, compared with the healthy control (Table 4).

3.6. Photosynthetic Pigments. Chl a and phycobiliprotein content in *K. alvarezii* changed significantly (Table 5) after the seaweed was infected by *N. savatieri* ($P < 0.05$). The content of Chl a, phycocyanin (PC), phycoerythrin (PE), allophycocyanin (APC), and phycobiliprotein (PBP) in *N. savatieri*-infected *K. alvarezii* increased about 56.4%, 104.5%, 146.2%, 139.4%, and 130.9% compared with the healthy control, respectively (Table 5). The pigments increase in *N. savatieri*-infected *K. alvarezii* (Table 5) was much higher than the increase of ABS/CS and TR_O/CS (Table 4). The above results indicated a relative decrease in the light energy absorbed per pigment.

4. Discussion

The changes in PSII performance of the photosynthetic apparatus caused by environmental stress or senescence have been explored widely by applying the chlorophyll fluorescence technique in higher plants [8, 26–31]. However, there is not detailed knowledge on the influence of epiphyte on the photosynthetic activity of its host. In the present study, we have demonstrated the response of PSII of *K. alvarezii* to *N. savatieri* infection. The Chl a fluorescence transient recorded with high time resolution was analyzed by the JIP-test in order to quantify the PSII behaviors in *K. alvarezii* after *N. savatieri* infection.

φ_{P_O} changed slightly; however, PI decreased significantly in *N. savatieri*-infected *K. alvarezii*. The PI was calculated from three components, which depend on the reaction center density, the trapping efficiency, and the electron transport efficiency. The above changes of PI showed that photosynthesis in the infected *K. alvarezii* was inhibited which could partly explain the phenomenon of stunted, rough, and poorly branched carrageenan producing seaweed arisen by epiphyte infection [7]. Moreover, our results proved that PI is more sensitive to environmental change than φ_{P_O}

Table 4: Performance indexes (PI) and quantum yields in the healthy and epiphyte-infected *K. alvarezii.*

	φ_{P_O}	ψ_O	φ_{E_O}	PI_{ABS}*	PI_{CS_O}*	PI_{CS_m}*
Healthy	0.57 ± 0.01	0.51 ± 0.08	0.29 ± 0.04	0.71 ± 0.23	411 ± 43	952 ± 97
Infected	0.57 ± 0.02	0.39 ± 0.07	0.22 ± 0.05	0.30 ± 0.15	230 ± 95	544 ± 237
RV	1	0.765	0.759	0.423	0.56	0.571

Values present mean ± SE of four replicates, *indicates significant differences at $P < 0.05$ between the healthy and infected *K. alvarezii*, and RV indicates the relative value of infected sample to the healthy sample.

Table 5: Effects of *N. savatieri* on the photosynthetic pigments of *K. alvarezii.*

	Chl a(μg/g)*	PC(mg/g)*	PE(mg/g)*	APC(mg/g)*	PBP(mg/g)*
Healthy	45.6 ± 6.8	0.22 ± 0.01	0.13 ± 0.01	0.33 ± 0.02	0.68 ± 0.04
Infected	71.3 ± 1.9	0.45 ± 0.03	0.32 ± 0.03	0.79 ± 0.07	1.57 ± 0.13
RV	1.564	2.045	2.462	2.394	2.309

Values present mean ± SE of four replicates, *indicates significant differences at $P < 0.05$ between the healthy and infected *K. alvarezii*, RV indicates the relative value of infected sample to the healthy sample.

and correlates well with plant vigor and performance again that agrees with the research by Hermans et al. [32].

Chlorophyll and phycobiliprotein content in *N. savatieri*-infected *K. alvarezii* was increased to 156% and 230% (Table 5). Therefore, the energy fluxes for absorption and trapping in *N. savatieri*-infected *K. alvarezii* were increased (Tables 2 and 3). However, the negligible changes of ET_O/CS (Table 3) and φ_{P_O} (Table 4) indicated that the trapped energy was not efficiently used for electron transport. The damage of OEC, decrease in RC number, and reduction of PQ pool could further explain why the light trapped in *N. savatieri*-infected *K. alvarezii* was not sufficiently consumed timely for photosynthesis.

The side impacts of epiphyte on *K. alvarezii* growth were not only limited to photochemical reactions. Largo et al. [33] reported that light intensity of less than 50 μmoL photon m^{-2} could induce the decay of *K. alvarezii*. *N. savatieri* occupied the outsurface of *K. alvarezii* and shielded the host from getting enough light. Moreover, both *N. savatieri* and *K. alvarezii* all belonged to Rhodophyta species and owned similar types of photosynthetic pigments that aggravated the competition of light absorption between them. The competition between *N. savatieri* and *K. alvarezii* seriously decreased the ambient light. However, the infected *K. alvarezii* tried to acclimate itself to the low-light conditions by increasing its photosynthetic pigments, especially phycobiliprotein (Table 5). Unfortunately, the adaptive regulation seemed to be meaningless for EFA-infected *K. alvarezii* because of the decrease in active RC number, damage of OEC, and reduction of PQ pool as mentioned above. Glenn and Doty [34] reported that culture of *K. alvarezii* required high levels of water motion provided by strong and consistent trade winds. *N. savatieri*, covered on the surface of *K. alvarezii*, were bound to reduce the water motion nearby the *K. alvarezii* as well as the materials exchange between *K. alvarezii* and external environment. Therefore, the production of oxygen by the photosynthesis of *N. savatieri* and *K. alvarezii* was easy to cause the surplus of oxygen during the daytime. Moreover, the consumption of oxygen by the respiration of *N. savatieri* and *K. alvarezii* was easy to cause the insufficiency of oxygen during the nighttime. In addition, the epiphyte *N. savatieri* competed with host *K. alvarezii* for absorbing nutrients (N, P, CO_2, and other mineral elements). Most of the nutrients dissolving in the water body were first filtered by *N. savatieri* before reaching to *K. alvarezii*, and so nutrient deficiency inevitably occurred in *K. alvarezii* after EFA infection. Dense *N. savatieri* were severe stress for the metabolism of *K. alvarezii* by shading, high O_2 concentrations in the light, anoxic conditions in the dark, and competition of nutrients. Therefore, heavy decay in *K. alvarezii* was usually found when the seaweed was infected by *N. savatieri*.

In conclusion, the dominant EFA on *K. alvarezii* in Lian Bay, Hainan province were *N. savatieri*. Damage of OECs, decrease of active RCs and the PQ pool and significant reduction in the performance indexes (PI) of PSII were caused by the infection of *N. savatieri* although the seaweed acclimated itself to the low-light condition by increasing its photosynthetic pigments to absorb more light energy. The influence of *N. savatieri* on photosynthetic activity of *K. alvarezii* was one of the important reasons to reduce the production of *K. alvarezii.*

Acknowledgments

The authors wish to thank Mr. Zhaoliang Zheng from Lingshui Haotian Company for the provision of algae. This work was supported by the National Natural Science Foundation of China (30771639), Special Project for Marine Public Welfare Industry (200705010).

References

[1] M. S. Doty and V. B. Alvarez, "Status, problem, advances and economics of Eucheuma farms," *Marine Technology Society Journal*, vol. 9, no. 4, pp. 30–35, 1975.

[2] E. Ask and V. Azanza, "Advances in cultivation technology of commercial eucheumatoid species: a review with suggestions for future research," *Aquaculture*, vol. 206, no. 3-4, pp. 257–277, 2002.

[3] H. S. Parker, "The culture of the red algal genus Eucheuma in the Philippines," *Aquaculture*, vol. 3, no. 4, pp. 425–439, 1974.

[4] A. Q. Hurtado, A. T. Critchley, A. Trespoey, and G. B. Lhonneur, "Occurrence of *Polysiphonia* epiphytes in *Kappaphycus* farms at Calaguas Is., Camarines Norte, Phillippines," *Journal of Applied Phycology*, vol. 18, no. 3–5, pp. 301–306, 2006.

[5] C. S. Vairappan, "Seasonal occurrences of epiphytic algae on the commercially cultivated red alga *Kappaphycus alvarezii* (Solieriaceae, Gigartinales, Rhodophyta)," *Journal of Applied Phycology*, vol. 18, no. 3–5, pp. 611–617, 2006.

[6] C. S. Vairappan, C. S. Chung, A. Q. Hurtado, F. E. Soya, G. B. Lhonneur, and A. Critchley, "Distribution and symptoms of epiphyte infection in major carrageenophyte-producing farms," *Journal of Applied Phycology*, vol. 2, no. 5, pp. 27–33, 2009.

[7] E. Ask, *Cottonii and Spinosum Cultivation Handbook*, FMC Food Ingredients Division, Philadelphia, Pa, USA, 1999.

[8] K. J. Appenroth, J. Stöckel, A. Srivastava, and R. J. Strasser, "Multiple effects of chromate on the photosynthetic apparatus of *Spirodela polyrhiza* as probed by OJIP chlorophyll a fluorescence measurements," *Environmental Pollution*, vol. 115, no. 1, pp. 49–64, 2001.

[9] G. H. Krause and E. Weis, "Chlorophyll fluorescence and photosynthesis: the basics," *Annual Review of Plant Physiology and Plant Molecular Biology*, vol. 42, no. 1, pp. 313–349, 1991.

[10] Govindjee, "Sixty-three years since Kautsky: chlorophyll a fluorescence," *Australian Journal of Plant Physiology*, vol. 22, no. 2, pp. 131–160, 1995.

[11] D. Lazar, "Chlorophyll a fluorescence induction," *Biochimica et Biophysica Acta*, vol. 1412, pp. 1–28, 1999.

[12] R. J. Strasser, M. Tsimilli-Michael, and A. Srivastava, "Analysis of the chlorophyll a fluorescence transient," in *Chlorophyll a Fluorescence: A Signature of Photosynthesis*, G. C. Papageorgiou and Govindjee, Eds., pp. 321–362, Springer, Rotterdam, The Netherlands, 2004.

[13] A. Srivastava and R. J. Strasser, "Constructive and destructive actions of light on the photosynthetic apparatus," *Journal of Scientific and Industrial Research*, vol. 56, no. 3, pp. 133–148, 1997.

[14] A. J. Clark, W. Landolt, J. B. Bucher, and R. J. Strasser, "Beech (*Fagus sylvatica*) response to ozone exposure assessed with a chlorophyll a fluorescence performance index," *Environmental Pollution*, vol. 109, no. 3, pp. 501–507, 2000.

[15] B. J. Strasser and R. J. Strasser, "Measuring fast fluorescence transients to address environmental questions: the JIP test," in *Photosynthesis: From Light to Biosphere*, P. Mathis, Ed., pp. 977–980, Kluwer Academic, Dodrecht, The Netherlands, 1995.

[16] A. Srivastava and R. J. Strasser, "Greening of peas: parallel measurements of 77 K emission spectra, OJIP chlorophyll a fluorescence transient, period four oscillation of the initial fluorescence level, delayed light emission, and P700," *Photosynthetica*, vol. 37, no. 3, pp. 365–392, 1999.

[17] B. J. Strasse, A. Srivastava, and M. Tsimilli-Michael, "The fluorescence transient as a tool to characterize and screen photosynthetic samples," in *Probing Photosynthesis: Mechanism, Regulation and Adaptation*, M. Yunus, U. Pathre, and P. Mohanty, Eds., pp. 445–483, Taylor and Francis, London, UK, 2000.

[18] R. J. Strasser and M. Tsimilli-Michael, "Structure function relationship in the photosynthetic apparatus: a biophysical approach," in *Biophysical Processes in Living Systems*, P. Pardha Saradhi, Ed., pp. 271–303, Science Publishers, Enfield, NH, USA, 2001.

[19] J. F. G. M. Wintermans and A. de Mots, "Spectrophotometric characteristics of chlorophylls a and b and their phenophytins in ethanol," *Biochimica et Biophysica Acta*, vol. 109, no. 2, pp. 448–453, 1965.

[20] L. V. Venkataraman, *Bluegreen Alga Spirulina*, Department of Science and Technology, New Delhi, India, 1983.

[21] M. S. Kim and I. K. Lee, "*Neosiphonia* flavimarina gen. et sp. nov. with a taxonomic reassessment of the genus *Polysiphonia* (Rhodomelaceae, Rhodophyta)," *Phycological Research*, vol. 47, no. 4, pp. 271–281, 1999.

[22] M. Masuda, T. Abe, S. Kawaguchi, and S. M. Phang, "Taxonomic notes on marine algae from Malaysia. VI. Five species of ceramiales (Rhodophyceae)," *Botanica Marina*, vol. 44, no. 5, pp. 467–477, 2001.

[23] M. Tani, Y. Yamagishi, M. Masuda, K. Kogame, S. Kawaguchi, and S. M. Phang, "Taxonomic notes on marine algae from Malaysia. IX. Four species of rhodophyceae, with the description of chondria decidua sp. nov," *Botanica Marina*, vol. 46, no. 1, pp. 24–35, 2003.

[24] B. Guissé, A. Srivastava, and R. J. Strasser, "The polyphasic rise of the chlorophyll a fluorescence (O-K-J-I-P) in heat stressed leaves," *Archives des Sciences Genève*, vol. 48, pp. 147–160, 1995.

[25] B. J. Strasser, "Donor side capacity of photosystem II probed by chlorophyll a fluorescence transients," *Photosynthesis Research*, vol. 52, no. 2, pp. 147–155, 1997.

[26] J. Dai, H. Gao, Y. Dai, and Q. Zou, "Changes in activity of energy dissipating mechanisms in wheat flag leaves during senescence," *Plant Biology*, vol. 6, no. 2, pp. 171–177, 2004.

[27] C. D. Jiang, H. Y. Gao, and Q. Zou, "Changes of donor and acceptor side in photosystem 2 complex induced by iron deficiency in attached soybean and maize leaves," *Photosynthetica*, vol. 41, no. 2, pp. 267–271, 2003.

[28] C. Lu and J. Zhang, "Changes in photosystem II function during senescence of wheat leaves," *Physiologia Plantarum*, vol. 104, no. 2, pp. 239–247, 1998.

[29] C. M. Lu, N. W. Qiu, B. S. Wang, and J. H. Zhang, "Salinity treatment shows no effects on photosystem II photochemistry, but increases the resistance of photosystem II to heat stress in halophyte Suaeda salsa," *Journal of Experimental Botany*, vol. 54, no. 383, pp. 851–860, 2003.

[30] E. H. Murchie, Y. Z. Chen, S. Hubbart, S. B. Peng, and P. Horton, "Interactions between senescence and leaf orientation determine in situ patterns of photosynthesis and photoinhibition in field-grown rice," *Plant Physiology*, vol. 119, no. 2, pp. 553–563, 1999.

[31] L. B. Thach, A. Shapcott, S. Schmidt, and C. Critchley, "The OJIP fast fluorescence rise characterizes Graptophyllum species and their stress responses," *Photosynthesis Research*, vol. 94, no. 2-3, pp. 423–436, 2007.

[32] C. Hermans, M. Smeyers, R. M. Rodriguez, M. Eyletters, R. Strasser, and J. P. Delhaye, "Quality assessment of urban's trees: a comparative study of physiological characterisation, airborne imaging and on site fluorescence monitoring by the OJIP-test," *Journal of Plant Physiology*, vol. 160, no. 1, pp. 81–90, 2003.

[33] D. B. Largo, K. Fukami, T. Nishijima, and M. Ohno, "Laboratory-induced development of the *ice-ice* disease of the farmed red algae *Kappaphycus alvarezii* and *Eucheuma denticulatum* (Solieriaceae, Gigartinales, Rhodophyta)," *Journal of Applied Phycology*, vol. 7, no. 6, pp. 539–543, 1995.

[34] E. P. Glenn and M. S. Doty, "Water motion affects the growth rates of *Kappaphycus alvarezii* and related red seaweeds," *Aquaculture*, vol. 108, no. 3-4, pp. 233–246, 1992.

Hindawi Publishing Corporation
Evidence-Based Complementary and Alternative Medicine
Volume 2011, Article ID 984080, 11 pages
doi:10.1155/2011/984080

Research Article

Identification and Characterization of Cell Wall Proteins of a Toxic Dinoflagellate *Alexandrium catenella* Using 2-D DIGE and MALDI TOF-TOF Mass Spectrometry

Da-Zhi Wang, Hong-Po Dong, Cheng Li, Zhang-Xian Xie, Lin Lin, and Hua-Sheng Hong

State Key Laboratory of Marine Environmental Science, Environmental Science Research Centre, Xiamen University, Xiamen 361005, China

Correspondence should be addressed to Da-Zhi Wang, dzwang@xmu.edu.cn

Received 20 January 2011; Accepted 30 June 2011

The cell wall is an important subcellular component of dinoflagellate cells with regard to various aspects of cell surface-associated ecophysiology, but the full range of cell wall proteins (CWPs) and their functions remain to be elucidated. This study identified and characterized CWPs of a toxic dinoflagellate, *Alexandrium catenella*, using a combination of 2D fluorescence difference gel electrophoresis (DIGE) and MALDI TOF-TOF mass spectrometry approaches. Using sequential extraction and temperature shock methods, sequentially extracted CWPs and protoplast proteins, respectively, were separated from *A. catenella*. From the comparison between sequentially extracted CWPs labeled with Cy3 and protoplast proteins labeled with Cy5, 120 CWPs were confidently identified in the 2D DIGE gel. These proteins gave positive identification of protein orthologues in the protein database using *de novo* sequence analysis and homology-based search. The majority of the prominent CWPs identified were hypothetical or putative proteins with unknown function or no annotation, while cell wall modification enzymes, cell wall structural proteins, transporter/binding proteins, and signaling and defense proteins were tentatively identified in agreement with the expected role of the extracellular matrix in cell physiology. This work represents the first attempt to investigate dinoflagellate CWPs and provides a potential tool for future comprehensive characterization of dinoflagellate CWPs and elucidation of their physiological functions.

1. Introduction

The dinoflagellates are a diverse group of unicellular algae that comprise a large part of the marine phytoplankton [1]. They are not only important primary producers and an important part of the food chain in the marine ecosystem, but also the major causative species of harmful algal blooms (HABs) in the coastal zone [2]. Moreover, many dinoflagellate species can produce various potent toxins that impact human health through the consumption of contaminated shellfish, coral reef fish, and finfish or through water or aerosol exposure [3]. In the past few decades, much effort has been devoted to the study of HABs and dinoflagellate toxins. However, many aspects of them are still not well elucidated due to the unusual physiological and molecular features of dinoflagellates, and this has impeded our understanding of dinoflagellate-caused HABs and subsequently their monitoring, mitigation, and prevention [4].

Dinoflagellates typically have an outer covering called the theca or amphiesma (Figure 1), which consists of a continuous outermost membrane, an outer plate membrane, and a single-membrane bounded thecal vesicle [5, 6]. Inside this vesicle, a number of cellulosic thecal plates are subtended by a pellicular layer. Thecal plates usually consist primarily of cellulose and polysaccharides with a small amount of proteins. Although much effort has been devoted to understanding the cell wall ultrastructure of dinoflagellates using electron microscopic and cytochemical approaches, molecular information on cell wall biogenesis and dynamics is lacking.

It is known that a number of proteins and enzymes reside on the cell wall and outer membrane of phytoplankton, such as high-affinity binding proteins [7, 8], transporters [9–14], stress proteins [15], signaling proteins [16], and ectoenzymes [17–25]. These proteins play important roles ranging from nutrient utilization, defense, signaling, and cell adhesion

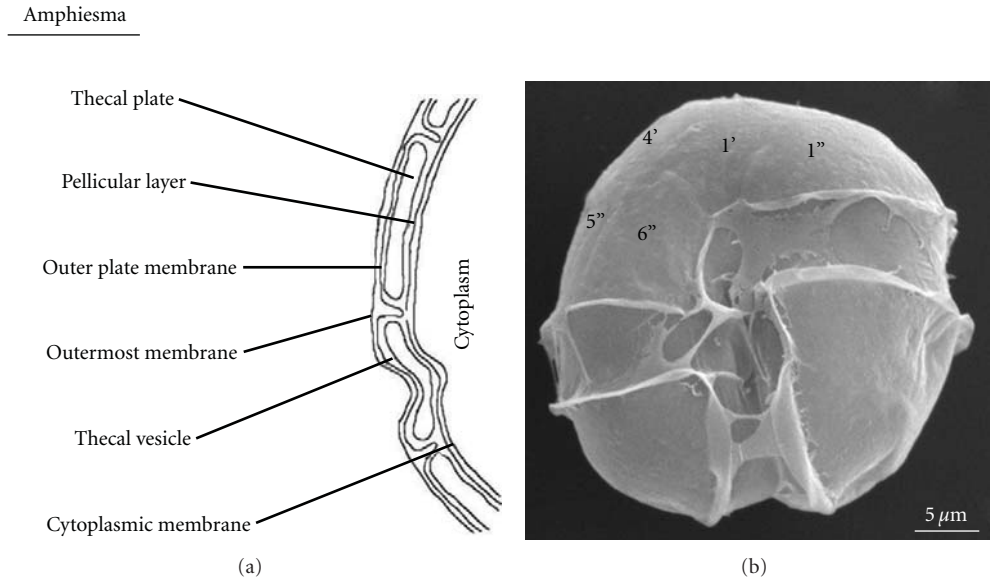

Figure 1: Schematic diagram of the amphiesma of a typical thecate dinoflagellate based on Morrill and Loeblich (1984). (a) Structure of the amphiesma, including a continuous outermost membrane, an outer plate membrane, a single-membrane bounded thecal vesicle, and a cytoplasmic membrane. Inside this vesicle, a number of cellulosic thecal plates are subtended by a pellicular layer. (b) Scanning electron micrograph of *A. catenella*, with the continuous outermost membrane obvious on the cell surface.

to cell-cell recognition. The cell wall of dinoflagellates is a subcellular component of substantial interest with regard to various aspects of cell surface associated ecophysiology. However, there are few experimental data available for the cell wall of dinoflagellates compared with other organisms due to the lack of the whole genome. So far, only a limited number of cell wall proteins (CWPs) and enzymes have been identified and characterized at the biochemical and functional level, and neither the mechanism of their functions nor their locations have been elucidated [26–30]. A few studies indicate that cell wall-associated proteins and their activities are known to be induced or increased by factors limiting the growth of these members of the eukaryotic phytoplankton, because they may enhance cell scavenging of nutrients. Moreover, dinoflagellate CWPs may also be involved in signaling pathways [16]. Clearly, the cell wall presents an important site of interaction between algal cells and their environment. In light of this, a better understanding of dinoflagellate CWPs composition may help to reveal various physiological activities on the cell wall as well as in the blooming mechanism of dinoflagellates.

Study of CWPs has often relied on the methods used for their isolation from the cell wall of dinoflagellates. However, at present, there is no ideal method for the isolation of CWPs although many studies have been devoted to various membrane proteins. One of the current strategies is to extract CWPs from whole cells using a sequential extraction method [31–33]. However, this approach causes the cells to break during the long chemical extraction, and this results in potential cross-contamination of the CWPs [32]. Specific labeling methods, for example, biotinylation or the use of the radioisotope Na125I, are also developed to recognize and isolate the cell surface proteins (CSPs) from dinoflagellates [26, 30]. However, these methods led to a loss of solubility of the proteins due to the multiple additions of large hydrophobic groups, and, moreover, these methods only address CSPs and not the CWPs.

Global techniques such as proteomics provide effective strategies and tools for profiling and identifying proteins of dinoflagellates [34–38]. In contrast to conventional biochemical approaches that address one or a few specific proteins at a time, proteomic techniques allow simultaneous isolation and identification of hundreds to thousands of proteins in one sample. Fluorescence difference gel electrophoresis (DIGE) technology is a newly developed 2D gel-based approach that employs three fluorescent succinimidyl esters, termed CyDyes, to differentially label proteins prior to electrophoretic separation [39]. Because of the sensitivity and extended linear dynamic range of these dyes, this technique facilitates not only quantification over a comparatively wide dynamic range with high accuracy, but also enables relative quantification with reference to an internal standard, thereby also facilitating the analysis of an adequate set of biological replicates in order to obtain the most significant data on protein regulation. This technique is recently applied for identifying biomarkers, designing novel drug targets, and monitoring therapeutic processes [40–43].

In this study, we present a newly developed method for the identification and characterization of CWPs from *A. catenella* DH01, an HAB-causing dinoflagellate species widely spread in the coastal waters of China[44]. By comparing sequentially extracted CWPs labeled with Cy3 and protoplast proteins labeled with Cy5, 120 CWPs were confidently identified on the 2D DIGE gel, and the majority gave positive identification of protein orthologues in the protein database by *de novo* sequence analysis and database

searching (MS-BLAST). The goal of this study was to establish an efficient and reliable method to identify CWPs from dinoflagellates and to characterize putative proteins in order to provide a foundation for future investigation of the functions and expression of CWPs in *A. catenella* as well as other dinoflagellates.

2. Materials and Methods

2.1. Organism and Culture Conditions. *A. catenella* DH01 was provided by the Culture Collection Center of Marine Bacteria and Algae of the State Key Laboratory of Marine Environmental Science, Xiamen University, China. A unialgal isolate was routinely maintained in K medium [45] at 20°C under a 10 : 14 h light: dark photoperiod at a light intensity of approximately 100 μmol photons m^{-2} s^{-1} provided using fluorescent lamps. The cells for the experiments were grown in 5,000 mL flasks containing 4,000 mL of K medium, and the culture conditions were the same as above. The K medium did not contain any protein. Approximately 2×10^7 cells of *A. catenella* in their exponential growth phase were collected with centrifugation at 3,000 × g for 30 minutes at 4°C. The cell pellets were rinsed twice with precooled sterilized seawater to avoid any carryover of culture medium and extracellular proteins and were used for the extraction of CWPs and protoplast proteins.

2.2. Preparation of Sequentially Extracted CWPs. For CWP extraction, the cell pellets were sequentially extracted with 0.2 M $CaCl_2$, 50 mM CDTA in 50 mM sodium acetate (pH 6.5), 2 mM DTT, and 1 M NaCl at 4°C for 30 min each, and finally to 0.2 M borate (pH 7.5) at room temperature for 30 min, with gentle vortexing. The extracts were pooled together and precipitated with three volumes of ice-cold 20% TCA (v/v) in acetone overnight at −20°C and centrifuged at 20,000 g for 30 min at 4°C (Hettich ROTINA 38R Refrigerated Centrifuges, Germany). The supernatant was discarded, and the precipitate was washed twice with ice-cold 90% acetone (v/v) containing 20 mM DTT and then twice with ice-cold 100% acetone. The protein obtained was air-dried to remove residual acetone and subsequently dissolved in 50 μL rehydration buffer (pH 8.5) containing 7 M urea, 2 M thiourea, 4% CHAPS (w/v), and 30 mM Tris and then stored at −80°C for proteomic analysis. This protein sample was termed sequentially extracted CWPs.

2.3. Preparation of Protoplast Proteins. 1×10^7 cells were resuspended in sterilized sea water and maintained at 4°C for one and a half hours then at 20°C for 10 min. After this treatment, the cell walls became detached from the protoplasts without the cell being broken (Figure 2). The suspension was centrifuged at 4,000 g for 30 min at 4°C. After removing the supernatant, the pellet was separated into two layers, cell walls in the upper layer and protoplasts in the lower layer (Figure 2(e)). The cell wall layer was introduced to a membrane filter of 5 μM diameter pore size (Whatman) with a pipette and gently washed three times with sterilized sea water to avoid contamination by extracellular proteins. The protoplasts were removed on a 10 μM diameter pore size filter (Whatman) and washed three times with sterilized sea water to avoid contamination by the cell walls. 1 mL Trizol reagent was added to the protoplast pellet collected using centrifugation, and it was subjected to sonication on ice. Subsequently, 200 μL of chloroform was added to the cell lysate before shaking it vigorously for 15 s. The mixture was allowed to stand for 5 min at room temperature before being centrifuged at 12000 × g for 15 min at 4°C. The top pale-yellow or colorless layer was removed, and 300 μL of ethanol was added to resuspend the reddish bottom layer and this mixture centrifuged at 2000 × g for 5 min at 4°C. The supernatant was transferred to a new tube and 1.5 mL of isopropanol was added. The mixture was allowed to stand for at least 20 min for precipitation of proteins at room temperature. It was then centrifuged at 14000 × g for 10 min at 4°C, and the pellet obtained was briefly washed with 95% ethanol before being allowed to air dry. 500 μL of rehydration buffer with 7 M urea, 2 M thiourea and 4% W/V CHAPS was added to solubilize the protein pellet before loading onto the first dimension isoelectric focusing (IEF).

2.4. Minimal Labeling of Proteins Using Fluorescent Dye. Sequentially extracted CWPs and protoplast proteins were subjected to minimal labeling using the fluorescent dyes Cy3 and Cy5 according to the manufacturer's instructions. Aliquots of 50 μg of each sample were separately labeled. Briefly, stock cyanine dyes (14 nmol/μL) were diluted in freshly prepared DMF to 400 pmol/μL and 8 pmol dye was added per 1 μg of protein in the cell lysate. The sample was vortexed, briefly centrifuged, and left on ice for 30 min in the dark. No primary amines, DTT, or carrier ampholytes were included in the lysis buffer as such components could potentially react with the *N*-hydroxy succinimide ester group of the cyanine dyes. The labeling reaction was quenched by adding 1 μL of 10 mML-lysine per 400 pmol of dye. The sequentially extracted CWPs and protoplast proteins were labeled with Cy3and Cy5, respectively. Thereafter, the Cy3- and Cy5-labeled samples were mixed at a ratio of 1 : 1 (equating to 100 μg of total protein) and prepared for IEF.

2.5. Two-Dimensional Gel Electrophoresis. For 2D DIGE, the labeling protein samples were mixed with a rehydration buffer (7 M urea, 2 M thiourea, 4% w/v CHAPS, 1% DTT, and 0.5% v/v IPG) before loading onto IPG strips with a linear pH gradient from 4–7 (Immobiline Drystrip, GE Healthcare Life Science, Piscataway, US). The sample was subjected to IEF using an IPGphor III system with 24 cm IPG strips and the following protocol: 6 h at 40 V (active rehydration), 6 h at 100 V, 0.5 h at 500 V, 1 h at 1000 V, 1 h at 2000 V, 1.5 h at 10000 V, and 6 h at 10000 V for 60000 Vh. The minimal Vh applied was 60000 units. Subsequently, the immobilized pH gradient strips were equilibrated for 15 min in reducing buffer containing 6 M urea, 2% SDS, 50 mM Tris-Cl (pH 8.8), 30% glycerol, and 1% DTT, followed by equilibration for 15 min in alkylation buffer containing 6 M urea, 2% SDS, 50 mM Tris-Cl (pH 8.8), 30% glycerol, and 2.5% iodoacetamide. Second-dimension SDS-PAGE gels (12.5%) were run on a GE Ettan DALT six at 0.5 w/gel for 1 h and then at 17 w/gel for 6 h.

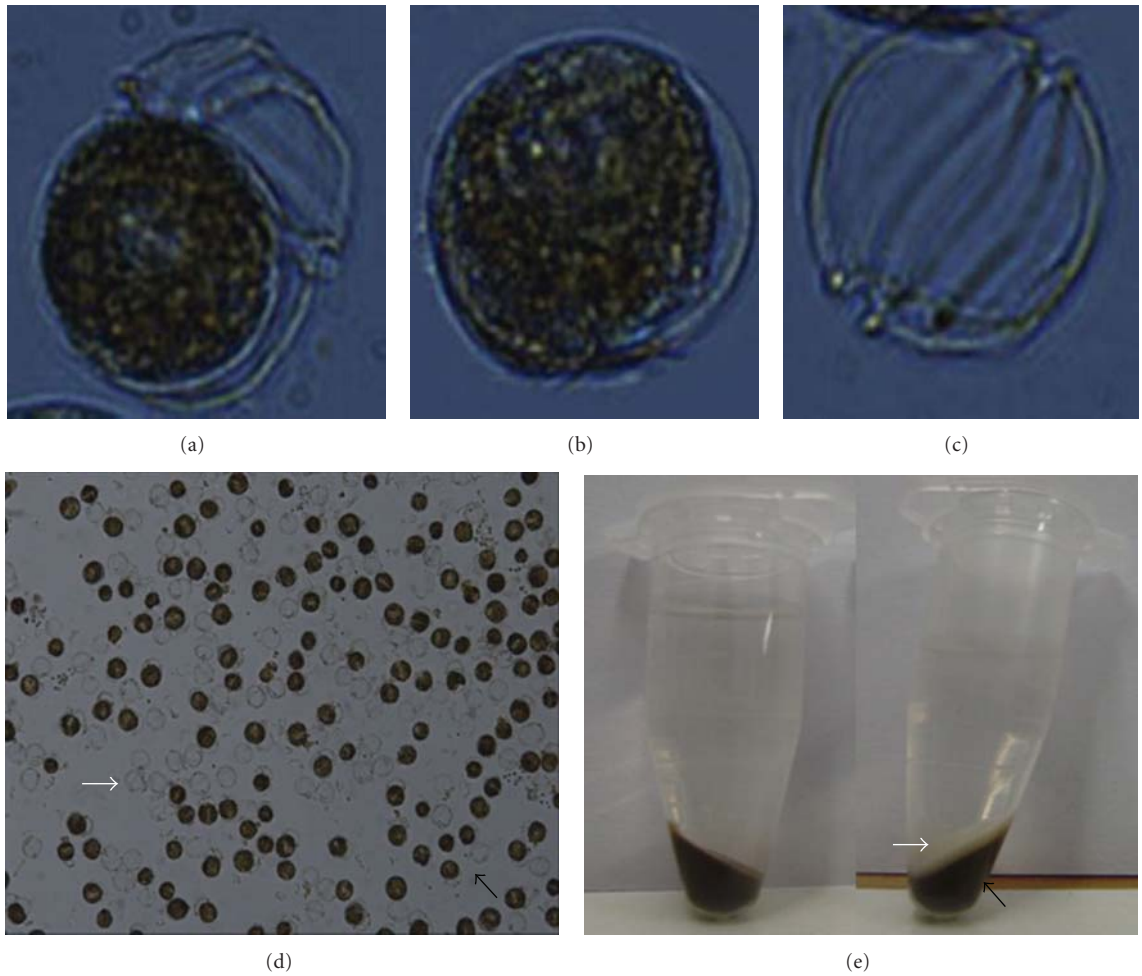

Figure 2: Preparation of protoplasts of *A. catenella* DH01 using the temperature shock method. (a), (b), and (c) are photographs of the intact cell, the protoplast and the cell wall of *A. catenella* DH01 under the light microscope. (d) A mixture of cell walls (white arrow) and protoplasts (black arrow). (e) Concentrated cell walls (white arrow) and protoplasts (black arrow). (The magnitude was 10 × 20).

2.6. Gel Scanning, Digitizing, and Data Analysis. The resultant analytical gels were scanned using a Typhoon 9400 scanner (Amersham 4 Biosciences/GE Healthcare). The specific excitation and emission wavelengths for each of the fluorescent dyes were recommended by the manufacturer. Gel images were scanned at a resolution of 100 μm and preprocessed using ImageQuant software (version 5.2, Amersham Biosciences/GE Healthcare). Cropped gel images were analyzed using DeCyder 2D software (version 6.5, Amersham Biosciences/GE Healthcare). The differential in-gel analysis (DIA) algorithm detected overlapping spots on a combined image derived from merging individual images from the two samples tagged by Cy3 and Cy5. Protein spots which were identified as CWPs between the sequentially extracted CWPs and protoplast proteins were marked for spot excision and subsequent protein identification using MALDI TOF-TOF.

2.7. In-Gel Digestion. 120 CWPs identified using 2D DIGE were manually excised from the prepared silver stained 2-DE gels (Figure 4), and the silver-stained gel pieces were rinsed once with MilliQ water and destained in 100 mM sodium thiosulfate and 30 mM potassium ferricyanide until the gel pieces became white. They were then rinsed three times in Milli-Q water, shrunk with 100% acetonitrile for 15 min, and air-dried at room temperature for 30 min. All gel pieces were incubated with 12.5 ng/μL sequencing grade trypsin (Roche Molecular Biochemicals) in 20 mM NH_4HCO_3 overnight at 37°C. After digestion, 1 μL of supernatant was pipetted and spotted on the target plate then air-dried at room temperature. 1 μL of matrix (4-hydroxy–cyanocinnamic acid in 30% CAN, 0.1% TFA) was laid over the samples on the target plate until they dried completely.

2.8. Mass Spectrometric Analysis. MALDI-TOF mass spectrometry and tandem TOF/TOF mass spectrometry were carried out with a 4800 Plus MALDI TOF-TOF Analyzer (Applied Biosystems, Foster City, USA) equipped with a neodymium: yttrium-aluminum-garnet laser. The laser wavelength and the repetition rate were 355 nm and 200 Hz. The MS spectra were processed using the Peak Explorer (Applied Biosystems) software allowing nonredundant and fully automated selection of precursors for tandem mass

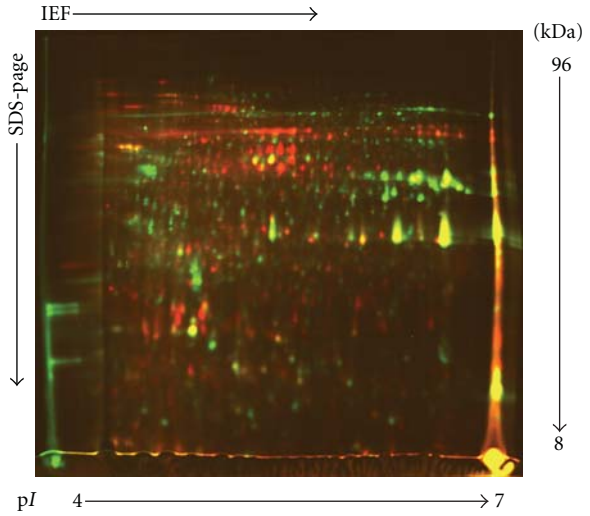

Figure 3: 2D DIGE analysis of sequentially extracted CWPs and protoplast proteins labeled using the fluorescent dyes Cy3 (green) and Cy5 (red), respectively. This representative 2D DIGE image for protein expression maps used a 12.5% homogenous SDS-PAGE gel in the pH range 4 to 7.

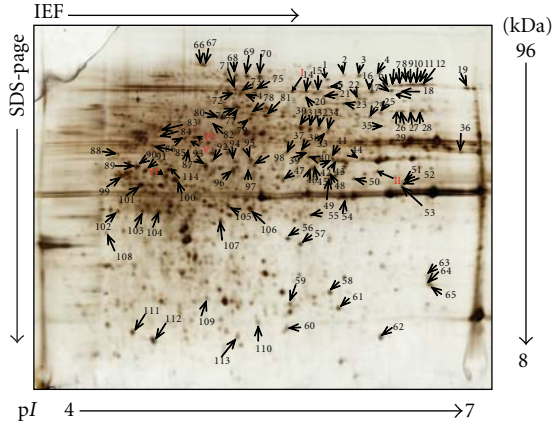

Figure 4: Representative 2-DE gel of CWPs from an *A. catenella* DH01 sample stained with silver. The proteins were resolved in 4–7 linear pH gradient (Immobiline DryStrips; 240 × 3 × 0.5) and 12.5% SDS-PAGE (2400 × 2000 × 1 mm). 120 CWPs were separated and identified (indicated by arrows) from *A. catenella* DH01.

spectrometry (MS/MS) acquisition. At least 2000 laser shots were typically accumulated in the MS mode, whereas in the MS/MS mode spectra from up to 5000 laser shots were acquired and averaged. The peak detection criteria used were a minimum S/N of 10, a local noise window width mass/charge (m/z) of 250 and a minimum full-width half-maximum (bins) of 2.9. The mass spectra were internally calibrated using porcine trypsin autolytic products (m/z 842.51, 1045.564, and 2211.104 Da) resulting in mass errors of less than 30 ppm. A maximum of the five strongest precursor ions per protein spot were chosen for MS/MS analysis. The following monoisotopic precursor selection criteria were used for MS/MS: minimum S/N filter of 50, excluding the most commonly observed peptide peaks for trypsin and keratin, and excluding the precursors within 200 resolution. In the TOF1 stage, all ions were accelerated to 1 kV under conditions promoting metastable fragmentation. The peak detection criteria used were an S/N of 10 and a local noise window width of 250 (m/z).

2.9. Database Search. A combined MS and MS/MS search was first performed against the NCBI nonredundant database with no taxonomic restriction using an in-house MASCOT server (Version 2.2). The raw MS and MS/MS spectra were processed using GPS Explorer software (Version 3.5, Applied Biosystems). For protein spots with a scores confidence interval below 95%, their MS/MS spectra were used for automated *de novo* sequencing using the Applied Biosystems DeNovo Explorer software [46]. Briefly, each MS/MS spectrum produced ten peptide sequence candidates, and each peptide sequence had a score associated with it that indicated how much of the total ion abundance in the MS/MS spectrum was accounted for by the typical fragment ions that could be calculated for the particular sequence. The closer to 100 was the score, the greater the likelihood that all or most of the sequence generated by DeNovo Explorer was correct.

De novo generated peptide sequences were performed for similarity searches using the MS-BLAST algorithms [46]. The MS-BLAST searches were conducted at the Heidelberg server (http://dove.embl-heidelberg.de/Blast2/msblast.html) against the NCBI nonredundant database using standard settings with no taxonomic restriction. All sequences obtained from an MS/MS spectrum were spaced with the minus symbol (−) and were merged into a single string, and submitted to an MS BLAST search as reported above. The MS-BLAST search results were considered significant if the resulting scores were higher than the threshold score indicated in the MS-BLAST scoring scheme.

3. Results

3.1. Identification of CWPs Using 2D DIGE. In this study, two protein fractions were obtained from *A. catenella*: one fraction was sequentially extracted CWPs prepared using a sequential chemical extraction method, a traditional plant CWP preparation method; the other was protoplast proteins prepared using a temperature shock method. The former was labeled with Cy3 and the latter with Cy5, and then, they were pooled together to run 2D DIGE. An overview of the fluorescent DIGE images of the sequentially extracted CWPs and protoplast proteins of *A. catenella*, and the overlaying of these two images are shown in Figure 3. The differentially expressed proteins were evaluated using DeCyder 2D software. This software identifies protein spots and compares the spot intensities for up to three samples run simultaneously on a single 2-DE gel. Figure 3 shows qualitative comparisons of sequentially extracted CWPs and protoplast proteins run on a single gel. Overlaying the images allowed direct comparison of the two. Green spots were sequentially extracted CWPs; red spots were protoplast proteins; yellow spots were the same proteins presented in

both sequentially extracted CWPs and protoplast proteins. Using DIA software analysis, 120 candidate protein spots were identified as CWPs (green spots) in the CyDye staining gel, and the majority of these CWPs was separated in the apparent molecular mass range of 14–50 kDa, and they had p*I* ranges of 4.0–7.0.

3.2. Categorization of the A. catenella CWPs. To further characterize the samples, 120 confidently identified CWPs of *A. catenella* DH01 were excised from the silver-staining gels (Figure 4) and trypsinized, before subjection to MALDI-TOF-TOF MS analysis. By searching against the NCBI nonredundant database using the MASCOT algorithm, no CWPs could be identified which were able to meet statistical significance. This is not surprising, however, since no dinoflagellate genome has been established at present. Furthermore, *de novo* sequencing and MS-BLAST similarity searches were used for protein identification. A total of 42 proteins were identified, most of which were associated with cell wall modifying enzymes, cell wall structure, transport/binding, signaling, and defense (Table 1). Among them, 15 proteins were putative cell wall-modifying enzymes, including four hydrolases, two dehydratases, two dehydrogenases, four oxidoreductases, two acyltransferases, and one protease. These proteins are involved in various physiological processes on the cell wall during cell growth and development. Three putative proteins, D-alanyl-D-alanine ligase A, UDP-glucose 4-epimerase and penicillin-binding protein (PBP) were possibly involved in cell wall construction. Transport/binding proteins, and lipoprotein represented another major group of proteins present in the cell wall. Of these, three belonged to ATP-binding cassette (ABC) family, three were other types of transport/binding proteins, and the other was lipoprotein. These proteins were involved in transporting various substrates across the cell wall membranes. The signaling proteins were another important component in CWPs of *A. catenella*, four of them were receptors, one was a binding protein, and two were other signal proteins. Five proteins related to cell defense were identified, they were polymorphic membrane protein B/C family (PMP), dihydropteroate synthase (DHPS), Vpu protein, FmtA-like protein, and SPAC328.04 protein.

In addition to the above proteins, several other proteins such as At2g46420/F11C10.11, CG2962, hypothetical membrane protein, and PB407L were also characterized amongst the CWPs of *A. catenella*, which reflects the roles of CWPs in cell surface physiology and in interactions between cell and environment.

4. Discussion

4.1. Isolation and Identification of CWPs. In this study, we prepared CWPs using a sequential extraction method. The cells were extracted first with $CaCl_2$, then sequentially with CDTA, DTT, borate, and NaCl, which can efficiently extract weak bound, strongly ionically bound, and pectin-bound proteins as well as glycoproteins. This method was successfully used to extract CWPs from suspension-cultured cells of plant species and did not cause contamination of the proteins [31]. However, we found that the extracts became red during the extraction process and a few broken cells were also observed under the microscope (data not shown), indicating that cytosolic proteins might have been released during extraction and so contaminated the CWPs. Continuous extraction with chemical regents might also increase the permeability of the cell wall (theca) membrane and protoplast membrane which would have led to the leakage of intracellular proteins and subsequently contamination of the CWPs. A study on cell wall proteomics of a green alga, *Haematococcus pluvialis*, demonstrates that the sequential extraction method results in contamination of CWPs with intracellular proteins [32]. Several intracellular proteins, RuBisco small subunit orthologue, and ATP synthase-chain orthologue were found in the SDS-PAGE of the CWPs, although the contamination was relatively minor. Thus, the sequential extraction method is not a reliable approach for the extraction of CWPs for a cell wall proteomic study of dinoflagellates, and so, our study used the 2D DIGE method to identify CWPs by combining the sequential extraction method with the protoplast preparation method. The sequentially extracted CWPs were labeled by Cy3, while the protoplast proteins were labeled by Cy5. By comparing the differential expressed proteins to exclude overlayed proteins run on a single gel, the contamination of the intracellular proteins resulting from broken cells was excluded, and the CWPs were confidently identified. This approach provided a reliable and efficient tool to prepare and identify the CWPs of dinoflagellates.

4.2. Functions of CWPs in A. catenella . In this study, 42 proteins associated with cell wall-modifying enzymes, cell wall structure, transport/binding, signaling, and defense were tentatively identified from *A. catenella* using *de novo* sequencing and MS-BLAST similarity searches. These proteins reflected their roles in cell wall physiology.

It is known that several reactions (hydrolysis, transglycosylation, transacylation, and redox reactions) are catalyzed by cell wall-modifying enzymes [47, 48]. In our study, 15 putative cell wall-modifying enzymes were identified from the *A. catenella* cell wall, including hydrolases, dehydratases, dehydrogenases, oxidoreductases, acyltransferases, and protease. Hydrolases are classified as EC 3 in the EC number classification of enzymes and catalyze the hydrolysis of various chemical bonds, for example, carbon-nitrogen, ester, and peptide. Various hydrolases are reported in bacteria and higher plant cell walls and play important roles in fruit ripening and tissue softening of plants as well as bacterial germination, vegetative growth, and sporulation [49, 50]. However, little information is available concerning dinoflagellates. In our study, four hydrolases, the carbon-nitrogen family, competence protein comA, BH3453 protein, and probable transmembrane protein, were identified from *A. catenella* cell walls. Two of them are involved in breaking carbon-nitrogen bonds and appear to be involved in the reduction of organic nitrogen compounds and ammonia production. Aside from these hydrolase proteins, a protease, methionine aminopeptidase (MAP), was identified from the cell wall. MAP is responsible for the removal of the amino-terminal

Table 1: Functional categorization of CWPs from *A. catenella* DH01.

Spot no.	Accession no.	Identification of MS-blast	MS-blast score (HSPs)
		Cell wall modifying enzymes	
III	AACY01006738	Quinoprotein ethanol dehydrogenase	114 (2)
V	Q7S9I3	Acyl-CoA dehydrogenase	107 (2)
5	Q9F1X6	Phosphotransacetylase	100 (2)
8	Q8XTK4	Probable transmembrane protein	135 (3)
24	Q5WKD5	Mannonate dehydratase	104 (2)
27	Q635P5	Hydrolase, carbon-nitrogen family	59 (1)
37	Q7NLM8	Gll1094 protein	65 (1)
43	Q88D51	5,10-methylenetetrahydrofolate reductase	80 (1)
46	D00131	Tyrosinase	73 (1)
66	CP000025	8-amino-7-oxononanoate synthase	64 (1)
69	P51973	Competence protein comA	65 (1)
80	Q63QT9	Gamma-glutamyl phosphate reductase	107 (2)
81	Q5UU97	Enolase	141 (3)
98	Q9K7B3	BH3453 protein	102 (2)
102	Q72CF9	Methionine aminopeptidase	64 (1)
		Transport/binding proteins and lipoproteins	
I	Q39909	Luciferin-binding protein	110 (2)
17	O73697	Calcium channel alpha-1 subunit homolog	75 (1)
36	Q6FPN9	Similar to uniprot|P40548 Saccharomyces cerevisiae YIL016w SNL1	76 (1)
85	Q926C3	Outer membrane lipoprotein omp16 homolog	97 (2)
97	CP000009	Carbamoyl-phosphate synthase large chain	70 (1)
100	Q833S0	ABC transporter, ATP-binding protein	97 (2)
112	Q6IV89	F1Fo-ATPase synthase f subunit	59 (1)
		Signaling proteins	
II	Q01369	Guanine nucleotide-binding protein beta subunit-like protein	152 (3)
18	Q7T0K6	Melanocortin 4 receptor	64 (1)
25	CAAJ01000020	Cg1 protein, putative	70 (1)
57	Q6WQQ4	Translocon-associated protein beta	67 (1)
72	AE006464	possible G-protein receptor	99 (2)
88	Q9VQM8	CG34393	68 (1)
103	Q98TY6	Tyrosine kinase negative regulator Cbl	137 (3)
		Cell wall structure-related proteins	
VI	Q8H6H9	Cell division inhibitor MinD	66 (1)
1	Q6N415	Putative D-alanyl-D-alanine ligase A	105 (2)
99	Q82D96	Putative UDP-glucose 4-epimerase	64 (1)
111	*C2Q9T5*	Penicillin-binding protein	66 (1)
		Defense	
IV	AE002181	polymorphic membrane protein B/C family	67 (1)
31	Q9WXP7	Dihydropteroate synthase	101 (2)
63	Q9Q6Y7	Vpu protein	65 (1)
74	Q8TR39	FmtA-like protein	70 (1)
109	Q9P3U2	SPAC328.04 protein	60 (1)
		Uncharacterized proteins	
32	Q9SKD8	At2g46420/F11C10.11	106 (2)
49	Q9W2X5	CG2962	60 (1)
15	Q89W76	hypothetical membrane protein	73 (1)
78	Q65173	PB407L	104 (2)

(initiator) methionine from nascent eukaryotic cytosolic and cytoplasmic prokaryotic proteins if the penultimate amino acid is small and uncharged. The occurrence of protease in cell walls is reported in bacteria, green algae, and higher plants. In a green alga, *H. pluvialis*, six putative proteases are identified and are postulated to be involved in processing and/or turnover of CWPs during cell growth and development [32].

Two dehydratases, mannonate dehydratase and enolase, were identified from the *A. catenella* cell wall. Mannonate dehydratase belongs to the family of lyases, specifically the hydrolases, which cleave carbon-oxygen bonds and participate in pentose and glucuronate interconversions. Enolase, also known as phosphopyruvate dehydratase, is a metalloenzyme responsible for the catalysis of 2-phosphoglycerate to phosphoenolpyruvate, the ninth and penultimate step of glycolysis. The two enzymes may exert a role in energy provision for cell wall formation.

A number of oxidoreductases were identified amongst the CWPs of *A. catenella*, including Gll1094 protein, 5, 10-methylenetetrahydrofolate reductase, tyrosinase, and gamma-glutamyl phosphate reductase. Aside from these proteins, two dehydrogenases (ethanol dehydrogenase and acyl-CoA dehydrogenase) were also detected in *A. catenella*. Acyl-CoA dehydrogenase catalyzes the initial step in each cycle of fatty acid β-oxidation and results in the introduction of a trans double bond between C2 and C3 of the acyl-CoA thioester substrate. Recently, several oxidoreductases, such as peroxidase, peptide Met (O) reductase 3, cytokinin oxidase, thioredoxin H-type 5, and UDP-*N*acetylmuramate-dehydrogenase, are identified in *H. pluvialis* cell wall extract [32]. It is suggested that oxidoreductases might cause reduction of cell wall extensibility by forming bridges across phenolic residues and adjacent CWPs or polysaccharides [51].

Two acyltransferases, phosphotransacetylase and 8-amino-7-oxononanoate synthase, were found in *A. catenella*. These two enzymes belong to the family of transferases, specifically the acyltransferase transferring groups rather than the aminoacyl groups. The former participates in taurine and hypotaurine metabolism, pyruvate metabolism, and propanoate metabolism, while the latter participates in biotin metabolism. Both of them might play important roles in the formation and stability maintenance of the cell wall.

Three putative proteins identified in this study were possibly involved in cell wall construction. PBP is the primary enzyme involved in cell wall biosynthesis including muramoylpentapeptide carboxypeptidase, peptide syntheses, transpeptidases, and hexosyltransferases. In bacteria, PBP is involved in the final stage of the synthesis of peptidoglycan, the major component of bacterial cell walls. Occurrence of the three proteins suggested that the cell wall of dinoflagellates may contain components similar to bacterial peptidoglycan, which can form a strong and rigid lattice-like structure. Recently, three proteins associated with cell wall construction, S-layer protein, cellulose synthase, and 1UDP-N-acetylmuramoyl-alanine-D-glutamateligas, were identified from a green alga *H. pluvialis* [32]. Moreover, cell division inhibitor MinD, a peripheral protein, was identified in our study. MinD is a ubiquitous ATPase that plays a crucial role in the selection of the division site in eubacteria, chloroplasts, and probably Archaea and cooperates with MinC to form a division inhibitor at the cell division site that is topologically regulated by MinE. Recently, MinD has been found in four green algae, and the overexpression of MinD results in the MinCD complex binding all cell division sites and inhibiting cell division and leads to a long and nonseptate filamentous cell [52]. Moreover, MinD affects the diameters of cells. Since in dinoflagellates with a theca (amphiesma) little is known about the cell wall biogenesis and dynamics, identification of MinD suggested that this protein might act as a mediator to regulate cell wall growth and cell size when exposed to environmental stresses.

Seven putative transport/binding proteins and lipoprotein represented another major group of proteins present in the cell wall of *A. catenella*. ABC family proteins are transmembrane proteins that utilize the energy of ATP hydrolysis to carry out various biological processes including translocation of various substrates across membranes, and nontransport-related processes such as translation of RNA and DNA repair. They transport a wide variety of substrates across extra- and intracellular membranes, including metabolic products, lipids and sterols, and drugs. Recently, six ATP-binding cassette transporters are identified in the cell wall of *H. pluvialis* [32]. In *Synechocystis*, ABC-type transporters represent the most abundant transporters in the periplasmic space that are involved in the uptake of inorganic nutrients [33]. These studies indicate that ATP-binding cassette transporters might play important roles in the nutrient transport of dinoflagellates. Aside from these proteins, outer membrane lipoprotein OMP 16, similar to uniprot P40548 and calcium channel alpha-1 subunit homolog, were also identified in the CWPs of *A. catenella*, and these proteins played important roles in protein binding, lipid anchor, and calcium binding of the cell walls. Interestingly, luciferin-binding protein, a protein involved in the bioluminescence reaction, was identified from the CWPs of *A. catenella*. It is interesting to note that most of the proteins described above were previously found to be associated with the plasma membrane. This suggests that potential direct physical connections may occur between the plasma membrane and the cell wall and/or interactions at the plasma-cell wall interface [53].

The signaling proteins are another important component in plant cell walls, which regulate various biological processes occurring in the cell wall, such as signal transduction, cell shape and size regulation, stress response, and defense. Melanocortin 4 receptor and G-protein receptor are two transmembrane receptors that sense molecules outside the cell and activate inside signal transduction pathways and, ultimately, cellular responses. G protein-coupled receptors are found only in eukaryotes. Translocon-associated protein beta and tyrosine kinase negative regulator Cb1 are a signal sequence receptor and a cell surface receptor linked to signal transduction, respectively. Guanine nucleotide-binding proteins are glycoproteins anchored on the cytoplasmic cell membrane. They are mediators for many cellular processes, including signal transduction, protein transport, growth regulation, and polypeptide chain elongation. They are also

known as GTP-binding proteins and GTPases. Almost all members of this super family of proteins act as a molecular switch, which is on when GTP is bound and off when GDP is bound. CG34393 was involved in regulation of small GTPase-mediated signal transduction. Our study also found one light signal transduction protein, Cg1 protein, which is a light induced protein and regarded as a possible member of a light signal transduction chain in parsley [54], indicating that Cg1 protein might function as a light-driven proton pump and take advantage of light energy directly as proteorhodopsin in *A. catenella*.

Proteins related to cell defense were also identified in cell wall of *A. catenella*. PMP is a bacterial outer membrane protein which might play important roles in the growth and development of *Chlamydia pneumoniae* [55]. DHPS, which has been found in bacteria, is a key enzyme in producing dihydropteroate. In the lower eukaryote *Pneumocystis carinii*, DHPS is the C-terminal domain of a multifunctional folate synthesis enzyme [56]. Finding DHPS in *A. catenella* suggested that this protein might have originated from the symbiotic bacteria which are hosted on the surface of *A. catenella* cells. Vpu protein and FmtA-like protein are two important proteins which play important roles in resisting bacteria and viruses.

4.3. Protein Identification Using De Novo Analysis and Database Searching. *De novo* analysis coupled with database searching is regarded as a powerful proteomic technique for protein identification, particularly for species with an unknown or incomplete genome [57–59]. Comparative genomic and proteomic studies have demonstrated that the amino acid sequence of proteins is significantly conserved across species boundaries. The conserved nature of many biosynthetic, metabolic, and regulatory pathways in different organisms was the basis for earlier studies of cross-species protein identification for species whose genome sequence were unknown or incomplete. Molecular information on cell wall biogenesis and dynamics of dinoflagellates is totally lacking due to the lack of a dinoflagellate genome at the present. For example, not a single CWP has been identified from dinoflagellates. In this study, approximately two thirds of the tested protein spots failed to be characterized in the protein databases, which might be caused by the low sequence homology matching for unambiguous protein identification across species boundaries. Studies have shown that amino acid residue substitutions occur in many positions of a specific protein across species boundaries resulting from evolutionary divergence as well as numerous posttranslational modifications, for example, phosphorylation, glycosylation, and acetylation, which might reduce or diminish the probability or efficiency of cross-species identification. In addition, low abundance and limited number of CWP sequences present in the available databases might further contribute to the limitations of the technique.

In summary, our study provided a newly developed method for identifying and characterizing CWPs from *A. catenella*. By combining the sequential extraction method for CWPs and the protoplast preparation method, the CWPs were separated from cytosolic proteins using the 2D DIGE method. This method has the potential to become a reliable complement to other methods currently used in studies of dinoflagellate CWPs. As a preliminary study, 120 CWPs were recognized, and 42 were characterized, such as cell wall-modifying enzymes, cell wall structural proteins, transport/binding proteins, signaling, and defense proteins. More insights can be expected; for example, the rapid analysis of many CWPs as well as the characterization of the proteomic changes occurring at the cell wall in response to environmental stresses are expected to facilitate the identification of new surface-exposed targets, and this can certainly improve our understanding of the relationship between cells and environmental variations.

Acknowledgments

This work was partially supported by research grants from the Specialized Research Fund for the Doctoral Program of Higher Education (no. 20070384014), the National Natural Science Foundation of China (nos. 40776068 and 40876059), the Ministry of Science and Technology of the People's Republic of China (Project no. 2010CB428703), the Excellent Group and the Program for New Century Excellent Talents in University to D.-Z. Wang. Professor John Hodgkiss is thanked for his help in polishing the English in this paper.

References

[1] F. J. R. Taylor, *The Biology of Dinoflagellates*, Black Well Scientific Publications, Oxford, UK, 1987.

[2] M. Kodama, "Ecobiology, classification, and origin," in *Seafood and Freshwater Toxins: Pharmacology, Physiology and Detection*, L. M. Botana, Ed., pp. 125–151, Marcel Dekker, New York, NY, USA, 2000.

[3] G. M. Hallegraeff, "Harmful algal blooms: a global overview," in *Manual on Harmful Marine Microalgae*, G. M. Hallegraeff, D. M. Anderson, and A. D. Cembella, Eds., pp. 25–49, Imprimerie Landais, Paris, France, 2005.

[4] D. M. Anderson, A. D. Cembella, and G. M. Hallegraeff, *Physiological Ecology of Harmful Blooms*, Springer, Berlin Heidelberg, Germany, 1998.

[5] A. R. Loeblich, "The amphiesma or dinoflagellate cell covering," in *Proceedings of the North American Paleont. Convention, Chicago*, pp. 867–929, Allen Press, Lawrence, Kan, USA, 1969.

[6] A. R. Loeblich and L. A. Loeblich, "Dinoflagellates: structure of the amphiesma and re-analysis of thecal plate patterns," *Hydrobiologia*, vol. 123, no. 2, pp. 177–179, 1985.

[7] D. J. Scanlan, N. H. Mann, and N. G. Carr, "The response of the picoplanktonic marine cyanobacterium *Synechococcus* species WH7803 to phosphate starvation involves a protein homologous to the periplasmic phosphate-binding protein of *Escherichia coli*," *Molecular Microbiology*, vol. 10, no. 1, pp. 181–191, 1993.

[8] B. Song and B. B. Ward, "Molecular cloning and characterization of high-affinity nitrate transporters in marine phytoplankton," *Journal of Phycology*, vol. 43, no. 3, pp. 542–552, 2007.

[9] Y. Tamai, A. Toh-e, and Y. Oshima, "Regulation of inorganic phosphate transport systems in Saccharomyces cerevisiae," *Journal of Bacteriology*, vol. 164, no. 2, pp. 964–968, 1985.

[10] H. M. ElBerry, M. L. Majumdar, T. S. Cunningham, R. A. Sumrada, and T. G. Cooper, "Regulation of the urea active transporter gene (DUR3) in *Saccharomyces cerevisiae*," *Journal of Bacteriology*, vol. 175, no. 15, pp. 4688–4698, 1993.

[11] M. T. Maldonado and N. M. Price, "Reduction and transport of organically bound iron by *Thalassiosira oceanica* (Bacillariophyceae)," *Journal of Phycology*, vol. 37, no. 2, pp. 298–309, 2001.

[12] C. C. Chung, S. P. Hwang, and J. Chang, "Identification of a high-affinity phosphate transporter gene in a Prasinophyte alga, *Tetraselmis chui*, and its expression under nutrient limitation," *Applied and Environmental Microbiology*, vol. 69, no. 2, pp. 754–759, 2003.

[13] M. Hildebrand, "Cloning and functional characterization of ammonium transporters from the marine diatom *Cylindrotheca fusiformis* (Bacillariophyceae)," *Journal of Phycology*, vol. 41, no. 1, pp. 105–113, 2005.

[14] A. E. Allen, "Beyond sequence homology: redundant ammonium transporters in a marine diatom are not functionally equivalent," *Journal of Phycology*, vol. 41, no. 1, pp. 4–6, 2005.

[15] A. K. Davis, M. Hildebrand, and B. Palenik, "A stress-induced protein associated with the girdle band region of the diatom *Thalassiosira pseudonana* (Bacillariophyta)," *Journal of Phycology*, vol. 41, no. 3, pp. 577–589, 2005.

[16] C. M. West, P. Zhang, A. C. McGlynn, and L. Kaplan, "Outside-in signaling of cellulose synthesis by a spore coat protein in *Dictyostelium*," *Eukaryotic Cell*, vol. 1, no. 2, pp. 281–292, 2002.

[17] D. M. Landry, T. Gaasterland, and B. P. Palenik, "Molecular characterization of a phosphate-regulated cell-surface protein from the coccolithophorid, *Emiliania huxleyi* (Prymnesiophyceae)," *Journal of Phycology*, vol. 42, no. 4, pp. 814–821, 2006.

[18] B. Palenik and F. M. M. Morel, "Amino acid utilization by marine phytoplankton: a novel mechanism," *Limnology and Oceanography*, vol. 35, no. 2, pp. 260–269, 1990.

[19] B. Palenik and F. M. M. Morel, "Comparison of cell-surface L-amino acid oxidases from several marine phytoplankton," *Marine Ecology Progress Series*, vol. 29, pp. 195–201, 1990.

[20] B. Palenik and F. M. M. Morel, "Amine oxidases of marine phytoplankton," *Applied and Environmental Microbiology*, vol. 57, no. 8, pp. 2440–2443, 1991.

[21] A. Strojsova, J. Vrba, J. Nedoma, and K. Simek, "Extracellular phosphatase activity of freshwater phytoplankton exposed to different in situ phosphorus concentrations," *Marine and Freshwater Research*, vol. 56, no. 4, pp. 417–424, 2005.

[22] S. T. Dyhrman and B. Palenik, "Characterization of ectoenzyme activity and phosphate-regulated proteins in the coccolithophorid *Emiliania huxleyi*," *Journal of Plankton Research*, vol. 25, no. 10, pp. 1215–1225, 2003.

[23] J. K. Middlemiss, A. M. Anderson, C. W. Stratilo, and H. G. Weger, "Oxygen consumption associated with ferric reductase activity and iron uptake by iron-limited cells of *Chlorella kessleri* (Chlorophyceae)," *Journal of Phycology*, vol. 37, no. 3, pp. 393–399, 2001.

[24] Y. Xu, T. M. Wahlund, L. Feng, Y. Shaked, and F. M. M. Morel, "A novel alkaline phosphatase in the coccolithophore *Emiliania huxleyi* (Prymnesiophyceae) and its regulation by phosphorus," *Journal of Phycology*, vol. 42, no. 4, pp. 835–844, 2006.

[25] A. E. Gau, A. Heindl, A. Nodop, U. Kahmann, and E. K. Pistorius, "L-amino acid oxidases with specificity for basic L-amino acids in cyanobacteria," *Journal of Biosciences*, vol. 62, no. 3-4, pp. 273–284, 2007.

[26] B. Palenik and J. A. Koke, "Characterization of a nitrogen-regulated protein identified by cell surface biotinylation of a marine phytoplankton," *Applied and Environmental Microbiology*, vol. 61, no. 9, pp. 3311–3315, 1995.

[27] S. T. Dyhrman and B. Palenik, "The identification and purification of a cell-surface alkaline phosphatase from the dinoflagellate *Prorocentrum minimum* (Dinophyceae)," *Journal of Phycology*, vol. 33, no. 4, pp. 602–612, 1997.

[28] D. K. Stoecker and D. E. Gustafson, "Cell-surface proteolytic activity of photosynthetic dinoflagellates," *Aquatic Microbial Ecology*, vol. 30, no. 2, pp. 175–183, 2003.

[29] S. T. Dyhrman, "Ectoenzymes in *Prorocentrum minimum*," *Harmful Algae*, vol. 4, no. 3, pp. 619–627, 2005.

[30] T. Bertomeu, J. W. Hastings, and D. Morse, "Vectorial labeling of dinoflagellate cell surface proteins," *Journal of Phycology*, vol. 39, no. 6, pp. 1254–1260, 2003.

[31] D. Robertson, G. P. Mitchell, J. S. Gilroy, C. Gerrish, G. P. Bolwell, and A. R. Slabas, "Differential extraction and protein sequencing reveals major differences in patterns of primary cell wall proteins from plants," *Journal of Biological Chemistry*, vol. 272, no. 25, pp. 15841–15848, 1997.

[32] S. B. Wang, Q. Hu, M. Sommerfeld, and F. Chen, "Cell wall proteomics of the green alga *Haematococcus pluvialis* (Chlorophyceae)," *Proteomics*, vol. 4, no. 3, pp. 692–708, 2004.

[33] F. Huang, E. Hedman, C. Funk, T. Kieselbach, W. P. Schroder, and B. Norling, "Isolation of outer membrane of *Synechocystis* sp. PCC 6803 and its proteomic characterization," *Molecular and Cellular Proteomics*, vol. 3, no. 6, pp. 586–595, 2004.

[34] L. L. Chan, S. C. L. Lo, and I. J. Hodgkiss, "Proteomic study of a model causative agent of harmful red tide, *Prorocentrum triestinum* I: optimization of sample preparation methodologies for analyzing with two-dimensional electrophoresis," *Proteomics*, vol. 2, no. 9, pp. 1169–1186, 2002.

[35] L. L. Chan, I. J. Hodgkiss, and S. C. L. Lo, "Proteomic study of a model causative agent of harmful algal blooms, *Prorocentrum triestinum* II: the use of differentially expressed protein profiles under different growth phases and growth conditions for bloom prediction," *Proteomics*, vol. 4, no. 10, pp. 3214–3226, 2004.

[36] L. L. Chan, I. J. Hodgkiss, S. H. Lu, and S. C. L. Lo, "Use of 2-DE electrophoresis proteome reference maps of dinoflagellates for species recognition of causative agents of harmful algal blooms," *Proteomics*, vol. 4, no. 1, pp. 180–192, 2004.

[37] L. L. Chan, I. J. Hodgkiss, P. K. Lam et al., "Use of two-dimensional gel electrophoresis to differentiate morphospecies of *Alexandrium minutum*, a paralytic shellfish poisoning toxin-producing dinoflagellate of harmful algal blooms," *Proteomics*, vol. 5, no. 6, pp. 1580–1593, 2005.

[38] L. L. Chan, W. H. Sit, P. K. S. Lam et al., "Identification and characterization of a "biomarker of toxicity" from the proteome of the paralytic shellfish toxin-producing dinoflagellate *Alexandrium tamarense* (Dinophyceae)," *Proteomics*, vol. 6, no. 2, pp. 654–666, 2006.

[39] N. B. Larbi and C. Jefferies, "2D-DIGE: comparative proteomics of cellular signalling pathways," *Methods in Molecular Biology*, vol. 517, pp. 105–132, 2009.

[40] H. L. Huang, T. Stasyk, S. Morandell et al., "Biomarker discovery in breast cancer serum using 2-D differential gel electrophoresis/MALDI-TOF/TOF and data validation by routine clinical assays," *Electrophoresis*, vol. 27, no. 8, pp. 1641–1650, 2006.

[41] Y. Fan, T. B. Murphy, J. C. Byrne, L. Brennan, J. M. Fitzpatrick, and R. W. G. Watson, "Applying random forests to identify

biomarker panels in serum 2D-DIGE data for the detection and staging of prostate cancer," *Journal of Proteome Research*, vol. 10, no. 3, pp. 1361–1373, 2011.

[42] T. Kondo, "Tissue proteomics for cancer biomarker development—laser microdissection and 2D-DIGE," *Journal of Biochemistry and Molecular Biology Reports*, vol. 41, no. 9, pp. 626–634, 2008.

[43] R. Kramer and D. Cohen, "Functional genomics to new drug targets," *Nature Reviews Drug Discovery*, vol. 3, no. 11, pp. 965–972, 2004.

[44] D. Z. Wang, S. G. Zhang, H. F. Gu, L. L. Chan, and H. S. Hong, "Paralytic shellfish toxin profiles and toxin variability of the genus *Alexandrium* (Dinophyceae) isolated from the Southeast China Sea," *Toxicon*, vol. 48, no. 2, pp. 138–151, 2006.

[45] M. D. Keller, R. C. Selvin, W. Claus, and R. R. L. Guillard, "Media for the culture of oceanic ultraphytoplankton," *Journal of Phycology*, vol. 23, pp. 633–638, 1987.

[46] D. Z. Wang, C. Li, Z. X. Xie, P. D. Dong, L. Lin, and H. S. Hong, "Homology-driven proteomics of dinoflagellates with unsequenced genome by MALDI-TOF/TOF and automated *de novo* sequencing," *eCAM*. In press.

[47] D. J. Cosgrove, "Enzymes and other agents that enhance cell wall extensibility," *Annual Review of Plant Biology*, vol. 50, pp. 391–417, 1999.

[48] S. C. Fry, "Polysaccharide-modifying enzymes in the plant cell wall," *Annual Review of Plant Physiology and Plant Molecular Biology*, vol. 46, pp. 497–520, 1995.

[49] J. J. Gumucio and J. D. Ostrow, "Brown pigment gallstones: the role of bacterial hydrolases and another missed opportunity," *Hepatology*, vol. 13, no. 3, pp. 607–609, 1991.

[50] Z. Minic, "Physiological roles of plant glycoside hydrolases," *Planta*, vol. 227, no. 4, pp. 723–740, 2008.

[51] S. H. Kim, J. R. Shinkle, and S. J. Roux, "Phytochrome induces changes in the immunodetectable level of a wall peroxidase that precede growth changes in maize seedlings," *Proceedings of the National Academy of Sciences of the United States of America*, vol. 86, no. 24, pp. 9866–9870, 1989.

[52] W. Z. Liu, Y. Hu, R. J. Zhang et al., "Transfer of a eubacteria-type cell division site-determining factor CrMinD gene to the nucleus from the chloroplast genome in *Chlamydomonas reinhardtii*," *Chinese Science Bulletin*, vol. 52, no. 18, pp. 2514–2521, 2007.

[53] B. D. Kohorn, "Plasma membrane-cell wall contacts," *Plant Physiology*, vol. 124, no. 1, pp. 31–38, 2000.

[54] O. C. Silva, "CG-1, a parsley light-induced DNA-binding protein," *Plant Molecular Biology*, vol. 25, no. 5, pp. 921–924, 1994.

[55] J. Grimwood, L. Olinger, and R. S. Stephens, "Expression of *Chlamydia pneumoniae* polymorphic membrane protein family genes," *Infection and Immunity*, vol. 69, no. 4, pp. 2383–2389, 2001.

[56] F. Volpe, M. Dyer, J. G. Scaife, G. Darby, D. K. Stammers, and C. J. Delves, "The multifunctional folic acid synthesis fas gene of *Pneumocystis carinii* appears to encode dihydropteroate synthase and hydroxymethyldihydropterin pyrophosphokinase," *Gene*, vol. 112, no. 2, pp. 213–218, 1992.

[57] A. L. Yergey, J. R. Coorssen, P. S. Backlund et al., "*De novo* sequencing of peptides using MALDI/TOF-TOF," *Journal of the American Society for Mass Spectrometry*, vol. 13, no. 7, pp. 784–791, 2002.

[58] N. S. Tannu and S. E. Hemby, "*De novo* protein sequence analysis of *Macaca mulatta*," *BMC Genomics*, vol. 8, article 270, 2007.

[59] B. Samyn, K. Sergeant, S. Memmi, G. Debyser, B. Devreese, and J. Van Beeumen, "MALDI-TOF/TOF *de novo* sequence analysis of 2-D PAGE-separated proteins from *Halorhodospira halophila*, a bacterium with unsequenced genome," *Electrophoresis*, vol. 27, no. 13, pp. 2702–2711, 2006.

Hindawi Publishing Corporation
Evidence-Based Complementary and Alternative Medicine
Volume 2011, Article ID 471020, 16 pages
doi:10.1155/2011/471020

Research Article

Homology-Driven Proteomics of Dinoflagellates with Unsequenced Genomes Using MALDI-TOF/TOF and Automated *De Novo* Sequencing

Da-Zhi Wang, Cheng Li, Zhang-Xian Xie, Hong-Po Dong, Lin Lin, and Hua-Sheng Hong

State Key Laboratory of Marine Environmental Science/Environmental Science Research Center, Xiamen University, Xiamen 361005, China

Correspondence should be addressed to Da-Zhi Wang, dzwang@xmu.edu.cn

Received 20 January 2011; Accepted 30 June 2011

This study developed a multilayered, gel-based, and underivatized strategy for *de novo* protein sequence analysis of unsequenced dinoflagellates using a MALDI-TOF/TOF mass spectrometer with the assistance of DeNovo Explorer software. MASCOT was applied as the first layer screen to identify either known or unknown proteins sharing identical peptides presented in a database. Once the confident identifications were removed after searching against the NCBInr database, the remainder was searched against the dinoflagellate expressed sequence tag database. In the last layer, those borderline and nonconfident hits were further subjected to *de novo* interpretation using DeNovo Explorer software. The *de novo* sequences passing a reliability filter were subsequently submitted to nonredundant MS-BLAST search. Using this layer identification method, 216 protein spots representing 158 unique proteins out of 220 selected protein spots from *Alexandrium tamarense*, a dinoflagellate with unsequenced genome, were confidently or tentatively identified by database searching. These proteins were involved in various intracellular physiological activities. This study is the first effort to develop a completely automated approach to identify proteins from unsequenced dinoflagellate databases and establishes a preliminary protein database for various physiological studies of dinoflagellates in the future.

1. Introduction

Dinoflagellates are a diverse group of unicellular algae that comprise a large part of the marine and freshwater phytoplankton [1]. They are not only the important primary producers and an important part of the food chain in marine ecosystem, but also the major causative species resulting in harmful algal blooms (HABs) in the coastal zone [2]. Moreover, many dinoflagellate species can produce various potent toxins that impact human health through the consumption of contaminated shellfish, through coral reef fish and finfish, or through water or aerosol exposure [3]. At the present, four major seafood poisoning syndromes caused by toxins have been identified from the dinoflagellates: paralytic shellfish poisoning (PSP), diarrheic shellfish poisoning, neurotoxic shellfish poisoning, and ciguatera fish poisoning. It is estimated that dinoflagellate toxins result in more than 50,000–500,000 intoxication incidents per year, with an overall mortality rate of 1.5% on a global basis [4]. In addition to their adverse effects on human health, dinoflagellate toxins are responsible for the death of fish and shellfish and have caused episodic mortalities of marine mammals, birds, and other animals dependant on the marine food web [5–8]. Dinoflagellate causing HABs and toxin-producing dinoflagellates have become a global concern [3, 9, 10].

Dinoflagellates are notable for their unusual genome content and organization [11, 12]. It is estimated that the dinoflagellate DNA content ranges from 3 to 250 $pg \cdot cell^{-1}$ [13, 14], corresponding to approximately 3,000–215,000 Mb. Moreover, dinoflagellates have many chromosomes (up to 325) that are permanently condensed and attached to the nuclear envelope during cell division. These unique features of dinoflagellates have brought challenges to the use of traditional biochemical methods and molecular technology in the study of dinoflagellates [15], and so genetic information concerning dinoflagellates are lacking worldwide at present, which has seriously impeded our understanding of HABs and, consequently, the monitoring, mitigation, and prevention.

Proteins are the actual "machinery" that brings about cell growth, proliferation, and homeostasis, and it is logical, therefore, that the study of proteins should help uncover in broad terms the various mechanisms involved in the biological activities of dinoflagellates. Global techniques such as proteomics provide effective strategies and tools for profiling and identifying dinoflagellate proteins, and, in contrast to conventional biochemical approaches that addressed one or a few specific proteins at a time, the proteomic techniques allow simultaneous isolation and identification of hundreds to thousands of proteins in one sample. In the past few years, the proteomic approach has been applied to the study of dinoflagellates, and a few important proteins have been discovered or identified [16–18]. However, only 3,578 and 2,621 dinoflagellate proteins are annotated in the NCBI and UniProtKB (December, 2010), respectively. The highly uncharacterized nature of the dinoflagellate proteome makes it difficult to identify proteins, demonstrate differential regulation of proteins, and investigate their posttranslational modifications. The lack of a genome limits the use of dinoflagellates for proteomic studies which rely on database searches for protein identification. Recently, with the fast development of MALDI-TOF-TOF MS technology, this limitation has been overcome to some extent using a *de novo* sequencing strategy, in which partial or complete amino acid sequences are obtained using either manual or automated *de novo* peptide sequence analysis. This approach has been successfully applied in recent studies with incomplete- or nongenome organisms in order to characterize their proteins [19–23].

Alexandrium is a widely distributed dinoflagellate genus in many coastal regions around the world. It is well known that many species from this genus can produce potent neurotoxins which cause PSPs through the consumption of shellfish contaminated by toxins [24, 25]. The losses in mariculture and the threats to human life due to exposure to PSPs have been documented increasingly and have become economic and public health concerns around the world. Recently, many efforts have been devoted to establish the expressed sequence tag (EST) library of *Alexandrium* and other dinoflagellate species, which provides a powerful tool to predict protein families and to develop expression systems for new proteins and their functions [26–28]. Our study selected *A. tamarense* as the model dinoflagellate species, and a layered method combining MALDI-TOF-TOF MS with *de novo* sequence analysis and stringent homology-based searching tools was employed to identify the proteins. A highly specific and stringent MASCOT search was applied as the first layer to identify proteins with identical peptides in the present database; the remainder were searched against a dinoflagellate EST database combined with BLASTX analysis. In the last layer, those borderline and nonconfident hits were subjected to automated *de novo* sequencing and homology searches using the homology-based search algorithm, MS-BLAST. Using this strategy, 158 unique proteins in 220 selected protein spots were identified from *A. tamarense*, and these proteins were involved in various physiological activities. The current study validated a robust method to characterize proteins from an unsequenced database of *A. tamarense* thereby facilitating the use of this HAB model in various studies.

2. Materials and Methods

2.1. Organism and Growth Conditions. The strain of *A. tamarense* was provided by the Culture Collection Center of Marine Bacteria and Algae of the State Key Laboratory of Marine Environmental Science, Xiamen University, China. The unialgal isolate was routinely maintained in K medium [29] at 20°C under a 14 : 10 h light : dark photoperiod at a light intensity of approximately 100 μmoL photons m^{-2} s^{-1} provided by fluorescent lamps. The cells for the experiments were grown in 5,000 mL flasks containing 4,000 mL of K medium, the culture conditions were the same as above. The K-medium did not contain any protein. Approximately 2×10^7 cells of *A. tamarense* in the middle exponential growth phase were collected by centrifugation at 3,000 ×g for 30 minutes at 4°C. The cell pellets were rinsed twice with precooled sterilized seawater to avoid any carryover of culture medium and extracellular proteins, ready for protein extraction.

2.2. Protein Extraction and Determination. Protein extraction was performed according to the method developed by Lee and Lo [30]. Briefly, 1 mL Trizol reagent was added to the cell pellet and subjected to sonication (a total of 2 min with short pulses of 3–5 s) on ice. Lysis of cells was confirmed using light microscope. Subsequently, 200 μL of chloroform was added to the cell lysate before shaking vigorously for 15 s. The mixture was allowed to stand for 5 min at room temperature before being centrifuged at 12,000 ×g for 15 min at 4°C The top pale yellow or colorless layer was removed, and then 300 μL of ethanol was added to resuspend the reddish bottom layer, and the mixture centrifuged at 2,000 ×g for 5 min at 4°C. The supernatant was transferred to a new tube, and 2 mL of isopropanol was added. The mixture was allowed to stand for at least 1 hr for precipitation of proteins at −20°C. It was then centrifuged at 14,000 ×g for 30 min at 4°C. The pellet obtained was briefly washed with 95% ethanol before being allowed to air dry. 30 μL of rehydration buffer (7 M urea, 2 M thiourea, 4% w/v CHAPS, 1% DTT, and 0.5% v/v IPG) was added to solubilize the protein pellet. Protein quantification in the urea-containing protein samples was performed using a 2D Quant kit (GE Healthcare, USA).

2.3. 2-DE and Analysis. Exactly 400 μg of protein sample was mixed with a rehydration buffer (7 M urea, 2 M thiourea, 4% w/v CHAPS, 1% DTT, and 0.5% v/v IPG) before being loaded onto IPG strips with a linear pH gradient of 4–7 (Immobiline Drystrip, pH 4–7, GE Healthcare Life Science, Piscataway, USA). The sample was subjected to isoelectric focusing using an IPGphor III system with 24 cm IPG strips following the manner: 6 h at 40 V (active rehydration), 6 h at 100 V, 0.5 h at 500 V, 1 h at 1,000 V, 1 h at 2,000 V, 1.5 h at 10,000 V, and 60,000 Vh at 10,000 V. The minimal Vh applied was at least 60,000 units. Subsequently, the

immobilized pH gradient strips were equilibrated for 15 min in reducing buffer containing 6 M urea, 2% SDS, 50 mM Tris-Cl (pH 8.8), 30% glycerol, and 1% DTT, followed by equilibration for 15 min in alkylation buffer containing 6 M urea, 2% SDS, 50 mM Tris-Cl (pH 8.8), 30% glycerol, and 2.5% iodoacetamide. Two-dimension SDS-PAGE (2-DE) gels (12.5%) were run in an EttanDalt system (GE Healthcare) at 1 w/gel for 30 min and then at 15 w/gel for 6 h. The 2-DE gels were visualized using Coomassie Blue (CBB) staining and digitized using a gel documentation system on a GS-670 Imaging Densitometer from Bio-Rad (USA) with 2-DE electrophoretogram-matching software.

2.4. In-Gel Trypsin Digestion. Two hundred and twenty protein spots were manually excised from preparative CBB stained 2-DE gels (Figure 2). CBB-stained gel pieces were washed with MilliQ water for 10 min, destained three times in 200 μL of 25 mM NH_4HCO_3 in 50% acetonitrile (ACN) for 20 min at 37°C, and then incubated in 200 μL of 100% ACN at room temperature with occasional vortexing, until the gel pieces became white and shrunken. They were then air dried at room temperature for 30 min. All gel pieces were incubated with 12.5 ng/μL sequencing-grade trypsin (Roche Molecular Biochemicals) in 10 mM NH_4HCO_3 overnight at 37°C. After digestion, the supernatants were discarded. Peptides were extracted from the gel pieces first into 50% ACN, 0.1% trifluoroacetic acid, and then into 100% ACN. All extracts were pooled and dried completely by SpeedVac. Peptide mixtures were redissolved in 0.1% TFA, and 1 μL of peptide solution was mixed with 1 μL of matrix (α-cyano-4-hydroxycinnamic acid (CHCA) in 30% ACN, 0.1% TFA) before spotting on the target plate.

2.5. Mass Spectrometric Analysis. Mass spectrometry analyses were conducted using an AB SCIEX MALDI TOF-TOF 5800 Analyzer (AB SCIEX, Shanghai, China) equipped with a neodymium: yttrium-aluminum-garnet laser (laser wavelength was 349 nm), in reflection positive-ion mode. With CHCA as the matrix, TFA for an ionization auxiliary reagent, and calibrated with Sequenzyme peptide standard kit (AB SCIEX), the MS spectra were processed using TOF/TOF Series Explorer software (AB SCIEX) allowing nonredundant and fully automated selection of precursors for MS/MS acquisition. At least 1,000 laser shots were typically accumulated with a laser pulse rate of 400 Hz in the MS mode, whereas in the MS/MS mode spectra up to 2,000 laser shots were acquired and averaged with a pulse rate of 1,000 Hz. Peptides were fragmented with collision-induced decomposition (CID) with an energy of 1 kV. For CID experiments, ambient air was used as collision gas with medium pressure of 10^{-6} Torr. The 20 most intense precursors per spot were selected with a minimum signal-to-noise (S/N) ratio of 50 and were fragmented in the CID mode. The peak detection criteria used were a minimum S/N of 10, a local noise window width mass/charge (m/z) of 200 and a minimum full-width half-maximum (bins) of 2.9. The contaminant m/z peaks originating from human keratin, trypsin autodigestion, or matrix were included in the exclusion list used to generate the peptide mass list for the database search.

2.6. De Novo Sequencing. The Applied Biosystem DeNovo Explorer software (AB SCIEX) was used for automated *de novo* sequencing followed by manual confirmation of most sequences generated. Those nonconfident fits were submitted to *de novo* sequencing analysis. The *de novo* sequencing parameters were set as follows: trypsin as the protease with one maximum missed cleavage allowed, the error tolerance of a parent- and fragment-mass was 0.08 u, deconvolute the charge state in the spectra to generate a spectrum in which each monoisotopic peak becomes singly charged, carbamidomethylation of cysteine as fixed modification and methionine oxidation as variable modification. The most abundant peptide fragments "*b-ions* and *y-ions*", the less abundant peptide fragments "*a-ions*", the neutral losses of water and ammonia for *b-ions* and *y-ions*, as well as the *immonium ions* were used to deduce confident and complete peptide sequences *de novo* from MS/MS spectra. Each MS/MS spectrum produced ten peptide sequence candidates, and each peptide sequence had a score associated with it that indicated how much of the total ion abundance in the MS/MS spectrum was accounted for by the typical fragment ions that can be calculated for the particular sequence; the closer the score was to 100, the greater the likelihood that all or most of the sequence generated by the DeNovo Explorer was corrected. In order to minimize randomness, only those peptides with a score higher than 50 were considered in this study.

2.7. Database Searches. A combined MS and MS/MS search was first performed against the NCBI database with no taxonomic restriction (updated December, 2010, containing 4,607,655 entries) using an in-house MASCOT server (Version 2.2). The raw MS and MS/MS spectra were processed using GPS Explorer software (Version 3.5, Applied Biosystems, USA) with the following criteria: MS peak filtering mass range, 850–4,000 Da; minimum signal-to-noise ratio, 10; peak density filter, 50 peaks per 200 Da; maximum number of peaks, 65; MS/MS peak filtering-mass range, 60–200 Da. The searches were conducted using the following setting: one missed cleavage, $P < 0.05$ significance threshold, 50 ppm peptide mass tolerance, 0.25 Da fragment mass tolerance peptide mass tolerance of 50 ppm, MS/MS ion tolerance of 0.1 Da, carbamidomethylation of cysteine as fixed modification, and methionine oxidation as variable modification. For a protein scores confidence interval (C.I.) below 95%, the MS/MS spectra were subjected to similarity searches against the dinoflagellate EST database (downloaded from NCBI, updated December, 2010, containing 171,550 entries) using the BLASTX algorithm [31]. The similarities were considered to be significant when the total ion C.I. % was $\geq$95, and the E value was below e^{-20}. Nonetheless, the remaining hits were further identified using *de novo* sequencing and homology-based search as previously described [32].

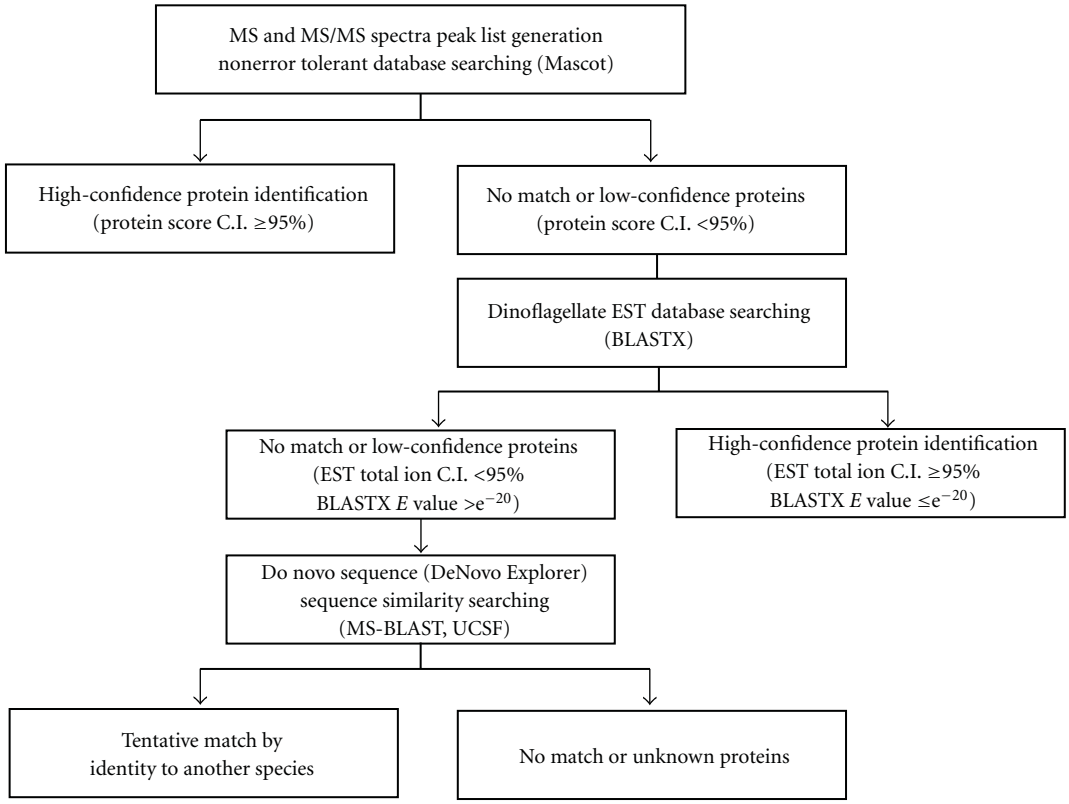

Figure 1: Multilayered protein identification workflow. After MASCOT search against the NCBI database, confident hits were identified with at least two peptides and protein scores above the minimum C.I. of 95%. Cross-species hits matching one peptide or protein scores below C.I. 95% were considered as borderline and were subjected to similarity searches against the dinoflagellate EST database using the BLASTx algorithm. The sequence similarities were considered to be significant if total ions score C.I. was ≥95% and the *E* value was $\leq e^{-20}$ at the amino acid sequence level. Nonconfident hits were interpreted using DeNovo Explorer software and MS-BLAST searches. Only HSPs with a score of 62 or above were considered confident.

De novo generated peptide sequences were used for homology searches using the MS BLAST algorithm. The MS-BLAST searches were conducted via the Washington University server (http://genetics.bwh.harvard.edu/msblast/disclaimer_ms.html) against the NCBI nonredundant database using standard settings with no taxonomic restriction. All sequences obtained from a MS/MS spectrum were spaced with the minus symbol (−) and were merged into a single string and submitted to an MS-BLAST search as reported before [33, 34]. The MS-BLAST search results were regarded as significant if the resulting scores were higher than the threshold score indicated in the MS-BLAST scoring scheme. However, only high-scoring segment pairs (HSSPs) with a score of 62 or above were considered. The clusters of orthologous groups [35] databases were used to infer the functional classification of the proteins identified.

3. Results

3.1. The Workflow of Protein Identification. The multilayered workflow integrated mass spectra processing with conventional and homology-based searches is outlined in Figure 1. Briefly, the MS and MS/MS spectra of each protein spot obtained from MALDI-TOF-TOF MS were first submitted to MASCOT search against the NCBI database with no taxonomic restriction. If the database entries were matched with at least two peptides and the protein scores taken from MS combined MS/MS search had a minimum C.I. of 95%, the protein hits were regarded as confident identifications. Cross-species hits matching one peptide or protein scores below a C.I. of 95% were considered as low-confidence identifications, and the MS/MS spectra were subjected to similarity searches against the dinoflagellate EST database. The sequences were then subjected to similarity searches against the NCBI nonredundant protein database (nr) using the BLASTX algorithm [31]. If the total ions score C.I. was above 95% and the *E* value was below e^{-20} at the amino acid sequence level, the sequence similarities were considered to be significant. In the last layer, those nonconfident hits were sequenced using *de novo* sequencing software to obtain candidate sequences and submitted to MS-BLAST searches. In the homology-based search, the statistical significance of hits was evaluated according to the MS BLAST scoring scheme. Only HSSPs with a score of 62 or above were considered to be confident [36, 37].

3.2. Protein Identification Using Mascot and Dinoflagellate EST Searches. The protein extract from *A. catenella* was

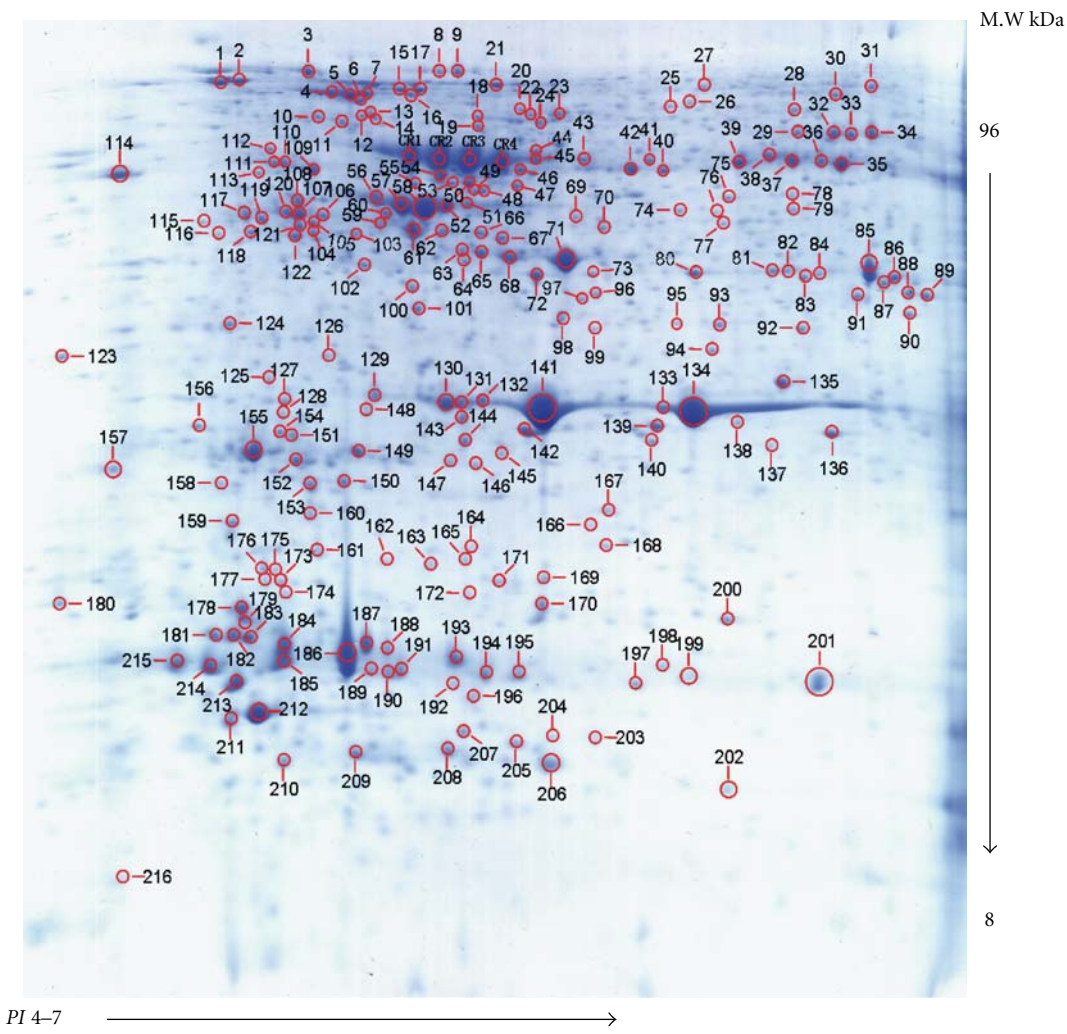

Figure 2: Representative 2-DE gel of an *A. tamarense* protein sample stained with CCB. The proteins were resolved in a linear 4–7 pH gradient (Immobiline DryStrips) and 12.5% SDS-PAGE.

separated using 2-DE and visualized using the modified CBB stain method. An average of about 880 protein spots was detected in the 2-DE gel (Figure 2). Among them, 220 representing low, moderate, and high abundance intracellular proteins were randomly excised from the 2-DE gel and were in-gel digested using trypsin after destaining the gel plugs. The peptide fragments extracted from the gel plugs were subjected to tandem mass spectrometry using the AB SCIEX MALDI-TOF/TOF 5800 System. Tandem mass spectra excluding contaminant peaks from human keratin, trypsin autodigestion, or matrix were directly submitted for database searching (GPS Explore: MASCOT) for protein characterization using the NCBInr database with or without all known posttranslational modifications. Out of the 220 protein spots, 104 were identified statistically as cross-species matches yielding positive characterization and high matching score in MASCOT searches and accounted for a half of the totally identified proteins (see Supplemental file 1 available online at doi:10.1155/2011/471020). Among them were 100 protein spots with two or more MS/MS significant hits, and four protein spots with one MS/MS significant hit which was regarded as the borderline. A large proportion of the identified proteins showed a high level of similarity to the proteins of dinoflagellates (49.0%), nondinoflagellate algae (8.7%), and other species of organisms (42.3%) (Figure 5(a)).

The remaining 116 protein spots with low protein scores (<C.I 95%) as well as those proteins with one MS/MS hit were subjected to search against the EST database about dinoflagellate sequences, combining with BLASTX analysis. With a stringent cut-off *E* value of e^{-20} or less and a total ion C.I. % of ≥95, a total of 72 sequence similarities were confidently identified in *A. tamarense* (Supplemental file 1). A large proportion of the identified proteins showed a high level of similarity to dinoflagellate proteins (59.7%), nondinoflagellate algae (11.1%), and other species of organisms (29.2%) (Figure 5(b)). The rest of the protein spots with nonconfident hits were subsequently identified using a combination of *de novo* sequencing and MS-BLAST searches.

3.3. Protein Identification Using De Novo Sequencing and MS-BLAST Searches. Typically, the 20 most intense peaks

in the PMF were selected for MS/MS analysis. The tandem mass spectra were analyzed using DeNovo Explorer software to generate amino acid sequences and deconvoluted to minimize the error in *de novo* sequencing. DeNovo Explorer works in the same way as PEAKS: briefly, the algorithm first computes a *y*-ion matching score and a *b*-ion matching score at each mass value according to the peaks around it. If there are no peaks around a mass value, a penalty value is assigned. The algorithm then efficiently computes many amino acid sequences, and each candidate peptide sequence is assigned a score that indicates the degree of matching of the peaks and the intensity of the peaks between the theoretical fragmentation spectrum and the fragmentation spectrum that corresponds to the peaks in the peak list. The scores in the Denovo Explorer are calculated based on the percent peak intensity match of the fragments between the actual data and the candidate peptide. These candidate sequences are further evaluated by a more accurate scoring function, which also considers other ion types such as *immonium* ions and internal cleavage ions [32].

In most spots, 100 to 200 amino acid sequences, with a length varying between seven and 37 amino acids, were obtained *de novo*. In this study, the *de novo* sequencing selects the most abundant peptide fragments "*b-ions*" and "*y-ions*", less abundant peptide fragments "*a-ions*", and the neutral losses of water and ammonia for *b-ions* and *y-ions* as well as *immonium* ions to generate confident peptide sequences *de novo* from MS/MS spectra. Figure 3 shows the MS spectrum of the in-gel tryptic peptide mixture of spot 124, and displays the fragmentation pattern of a precursor ion with *m/z* of 1755.6631 from spot 124 and the *b*-, *y*-, *a*-, and *immonium ions* as well as the neutral losses of water and ammonia for *y-ions* and *b-ions* (Figure 4(a)). Ten possible peptide sequences for this precursor were deduced from DeNovo Explorer *de novo* sequencing and are listed in the order according to their scores in Figure 4(b). The peptide sequence candidate with the highest score for this precursor was "NNHDENVGAVIVGFDR" deduced from DeNovo Explorer *de novo* sequencing. A similar analysis was performed on the other selected protein spots.

The *de novo* deduced peptide sequences were used to identify the proteins using sequence similarity searching. Several database searching tools have been developed that accommodate the specific requirements of MS/MS sequencing [27, 38]. In our study, the homology-based data search approach MS-BLAST was used. This is the most popular database search approach for identifying unknown proteins using sequence similarity to homologous proteins available in a database. The redundant, degenerate, and partially inaccurate peptide sequences obtained by *de novo* interpretation of MS/MS spectra are assembled into a single searching string in arbitrary order [33, 37]. The quality of the results is dependent on the number of peptides sequenced and the accuracy of the sequence information entered, as well as database completeness and species-to-species sequence variability for the peptides entered. It is also possible to enter a part of the sequence as a mass, along with a tolerance factor.

The *de novo* derived sequence information from each protein spot with nonconfident hits was combined in one search query and analyzed using the MS BLAST algorithm. The results were chosen according to the number of HSSPs from different MS/MS spectra [37], and phylogenetic closeness to dinoflagellates was also considered. Using this strategy, 40 protein spots out of 44 protein spots were tentatively identified, 32 of them obtaining two or more HSSP significant hits and eight only one. However, four protein spots could not obtain positive identification and were assigned to unknown proteins (Supplemental file 1). A large proportion of the identified proteins showed a high level of similarity to proteins of dinoflagellates (15.0%), non-dinoflagellate algae (2.5%) and other species of organisms (82.5%) (Figure 5(c)).

3.4. Validation of MASCOT Cross-Species Identifications with Borderline Statistical Confidence. Cross-species identification of proteins by matching identical peptides in known homologous proteins is a conventional proteomic methodology. However, such identification often results in borderline statistical confidence due to the relatively rare peptides and only a few peptide sequences matching. Here, we demonstrate how *de novo* sequencing and MS BLAST searches provided independent validation of borderline cross-species MASCOT hits [39]. The MS BLAST scoring scheme and its validation are described elsewhere [37].

In spot 187 of the above sample of *A. tamarense* proteins, a MASCOT search identified a plausible homologue of the chloroplast light harvesting complex protein from another algal species, *Heterocapsa triquetra*. However, this identification relied upon a single exactly matching peptide, and, in line with current proteomics guidelines [40], it should be considered as borderline. To validate this hit, the MS/MS spectrum was then interpreted *de novo* (Figures 6(a1) and 6(b)), and the top ten candidate sequences were linked in a string and submitted to MS BLAST search (Figure 6(e)), which produced a statistically confident hit from *A. carterae* to the overlapping sequence stretch in a related database entry. It should be noted that peptide sequences of the MASCOT hit and *de novo* candidates differed in their length of amino acid sequence, and, currently, it is not possible to judge which peptide sequence was correct, since the full sequence of the *A. tamarense* protein remains unknown. The two proteins from the MASCOT hit and MS BLAST search were homologous. However, this did not affect the confidence of the MS BLAST hit assignment, which relies upon an independent scoring scheme that only considers the local similarity of sequence stretches aligned within the HSP. In regard to spot 214, the MASCOT hit and the result of MS BLAST search using *de novo* candidates were identical using validated methods [36] (Figures 6(a2), 6(a3), 6(c) and 6(e)). Additionally, MS BLAST searches also revealed one new peptide (precursor MW 2480.3132) from a protein already matched by MASCOT (spot 214) thus improving the sequence coverage and confidence of identification.

3.5. Functional Categorization of the Proteins Identified from A. tamarense. Using the multilayer, stringent, and homology-similarity database searching strategy, 216 protein

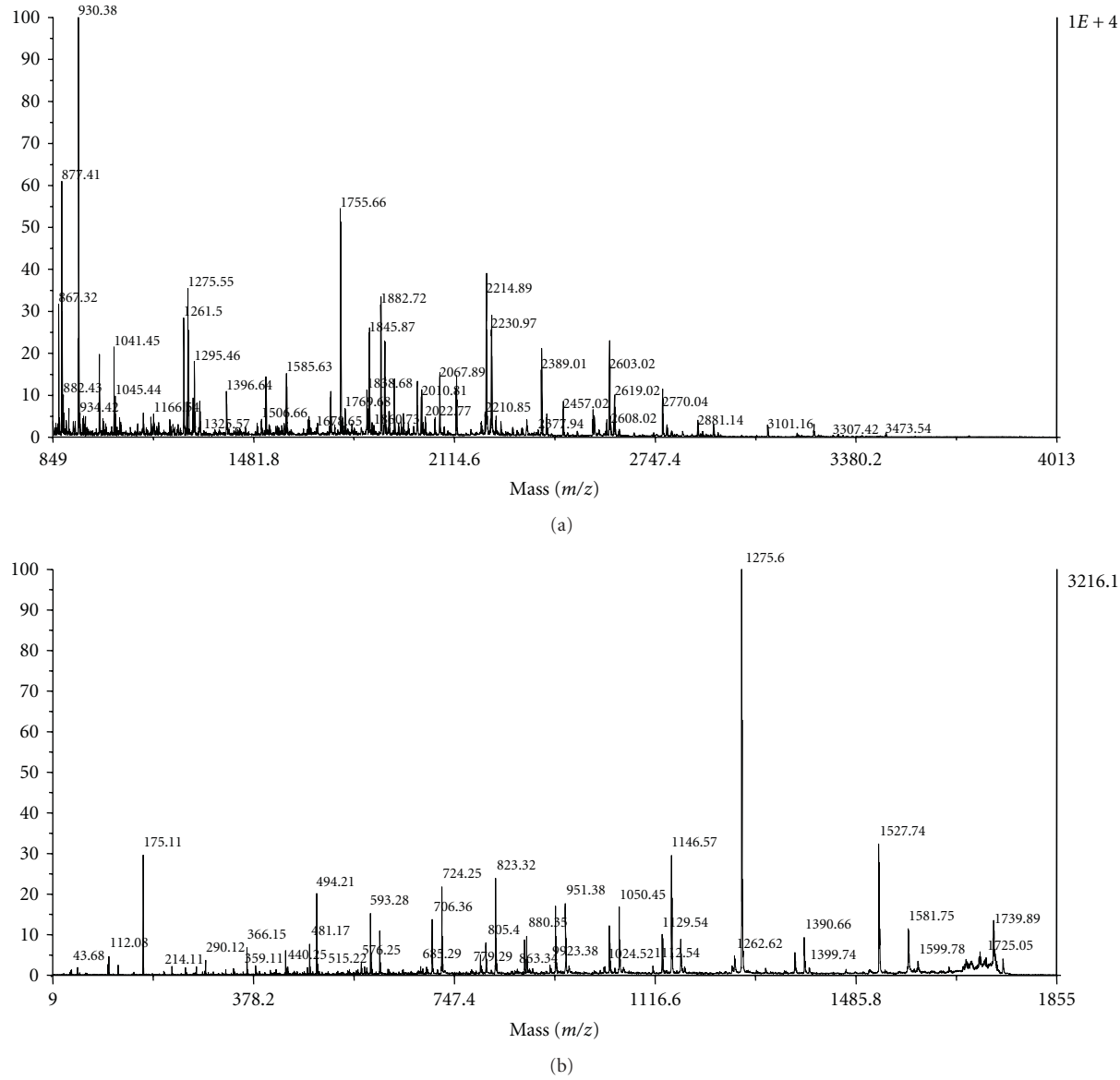

Figure 3: Peptide mass fingerprint and MS/MS spectrum (peptide 1755.6631) derived from spot 124 in Figure 2.

spots (representing 158 unique proteins) were identified from *A. tamarense* out of the 220 protein spots isolated. The remaining four protein spots did not give positive identification and were assigned to unknown proteins. The NCBI accession number, protein name, protein score and C.I. %, total ion score and C.I. %, number of unique peptides and total spectra used in the identification; and the theoretical MW and isoelectric point of the proteins identified are listed in the Web Appendix.

It should be pointed out that many of the proteins identified presented multiple isoforms in 2-DE gel with different *PI* and MW values, thus forming a train of spots horizontally or scattering on the 2-DE gel. For example, four isoforms of ribulose-1,5-bisphosphate carboxylase oxygenase (RuBisCO), CR1, CR2, CR3, and CR4 were identified in 2-DE gel with different *PI* values, but they matched the same amino acid sequence. It is known that a large number of isoforms are caused by single-nucleotide polymorphisms or SNPs, small genetic differences between alleles of the same gene. Currently, we cannot determine whether these isoforms are physiologically relevant, but the existence of multiple isoforms opens new areas for understanding gene functions in dinoflagellates.

Based on the functional categories established [28], 158 unique proteins were classified into 23 groups (Figure 7). Among the unique proteins identified, 21.6% were involved in photosynthesis, 6.4% were in glycolysis, 6.4% in amino acid metabolism, 5.7% in other enzymatic processes, 5.7% were transporters, and 5.1% were involved in stress response or as chaperones. Other proteins, accounting for small number of the total, were related to protein synthesis and degradation (4.5%), cell structure and motility

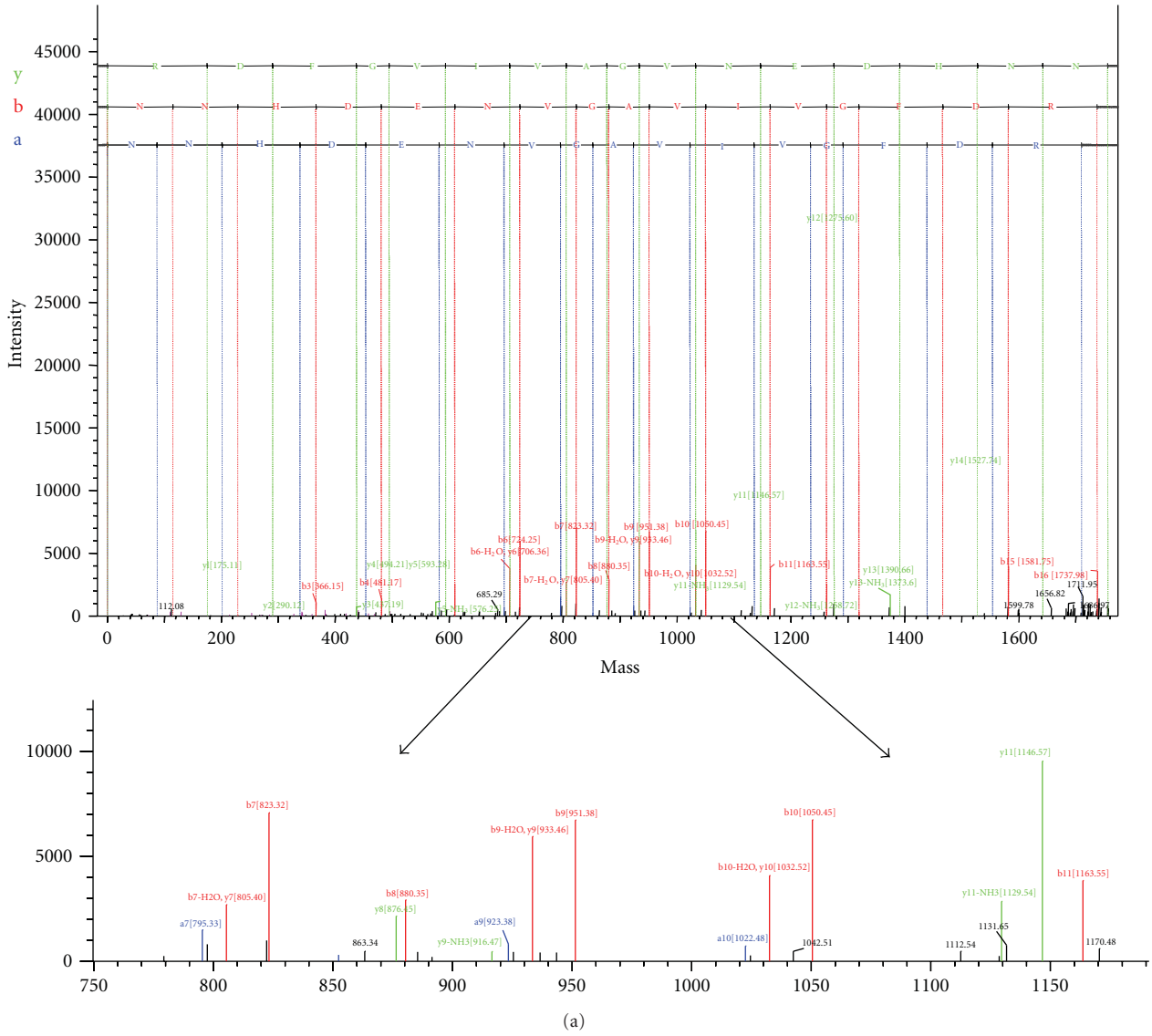

(a)

Precursor ion1755.6631

Rank	Sequence	Score
1	NNHDENVGAVIVGFDR	84.1073
2	NNHDENVGAVLRFDR	81.1464
3	PMHDENVGAVLRFDR	81.1464
4	VEHDENVGAVPDGFDR	79.9413
5	PMHDNEVGAVLRFDR	72.6614
6	NNHDNEVGAVLRFDR	72.6614
7	NNHDENVLNLRFDR	72.6604
8	PMHDENVLNLRFDR	72.6604
9	VEHDTAAVGAVPDGFDR	71.3905
10	VEHDENVGPWRFDR	69.196

(b)

Figure 4: *De novo* analysis of an unknown protein from *A. tamarense*. (a) The *x*- and *y*-axes show the mass-to-charge (*m/z*) ratio and the % abundance of the precursor ion fragments (*m/z* of 1755.6631), respectively. The MS/MS spectrum was analyzed using DeNovo Explorer software to generate "NNHDENVGAVIVGFDR", and (b) the table details ten peptide sequence candidates for this precursor deduced from DeNovo Explorer *de novo* sequencing.

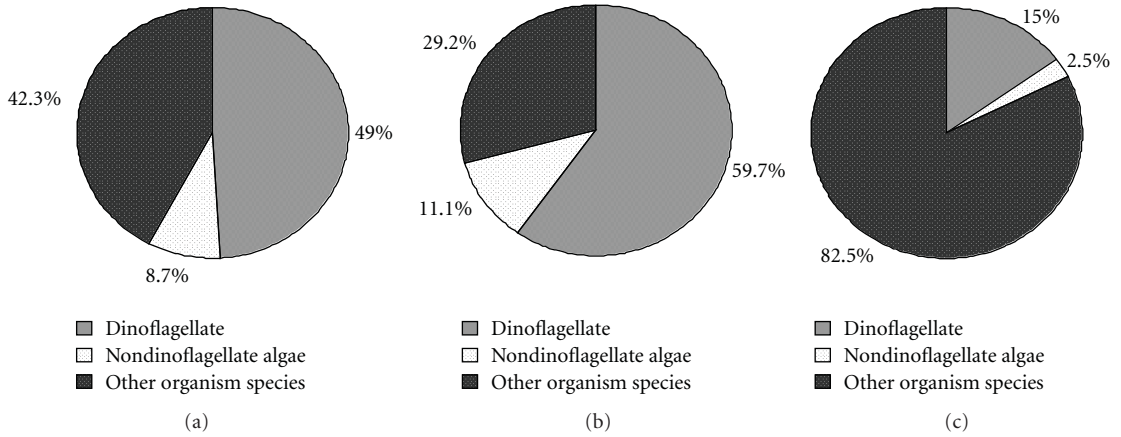

Figure 5: Taxonomic group distribution of proteins from *A. tamarense*. (a) Proteins identified using MASCOT search against the NCBInr database, (b) proteins identified against the dinoflagellate EST database, and (c) proteins identified with *de novo* and MS-BLAST search.

(3.8%), the TCA cycle (3.8%), protein modification and folding (3.8%), antioxidant activities (2.5%), carbohydrate metabolism (2.5%), nucleotide metabolism (2.5%), transcription (1.9%), the glyoxylate cycle (1.3%), the cell cycle and division (1.3%), intracellular trafficking (1.3%), DNA replication and repair (0.6%), lipid metabolism (0.6%), the electron transport chain (0.6%) and signaling (0.6%). Other functional and unknown function proteins accounted for 4.5% and 13.4% of the total protein, respectively.

4. Discussion

4.1. Protein Identification Strategy for Genome-Unsequenced Dinoflagellates. Dinoflagellates are not only the major causative agents of worldwide HABs but also are the producers of various potent biotoxin. However, a worldwide lack of available genetic information limits our understanding of HABs and consequently our ability to monitor, mitigate and prevent them. Proteomics provides effective strategies and tools for profiling and identifying dinoflagellate proteins in order to elucidate the biochemical and molecular mechanisms of bloom formation and toxin biosynthesis. Contemporary proteomics requires prompt and confident protein identification of proteins of interest. A sequence similarity search is a powerful tool for the identification of proteins from organisms with unsequenced genomes [33, 42–46]. In the past few years, various sequence similarity search engines, such as MS-BLAST [33], FASTS [43], CIDentify [41], MS-Homology [47], and OpenSea [48], have been developed and successfully applied in various proteomic studies. Partial sequence tags or complete peptide sequences were deduced directly from MS/MS spectra with no recourse to database resources [49] and then searched against a database in an error-tolerant fashion. In this way, even proteins with only marginal sequence similarity to reference database entries could be identified [42, 45, 46]. Recently, a layered manner combining LS-MS/MS analysis with stringent data processing and sequence similarity database search was developed and successfully applied to identify proteins in organisms with unsequenced genomes [34].

De novo sequencing analysis is a newly developed strategy for protein identification from incomplete- or nongenome organisms, which is regarded as the only alternative choice for the study of organisms with incomplete databases or databases not included in the public domain [20, 50–52]. This approach has been successfully applied in recent studies with incomplete- or nongenome organisms in order to characterize their proteins [19–23]. In this way, partial or complete amino acid sequences are obtained using either manual or automated *de novo* peptide sequence analysis. Manual protein sequencing can yield exact amino acid sequences without ambiguity via Edman degradation, but this procedure is time consuming and laborious. Moreover, its sensitivity is lower than mass spectrometry, and it is halted by the presence of blocked amino acids. Several automated software tools have been developed to deduce the amino acid sequences from an MS/MS spectrum [53–55], which consists of a ladder of peaks for *y-ions* (ions containing a *C*-terminus) and *b-ions* (ions containing an *N*-terminus). Interpretation of MS/MS spectra relies on calculating the mass differences between adjacent fragment ion peaks of *y*-series or *b*-series, which are common in tryptic peptides. *De novo* sequencing enables the analysis of quality MS/MS spectra which fail to generate protein identifications after database searches, which is the case for the majority of dinoflagellate proteins.

In the present study, a multilayer, stringent and sequence similarity database searching strategy combining MALDI-TOF-TOF MS with *de novo* sequence analysis and stringent homology-based searching tools was developed, which provided a rapid and reliable means to identify proteins in *A. tamarense* with an unsequenced database. This data interpretation pipeline has no need for chemical derivatization or isotopic labeling of analyzed peptides or for repetitive MALDI-FOF-TOF analysis under specific settings, and is applicable to all two dimensional gel-based proteomic approaches for studying dinoflagellates. Moreover, it might also have important implications for proteomics in fully

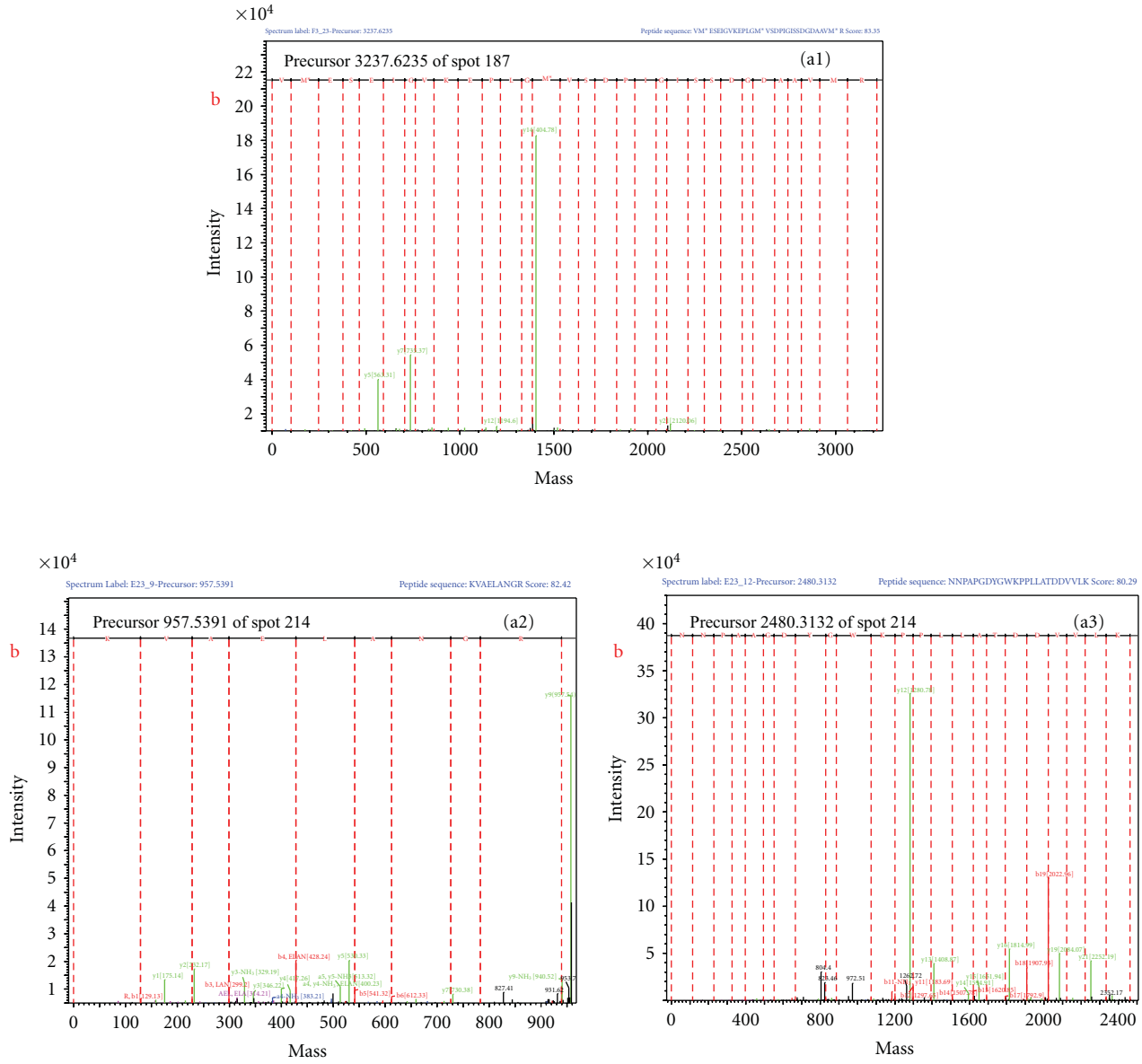

(a)

Precursor MW	Peptide sequence candidate	Score	Modifications
	VM*ESEIGVKEPLGM*VSDPIGISSDGDAAVM*R	93.3536	
	VM*ESEIRKEPLGM*VSDPIGISSDGDAAVM*R	92.8288	
	VPAIPNIGVKEPLGM*VSDPIGISSDGDAAVM*R	92.7511	
	VM*ESEIRKEPLGM*VSDPIGISSDGDAIGM*R	92.7233	
3237.6235	AVPIPNIGVKEPLGM*VSDPIGISSDGDAAVM*R	92.716	*Oxidation
	VPAIPNIRKEPLGM*VSDPIGISSDGDAAVM*R	92.2264	
	SSM*VAADGDSSIGIPDVSM*GPLEKVGVVMENN	83.4756	
	VM*ESEIRKEPLGM*VSDPIGISSDGVSAVM*R	82.9515	
	VM*ESEIRKEPLGM*VSDPIGISSDENAVM*R	82.5414	

(b)

Figure 6: Continued.

Precursor MW	Peptide sequence candidate	Score	Remarks
957.5391	KVAELANGR	82.42	
			Matching peptide in MASCOT
2480.3132	NNPAPGDYGWKPPLLATDDVVLK	80.29	

(c)

```
^ = gi|3355306|emb|CAA08771.1| light-harvesting polyprotein precursor
                    [Amphidinium carterae]
          Length = 820

Total score: 640

                                0         170         340         510         680
                                |         |           |           |           |          |820
gi|3355306|emb|CAA087          |
Local hits (HSPs)               |

 Score = 79 (39.9 bits)
 Identities = 9/11 (81%), positives = 10/11 (90%)

Query: 399 ISMIATMGYIT 409
           I M+ATMGYIT
Sbjct: 654 IAMLATMGYIT 664

 Score = 79 (39.9 bits)
 Identities = 9/11 (81%), positives = 10/11 (90%)

Query: 381 ISMIATMGYIT 391
           I M+ATMGYIT
Sbjct: 310 IAMLATMGYIT 320
```

(d)

```
^ = gi|53748880|dbj|BAD52338.1| chlorophyll a/c-binding protein [Alexandrium
                                tamarense]
          Length = 110

Total score: 147

                                0         30          60          90
                                |         |           |           |          |110
gi|53748880|dbj|BAD52          |
Local hits (HSPs)               |

 Score = 100 (51.3 bits)
 Identities = 14/16 (87%), positives = 14/16 (87%)

Query: 14 APGDYGWKPPLLATDD 29
          APGD GWKPP LATDD
Sbjct: 43 APGDCGWKPPVLATDD 58

 Score = 47 (25.1 bits)
 Identities = 7/7 (100%), positives = 7/7 (100%)

Query: 3 AELANGR 9
          AELANGR
Sbjct: 67 AELANGR 73
```

(e)

Figure 6: *De novo* sequencing and an MS-BLAST search validated a borderline hit produced using the MASCOT search. (a) The *x*- and *y*-axes show the mass-to-charge (*m/z*) ratio and the % abundance of the precursor ion fragments, respectively. The MS/MS spectrum was analyzed using DeNovo Explorer software to generate peptide (precursor 957.5391, 2480.3132, and 3237.6235) sequence candidates, (b) the table details ten peptide sequence candidates for the precursor 3237.6235 deduced from *de novo* sequencing, (c) the file corresponding to the spectrum in a2 and a3 and their *de novo* interpretation produced two candidate sequences with the quality score, and (d) and (e) the peptide sequence candidates from (b) and (c) were merged into an MS-BLAST query, and the search hit the same protein from *A. tamarense*. According to the MS-BLAST scoring scheme, the hits were confident.

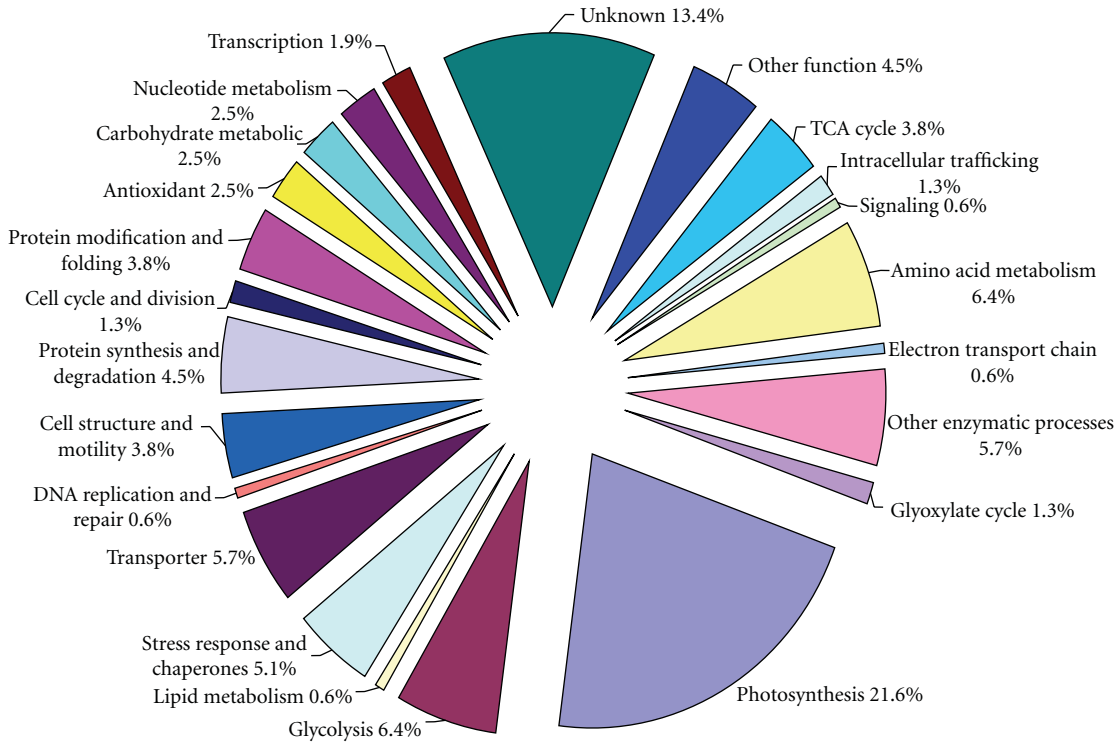

Figure 7: GO functional classification of the proteins identified in *A. tamarense*. The functional categories were defined according to Taylor and Johnson [41].

sequenced organisms, as it validates borderline hits produced by conventional database searches and has the potential for unbiased screening for PTMs, sequence polymorphism and unrecognized splicing variants.

4.2. Protein Functions of Dinoflagellates. *A. tamarense* is an autotrophic microalgae which uses CO_2 and light as carbon and light sources. This study identified various light-harvesting proteins, chloroplast light-harvesting complex proteins, chl *a*- or *c*-binding proteins, and peridinin-chl *a*-binding proteins, which have been reported in many dinoflagellate species at the transcriptional level [27]. RuBisCO is the most abundant protein on earth and triggers reactions to make the carbohydrates, proteins, and fats used to sustain all forms of life. In our study, four isoforms of RuBisCO (spots CR1, CR2, CR3, and CR4) were identified abundantly in *A. tamarense*. Beside these isoforms, RuBisCO large subunits were also found in *A. tamarense*. RuBisCO has also been found widely in many dinoflagellate species. Moreover, several other proteins involved in the Calvin cycle, that is, chloroplast transketolase, ribulose-5-phosphate 3-epimerase, chloroplast phosphoribulokinase, ribulose bisphosphate carboxylase were also identified in *A. tamarense* these proteins are involved in various processes of the Calvin cycle and participate in carbon fixation. Glyceraldehyde-3-phosphate dehydrogenase (GAPDH) was another major component of the proteins identified. Nine spots (spots 51, 60, 63, 68, 71, 82, 85, 86, and 146) were identified as GAPDH, and they presented different cellular locations in *A. tamarense*. GAPDH is an enzyme that catalyzes the sixth step of glycolysis and thus serves to break down glucose for energy and carbon molecules. In addition to this function, GAPDH has recently been implicated in several nonmetabolic processes, including transcription activation, initiation of apoptosis and ER to Golgi vesicle shuttling. Sequences coding for this enzyme has also been reported amongst the highest expressed in the EST libraries of other dinoflagellates such as *A. catenella* [27], *L. polyedrum* [56], *A. tamarense* [26], *K. brevis* [57], and *A. fundyense* [58]. Another transferase enzyme, chloroplast phosphoglycerate kinase involved in glycolysis, was identified. It transfers a phosphate group from 1,3-biphosphoglycerate to ADP, forming ATP and 3-phosphoglycerate. Beside these proteins, a number of proteins involved in the light phase of photosynthesis, such as chloroplast ferredoxin-NADP (+) reductase, photosystems I subunit VII, cytochrome b6, PsbV, and chloroplast ATP synthase gamma-subunit, were identified in *A. tamarense*. Two proteins involved in chlorophyll synthesis, geranylgeranyl reductase, and plastid fructose-1,6-bisphosphate aldolase class II protein precursor were also identified.

Protein synthesis is a complex biological process, including amino acid elongation, protein folding, posttranslational modification, and protein degradation. Our study identified translational initiation inhibitor, peptidase, ribosomal protein, elongation factor, calretulin, protease, proteasome, and other protein-synthesis-related proteins in *A. tamarense*. These proteins participate in amino acid elongation, protein modification, folding, and degradation in *A. tamarense*

cells. Moreover, two proteins (signal peptidase I and ADP-ribosylation factor-like 2) involved in intracellular trafficking were also identified in *A. tamarense*. These two proteins participate in the proteolytic processing of proteins or folding of tubulin peptides.

Seven proteins involved in amino acid metabolism were identified in *A. tamarense*, that is, methionine S-adenosyl transferase, S-adenosyl-homocysteine hydrolase-like protein, adenylyl sulfate kinase, glutamine synthetase, glutamate semialdehyde synthase, adenosylhomocysteinase, and ketol-acid reductoisomerase. These proteins participate in the biosynthesis and conversion of various amino acids in dinoflagellate cells.

Glycolysis is thought to be the archetype of a universal metabolic pathway that converts glucose $C_6H_{12}O_6$, into pyruvate, CH_3COCOO^- and H^+. The free energy released in this process is used to form the high-energy compounds ATP and NADH. It occurs, with variations, in nearly all organisms, both aerobic and anaerobic. In this study, six proteins involved in different steps of glycolysis were identified; they were enolase, fructose bisphosphate aldolase, GAPDH, phosphoglucomutase, phosphoglycerate kinase, and triose-phosphate isomerase.

Four proteins, peptidoglycan interpeptide bridge formation enzyme, alcohol dehydrogenase GroES domain protein, glucose-methanol-choline oxidoreductase, and a predicted protein were identified in *A. tamarense*. These proteins might be involved in cell wall formation, peptidoglycan synthesis, as glucose oxidase, and other functions.

In eukaryotic cells, the citric acid cycle (TCA) is part of a metabolic pathway involved in the chemical conversion of carbohydrates fats, and proteins into carbon dioxide and water to generate a form of usable energy. Our study identified six proteins involved in the TCA cycle, that is, malate dehydrogenase, and its precursor, dihydrolipoamide acetyltransferase, isocitrate dehydrogenase and two hypothetical proteins. Furthermore, two proteins, phosphoglycolate phosphatase precursor and isocitrate lyase, involved in the glyoxylate cycle, were also identified, and these two proteins participate in glyoxylate and dicarboxylate metabolism.

Five ATPase regulating cation and calcium transports were identified in *A. tamarense*. ATPases are a class of enzymes that catalyze the decomposition of adenosine triphosphate (ATP) into adenosine diphosphate (ADP) and a free phosphate ion. This dephosphorylation reaction releases energy, which the enzyme (in most cases) is harnessed to drive other chemical reactions that would not otherwise occur. Some such enzymes are transmembrane ATPases which move solutes across the membrane, typically against their concentration gradient. Three other hypothetical transport proteins were also identified in our study, but their functions were not well known.

Little is known concerning the cell cycle regulation of dinoflagellate cells although a few cyclin-like proteins have been found in some dinoflagellate species. Our study identified two cell cycle regulating proteins, cell division protein FtsZ, and DNA damage checkpoint protein rad24. The former is the key protein in cell division while the latter is essential for DNA damage checkpoint control. Another cell cycle regulation protein, DNA polymerase, was also identified in this study which plays an important role in DNA replication and repair in eukaryotes.

Three transcriptional proteins, pseudouridine synthase, ATP-dependent helicase, and hypoxia-inducible factor 1 alpha inhibitor were identified from *A. tamarense*. These proteins play critical roles in maintaining the structure and integrity of DNA or RNA.

A. tamarense is a motile organism with two flagella which propel the cells through the water. In our study, actin, tubulin, and flagellin were identified from *A. tamarense*. Actin and tubulin being two major components of flagella and cilia in protists including dinoflagellates, while flagellin is a protein forming the filament in the bacterial flagellum. The presence of theses proteins indicated that they play important roles in the cell structure and motility of *A. tamarense*.

Stress proteins and antioxidant enzymes have been identified in dinoflagellate species [59]. In our study, two antioxidative enzymes, copper/zinc superoxide dismutase and superoxide dismutase, and two antioxidant proteins, peroxiredoxin V protein and a conserved hypothetical protein, were identified in *A. tamarense*. Heat shock proteins (HSPs) are highly regulated proteins that are involved in normal cellular activity and are upregulated when the cell is exposed to stress such as heat or excess ROS production. This study identified three HSPs, HSP60, 70 and 90, and one HSP chaperone, GroEL-like chaperone, ATPase in *A. tamarense*. A previous study demonstrates HSP 60, together with Mn SOD and Fe SOD in a dinoflagellate species, *Karenia brevis*, and these play an important role in the survival of this species.

Beside the above functional groups, numerous proteins involved in transcription, the electron transport chain, nucleotide metabolism, signaling, and lipid metabolism together with some other functional proteins were also identified from *A. tamarense*. It should be emphasized that most of the proteins identified in the present study have been predicted at transcriptional levels in various dinoflagellates [60, 61], which further demonstrated that the protein identifying method developed in this study was rapid and reliable, although some proteins were identified with unknown functions. In future, more effort should be devoted to both transcriptomic and genomic studies of dinoflagellates, which will facilitate protein identification, and to proteomic studies which will aid in gaining an understanding of HABs and the subsequent monitoring, mitigation, and prevention of HABs.

In summary, the current study was undertaken to delineate a proteomics scale methodology to identify proteins from dinoflagellates. Using this methodology, 116 out of the 220 excised protein spots, representing high, moderate, and low abundant proteins, gave positive identification. Most of them have been predicted at the transcriptional level or have been identified from various dinoflagellate species and play important roles in the various physiological activities of dinoflagellates. Nevertheless, the present results provided the first preliminary proteomic profile and 2-DE gel reference map of *A. tamarense* and will form the basis of future

proteomics scale studies using the unsequenced database of *A. tamarense*.

5. Supporting Information

List of all peptide sequences deduced from each MS/MS spectrum using DeNovo Explorer software *de novo* sequencing.

Acknowledgments

The authors thank Professor John Hodgkiss from the University of Hong Kong for his help with English. They also thank Drs. Yong-Ming Xie and Li-Hai Guo from AB SCIEX Company (Shanghai, China) for their assistance during mass spectrometric analysis. This work was partially supported by research grants from the National Natural Science Foundation of China (40776068, 40876059, and 40821063), the Ministry of Science and Technology of the People's Republic of China (Project No. 2010CB428703), the Excellent Group, and the Program for New Century Excellent Talents in University to D.-Z. Wang.

References

[1] M. O. Soyer-Gobillard, "Dinoflagellates," in *Encyclopedia of Microbiology*, S. Moselio, Ed., pp. 617–633, Academic Press, New York, NY, USA, 2009.

[2] G. M. Hallegraeff, "Harmful algal blooms: a global review," in *Manual on Harmful Marine Microalgae*, G. M. Hallegraeff, D. M. Anderson, and A. D. Cembella, Eds., pp. 25–49, UNESCO, Landais, France, 2005.

[3] F. M. VanDolah, "Diversity of marine and freshwater algal toxins," in *Seafood and Freshwater Toxins: Pharmacology, Physiology, and Detection*, L. M. Botana, Ed., pp. 19–44, CRC Press, New York, NY, USA, 2000.

[4] J. P. Quod and J. Turquet, "Ciguatera in Reunion Island (SW Indian Ocean): epidemiology and clinical patterns," *Toxicon*, vol. 34, no. 7, pp. 779–785, 1996.

[5] J. R. Geraci, D. M. Anderson, R. J. Timperi et al., "Humpback whales (*Megaptera novaeangliae*) fatally poisoned by dinoflagellate toxin," *Canadian Journal of Fisheries and Aquatic Sciences*, vol. 46, pp. 1895–1898, 1989.

[6] J. H. Landsberg and K. A. Steidinger, "A historical review of red tide events caused by Gymnodinium breve as related to mass mortalities of the endangered manatee (Trichechus manatus latirostris) in Florida, USA," in *Proceedings of the Eighth International Conference on Harmful Algae*, B. Reguera, J. Blanco, M. Fernandez, and T. Wyatt, Eds., pp. 97–100, Xunta de Galicia and IOC of UNESCO Publishers, Santiago de Compostela, Spain, 1997.

[7] C. A. Scholin, F. Gulland, G. J. Doucette et al., "Mortality of sea lions along the central California coast linked to a toxic diatom bloom," *Nature*, vol. 403, no. 6765, pp. 80–84, 2000.

[8] L. J. Flewelling, J. P. Naar, J. P. Abbott et al., "Red tides and marine mammal mortalities," *Nature*, vol. 435, no. 7043, pp. 755–756, 2005.

[9] D. M. Anderson, "Toxic algal blooms and red tides: a global perspective," in *Red Tides: Biology, Environmental Science, and Toxicology*, D. M. Okaichi, T. Anderson, and T. Nemoto, Eds., pp. 11–16, Elsevier, New York, NY, USA, 1989.

[10] T. J. Smayda, "Novel and nuisance phytoplankton blooms in the sea: evidence for a global epidemic," in *Toxic Marine Phytoplankton*, E. Graneli, B. Sundstrøm, L. Edler, and D. M. Anderson, Eds., pp. 29–40, Elsevier, New York, NY, USA, 1990.

[11] J. D. Hackett, D. M. Anderson, D. L. Erdner, and D. Bhattacharya, "Dinoflagellates: a remarkable evolutionary experiment," *American Journal of Botany*, vol. 91, no. 10, pp. 1523–1534, 2004.

[12] P. J. Rizzo, "The enigma of the dinoflagellate chromosome," *Journal of Eukaryotic Microbiology*, vol. 38, no. 3, pp. 246–252, 1991.

[13] T. C. LaJeunesse, G. Lambert, R. A. Andersen, M. A. Coffroth, and D. W. Galbraith, "Symbiodinium (Pyrrhophyta) genome sizes (DNA content) ARE smallest among dinoflagellates," *Journal of Phycology*, vol. 41, no. 4, pp. 880–886, 2005.

[14] D. L. Spector, "Dinoflagellate nuclei," in *Dinoflagellates*, pp. 107–147, Academic Press, New York, NY, USA, 1984.

[15] F. G. Plwnley, "Marine algal toxins: biochemistry, genetics, and molecular biology," *Limnology and Oceanography*, vol. 42, no. 5, pp. 1252–1264, 1997.

[16] L. L. Chan, I. J. Hodgkiss, J. M. F. Wan et al., "Proteomic study of a model causative agent of harmful algal blooms, *Prorocentrum triestinum* II: the use of differentially expressed protein profiles under different growth phases and growth conditions for bloom prediction," *Proteomics*, vol. 4, no. 10, pp. 3214–3226, 2004.

[17] L. L. Chan, I. J. Hodgkiss, P. K. S. Lam et al., "Use of two-dimensional gel electrophoresis to differentiate morphospecies of *Alexandrium minutum*, a paralytic shellfish poisoning toxin-producing dinoflagellate of harmful algal blooms," *Proteomics*, vol. 5, no. 6, pp. 1580–1593, 2005.

[18] L. L. Chan, W. H. Sit, P. K. S. Lam et al., "Identification and characterization of a "biomarker of toxicity" from the proteome of the paralytic shellfish toxin-producing dinoflagellate Alexandrium tamarense (Dinophyceae)," *Proteomics*, vol. 6, no. 2, pp. 654–666, 2006.

[19] D. F. Hunt, R. A. Henderson, J. Shabanowitz et al., "Characterization of peptides bound to the class I MHC molecule HLA-A2.1 by mass spectrometry," *Science*, vol. 255, no. 5049, pp. 1261–1263, 1992.

[20] M. Getie, C. E. Schmelzer, and R. H. Neubert, "Characterization of peptides resulting from digestion of human skin elastin with elastase," *Proteins*, vol. 61, no. 3, pp. 649–657, 2005.

[21] A. L. Yergey, J. R. Coorssen, P. S. Backlund et al., "*De novo* sequencing of peptides using MALDI/TOF-TOF," *Journal of the American Society for Mass Spectrometry*, vol. 13, no. 7, pp. 784–791, 2002.

[22] N. S. Tannu and S. E. Hemby, "*De novo* protein sequence analysis of *Macaca mulatta*," *BMC Genomics*, vol. 8, no. 1, article 270, 2007.

[23] B. Samyn, K. Sergeant, S. Memmi, G. Debyser, B. Devreese, and J. Van Beeumen, "MALDI-TOF/TOF *de novo* sequence analysis of 2-D PAGE-separated proteins from *Halorhodospira halophila*, a bacterium with unsequenced genome," *Electrophoresis*, vol. 27, no. 13, pp. 2702–2711, 2006.

[24] D. M. Anderson and D. L. Garrison, "The ecology and oceanography of harmful algal blooms: preface," *American Society of Limnology and Oceanography*, vol. 42, pp. 1007–1009, 1997.

[25] A. D. Cembella, "Ecophysiology and metabolism of paralytic shellfish toxins in marine microalgae," in *Physiological Ecology of Harmful Algal Blooms*, A. D. Anderson, D. M. Cembella, and G. M. Hallegraeff, Eds., pp. 381–403, Springer, New York, NY, USA, 1998.

[26] J. D. Hackett, T. E. Scheetz, H. S. Yoon et al., "Insights into a dinoflagellate genome through expressed sequence tag analysis," *BMC Genomics*, vol. 6, no. 1, p. 80, 2005.

[27] P. Uribe, D. Fuentes, J. Valdés et al., "Preparation and analysis of an expressed sequence tag library from the toxic dinoflagellate *Alexandrium catenella*," *Marine Biotechnology*, vol. 10, no. 6, pp. 692–700, 2008.

[28] E. Toulza, M. S. Shin, G. Blanc et al., "Gene expression in proliferating cells of the dinoflagellate alexandrium catenella (Dinophyceae)," *Applied and Environmental Microbiology*, vol. 76, no. 13, pp. 4521–4529, 2010.

[29] M. D. Keller, R. C. Selvin, W. Claus, and R. R. L. Guillard, "Media for the culture of oceanic ultraphytoplankton," *Journal of Phycology*, vol. 23, no. 4, pp. 633–638, 1987.

[30] F. W. F. Lee and S. C. L. Lo, "The use of Trizol reagent (phenol/guanidine isothiocyanate) for producing high quality two-dimensional gel electrophoretograms (2-DE) of dinoflagellates," *Journal of Microbiological Methods*, vol. 73, no. 1, pp. 26–32, 2008.

[31] S. F. Altschul, W. Gish, W. Miller, E. W. Myers, and D. J. Lipman, "Basic local alignment search tool," *Journal of Molecular Biology*, vol. 215, no. 3, pp. 403–410, 1990.

[32] V. Dančík, T. A. Addona, K. R. Clauser, J. E. Vath, and P. A. Pevzner, "De novo peptide sequencing via tandem mass spectrometry," *Journal of Computational Biology*, vol. 6, no. 3-4, pp. 327–342, 1999.

[33] A. Shevchenko, S. Sunyaev, A. Loboda et al., "Charting the proteomes of organisms with unsequenced genomes by MALDI-quadrupole time-of-flight mass spectrometry and BLAST homology searching," *Analytical Chemistry*, vol. 73, no. 9, pp. 1917–1926, 2001.

[34] P. Waridel, A. Frank, H. Thomas et al., "Sequence similarity-driven proteomics in organisms with unknown genomes by LC-MS/MS and automated *de novo* sequencing," *Proteomics*, vol. 7, no. 14, pp. 2318–2329, 2007.

[35] R. L. Tatusov, N. D. Fedorova, J. D. Jackson et al., "The COG database: an updated version includes eukaryotes," *BMC Bioinformatics*, vol. 4, pp. 1–14, 2003.

[36] P. Waridel, A. Frank, H. Thomas et al., "Sequence similarity-driven proteomics in organisms with unknown genomes by LC-MS/MS and automated *de novo* sequencing," *Proteomics*, vol. 7, no. 14, pp. 2318–2329, 2007.

[37] B. Habermann, J. Oegema, S. Sunyaev, and A. Shevchenko, "The power and the limitations of cross-species protein identification by mass spectrometry-driven sequence similarity searches," *Molecular & Cellular Proteomics*, vol. 3, no. 3, pp. 238–249, 2004.

[38] A. J. Liska and A. Shevchenko, "Expanding the organismal scope of proteomics: cross-species protein identification by mass spectrometry and its implications," *Proteomics*, vol. 3, no. 1, pp. 19–28, 2003.

[39] N. Wielsch, H. Thomas, V. Surendranath et al., "Rapid validation of protein identifications with the borderline statistical confidence via *de novo* sequencing and MS BLAST searches," *Journal of Proteome Research*, vol. 5, no. 9, pp. 2448–2456, 2006.

[40] S. Carr, R. Aebersold, M. Baldwin, A. Burlingame, K. Clauser, and A. Nesvizhskii, "The need for guidelines in publication of peptide and protein identification data," *Molecular & Cellular Proteomics*, vol. 3, no. 6, pp. 531–532, 2004.

[41] J. A. Taylor and R. S. Johnson, "Sequence database searches via de Novo peptide sequencing by tandem mass spectrometry," *Rapid Communications in Mass Spectrometry*, vol. 11, no. 9, pp. 1067–1075, 1997.

[42] S. Sunyaev, A. J. Liska, A. Golod, A. Shevchenko, and A. Shevchenko, "MultiTag: multiple error-tolerant sequence tag search for the sequence-similarity identification of proteins by mass spectrometry," *Analytical Chemistry*, vol. 75, no. 6, pp. 1307–1315, 2003.

[43] A. Mackey, T. Haystead, and W. Pearson, "Getting more from less," *Molecular & Cellular Proteomics*, vol. 1, no. 2, pp. 139–147, 2002.

[44] L. Huang, R. J. Jacob, S. C. H. Pegg et al., "Functional assignment of the 20S proteasome from Trypanosoma brucei using mass spectrometry and new bioinformatics approaches," *Journal of Biological Chemistry*, vol. 276, no. 30, pp. 28327–28339, 2001.

[45] A. Frank, S. Tanner, V. Bafna, and P. Pevzner, "Peptide sequence tags for fast database search in mass-spectrometry," *Journal of Proteome Research*, vol. 4, no. 4, pp. 1287–1295, 2005.

[46] D. L. Tabb, C. Narasimhan, M. B. Strader, and R. L. Hettich, "DBDigger: reorganized proteomic database identification that improves flexibility and speed," *Analytical Chemistry*, vol. 77, no. 8, pp. 2464–2474, 2005.

[47] R. J. Chalkley, P. R. Baker, L. Huang et al., "Comprehensive analysis of a multidimensional liquid chromatography mass spectrometry dataset acquired on a quadrupole selecting, quadrupole collision Cell, time-of-flight mass spectrometer," *Molecular & Cellular Proteomics*, vol. 4, no. 8, pp. 1194–1204, 2005.

[48] B. O. Searle, S. Dasari, M. Turner et al., "High-throughput identification of proteins and unanticipated sequence modifications using a mass-based alignment algorithm for MS/MS *de novo* sequencing results," *Analytical Chemistry*, vol. 76, no. 8, pp. 2220–2230, 2004.

[49] K. G. Standing, "Peptide and protein de novo sequencing by mass spectrometry," *Current Opinion in Structural Biology*, vol. 13, no. 5, pp. 595–601, 2003.

[50] C. Xu and B. Ma, "Software for computational peptide identification from MS-MS data," *Drug Discovery Today*, vol. 11, no. 13-14, pp. 595–600, 2006.

[51] G. W. Birrell, S. Earl, P. P. Masci et al., "Molecular diversity in venom from the Australian Brown Snake," *Molecular & Cellular Proteomics*, vol. 5, no. 2, pp. 379–389, 2006.

[52] C. E. H. Schmelzer, M. Getie, and R. H. H. Neubert, "Mass spectrometric characterization of human skin elastin peptides produced by proteolytic digestion with pepsin and thermitase," *Journal of Chromatography A*, vol. 1083, no. 1-2, pp. 120–126, 2005.

[53] B. Ma, K. Zhang, C. Hendrie et al., "PEAKS: powerful software for peptide de novo sequencing by tandem mass spectrometry," *Rapid Communications in Mass Spectrometry*, vol. 17, no. 20, pp. 2337–2342, 2003.

[54] A. Frank and P. Pevzner, "PepNovo: de novo peptide sequencing via probabilistic network modeling," *Analytical Chemistry*, vol. 77, no. 4, pp. 964–973, 2005.

[55] B. Fischer, V. Roth, F. Roos et al., "NovoHMM: a hidden Markov model for de novo peptide sequencing," *Analytical Chemistry*, vol. 77, no. 22, pp. 7265–7273, 2005.

[56] T. R. Bachvaroff, G. T. Concepcion, C. R. Rogers, E. M. Herman, and C. F. Delwiche, "Dinoflagellate expressed sequence tag data indicate massive transfer of chloroplast genes to the nuclear genome," *Protist*, vol. 155, no. 1, pp. 65–78, 2004.

[57] K. B. Lidie, J. C. Ryan, M. Barbier, and F. M. Van Dolah, "Gene expression in Florida red tide dinoflagellate *Karenia brevis*: analysis of an expressed sequence tag library and development

of DNA microarray," *Marine Biotechnology*, vol. 7, no. 5, pp. 481–493, 2005.

[58] C. Taroncher-Oldenburg and D. M. Anderson, "Identification and characterization of three differentially expressed genes, encoding S-adenosylhomocysteine hydrolase, methionine aminopeptidase, and a histone-like protein, in the toxic dinoflagellate *Alexandrium fundyense*," *Applied and Environmental Microbiology*, vol. 66, no. 5, pp. 2105–2112, 2000.

[59] J. S. Miller-Morey and F. M. Van Dolah, "Differential responses of stress proteins, antioxidant enzymes, and photosynthetic efficiency to physiological stresses in the Florida red tide dinoflagellate, *Karenia brevis*," *Comparative Biochemistry and Physiology-C*, vol. 138, no. 4, pp. 493–505, 2004.

[60] N. J. Patron, R. F. Waller, J. M. Archibald, and P. J. Keeling, "Complex protein targeting to dinoflagellate plastids," *Journal of Molecular Biology*, vol. 348, no. 4, pp. 1015–1024, 2005.

[61] F. M. Van Dolah, T. A. Leighfield, H.D. Sandel, and C. K. Hsu, "Cell division in the dinoflagellate Gambierdiscus toxicus is phased to the diurnal cycle and accompanied by activation of the cell cycle regulatory protein, CDC2 kinase," *Journal of Phycology*, vol. 31, no. 3, pp. 395–406, 1995.

Hindawi Publishing Corporation
Evidence-Based Complementary and Alternative Medicine
Volume 2011, Article ID 140462, 8 pages
doi:10.1155/2011/140462

Research Article

Dieckol from *Ecklonia cava* Regulates Invasion of Human Fibrosarcoma Cells and Modulates MMP-2 and MMP-9 Expression via NF-κB Pathway

Chen Zhang,[1,2] Yong Li,[3,4] Zhong-Ji Qian,[3] Sang-Hoon Lee,[3] Yong-Xin Li,[1] and Se-kwon Kim[1,3]

[1] *Department of Chemistry, Pukyong National University, Busan 608-737, Republic of Korea*
[2] *Key Laboratory of Molecular Enzymology and Enzyme Engineering of Ministry Education, College of Life Science, Jilin University, Changchun 130021, China*
[3] *Marine Bioprocess Research Center, Pukyong National University, Busan 608-737, Republic of Korea*
[4] *School of Pharmaceutical Sciences, Changchun University of Chinese Medicine, Changchun 130117, China*

Correspondence should be addressed to Se-kwon Kim, sknkim@pknu.ac.kr

Received 28 December 2010; Revised 17 March 2011; Accepted 3 June 2011

The matrix metalloproteinase (MMP) family is involved in the breakdown of extracellular matrix in normal physiological processes, as well as in the disease processes such as arthritis and cancer metastasis. In the present study, dieckol was obtained with high yield from marine brown alga *Ecklonia cava* (EC), and its effect was assessed on the expression of MMP-2 and -9 and morphological changes in human fibrosarcoma cell line (HT1080). Dieckol inhibited the expression of MMP-2 and -9 in a dose-dependent manner and also suppressed the cell invasion and the cytomorphology in 3D culture system on HT1080 cells. Moreover, dieckol may influence nuclear factor kappa B (NF-κB) pathway without obvious influence on activator protein-1 (AP-1) pathway and tissue inhibitor of metalloproteinases (TIMPs). In conclusion, dieckol could significantly suppress MMP-2 and -9 expression and alter cytomorphology of HT1080 cell line via NF-κB pathway.

1. Introduction

The past few decades of cancer research has revealed that matrix metalloproteinases (MMPs) play a significant role in a variety of pathologic conditions. Especially in malignant tumors, the activities of MMPs are deregulated and their expressions are often associated with poor prognosis. Among all the MMPs, MMP-2 and -9 have demonstrated to play a major role in the establishment of metastasis, which substantially increases in majority of malignant tumors. Therefore, inhibition of MMP-2 and -9 is thought to have a therapeutic benefit for cancer [1–8].

Recently, significant achievements have been made in synthetic bioactive applications. However, natural compounds and their derivatives are still known as the richest source of bioactive compounds with huge pharmaceutical application potential [9]. Dieckol (Figure 1) is a phloroglucinal derivative isolated from marine brown alga *Ecklonia cava* (EC) with a variety of biological functions *in vitro* and *in vivo*, for example, antioxidant, antitumor, antihuman immunodeficiency virus (-HIV), and anti-inflammatory activities. For instance, dieckol is a novel safe phloroglucinal derivative which inhibited the cytopathic effects of HIV-1 including HIV-1-induced syncytia formation, lytic effects, and viral p24 antigen production, as well as exhibited reverse transcriptase enzymes inhibitory and HIV-1 entry activity in addition to its other biological properties [10, 11].

In the present study, effect of dieckol on the expression of MMP-2 and -9, cytotoxicity, and cellular invasiveness was evaluated in HT1080 cells. The selectivity of this cell line was based on the extensive studies performed previously on MMPs expression [12]. In addition, the mechanism of dieckol regulating MMP-2 and -9 via the influence on nuclear factor kappa B (NF-κB) pathway has also been investigated.

2. Materials and Methods

2.1. General Materials. ^{1}H NMR (400 MHz) and ^{13}C NMR (100 MHz) spectra were recorded on a JEOL JNM-ECP

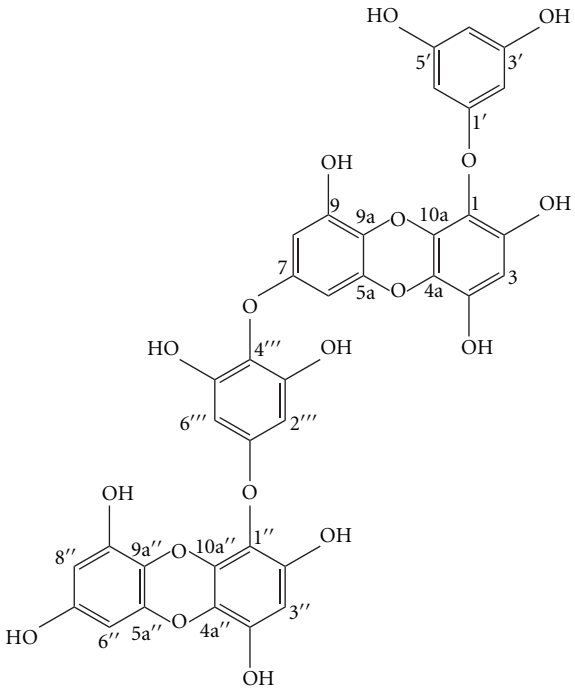

Figure 1: Chemical structure of dieckol.

400 NMR spectrometer (JEOL, Japan), using DMSO-d_6 solvent peak (2.50 ppm in ^{1}H and 39.5 ppm in ^{13}C NMR) as an internal reference standard. For some signals, the chemical shifts approximated at the third decimal place. This is to distinguish between signals of very close value, but which could nevertheless be clearly differentiated by visual inspection of the spectra. MS spectra were obtained on a JEOL JMS-700 spectrometer (JEOL, Japan). Extraction of EC was performed using extraction unit (Dongwon Scientific Co., Republic of Korea). Column chromatography was carried out by silica gel 60 (230–400 mesh, Merck, Germany) and Sephadex LH-20 (Sigma, St. Louis, Mo). Thin-layer chromatography (TLC) was run on precoated Merck Kieselgel 60 F_{254} plates (0.25 mm), and the spots on the TLC plate were detected under UV lamp (254 and 365 nm) using $CHCl_3$/MeOH/H_2O/acetic acid (65 : 25 : 4 : 3, v/v/v/v) as a development solvent system. Vanillin-H_2SO_4 was employed as the detecting agent for phenolic compounds. All the solvent and chemicals used in this study were of reagent grade from commercial sources (Duksan Pure Chemicals Co., Ltd., Republic of Korea).

2.2. Extraction, Isolation, Purification, and Elucidation of Dieckol. *Ecklonia cava* was collected from Jeju Island coast of Republic of Korea, washed three times with water to remove salt, and subjected to lyophilization. The lyophilized EC was ground into powder before extraction. The dried EC powder (10 kg) was extracted by stirring extraction unit with MeOH (3 × 5 L) for 10 days at room temperature (25°C). The extract (273 g) was suspended in water and partitioned with n-hexane (35.92 g), CH_2Cl_2 (20.49 g), EtOAc (24.87 g), and n-BuOH (106 g) in a sequence. The EtOAc fraction (24.87 g) was subjected to a silica gel flash chromatography eluted with Hexane/EtOAc/MeOH/CH_2Cl_2 (gradient) to yield ten subfractions (F1–F10). The F5 subfraction was further purified by Sephadex LH-20 with MeOH obtained dieckol (58.30 mg).

2.3. Cell Culture and Cell Viability Assay. Human fibrosarcoma cells (HT1080) from ATCC were cultured in Dulbecco's Modified Eagle's Medium (DMEM), supplemented with 10% fetal bovine serum (FBS), 2 mM glutamine, and 100 U/mL penicillin-streptomycin, and incubated at 5% CO_2 and 37°C humidified atmosphere. For experiments, cells were passaged at least for 5 times and detached with Trypsin-EDTA. For cell viability assay, cells were seeded in 96-well plates at a density of 1×10^4 cells/well in 200 μL DMEM containing 10% fetal bovine serum. After 24 hours, the medium was removed and the cells were incubated for 48 h with DMEM containing 1% FBS in the absence or presence of various concentrations of dieckol. Forty-eight hours later, 100 μL 3-(4,5)-dimethylthiahiazol (-z-y1)-3,5-di-phenytetrazoliumromide (MTT) (0.5 mg/mL final concentration) was added to each well and incubated for another 4 hours at 37°C in 5% CO_2. Finally, DMSO (150 μL) was added to solubilize the formazan salt formed and amount of formazan salt was determined by measuring the OD at 540 nm using GENios microplate reader (Tecan Austria GmbH, Austria). Relative cell viability was determined by the amount of MTT converted into formazan salt. Viability of cells was quantified as a percentage compared to the control and dose response curves were developed. The data were expressed as mean (±SD) from three independent experiments.

2.4. In Vitro Invasion Assay. An *in vitro* invasion assay was performed using a 24-well transwell unit (8 μm pore size) with polyvinylpyrrolidone-free polycarbonate filters coated with 500 μg/mL of Matrigel and placed in transwell chambers. The coated filters were washed thoroughly in PBS and dried immediately before use. Cells were placed in the upper part of the transwell plate and allowed cell attachement for 24 hours, then incubated with dieckol for 36 hours at 37°C. The cells that invaded the lower surface of the membrane were fixed with methanol and stained with 0.5% crystal violet for 10 min. Finally, we determined invasive phenotypes by counting the cells that migrated to the lower side of the filter using Leica DM6000B microscopy at 200 × (Leica Microsystems Wetzlar GmbH, Germany) in at least 5 bright fields [13].

2.5. Three-Dimensional (3D) Culture of HT1080 Cell Line. The cells behavior and morphology in 3D culture system is quite different from that observed in the 2D system [14]. The 3D culture model was established as described previously [15]. Briefly, HT1080 cells (1.5×10^3) were suspended with a neutralized solution of type I collagen (1 mg/mL) (Sigma, St. Louis, Mo) and 1/5 volume of a 5 × DMEM. The cell suspension containing various final concentrations of dieckol was added to 24-well plates and kept at 37°C until

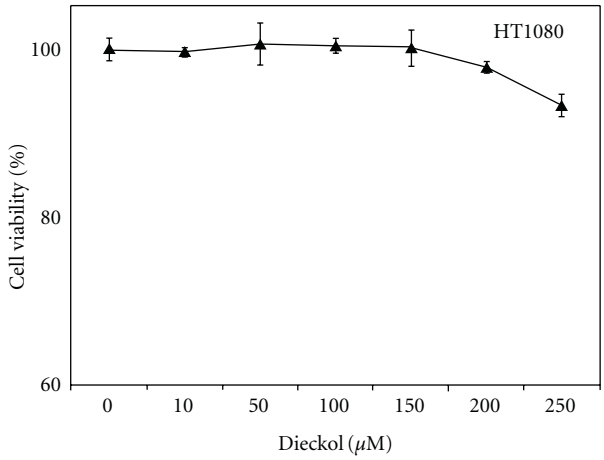

Figure 2: Effect of dieckol on the viability of HT1080 cells. Data represented as mean ± SD of three independent experiments.

gelled. The plates were then incubated at 37°C for 24 hours. The results were observed under microscope at 200 × (Leica Microsystems Wetzlar GmbH, Germany).

2.6. Gelatin Zymography. For gelatin zymography, HT1080 cells were seeded in 24-well plates using serum-free media and pretreated with different concentrations of dieckol for 1 hour. MMP expression was stimulated by 12-O-tetradecanoylphorbol 13-acetate (PMA) (10 ng/mL) and incubation was continued for 48 hours. After incubation, conditioned media were collected and their protein contents were determined by the Bradford method [16]. After normalizing the protein content, equal amounts of proteins were electrophoresed under nonreducing conditions on 10% polyacrylamide gels containing 1.5 mg/mL gelatin. Following electrophoresis, polyacrylamide gels were washed with 50 mM Tris-HCl (pH 7.5) containing 2.5% Triton X-100 to remove sodium dodecyl sulfate. Gels were then incubated overnight at 37°C in a developing buffer containing 10 mM $CaCl_2$, 50 mM Tris-HCl, and 150 mM NaCl to digest gelatin by MMPs. Areas of gelatin hydrolyzed by MMPs were visualized as clear zones against blue background by Coomassie blue staining and the intensities of the bands were estimated by densitometry (Multi Gauge V3.0 software, Fujifilm Life Science, Japan) [12].

2.7. Reverse Transcription-PCR. Total RNA from each sample was isolated by TRIzol reagent and subjected for reverse transcription-PCR (RT-PCR). For RT-PCR analysis, total RNA was reverse-transcribed to synthesize cDNA using a commercial kit (TaKaRa RNA PCR kit (AMV)) according to the manufacturer's protocol. PCR was then carried out in 50 μL of reaction volumes containing RNA PCR buffer, 2.5 mM $MgCl_2$, 0.2 μM of each primer, and 2.5 units of TaKaRa Taq polymerase. Samples were predenatured at 94°C for 4 min, followed by amplification at 94°C for 1 min, at 55°C for 30 s, and at 72°C for 1 min for 25 cycles, followed by a final 10 min extension step at 72°C. The primers for GAPDH were 5′-GTCAACGGATTTGGTCGTATT-3′′ and 5′-AGTCTTCTGGGTGGCAGTGAT-3′ with an expected amplified product of 300 bp. The MMP-2 primers were 5′-CTCAGATCCGTGGTGAGATCT-3′ and 5′-CT TTGGT-TCTCCAGCTTCAGG-3 with an expected amplified product of 496 bp. The MMP-9 primers were 5′-ATCCAGTTT-GGTGTCGCGGAGC-3′ and 5′-GAAGGGGAAGACGCA-CA GCT-3′ with an expected amplified product of 552 bp.

2.8. Extraction of Nuclear and Plasma Proteins and Western Blot Analysis. HT1080 cells were pretreated without or with different concentrations of dieckol for 1 hour followed by the stimulation with PMA, and the incubation was continued for another 48 hours. For separate extraction of nuclear and cytoplasm proteins, CelLytic NuCLEAR Extraction kit (S26-36-23, Sigma-Aldrich Co., Mo, USA) was used by following manufacturer's instructions. The cells were lysed with 0.5 mL of lysis buffer (500 μL hypotonic lysis buffer, 5 μL 0.1 M dithiothreitol (DTT), and 5 μL protease inhibitor cocktail, proteasome inhibitor, MG132) for 15 min on the ice. Igepal CA-630 solution (4 μL) was added and vortexed for 20 s. nuclei were separated by centrifugation at 10,000 × g for 10 min and supernatant (cytoplasm protein) was collected. Precipitated nuclei were lysed with 100 μL of extraction buffer mix (98 μL of extraction buffer, 1 μL of 0.1 M, DTT and 1 μL of protease inhibitor cocktail) for 10 min and nuclei protein were collected by centrifugation at 12,000 × g for 10 min. Proteins were separated by 12% SDS-PAGE and electrotransferred onto PVDF membranes (Millipore, Bedford, Mass). After blocking with 5% skim milk in PBST (PBS, pH 7.6, containing 0.2% Tween-20), the membranes incubated with primary antibody (Santa Cruz Biotechnology, Inc. us). for 1 hours, washed with 0.2% Tween-20 in PBS, and then incubated with horseradish peroxidase-linked secondary antibody (Santa Cruz Biotechnology, Inc., Calif, USA). The reactive signals were visualized by ECL kit (PE Applied Biosystems).

2.9. Statistical Analysis. All the experiments were repeated at least three times. All results were expressed as the mean of three replicates determination and standard deviation (SD). Statistical comparisons were made with Student's *t*-test and P values < 0.05 were considered to be significant.

3. Results

3.1. Cell Viability Assay. Cell viability assay was introduced for determining whether dieckol can have toxic effect on HT1080 cells at high concentration. Comparison of cell growth over 48 h with various dieckol concentrations (0–250 μM) were showed in Figure 2. The values for all concentrations were similar with control (dieckol 0 μM) indicating that dieckol does not affect cell viability below the concentrations of 200 μM.

3.2. Transwell Invasion Assay. Although no cytotoxic effect was observed even below 200 μM concentration of dieckol on HT1080 cell line, ideally, 0 to 100 μM of dieckol was

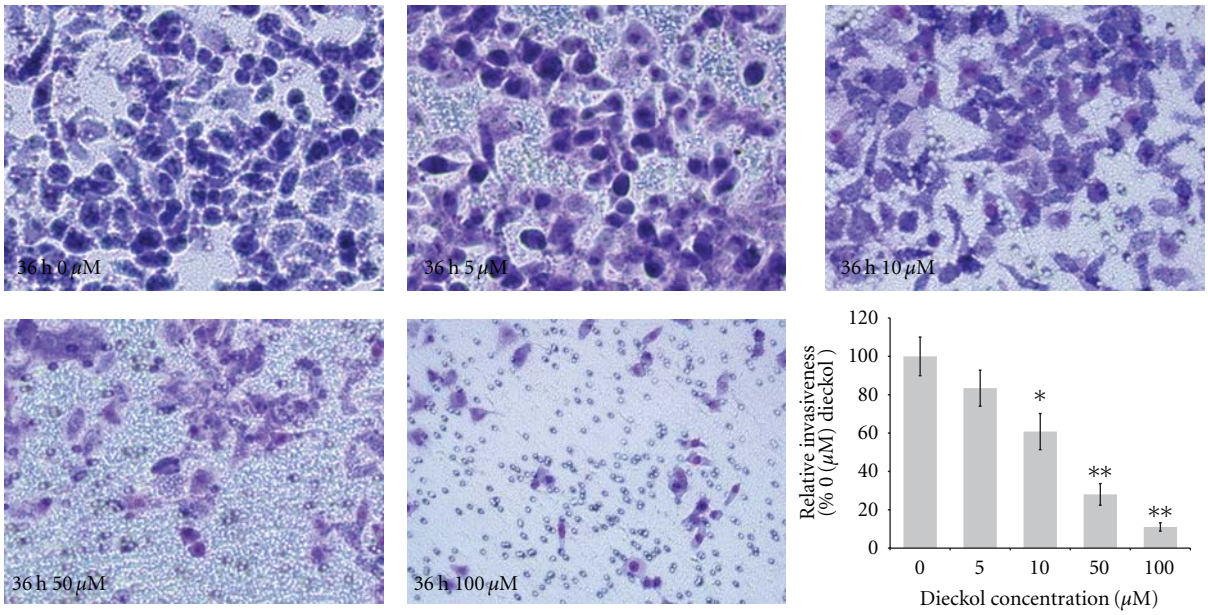

(a)

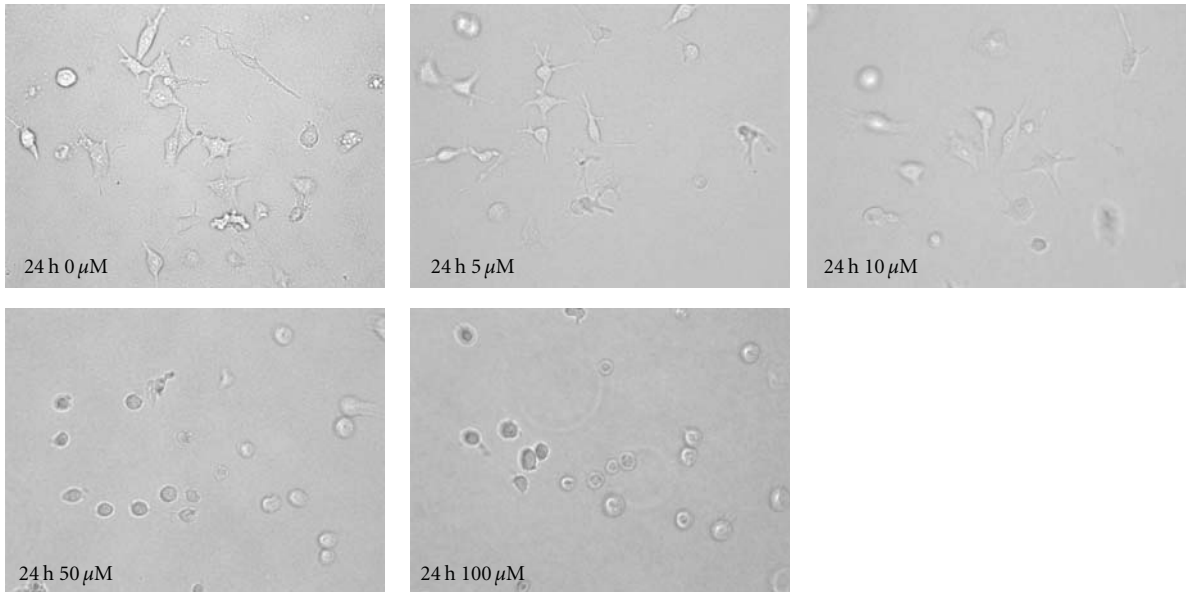

(b)

Figure 3: Effect of dieckol on invasion in HT1080 cells. (a) Microphotographs of filters of the Matrigel chamber invasion assay. Inset (a) represents the conclusive data of cellular invasion. (b) Dieckol Effect on the morphology of HT1080 cells in three-dimensional (3D) cultures system. The data presented are mean ± SD of three independent experiments. Values are compared with the 0 μM dieckol, which are significant at $^{*}P < 0.05$ and $^{**}P < 0.01$.

used in the cell invasion and the subsequent experiments. To investigate whether dieckol inhibits tumor invasion, Matrigel invasion assays were performed for dieckol-treated HT1080 cells. It was observed that dieckol treatment reduced the cell invasion, and 100 μM of dieckol concentration significantly blocked tumor invasion (Figure 3(a)) [13, 17].

3.3. Effects of Dieckol on the 3D Culture in HT1080 Cell Line. To investigate the effect of dieckol on the 3D culture system of HT1080 cells, same density of cells were seeded into 3D collagen gel with various final concentrations of the dieckol. After 36 h, the control (without dieckol) stretched out in the gel and formed many branched and elongated structures in type I collagen matrix (Figure 3(b)). In contrast, the branches were reduced in the cells treated with 5 μM concentration of dieckol. As the concentration increased to 100 μM, these branches disappeared and cells changed to spherical shape.

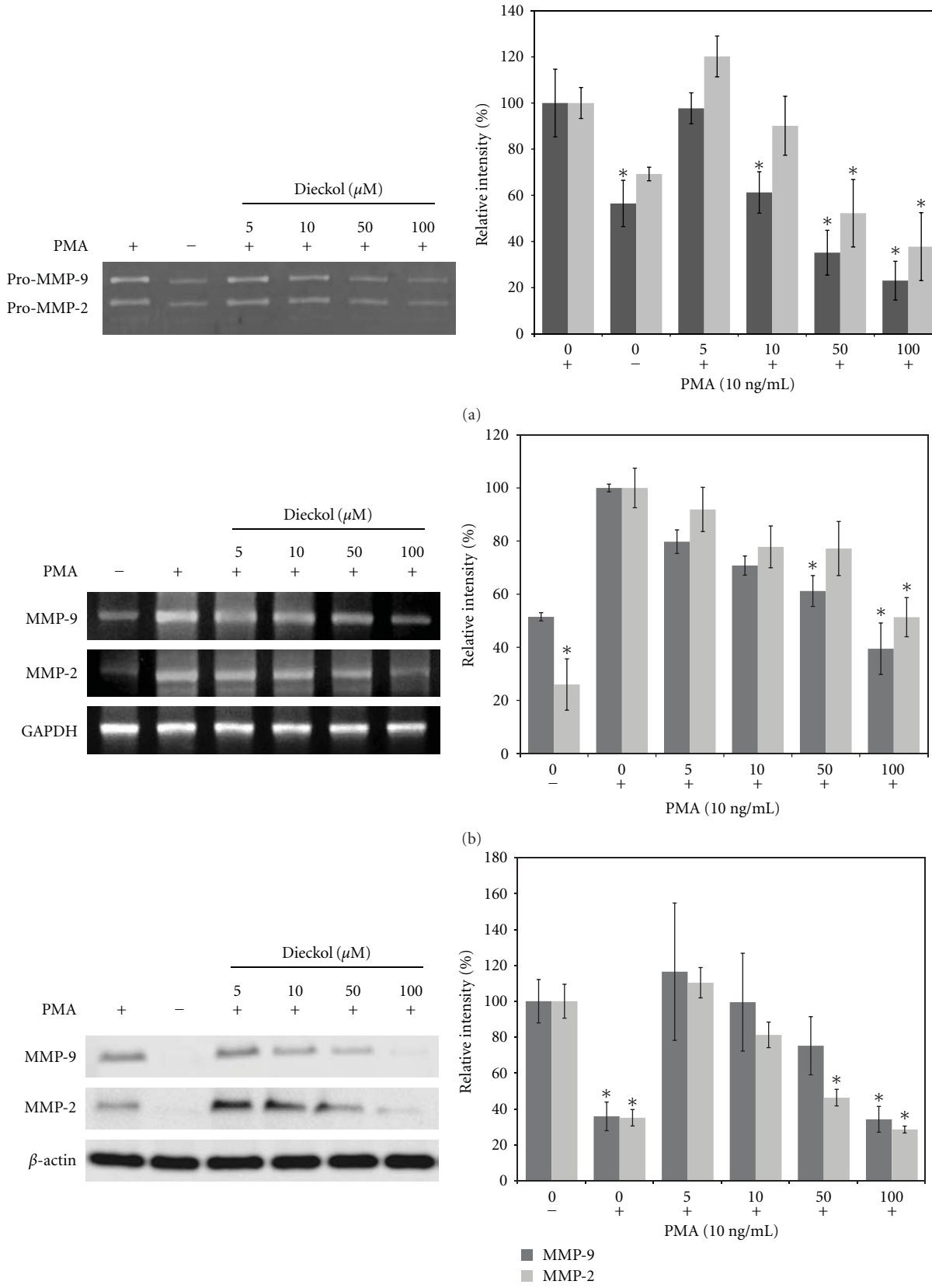

Figure 4: Effects of dieckol on the MMP expression. (a) Expression of MMP-2, -9 in dieckol-treated HT1080 cells by gelatin zymography. (b) mRNA transcription levels of MMP-2, -9 in HT1080 cells by RT-PCR analysis. (c) MMP-2, -9 protein expressions in the dieckol-treated HT1080 cells by western blot analysis. The columns presented in (a), (b), and (c) were the representative of three independent experiments. *, $P < 0.05$, Compared with the 0 μM dieckol with PMA 10 ng/mL.

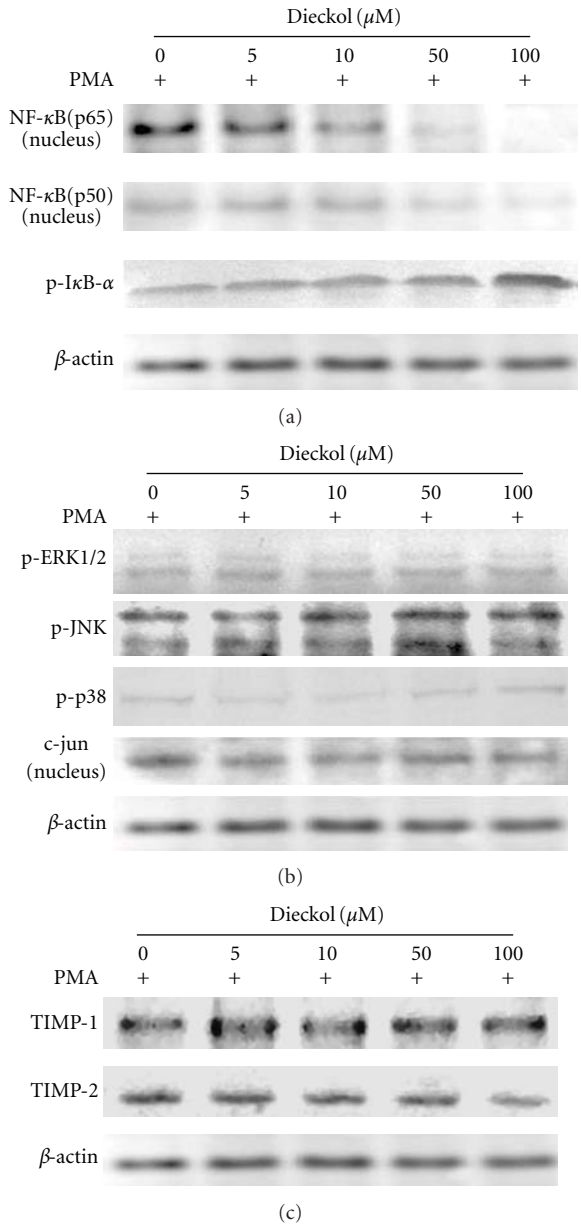

Figure 5: Effect of dieckol on the NF-κB and AP-1 cell signaling pathway and TIMP-1, -2 expressions in HT1080 cells. (a) Nucleus NF-κB (p65 and p50) and IκB (p-IκB-α) protein expressions in the dieckol treated HT1080 cells. (b) (c-jun), MAPK pathway (ERK, JNK, p38). (c) Western blot analysis of TIMP-1 and TIMP-2.

3.4. Effects of Dieckol on the MMP-2, -9 Transcription and Expression Levels in HT1080 Cell Line. Gelatin zymography analysis was performed, for investigating whether dieckol could inhibit protein levels of MMP-2 and MMP-9. As shown in Figure 4(a), protein expressions for MMP-2 and MMP-9 were significantly inhibited by dieckol in a dose-dependent manner. In addition, results from the RT-PCR and western blot revealed that the expression of MMP-2 and -9 was inhibited at transcription levels by dieckol, more or less similar manner with zymography analysis (Figures 4(b) and 4(c)).

3.5. Effects of Dieckol Influenced AP-1, NF-κB, and IκB Expressions on HT1080 Cell Line. Western blot studies were carried out to assay the downregulation effects of dieckol on the possible mechanism of expression of activator protein-1 (AP-1) and nuclear factor-kappa B (NF-κB). Meanwhile, the tissue inhibitor of metalloproteinases (TIMP) was been checked by western blot. As shown in Figure 5(b), dieckol did not exhibit a clear influence of activator protein-1 (AP-1) (c-jun) expression and mitogen-activated protein kinase (MAPK) (ERK, JNK, p38), which mediated the AP-1. The NF-κB transcription family proteins consist of several protein subunits, and it was clear that the level of NF-κB (p65 and p50) was decreased in a dose-dependent manner. The p-IκB-α expression was increased significantly, when treated with high concentration of dieckol (100 μM) (Figure 5(a)). As observed in Figure 5(c), there is no distinct change in the expressions of TIMP-1 and TIMP-2 when treated with different concentrations of dieckol.

4. Discussion

MMPs, a family of zinc-dependent endopeptidases, participate in many physiological and pathological processes. An imbalance between the inhibition and activation of MMPs is related to some diseases such as osteoarthritis, rheumatoid arthritis, tumor metastasis, cardiovascular diseases and congestive heart failure [18–20]. Finding MMP inhibitors (MMPIs) for treatment of these prevalent diseases has been an important aspect of present day cancer research [21]. MMPIs regulate MMPs at several biochemical pathways, but most of them directly inhibit the activity of enzyme. Till now, MMPIs entering clinical trial are only of synthetic origin (organic compounds) and have failed to enter the pharmaceutical market owing to their side effects [22]. The search for novel and natural compounds has led to the discovery of oceans as the treasure house of substances with amazing pharmacological potential. Therefore, discovering the ideal MMPIs from marine natural sources is feasible and more advantageous [23].

Ecklonia cava (a marine alga), one of the marine floral members, produces dieckol which has been well studied previously to inhibit the expression of various MMPs [12, 24]. In this study, dieckol did not show any cytotoxic effect on HT1080 cells at the concentrations below 200 μM. However, dieckol influenced the cell mobility as measured by transwell invasion assay; it also suppressed HT1080 cells crossing the matrix gel in a dose-dependent manner. In addition, we have examined the effect of dieckol on the organization of HT1080 cells in a 3D culture environment. *In vivo*, cells experience a 3D environment and are surrounded by other cells and ECM. The traditional 2D monolayer culture system cannot emulate the complexities of the 3D tissue microenvironment and will always represent a suboptimal milieu for studying physiological ECM interactions with connective tissue cells [25, 26]. MMPs also affect cell morphology in 3D culture environment. MMPs cleave the matrix proteins fibronectin, vitronectin, and collagen I into smaller fragments. The cleaved ECM fragments then facilitate and accelerate cancer

cell adhesion and invasion [15]. HT1080 cells formed the stellate structures in the 3D culture environment, and these structures migrated into the collagen matrix cleaving the ECM with the help of the MMPs. However, dieckol treatment significantly reduced the number and length of stellate structures. The cultured HT1080 cells were treated with dieckol with selected concentrations (0–200 μM) and the expression of MMP-2, -9 was induced by PMA. Several studies have shown that PMA can induce expression of MMP-2, -9 [27]. Dieckol inhibited the expression of MMP-2, -9 in a dose-dependent manner, according to the results of RT-PCR, western blot and zymography assays.

AP-1 and NF-κB are major transcription factors that regulate MMP-2, -9 expression [28–30]. Members of the MAPK superfamily (ERK1/2, JNKs, and p38 kinase) are known to regulate AP-1 transactivation by increasing the level of AP-1 components or altering the phosphorylation of their subunits (c-jun, c-fos) and then regulate MMPs expression and activity in various cell types [31]. NF-κB, in its inactive form, it is sequestered in the cytoplasm, bound by members of the inhibitor of kappa B (IκB) family of inhibitor proteins (including IκBa, IκBb, IκBg, and IκBe). Various stimuli that activate NF-κB result in phosphorylation of IκB, is followed by its ubiquitination and subsequent degradation [32, 33]. Dieckol suppress NF-κB (p65 and p50) expression in a dose-dependent manner. However, dieckol did not show any clear effect on AP-1 and ERK1/2, JNKs, and p38 kinase expressions. It has been found that p-IκB-α expression increased when treated with high concentration of dieckol (100 μM), but not in low concentration [34]. It may suggest that the inhibitor of kappa B family could be upregulated by high concentration of dieckol, and this may be another reason for NF-κB suppression by dieckol. Western blot resulted from TIMP-1 and TIMP-2 depicted that TIMP have not been influenced by different concentrations of dieckol. It is indicating that inhibition of MMP-2, -9 activity by dieckol is not because of the TIMP at the test concentrations.

At the promoter site of MMP-2 and -9 genes, several putative binding sites for transcription factors are present, which regulate gene expression. This promoter contains an AP-1 binding consensus site at -79 upstream from the starter site and further upstream, there is a cluster of regulatory elements including another AP-1 binding site called AP-2 and NF-κB binding site [35]. It is commonly known that MMP-9 transcription is mainly regulated via AP-1 [36, 37]. In addition to this, under some inflammatory and other pathology conditions, MMP-2, -9 transcription can be regulated via NF-κB signaling pathways. Interestingly, dieckol inhibited NF-κB expression with a similar dose-dependent manner as observed for MMP-2, -9 expressions. However, it did not significantly influence the expression of AP-1. This mode of action may be contributed to the unique chemical structure of dieckol [38–40]. The reasons could be discussed based on the structural features of the isolated dieckol and the structure-activity relationship could be described due to its unique skeleton. For example, the number of hydroxyl groups present in its chemical structure probably plays an important role because of the higher polymerization of phloroglucinal units and on the other hand, the O-bridge linkages (ether linkage) among phloroglucinals donate more free anions to attract responsible receptors.

5. Conclusion

Dieckol was isolated from an edible marine brown alga *Ecklonia cava* has been characterized according to the MS and NMR data. It acts as an inhibitor of MMP-2, -9 expressions by the downregulation of NF-κB pathway without significant influence on AP-1, MAPK pathway. Furthermore, the modulation of MMP-2 and -9 expressions could be one reason for the suppression of invasiveness and 3D culturing of HT1080 cell line. Hence, this study suggested that dieckol could be an effective candidate for the suppression of cancer invasion.

Acknowledgment

This paper was supported by a grant from Marine Bioprocess Research Center of the Marine Biotechnology program funded by the Ministry of Land, Transport and Maritime, Republic of Korea.

References

[1] A. H. Baker, D. R. Edwards, and G. Murphy, "Metalloproteinase inhibitors: biological actions and therapeutic opportunities," *Journal of Cell Science*, vol. 115, no. 19, pp. 3719–3727, 2002.

[2] S. Tanimura, R. Kadomoto, T. Tanaka, Y. J. Zhang, I. Kouno, and M. Kohno, "Suppression of tumor cell invasiveness by hydrolyzable tannins (plant polyphenols) via the inhibition of matrix metalloproteinase-2/-9 activity," *Biochemical and Biophysical Research Communications*, vol. 330, no. 4, pp. 1306–1313, 2005.

[3] L. J. McCawley and L. M. Matrisian, "Matrix metalloproteinases: multifunctional contributors to tumor progression," *Molecular Medicine Today*, vol. 6, no. 4, pp. 149–156, 2000.

[4] R. A. Ashley, "Clinical trials of a matrix metalloproteinase inhibitor in human periodontal disease," *Annals of the New York Academy of Sciences*, vol. 878, pp. 335–346, 1999.

[5] H. S. Kang, H. Y. Chung, J. Y. Kim, B. W. Son, H. A. Jung, and J. S. Choi, "Inhibitory phlorotannins from the edible brown alga Ecklonia stolonifera on total reactive oxygen species (ROS) generation," *Archives of Pharmacal Research*, vol. 27, no. 2, pp. 194–198, 2004.

[6] S. Das, A. Banerji, E. Frei, and A. Chatterjee, "Rapid expression and activation of MMP-2 and MMP-9 upon exposure of human breast cancer cells (MCF-7) to fibronectin in serum free medium," *Life Sciences*, vol. 82, no. 9-10, pp. 467–476, 2008.

[7] J. Westermarck and V. M. Kähäri, "Regulation of matrix metalloproteinase expression in tumor invasion," *FASEB Journal*, vol. 13, no. 8, pp. 781–792, 1999.

[8] Q. T. Le, Y. Li, Z. J. Qian, M. M. Kim, and S. K. Kim, "Inhibitory effects of polyphenols isolated from marine alga *Ecklonia cava* on histamine release," *Process Biochemistry*, vol. 44, no. 2, pp. 168–176, 2009.

[9] J. D. McChesney, S. K. Venkataraman, and J. T. Henri, "Plant natural products: back to the future or into extinction?" *Phytochemistry*, vol. 68, no. 14, pp. 2015–2022, 2007.

[10] M. Artan, Y. Li, F. Karadeniz, S. H. Lee, M. M. Kim, and S. K. Kim, "Anti-HIV-1 activity of phloroglucinol derivative, 6,6′-bieckol, from *Ecklonia cava*," *Bioorganic and Medicinal*

Chemistry, vol. 16, no. 17, pp. 7921–7926, 2008.
[11] A. John and G. Tuszynski, "The role of matrix metalloproteinases in tumor angiogenesis and tumor metastasis," *Pathology and Oncology Research*, vol. 7, no. 1, pp. 14–23, 2001.
[12] M. M. Kim, Q. V. Ta, E. Mendis et al., "Phlorotannins in *Ecklonia cava* extract inhibit matrix metalloproteinase activity," *Life Sciences*, vol. 79, no. 15, pp. 1436–1443, 2006.
[13] S. Pasco, B. Brassart, L. Ramont, F. X. Maquart, and J. C. Monboisse, "Control of melanoma cell invasion by type IV collagen," *Cancer Detection and Prevention*, vol. 29, no. 3, pp. 260–266, 2005.
[14] K. B. Hotary, E. D. Allen, P. C. Brooks, N. S. Datta, M. W. Long, and S. J. Weiss, "Membrane type I matrix metalloproteinase usurps tumor growth control imposed by the three-dimensional extracellular matrix," *Cell*, vol. 114, no. 1, pp. 33–45, 2003.
[15] T. Frisk, S. Rydholm, T. Liebmann, H. Andersson Svahn, G. Stemme, and H. Brismar, "A microfluidic device for parallel 3-D cell cultures in asymmetric environments," *Electrophoresis*, vol. 28, no. 24, pp. 4705–4712, 2007.
[16] M. M. Bradford, "A rapid and sensitive method for the quantitation of microgram quantities of protein utilizing the principle of protein dye binding," *Analytical Biochemistry*, vol. 72, no. 1-2, pp. 248–254, 1976.
[17] K. J. Lee, J. Y. Kim, J. H. Choi et al., "Inhibition of tumor invasion and metastasis by aqueous extract of the radix of *Platycodon grandiflorum*," *Food and Chemical Toxicology*, vol. 44, no. 11, pp. 1890–1896, 2006.
[18] F. G. Spinale, M. L. Coker, S. R. Krombach et al., "Matrix metalloproteinase inhibition during the development of congestive heart failure: effects on left ventricular dimensions and function," *Circulation Research*, vol. 85, no. 4, pp. 364–376, 1999.
[19] Y. Yoshihara, H. Nakamura, K. Obata et al., "Matrix metalloproteinases and tissue inhibitors of metalloproteinases in synovial fluids from patients with rheumatoid arthritis or osteoarthritis," *Annals of the Rheumatic Diseases*, vol. 59, no. 6, pp. 455–461, 2000.
[20] G. P. Stricklin and H. G. Welgus, "Human skin fibroblasts collagenase inhibitor. Purification and biochemical characterization," *Journal of Biological Chemistry*, vol. 258, no. 20, pp. 12252–12258, 1983.
[21] C. Zhang and S. K. Kim, "Matrix metalloproteinase inhibitors (MMPIs) from marine natural products: the current situation and future prospects," *Marine Drugs*, vol. 7, no. 2, pp. 71–84, 2009.
[22] C. M. Overall and C. López-Otín, "Strategies for MMP inhibition in cancer: innovations for the post-trial era," *Nature Reviews Cancer*, vol. 2, no. 9, pp. 657–672, 2002.
[23] A. M. S. Mayer and K. R. Gustafson, "Marine pharmacology in 2000: antitumor and cytotoxic compounds," *International Journal of Cancer*, vol. 105, no. 3, pp. 291–299, 2003.
[24] S. O. Kim and Y. H. Choi, "The ethyl alcohol extract of *Hizikia fusiforme* inhibits matrix metalloproteinase activity and regulates tight junction related protein expression in Hep3B human hepatocarcinoma cells," *Journal of Medicinal Food*, vol. 13, no. 1, pp. 31–38, 2010.
[25] D. B. Edelman and E. W. Keefer, "A cultural renaissance: in vitro cell biology embraces three-dimensional context," *Experimental Neurology*, vol. 192, no. 1, pp. 1–6, 2005.
[26] E. Cukierman, R. Pankov, D. R. Stevens, and K. M. Yamada, "Taking cell-matrix adhesions to the third dimension," *Science*, vol. 294, no. 5547, pp. 1708–1712, 2001.
[27] S. O. Yoon, S. J. Park, S. Y. Yoon, C. H. Yun, and A. S. Chung, "Sustained production of H2O2 activates pro-matrix metalloproteinase-2 through receptor tyrosine kinases/phosphatidylinositol 3-kinase/NF-κB pathway," *Journal of Biological Chemistry*, vol. 277, no. 33, pp. 30271–30282, 2002.
[28] Z. Xie, M. Singh, and K. Singh, "Differential regulation of matrix metalloproteinase-2 and -9 expression and activity in adult rat cardiac fibroblasts in response to interleukin-1β," *Journal of Biological Chemistry*, vol. 279, no. 38, pp. 39513–39519, 2004.
[29] J. Westermarck and V. M. Kähäri, "Regulation of matrix metalloproteinase expression in tumor invasion," *FASEB Journal*, vol. 13, no. 8, pp. 781–792, 1999.
[30] Q. Huang, H. M. Shen, and C. N. Ong, "Inhibitory effect of emodin on tumor invasion through suppression of activator protein-1 and nuclear factor-κB," *Biochemical Pharmacology*, vol. 68, no. 2, pp. 361–371, 2004.
[31] U. H. Jin, S. J. Suh, W. C. Hyen et al., "Tanshinone IIA from Salvia miltiorrhiza BUNGE inhibits human aortic smooth muscle cell migration and MMP-9 activity through AKT signaling pathway," *Journal of Cellular Biochemistry*, vol. 104, no. 1, pp. 15–26, 2008.
[32] S. Ghosh and D. Baltimore, "Activation in vitro of NF-κB by phosphorylation of its inhibitor IκB," *Nature*, vol. 344, no. 6267, pp. 678–682, 1990.
[33] T. Henkel, T. Machleidt, I. Alkalay, M. Kronke, Y. Ben-Neriah, and P. A. Baeuerle, "Rapid proteolysis of IκB-α is necessary for activation of transcription factor NF-κb," *Nature*, vol. 365, no. 6442, pp. 182–185, 1993.
[34] P. Wisniewski, A. Ellert-Miklaszewska, A. Kwiatkowska, and B. Kaminska, "Non-apoptotic Fas signaling regulates invasiveness of glioma cells and modulates MMP-2 activity via NFκB-TIMP-2 pathway," *Cellular Signalling*, vol. 22, no. 2, pp. 212–220, 2010.
[35] S. K. Moon, H. M. Kim, and C. H. Kim, "PTEN induces G1 cell cycle arrest and inhibits MMP-9 expression via the regulation of NF-κB and AP-1 in vascular smooth muscle cells," *Archives of Biochemistry and Biophysics*, vol. 421, no. 2, pp. 267–276, 2004.
[36] J. S. Shim, E. J. Choi, C. W. Lee, H. S. Kim, and J. K. Hwang, "Matrix metalloproteinase-1 inhibitory activity of *kaempferia pandurata* roxb," *Journal of Medicinal Food*, vol. 12, no. 3, pp. 601–607, 2009.
[37] C. Yan, H. Wang, and D. D. Boyd, "KiSS-1 represses 92-kDa type IV collagenase expression by down-regulating NF-κB binding to the promoter as a consequence of IκBα-induced block of p65/p50 nuclear translocation," *Journal of Biological Chemistry*, vol. 276, no. 2, pp. 1164–1172, 2001.
[38] J. Lee, E. Jung, J. Lee et al., "Emodin inhibits TNF α-induced MMP-1 expression through suppression of activator protein-1 (AP-1)," *Life Sciences*, vol. 79, no. 26, pp. 2480–2485, 2006.
[39] N. Matsunaga, Y. Chikaraishi, M. Shimazawa, S. Yokota, and H. Hara, "Vaccinium myrtillus (bilberry) extracts reduce angiogenesis *in vitro* and *in vivo*," *Evidence-Based Complementary and Alternative Medicine*, vol. 7, no. 1, pp. 47–56, 2010.
[40] E. L. Cooper, "Drug discovery, CAM and natural products," *Evidence-Based Complementary and Alternative Medicine*, vol. 1, no. 3, pp. 215–217, 2004.

Hindawi Publishing Corporation
Evidence-Based Complementary and Alternative Medicine
Volume 2011, Article ID 452621, 7 pages
doi:10.1155/2011/452621

Research Article

Protective Effects of Emodin and Chrysophanol Isolated from Marine Fungus *Aspergillus sp.* on Ethanol-Induced Toxicity in HepG2/CYP2E1 Cells

Zhong-Ji Qian,[1] Chen Zhang,[2,3] Yong-Xin Li,[2] Jae-Young Je,[4] Se-Kwon Kim,[2] and Won-Kyo Jung[1]

[1] *Department of Marine Life Science and Marine Life Research and Education Center, Chosun University, Gwangju 501-759, Republic of Korea*
[2] *Department of Chemistry, Pukyong National University, Busan 608-737, Republic of Korea*
[3] *Key Laboratory of Molecular Enzymology and Enzyme Engineering of Ministry Education, College of Life Science, Jilin University, Changchun 130021, China*
[4] *School of Food Technology and Nutrition, Chonnam National University, Yeosu 550-749, Republic of Korea*

Correspondence should be addressed to Won-Kyo Jung, wkjung@chosun.ac.kr

Received 14 January 2011; Revised 31 March 2011; Accepted 3 June 2011

Alcohol-induced liver injury progresses from fatty infiltration followed by a harmful cause of inflammation leading to an irreversible damage. In this study, two compounds (emodin and chrysophanol) isolated from marine fungus *Aspergillus sp.* were examined for their protective effects against ethanol-induced toxicity *in vitro*. Ethanol-induced HepG2/CYP2E1 cells were treated with the compounds at various concentrations, and the results showed that there was a dose-dependent decrease of gamma-glutamyl transpeptidase (GGT) activity and increase of glutathione (GSH) in the culture media with an increase in cell viability. Furthermore, the protective effects of the compounds were evaluated by protein expression levels of GGT, GSH, and CYP2E1 using Western blot. Among the compounds, emodin addressed to the ethanol-induced cytotoxicity more effectively compared to the chrysophanol. It could be suggested that emodin isolated from this genus would be a potential candidate for attenuating ethanol induced liver damage for further industrial applications such as functional food and pharmaceutical developments.

1. Introduction

Alcohol toxicity is one of the world's major health problems as significant numbers of people are affected due to several fatal diseases caused by alcohol [1]. Alcohol is mostly metabolized in the liver, and excessive alcohol use can lead to acute and chronic liver diseases including hepatitis, liver cirrhosis, fatty liver, and liver cancer [2]. Chronic alcohol abuse is a major health problem causing liver and pancreatic diseases and is known to impair hepatic alcohol dehydrogenase, myocardial infarction, pancreatitis, and disorders of the immune, endocrine, and reproductive systems. The diverse mechanisms are involved in the ethanol-induced hepatotoxicity while accumulating evidence shows the importance of oxidative stress mediated by reactive nitrogen species (RNS) or reactive oxygen species (ROS) [3]. Ethanol-induced oxidative stress leads to a decrease in intracellular antioxidative capacity of the liver cells including small molecular antioxidants and antioxidant enzymes such as superoxide dismutase (SOD) and glutathione (GSH). Therefore, supplementation with exogenous antioxidants has been an attractive approach to prevent or reduce ethanol-induced hepatotoxicity [4–6]. Ethanol can also be metabolized by catalase and more selectively by cytochrome P-450 2E1 (CYP2E1). Induction of CYP2E1 is proposed as a mechanism augmenting the formation of reactive paracetamol metabolites [7].

Gamma-glutamyltransferase (GGT) is a plasma membrane enzyme which catalyses extracellular glutathione (GSH); it plays a key role in the maintenance of GSH homeostasis, detoxification of xenobiotic compounds, and metabolism of endogenous biomolecules. GGT elevation indicates the involvement of GSH in metabolism since GGT facilitates GSH conjugate disposition and ensures high intracellular GSH [8]. Recent studies have shown that GGT expression is

also positively regulated by iron-dependent oxidative stress. Therefore GGT appears to be a marker of oxidative stress in general [9].

Marine microorganisms have proven to be a rich source of biologically active natural products required for developing fine chemical agents [10]. Particularly, fungi from marine environment have shown to produce diverse secondary metabolites which are more or less similar to those produced by terrestrial fungi [11].

As a part of our ongoing studies on protective effects of metabolites from marine microorganisms on ethanol-induce toxicity, this study is focused on the metabolites isolated from a marine fungi isolated from the surface of the marine brown alga collected in the Ulsan City, Korea in 2009 and was identified as an *Aspergillus sp.* The *Aspergillus* is a ubiquitous group of filamentous fungi spanning over 200 million years of evolution. They have an impact on human health and society, and there are more than 180 officially recognized species, including 20 human pathogens as well as beneficial species used to produce foodstuffs and industrial enzymes [12].

In this study, two compounds, emodin and chrysophanol, isolated from marine fungus *Aspergillus sp.* and their chemical characteristics and protective effects on ethanol-induced toxicity in HepG2/CYP2E1 cells were investigated.

2. Regents

2.1. Materials. Dulbecco's modified Eagle's medium (DMEM), fetal bovine serum (FBS), YPG medium, dimethyl sulfoxide (DMSO), penicillin, 3-(4,5-dimethylthiazol-2-yl)-2, 5-diphenyltetrazolium bromide (MTT), streptomycin, metaphosphoric acid, 2-nitro-5-thiobenzoic acid, gamma-glutamyl-p-nitroanilide, glycylglycine, naphthylethylene diamine, glutathione (GSH), *N*-acetyl-L-cysteine (NAC), 5,5′-dithiobis [2-nitrobenzoic acid] (DTNB), and nicotinamide adenine dinucleotide phosphate-oxidase (NADPH) were purchased from Gibco BRL (Grand Island, NY, USA) and Sigma-Aldrich (St Louis, MO, USA). Antibodies for GGT and GSH were obtained from Santa Cruz Biotechnology (CA), and cytochrome P450 (CYP2E1, human) was obtained from Rockland (Gilbertsville, PA). BCA protein assay kit, electrophoresis reagents, and goat antirabbit peroxidase IgG were purchased from Pierce Biotechnology Inc. (Rockford, IL). All other chemicals and solvents were of analytical grade.

2.2. Extraction and Isolation. The fungal strain (stock no. YL-06) was isolated from the surface of the marine brown alga collected in the Ulsan City, Korea in 2009 and identified as an *Aspergillus sp.* The fungal strain (YL-06) was stored in the 10% glycerol YPG medium at −75°C. The further culture for investigation was completed on YPG medium from 10 mL to large scale (1.0 L and 10.0 L). The fungus was cultured (30.0 L) for 30 days at 29°C in YPG medium. The culture broth and mycelium were separated, and the filtered broth was extracted with ethyl acetate to provide the broth extract (1.58 g). The broth extract extracted with ethyl acetate to provide the broth extract (1.58 g), which was fractionated by silica gel chromatography (n-5hexane/EtOAc) to generate

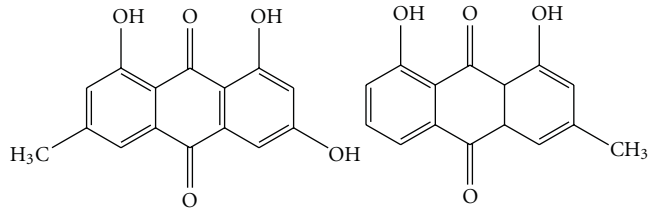

Figure 1: Chemical structures of emodin and chrysophanol from marine fungus *Aspergillus sp*.

six fractions. The further purification of the active fractions by ODS column chromatography (H_2O in MeOH), followed by HPLC (YMC ODS-A, MeOH), yielded two compounds emodin (5.0 mg) and chrysophanol (7.0 mg).

Emodin (1,3,8-trihydroxy-6-methylanthraquinone). Orange needles, 1H NMR ($CDCl_3$) δ 2.37 (3H, s, 3-Me), 6.26 (1H, d, J = 2.45, H-5), 6.95 (1H, br s, H-2), 7.00 (1H, d, J = 2.45, H-7), 7.43 (1H, br s, H-4), 12.08 and 12.20 (2H, s, 1/8-OH) (Figure 1).

Chrysophanol (1,8-dihydroxy-3-methylanthraquinone). Orange needles, 1H NMR ($CDCl_3$, 400 MHz) δ (ppm) 12.03 (1H, s, OH-8), 11.93 (1H, s, OH-1), 7.72 (1H, dd, J = 0.76 and 7.52,H-5), 7.56 (1H, d, J = 8.1, H-6), 7.55 (1H, d, J = 0.4, H-4), 7.19 (1H, dd, J = 0.74 and 8.4, H-7), 7.00 (1H, d, J = 0.4, H-2), 2.36 (3H, s, H-3) (Figure 1).

3. Methods

3.1. Cell Culture and Viability Assay. Human hepatocellular carcinoma (HepG2) cells obtained from the American Type Culture Collection (Manassas, VA, USA) were grown in Dulbecco's modified Eagle's medium (DMEM) as described earlier containing 10% fetal bovine serum (FBS), 100 U mL^{-1} penicillin, and 100 μg mL^{-1} streptomycin in a humidified atmosphere containing 5% CO_2 and 95% air at 37°C. HepG2/CYP2E1 cell lines (HepG2 cell transfected with human CYP2E1 cDNA) were generously provided by Professor Kim from Kyunghee University Medical Center. The full length of human CYP2E1 cDNA was inserted into the *Hind*III and *Nde*I restriction sites of modified plncx (inserted *Nde*I site) expression vector (Clontech) and mapped. The HCYP2E1F-LNCX, a retroviral vector containing human CYP2E1 cDNA, was used to transfect the packaging cell line 293GPG by lipofectamine, generating a stable transfected tool to produce CYP2E1 in the virus. Virus infection of HepG2 cells was carried out by supplying a medium previously collected and filtered [13]. The cells were seeded in 24-well culture plates at a density of 1×10^4 cells/mL and grown in 1 mL of growth media for 48 hr to reach 50–60% confluency and subcultured at appropriate intervals and maintained at subconfluent densities. The protein was determined using a BCA protein assay kit using bovine serum albumin as standard. All the experiments were done in triplicate.

Cytotoxic levels of the compound cultured cells were measured using MTT assay [14]. The HepG2/CYP2E1 cells were grown in 48-well plates at a density of 1×10^4 cells well^{-1}. After 24 h, cells were washed with fresh medium and treated with different concentrations of compound. After incubation for 48 h, the cells were rewashed and incubated with 100 μL of MTT (1 mg mL^{-1}) for 4 h at 37°C. Finally, 100 μL of DMSO were added to solubilize the formed formazan crystals, and the amount of formazan crystal was determined by measuring the absorbance at 540 nm using a multidetection microplate reader (GENios microplate reader, Tecan Austria GmbH, Austria). The data were expressed as means of at least three independent experiments. Each value was expressed as the mean ± S.D triplicate experiments.

3.2. GGT Assay. GGT activity was assayed colorimetrically on a microtiter plate using gamma-glutamyl-*p*-nitroanilide as an artificial substrate. The assay is based on the GGT catalysed breakdown of artificial substrate gamma-glutamyl-*p*-nitroanilide to *p*-nitroaniline which further reacts with nitrite and naphthylethylene diamine to form a red chromogenic compound [15]. Briefly, a 20 μL aliquot of conditioned cell culture media was added to 180 μL of the assay mixture consisting of 185 mM Tris-Cl (pH 8.2), 2 mM gamma-glutamyl-*p*-nitroanilide, 20 mM glycylglycine, 0.8 mM $NaNO_2$, and 3.2 mM naphthylethylene diamine. The assay was also run using the assay mixture without the substrate, gamma-glutamyl-*p*-nitroanilide, to correct for any potential interference by the compound. After incubating the plate at 37°C for 60 min, the reaction was stopped by addition of 40 μL of 1.0 N HCl. The red chromogen formation was estimated at 520 nm using a multiwell scanning spectrophotometer and corrected for the value obtained from the assay mixture devoid of the substrate.

3.3. Determination of Intracellular GSH Contents. The cells were ruptured in 100 μL of 5% metaphosphoric acid and centrifuged at 10,000 ×g for 15 min to obtain clear supernatants. The supernatants were used for the determination of total GSH by the enzymatic recycling method using DTNB [16]. The assay was carried out on a microtiter plate. The reaction mixture (100 μL) consisted of 143 mM NaPO4 (pH 7.5), 6.3 mM EDTA, 0.6 mM DTNB, 0.25 mM NADPH, 0.25 U mL^{-1} GSH reductase, and 2.0 μL compound. The plate was incubated at 37°C for 60 min, and the formation of 2-nitro-5-thiobenzoic acid was monitored by absorbance at 415 nm and converted to GSH concentration using a calibration curve with known amounts of GSH.

3.4. Western Blot Analysis. Western blotting was performed according to standard procedures. Briefly, cells were cultured at a density of 1×10^4 cells mL^{-1} in 6-well plate culture dishes with serum-free medium. After incubation for 48 h, the cells were treated with different concentrations of compound for 1 h and then treated with 1.0 M ethanol for 48 h with serum-free medium. Cells were lysed in lysis buffer containing 50 mM Tris-HCl (pH 8.0), 0.4% Nonidet P-40, 120 mM NaCl, 1.5 mM $MgCl_2$, 2 mM phenylmethylsulfonyl fluoride, 80 μg mL^{-1} leupeptin, 3 mM NaF, and 1 mM DTT at 4°C for 30 min. Total protein was extracted, and 100 μg mL^{-1} of protein were separated using a 10% SDS-polyacrylamide gel and 5% stacking gels and transferred onto a nitrocellulose membrane (Amersham Pharmacia Biotech., England, UK). The membrane was blocked for 1.5 h at 37°C using TBS-T buffer containing 0.1% Tween-20 and 3% BSA. After washing the membrane with TBS-T twice, the blots were incubated for 1 hr with suitable antibodies at 25°C. The respective proteins were detected with a chemiluminescent ECL assay kit (Amersham Pharmacia Biosciences, NJ, USA) according to the manufacturer's instructions. The western blot bands were visualized using a LAS-3000 system and quantified by Multi-Gauge V3.0 software (Fujifilm Life Science, Tokyo, Japan).

3.5. Statistical Analysis. Each value was expressed as means ± S.E.M ($n = 3$). The statistical significance of differences was analyzed by Student's *t*-test using SPSS (Chicago, IL, USA).

4. Results

4.1. Cytotoxic Effects of Ethanol and Compound (Emodin and Chrysophanol on HepG2/CYP2E1 Cells and Ethanol Induced HepG2/CYP2E1 Cells). The study first examined the cytotoxicity of different concentrations of ethanol on HeG2 and HeG2/CYP2E1 cell lines. The cells were treated with 0.1–2.0 M ethanol for 48 h and subjected to MTT assay to assess cell viability. As shown in Figure 2(a), the cells appeared to be quite resistant to ethanol up to 0.1 M but 2.0 M ethanol induced a severe loss of cell viability. Therefore, based on this viability data, the tested concentration of ethanol was 1.0 M, and HepG2/CYP2E1 cell lines can be transfected with human CYP2E1 cDNA; so we selected HeG2/CYP2E1 cell line for further experiments. The cytotoxic effects of emodin and chrysophanol on HepG2/CYP2E1 cells were determined by MTT assay. As shown in Figure 2(b), both emodin and chrysophanol exhibited no significant effects of cell proliferation at the tested concentrations (10–100 μM) after treatment for 48 h. Based on this viability data, the tested concentrations of emodin and chrysophanol were selected in the range of 10–100 μM for investigating the protective effects on ethanol-induced cytotoxicity.

The HepG2/CYP2E1 cells were pretreated with compound at various concentrations (10–100 μM) for 1 h prior to the treatment with 1.0 M ethanol for 48 h. The cells were then subjected to cell viability test. As expected (Figure 3), ethanol treat cell death (23.5% cell survival); however, the effect was almost completely abrogated when the cells were cotreated with emodin, chrysophanol together with ethanol (1.0 M) (emodin, 78.2% at 100 μM; chrysophanol, 72.1% at 100 μM cell survival), suggesting that emodin and chrysophanol have protective effect against ethanol-induced cytotoxicity in HepG2/CYP2E1 cells.

4.2. Effect of Emodin and Chrysophanol on Ethanol-Induced GGT and GSH Depletion in HepG2/CYP2E1 Cells. Serum gamma-glutamyltransferase (GGT) appeared to attenuate

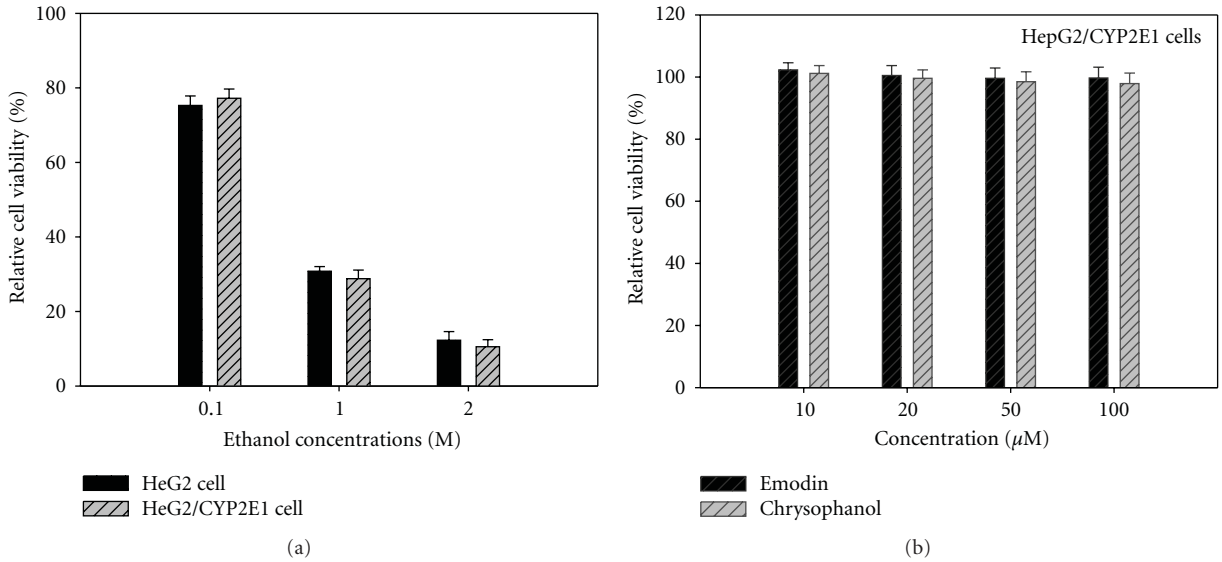

Figure 2: (a) Cytocompatibility of different concentrations (0.1–2 M) of ethanol on HeG2 and HeG2/CYP2E1 cells. (b) Cytocompatibility of emodin and chrysophanol on HepG2/CYP2E1 cells. Different concentrations of compounds were applied to the cells for 48 h, and cell viability was assessed by MTT assay as described in the text. Results are means ± standard error of three independent experiments.

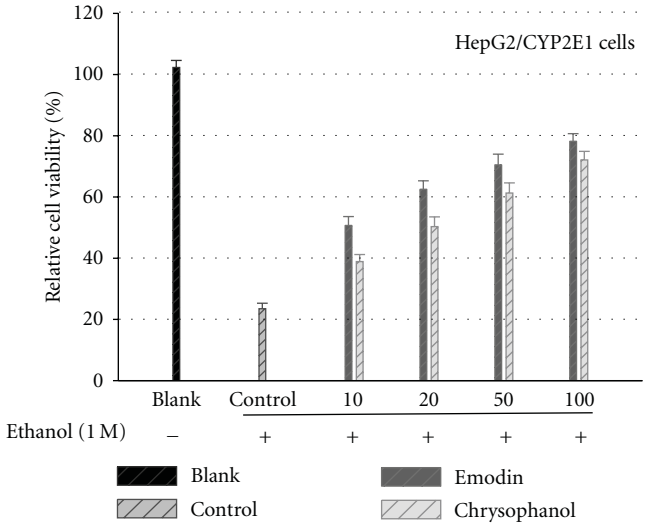

Figure 3: Effects of emodin and chrysophanol on the ethanol-induced cytotoxicity. The HepG2/CYP2E1 cells pretreated with compound at various concentrations for 1 h prior to the treatment with 1.0 M ethanol for 48 h. The cells were then subjected to cell viability test. Results are means ± standard error of three independent experiments.

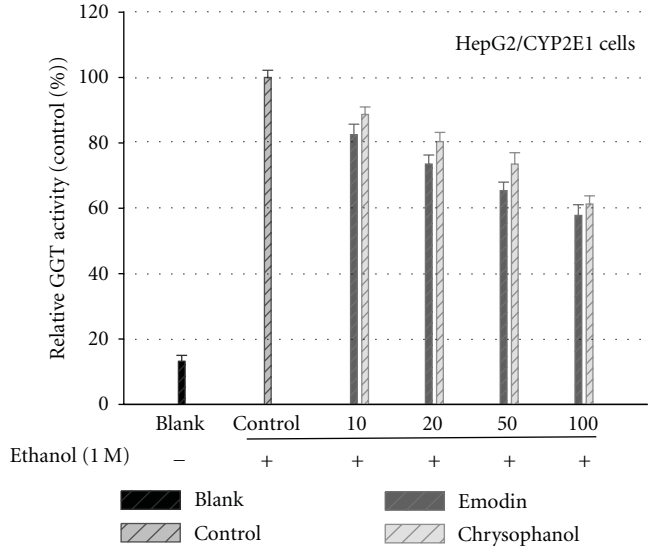

Figure 4: Constituents on the ethanol-induced GGT release. The HepG2/CYP2E1 cells pretreated with emodin and chrysophanol at various concentrations for 1 h prior to the treatment with 1.0 M ethanol for 48 h. The culture media were used for GGT assay. Results are means ± standard error of three independent experiments.

the ethanol-induced cytotoxicity; therefore the potential influence of emodin and chrysophanol on GGT activity was examined. As shown in Figure 4, ethanol (1.0 M) treatment of the cells increased GGT activity in the culture media of HepG2/CYP2E1 cell. Both emodin and chrysophanol inhibited the GGT increase dose-dependent manner (10–100 μM) after 48 h.

Cellular GSH levels at different concentrations (10–100 μM) of emodin and chrysophanol are shown in Figure 5. At the high concentration of the compound the GSH levels were significantly higher than those at the low concentration of the compound. Parallel to GGT activity results, both compounds (emodin and chrysophanol) exhibited elevation of GSH activity in dose dependent manner after 48 h.

4.3. Effects on GGT, GSH, and CYP2E1 Protein Expression of Emodin and Chrysophanol Evaluated by Western Blot. Besides

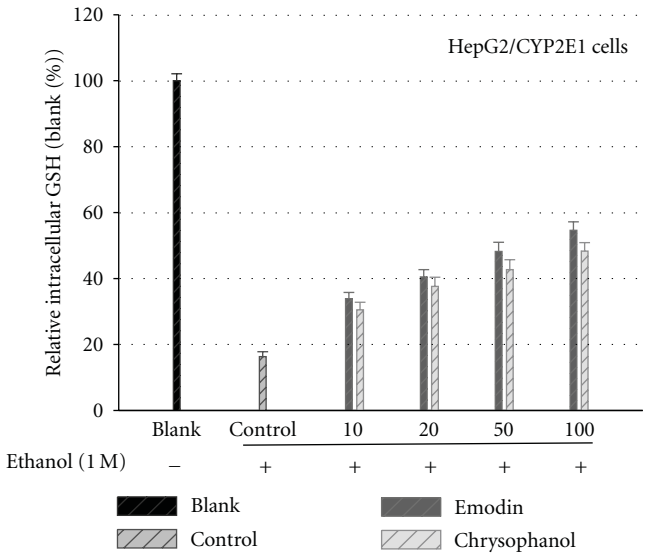

Figure 5: Effects of emodin and chrysophanol on the intracellular glutathione contents in the absence and presence of ethanol treatments. The HepG2/CYP2E1 cells pretreated with emodin and chrysophanol at various concentrations for 1 h prior to the treatment with 1.0 M ethanol for 48 h. The cell lysates in 5% metaphosphoric acid were used for the determination of intracellular GSH content for 48 h. Results are means ± standard error of three independent experiments.

the activity assays, levels of GGT, GSH, and CYP2E1 proteins were also examined by Western blot analysis after treatment with emodin and chrysophanol on ethanol-induced HepG2/CYP2E1 cells. Compounds treatment decreased the ethanol-induced elevated GGT and CYP2E1 protein levels in a dose-dependent manner. And both of the compounds increased the GSH protein levels dose-dependently against ethanol-induced depletion (Figure 6).

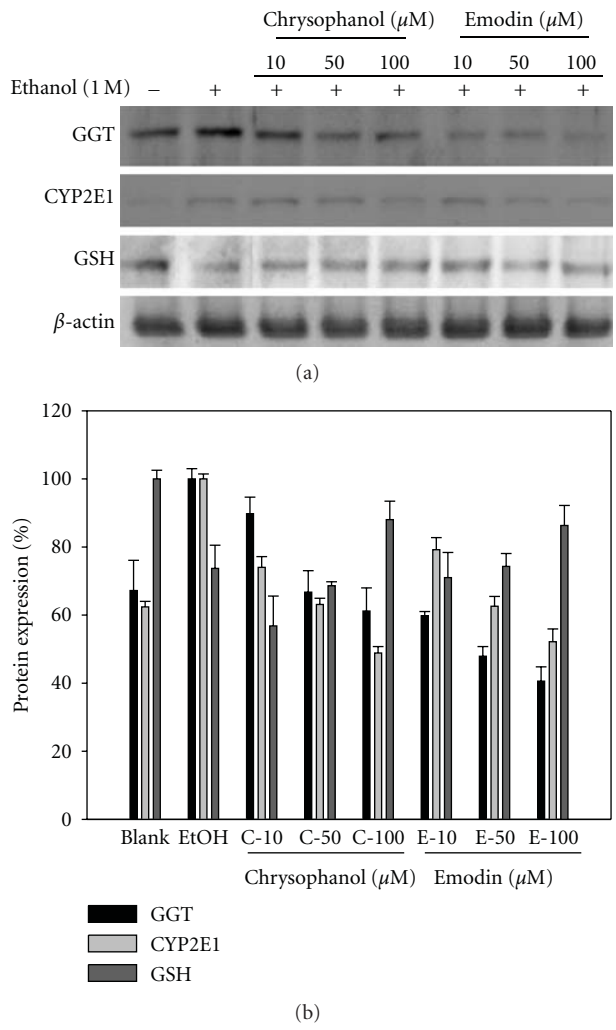

Figure 6: Effects of emodin and chrysophanol on the protein levels of GGT, GSH, and CYP2E in ethanol-induced HepG2/CYP2E1. Cells were treated with the compounds at different concentrations (10, 50, and 100 μM) and compared with ethanol nontreated group. The expression levels of protein were determined using Western blot analysis.

5. Discussion

Human hepatocellular carcinoma (HepG2) cells are known to metabolize ethanol nonoxidatively to fatty acid ethyl esters (FAEEs) [17]. Also, due to their many genotypic and phenotypic similarities to human hepatocytes, HepG2 cells are being often used for a variety of drug metabolism and toxicity studies, such as hepatic alcohol dehydrogenase (ADH) and CYP2E1 [18]. Previous studies have demonstrated that CYP2E1 was detectable in HepG2/CYP2E1 cells and HepG2 cells were not detectable. Consequently, our used HepG2 cells transfected with CYP2E1 in the present study to understand the metabolic basis of ethanol-induced hepatocellular injury. Western blot analysis clearly demonstrates over-expression of CYP2E1 in HepG2/CYP2E1 cells and HepG2 cell was not detectable (data not shown).

Ethanol consumption is known to increase the serum GGT level by inducing its expression, although it is also evident that alcohol-induced cellular damage leads to the enzyme release from the membranes. Many factors other than alcohol intake are associated with increased levels of GGT, in particular body mass index, diabetes mellitus, and serum total cholesterol [19]. GGT is one of the longest established biochemical tests for excessive alcohol consumption. Even though GGT is widely used as a marker of liver damage or alcohol abuse in clinics, its role in the ethanol toxicity has been elusive [20]. It is possibly involved in reabsorption of glutathione from the glomerular filtrate and protection against oxidative stress, via maintenance of intracellular glutathione levels [21]. GGT levels increase in response to exposure to a variety of drugs and alcohol. This suggests that GGT inhibition can provide positive effects on cell survival under stressed conditions. Therefore, the protective effects of emodin and chrysophanol could be attributed at least partly to its inhibition of GGT activity that appears to play a critical role in the ethanol toxicity. GGT catalyses extracellular GSH breakdown and produces the metabolites used for GSH synthesis inside the cells. Therefore, GGT activity might be

in great demand if intracellular GSH is depleted by ethanol toxicity [22]. However, GGT expression or activation may not lead to a restoration of intracellular GSH because the reaction products of GGT could potentially induce oxidative stress [23].

GSH, the most abundant antioxidant in cells, plays a major role in the defense against oxidative stress-induced cellular injury and is essential for the maintenance of intracellular redox balance [2]. Neuman et al. [24] reported a dramatic decrease in mitochondrial GSH in isolated hepatocytes exposed to alcohol. Ethanol increased ROS production, decreased GSH, and increased lipid peroxidation [25]. Incubation of HepG2 cells with ethanol induced oxidative stress and leaves the cells vulnerable to further injury by ROS. The results showed that the levels of GSH in HepG2 cells exposed to ethanol were significantly lower than GSH levels in nontreated cells. And also the data showed that the GSH levels decreased in ethanol-induced HepG2 cells while it increased in compounds (emodin and chrysophanol) treated cells. A dose-dependent GSH elevation was observed in compounds-treated cells after 48 h exposure to ethanol. Therefore, it is evident that compound treatment can relieve ethanol-induced cellular injury in HepG2/CYP2E1 cells which causes imbalance of cellular antioxidative system due to incubation with ethanol. The cytoprotective effects of emodin and chrysophanol are thus likely to be associated with these enzymes.

CYP2E1 could be induced by a broad variety of chemicals, such as ethanol. Ethanol increases the activity of cytochrome P450 2E1 (CYP2E1), which can metabolize alcohol and generate ROS [26, 27]. The CYP2E1 constitutes the microsomal ethanol oxidizing system, which is inducible by higher amounts of ethanol and other xenobiotics. Ethanol can also be metabolized by catalase and more selectively by cytochrome P-450 2E1 (CYP2E1) [28]. Acetaldehyde is the first oxidation product of ethanol. Due to high reactivity it is responsible for many aspects of alcohol-related liver injury. In a recent study CYP2E1 activity, cellular GSH and GGT levels were chosen to assess hepatocyte damage caused by ethanol exposure [29]. Due to the complicated nature of ethanol toxicity, various strategies have been suggested to protect cells from it. They include inhibition of ethanol metabolism leading to the production of toxic metabolites such as acetaldehyde and inhibition of ROS production from nitric oxide synthases, NADPH oxidase, and mitochondrial electron transport [4]. GGT catalyses extracellular GSH breakdown and produces the metabolites used for GSH synthesis inside the cells. Thus GGT activity might be in great demand if intracellular GSH is depleted by ethanol toxicity.

Recently, marine microorganisms have been well known as an important source to produce naturally bioactive secondary metabolites including phenols and polyphenols with unique linkages (ether and/or phenyl). In our results, emodin attenuated the ethanol cytotoxicity effectively compared to the chrysophanol. The active focus of emodin and chrysophanol components is ascribed to the phenolic hydroxyl groups attached to the ring structure. The structural diversity in each compound is determined by the number and the arrangement of hydroxyl groups and by the methyl groups. They were found to rule the biological effect of such systems. Therefore it could be suggested that structure-activity relationships (SARs) mainly depend on the number of phenolic ring substituents and phenyl ether linkages. The protecting effect of emodin with three hydroxyl groups was stronger than that of chrysophanol containing two hydroxyl group-substituted compounds on ethanol-induce cytotoxicity. Emodin is a natural anthraqinone compound, that is, an active component of the dried root of Rhei Rhizoma (Rheum palmatum, Daehwang in Korean) and is also present in many herbs and vegetables including cabbage, lettuce, beans, and peas [30]. Emodin is known to have immunosuppressive effect, hepatoprotective effect, antiinflammatory, antimicrobial, antiviral, anticancer and wound healing properties [31]. It could be suggested that emodin from this genus would be more potential candidate for attenuating ethanol-induced liver damage for further industrial applications such as in functional foods and pharmaceuticals.

6. Conclusion

In conclusion, our study demonstrated that emodin and chrysophanol isolated from marine fungus *Aspergillus sp.* are attenuating the ethanol-induced cytotoxicity of HepG2/CYP2E1 cells. Moreover, the ethanol-induced cytotoxicity could be attenuated by inhibition of GGT activity and CYP2E1 protein expression and providing increased levels of intracellular GSH. Therefore, it suggests that emodin and chrysophanol may provide a novel strategy for attenuating ethanol-induced liver damage.

Acknowledgment

This study was supported by research funds from Chosun University 2011.

References

[1] M. F. Fleming, L. B. Manwell, K. L. Barry, and K. Johnson, "At-risk drinking in an HMO primary care sample: prevalence and health policy implications," *American Journal of Public Health*, vol. 88, no. 1, pp. 90–93, 1998.

[2] A. Dey and A. I. Cederbaum, "Alcohol and oxidative liver injury," *Hepatology*, vol. 43, no. 2, pp. S63–S74, 2006.

[3] E. Albano, "Alcohol, oxidative stress and free radical damage," *Proceedings of the Nutrition Society*, vol. 65, no. 3, pp. 278–290, 2006.

[4] O. R. Koch, G. Pani, S. Borrello et al., "Oxidative stress and antioxidant defenses in ethanol-induced cell injury," *Molecular Aspects of Medicine*, vol. 25, no. 1-2, pp. 191–198, 2004.

[5] R. K. Dhiman and Y. K. Chawla, "Herbal medicines for liver diseases," *Digestive Diseases and Sciences*, vol. 50, no. 10, pp. 1807–1812, 2005.

[6] B. J. Xu, Y. N. Zheng, and C. K. Sung, "Natural medicines for alcoholism treatment: a review," *Drug and Alcohol Review*, vol. 24, no. 6, pp. 525–536, 2005.

[7] D. Wu and A. I. Cederbaum, "Ethanol cytotoxicity to a transfected HepG2 cell line expressing human cytochrome P4502E1," *The Journal of Biological Chemistry*, vol. 271, no. 39, pp. 23914–23919, 1996.

[8] K. M. Conigrave, P. Davies, P. Haber, and J. B. Whitfield, "Traditional markers of excessive alcohol use," *Addiction*, vol. 98, no. 2, pp. 31–43, 2003.

[9] H. Zhang, H. Jay Forman, and J. Choi, "γ-glutamyl transpeptidase in glutathione biosynthesis," *Methods in Enzymology*, vol. 401, article 28, pp. 468–483, 2005.

[10] D. J. Faulkner, "Marine natural products," *Natural Product Reports*, vol. 19, no. 1, pp. 1–48, 2002.

[11] T. S. Bugni and C. M. Ireland, "Marine-derived fungi: a chemically and biologically diverse group of microorganisms," *Natural Product Reports*, vol. 21, no. 1, pp. 143–163, 2004.

[12] W. E. Timberlake and M. A. Marshall, "Genetic engineering of filamentous fungi," *Science*, vol. 244, no. 4910, pp. 1313–1317, 1989.

[13] Y. H. Lee, J. N. Ho, M. S. Dong et al., "Transfected HepG2 cells for evaluation of catechin effects on alcohol-induced CYP2E1 cytotoxicity," *Journal of Microbiology and Biotechnology*, vol. 15, no. 6, pp. 1310–1316, 2005.

[14] F. Denizot and R. Lang, "Rapid colorimetric assay for cell growth and survival—modifications to the tetrazolium dye procedure giving improved sensitivity and reliability," *Journal of Immunological Methods*, vol. 89, no. 2, pp. 271–277, 1986.

[15] P. J. M. J. Kok, B. Seidel, H. C. Holtkamp, and J. Huisman, "A new procedure for the visualization of multiple forms of gamma-glutamyl transferase (GGT). Results in normals, patients receiving enzyme-inducing drugs and patients having liver parenchymal lesions," *Clinica Chimica Acta*, vol. 90, no. 3, pp. 209–216, 1978.

[16] M. E. Anderson, "Determination of glutathione and glutathione disulfide in biological samples," *Methods in Enzymology*, vol. 113, pp. 548–555, 1985.

[17] C. F. Lima, M. Fernandes-Ferreira, and C. Pereira-Wilson, "Phenolic compounds protect HepG2 cells from oxidative damage: relevance of glutathione levels," *Life Sciences*, vol. 79, no. 21, pp. 2056–2068, 2006.

[18] D. Wu and A. I. Cederbaum, "Ethanol-induced apoptosis to stable HepG2 cell lines expressing human cytochrome P-4502E1," *Alcoholism: Clinical and Experimental Research*, vol. 23, no. 1, pp. 67–76, 1999.

[19] T. R. Banciu, H. Weidenfeld, E. Marcoane, and L. Berinde, "Serum gama-glutamyltranspeptidase assay in the detection of alcohol consumers and in the early and stadial diagnosis of alcoholic liver disease," *Medecine Interne*, vol. 21, no. 1, pp. 23–29, 1983.

[20] J. B. Whitfield, "Gamma glutamyl transferase," *Critical Reviews in Clinical Laboratory Sciences*, vol. 38, no. 4, pp. 263–355, 2001.

[21] D. H. Lee, R. Blomhoff, and D. R. Jacobs, "Is serum gamma glutamyltransferase a marker of oxidative stress?" *Free Radical Research*, vol. 38, no. 6, pp. 535–539, 2004.

[22] S. J. Chinta, J. M. Kumar, H. Zhang, H. J. Forman, and J. K. Andersen, "Up-regulation of γ-glutamyl transpeptidase activity following glutathione depletion has a compensatory rather than an inhibitory effect on mitochondrial complex I activity: implications for Parkinson's disease," *Free Radical Biology and Medicine*, vol. 40, no. 9, pp. 1557–1563, 2006.

[23] A. Paolicchi, R. Tongiani, P. Tonarelli, M. Comporti, and A. Pompella, "Gamma-glutamyl transpeptidase-dependent lipid peroxidation in isolated hepatocytes and HepG2 hepatoma cells," *Free Radical Biology and Medicine*, vol. 22, no. 5, pp. 853–860, 1997.

[24] M. G. Neuman, N. H. Shear, S. Bellentani, and C. Tiribelli, "Role of cytokines in ethanol-induced cytotoxicity in vitro in Hep G2 cells," *Gastroenterology*, vol. 115, no. 1, pp. 157–166, 1998.

[25] I. Kurose, H. Higuchi, S. Kato, S. Miura, and H. Ishii, "Ethanol-induced oxidative stress in the liver," *Alcoholism: Clinical and Experimental Research*, vol. 20, no. 1, pp. 77–85, 1996.

[26] E. Albano, P. Clot, M. Morimoto, A. Tomasi, M. Ingelman-Sundberg, and S. W. French, "Role of cytochrome P4502E1-dependent formation of hydroxyethyl free radical in the development of liver damage in rats intragastrically fed with ethanol," *Hepatology*, vol. 23, no. 1, pp. 155–163, 1996.

[27] J. M. Jimenez-Lopez and A. I. Cederbaum, "Green tea polyphenol epigallocatechin-3-gallate protects HepG2 cells against CYP2E1-dependent toxicity," *Free Radical Biology and Medicine*, vol. 36, no. 3, pp. 359–370, 2004.

[28] A. I. Cederbaum, D. Wu, M. Mari, and J. Bai, "CYP2E1-dependent toxicity and oxidative stress in HepG2 cells," *Free Radical Biology and Medicine*, vol. 31, no. 12, pp. 1539–1543, 2001.

[29] I. L. Sang, J. K. Hyo, and Y. C. Boo, "Effect of green tea and (-)-epigallocatechin gallate on ethanol-induced toxicity in HepG2 cells," *Phytotherapy Research*, vol. 22, no. 5, pp. 669–674, 2008.

[30] Q. Huang, G. Lu, H. M. Shen, M. C. M. Chung, and N. O. Choon, "Anti-cancer properties of anthraquinones from rhubarb," *Medicinal Research Reviews*, vol. 27, no. 5, pp. 609–630, 2007.

[31] T. Tang, L. Yin, J. Yang, and G. Shan, "Emodin, an anthraquinone derivative from Rheum officinale Baill, enhances cutaneous wound healing in rats," *European Journal of Pharmacology*, vol. 567, no. 3, pp. 177–185, 2007.

Hindawi Publishing Corporation
Evidence-Based Complementary and Alternative Medicine
Volume 2011, Article ID 196190, 8 pages
doi:10.1155/2011/196190

Research Article

Purification and the Secondary Structure of Fucoidanase from *Fusarium* sp. LD8

Wu Qianqian, Ma Shuang, Xiao Hourong, Zhang Min, and Cai Jingmin

Department of Biological and Environmental Sciences, Hefei University, Hefei 230022, China

Correspondence should be addressed to Cai Jingmin, caijingmin@hfuu.edu.cn

Received 15 January 2011; Revised 25 April 2011; Accepted 25 July 2011

The fucoidanase from *Fusarium* sp. (LD8) was obtained by solid-state fermentation. The fermented solid medium was extracted by citric acid buffer, and the extracts were precipitated by acetone and purified by Sephadex G-100 successively. The results showed that the specific fucoidanase activity of purified enzyme was 22.7-fold than that of the crude enzyme. The recovery of the enzyme was 23.9%. The purified enzyme gave a single band on SDS-PAGE gel, and the molecular weight of fucoidanase was about 64 kDa. The isoelectric point of the enzyme was 4.5. The enzyme properties were also studied. The results showed that the optimum temperature and pH were 60°C and 6.0, respectively; the temperature of half inactivation was 50°C, and the most stable pH for the enzyme was 6.0. K_M, and the $V_{\max}$ of the enzyme was 8.9 mg·L^{-1} and 2.02 mg·min^{-1}·mL^{-1} by using fucoidan from *Fucus vesiculosus* as substrate. The compositions of the secondary structure of fucoidanase were estimated by FTIR, the second derivative spectra, and the curve-fitting analysis of the amide I bands in their spectra. The results showed that β-sheet was the dominant component (58.6%) and α-helix was the least (12%); the content of β-turn and random coil were 15.39% and 14.5%, respectively.

1. Introduction

Sulfated polysaccharides, named fucoidan, could be extracted from many marine brown algae. The main differences of structural characterization in algal fucoidan originate from their species; the backbone of fucoidan isolated from *Laminaria cichorioides* [1] was consisting of α (1–3) linked fucopyranose residues, and that from *L. japonica* was primarily α (1–3) linked fucopyranose residues (75%) and a few α (1–4) fucopyranose linkages (25%) [2]; The fucoidan from *Fucus serratus* [3], *F. evanescens* [4], and *F. distichus* [5] was shown to contain a backbone consisting of alternating (1–3) and (1–4) linked a-L-fucopyranose residues.

Investigators were interested in screening fucoidan which was isolated from different brown algal species; fucoidan was attributed several different bioactivities including anticoagulant [6–8], antithrombotic/antithrombin activity [9], antiviral [10], and other activities [11]. The biological effects of fucoidan depended on the molecular mass, sulfate content, and sugar constituents [12, 13]. The low molecular weight fucoidan (LMWF) could be obtained by fucoidanase (E.C.3.2.1.44) enzymolysis, and it could hydrolyze fucoidan to sulfated LMWF without removal of its side substitute groups.

Fucoidanase could be extracted from hepatopancreas of invertebrates [14, 15], marine bacteria [16–25], and marine fungi [26–28].

There were some papers focusing on fermentation conditions of fucoidanase from marine fungus [26–28] and marine bacteria [23, 29], a few papers concerning purifications of fucoidanase from hepatopancreas [14] and marine bacteria reported [17, 20–22]. In order to elucidate the structure of fungal fucoidanase, we investigate fucoidanases isolated from different species of fungi. The present work is devoted to purification and the structure analysis of a fucoidanase from marine fungus *Fusarium* sp. LD8.

2. Materials and Methods

2.1. Chemicals. Fucoidan from *Fucus vesiculosus* was obtained from Sigma Chemical Co., Sephadex; G-100 was purchased from Pharmacia Biotech Corporation (Sweden). Fucoidan from *Laminaria* sp. was purchased from Rizhao Jiejing Ocean Biotechnology Development Co., Ltd (PRC). All of the other chemical reagents were analytical pure grade made in China.

2.2. Microorganism. The marine fungus LD8 was isolated from sand of North Sea in German which was identified as *Fusarium* sp. (LD8), and it could be used for the synthesis of fucoidanase. Solid-state medium for LD8 consisted of 7.5 g wheat bran, 0.5 g kelp powder, 0.1 g glucose, 0.04 g $NaNO_3$, and 7.5 mL artificial sea water in 250 mL flasks [27].

2.3. Chemical Analysis. The protein concentration was determined by the Bradford method [30].

2.4. Enzyme Assay

2.4.1. Fucoidanase Activity. Fucoidanase activity was measured by the dinitrosalicylic acid technique [31] to estimate the release of reducing sugars at 540 nm as follows: a mixture consisting of 1 mL substrate solution (1% fucoidan (w/v) from Fucus vesiculosus dissolved with 0.02 mol·L^{-1} citric acid-sodium citric buffer, pH 6.0) and 0.1 mL enzyme solution (crude extract or pure enzyme) was incubated at 50°C for 10 min, using inactivated enzyme solution as blank CK. Using fucose as standard, the calibration curve function was $y = 1.611x$ (x: the quantity of fucose, mg; y: the absorbance at 540 nm, $R^2 = 0.9983$).

One unit (IU) of fucoidanase activity is defined as the amount of enzyme that releases 1 μmol of fucose per minute under the assay conditions.

2.4.2. Fucosidase Activity. Fucosidase activity was measured under the following conditions: the reaction mixture contained 1 mL substrate solution (1% ρ-nitrophenyl-α-L-fucoside (w/v) dissolved with 0.02 mol·L^{-1} citric acid-sodium citric buffer, pH 6.0) and 0.1 mL enzyme solution (purified enzyme) was incubated at 40°C for 2 h. One unit (IU) of fucosidase activity is defined as the amount of enzyme that releases 1 μmol of ρ-nitrophenyl per minute under the assay conditions.

2.4.3. Amylase Assay. The reaction mixture containing 1 mL of 2% soluble starch (w/v) in acetate buffer (pH 5.5) and 1 mL of enzyme solution was incubated with shaking at 40°C for 30 min. The reaction was stopped by boiling water for 5 min, and after centrifugation the released reducing sugar was measured by the dinitrosalicylic acid method [31]. One unit (IU) of amylase activity is defined as the amount of enzyme that liberated 1 μmol reducing sugar (as glucose) per min under the assay conditions.

2.5. Extraction, Purification, and Purity Identification of Fucoidanase. The LD8 was cultivated at 28°C for 48 h on the solid-state medium in 250 mL flask.

All the following steps were accomplished at 4°C except being indicated specifically.

50 g fermented culture medium was extracted with citric acid-citric sodium buffer (pH 6.0) for 0.5 h. After being filtrated through six-layer carbasus, the filtrate was centrifuged at 15,000 g for 0.5 h, and then ice-cold acetone was added to the supernatant to a final concentration of 66.7% (v/v) with gentle stirring. Insoluble material was obtained by centrifugation at 15,000 g for 0.5 h. The precipitate was dissolved in pH 6.0, 0.02 mol·L^{-1} citric acid-citric sodium buffer and was centrifuged at 15,000 g for 0.5 h, and the clear solution was collected for use. The enzyme solution was concentrated to about 10 mL by low-temperature vacuum concentration and then loaded to Sephadex G-100 column (2.5 × 100 cm), which has been balanced well with 0.1 mol·L^{-1} citric acid-citric sodium buffer. The enzyme was eluted at room temperature at the flow rate of 0.33 mL·min^{-1}; fractions were collected at 20 min intervals. The fractions with the highest enzymatic activity were pooled, concentrated by low-temperature vacuum concentration to 10 mL, dialyzed in deionized water, lyophilized, and stored at −18°C.

SDS-PAGE was performed to identify the purity of the purified enzyme and calculate the M_w of the proteins in the gel. SDS-PAGE was 7% (w/v) polyacrylamide gel containing 10% (w/v) SDS; molecular markers were myosin (220 kDa), α-2 macroglobulin (170 kDa), β-galactosidase (116 kDa), transferrin (76 kDa), and glutamic dehydrogenase (53 kDa), respectively. The protein was stained by Coomassie bright blue R-250.

2.6. Characteristics of the Purified Enzyme. Isoelectrofocusing was performed on gel rods. The electrode solutions were 2% (w/v) sodium hydroxide solution at the cathode and 5% (v/v) phosphoric acid solution at the anode. Each gel was focused in 100 V, 2 mA for 2 h, followed by 150–160 V, 4 mA for 5 h, which allowed for a sharp focalisation of fucoidanase. Following isoelectric focusing, the gels were cut into 0.5 cm for measuring pH and enzyme activity. The protein was stained by 0.5% amino black (w/v).

The pH relative activity of the fucoidanase was determined by detecting the fucoidanase activity over a pH range of 3–8 with three kinds of buffer solutions (50 mmol·L^{-1} sodium citrate buffer, 50 mmol·L^{-1} sodium phosphate buffer, 50 mmol·L^{-1} sodium carbonate buffer) at 50°C. The pH stability of the enzyme was studied by detecting the residual activity after the enzyme being incubated for 3 h at room temperature under different pH value. To obtain optimal reactive temperature, a mixture consisting of 1 mL substrate solution (1% fucoidan (w/v) from *Fucus vesiculosus* dissolved with 0.02 mol·L^{-1} citric acid-sodium citric buffer, pH 6.0) and 0.1 mL enzyme solution was incubated at different temperatures for 10 min. For thermal stability study, 0.1 mL of enzyme solution was incubated at temperature range from 30 to 80°C for 1 h, then cooled rapidly in ice bath for 5 min, and then removed to 25°C. The residual enzyme activity was detected at 50°C for 10 min.

The substrate specificity of the enzyme was examined by using different fucoidan from *Fucus vesiculosus* and *Laminaria* sp. as substrates. Michaelis constants (K_M) and maximum reaction velocities (V_{max}) were calculated by the double-reciprocal plot method of Lineweaver and Burk [32].

2.7. FTIR Assessment of the Secondary Structure of Fucoidanase. Infrared spectra were recorded on a MAGNA-IR750 Fourier transform spectrometer (INCOLET

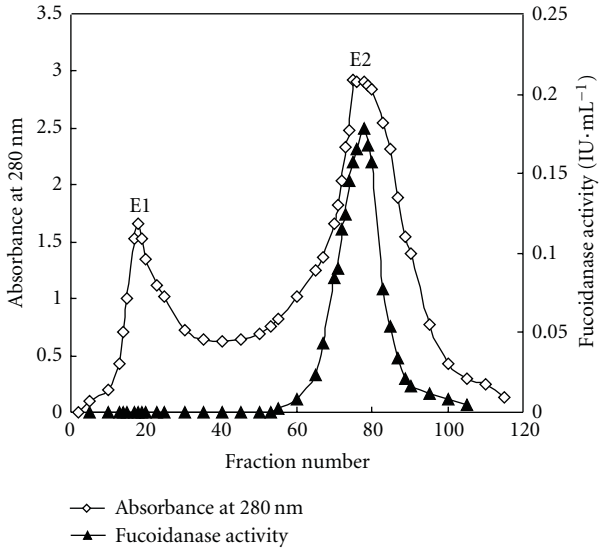

FIGURE 1: Gel filtration column chromatography. Chromatography of fucoidanase obtained from the column of Sephadex G-100 (2.5 × 100 cm). After the column had been washed well with 0.1 mol·L^{-1} citric acid-citric sodium buffer (pH 6.0), it was eluted with 2000 mL of the same buffer solution at a flow rate of 0.33 mL·min^{-1} with 6.6 mL elute in each fraction.

INSTRVMENTW, USA). For the spectrum range from 1500~2200 cm^{-1}, 32 scans were collected at a spectral resolution of 4 cm^{-1}. Pure fucoidanase (10 mg) was mixed with 100 mg of dried potassium bromide (KBr). Water vapor was purged from sample room. The spectrum of the amide I band of fucoidanase was obtained, and self-deconvolution and curve-fitting methods were used to analyze the secondary structure of the fucoidanase.

3. Result

3.1. Purification of Fucoidanase. Two protein peaks (E1 and E2) were observed. E2 peak showed fucoidanase activities (Figure 1) whose purity had been detected by SDS-PAGE (see below). The crude enzyme extraction was purified by 66.7% acetone precipitation and Sephadex G-100 gel chromatography (Table 1). The purification fold of fucoidanase activity of 1 mg protein was enhanced from 1-fold to 23.9-folds while recovery rate was decreased from 100% to 22.7%. The fractions with higher fucoidanase activity (tube no. 65 to 87) were pooled and concentrated to 10 mL. To exclude the reducing carbohydrates from carbon sources used for cultivation (starch, kelp polysaccharides), fucoidanase-related enzymes such as fucosidase and amylase activity of purified protein were determined, but there is no fucosidase or amylase activity (Table 2).

3.2. Determination of Isoelectric Point and Molecular Mass of Fucoidanase. The result exhibited that the purified fucoidanase gave a single band on isoelectric electrophoresis, and the isoelectric point of the enzyme was pH 4.5 (Figure 2).

The purified fucoidanase gave a single band on SDS-PAGE gel, which suggested that relatively pure fucoidanase had been obtained. The molecular mass of the fucoidanase was about 64 kDa by SDS-PAGE (Figure 3) which was different from that of *Dendryphiella arenaria* TM94 (180 kDa). Molecular markers used were myosin (220 kDa), α-2 macroglobulin (170 kDa), β-galactosidase (116 kDa), transferrin (76 kDa), and glutamic dehydrogenase (53 kDa), respectively.

3.3. Effect of pH on Fucoidanase Activity and Stability. Effect of pH on the activity of fucoidanase obtained from *Fusarium* sp. LD8 was shown in Figure 4. The maximum enzyme activity was at pH 6. The optimal pH of this enzyme was very close to that from marine fungus *Dendryphiella arenaria* TM94 and *Vibrio* sp. N-5, while the optimal pH of fucoidanase from Hepatopancreas of *Patinopecten yessoensis* was 5.5.

The effect of pH on stability was also determined. The results showed that the enzyme displayed stability at pH 6.0, whereas at pH 5.0 and 8.0, an activity loss of about 50% occurred after 6 h incubation at room temperature (25°C), respectively.

3.4. Effect of Temperature on Fucoidanase Activity and Stability. The optimum temperature for maximal activity of the fucoidanase was 60°C at pH 6.0 (Figure 5(a)). At 30°C the activity of fucoidanase decreased to 12.5%, while at 80°C to 18.75%. The result showed that the optimal temperature of fucoidanase from TM94 was higher than that of the fucoidanase in *Vibrio* sp. N-5, whose optimum temperature was 40°C [33].

The residual activity of fucoidanase was examined after preincubating it at different temperatures for 1 hr, and the temperature at which enzyme lost half activity was 50°C (Figure 5(b)). It was completely inactivated at above 80°C. The temperature of lost half activity is different from those of *Vibrio* sp. N-5 and *Dendryphiella arenaria* TM94. The enzyme of *Dendryphiella arenaria* TM94 and *Vibrio* sp. N-5 showed that their optimal temperature of half lost inactivation was at 56°C and 40°C, respectively [33].

3.5. Determination of K_M, V_{max} and Affinity for Fucoidanase. The kinetic parameters of fucoidanase were examined using *Fucus vesiculosus* fucoidan and *Laminaria* sp. fucoidan as substrates. The K_M values of the enzyme determined by Lineweaver-Burk method were 8.9 mg·L^{-1} and 10.9 mg·mL^{-1}, respectively. At the same time, the V_{max} values for both substrates were 2.02 mg·min^{-1}·mL^{-1} and 2.06 mg·min^{-1}·mL^{-1}, respectively. The enzyme showed higher affinity to fucoidan from *Fucus vesiculosus.*

3.6. The Second Structure of Fucoidanase. The original IR spectrum for the fucoidanase was showed in Figure 6. The

Table 1: Summary of Purification of Fucoidanase.

Purification step	Total protein (mg)	Total activity (IU)	Specific activity (IU·mg^{-1})	Purification (fold)	Yield (100%)
Crude enzyme	11668.43	127.96	0.011	1	100
Acetone precipitation	509.23	80.43	0.16	14.5	62.8
Sephadex G-100	120.43	30.64	0.25	22.7	23.9

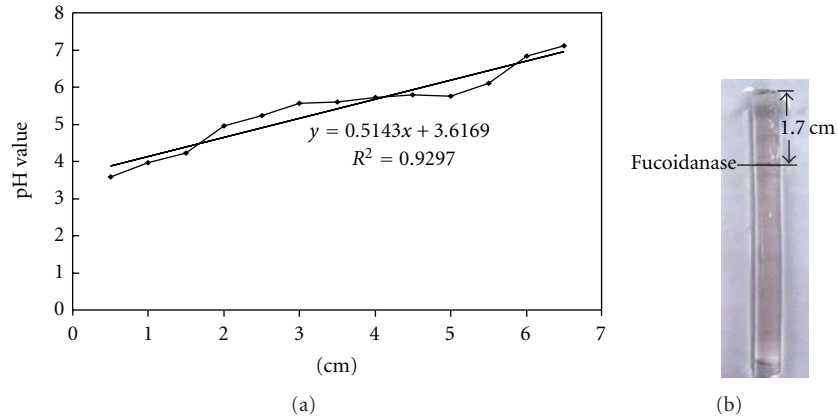

Figure 2: Determination of isoelectric point of the fucoidanase (a) R_f value of the pH; (b) R_f of the purified fucoidanase on original isoelectric focusing gel isoelectrofocusing was performed on gel rods. The electrode solutions were 2% (w/v) sodium hydroxide solution at the cathode and 5% (v/v) phosphoric acid solution at the anode. Each gel was focused in 100 V, 2 mA for 2 h, followed by 150–160 V, 4 mA for 5 h. Following isoelectric focusing, the gels were cut into 0.5 cm for measuring pH and enzyme activity. The protein was stained by 0.5% amino black.

Table 2: Fucoidanase and fucoidanase-related activity of purified protein.

Enzyme activity	Fucoidanase	E2 Fucosidase	Amylase
IU·mL^{-1}	1.88	—	—

—: no enzyme activity.

bands at about 1620~1700 cm^{-1} can be mainly attributed to the (ν(C=O)) and is called amide I. The shape of the amide I band is representative of fucoidanase secondary structure. The bands of the 1650~1658 cm^{-1}, 1600~1640 cm^{-1}, 1640~1650 cm^{-1}, 1660~1695 cm^{-1} regions were, respectively, assigned to α-helix, β-sheet, random coil, and β-turn structure.

The second derivative and a curve-fitting treatment can be carried out to estimate quantitatively the relative proportion of each component representing a type of secondary structure. The fourth derivative function was calculated by the PeakFit 4.12 software to determine the number of components in the amide I region for the second derivative spectra and the curve-fitting process (Table 3). According to this band composition, the amide I profile of fucoidanase contains four major components that can be linked with α-helix, β-sheet, random coil, and β-turn structure where β-sheet is evidently the most intense component. The results showed that β-sheet was the dominant component (58.6%), α-helix was the least (12%), and the content of β-turn and random coil were 15.39% and 14.5%.

4. Discussion

Fucoidanase could be isolated from marine invertebrates as *Haliotis* sp., sea cucumber, sponges, and molluscs [34] and was produced by marine bacteria as *Pseudomonas atlanica*, *P. carrageenovora*, *P. alteromonas*, *Vibrio* sp., *Bacillus* sp. HTP2, *Pseudoalteromonas citrea*, Family flavobacteriaceae [19, 24] and marine fungi *Dendryphiella arenaria* TM94 [26], *Fusarium* sp. LD8 [27], *Aspergillus niger, Penicillium purpurogenum*, *Mucor* sp. [28].

Fucoidanase had different molecular weight in different organisms. The molecular weight (M_w) of LD8 fucoidanase was 64 kDa; it is close to that of fucoidanase E1, E2, and E3 of *Vibrio* sp. N-5 (39 kDa, 68 kDa, and 68 kDa, resp.) [33], while the M_w of LD8 fucoidanase was lower than that of fucoidanase from hepatopancreas of *Patinopecten yessoensis* (100–200 kDa) [14] and *Dendryphiella arenaria* TM94 (180 kDa) [35].

Fucoidanase from *Fusarium* sp. LD8 was more sensitive to pH and temperature. The catalytic activity of the fucoidanase of LD8 reached maximum at pH 6.0, which is very close to that of the fucoidanases from bacteria *Vibrio* sp. N-5 and *Dendryphiella arenaria* TM94. The enzyme activity decreased rapidly in LD8 when pH is below or above 6.0. At pH 5.0 and 7.0, the enzyme retained 68.2% and 86.4% of the enzyme activity at pH 6, respectively. The fucoidanase from LD8 had a relatively higher optimal temperature (60°C) compared with that of bacteria *Vibrio* sp. N-5 (37°C), Flavobacteriaceae SW5 (room temperature),

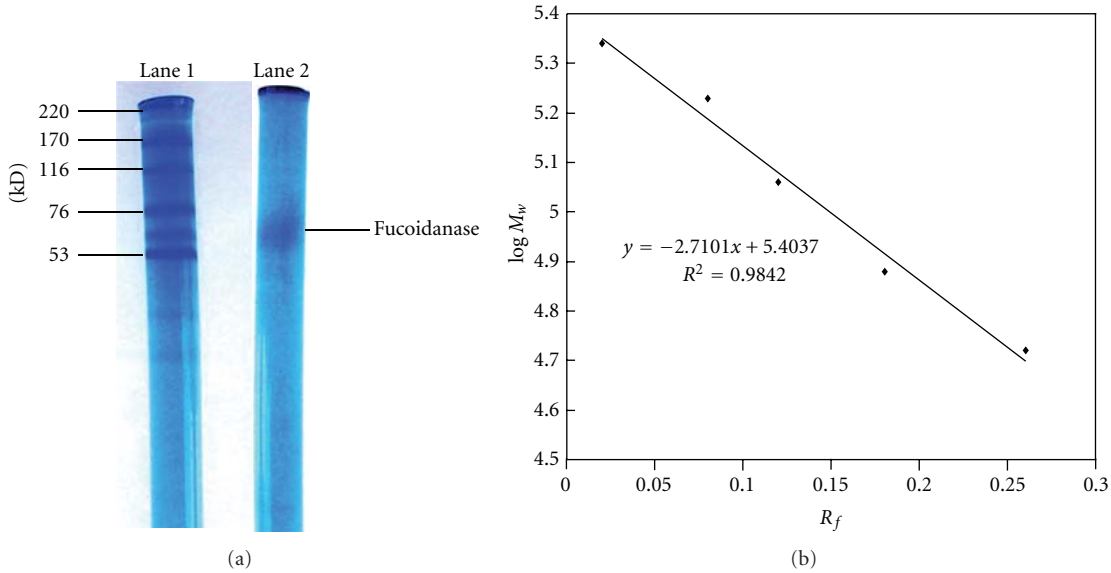

Figure 3: Determination of the M_w of the fucoidanase by SDS-PAGE. Picture of electrophoresis of fucoidanase: lane 1 is M_w marker; lane 2 is the fucoidanase; (b) standard curve and M_w function of the M_w marker SDS-PAGE was conducted using discontinuous electrophoresis method with Phastsystem, 5.5% (w/v) polyacrylamide, pH 8.3, 250 V, 10 mA, in the concentration gel with 7.0% polyacrylamide (w/v), 250 V, 30 mA, in the separation gel. Protein was stained with Coomassie brilliant blue R-250. Molecular markers used were (220 kDa), α-2 macroglobulin (170 kDa), β-galactosidase (116 kDa), transferring (76 kDa), and glutamic dehydrogenase (53 kDa).

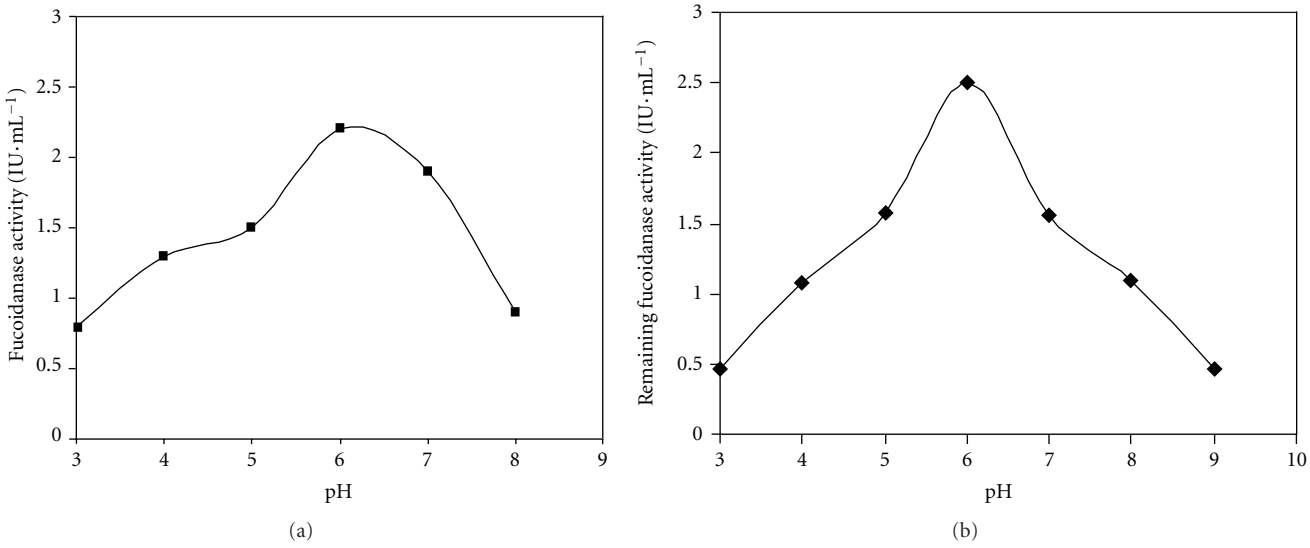

Figure 4: Effects of pH on fucoidanase activity (a) and stability. (b) Effects of pH on fucoidanase activity was determined under the following method: 1.0 mL substrate solution (pH 3–8) in buffer solutions (50 mmol·L^{-1} sodium citrate buffer, 50 mmol·L^{-1} sodium phosphate buffer, 50 mmol·L^{-1} sodium carbonate buffer) was added to 0.1 mL enzyme solution and then was incubated at 50°C for 10 min. The pH stability of the enzyme was determined by assaying the residual activity after incubating enzyme for 3 h at the room temperature at different pH levels ranging from 3 to 9. Residual fucoidanase activity was determined by adding 0.1 mL enzyme solution to 1.0 mL of substrate solution (citric acid-citric sodium buffer, pH 6.0) and then was incubated at 50°C for 10 min.

and marine fungi *Dendryphiella arenaria* TM94 (50°C). The temperature of half inactivation of LD8 fucoidanase was 50°C, while that of bacteria *Vibrio* sp. N-5 was 65°C [33].

Effects of temperature on the secondary structure of LD8 fucoidanase were studied by Gaussian fitting to the deconvoluted spectra of fucoidanase at amide I kregion [36, 37]. A decrease of the β-turn structure and an increase of α-helix of amide I region had been observed when treated temperature was below 60°C. While treated temperature was above 60°C, the contents of α-helix, β-sheet, random coil, and β-turn had no changes. The above result was consistent with our conclusion that the optimal enzyme reaction tem-

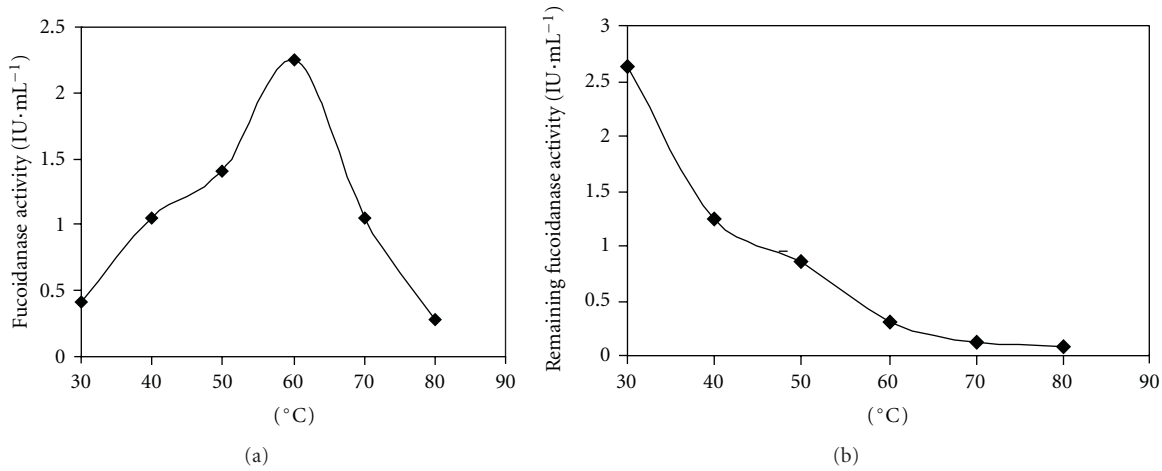

Figure 5: Effects of temperature on fucoidanase activity (a) and stability. (b) Effects of temperature on fucoidanase activity was obtained by the following method: adding 0.1 mL of enzyme solution to 1.0 mL of substrate solution (citric acid-citric sodium buffer, pH 6.0), then incubating for 10 min at different temperatures from 30°C to 80°C, respectively. Temperature on stability of the fucoidanase was determined by assaying the residual activity under the following method: 0.1 mL of enzyme solution was incubated at 30 to 80°C for 1 h, rapidly cooled in an ice bath for 5 min, and then removed to 25°C. When the sample reached 25°C, 1.0 mL of substrate solution was added, and the residual enzyme activity was determined and expressed relative to the maximum activity.

Table 3: The results of Gaussian fitting of fucoidanase in amide I region.

Position	Area	Content (%)	Components (assignments)
1606	7.89140	21.1	β-sheet
1618	7.40320	19.8	β-sheet
1631	2.36538	17.7	β-sheet
1645	5.40532	14.5	random
1658	4.31620	11.5	α-helix
1672	3.38760	9.06	β-turn
1685	6.60977	6.33	β-turn

perature was 60°C; The enzyme activity decreased rapidly in LD8 below or above pH 6.0. It was suggested that the enzyme activity of fucoidanase was closely related to the proportion of α-helix and β-turn structure with no direct relation to β-sheet and random coil structure.

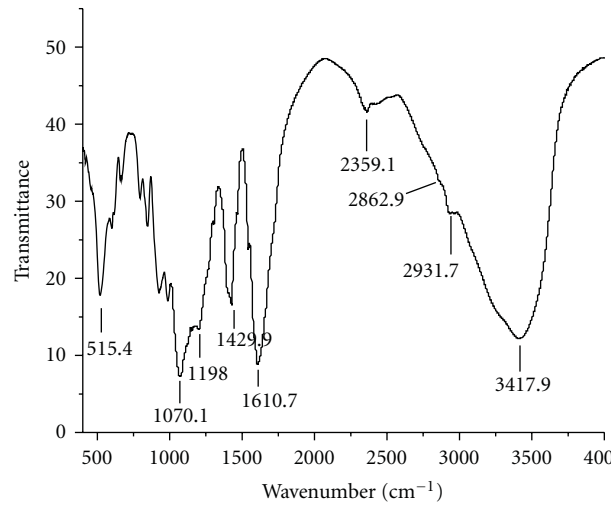

Figure 6: The FTIR spectra of fucoidanase. Fucoidanase (10 mg) was mixed with 100 mg of dried potassium bromide (KBr). Water vapor was purged from sample room. A baseline drawn between the spectra data points at 1500 and 2200 cm^{-1}; 32 scans were collected at a spectral resolution of 4 cm^{-1}.

Abbreviations

LMWF: The low molecular weight fucoidan
K_M: Michaelis constants
V_{max}: Maximum reaction velocities
M_w: Molecular weight.

Acknowledgments

This work was supported by funds from Anhui Provincial Nature Science Foundation (no. 03043104), Anhui Provincial Excellent Youth Science and Technology Foundation (no. 04043051), Anhui Advanced School Science and Research Fund Project for Young Teacher, Hefei University Scientific Research and Development Fund.

References

[1] S. D. Anastyuk, N. M. Shevchenko, E. L. Nazarenko et al., "Structural analysis of a highly sulfated fucan from the brown alga *Laminaria cichorioides* by tandem MALDI and ESI mass

spectrometry," *Carbohydrate Research*, vol. 345, no. 15, pp. 2206–2207, 2010.

[2] J. Wang, Q. Zhang, Z. Zhang, H. Zhang, and X. Niu, "Structural studies on a novel fucogalactan sulfate extracted from the brown seaweed *Laminaria japonica*," *International Journal of Biological Macromolecules*, vol. 47, no. 2, pp. 126–131, 2010.

[3] M. I. Bilan, A. A. Grachev, A. S. Shashkov, N. E. Nifantiev, and A. I. Usov, "Structure of a fucoidan from the brown seaweed *Fucus serratus* L," *Carbohydrate Research*, vol. 341, no. 2, pp. 238–245, 2006.

[4] S. D. Anastyuk, N. M. Shevchenko, E. L. Nazarenko, P. S. Dmitrenok, and T. N. Zvyagintseva, "Structural analysis of a fucoidan from the brown alga *Fucus evanescens* by MALDI-TOF and tandem ESI mass spectrometry," *Carbohydrate Research*, vol. 344, no. 6, pp. 779–787, 2009.

[5] M. I. Bilan, A. A. Grachev, N. E. Ustuzhanina, A. S. Shashkov, N. E. Nifantiev, and A. I. Usov, "A highly regular fraction of a fucoidan from the brown seaweed *Fucus distichus* L," *Carbohydrate Research*, vol. 339, no. 3, pp. 511–517, 2004.

[6] I. R. L. Albuquerque, K. C. S. Queiroz, L. G. Alves, E. A. Santos, E. L. Leite, and H. A. O. Rocha, "Heterofucans from Dictyota menstrualis have anticoagulant activity," *Brazilian Journal of Medical and Biological Research*, vol. 37, no. 2, pp. 167–171, 2004.

[7] P. A. S. Mourão, "Use of sulfated fucans as anticoagulant and antithrombotic agents: future perspectives," *Current Pharmaceutical Design*, vol. 10, no. 9, pp. 967–981, 2004.

[8] W. J. Kim, Y. K. Koo, M. K. Jung et al., "Anticoagulating activities of low-molecular weight fuco-oligosaccharides prepared by enzymatic digestion of fucoidan from the sporophyll of Korean *Undaria pinnatifida*," *Archives of Pharmacal Research*, vol. 33, no. 1, pp. 125–131, 2010.

[9] T. Nishino, T. Yamauchi, M. Horie, T. Nagumo, and H. Suzuki, "Effects of a fucoidan on the activation of plasminogen by u-PA and t-PA," *Thrombosis Research*, vol. 99, no. 6, pp. 623–634, 2000.

[10] D. J. Schaeffer and V. S. Krylov, "Anti-HIV activity of extracts and compounds from algae and cyanobacteria," *Ecotoxicology and Environmental Safety*, vol. 45, no. 3, pp. 208–227, 2000.

[11] H. Maruyama, H. Tamauchi, M. Hashimoto, and T. Nakano, "Antitumor activity and immune response of Mekabu fucoidan extracted from Sporophyll of *Undaria pinnatifida*," *In Vivo*, vol. 17, no. 3, pp. 245–249, 2003.

[12] T. Nishino, C. Nishioka, H. Ura, and T. Nagumo, "Isolation and partial characterization of a novel amino sugar-containing fucan sulfate from commercial *Fucus vesiculosus* fucoidan," *Carbohydrate Research*, vol. 255, pp. 213–224, 1994.

[13] L. Chevolot, A. Foucault, F. Chaubet et al., "Further data on the structure of brown seaweed fucans: relationships with anticoagulant activity," *Carbohydrate Research*, vol. 319, no. 1–4, pp. 154–165, 1999.

[14] T. Fujikawa, K. Koyabu, and M. Wada, "Enzymes in hepatopancreas of abalone active on fucoidan(1), Crude enzyme and unabsorbed fraction on CM-cellulose," *Nippon Nogeikagaku Kaishi*, vol. 53, pp. 87–95, 1979 (Japanese).

[15] K. Kitamura, M. Masaru, and T. Yasui, "Enzymic degradation of fucoidan by fucoidanase from the hepatopancreas of *Patinopecten yessoensis*," *Bioscience, Biotechnology, and Biochemistry*, vol. 56, pp. 490–494, 1992.

[16] W. Yaphe and K. Morgan, "Enzymic hydrolysis of fucoidin by *Pseudomonas atlantica* and *pseudomonas carrageenovora*," *Nature*, vol. 183, no. 4663, pp. 761–762, 1959.

[17] S. Furukawa, T Fujikawa, D. Koga, and A. Ide, "Production of fucoidan-degrading enzymes, fucoidanase, and fucoidan sulfatase by *Vibrio* sp. N-5," *Nippon Suisan Gakkaishi*, vol. 58, pp. 1499–1503, 1992 (Japanese).

[18] I. Y. Bakunina, O. I. Nedashkovskaya, S. A. Alekseeva et al., "Degradation of fucoidan by the marine proteobacterium *Pseudoalteromonas citrea*," *Mikrobiologiya*, vol. 71, pp. 41–47, 2002.

[19] T. Sakai, H. Kimura, and I. Kato, "A marine strain of Flavobacteriaceae utilizes brown seaweed fucoidan," *Marine Biotechnology*, vol. 4, no. 4, pp. 399–405, 2002.

[20] T. Sakai, K. Ishizuka, and I. Kato, "Isolation and characterization of a fucoidan-degrading marine bacterium," *Marine Biotechnology*, vol. 5, no. 5, pp. 409–416, 2003.

[21] T. Sakai, K. Ishizuka, K. Shimanaka, K. Ikai, and I. Kato, "Structures of oligosaccharides derived from *Cladosiphon okamuranus* fucoidan by digestion with marine bacterial enzymes," *Marine Biotechnology*, vol. 5, no. 6, pp. 536–544, 2003.

[22] T. Sakai, H. Kimura, and I. Kato, "Purification of sulfated fucoglucuronomannan lyase from bacterial strain of Fucobacter marina and study of appropriate conditions for its enzyme digestion," *Marine Biotechnology*, vol. 5, no. 4, pp. 380–387, 2003.

[23] P. Wang, J. Cai, S. Qin et al., "Fermentation of marine bacterium *Bacillus* sp. H-TP2 for fucoidanase and enzyme properties," *Food and Fermentation Industry*, vol. 30, pp. 13–15, 2004 (Chinese).

[24] A. M. Urvantseva, I. Y. Bakunina, O. I. Nedashkovskaya, S. B. Kim, and T. N. Zvyagintseva, "Distribution of intracellular fucoidan hydrolases among marine bacteria of the family Flavobacteriaceae," *Applied Biochemistry and Microbiology*, vol. 42, no. 5, pp. 484–491, 2006.

[25] V. Descamps, S. Colin, M. Lahaye et al., "Isolation and culture of a marine bacterium degrading the sulfated fucans from marine brown algae," *Marine Biotechnology*, vol. 8, no. 1, pp. 27–39, 2006.

[26] K. Wu, Q. Wu, J. Yan et al., "Production of fucoidanase from the marine fungus *Dendryphiella arenaria* TM94 by solid substrate fermentation," *ESMB*, vol. 5, pp. 12–14, 2002.

[27] Q. Wu, J. Cai, K. Wu, and S. Qin, "Solid state fermentation of fucoidanase of marine fungus LD8. Marine Sciences," *Marine Sciences*, vol. 28, pp. 23–27, 2004 (Chinese).

[28] R. M. R. Jasso, C. N. A. Gonzalez, L. Pastrana, and J. A. Teixeira, "Identification and evaluation of fungal strains with fucoidan degradation potential," in *Proceedings of the 10th International Chemical and Biological Engineering Conference (CHEMPOR '08)*, pp. 2106–2109, Braga, Portugal, September 2008.

[29] T. Sakai, T. Kawai, and I. Kato, "Isolation and characterization of a fucoidan-degrading marine bacterial strain and its fucoidanase," *Marine Biotechnology*, vol. 6, no. 4, pp. 335–346, 2004.

[30] M. M. Bradford, "A rapid and sensitive method for the quantitation of microgram quantities of protein utilizing the principle of protein dye binding," *Analytical Biochemistry*, vol. 72, no. 1-2, pp. 248–254, 1976.

[31] G. L. Miller, "Use of dinitrosalicylic acid reagent for determination of reducing sugar," *Analytical Chemistry*, vol. 31, no. 3, pp. 426–428, 1959.

[32] H. Lineweaver and D. Burk, "The determination of enzyme dissociation constants," *Journal of the American Chemical Society*, vol. 56, no. 3, pp. 658–666, 1934.

[33] S. Furukawa, T. Fujikawa, D. Koga, and A. Ide, "Purification and some properties of exo-type fucoidanase from *Vibrio* sp. N-5," *Bioscience, Biotechnology, and Biochemistry*, vol. 56, pp. 1829–1834, 1992.

[34] R. Daniel, O. Berteau, J. Jozefonvicz, and N. Goasdoue, "Degradation of algal (*Ascophyllum nodosum*) fucoidan by an enzymatic activity contained in digestive glands of the marine mollusc Pecten maximus," *Carbohydrate Research*, vol. 322, no. 3-4, pp. 291–297, 1999.

[35] Q. Wu, M. Zhang, K. Wu, B. Liu, J. Cai, and R. Pan, "Purification and characteristics of fucoidanase obtained from *Dendryphiella arenaria* TM94," *Journal of Applied Phycology*, vol. 23, no. 2, pp. 197–203, 2011.

[36] S. Ma, *The studies on the preparation, enzymatic properties and characterization of fucoidanase from marine Fusarium*, M.S. thesis, Anhui Agriculture University, China, 2006.

[37] S. Ma, H. Xiao, Q. Wu, R. Pan, and J. Cai, "Investigation of fucoidanase by FTIR spectra," *Spectroscopy and Spectral Analysis*, vol. 28, pp. 590–593, 2010 (Chinese).

Hindawi Publishing Corporation
Evidence-Based Complementary and Alternative Medicine
Volume 2011, Article ID 806485, 8 pages
doi:10.1155/2011/806485

Research Article

A Preliminary Study of the Microbial Resources and Their Biological Activities of the East China Sea

Xiaoling Lu, Xiaoyu Liu, Cong Long, Guoxiang Wang, Yun Gao, Junhua Liu, and Binghua Jiao

Department of Biochemistry and Molecular Biology, College of Basic Medical Sciences, Second Military Medical University, Shanghai 200433, China

Correspondence should be addressed to Binghua Jiao, jiaobh@uninet.com.cn

Received 15 January 2011; Revised 15 April 2011; Accepted 16 May 2011

East China Sea is one of the four sea areas in China, which possesses peculiar ecological environment and many kinds of living creatures, especially the microorganisms. We established the East China Sea microorganism library (during 2006–2010) for the first time, which stored about 30000 strains that covered most kinds of the species. In this paper, 395 pure strains of East China Sea microorganism library which belong to 33 different genera were mainly introduced. *Sulfitobacter*, *Halomonas*, *Bacillus*, *Pseudoalteromonas*, and *Idiomarina* were the most dominant species. On the large-scale biological activity screening of the 395 strains, 100 strains possess different biological activities based on different screening models, of which 11.4% strains have antibacterial activities, 15.9% have cytotoxicity activities, and 6.1% have antioxidation activities. Besides, the secondary metabolites of 6 strains with strong biological activities were studied systematically; diketopiperazines and macrocyclic lactones are the active secondary metabolites. The species and the biological activity of microorganisms diversity, the abundant structure type of the secondary metabolites, and their bioactivities all indicate that East China Sea is a potent marine microorganisms-derived developing resource for drug discovery.

1. Introduction

Since the Scottish scientist Alexander Fleming discovered penicillin from the *penicillum* fungi in 1929, bioactive secondary metabolites isolated from the microorganisms have been the abundant resources for the drug discovery. The traditional sources of bioactive compounds were terrestrial microorganisms which could be easily obtained and readily explored. In comparison, the ocean source was scarcely studied. However, since the 1970s, as a consequence of the advanced technology, the ocean has become an attracting area of drug development because of the structural diversity and pharmacological potential which were presented by the novel scaffold molecules isolated from this environment [1]. In 2009, scientists wrote a report that the distribution by phylum for 2006 and 2007 is compared with the historic average derived for the period 1965–2005, the production of marine natural products of microorganisms took a spectacular rise, especially the fungi and bacteria of marine origin [2]. It had also been known that the geographic region of collection sources in output mainly focused on the Caribbean, the China Sea, the Indian Ocean, Japan, and the Western Pacific. The emergence of the China Sea as a significant source of new compounds is particularly obvious.

China is a vast ocean country, which includes four sea areas, such as Bohai Sea, Yellow Sea, South China Sea, and East China Sea. Our country possesses coastline of 18,000 kilometers and the island coastline of 14,000 kilometers, and has the sovereignty and jurisdiction over the sea area of about 3 million square kilometers spanning the tropical zone, subtropical zone, temperate zone, and cold zone. Besides, China Sea possesses four kinds of marine ecosystems, including coastal wetland ecosystems, coral reef ecosystems, upwelling ecosystems, and deep sea ecosystems, which produce many kinds of microorganisms and have abundant resources. The rest three sea areas, except for East China Sea, have been systematically studied [3, 4], while microbial resources of the large-scale survey and the study of the strains with biological activities in the East China Sea have not been reported.

East China Sea mainly has the upwelling ecosystems and deep sea ecosystems. On one hand, upwelling marine ecosystem possesses higher biological diversity than other ecosystem because of the rich nutrients; on the other hand, some animals and microorganisms with specific structures

mainly exist in the deep-sea ecosystem. Overall, the East China Sea has great potential for drug development because of its rich and unique microbial resources.

In order to discover the bioactive secondary metabolites of the microorganisms from the East China Sea, it is essential to do the large-scale survey of the microbial resources of East China Sea. In this paper, we mainly reported the marine microorganisms, their biological activities such as antimicrobial, antitumor, antioxidant activities, and some secondary metabolites of the strains with biological activities in the East China Sea.

2. Materials and Methods

2.1. Sampling. The sea water and sea sediment samples were collected in 2006 at a depth of 30 m in the East China Sea (27°15′50″ N120°45′22″ E ~ 31°24′7″ N122°40′48″ E), and we totally obtained 100 sea sediment sample and 122 sea water sample, which were all stored in refrigerator at −80°C. Weigh 5 g sea sediment, add 45 mL sterile artificial water, shake and mix fully, and stand settlement. Sterile sea water and the supernatant of the sea sediment were progressively diluted with sterilized artificial seawater step by step into 10^{-1}, 10^{-2}, 10^{-3}, 10^{-4}, and 10^{-5}. Take 0.2 mL every gradient diluent and spread them into different medium plates, incubate at 25°C for 7–14 days, and then pick the single colony according to the differences of the sample and the morphological of the strains. Streak plate method combined with the microscope observation is used during the separation process. All these pure strains were now conserved by freezing at −80°C and at 4°C in our laboratory.

2.2. Determination of 16S rRNA Sequence. According to the method described by Rainey et al. [5], the genomic RNAs of all the pure strains were prepared by Genomic RNA Isolation kit (Watson). Then, gene encoding 16S rRNA was amplified by PCR with 16S rRNA Bacterial Identification PCR kit (TaKaRa). An ABI BigDye and Terminator 3.1 cycle sequencing kit (Applied Biosystems) and an automated RNA sequencer (model ABI 3730; Applied Biosystems) were used to determine 16S rRNA gene sequence.

2.3. Activity Assays

2.3.1. Assay of Antibacterial Activities. All strains were respectively inoculated in tubes containing 5 mL corresponding liquid medium and cultured on a rotary shaker (150 rpm) at 28°C for 3 ~ 5 days. The fermented broth was filtered through cheese cloth to separate the supernatant and thallus. Antibacterial activity of all the supernatants was evaluated by zone of inhibition using the agar well diffusion assay. The indicator strains are *B. subtilis* (ATCC 6633), *E. coli* (ATCC 25922), and *S. aureus* (ATCC 25923). In this part, ampicillin and blank medium were used as the positive and negative control, respectively.

2.3.2. Assay of Cytotoxic Activities. The entire supernatants of cultured broth were prepared as described above. Cytotoxic activities of these supernatants were evaluated by MTT method [6] using HepG2, HL-60, SMMC 7721, MCF, P388, S180, and SW1990 cell lines. In MTT assay, the cell lines were grown in RPMI-1640 supplemented with 10% fetal bovine serum (FBS) under a humidified atmosphere of 5% CO_2 and 95% air at 37°C. Cell suspension (90 μL) at a density of 5×10^4 cell/mL was plated in 96-well microtiter plates and incubated for 24 h under the mentioned condition. The supernatants (10 μL) of cultured broth was added to each well and further incubated for additional 72 h in the same condition. Then, 10 μL of MTT solution (5 mg/mL in IPMI-1640 medium) was added to each well and incubated for 4 h. The old medium (110 μL) containing MTT in 96-well microtiter plates was gently replaced by DMSO and pipetted to dissolve any formazan crystals. Absorbance was then determined on a Spectra Max Plus plate reader at 540 nm. In this part, actinomycin D was used as the positive control, normal saline was used as negative control, and 10% DMSO solution was used as blank control.

2.3.3. Assay of Antioxidant Activities. Seed culture (50 mL) of all strains was inoculated into Erlenmeyer flask (2000 mL) containing the liquid medium (500 mL) and cultured on a rotary shaker (150 rpm) at 28°C for 5 days. The fermented whole broth was centrifugated at 12000 rpm for 5 min and separated from supernatant and thallus. The supernatant was extracted with ethyl acetate for 3 times, and the combined extracts were evaporated in vacuum at 30°C to dryness to yield the crude extract, which was dissolved at a concentration of 1 mg/mL in methanol for further analyses.

The DPPH assay was evaluated according to the method described by Hu and Kitts [7] with a little modify. Briefly, crude extract in methanol solution (0.3 mL) mixed with 0.06 mmol/L DPPH (0.5 mL) dissolving in ethanol solution and stood at room temperature in the dark for 20 min when the absorbance at 517 nm was taken. Capacity of free-radical scavenging was evaluated by the inhibition percentage, calculated from the following equation: Inh% = $[(A_{control} - A_{sample})/A_{control}] \times 100$, where $A_{control}$ = absorbance of 0.06 mmol/L DPPH (0.5 mL) with methanol (0.3 mL), A_{sample} = absorbance of 0.06 mmol/L DPPH (0.5 mL) with sample solution (0.3 mL).

The ABTS assay was evaluated according to the method of Kajal and Paulraj [8] with a little modify. Briefly, a stock solution of ABTS radical cation was prepared by dissolving ABTS (0.25 mmol/L, 5 mL in water) with potassium persulfate (2 mmol/L, 88 mL). The reaction mixture was diluted to 25 times volume with EtOH and left to stand at room temperature overnight (13 h) in the dark. The ABTS assay was started by mixing the diluted ABTS solution (0.9 mL) with crude extract in methanol solution (0.1 mL) and stood at room temperature in the dark for 20 min when the absorbance at 734 nm was taken. Capacity of free-radical scavenging was evaluated by the inhibition percentage, calculated from the following equation; Inh% = $[(A_{control} - A_{sample})/A_{control}] \times 100$, where $A_{control}$ = absorbance of diluted ABTS solution (0.9 mL) with methanol (0.1 mL), A_{sample} = absorbance of diluted ABTS solution (0.9 mL) with sample solution (0.1 mL). Quercetin was used as positive control in the two tests.

Table 1: Taxonomy of 395 strains.

Genus	No.	Genus	No.	Genus	No.
Agrococcus	8	*Alcanivorax*	3	*Alphaproteobacterium*	4
Bacillus	30	*Brachybacterium*	7	*Brevibacterium*	6
Dietzia	2	*Erythrobacter*	1	*Exiguobacterium*	10
Gamma proteobacterium	5	*Halomonas*	42	*Idiomarina*	36
Kocuria	9	*Kurthia*	2	*Loktanella*	3
Lysobacter	2	*Marinobacter*	4	*Marinococcus*	3
Methylarcula	5	*Micrococcus*	1	*Oceanicola*	4
Paracoccus	6	*Photobacterium*	7	*Planococcus*	5
Pseudoalteromonas	69	*Pseudomonas*	12	*Psychrobacter*	2
Rheinheimera	5	*Salegentibacter*	2	*Staphylococcus*	10
Sulfitobacter	62	*Vibrio*	8	*Virgibacillus*	20

2.4. Fermentation of the Pure Cultured Strains. The strains F81612, F201721, F8712, F321122, F121122, and M44 have been isolated from sea sediment and sea water of East China Sea, respectively. They were all isolated on F1 medium with incubation at 28°C. F1 Medium: Glucose (6 g), peptone (5 g), and yeast extract (1 g) were dissolved in artificial seawater (1 L). A statistical methodology, combining Plackett-Burman design (PBD) with response surface methodology (RSM), was applied to optimize the biological activity of the strains in the fermentation [9]. Each strain was fermented as follows: 40 2 L Erlenmeyer flasks each containing 700 mL F1 medium (set to the pH 6.5 before sterilization) were inoculated and grown for 4 ~ 7 days at 28°C while shaking at 90 rpm.

2.5. Isolation of the Secondary Metabolites. The 6 entire culture broths were all centrifugated at 12000 rpm for 15 minutes, respectively, got the supernatants. The each supernatant was extracted with ethyl acetate for 3 times. The combined extracts were evaporated in vacuum at 30°C to dryness to yield crude extract. Then, the each crude extract was subjected to Sephadex LH-20 and silica gel column, middle-pressure LC with the gradient elution, and chromatographed on preparative HPLC columns repeatedly, which yielded many secondary metabolites.

3. Results

3.1. Taxonomy of the Studied Pure Strains. The 16S rRNA gene sequence has been determined for a large number of strains. GenBank, the largest databank of nucleotide sequences, has over 20 million deposited sequences, of which over 90,000 are of 16S rRNA gene. This means that there are many previously deposited sequences against which to compare the sequence of an unknown strain [10]. 16S rRNA sequences of 416 pure strains have been determined. After blasting with the GenBank sequences, it is known that a total of 395 strains can be determined their taxonomic status (Table 1). 395 strains belong to 33 different genera, which *Sulfitobacter*, *Halomonas*, *Bacillus*, *Pseudoalteromonas*, and *Idiomarina* were the most dominant species.

3.2. Antibacterial Activities. 45 strains of the tested pure isolated microorganisms exhibited antibacterial activities, among of which most strains belong to the *Bacillus*, *Sulfitobacter*, and *Pseudoalteromonas* (Table 2). The antibacterial activities of marine *Bacillus* mainly focused on the killing *S.aureus* and *B.subtilis*, while the *Sulfitobacter* mainly showed the strong activities of killing *S.aureus*, and *Pseudoalteromonas* mainly showed the strong activities of killing *E.coli*.

3.3. Cytotoxic Activities. The tested pure isolated microorganisms exhibited good cytotoxicity activities to several cell lines, like HepG2, Hela, MCF, and SMMC 7721. It means not all the strains are susceptible to all the tested cell lines, which signifies the differences between the genus and the strains. 63 strains of the tested pure isolated microorganisms exhibited cytotoxicity, among of which most strains were sensitive to the HepG2 cell line and their inhibitory ratio mostly exceed 20% (Table 3).

Most strains of *Sulfitobacter*, *Pseudoalteromonas*, and *Halomonas* exhibited good cytotoxic activities. For example, *Sulfitobacter* sp. is the common species of pure cultured strains. In this species, most strains show good cytotoxic activities to HepG2 cell line (Figure 1). About 25% strains of this species possess strong cytotoxicity activities, whose inhibitory ratios exceed 30%, while the inhibitory ratios of another 30% strains exceed 25%. Thus, it can be seen that *Sulfitobacter* sp. is the potential ones which may produce cytotoxic secondary metabolites.

3.4. Antioxidant Activities. The antioxidant activity of the pure cultured strains was determined by the method of spectrophotometry DPPH· radical scavenging assay and ABTS·+ radical cation decolorization assay. We screened 395 fermented liquid extract of strains, among of which 24 strains show antioxidant activity using the DPPH· radical scavenging assay, while 30 strains exhibit antioxidant activity using the ABTS+· radical cation decolorization assay (Figures 2 and 3). In the DPPH· assay, inhibitory ratio of the 11 strains exceed 40%, and 3 strains exceed 90%. In the ABTS·+ assay, inhibitory ratio of the 10 strains exceed 40%, among of which strain F7 has the highest inhibitory ration 98.97%. It can be seen that strains F19, F12, and F23 all exhibit good antioxidant activity in the both methods, which deduce that these 3 strains may have 2 antioxidant mechanisms at least.

Table 2: Strains with strongest antibacterial activities.

Strain no.	Genus	*E. coli*	*B. subtilis*	*S. aureus*
ZJ8112	*Pseudoalteromonas*	++	−	−
F121112	*Pseudoalteromonas*	+	−	−
F8712	*Halomonas*	−	−	−
F321122	*Halomonas*	−	−	−
201721	*Pseudoalteromonas*	++	−	+
XB16	*Idiomarina*	−	−	−
MZ0306A2	*Bacillus*	+	+	++
MZ0208A2	*Bacillus*	−	+	++
MZ0204A3	*Bacillus*	−	+	+
P3001	*Bacillus*	−	+	+++
P4004A	*Bacillus*	−	+	+
P16006B	*Idiomarina*	−	+++	−
P3009B	*Idiomarina*	−	+++	−
P16011A	*Bacillus*	−	+	−
P16010C	*Halomonas*	−	++	−
P4004C	*Bacillus*	−	++	++
XF22−2	*Sulfitobacter*	−	−	++
P4003B	*Sulfitobacter*	−	−	+
P12012B	*Sulfitobacter*	−	−	++

Note: "+++"means the diameters of the inhibition zone exceeding 15 mm; "++" means the diameters of the inhibition zone 10–15 mm; "+" means the diameter of the inhibition zone exceeding 6–10 mm; "−"means no antibacterial activities.

Table 3: Strains with strongest cytotoxic activities of the 395 strains.

Strain no.	Genus	Sensitive tumor strain	Inhibitory ratio
F321121	*Halomonas*	SMMC 7721	17.6%
P12002	*Sulfitobacter*	HeLa, MCF	35%, 12%
F81612	*Bacillus*	HeLa, SW1990	39%, 9.3%
F81611	*Bacillus*	HeLa	29.1%
P3001	*Vibrio*	HepG2	28%
P3002	*Rheinheimera*	HepG2, MCF	27%
P16006A	*Kocuria*	HepG2	29%
P16006B	*Idiomarina*	HepG2	32%
P16001	*Halomonas*	HeLa, MCF	18.4%, 20.4%
P4003B	*Sulfitobacter*	HepG2, P388	31%, 7.9%
P12006A2	*Sulfitobacter*	HepG2	31%
P4006B	*Marinobacter*	HepG2, P388	42%, 13%
MZ0206A2	*Bacillus*	SMMC7721, S180	11%, 19%
MZ0208A2	*Bacillus*	SMMC 7721	21%
P16003	*Kocuria*	HepG2	23%
P4004B	*Idiomarina*	HepG2	31%
P12002	*Idiomarina*	HepG2	28.7%
P12012B	*Sulfitobacter*	HepG2, SW1990	14.9%, 17%
P12004D	*Sulfitobacter*	HepG2, S180	16.7%, 23%

All the cultured broths of the strains were tested at a fixed concentration 500 μg/mL. Each experiment was repeated 3 times, and the inhibitory ratio was the average of the 3 results.

3.5. The Study of the Secondary Metabolites of the Strains. In our screening program for bioactive principles from marine microorganisms, we pick up 6 strains (F81612, F201721, F8712, F321122, F121122, and M44) of different genus with strong biological activities to study their bioactive secondary metabolites (Table 4, Figure 4). These 6 strains mainly belong to 3 species which is *Bacillus*, *Pseudoalteromonas*, and *Sulfitobacter*. From the isolated secondary metabolites, it is known that: (1) the main type of the metabolites of these species is cyclopeptide, especially cyclodipeptide, (2) some strains have the common secondary metabolites, for example, macrolactins, cylco(Phe-Ile), cylco(Pro-Ile), and

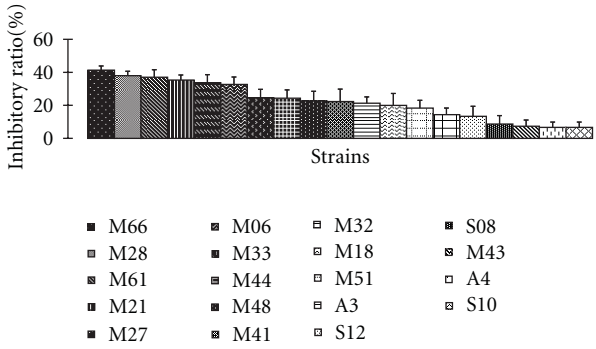

Figure 1: Strains of *Sulfitobacter* sp. with cytotoxicity activities to HepG2 cell line. All the cultured broth of the strains were tested at a fixed concentration 500 μg/mL. Each experiment was repeated 3 times, and the inhibitory ratio was the average of the 3 results.

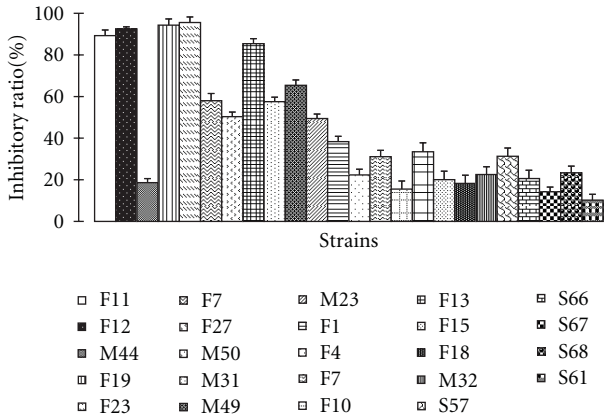

Figure 2: 24 strains with best antioxidant activity in DPPH· assay. All the cultured broths of the strains were tested at a fixed concentration 375 μg/mL. Each experiment was repeated 3 times, and the inhibitory ratio was the average of the 3 results.

cyclo (Pro-Leu) et al., and (3) the secondary metabolites isolated from different strains signify the different metabolite mechanisms between the genus and the strains.

From the secondary metabolites of our finding, another important kind of the metabolites is macrolide. In 2007, our group found a new macrolactin named macrolactin Q which was isolated from a marine *Bacillus subtilis* [11, 12], and besides, we also isolated macrolactin A and macrolactin B from the same marine *Bacillus subtilis*. Macrolactin Q, macrolactin A and macrolactin B all exhibited antimicrobial activity, macrolactin Q showing stronger antibacterial activity against *E. coli* than *S. aureus* and *B. subtilis*. Macrolactin Q inhibited bacterial growth against *E.coli* with a MIC of 0.2 μg/mL, while inhibiting weaker bacterial growth against *S. aureus* and *B. subtilis* with a MIC of 0.7 μg/mL and 100 μg/mL, respectively.

4. Discussion

According to the different sampling points and the different characteristics (morphous, sizes, and colours) of the pure strains, we totally obtained about 30000 pure strains, of

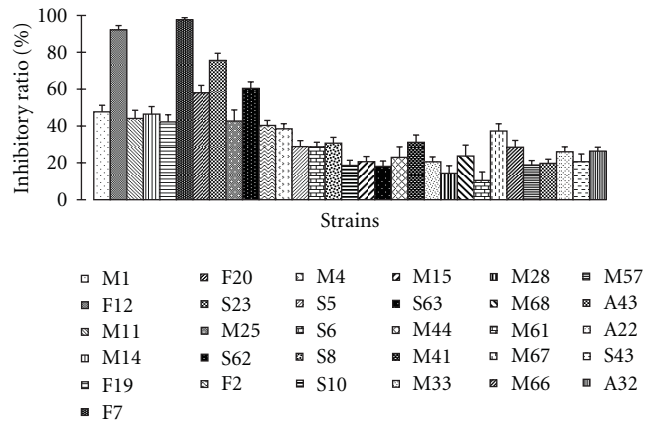

Figure 3: 30 strains with best antioxidant activity in ABTS·+ assay. All the cultured broths of the strains were tested at a fixed concentration 375 μg/mL. Each experiment was repeated 3 times, and the inhibitory ratio was the average of the 3 results.

which 52% strains belong to the actinomycete, 15% belong to the fungus, and 33% are bacteria. Firstly, we picked up 416 isolated bacteria according to their different morphologic and cultural characteristics to further study their taxonomy, biological activities, and secondary metabolites.

Based on the morphologic and cultural characteristics of the strains, firstly, it is known that majority of them belong to the Gram-negative bacteria. Secondly, more than 85% strains must be cultured in the medium with different concentrations of NaCl, the concentrations of NaCl which range from 2.5% to 15%. Thirdly, it is shown that these strains only need simple nutritional requirements, most of which possess extracellular enzymes and do not use sugar as carbon source and so on. Besides, 395 strains can be determined their taxonomic status, which belong to 33 different genera, and *Sulfitobacter*, *Halomonas*, *Bacillus*, *Pseudoalteromonas*, and *Idiomarina* were the most dominant species.

In the recent years, there are many studies about the biological activities of the secondary metabolites isolated from the marine microorganisms, and these studies mainly focus on the antibacterial, cytotoxic, antioxidation, and antiviral, immunosuppressant activities [13]. In our screening program for bioactive principles from marine microorganisms, it is essential to study the biological activities of the marine microorganisms producing the bioactive secondary metabolites. We mainly studied the activity screening of marine microorganisms referring to the antimicrobial, cytotoxicity, and antioxidant activities.

On the large-scale activity screening of the 395 strains, 100 strains possess different biological activities, of which 45 strains have antibacterial activities, 63 strains have cytotoxicity activities, and 24 strains have antioxidant activities. By this screening, we found that the microorganisms of East China Sea have a wide range of biological activities, including antibacterial activities, cytotoxicity activities, and antioxidant activities, which possess the good potential for the development and utilization. It is good for us to further develop the medicinal microbial use of East China Sea on the

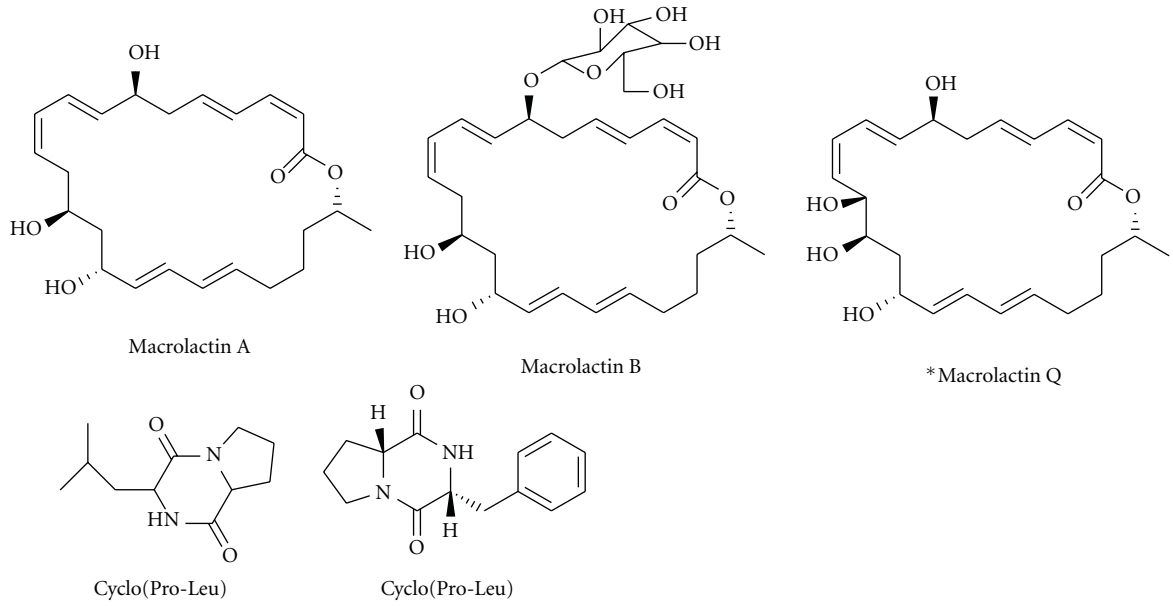

Figure 4: The new secondary metabolites and the compounds with the good biological activities isolated from the strain F201721, F81612, F8712, F321122, F121122, and M44.

Table 4: Overview of the 6 strains with biological activities.

No.	Genus	Biological activity	Main type of the secondary metabolites
F81612	*Bacillus*	Antibacterial	cyclopeptide, indole derivatives, and macrolide
F201721	*Bacillus*	Antibacterial	cyclopeptide, indole derivatives, and macrolide
F8712	*Pseudoalteromonas*	Cytotoxicity	cyclopeptide
F321122	*Pseudoalteromonas*	Cytotoxicity	cyclopeptide and indole derivatives
F121122	*Sulfitobacter*	Cytotoxicity	cyclopeptide
M44	*Sulfitobacter*	Cytotoxicity	cyclopeptide

foundation of the biological activity screening of the isolated pure strains.

In our screening program for bioactive principles from marine microorganisms, diketopiperazine and macrolide are the two important bioactive secondary metabolites. Diketopiperazines (DKPs), the smallest cyclic peptides, have been isolated from marine microorganisms (bacteria, fungi, and actinomycete) [14–17] or the microorganisms associated with sponge [18–20]. As cyclic peptide derivatives, DKPs have been considered as cell-cell signalling compounds. Some L, L-diketopiperazines have recently been known as quorum-sensing bacterial sensors [21, 22], which are used by Gram-negative bacteria for cell-cell communication and regulating gene expression in response to population density. For example, cyclo (L-Pro-L-Phe) and cyclo (L-Pro-L-Leu) are capable of activating or antagonizing LuxR-mediated quorum-sensing system of bacteria [23, 24]. Therefore, the diketopiperazines, which were produced by many species of the microorganisms, suggest a probable role of these compounds in bacterial-bacterial interaction.

Besides, DKPs represent an important class of biologically active natural products, which play an important ecological role in antifouling [25, 26], antifungal [27] and antibacterial [16]. For example, cyclo (D-Pro-D-Phe) was previously found in marine bacteria associated with *Pecten maximus* and proved to exhibit bioactivity against *Vibrio anguillarum* [16], and meanwhile, it was also proved to have antifouling activity [28]. Cyclo (L-Pro-L-Phe) and cyclo-(L-Pro-L-Leu), isolated from the bacterium *Alcaligenes faecalis* A72, showed moderate inhibitory activity against *S. aureus* [29]. Therefore, the diketopiperazines, which were isolated from the microorganisms of East China Sea, may show many kinds of biological activities, which indicated the biological activities of the microorganisms.

Macrolactins are a group of 24-membered lactones with potent antibacterial or other activities, most of which were derived from the second metabolites of the marine microorganisms, while several of them were also produced by some soil microorganisms as well. There were total 22 isolated macrolactins reported, since the first one was isolated in 1989. Our group found a new macrolactin named macrolactin Q, which possesses strong antibacterial activity against *E. coli* than *S. aureus*

5. Conclusion

The East China Sea marine microorganism library (during 2006–2010) was established for the first time, which stored about 30000 strains that covered most kinds of the species. In this paper, 395 strains were mainly described, which belong to 33 different genera. *Sulfitobacter*, *Halomonas*, *Bacillus*, *Pseudoalteromonas*, and *Idiomarina* were the most dominant species, which may signify the genera diversity of the microorganisms of East China Sea. According to the results, 25.3% strains possess different biological activities, like antibacterial, cytotoxicity, and antioxidant activities. The diversity of the species of microorganisms, the biological activities of their secondary metabolites, and the abundant structure type of the secondary metabolites all indicate that East China Sea is a potent microorganism-derived medical resource for drug development.

Conflict of Interests

The authors declare that there is no conflict of interests.

Abbreviations

DPPH: Diphenyl-1-picrylhydrazyl
ABTS·+: 2,2′-azino-bis (3-ethylbenzthiazoline-6-sulphonic acid)
DKPs: Diketopiperazines
MIC: Minimal inhibitory concentration.

Acknowledgments

This work was supported by National Hi-tech R&D Program to B. Jiao (no. 2007AA091501), X. Liu (no. 2006AA09Z416), and Q. Xu (no. 2006AA09Z425), Science and Technology Commission of Shanghai Municipality Program to B. Jiao (no. 09431901900).

References

[1] D. J. Faulkner, "Marine natural products," *Natural Product Reports*, vol. 16, no. 2, pp. 155–198, 1999.
[2] J. W. Blunt, B. R. Copp, W. P. Hu, M. H. G. Munro, P. T. Northcote, and M. R. Prinsep, "Marine natural products," *Natural Product Reports*, vol. 26, no. 2, pp. 170–244, 2009.
[3] S. Wang et al., "Study of marine microbial resources in Huanghai, Bohai and Liaoning offshore of China," *Journal of Jinzhou Normal College*, vol. 22, no. 1, pp. 1–5, 2001.
[4] F. Sun, B. Wang, G. Li et al., "Diversity of bacteria isolated from the South China Sea sediments," *Acta Microbiologica Sinica*, vol. 48, no. 12, pp. 1578–1587, 2008.
[5] F. A. Rainey, N. Ward-Rainey, R. M. Kroppenstedt, and E. Stackebrandt, "The genus Nocardiopsis represents a phylogenetically coherent taxon and a distinct actinomycete lineage: proposal of nocardiopsaceae fam. nov," *International Journal of Systematic Bacteriology*, vol. 46, no. 4, pp. 1088–1092, 1996.
[6] F. Z. Wang, Y. Fang, T. Zhu et al., "Seven new prenylated indole diketopiperazine alkaloids from holothurian-derived fungus *Aspergillus fumigatus*," *Tetrahedron*, vol. 64, no. 34, pp. 7986–7991, 2008.
[7] C. Hu and D. D. Kitts, "Studies on the antioxidant activity of echinacea root extract," *Journal of Agricultural and Food Chemistry*, vol. 48, no. 5, pp. 1466–1472, 2000.
[8] C. Kajal and R. Paulraj, "Sesquiterpenoids with free-radical-scavenging properties from marine macroalga Ulva fasciata Delile," *Food Chemistry*, vol. 122, no. 1, pp. 31–41, 2010.
[9] D. Chen, Y. Han, and Z. Gu, "Application of statistical methodology to the optimization of fermentative medium for carotenoids production by Rhodobacter sphaeroides," *Process Biochemistry*, vol. 41, no. 8, pp. 1773–1778, 2006.
[10] H. Stan-Lotter, M. Pfaffenhuemer, A. Legat, H. J. Busse, C. Radax, and C. Gruber, "Halococcus dombrowskii sp. nov., an archaeal isolate from a Permian alpine salt deposit," *International Journal of Systematic and Evolutionary Microbiology*, vol. 52, no. 5, pp. 1807–1814, 2002.
[11] X. L. Lu et al., "Marine drugs—macrolactins," *Chemistry & Biodiversity*, vol. 5, no. 9, pp. 1669–1674, 2008.
[12] X. L. Lu, Q. Z. Xu, Y. H. Shen et al., "Macrolactin S, a novel macrolactin antibiotic from marine Bacillus sp," *Natural Product Research*, vol. 22, no. 4, pp. 342–347, 2008.
[13] P. Vaishnav and A. L. Demain, "Unexpected applications of secondary metabolites," *Biotechnology Advances*, vol. 29, no. 2, pp. 223–229, 2011.
[14] M. Adamczeski, A. R. Reed, and P. Crews, "New and known diketopiperazines from the Caribbean sponge, Calyx cf. podatypa," *Journal of Natural Products*, vol. 58, no. 2, pp. 201–208, 1995.
[15] S. De Rosa, M. Mitova, and G. Tommonaro, "Marine bacteria associated with sponge as source of cyclic peptides," *Biomolecular Engineering*, vol. 20, no. 4–6, pp. 311–316, 2003.
[16] F. Fdhila, V. Vazquez, J. L. Sánchez, and R. Riguera, "DD-diketopiperazines: antibiotics active against Vibrio anguillarum isolated from marine bacteria associated with cultures of Pecten maximus," *Journal of Natural Products*, vol. 66, no. 10, pp. 1299–1301, 2003.
[17] S. P. B. Ovenden, G. Sberna, R. M. Tait et al., "A diketopiperazine dimer from a marine-derived isolate of *Aspergillus niger*," *Journal of Natural Products*, vol. 67, no. 12, pp. 2093–2095, 2004.
[18] X. Fu, M. L. G. Ferreira, F. J. Schmitz, and M. Kelly-Borges, "New diketopiperazines from the sponge *Dysidea chlorea*," *Journal of Natural Products*, vol. 61, no. 10, pp. 1226–1231, 1998.
[19] X. Fu, L. M. Zeng, J. Y. Su, and M. Pais, "A new diketopiperazine derivative from the South China Sea sponge *Dysidea fragilis*," *Journal of Natural Products*, vol. 60, no. 7, pp. 695–696, 1997.
[20] C. Vergne, N. Boury-Esnault, T. Perez et al., "Verpacamides A-D, a sequence of $C_{11}N_5$ diketopiperazines relating cyclo(Pro-Pro) to cyclo(Pro-Arg), from the marine sponge *Axinella vaceleti*: possible biogenetic precursors of pyrrole-2-aminoimidazole alkaloids," *Organic Letters*, vol. 8, no. 11, pp. 2421–2424, 2006.
[21] T. R. De Kievit and B. H. Iglewski, "Bacterial quorum sensing in pathogenic relationships," *Infection and Immunity*, vol. 68, no. 9, pp. 4839–4849, 2000.
[22] S. De Rosa, M. Mitova, and G. Tommonaro, "Marine bacteria associated with sponge as source of cyclic peptides," *Biomolecular Engineering*, vol. 20, no. 4–6, pp. 311–316, 2003.
[23] G. Degrassi, C. Aguilar, M. Bosco, S. Zahariev, S. Pongor, and V. Venturi, "Plant growth-promoting *Pseudomonas putida* WCS358 produces and secretes four cyclic dipeptides: cross-talk with quorum sensing bacterial sensors," *Current Microbiology*, vol. 45, no. 4, pp. 250–254, 2002.

[24] M. T. G. Holden, S. R. Chhabra, R. De Nys et al., "Quorum-sensing cross talk: isolation and chemical characterization of cyclic dipeptides from *Axinella vaceleti* and other Gram-negative bacteria," *Molecular Microbiology*, vol. 33, no. 6, pp. 1254–1266, 1999.

[25] Y. Wang, U. G. Mueller, and J. Clardy, "Antifungal diketopiperazines from symbiotic fungus of fungus-growing ant *Cyphomyrmex minutus*," *Journal of Chemical Ecology*, vol. 25, no. 4, pp. 935–941, 1999.

[26] Z. Y. Li and Y. Liu, "Marine sponge *Craniella austrialiensis*-associated bacterial diversity revelation based on 16S rDNA library and biologically active actinomycetes screening, phylogenetic analysis," *Letters in Applied Microbiology*, vol. 43, no. 4, pp. 410–416, 2006.

[27] R. Musetti, R. Polizzotto, A. Vecchione et al., "Antifungal activity of diketopiperazines extracted from *Alternaria alternata* against *Plasmopara viticola*: an ultrastructural study," *Micron*, vol. 38, no. 6, pp. 643–650, 2007.

[28] L. H. Yang, L. Miao, O. O. Lee et al., "Effect of culture conditions on antifouling compound production of a sponge-associated fungus," *Applied Microbiology and Biotechnology*, vol. 74, no. 6, pp. 1221–1231, 2007.

[29] Z. Y. Li, C. Peng, Y. Shen, X. Miao, H. Zhang, and H. Lin, "L,L-diketopiperazines from *Alcaligenes faecalis* A72 associated with South China Sea sponge *Stelletta tenuis*," *Biochemical Systematics and Ecology*, vol. 36, no. 3, pp. 230–234, 2008.

Hindawi Publishing Corporation
Evidence-Based Complementary and Alternative Medicine
Volume 2011, Article ID 384572, 11 pages
doi:10.1155/2011/384572

Review Article

Genome-Based Studies of Marine Microorganisms to Maximize the Diversity of Natural Products Discovery for Medical Treatments

Xin-Qing Zhao

School of Life Science and Biotechnology, Dalian University of Technology, Linggong Road 2, Dalian 116024, China

Correspondence should be addressed to Xin-Qing Zhao, xqzhao@dlut.edu.cn

Received 15 January 2011; Revised 15 April 2011; Accepted 3 June 2011

Marine microorganisms are rich source for natural products which play important roles in pharmaceutical industry. Over the past decade, genome-based studies of marine microorganisms have unveiled the tremendous diversity of the producers of natural products and also contributed to the efficiency of harness the strain diversity and chemical diversity, as well as the genetic diversity of marine microorganisms for the rapid discovery and generation of new natural products. In the meantime, genomic information retrieved from marine symbiotic microorganisms can also be employed for the discovery of new medical molecules from yet-unculturable microorganisms. In this paper, the recent progress in the genomic research of marine microorganisms is reviewed; new tools of genome mining as well as the advance in the activation of orphan pathways and metagenomic studies are summarized. Genome-based research of marine microorganisms will maximize the biodiscovery process and solve the problems of supply and sustainability of drug molecules for medical treatments.

1. Introduction

The marine environment covers more than 70% of the Earth's surface and has been proven to be a rich source for both biological and chemical diversity. Marine natural products have become fascinating targets for biologists and chemists for discovery of lead compounds for clinical development for the past five decades [1–10]. Marine microorganisms comprise an important group of natural product producers, and the natural products isolated from marine microorganisms presented diverse activities, such as antibacterial, antifungal, anticancer, and antiviral activities. Of the major producers of useful natural products, marine actinobacteria are especially notable for the capability of producing diverse useful natural products [5–7], and marine cyanobacteria are also an important group of bioactive metabolites [5]. Currently 13 marine-derived compounds are reported in clinical development, and those belong to the authentic or derivatives of marine natural products of microbial origin and are listed in Table 1, and the structures are displayed in Figure 1. Of these compounds, soblidotin (TZT 1027), the synthetic derivative of dolastatin 10, was isolated from the marine cyanobacterium *Symploca* sp. VP642 from Palau, and the synthesis of plinabulin (NPI-2358) was inspired by halimide and phenylahistin, the former of which was isolated from a marine fungus *Aspergillus* sp. CNC-139. The structures of other interesting compounds with novel structures or potent activities can be retrieved from the recent literatures and review papers [8–17].

Although natural products embrace a wide range of entities such as biomaterials and biocatalysts as well as biocontrol agents other than drug molecules, due to space limitation, in this paper, most of the cited natural products focused upon are compounds with the potential to be developed as drugs and used in medical treatments. Taking the advantage of established microbial cultivation technology, the promising natural products identified from marine microorganisms provide great potential to solve the supply and sustainability problem of useful drugs to cure human diseases.

High-throughput screening (HTS) of drug molecules demands abundant diversity of the compound libraries to get more hits for drug discovery. To combat the emergence of drug-resistant pathogens, as well as to improve the efficacy and safety of medical treatment, new drug leads are urgently needed. The key point of improving the success of natural

Table 1: Active natural products isolated from marine microorganisms.

Metabolites	Source	Activity	Reference	Clinical status
Soblidotin (TZT1027)	Synthetic derivative of dolastatin 10 isolated from marine cyanobacterium *Symploca* sp. VP642	Anticancer	[12]	Phase III
Plinabulin (NPI-2358)	Synthetic analog of halimide isolated from the marine fungus *Aspergillus* sp. CNC-139	Anticancer	[13]	Phase II
Bryostatin 1	Identified from bryozoan and also marine symbiotic bacteria *Candidatus Endobugula sertula*	Anticancer, Anti-Alzheimer	[14]	Phase I
Marizomib (salinosporamide A, NPI-0052)	Marine actinobacteria *Salinispora arenicola*	Anticancer	[15]	Phase I
Compound 4 (curacin A synthetic derivative)	Curacin A was isolated from the marine cyanobacterium *Lyngbya majuscula*	Anticancer	[16]	Preclinical

product screening and development is to improve the diversity and the size of natural product library for new drug discovery. In this paper, the recent progress in the genomic research for natural compound discovery is summarized, with the focus on the important roles of genetic diversity deduced from genome mining on new drug discovery.

2. Genomic Sequencing of Natural-Product-Producing Microorganisms

Genomic sequencing of microorganisms in the recent years has unveiled unprecedented insights into the biosynthetic potential of microbial cells, and thus the discovery of natural products has entered into the new postgenomic era. The genomic sequencing data of various living organisms have been accumulating rapidly in recent years. According to the Genomes On Line Database (GOLD), there are 5831 genome sequencing projects registered in GOLD, while according to the last update (April 11, 2011), 10298 genome projects are documented currently in GOLD (http://www.genomesonline.org), of which 1674 complete genomes are registered. And in the mean time, 204 archaeal, 6087 bacterial, and 2003 eukaryal genome projects are ongoing, which are double of those reported in 2009 [18]. The same case is the genome project numbers in 2009 comparing with those in 2007 [19]. Genome sequencing projects supported by the Gordon and Betty Moore Foundation resulted in the release of about 150 marine bacterial genomes [20]. Draft or complete genomic sequences of more than 35 marine cyanobacterial strains of six different species have been released, and some gene clusters for polyketide and nonribosomal peptide biosynthesis were identified [21]. It can be anticipated that more marine microbial genomic sequences will be available in the near future, and more relevance of natural product biosynthesis to the microbial genomes will be disclosed. For instance, the genomes of marine *Nocardiopsis* sp. strain TFS65-07 and marine-derived fungus strain *Aspergillus* sp. MF297-2 were reported to be sequenced, and studies on the biosynthesis of thiopeptide antibiotic TP-1161 and prenylated indole alkaloids, stephacidin and notoamide metabolites, were subsequently guided by the bioinformatics analysis of gene clusters located in these genomes [22, 23]. Despite the fact that comparing to the studies on terrestrial species and strains, genomic studies of marine-derived microorganisms are still well performed, the knowledge accumulated from the terrestrial microorganisms can be used also in the marine-derived strains. Actinobacteria are major producers of various useful antibiotics and antitumor agents. In the below section, I gave some examples on the investigations on the genomes of some model or natural-product-producing strains, which will shed light on their marine-derived counterparts.

Streptomyces is the largest genus of actinobacteria, and, species of streptomycetes are major producers of antibiotics which have wide range of utilities in medical treatments and agricultural applications. The first genomic sequencing of the model streptomycete, *Streptomyces coelicolor* A3 [2], was reported in 2002 [24], and the genome contains about 31 biosynthetic gene clusters that were predicted to contribute to the biosynthesis of secondary metabolites, which are the major source of bioactive natural products. Surprisingly, only half a dozen of these secondary metabolites in *S. coelicolor* have by that time been identified, which implies that microbial cells can produce much larger chemical diversity than previously anticipated. Later on, the genome sequence of *S. avermitilis* was also reported [25], followed by the blooming uncover of genomic sequences of various antibiotic producers [26–31].

The genome sequence of the first seawater-requiring marine actinomycete, *Salinispora tropica,* was reported [26]. Bioinformatics analysis revealed that this marine bacterial species owns a large proportion of genes (about 9.9%) responsible for natural product biosynthesis, while the corresponding numbers in *S. coelicolor* and *S. avermitilis* are 4.5% and 6%, respectively [32]. The genome of *S. tropica* contains amazingly large size of genes (516 Kb) dedicated to polyketide synthase (PKS) and/or nonribosomal peptide synthetase (NRPS) biosynthesis, which are megasynthases that are responsible for many active natural product biosynthesis and are especially popular tools for combinational biosynthesis [33–35]. The majority of the gene loci are novel, indicating that *S. tropica* has great potential to produce novel natural products and that the biosynthetic potential of this species, like that of many other actinomycetes that were genomically sequenced, is considerably greater than

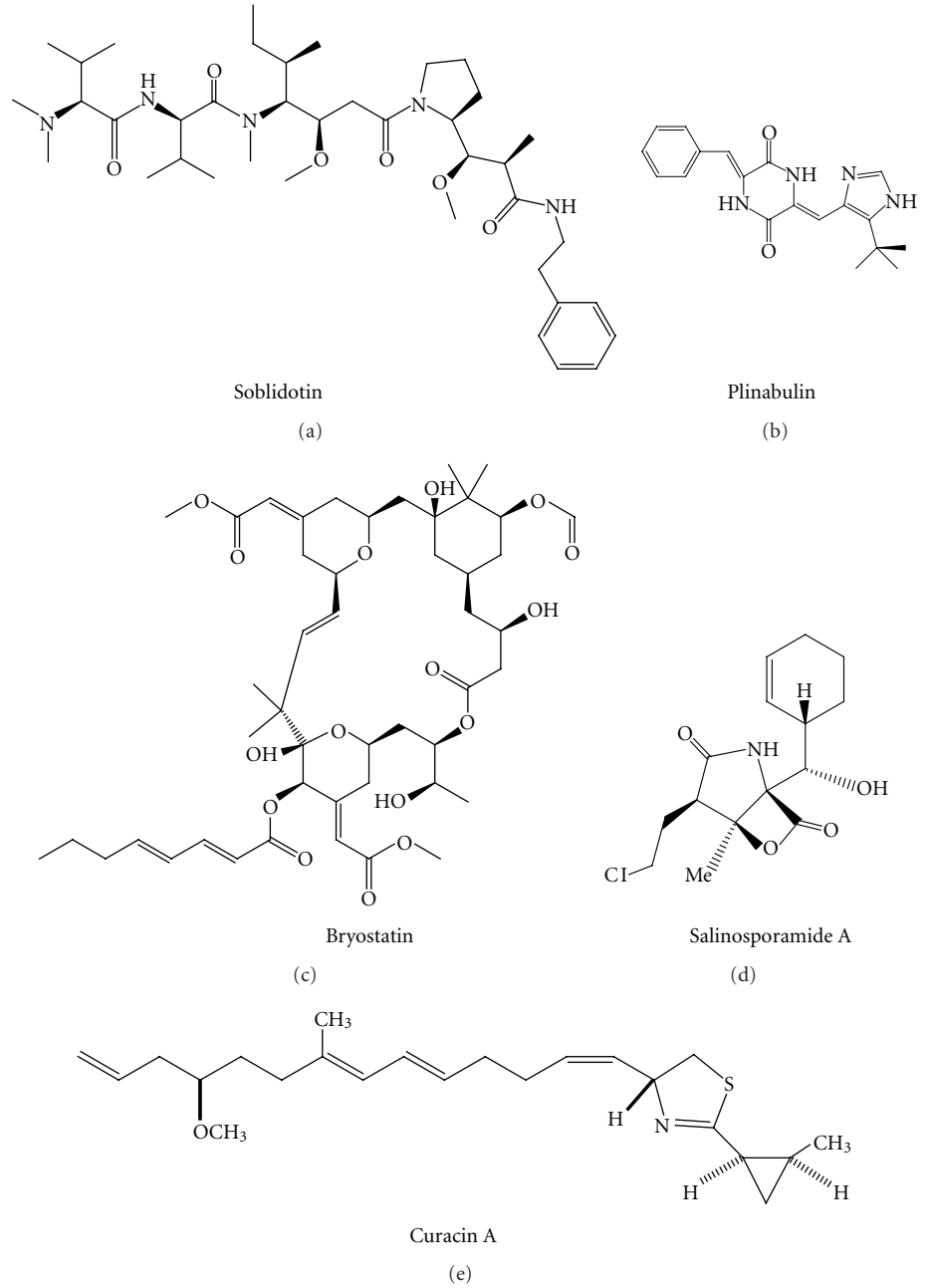

Figure 1: Structures of the marine microbial-derived compounds in clinical development.

that has been observed by cultivation and chemical analysis [26], which provided basis for mining of these novel genetic sources for new natural products.

3. Important Roles of Genetic Studies to Maximize the Diversity for Natural Product Discovery

Although natural products from marine microorganisms have already widened the spectrum of chemical diversity, increasing the diversity of natural compounds is still the prerequisite for HTS to get enough new hits for drug discovery. And in the meantime, the classical activity-based screening is increasingly challenged by repeated discovery of known compounds, as well as the limitation of available assay methods. Therefore, new techniques are needed to maximize the diversity of natural products for the discovery of new therapeutic agents, not only to increase the efficacy and decrease the toxicity, but also to combat the emergence of drug resistance.

The development of genomic sequencing techniques as well as the bioinformatics tools in recent years has profound influence on the discovery of new drugs. Nowadays it is much easier to have the genome of the interested organisms sequenced, especially for relatively small genomes of microorganisms. The availability of genomic sequences and the

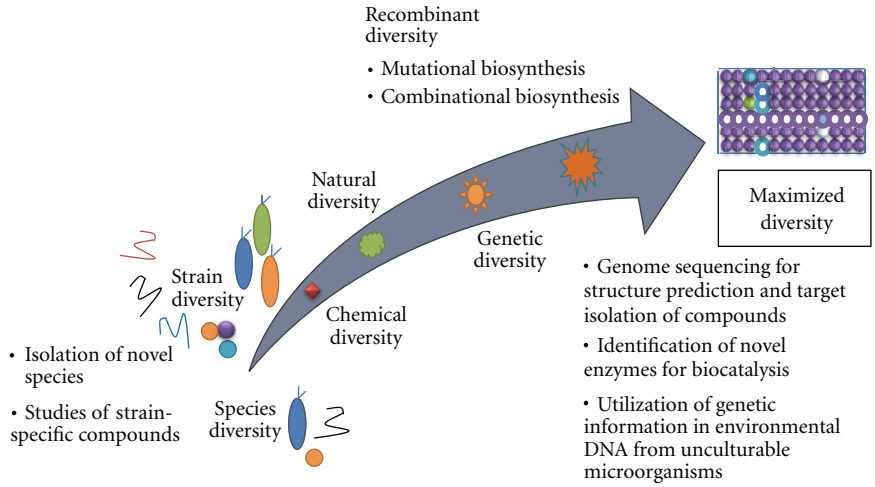

Figure 2: Important tools to maximize the diversity for new drug discovery.

subsequent genome mining of microorganisms have provided new insights in the biosynthetic potential of the cells, and thus the studies of marine natural products have entered into the new postgenomic era. There is an increasing trend to expand the studies on the chemical diversity of natural products from bioassay-based screening to genetic diversity studies, from the studies of natural diversity to creation and utilization of recombinant diversity (e.g., to use genetic tools to produce new "unnatural" natural products), and in the meantime, it is well accepted that the chemical diversity and genetic diversity not only exist in different microbial species, but also exist in the different strains in one species [36]. Therefore, the chemical diversity for useful natural products can be maximized by the integration of genomic research and genetic engineering with the efforts of chemists. The important strategies to maximize biodiversity of marine natural products are illustrated in Figure 2, and will be depicted in detail in the following sections.

4. "Gene-to-Compound" Procedure for Genome-Based Screening of Natural Products

It has been observed that the genetic elements responsible for the biosynthesis of many, if not all, secondary metabolites are clustered in the bacterial or fungal genomes to form gene clusters, which include the genes encoding biosynthetic enzymes, as well as genes responsible for regulation and resistance [37]. This genetic feature has not only greatly facilitated the molecular cloning and characterization of the biosynthetic genes, but has also provided basis for the generation of novel compounds through combinational biosynthesis. Traditionally, to identify and isolate the gene cluster for natural product biosynthesis, knowledge on the chemical structures of the compounds must be obtained prior to the genetic studies. However, this "compound-to-gene" route is facing challenges in that (1) the cultivation media and conditions have great impact on the searching of the chemicals; therefore, a lot of efforts have to be made to test different media and cultivation parameters; (2) the bioassay-based screening results in the rediscovery of known compounds from the screening of natural products; (3) the elucidation of complex structures; (4) the isolation of the natural products is hampered by low production yields and complex purification procedures.

In the recent years, more and more studies have focused on the "from genetics-to-chemistry" route for natural product research, that is, to use gene-based screening strategy to study the biosynthetic potential of the microbial strains, followed by molecular cloning experiments and chemical purifications [38, 39]. A good example is the studies on the identification of active halogenated compounds from 550 randomly selected actinomycetes based on the conserved sequences from diverse halogenase genes. Using this "genome-based" strategy, novel halogenase genes were identified and novel halometabolites were isolated by the cloning of related gene cluster in heterologous host [38]. We used the same strategy to screen the marine actinobacteria strain library in our lab and isolated a gene cluster putatively involved in the biosynthesis of glycopeptide antibiotics. Furthermore, the genomic sequence of a new marine-derived *Streptomyces* sp. S187 was obtained, and bioinformatics analysis guided the identification of the gene cluster responsible for a new glycopeptide antibiotic (unpublished data). Genome scanning is another successful approach, in which the random genome sequence tags (GSTs) prepared from the genomic DNA library are screened using degenerate primers to identify the gene cluster, and the products of the gene cluster can be subsequently searched using various genomics-guided strategies [40, 41], which will be detailed in the following section. Using this "gene-to-compound" strategy, screening of a large strain library can be rapidly focused on small group of strains with high possibility to produce new compounds. However, the success of this strategy is dependent on multifaceted factors, including the selection of target genes for genome-based screening, the design of suitable degenerate primers, the quality of template DNA (especially

environmental DNA), PCR conditions, and sequence degeneracy, and thus is limited to the detection of chemical diversities with diverse structures.

5. Genome Mining of Microbial Natural Product Producers

Although the cost of genome sequencing is declining, it is still not affordable for every lab for natural product research. Two questions may arise concerning the whole genomic sequencing. Why do we need to know all the sequences on the genome? What can we do next after obtaining the genomic sequence?

To answer the first question, it is well accepted that the genetic loci in the genome can be roughly grouped by genes involved in primary metabolism and genes involved in secondary metabolism. Because not all genes are expressed in all the conditions, the chemical analysis of the cultivation broth under certain conditions cannot fully explore the biosynthetic potential of the cells. Furthermore, not all genes can be fished out by gene-based screening using degenerate PCR; therefore, sequencing the genome can fully access the genetic loci responsible for natural product biosynthesis. At the same time, genetic loci involved in primary metabolism are also tightly linked to the biosynthesis of natural product by providing precursors and cofactors [42]; therefore, the production of natural products requires the balanced interaction of metabolic network of both primary metabolism and secondary metabolism. Knowing the genomic sequence is the prerequisite to understand and harness the diversity of the natural product producers. The availability of genomic sequence also enables the studies of natural product producer using systems biological approaches, which are exemplified by the metabolome studies [43] and transcriptome studies [44] in *S. coelicolor*.

The answer to the second question relies on the rapid development of tools for genome mining, which were presented in several excellent reviews elsewhere [45–51]. Several strategies for genome mining for novel natural products identification are summarized below with the addition of recent reports:

(1) Genome-Guided Structural Prediction of the Products and Target Isolation. As indicated above, the polyketides and nonribosomal peptides are synthesized by modular PKS or NRPS system, and extensive knowledge has been accumulated on the relationship between the structures of these compounds and the organization of the multienzymes. Successful mining of ribosomally synthesized peptides has also been reported and summarized [51]. Bioinformatics analysis of these groups of genes thus can give important insight into the structural features of the biosynthetic products. The genome-guided discovery of salinilactam A in marine actinomycete *S. tropica* strain CNB-440 is one good example [27]. Initial bioinformatises analysis indicated that the *slm* gene cluster codes for polyene macrolactam polyketide, and investigation of the fermentation broth using characteristic UV chromophores of polyene units led to the identification

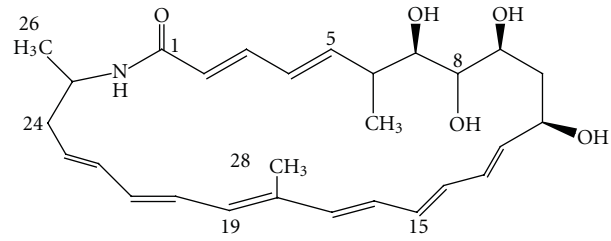

Salinilactam A

(a)

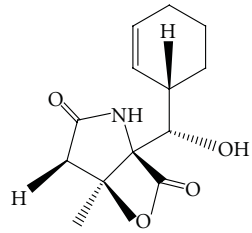

Salinosporamide K

(b)

Figure 3: Structures of salinilactam A and salinosporamide K discovered by genome mining.

of structural fragments of salinilactam A series compounds. Inspection of the structure fragments suggested that salinilactam A was derived from a PKS with at least 10 extension modules. This information was useful to help resolve and properly assemble the repetitive DNA sequences associated with the *slm* PKS, which was used in combination of partial NMR-based structural fragments to accurately predict the gross chemical structure of salinilactam A. What is more, bioinformatics analysis also assisted in the correction of the initial assignment of the C-28 methyl group complicated by overlapping olefinic NMR signals. The salinilactam A structure was later verified by comprehensive NMR analyses of the purified natural product to confirm the bioinformatics-based total structure assignment.

In another recent report, salinosporamide K was discovered by comparative genomic analysis of "*S. pacifica*" with that of *S. tropica* [52]. A truncated biosynthetic gene cluster was identified in the draft genome of "*S. pacifica*", which is related to the 41 kb gene cluster in *S. tropica* for salinosporamide A biosynthesis, but the genes coding for the enzymes in the chloroethylmalonyl-CoA pathway are absent in "*S. pacifica.*" This information guided the isolation of salinosporamide K, which structurally resembles salinosporamide A [26].

The structures of salinilactam A and salinosporamide K described above were presented in Figure 3.

(2) Comparative Metabolic Profiling of the Mutants with the Addition or Inactivation of the Biosynthetic Genes. Biosynthetic gene clusters that are related to the production of yet-unknown metabolites are often referred to as "orphan" [46].

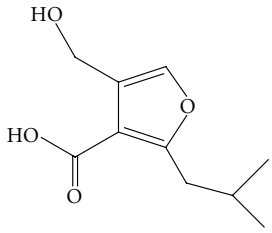

2-alkyl-4-hydroxymethylfuran-3-carboxylic acid (AHFCA 3)

(a)

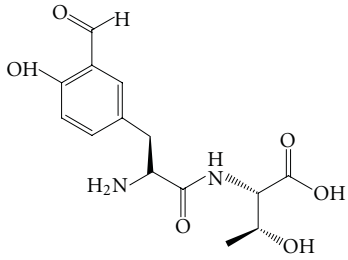

3-formyl-L-tyrosine-L-threonine dipeptide

(b)

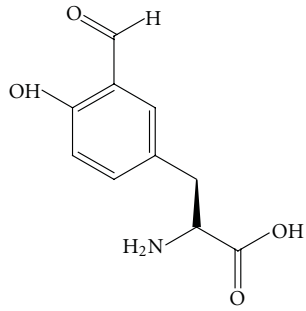

3-formyl-L-tyrosine

(c)

Figure 4: Structures of MMF1, 3-formyl-L-tyrosine-L-threonine dipeptide and 3-formyl-L-tyrosine.

The biosynthetic genes in the orphan gene cluster can be inactivated by deletion or disruption, and the comparison of the metabolic profiling using HPLC or LC-MS of the mutant with that of the wild type strain will identify the product of the gene cluster. The discovery of coelichelin in *S. coelicolor* is the early example in which this approach was employed [53]. Alternatively, the biosynthetic gene clusters can be heterologously expressed in a well-characterized "clean" host with no background production of similar metabolites, and the comparative metabolic profiling will help to identify the novel products. The 5 new 2-alkyl-4-hydroxymethylfuran-3-carboxylic acids termed as Mm furans (MMFs), which are new autoinducers to regulate antibiotic production, were discovered by this heterologous expression approach [54]. In a recent report, a gene cluster containing ATP-grasp enzymes identified by genome mining of the marine gamma proteobacterium *Pseudoalteromonas tunicata* D2 was overexpressed in *E. coli*, which led to the isolation of two new metabolites, 3-formyl-L-tyrosine-L-threonine dipeptide and 3-formyl-L-tyrosine [55]. This work emphasized the studies of smaller pathways (comparing to PKS and NRPS) employing less familiar biosynthetic strategies for the discovery of novel natural products. The structures of one Mm furans (MMF1), 3-formyl-L-tyrosine-L-threonine dipeptide, and 3-formyl-L-tyrosine were shown in Figure 4.

(3) Activation of the Biosynthetic Genes by Manipulation of Regulatory Genes. The failure of producing certain natural products can be attributed to the poor expression or silence of the biosynthetic gene cluster. Therefore, overexpression of the regulatory genes, either pathway-specific regulatory genes or global regulatory genes, can lead to the production of novel compounds. One example is the discovery of aspyridones in *Aspergillus nidulans*. Overexpression of the putative pathway-specific regulatory gene located in the silent gene cluster resulted in the identification of the novel hybrid PKS-NRPS product aspyridone [56]. Alternatively, the promoter of the pathway-specific regulatory gene can be replaced by strong constitutive promoter, so that the expression of regulatory gene can be deregulated by repression.

On the other hand, some regulatory genes can also exert inhibitory effect on the production of certain compounds; in this case, the deletion of such regulatory genes readily results in the activation of silent pathways and production of novel compounds. In a recent report, a new yellow-pigmented secondary metabolite was observed in *S. coelicolor* after deleting a putative pathway-specific regulatory gene (*scbR2*) that encodes gamma-butyrolactone receptor protein [57]. This strategy can be used for the discovery of novel natural products from marine microorganisms, although no known literature in this aspect has been reported so far.

Other strategies for genome mining including genomisotopic studies and in vitro reconstitution of biosynthetic enzymes were described in reviews elsewhere [58, 59]. It can be predicted that genome mining of marine microorganisms will unveil the tremendous diversity of natural products produced by microorganisms. What is more, it should be mentioned that only 1% of the microbial community is estimated to be culturable in lab conditions [60–62], pointing out the importance the area of biodiversity research in the yet "unculturable" microorganisms, which will be addressed in the following section.

6. Metagenomic Studies of "Unculturable" Marine Microorganisms

Marine symbiotic microorganisms are rich source of active natural products and are thought in some cases to be the true producers of potent drug candidates instead of the marine invertebrate including sponges, tunicates, and bryozoans [63]. Shotgun sequencing of the environmental genome in the seawater samples collected from the Sargasso Sea near Bermuda also revealed tremendous diversity of the commonly thought tobe nutrient-limited environment [64],

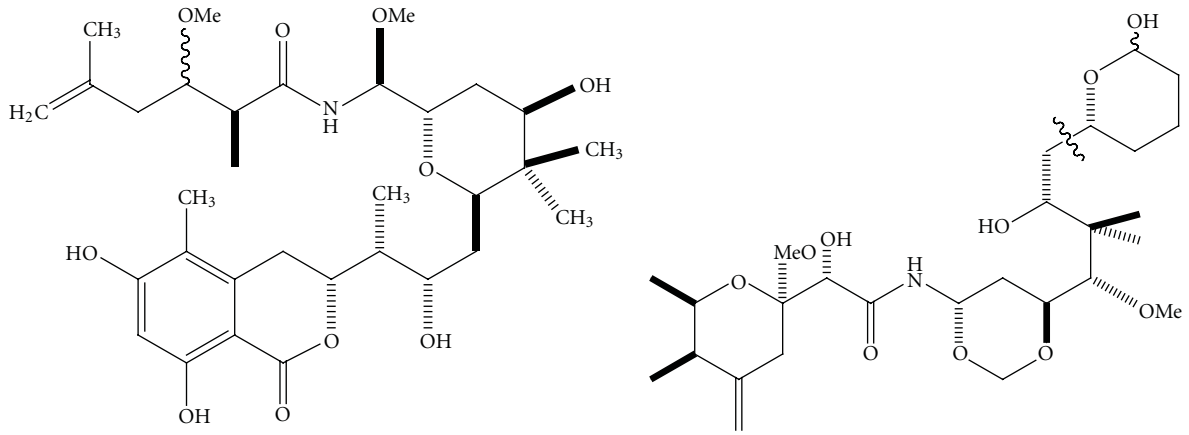

(a) (b)

Figure 5: Structures of antitumor agents psymberin and theopederins A studied in metagenomic analysis.

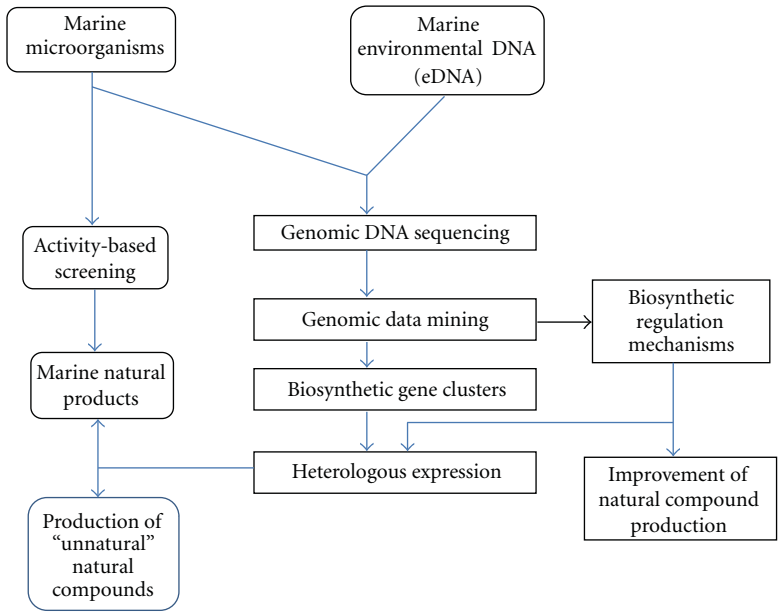

Figure 6: Combination of genome mining with classical activity-based screening for natural product discovery, generation, and hyperproduction.

which unveiled 148 previously unknown bacterial phylotypes and 1.2 million previously unknown genes. However, the majority of the marine symbionts and 99% of the microbial population in environment are difficult to grow or are slowly growing as pure culture. To fully access the valuable chemical diversity and explore the biosynthetic potential of all the microbial communities, the environmental DNA (eDNA) is extracted directly from a given environment, and packed into vectors, following by transformation to various hosts, including *E. coli* and *Streptomyces lividans*. Clone libraries are produced independently of the host cultivation or fermentation and then subjected to sequence-based screening or function-based screening. This cultivation-independent approach is termed metagenomics. During the past decade, many successful metagenomic studies have been reported. Onnamides and theopederins are antitumor polyketides produced by an uncultured *Pseudomonas* sp. symbiont of marine sponge *Theonella swinhoei*. Biosynthesis genes of onnamides and theopederins were isolated from the metagenome of the marine sponge, and bioinformatics analysis of the biosynthetic genes strongly indicated a prokaryotic origin, suggesting that these potent antitumor agents may be produced by the symbiotic bacteria [65]. An entire putative gene cluster responsible for the biosynthesis of bryostatin, which has been evaluated for the treatment of various leukemias, ovarian cancers, and prostate cancers, has been

implicated to be produced by a symbiotic bacteria, *Candidatus Endobugula sertula* from the marine bryozoan [66]. In another study, gene cluster for the biosynthesis of potent antitumor agent psymberin was isolated from the metagenomic library of marine sponge *Psammocinia* aff. *Bulbosa* [67]. Combining with the research development in heterologous expression [68], active compounds can be produced in large quantities by overexpressing the biosynthetic gene clusters isolated from metagenomic libraries in the heterologous hosts, which will solve the supply and sustainability problem of the precious compounds produced by marine symbionts and the yet "unculturable" marine microorganisms.

The structures of some compounds studied by metagenomic analysis were presented in Figure 5.

7. Updating Tools for Exploration of Diversities of Natural Compounds

Exploration of the diversity of marine natural products is greatly promoted by various genome-based strategies described in this paper, and new chemical structures and novel bioactivities unveiled by these methods are complementing the traditional bioassay-guided studies. However, as indicated by Glöckner and Joint [69], the success of the genome-based methods is largely dependent on the accuracy of bioinformatics analysis, and the bioinformatics tools are often the limiting factor. Researchers are now developing various bioinformatics tools such as ClustScan [70], NP.searcher [71], SBSPKS [72], to name a few, for the analysis of PKS or NRPS modular sequences and structure predictions.

On the other hands new tools in the detection of natural products are continuously being developed to explore the chemical diversity of microbial natural products. The imaging mass spectrometry (IMS) tools were used to visualize the spatial distribution of secondary metabolites produced by marine cyanobacteria [73], providing information for dereplication and discovery of novel natural products. The PrISM (Proteomic Investigation of Secondary Metabolism) approach employs mass-spectrometry-based proteomics to localize expressed PKS or NRPS clusters, which resulted in the discovery of new NRPS gene cluster in *Bacillus* strain NK2018 [74]. Single-cell genomics approach was used to study the lifestyle of marine symbiotic bacteria, *Poribacteria* [75], and this strategy also holds promise in studying the biosynthetic potential of unculturable microorganisms in the near future. All these updated bioinformatics tools and detection tools can be combined to facilitate new marine natural products.

The exploration of the diversity of marine microorganisms using the combined classical activity-based screening with the genome mining in both the culturable and unculturable microorganisms is presented in Figure 6.

8. Conclusion and Prospects

Recent years have witnessed the exponentially increasing genome sequencing information, and genome mining analyses have revealed tremendous capability of marine microorganisms to produce active natural products as therapeutic agents. Studies on the biosynthetic machinery and regulatory mechanisms of natural product biosynthesis will greatly maximize the diversity exploration of marine natural products. Nowadays the diversity studies of natural products have been shift from pure chemical analysis to the combination of genetic manipulations and chemical synthesis, and the diversity of natural products can be further enlarged by genetic engineering of biosynthetic genes. Genomic research of marine microorganisms will have great impact on the discovery of novel natural products for medical treatments and will contribute to efficient drug discovery from marine environment.

Acknowledgments

This work is financially supported by Open Funding Project of the State Key Laboratory of Bioreactor Engineering, East China University of Science and Technology on marine halogenase to the author. The author also thanks the Alexander von Humboldt Foundation for the support of the research in the regulation of antibiotic biosynthesis in Germany. The comments and suggestions of three anonymous reviewers are sincerely appreciated, which helped to enrich the manuscript in marine aspects.

References

[1] E. L. Cooper, "Drug discovery, CAM and natural products," *Evidence-Based Complementary and Alternative Medicine*, vol. 1, pp. 215–217, 2004.

[2] P. Bhadury, B. T. Mohammad, and P. C. Wright, "The current status of natural products from marine fungi and their potential as anti-infective agents," *Journal of Industrial Microbiology and Biotechnology*, vol. 33, no. 5, pp. 325–337, 2006.

[3] A. T. Bull and J. E. M. Stach, "Marine actinobacteria: new opportunities for natural product search and discovery," *Trends in Microbiology*, vol. 15, no. 11, pp. 491–499, 2007.

[4] P. G. Williams, "Panning for chemical gold: marine bacteria as a source of new therapeutics," *Trends in Biotechnology*, vol. 27, no. 1, pp. 45–52, 2009.

[5] A. C. Jones, L. Gu, C. M. Sorrels, D. H. Sherman, and W. H. Gerwick, "New tricks from ancient algae: natural products biosynthesis in marine cyanobacteria," *Current Opinion in Chemical Biology*, vol. 13, no. 2, pp. 216–223, 2009.

[6] T. A. Gulder and B. S. Moore, "Chasing the treasures of the sea—bacterial marine natural products," *Current Opinion in Microbiology*, vol. 12, no. 3, pp. 252–260, 2009.

[7] A. M. S. Mayer, A. D. Rodríguez, R. G. S. Berlinck, and N. Fusetani, "Marine pharmacology in 2007-8: marine compounds with antibacterial, anticoagulant, antifungal, anti-inflammatory, antimalarial, antiprotozoal, antituberculosis, and antiviral activities; Affecting the immune and nervous system, and other miscellaneous mechanisms of action," *Comparative Biochemistry and Physiology Part C*, vol. 153, no. 2, pp. 191–222, 2011.

[8] A. M. S. Mayer, K. B. Glaser, C. Cuevas et al., "The odyssey of marine pharmaceuticals: a current pipeline perspective,"

Trends in Pharmacological Sciences, vol. 31, no. 6, pp. 255–265, 2010.

[9] F. A. Villa and L. Gerwick, "Marine natural product drug discovery: leads for treatment of inflammation, cancer, infections, and neurological disorders," *Immunopharmacology and Immunotoxicology*, vol. 32, no. 2, pp. 228–237, 2010.

[10] A. L. Waters, R. T. Hill, A. R. Place, and M. T. Hamann, "The expanding role of marine microbes in pharmaceutical development," *Current Opinion in Biotechnology*, vol. 21, no. 6, pp. 780–786, 2010.

[11] T. L. Simmons, E. Andrianasolo, K. McPhail, P. Flatt, and W. H. Gerwick, "Marine natural products as anticancer drugs," *Molecular Cancer Therapeutics*, vol. 4, no. 2, pp. 333–342, 2005.

[12] H. Luesch, R. E. Moore, V. J. Paul, S. L. Mooberry, and T. H. Corbett, "Isolation of dolastatin 10 from the marine cyanobacterium *Symploca* species VP642 and total stereochemistry and biological evaluation of its analogue symplostatin 1," *Journal of Natural Products*, vol. 64, no. 7, pp. 907–910, 2001.

[13] W. Fenical, P. R. Jensen, and X. C. Cheng, "Halimide, a cytotoxic marine natural product, and derivatives thereof," WO/1999/048889, The Regents of the University of California, September 1999.

[14] S. K. Davidson, S. W. Allen, G. E. Lim, C. M. Anderson, and M. G. Haygood, "Evidence for the biosynthesis of bryostatins by the bacterial symbiont "*Candidatus Endobugula sertula*" of the bryozoan *Bugula neritina*," *Applied and Environmental Microbiology*, vol. 67, no. 10, pp. 4531–4537, 2001.

[15] R. H. Feling, G. O. Buchanan, T. J. Mincer, C. A. Kauffman, P. R. Jensen, and W. Fenical, "Salinosporamide A: a highly cytotoxic proteasome inhibitor from a novel microbial source, a marine bacterium of the new genus Salinospora," *Angewandte Chemie International Edition*, vol. 42, no. 3, pp. 355–357, 2003.

[16] W. H. Gerwick, L. T. Tan, and N. Sitachitta, "Nitrogen-containing metabolites from marine cyanobacteria," in *The Alkaloids: Chemistry and Biology*, G. A. Cordell, Ed., vol. 57, pp. 75–184, Academic Press, San Diego, Calif, USA, 2001.

[17] M. E. Rateb and R. Ebel, "Secondary metabolites of fungi from marine habitats," *Natural Product Reports*, vol. 28, no. 2, pp. 290–344, 2011.

[18] K. Liolios, I. A. Chen, K. Mavromatis et al., "The Genomes On Line Database (GOLD) in 2009: status of genomic and metagenomic projects and their associated metadata," *Nucleic Acids Research*, vol. 38, no. 1, pp. D346–D354, 2009.

[19] K. Liolios, K. Mavromatis, N. Tavernarakis, and N. C. Kyrpides, "The Genomes On Line Database (GOLD) in 2007: status of genomic and metagenomic projects and their associated metadata," *Nucleic Acids Research*, vol. 36, no. 1, pp. D475–D479, 2008.

[20] Moore, "Microbial Genome Sequencing Project," http://camera.calit2.net/microgenome.

[21] A. C. Jones, E. A. Monroe, E. B. Eisman, L. Gerwick, D. H. Sherman, and W. H. Gerwick, "The unique mechanistic transformations involved in the biosynthesis of modular natural products from marine cyanobacteria," *Natural Product Reports*, vol. 27, no. 7, pp. 1048–1065, 2010.

[22] K. Engelhardt, K. F. Degnes, and S. B. Zotchev, "Isolation and characterization of the gene cluster for biosynthesis of the thiopeptide antibiotic TP-1161," *Applied and Environmental Microbiology*, vol. 76, no. 21, pp. 7093–7101, 2010.

[23] Y. Ding, J. R. de Wet, J. Cavalcoli et al., "Genome-based characterization of two prenylation steps in the assembly of the stephacidin and notoamide anticancer agents in a marine-derived *Aspergillus sp*," *Journal of the American Chemical Society*, vol. 132, no. 36, pp. 12733–12740, 2010.

[24] S. D. Bentley, K. F. Chater, A. M. Cerdeño-Tárraga et al., "Complete genome sequence of the model actinomycete *Streptomyces coelicolor* A3(2)," *Nature*, vol. 417, no. 6885, pp. 141–147, 2002.

[25] H. Ikeda, J. Ishikawa, A. Hanamoto et al., "Complete genome sequence and comparative analysis of the industrial microorganism *Streptomyces avermitilis*," *Nature Biotechnology*, vol. 21, no. 5, pp. 526–531, 2003.

[26] M. Oliynyk, M. Samborskyy, J. B. Lester et al., "Complete genome sequence of the erythromycin-producing bacterium *Saccharopolyspora erythraea* NRRL23338," *Nature Biotechnology*, vol. 25, no. 4, pp. 447–453, 2007.

[27] D. W. Udwary, L. Zeigler, R. N. Asolkar et al., "Genome sequencing reveals complex secondary metabolome in the marine actinomycete *Salinispora tropica*," *Proceedings of the National Academy of Sciences of the United States of America*, vol. 104, no. 25, pp. 10376–10381, 2007.

[28] Y. Ohnishi, J. Ishikawa, H. Hara et al., "Genome sequence of the streptomycin-producing microorganism *Streptomyces griseus* IFO 13350," *Journal of Bacteriology*, vol. 190, no. 11, pp. 4050–4060, 2008.

[29] X. J. Wang, Y. J. Yan, B. Zhang et al., "Genome sequence of the milbemycin-producing bacterium *Streptomyces bingchenggensis*," *Journal of Bacteriology*, vol. 192, no. 17, pp. 4526–4527, 2010.

[30] J. Y. Song, H. Jeong, D. S. Yu et al., "Draft genome sequence of Streptomyces clavuligerus NRRL 3585, a producer of diverse secondary metabolites," *Journal of Bacteriology*, vol. 192, no. 23, pp. 6317–6318, 2010.

[31] N. Ichikawa, A. Oguchi, H. Ikeda et al., "Genome sequence of kitasatospora setae NBRC 14216T: an evolutionary snapshot of the family *Streptomycetaceae*," *DNA Research*, vol. 17, no. 6, pp. 393–406, 2010.

[32] M. Nett, H. Ikeda, and B. S. Moore, "Genomic basis for natural product biosynthetic diversity in the actinomycetes," *Natural Product Reports*, vol. 26, no. 11, pp. 1362–1384, 2009.

[33] D. E. Cane, C. T. Walsh, and C. Khosla, "Harnessing the biosynthetic code: combinations, permutations, and mutations," *Science*, vol. 282, no. 5386, pp. 63–68, 1998.

[34] H. G. Floss, "Combinatorial biosynthesis-potential and problems," *Journal of Biotechnology*, vol. 124, no. 1, pp. 242–257, 2006.

[35] L. Du, C. Sánchez, and B. Shen, "Hybrid peptide-polyketide natural products: biosynthesis and prospects toward engineering novel molecules," *Metabolic Engineering*, vol. 3, no. 1, pp. 78–95, 2001.

[36] P. R. Jensen, P. G. Williams, D.-C. Oh, L. Zeigler, and W. Fenical, "Species-specific secondary metabolite production in marine actinomycetes of the genus *Salinispora*," *Applied and Environmental Microbiology*, vol. 73, no. 4, pp. 1146–1152, 2007.

[37] J. F. Martin, "Clusters of genes for the biosynthesis of antibiotics: regulatory genes and overproduction of pharmaceuticals," *Journal of Industrial Microbiology*, vol. 9, no. 2, pp. 73–90, 1992.

[38] A. Hornung, M. Bertazzo, A. Dziarnowski et al., "A genomic screening approach to the structure-guided identification of drug candidates from natural sources," *ChemBioChem*, vol. 8, no. 7, pp. 757–766, 2007.

[39] T. Toyomasu, A. Kaneko, T. Tokiwano et al., "Biosynthetic gene-based secondary metabolite screening: a new diterpene, methyl phomopsenonate, from the fungus *Phomopsis amygdali*," *Journal of Organic Chemistry*, vol. 74, no. 4, pp. 1541–1548, 2009.

[40] E. Zazopoulos, K. Huang, A. Staffa et al., "A genomics-guided approach for discovering and expressing cryptic metabolic pathways," *Nature Biotechnology*, vol. 21, no. 2, pp. 187–190, 2003.

[41] L. C. Foulston and M. J. Bibb, "Microbisporicin gene cluster reveals unusual features of lantibiotic biosynthesis in actinomycetes," *Proceedings of the National Academy of Sciences of the United States of America*, vol. 107, no. 30, pp. 13461–13466, 2010.

[42] I. Borodina, J. Siebring, J. Zhang et al., "Antibiotic overproduction in *Streptomyces coelicolor* A3(2) mediated by phosphofructokinase deletion," *Journal of Biological Chemistry*, vol. 283, no. 37, pp. 25186–25199, 2008.

[43] I. Borodina, P. Krabben, and J. Nielsen, "Genome-scale analysis of *Streptomyces coelicolor* A3(2) metabolism," *Genome Research*, vol. 15, no. 6, pp. 820–829, 2005.

[44] M. Castro-Melchor, S. Charaniya, G. Karypis, E. Takano, and W. S. Hu, "Genome-wide inference of regulatory networks in *Streptomyces coelicolor*," *BMC Genomics*, vol. 11, no. 1, article 578, 2010.

[45] S. G. van Lanen and B. Shen, "Microbial genomics for the improvement of natural product discovery," *Current Opinion in Microbiology*, vol. 9, no. 3, pp. 252–260, 2006.

[46] H. Gross, "Strategies to unravel the function of orphan biosynthesis pathways: recent examples and future prospects," *Applied Microbiology and Biotechnology*, vol. 75, no. 2, pp. 267–277, 2007.

[47] J. B. McAlpine, "Advances in the understanding and use of the genomic base of microbial secondary metabolite biosynthesis for the discovery of new natural products," *Journal of Natural Products*, vol. 72, no. 3, pp. 566–572, 2009.

[48] H. Gross, "Genomic mining—a concept for the discovery of new bioactive natural products," *Current Opinion in Drug Discovery and Development*, vol. 12, no. 2, pp. 207–219, 2009.

[49] J. E. Velásquez and W. A. van der Donk, "Genome mining for ribosomally synthesized natural products," *Current Opinion in Chemical Biology*, 2010.

[50] A. L. Lane and B. S. Moore, "A sea of biosynthesis: marine natural products meet the molecular age," *Natural Product Reports*, vol. 28, no. 2, pp. 411–428, 2011.

[51] J. E. Velásquez and W. A. van der Donk, "Genome mining for ribosomally synthesized natural products," *Current Opinion in Chemical Biology*, vol. 15, pp. 11–12, 2010.

[52] A. S. Eustáquio, S. J. Nam, K. Penn et al., "The discovery of salinosporamide K from the marine bacterium "*Salinispora pacifica*" by Genome mining gives insight into pathway evolution," *ChemBioChem*, vol. 12, no. 1, pp. 61–64, 2011.

[53] S. Lautru, R. J. Deeth, L. M. Bailey, and G. L. Challis, "Discovery of a new peptide natural product by *Streptomyces coelicolor* genome mining," *Nature Chemical Biology*, vol. 1, no. 5, pp. 265–269, 2005.

[54] C. Corre, L. Song, S. O'Rourke, K. F. Chater, and G. L. Challis, "2-Alkyl-4-hydroxymethylfuran-3-carboxylic acids, antibiotic production inducers discovered by *Streptomyces coelicolor* genome mining," *Proceedings of the National Academy of Sciences of the United States of America*, vol. 105, no. 45, pp. 17510–17515, 2008.

[55] L. C. Blasiak and J. Clardy, "Discovery of 3-formyl-tyrosine metabolites from *Pseudoalteromonas tunicata* through heterologous expression," *Journal of the American Chemical Society*, vol. 132, no. 3, pp. 926–927, 2010.

[56] S. Bergmann, J. Schümann, K. Scherlach, C. Lange, A. A. Brakhage, and C. Hertweck, "Genomics-driven discovery of PKS-NRPS hybrid metabolites from *Aspergillus nidulans*," *Nature Chemical Biology*, vol. 3, no. 4, pp. 213–217, 2007.

[57] M. Gottelt, S. Kol, J. P. Gomez-Escribano, M. Bibb, and E. Takano, "Deletion of a regulatory gene within the cpk gene cluster reveals novel antibacterial activity in *Streptomyces coelicolor* A3(2)," *Microbiology*, vol. 156, no. 8, pp. 2343–2353, 2010.

[58] H. Gross, V. O. Stockwell, M. D. Henkels, B. Nowak-Thompson, J. E. Loper, and W. H. Gerwick, "The genomisotopic approach: a systematic method to isolate products of orphan biosynthetic gene clusters," *Chemistry and Biology*, vol. 14, no. 1, pp. 53–63, 2007.

[59] A. L. McClerren, L. E. Cooper, C. Quan, P. P. Thomas, N. L. Kelleher, and W. A. van der Donk, "Discovery and in vitro biosynthesis of haloduracin, a two-component lantibiotic," *Proceedings of the National Academy of Sciences of the United States of America*, vol. 103, no. 46, pp. 17243–17248, 2006.

[60] P. D. Schloss and J. Handelsman, "Metagenomics for studying unculturable microorganisms: cutting the Gordian knot," *Genome Biology*, vol. 6, no. 8, article 229, 2005.

[61] S. F. Brady, L. Simmons, J. H. Kim, and E. W. Schmidt, "Metagenomic approaches to natural products from free-living and symbiotic organisms," *Natural Product Reports*, vol. 26, no. 11, pp. 1488–1503, 2009.

[62] A. Uria and J. Piel, "Cultivation-independent approaches to investigate the chemistry of marine symbiotic bacteria," *Phytochemistry Reviews*, vol. 8, no. 2, pp. 401–414, 2009.

[63] C. Gurgui and J. Piel, "Metagenomic approaches to identify and isolate bioactive natural products from microbiota of marine sponges," *Methods in Molecular Biology*, vol. 668, pp. 247–264, 2010.

[64] J. C. Venter, K. Remington, J. F. Heidelberg et al., "Environmental genome shotgun sequencing of the Sargasso Sea," *Science*, vol. 304, no. 5667, pp. 66–74, 2004.

[65] J. Piel, D. Hui, G. Wen et al., "Antitumor polyketide biosynthesis by an uncultivated bacterial symbiont of the marine sponge *Theonella swinhoei*," *Proceedings of the National Academy of Sciences of the United States of America*, vol. 101, no. 46, pp. 16222–16227, 2004.

[66] S. Sudek, N. B. Lopanik, L. E. Waggoner et al., "Identification of the putative bryostatin polyketide synthase gene cluster from "*Candidatus Endobugula sertula*", the uncultivated microbial symbiont of the marine bryozoan *Bugula neritina*," *Journal of Natural Products*, vol. 70, no. 1, pp. 67–74, 2007.

[67] K. M. Fisch, C. Gurgui, N. Heycke et al., "Polyketide assembly lines of uncultivated sponge symbionts from structure-based gene targeting," *Nature Chemical Biology*, vol. 5, no. 7, pp. 494–501, 2009.

[68] H. Zhang, B. A. Boghigian, J. Armando, and B. A. Pfeifer, "Methods and options for the heterologous production of complex natural products," *Natural Product Reports*, vol. 28, no. 1, pp. 125–151, 2011.

[69] F. O. Glöckner and I. Joint, "Marine microbial genomics in Europe: current status and perspectives: minireview," *Microbial Biotechnology*, vol. 3, no. 5, pp. 523–530, 2010.

[70] A. Starcevic, J. Zucko, J. Simunkovic, P. F. Long, J. Cullum, and D. Hranueli, "ClustScan: an integrated program package for the semi-automatic annotation of modular biosynthetic gene

clusters and in silico prediction of novel chemical structures," *Nucleic Acids Research*, vol. 36, no. 21, pp. 6882–6892, 2008.

[71] M. H. T. Li, P. M. U. Ung, J. Zajkowski, S. Garneau-Tsodikova, and D. H. Sherman, "Automated genome mining for natural products," *BMC Bioinformatics*, vol. 10, article 185, 2009.

[72] S. Anand, M. V. R. Prasad, G. Yadav et al., "SBSPKS: structure based sequence analysis of polyketide synthases," *Nucleic Acids Research*, vol. 38, no. 2, pp. W487–W496, 2010.

[73] E. Esquenazi, C. Coates, L. Simmons, D. Gonzalez, W. H. Gerwick, and P. C. Dorrestein, "Visualizing the spatial distribution of secondary metabolites produced by marine cyanobacteria and sponges via MALDI-TOF imaging," *Molecular BioSystems*, vol. 4, no. 6, pp. 562–570, 2008.

[74] S. B. Bumpus, B. S. Evans, P. M. Thomas, I. Ntai, and N. L. Kelleher, "A proteomics approach to discovering natural products and their biosynthetic pathways," *Nature Biotechnology*, vol. 27, no. 10, pp. 951–956, 2009.

[75] A. Siegl, J. Kamke, T. Hochmuth et al., "Single-cell genomics reveals the lifestyle of *Poribacteria*, a candidate phylum symbiotically associated with marine sponges," *ISME Journal*, vol. 5, no. 1, pp. 61–70, 2011.

Hindawi Publishing Corporation
Evidence-Based Complementary and Alternative Medicine
Volume 2011, Article ID 487543, 8 pages
doi:10.1155/2011/487543

Research Article

Impact of Intensive Land-Based Fish Culture in Qingdao, China, on the Bacterial Communities in Surrounding Marine Waters and Sediments

Qiufen Li,[1] Yan Zhang,[1] David Juck,[2] Nathalie Fortin,[2] and Charles W. Greer[2]

[1] *Yellow Sea Fishery Research Institute, Chinese Academy of Fishery Science, 106 Nanjing Road, Shandong, Qingdao 266071, China*
[2] *Biotechnology Research Institute, National Research Council of Canada, 6100 Royalmount Avenue, Montreal, Québec, Canada H4P 2R2*

Correspondence should be addressed to Qiufen Li, liqf@ysfri.ac.cn

Received 15 January 2011; Revised 26 May 2011; Accepted 30 June 2011

The impact of intensive land-based fish culture in Qingdao, China, on the bacterial communities in surrounding marine environment was analyzed. Culture-based studies showed that the highest counts of heterotrophic, ammonium-oxidizing, nitrifying, and nitrate-reducing bacteria were found in fish ponds and the effluent channel, with lower counts in the adjacent marine area and the lowest counts in the samples taken from 500 m off the effluent channel. Denaturing gradient gel electrophoresis (DGGE) analysis was used to assess total bacterial diversity. Fewer bands were observed from the samples taken from near the effluent channel compared with more distant sediment samples, suggesting that excess nutrients from the aquaculture facility may be reducing the diversity of bacterial communities in nearby sediments. Phylogenetic analysis of the sequenced DGGE bands indicated that the bacteria community of fish-culture-associated environments was mainly composed of Flavobacteriaceae, gamma- and deltaproteobacteria, including genera *Gelidibacter, Psychroserpen, Lacinutrix,* and *Croceimarina*.

1. Introduction

Land-based intensive fish culture is developing at a high speed in China and has brought about the fourth mariculture fervor in recent years. While it is worth paying attention to the discharge of large quantity of untreated effluent, La Rosa and coworkers [1] have reported that in oligotrophic marine environments, addition of various nutrients through feed, detritus, and fecal matter can induce changes in the macro-, meio-, and micro-fauna community structure in the water column and sediment. Moreover, it has been proved that intensive fish husbandry often lead to environmental eutrophication, foreign species, and disease introduction [2, 3]. In 2006, intensive fish farming in the Philippines was demonstrated to be detrimental to the reef-building coral *Pocillopora damicornis*, since many biological aspects of coral were impaired by exposure to effluent from fish farms [4].

Bacterial communities play important roles in nutrient circulation and are sensitive to changes of environment. For example, accumulation of large amounts of organic matters can induce persistent alterations in bacterial assemblage [5]. Comprehensive characterization of microbial populations in regions adjacent to aquaculture operations is important for the prevention and treatment of various diseases of farmed fish and for the maintenance of water quality [6]. However, traditional culture-dependent approaches are time-consuming and costly, and the data cannot represent actual situations, as ~99.99% of the microorganisms in the natural environment are currently uncultivable [7]. Therefore, the composition of bacteria in aquaculture ecosystems is very poorly understood [8]. To our best knowledge, by far, there are few reports on the composition and structure of bacteria community associated with land-based intensive fish culture and the impact of such fish-culture performance to the nearby environment.

In recent years, many molecular biological approaches have been successfully applied to microbial ecology analysis, for example, denaturing gradient gel electrophoresis (DGGE), which was originally developed for analyzing gene mutation based on the sequence difference of PCR products by electrophoresis in the medicine research field. It was first applied by Muyzer et al. [9] to study the diversity of microbes

in 1993. Since then, DGGE has been widely used in microbial diversity analyses of different ecoenvironments, such as explosive-polluted soil [10], estuary [11], scallop early stage environment [12], shrimp guts [13], and the offshore cage fish farms [6]. However, it has never been utilized to examine the microbes in land-based fish-culture-associated environment. In this study, bacterial community composition of the environment associated with intensive land-based marine fish culture was investigated through culture-dependent and culture-independent approaches, with the aim to characterize the bacteria compositions of associated environment and to evaluate the effect of intensive fish culture on the bacteria community in nearby sea areas.

2. Materials and Methods

2.1. Description of Sites and Sampling. The intensive land-based fish-culturing farm is located in the suburb of Qingdao, China. It is a newly developed industry and mainly raises turbot (*Scophthalmus maximus*) and Japanese flounder (*Paralichthys olivaceus*) with natural and underground sea water. Most of the untreated effluent is discharged into the nearby Aoshan Bay. The samples were collected from the fish farming ponds, effluent channel, polluted sea areas 10 m off the effluent channel end, and unpolluted sea area 500 m off the channel end. Triplicate samples were collected with sterilized containers from each site, each including 2 L of sea water and 50 g of sediment, and were transferred to the laboratory on ice in time. Subsamples were then treated for bacteria cultivation. The remaining samples were stored at −20°C for molecular analysis.

2.2. Detection of Bacteria Groups with Different Physiological Functions. The sediment and water samples were serially diluted 10-fold with sterilized sea water, and 0.1 mL aliquots of the dilution were spread onto Zobell's 2216E medium for heterotrophic bacteria and other appropriate media for ammonia oxidizing bacteria and nitrifying bacteria [8]. Colonies on the plates were counted after 2-3 days incubation at 28°C.

Sulfate and nitrate reducing bacteria were detected with "Most Probable Number" method as described previously [6, 14]. Briefly, aliquots of 1 mL series dilution were added into series 10 mL of media. Triplicate tubes were prepared for each dilution. Cultures were detected after 7 days of incubation at 28°C for nitrate reducing bacteria and 14 days for sulfate reducing bacteria. The population size of bacteria was calculated by referring to the table, according to the tubes with positive outcomes at each dilution. The three counting results for each sampling site were averaged, and the standard deviations (STDEV) were shown.

2.3. Extraction of Genomic DNA of Bacteria. Genomic DNA was extracted using the chemical-enzymatic lyses protocol [15] with a few modifications. Briefly, the membrane for water sample or 10 g of each sediment sample with 5 mL of sterilized distilled water were vortexed at maximum speed for 5 min, then 1 mL lysozyme (100 mg/mL) and 4 mL DNA extraction buffer (100 mM Tris-HCl, 100 mM EDTA, 100 mM Na_3PO_4, 1.5 M NaCl, pH 8.0) were added to the tubes. The samples were incubated on shaking inoculators for 1 h at 30°C, and another 1 h at 37°C after 20 μL proteinase K (100 mg/mL) was added, followed by 5~15 min at 85°C with 100 μL 20% SDS. Subsequently, samples were then centrifuged at 4,100 g for 15 min. One-second volume of 7.5 M ammonium acetate was added to the supernatants, followed by incubation on ice for 15 min. Thereafter, tubes were centrifuged at 4°C and 9, 400 g for 15 min, and the supernatants were treated with cold 2-propanol overnight at −20°C. Pellets were raised with 70% and 95% ethanol, respectively. DNA was finally resuspended in sterilized distilled water. The crude DNA extract was purified with polyvinylpolypyrrolidone (PVPP) and sephacryl S-400 spin columns as described by Elliott [2] to remove PCR inhibitors, such as humid acid. Untreated and treated DNA were compared by electrophoresis 0.7% agarose gel at 60 V for 2 h and visualized on a MultiImage light Cabinet (Alpha Innotech Corporation, France).

2.4. Amplification of 16S rDNA. The bacterial universal primers, U341 and U758, were used to amplify a 418 bp fragment corresponding to position 341 to 758 bp of *Escherichia coli* 16S rDNA sequence [9]. To stabilize the melting behavior of the amplified fragments in the DGGE reaction, the forward primer contained a GC-clamp [10]. Sequences of the U341 and U758 were as follows: U341: 5-GCGGGCGGGGCGGGGGGCACGGGGGGCGCCGGC-GGGCGGGGCGGGGGCCTACGGGAGGCAGCAG-3′; U758: 5′-CTACCAGG GTATCTAATCC-3′. For optimum DGGE result, different PCR conditions were tested. The optimum PCR reaction was carried out in a 50 μL volume, including 5 μL of genomic DNA as the template, 5 μL 10 × PCR buffer, 25 pmol of each primer, 200 μM of each dNTP, 1 mM $MgCl_2$, and 2.5 units of Taq polymerase (Amersham Biosciences, Piscataway, USA). Before adding Taq polymerase, samples were denatured at 96°C for 5 min, followed by a touchdown PCR protocol [15] in which the annealing temperature was set to 65°C and decreased by 1°C every cycle until it reached 55°C. Each cycle included denaturation at 94°C for 1 min, anneal for 1 min, and extension at 72°C for 3 min. Twenty additional cycles were carried out with annealing at 55°C. Finally, 5 μL of each PCR product was loaded onto a 1.4% agarose gel with a 100 bp DNA ladder (MBI Fermentas, Amherst, USA). Bands were visualized with SYBR safe dye in the MultiImage light cabinet.

2.5. DGGE Analysis of Amplified DNA. DGGE was performed on the Decode Universal Mutation Detection System (Bio-Rad Inc., Mississauga, Canada) as described by the manufacturer. The separation was carried out on an 8% (W/V) acrylamide gel in 1X TAE (40 mM Tris-acetate, pH 8.0; 1 mM Na_2DETA) containing a linear gradient from 25% to 65% denaturant (100% denaturant consisted of 7 M urea and 40% formamide) as described by Muyzer et al. [9]. To avoid disturbance of the gradient during comb

insertion, a 6% acrylamide-N,N-methylene: bisacrylamide (37.5 : 1) stacking gel without denaturant was added [15]. Each purified PCR product (about 600 ng) with 15 μL of 2X loading buffer was applied to one lane of the denaturing gradient gel. The electrophoresis was run for 16 h at 80 V, then stained in 1 : 10000 dilution of Vistra Green staining solution (Amersham Pharmacia Biosciences Inc., Baie-d'Urfe, Canada) for 30 min, and visualized on a FluorImager system (Model 595, Amersham) with a 488 nm excitation filter and a 530 nm emission filter.

To analyze the bacterial diversity, the Shannon index of each sample was calculated according to the strength (shown as the absorbance) and position of the DGGE bands in every lane, and (1) was used

$$H = -\sum\left(\frac{n_i}{N}\right)\lg\left(\frac{n_i}{N}\right). \quad (1)$$

In (1), n_i means the area of absorbance peak of each band and N means the total area of absorbance peak of all bands in a lane.

Dendrogram analysis of DGGE band patterns was performed using the Dendron 2.2 software package (Soll-tech Inc., Oakdale, USA). The unweighted pair group method, based on a similarity matrix calculated from the presence/absence of DGGE bands, was used to analyze the similarity between the samples.

2.6. Reamplification and Sequencing of DGGE Bands. From the gels, 32 specific DGGE bands were excised with a sterile surgical scalpel. DNA from these bands was eluted by incubating overnight at 37°C in sterilized deionized water [16] and then purified with QIA quick PCR purification kit (Qiagen, Mississauga, Canada). The obtained DNA was used as template for reamplification. The standard PCR was performed in a 50 μL reaction volume, containing 1 μL DNA, 1 μL U341 primer (25 pmoL), 1 μL U758 primer (25 pmoL), 0.625 μL BSA (10 mg/mL), 5 μL 10X PCR buffer, 8.0 μL $MgCl_2$(100 mg), 8.0 μL dNTPs (1.25 mM), 24.9 μL sterile deionized water, and 0.5 μL Taq polymerase which was added separately when the temperature reached 80°C after initial denaturization for 5 min at 95°C. The PCR included 25 cycles of 1 min at 94°C, 1 min at 64°C, and 1 min at 72°C. In order to get single bands for clean sequencing results, the quantity of template, annealing temperature, and cycle number were adjusted according to the result of standard PCR protocol for individual samples. Amplicants showing single bands in a 1.4% agarose gel were purified with GFX Purification Kit (Amersham, Piscataway, USA) and quantified by loading 1 μL onto a 1.4% agarose gel in comparison with dilution series of 100 bp DNA ladder. Samples (20 μL, 2 ng/μL) were sent to Laval University for sequencing.

2.7. Phylogenetic Analysis of Bacterial Communities. The obtained sequences were manually corrected by comparing the consensus of forward and reverse sequences with software Macvector 8.1 (MacVector Inc., Cary, USA). The length of the corrected sequences varied in the range from 352 to 387 bp. The sequences were initially aligned using the Clustal W program, then they were analyzed referring to the closely related sequences retrieved from the NCBI website: http://blast.ncbi.nlm.nih.gov/Blast.cgi?PROGRAM=blastn. Identical sequences with the same migration on DGGE were treated as one. Further manual amendments to the alignment were performed using the multicluster function.

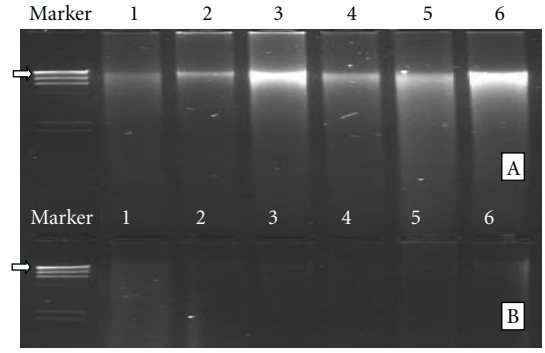

Figure 1: Electrophoresis of genomic DNA isolated from bacterial community in water and sediments of fish-culture-associated environments in Qingdao, China. Showing PVPP and Sephacryl is effective to purify the crude DNA extracts. (A) purified DNA extracts with PVPP and Sephacryl; (B) crude DNA before purification. Marker: λDNA digested with HindIII (arrow indicates a 23.1 kb fragment), 1: water from the fish culture pond; 2: water in effluent channel; 3: water from polluted sea area; 4: sediment from polluted sea area; 5: water from unpolluted sea area; 6: sediment from unpolluted sea area.

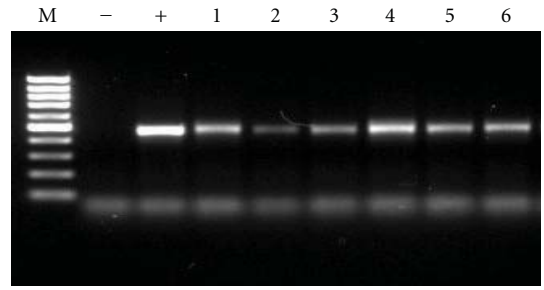

Figure 2: Gel electrophoresis of PCR-amplified 16S rDNA of genomic DNA, indicating the target DNA fragment was successfully amplified in the 6 samples. M: 100 bp DNA ladder; −: negative control; +: positive control; 1; water from the fish-culture pond; 2: water in effluent channel; 3: water from polluted sea area; 4: sediment from polluted sea area; 5: water from unpolluted sea area; 6: sediment from unpolluted sea area.

3. Results

3.1. Number of Bacteria Detected with the Culture-Dependent Method. Bacteria from 5 important physiologically defined groups were found in all sediment and water samples. As shown in Table 1, the counts for total heterotrophic bacteria in the fish pond and effluent channel were the highest (1.25 to 1.29 $\times$ 10^5 CFU/g), followed by polluted sea areas accepting fish culture effluent (1.23 to 4.7 $\times$ 10^4 CFU/g), and that of unpolluted sea areas 500 m off the

Table 1: Population size of various bacteria groups in sediment and water samples.

Sampling site	Total no. of heterotrophic bacteria (CFU/g or mL)	No. of ammonium-oxidizing bacteria (CFU/g or mL)	No. of nitrifying bacteria (CFU/g or mL)	No. of sulfate-reducing bacteria (cells/g or mL)	No. of nitrate-reducing bacteria (cells/g or mL)
Sediment of polluted sea area	$6.70 \pm 0.05 \times 10^4$	$1.90 \pm 0.01 \times 10^3$	$9.80 \pm 0.03 \times 10^3$	$4.60 \pm 0.04 \times 10^2$	$1.20 \pm 0.10 \times 10^3$
Sediment of unpolluted sea area	$4.30 \pm 0.10 \times 10^3$	$1.50 \pm 0.12 \times 10^3$	$4.60 \pm 0.14 \times 10^3$	$2.30 \pm 0.20 \times 10^1$	$2.10 \pm 0.03 \times 10^3$
Water of fish pond	$1.25 \pm 0.13 \times 10^5$	$7.50 \pm 0.01 \times 10^2$	$4.40 \pm 0.17 \times 10^4$	<3	$4.30 \pm 0.20 \times 10^3$
Water of effluent channel	$1.29 \pm 0.32 \times 10^5$	$2.10 \pm 0.05 \times 10^2$	$4.90 \pm 0.06 \times 10^3$	<3	$1.50 \pm 0.09 \times 10^4$
Water of polluted sea area	$1.23 \pm 0.15 \times 10^4$	$6.20 \pm 0.08 \times 10^2$	$4.60 \pm 0.09 \times 10^3$	$7.50 \pm 0.21 \times 10^1$	$1.10 \pm 0.05 \times 10^3$
Water of unpolluted sea area	$1.60 \pm 0.08 \times 10^3$	$4.00 \pm 0.20 \times 10^1$	$1.00 \pm 0.05 \times 10^2$	<3	$9.00 \pm 0.15 \times 10^2$

effluent channel was the lowest (1.6 to 4.3×10^3 CFU/g). Bacteria numbers in sediment were all higher than those of related water environments. The numbers of ammonium-oxidizing bacteria, nitrifying bacteria, and nitrate-reducing bacteria showed similar distribution trend to heterotrophic bacteria, varied from 4.0×10^1 cells/g to 1.5×10^5 cells/g, suggesting active nitrogen circulations in the polluted areas. The numbers of sulfate-reducing bacteria, however, were only 2.3×10^1 cells/g to 4.6×10^2 cells/g in the sediments and $3 \sim 7.5 \times 10^1$ cells/g in the waters, significantly lower than those of other bacteria.

3.2. Genomic DNA of Bacteria Isolated from Fish-Culture-Associated Environments. The size of obtained Genomic bacterial DNA fragment was about 23 kb. The extracts became colorless from brown, and their electrophoresis bands became much clearer after purification with PVPP and Sephacryl (S-400) columns (Figures 1(A) and 1(B)), indicating that PVPP and Sephacryl purification were effective in removing inhibiting factors in the crude extracts.

3.3. Amplification of 16S rDNA. A 417 bp fragment of 16S rRNA gene was amplified with primers GC U341 and U758. The touch-down protocol insured single-specific bands. The yield was reasonably high, as the bright bands shown in Figure 2.

3.4. DGGE Band Profiles of Samples from Various Environments. DGGE analysis of PCR products produced identical patterns, with more than 20 bands for each sample, indicating a high diversity of bacteria community. As shown in Figure 3, band patterns of sediments showed higher diversity and more homogenized distribution than that of waters. The bacterial diversity in water reduced with the increase of the distance from fish ponds. This can be demonstrated by their Shannon index, as shown in Table 2. The significance of

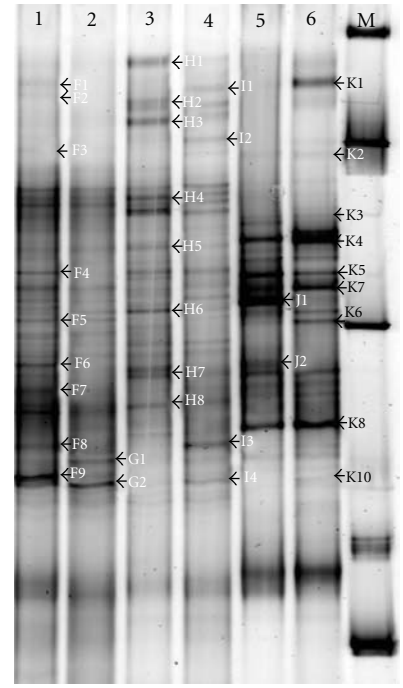

Figure 3: DGGE profiles of 16S rDNA fragments of bacterial communities in various water and sediment samples, showed the high diversity in fish culture associated environment and the difference between samples. 1: water from polluted sea area; 2: water from unpolluted sea area; 3: sediment from polluted sea area; 4: sediment from unpolluted sea area; 5: water from the fish culture pond; 6: water from effluent channel; M: Marker.

dominant bands in these samples also differed greatly, with water from fish ponds > water from effluent channel > water from polluted sea area > water from unpolluted sea area > sediment of polluted sea area > sediment of unpolluted sea area, suggesting that fish culture could lead to a reduction of

Table 2: The Shannon index of the bacteria in the water and sediment samples shown by DGGE bands.

Sample no.	1	2	3	4	5	6
Shannon index	1.25	1.27	1.37	1.46	1.15	1.19

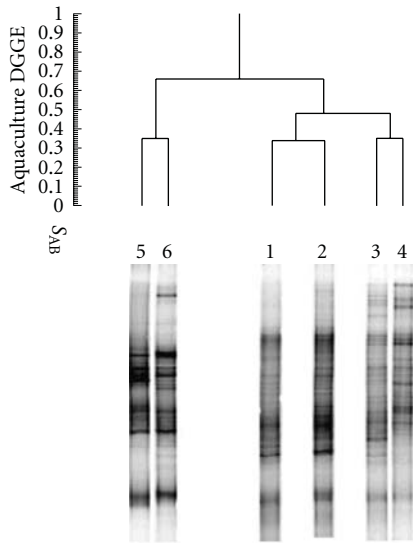

Figure 4: UPGMA dendron similarity assessment of the DGGE profile illustrated in Figure 3 showed the similarity between samples. 1: water from polluted sea area; 2: water from unpolluted sea area; 3: sediment from polluted sea area; 4: sediment from unpolluted sea area; 5: water from the fish-culture pond; 6: water from effluent channel.

bacterial diversity and some species could become absolutely dominant.

Dendrogram of the DGGE band patterns reflected the correlation/similarity of different DGGE lanes. As shown in Figure 4, the two sediment samples from polluted and unpolluted sea area were clustered into one group (S_{AB}, 0.67) and were clustered into one big group with the two water samples from the same sea area (S_{AB}, 0.52). However, the two water samples from fish ponds and effluent channel were clustered into the other group (S_{AB}, 0.65). Meanwhile, the similarity coefficient (S_{AB}) of samples from fish culture pond and samples from sea area was only 0.34, suggesting that composition of bacterial communities in the same habitat was more similar.

3.5. Phylogenetic Analysis of Sequenced DGGE Bands. In total, 32 bands in DGGE gel were selected and reamplified with the primers U341 and U758. Among them, 19 produced clean sequencing results. The closest matches of these sequences were then identified by NCBI BLAST analysis. Results were summarized in Table 3. The similarity of these sequences compared to references in database ranged from 93% to 100%.

Phylogenetic analysis of the sequences revealed the bacterial community structure of the land-based fish-culture-associated environments. In general, the communities were composed of Flavobacteria, Gammaproteobacteria and Deltaproteobacteria. Among them, Flavobacteria showed strong dominance, and it covered genera *Gelidibacter, Psychroserpen, Lacinutrix, Croceimarina, Actibacter, Maribacter, Winogradskyella, Zobellia, Formosa,* and *Polaribacter.* The two proteobacteria groups ranted a small part of the total population. Some of these species had not been cultured independently, such as I4 and K7. For individual environment, *Polaribacter* sp. (K3, K4), *Marinobacter* sp. (K5), thiotrophic endosymbiont of *Idas* sp. (J1), and *Pseudoalteromonas* sp. like bacteria (K8) were dominant in fish culture effluent and polluted sea water samples. In addition, *Formosa* sp. (K1) was also found to be significantly dominant in the polluted sea water. On the other hand, dominant bacteria in sediment samples of polluted sea area were not as significant as that in water samples. These dominant bacteria in sediment were composed of *Gelidibacter* sp. (H1), *Lacinutrix copepodicola* (H3), *Croceimarina litoralis* (H4), and *Maribacter polysiphoniae* (H6). The unpolluted sea area contained almost all bacteria species in the above-mentioned environments and distributed evener than them. At the same time, some unique species, such as *Winogradskyella thalassocola* (I2), *Desulfuromonas* sp. (I3), and uncultured delta proteobacterium (I4), presented in the unpolluted sea area. The phylogenetic relationship of the above-mentioned bacteria is shown in Figure 5.

4. Discussion

The feed conservation ratio of intensively cultured fish was reported to be 71.2–74.9%, and the faeces production ratio was 9.6–3.1%. These implied that 133 kg of nitrogen and 28.8 kg of phosphorous would be discharged into the environment for 1 ton of fish [17]. Discharge of detritus and fecal matters produced due to the addition of feed, to the oligotrophic marine environment can induce changes in the community structures of macro-, meio- and microfauna in the water columns and sediments [1], as well as the nutrient level, physical, and chemical conditions. The five physiologically defined bacteria groups chosen in this study have close relationship with the content of organic matter, levels of dissolved oxygen, and nitrogen and sulfur circulation activities in their environment. The results of our study showed that the counts for heterotrophic bacteria gradually reduced with the increase of distance from the fish ponds, suggesting that fish culture effluent could introduce abundant organic matters and heterotrophic bacteria to the sea area accepting it. The high numbers of ammonium-oxidizing bacteria, nitrifying bacteria, and nitrate-reducing bacteria in the effluent water and polluted sea area indicated active nitrogen circulation in these areas. This could be attributed to the abundant nitrogen brought forth by fish-culture effluent with fish metabolic excreta (feces, etc.) and waste feeds.

Yoza et al. [6] observed similar DGGE gradient profiles for a newly developed cage fish-culture sediment sample and a 300 m upcurrent control sample. However, they still expected that sufficient nutriment addition would impact the sediment environment. In our experiments, less diversity and

Table 3: Closest BLAST match for 16S rRNA genes of bacteria in fish-culture-associated environments.

Sampling sites	No. of DG E bands	Sizes of the DNA (bp)	Closest relative	Accession no. of BLAST closest match	% identity	Classification of strains
Sediment of polluted sea area	H1	408	*Gelidibacter* sp.	EF108219	99%	Flavobacteriaceae
	H2	415	*Psychroserpens mesophilus*	DQ001321	98%	Flavobacteriaceae
	H3	410	*Lacinutrix copepodicola*	AB261015	98%	Flavobacteriaceae
	H4	412	*Croceimarina litoralis*	EF108214	96%	Flavobacteriaceae
	H5	407	*Actibacter sediminis*	EF670651	100%	Flavobacteriaceae
	H6	415	*Maribacter polysiphoniae*	AM497875	98%	Flavobacteriaceae
Sediment of unpolluted sea area	I1	408	*Flavobacteriaceae bacterium*	EF527870	97%	Flavobacteriaceae
	I2	409	*Winogradskyella thalassocola*	AY771720	98%	Flavobacteriaceae
	I3	399	*Desulfuromonas* sp.	AY177801	97%	δ-proteobacterium
	I4	412	Uncultured deltaproteo-bacterium	DQ351798	99%	δ-proteobacterium
Water of fish ponds	J1	391	Thiotrophic endosymbiont of *Idas* sp.	AM402957	93%	Bacteria
	J2	410	*Zobellia laminariae*	AB121975	98%	Flavobacteriaceae
Water of effluent channel	K1	402	*Formosa* sp.	AY612758	97%	Flavobacteriaceae
	K2	405	*Winogradskyella thalassocola*	AY771720	97%	Flavobacteriaceae
	K3	397	*Polaribacter* sp.	AF493675	98%	Flavobacteriaceae
	K4	400	*Polaribacter dokdonensis*	DQ481463	98%	Flavobacteriaceae
	K5	411	*Marinobacter* sp.	DQ530471	98%	γ-proteobacteria
	K7	407	Uncultured *F. bacterium*	AM279213	98%	Flavobacteriaceae
	K8	409	*Pseudoalteromonas* sp.	EF673280	95%	γ-proteobacteria

evenness in species distribution was observed from sediment samples in polluted sea areas than that in unpolluted sea areas, with Shannon index 1.37 and 1.46, respectively. These observations proposed that intensive land-based fish-culture effluent have produced significant impact on the bacteria community, leading to reduction in bacterial diversity. Furthermore, both of the studies were carried out shortly after the development of fish culture. With a longer culturing time, it is reasonable to believe that the impact would be much more significant. Asami et al. [18] also reported that intensive shellfish aquaculture accelerated sulfur cycle in the beneath coastal marine sediment [17]. Moreover, the bacterial community was decided by the habitat rather than by its geographic location [19]. Namely, the impact of fish-culture effluent to the bacterial communities may occur by changing the chemical and physical conditions of their habitat, besides importing bacteria from effluent.

One of the dominant phylotype (K8) found in the fish culture effluent and polluted sea water area belonged to the genus, *Pseudoalteromonas* of Gammaproteobacteria. This genus had a widespread distribution in the marine environment [20]. It was reported that *Pseudoalteromonas* had both deleterious and beneficial effects on marine eukaryotes [21–23]. The dominant phylotype (I3) in the sediment of unpolluted sea area was similar to *Desulfuromonas sp.*, a sulfate-reducing bacterium in *Delta*-proteobacteria family. It was not surprising to find sulfate reducers in the marine sediment, since sulfate is a favored terminal electron acceptor in this environment [24], though the number of bacteria detected was very low through culture-dependent methods in this paper. Genus *Formosa* (K1) was found both in the effluent channel water and native sea water, and it was a heterotrophic, gram-negative, motile, aerobic, and brown alga-degrading bacterial group [25, 26], indicating its commitment to the marine environment.

Many of the main bacteria groups, such as *Aeromonadaceae, Pseudomonadaceae,* and *Vibrionaceae* detected as pathogens of farmed fish with traditional culture-depended methods, were not detected by molecular methods in this paper, suggesting that pathogenic bacteria might not be dominant in the whole community. So, the bacterial composition is still far more complex than we could imagine. Further study is necessary to determine whether and how long the aquaculture could change the composition and destroy balance of bacterial communities in its nearby sea area.

5. Conclusion

In the present paper, the impact of intensive land-based fish culture in Qingdao, China, on the bacterial communities in surrounding marine environment was analyzed through culture-based and molecular-based approaches. The result of culture-based studies showed that counts of heterotrophic,

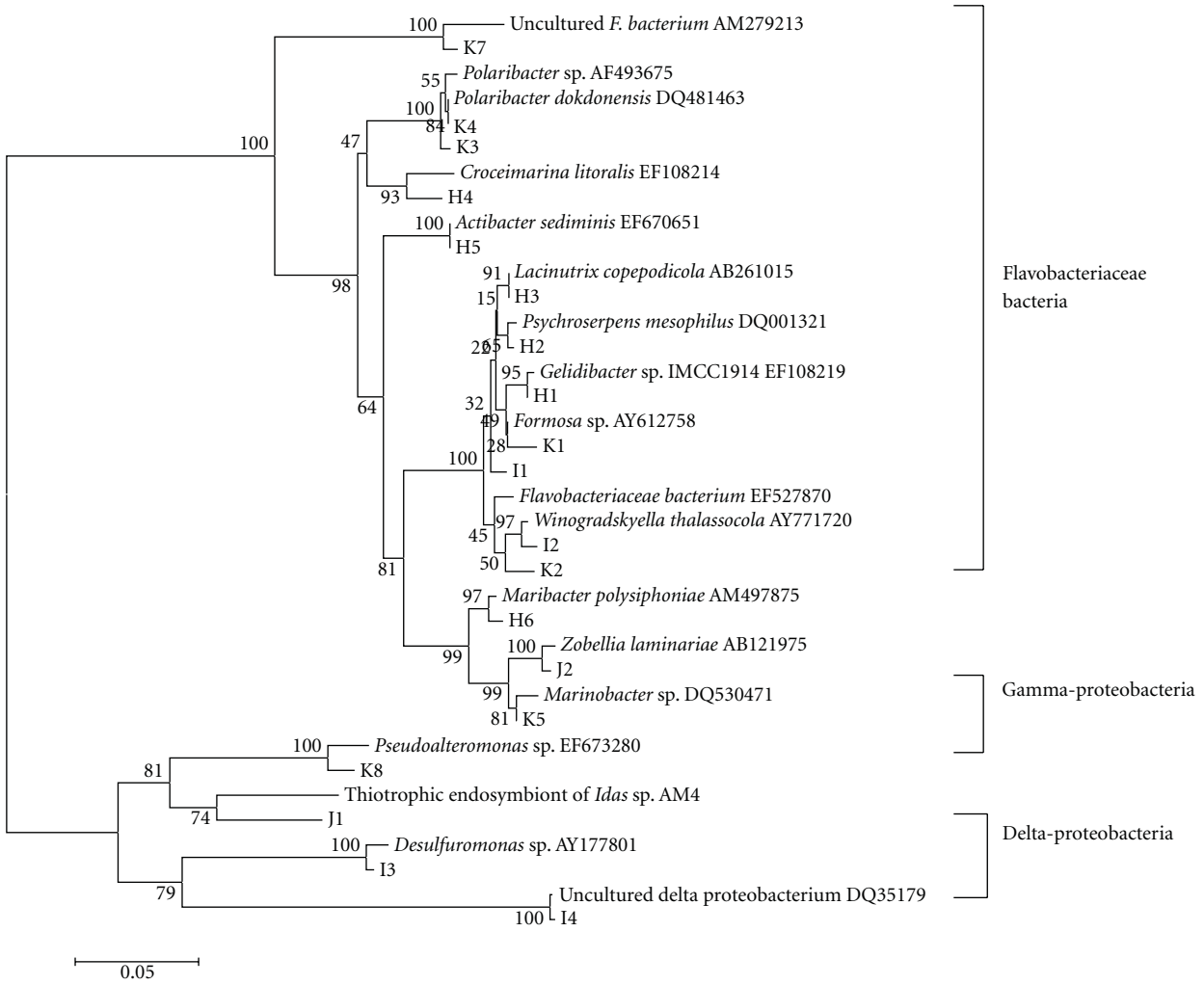

Figure 5: Phylogenetic tree of the sequences of 16S rDNA fragments separated by DGGE showed the classification positions of the bacteria and the phylogenetic relationship between each other. Reference sequences are shown with their respective Genbank accession numbers. The tree was built by MEGA bootstrap 1000 using neighbor joining.

ammonium-oxidizing, nitrifying, and nitrate-reducing bacteria reduced with the distance increasing from fish ponds to the unpolluted sea area. DGGE profiles showed fewer bands in the samples taken from near the effluent channel compared with more distant sediment samples. All the above suggested that excess nutrients from the intensive land-based fish culture facilities may import bacteria to and change the chemical and physical conditions of the nearby sea area and also reduce the diversity of bacterial communities in nearby waters and sediments.

Acknowledgments

The financial support of this paper was provided by the Fund for Postdoctoral Research of Shandong Province (200601011), the National High Technology Development Project of China (2006AA10Z414, 2006AA10Z415), and the National Marine Public Welfare Research Project (no. 200805069). The authors thank Professor Keming Qu for his assistance in sample collection.

References

[1] T. La Rosa, S. Mirto, A. Mazzola, and R. Danovaro, "Differential responses of benthic microbes and meiofauna to fish-farm disturbance in coastal sediments," *Environmental Pollution*, vol. 112, no. 3, pp. 427–434, 2001.

[2] M. Elliott, "Biological pollutants and biological pollution—an increasing cause for concern," *Marine Pollution Bulletin*, vol. 46, no. 3, pp. 275–280, 2003.

[3] C. A. McClure, K. L. Hammell, I. R. Dohoo, P. Nerette, and L. J. Hawkins, "Assessment of infectious salmon anaemia virus prevalence for different groups of farmed Atlantic salmon, *Salmo salar* L., in New Brunswick," *Journal of Fish Diseases*, vol. 27, no. 7, pp. 375–383, 2004.

[4] R. D. Villanueva, H. T. Yap, and M. N. E. Montaño, "Intensive fish farming in the Philippines is detrimental to the reef-building coral *Pocillopora damicornis*," *Marine Ecology Progress Series*, vol. 316, pp. 165–174, 2006.

[5] R. Danovaro, M. Armeni, A. Dell'Anno et al., "Small-scale distribution of bacteria, enzymatic activities, and organic matter in coastal sediments," *Microbial Ecology*, vol. 42, no. 2, pp. 177–185, 2001.

[6] B. A. Yoza, R. M. Harada, C. C. Nihous, Q. X. Li, and S. M. Masutani, "Impact of mariculture on microbial diversity in sediments near open ocean farming of Polydactylus sexfilis," *Ecological Indicators*, vol. 7, no. 1, pp. 108–122, 2007.

[7] R. I. Amann, W. Ludwig, and K. H. Schleifer, "Phylogenetic identification and *in situ* detection of individual microbial cells without cultivation," *Microbiological Reviews*, vol. 59, no. 1, pp. 143–169, 1995.

[8] Q. Li, B. Chen, K. Qu et al., "Variation of bacteria numbers in fish-shrimp mix-culturing ecosystem," *Chinese Journal of Applied Ecology*, vol. 13, no. 6, pp. 731–734, 2002.

[9] G. Muyzer, E. C. Waal, and A. G. Uitterlinden, "Profiling of complex microbial populations by denaturing gradient gel electrophoresis analysis of polymerase chain reaction-amplified genes coding for 16S rRNA," *Applied and Environmental Microbiology*, vol. 59, no. 3, pp. 695–700, 1993.

[10] D. Juck, B. T. Driscoll, T. C. Charles, and C. W. Greer, "Effect of experimental contamination with the explosive hexahydro-1,3,5-trinitro-1,3,5-triazine on soil bacterial communities," *FEMS Microbiology Ecology*, vol. 43, no. 2, pp. 255–262, 2003.

[11] T. E. Freitag, L. Chang, and J. I. Presser, "Changes in the community structure and activity of β-proteobacterial ammonia-oxidizing sediment bacteria along a freshwater-marine gradient," *Environmental Microbiology*, vol. 8, no. 4, pp. 684–696, 2006.

[12] R. Sandaa, T. Magnesen, L. Torkildsen, and O. Bergh, "Characterisation of the bacterial community associated with early stages of great scallop (*Pecten maximus*), using denaturing gradient gel electrophoresis (DGGE)," *Systematic and Applied Microbiology*, vol. 26, no. 2, pp. 302–311, 2003.

[13] P. Luo, C. Hu, Z. Xie et al., "PCR-DGGE analysis of bacterial community composition in brackish water *Litopenaeus vannamei* system," *Journal of Tropical Oceanography*, vol. 25, no. 2, pp. 49–50, 2006.

[14] S. Chen, W. Bao, B. Li et al., "Pollution situation of Rushan Bay and analysis of heterotrophic microorganisms," *Journal of Ocean College of Shandong* , vol. 17, no. 4, pp. 86–94, 1987.

[15] N. Fortin, D. Beaumier, K. Lee, and C. W. Greer, "Soil washing improves the recovery of total community DNA from polluted and high organic content sediments," *Journal of Microbiological Methods*, vol. 56, no. 2, pp. 181–191, 2004.

[16] K. J. Purdy, D. B. Nedwell, and T. M. Embley, "Analysis of the sulfate-reducing bacterial and methanogenic archaeal populations in contrasting antarctic sediments," *Applied and Environmental Microbiology*, vol. 69, no. 6, pp. 3181–3191, 2003.

[17] H. Cai, Y. Sun, and X. Zhang, "Environmental impact of cage aquaculture and the aquaculture environmental capacity in Xiangshan Harbor," *Techniques and Equipment for Environmental Pollution Control*, vol. 7, no. 11, pp. 71–76, 2006.

[18] H. Asami, M. Aida, and K. Watanabe, "Accelerated sulfur cycle in coastal marine sediment beneath areas of intensive shellfish aquaculture," *Applied and Environmental Microbiology*, vol. 71, no. 6, pp. 2925–2933, 2005.

[19] T. Staufenberger, V. Thiel, J. Wiese, and J. F. Imhoff, "Phylogenetic analysis of bacteria associated with *Laminaria saccharina*," *FEMS Microbiology Ecology*, vol. 64, no. 1, pp. 65–77, 2008.

[20] T. L. Skovhus, C. Holmstrom, S. Kjelleberg, and I. Dahllof, "Molecular investigation of the distribution, abundance and diversity of the genus *Pseudoalteromonas* in marine samples," *FEMS Microbiology Ecology*, vol. 61, no. 2, pp. 348–361, 2007.

[21] T. Sawabe, H. Makino, M. Tatsumi et al., "*Pseudoalteromonas bacteriolytica sp.* nov., a marine bacterium that is the causative agent of red spot disease of *Laminaria japonica*," *International Journal of Systematic Bacteriology*, vol. 48, no. 3, pp. 769–774, 1998.

[22] A. P. Negri, N. S. Webster, R. T. Hill, and A. J. Heyward, "Metamorphosis of broadcast spawning corals in response to bacteria isolated from crustose algae," *Marine Ecology Progress Series*, vol. 223, pp. 121–131, 2001.

[23] B. Migue and M. P. Combarro, "Bacteria associated with sardine (*Sardinapil chardus*) eggs in a natural environment (Ria de Vigo, Galicia, north western Spain)," *FEMS Microbiology Ecology*, vol. 44, no. 3, pp. 329–334, 2003.

[24] J. P. Gray and R. P. Herwig, "Phylogenetic analysis of the bacterial communities in marine sediments," *Applied and Environmental Microbiology*, vol. 62, no. 11, pp. 4049–4059, 1996.

[25] E. P. vanova, Y. V. Alexeeva, S. Flavier et al., "*Formosa algae gen.* nov., sp. nov., a novel member of the family *Flavobacteriaceae*," *International Journal of Systematic and Evolutionary Microbiology*, vol. 54, no. 3, pp. 705–711, 2004.

[26] O. I. Nedashkovskaya, S. B. Kim, M. Vancanneyt et al., "*Formosa agariphila sp.* nov., a budding bacterium of the family *Flavobacteriaceae* isolated from marine environments, and emended description of the genus *Formosa*," *International Journal of Systematic and Evolutionary Microbiology*, vol. 56, no. 1, pp. 161–167, 2006.

Hindawi Publishing Corporation
Evidence-Based Complementary and Alternative Medicine
Volume 2011, Article ID 408973, 6 pages
doi:10.1155/2011/408973

Research Article

Pyrolytic Characteristics and Kinetics of *Phragmites australis*

Hui Zhao,[1,2,3,4] Huaxiao Yan,[1] Congwang Zhang,[1,4] Xiaodong Liu,[1] Yanhui Xue,[1] Yingyun Qiao,[1,4] Yuanyu Tian,[1,4] and Song Qin[2,5]

[1] *College of Chemical and Environmental Engineering, Shandong University of Science and Technology, Qingdao, Shandong 266510, China*
[2] *Institute of Oceanology, Chinese Academy of Sciences, Qingdao, Shandong 266071, China*
[3] *Graduate University, Chinese Academy of Sciences, Beijing 100049, China*
[4] *Shandong Provincial Key Laboratory of Low-Carbon Energy Chemical Engineering, Qingdao 266510, China*
[5] *Yantai Institute of Coastal Zone Research, Chinese Academy of Sciences, Yantai, Shandong 264003, China*

Correspondence should be addressed to Hui Zhao, zhsdust@126.com and Song Qin, sqin@ms.qdio.ac.cn

Received 15 January 2011; Revised 25 May 2011; Accepted 24 July 2011

The pyrolytic kinetics of *Phragmites australis* was investigated using thermogravimetric analysis (TGA) method with linear temperature programming process under an inert atmosphere. Kinetic expressions for the degradation rate in devolatilization and combustion steps have been obtained for *P. australis* with Dollimore method. The values of apparent activation energy, the most probable mechanism functions, and the corresponding preexponential factor were determined. The results show that the model agrees well with the experimental data and provide useful information for the design of pyrolytic processing system using *P. australis* as feedstock to produce biofuel.

1. Introduction

The common reed, *Phragmites australis* (Cav.) Trin. exSteud., described as one of the most widely distributed angiosperms [1, 2] is commonly found in freshwater and marine wetlands and along the upland edge of tidal marshes. *P. australis* has increased in proportion in both tidal and nontidal wetlands in North America and has become a major concern to wetland ecologists [3, 4]. Expansion of *P. australis* into salt marshes reportedly caused a fivefold decrease in plant species richness [5], reductions in microtopography [6, 7], and reductions in biodiversity [3]. *P. australis* is actively colonizing wetlands raising concern about loss of biodiversity [8, 9]. In addition, the alternative source of energy contributes to the reduction of CO_2 emissions since the same amount of CO_2 is extracted from the air during the growth period of the plants [10]. *P. australis* seems to be especially a promising energy plant and chemical feedstock due to its high production potential. Various processes have been proposed for the integrated utilization of these powerful plants [11, 12]. The common reed can provide a large quantity of biomass and annual yields of 40–63 tons per hectare have been reported. *P. australis* is becoming very important as stable biomass source for China with its natural huge reserves and increasing artificial cultivation.

Pyrolysis is an effective method to harvest the energy in *P. australis*. However, pyrolytic characteristics studies of *P. australis* are little, which has led to the production of biofuel being far from commercialization. Both the development of the pyrolytic process and reactor design require complete elucidation of the pyrolytic mechanism. Therefore, the pyrolytic mechanisms of *P. australis* should be studied.

The specific objective of the present work was to study the pyrolytic characteristics of *P. australis* using a TG/DSC instrument. The kinetic parameters of decomposition were then obtained and the pyrolytic mechanism was illustrated, which can provide useful information for the design of pyrolysis system using *P. australis* biomass as feedstock to produce bio-fuel.

2. Materials and Methods

2.1. Materials. P. australis samples were harvested from a wetland beside the campus of Shandong University of Science and Technology, Qingdao, China, September 2010.

2.2. Analysis of P. australis Samples. Samples were ground into fine powders and sieved to less than 0.147 mm. Proximate and ultimate analyses were carried out to characterize

P. australis samples according to national standard GB212-91 (China) and element analyzer (Elementar Analysensysteme GmbH vario EL cube), respectively. In addition, cellulose, hemicelluloses, and lignin contents were analyzed according to methods from the literature [13]. The results were summarized in Table 1. All tests were carried out in triplicate.

2.3. Pyrolysis of the Samples. Thermogravimetric analyses were carried out using a thermal analyzer (TGA/DSC1/1600LF, METTLER TOLEDO Co., Switzerland). 10 mg of initial sample was pyrolyzed under a nitrogen flow rate of 50 cm^3/min with a heating rate of 25°C/min. The weight loss and calorific changes in response to temperature were then recorded and used to plot the thermogravimetric analysis (TGA), derivative thermogravimetric analysis (DTG), and differential scanning calorimetric (DSC) curves. All experiments were replicated three times.

2.4. The Kinetic Parameters of the Samples.

$$\frac{d\alpha}{dt} = \kappa f(\alpha), \tag{1}$$

where α is the conversion rate and is defined as

$$\alpha = \frac{m_0 - m}{m_0 - m_\infty}, \tag{2}$$

κ is the velocity constant, and $f(\alpha)$ is the mechanism function with different relative coefficient

$$T = T_0 + \beta t, \tag{3}$$

where β is the heating rate and T_0 is the initial temperature.

The reaction rate constant, κ, can be described by the following expression:

$$\kappa = CT^m. \tag{4}$$

By separation of variables and integration,

$$G(\alpha) = \int_0^\alpha \frac{d\alpha}{f(\alpha)} = \frac{C}{\beta \int_{T_0}^{T} T^m dT} = \frac{C}{\beta(m+1)} T^{m+1} + D = BT^{m+1} + D \overset{D=0}{\rightleftarrows} BT^{m+1}. \tag{5}$$

The expression of $G(\alpha)$ corresponding to each one of the mechanisms considered is also shown in Table 2

$$\lg G(\alpha_i) = \lg B + (m+1)\lg T_i. \tag{6}$$

This equation is used to estimate the most correct reaction mechanism function $G(\alpha)$. According to the plotting $\lg G(\alpha i)$ versus $\lg Ti$ and a linear regression, if the mechanism studied conforms to certain $G(\alpha)$ function, the slope of the straight line should be equal to −1.00000 and the linear correlation coefficient R^2 is high

$$B = \frac{C}{\beta(m+1)}. \tag{7}$$

Table 1: Proximate analysis, ultimate analysis, and component analysis of *P. australis* (/%wt).

Parameter	*P. australis*
Proximate analysis[a] (wt.%, ad. Basis)	
Moisture	5.89 ± 0.03
Ash	12.32 ± 1.12
Volatile matter	70.01 ± 2.40
Fix carbon[c]	11.78
Ultimate analysis[b] (wt.%, daf. Basis)	
Carbon	42.78 ± 1.53
Hydrogen	5.17 ± 0.02
Oxygen[c]	50.511
Nitrogen	1.31 ± 0.02
Sulfur	0.229 ± 0.01
C/H	8.31 ± 0.31
C/N	32.57 ± 1.55
Component analysis (wt.%, daf. Basis)	
Hemicellulose	30.68 ± 3.15
Lignin	20.34 ± 1.56
Cellulose	43.05 ± 3.98

[a] Dry-free basis; [b] Dry ash-free basis; [c] Calculated by difference.

Both of (5) and (6) are called Harcourt-Fission model of integral. m and B were constructed with deducing coefficients of least-square method

$$\lg\kappa_i = \lg C + m\lg T_i. \tag{8}$$

With a given value of $\lg Ti$, the constants C, m, $\lg\kappa_i$ can be determined

$$\ln \kappa_i = \ln A - \frac{E}{RT_i}. \tag{9}$$

Substituting the value of $\ln \kappa_i$ back into (9) in conjunction with $1/T$ allows $\ln A$ and E to be calculated [14].

All plots were generated and the lines were fitted using the Origin 8.0 software.

3. Results and Discussion

3.1. Characterization of Materials. The results of proximate, ultimate, and component analysis of *P. australis* samples are summarized in Table 1, which is in the same order of magnitude as energy crops. The comparison with other terrestrial materials shows a higher amount of ash and cellulose. The volatile matter and lignin contents of *P. australis* are lower, respectively, while the sulfur content of the samples is approximately equal [15].

3.2. Characteristics of the Thermal Degradation Process. Three stages in the pyrolytic process of *P. australis* are in accordance with the conclusion of oxidative pyrolysis curves of energy crops followed the usual shape for lignocellulosic materials [16–19]. The first stage (I) occurred as the temperature increased from 50 to 240°C, losing cellular water

Table 2: Algebraic expressions of functions $G(\alpha)$ and $f(\alpha)$ and mechanisms [23, 24].

No.	$G(a)$	$f(\alpha)$	Rate-determining mechanism
1	$1-(1-\alpha)^{2/3}$	$3/2(1-\alpha)^{1/3}$	Chemical reaction
2	$1-(1-\alpha)^{1/4}$	$4(1-\alpha)^{3/4}$	Chemical reaction
3	$(1-\alpha)^{-1/2}-1$	$2(1-\alpha)^{3/2}$	Chemical reaction
4	$(1-\alpha)^{-1}-1$	$(1-\alpha)^{2}$	Chemical reaction
5	$(1-\alpha)^{2}-1$	$1/2(1-\alpha)^{3}$	Chemical reaction
6	$(1-\alpha)^{3}-1$	$1/3(1-\alpha)^{4}$	Chemical reaction
7	$1-(1-\alpha)^{2}$	$1/2(1-\alpha)$	Chemical reaction
8	$1-(1-\alpha)^{3}$	$1/3(1-\alpha)^{2}$	Chemical reaction
9	$1-(1-\alpha)^{4}$	$1/4(1-\alpha)^{3}$	Chemical reaction
10	$\alpha^{3/2}$	$2/3\alpha^{-1/2}$	Nucleation
11	$\alpha^{1/2}$	$2\alpha^{1/2}$	Nucleation
12	$\alpha^{1/3}$	$3\alpha^{2/3}$	Nucleation
13	$\alpha^{1/4}$	$4\alpha^{3/4}$	Nucleation
14	lna	α	Nucleation
15	$-ln(1-\alpha)$	$1-\alpha$	Assumed random nucleation and its subsequent growth
16	$[-ln(1-\alpha)]^{2/3}$	$3/2(1-\alpha)[-ln(1-\alpha)]^{1/3}$	Assumed random nucleation and its subsequent growth
17	$[-ln(1-\alpha)]^{1/2}$	$2(1-\alpha)[-ln(1-\alpha)]^{1/2}$	Assumed random nucleation and its subsequent growth
18	$[-ln(1-\alpha)]^{1/3}$	$3(1-\alpha)[-ln(1-\alpha)]^{2/3}$	Assumed random nucleation and its subsequent growth
19	$[-ln(1-\alpha)]^{1/4}$	$4(1-\alpha)[-ln(1-\alpha)]^{3/4}$	Assumed random nucleation and its subsequent growth
20	$[-ln(1-\alpha)]^{2}$	$1/2(1-\alpha)[-ln(1-\alpha)]^{-1}$	Assumed random nucleation and its subsequent growth
21	$[-ln(1-\alpha)]^{3}$	$1/3(1-\alpha)[-ln(1-\alpha)]^{-2}$	Assumed random nucleation and its subsequent growth
22	$[-ln(1-\alpha)]^{4}$	$1/4(1-\alpha)[-ln(1-\alpha)]^{-3}$	Assumed random nucleation and its subsequent growth
23	$lna/(1-\alpha)$	$a/(1-a)$	Branching nuclei
24	α	$(1-a)^{0}$	Contracting disk
25	$1-(1-\alpha)^{1/2}$	$2(1-a)^{1/2}$	Contracting cylinder (cylindrical symmetry)
26	$1-(1-\alpha)^{1/3}$	$3(1-a)^{2/3}$	Contracting sphere (spherical symmetry)
27	α^{2}	$1/(2a)$	One-dimensional diffusion
28	$[1-(1-\alpha)^{1/2}]^{1/2}$	$4\{(1-\alpha)[1-(1-\alpha)]^{1/2}\}^{1/2}$	Two-dimensional diffusion
29	$a+(1-\alpha)ln(1-\alpha)$	$[-ln(1-\alpha)]^{-1}$	Two-dimensional diffusion
30	$[1-(1-\alpha)^{1/3}]^{2}$	$(3/2)(1-\alpha)^{2/3}[1-(1-\alpha)^{1/3}]^{-1}$	Three-dimensional diffusion, spherical symmetry
31	$1-2/3\alpha-(1-\alpha)^{2/3}$	$(3/2)[(1-\alpha a)^{-1/3}-1]^{-1}$	Three-dimensional diffusion, cylindrical symmetry
32	$[(1-\alpha)^{-1/3}-1]^{2}$	$(3/2)(1-\alpha)^{4/3}[(1-\alpha)^{-1/3}-1]^{-1}$	Three-dimensional diffusion
33	$[(1+\alpha)^{1/3}-1]^{2}$	$(3/2)(1+\alpha)^{2/3}[(1+\alpha)^{1/3}-1]^{-1}$	Three-dimensional diffusion
34	$1+2/3\alpha-(1+\alpha)^{2/3}$	$(3/2)[(1+\alpha)^{-1/3}-1]^{-1}$	Three-dimensional diffusion
35	$[(1+\alpha)^{-1/3}-1]^{2}$	$(3/2)(1+\alpha)4/3[(1+\alpha)^{-1/3}-1]^{-1}$	Three-dimensional diffusion
36	$[1-(1-\alpha)^{1/3}]^{1/2}$	$6(1-\alpha)2/3[1-(1-\alpha)^{1/3}]^{1/2}$	Three-dimensional diffusion

and the external water bound by surface tension. While the second stage (II), occurring as the temperature increased from 240 to 500°C was the devolatilization stage, during which the main pyrolytic process occurred and most of the organic materials are decomposed accompanied by various volatile components released gradually, resulting in a large weight loss which is more than 50% of total volatiles and formation of the main pyrolytic production. Specifically, stage II was composed of two zones for *P. australis* due to the different thermal stability of the components with zone I occurring as the temperature increased from 240 to 318°C which is a strong peak in the rate of weight loss curve, at which the rate of weight loss attains maximum with a maximum weight loss point at 288°C and zone II occurred as the temperature increased from 318 to 500°C with a maximum weight loss point at 346°C. The third stage (III) occurred as the temperature increased from 500 to 800°C with the residuals, the carbonaceous matters in the solid, slowly decomposed, resulting in the formation of a loose porous residual. A slight continued loss of weight is shown in the weight loss curve. *P. australis* is composed of many polysaccharides that have low polymerization. Moreover, the inorganic salts in *P. australis* presented a catalytic effect [20]. These findings indicate that the beginning of the decomposition occurs at a higher temperature for the samples evaluated in this study than for other terrestrial biomass with a high content of cellulose (straws and grasses) or lignin (woody biomass).

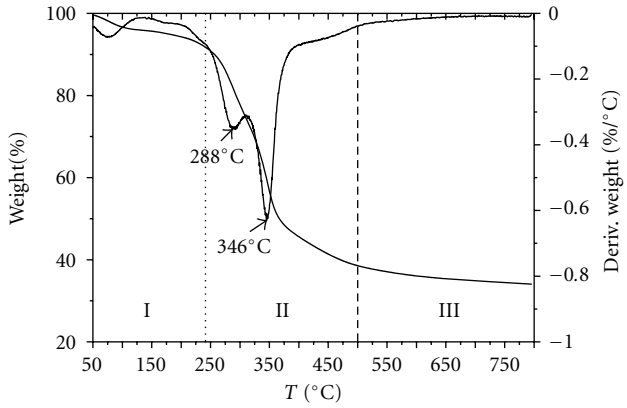

Figure 1: TG-DTG curves of *P. australis*.

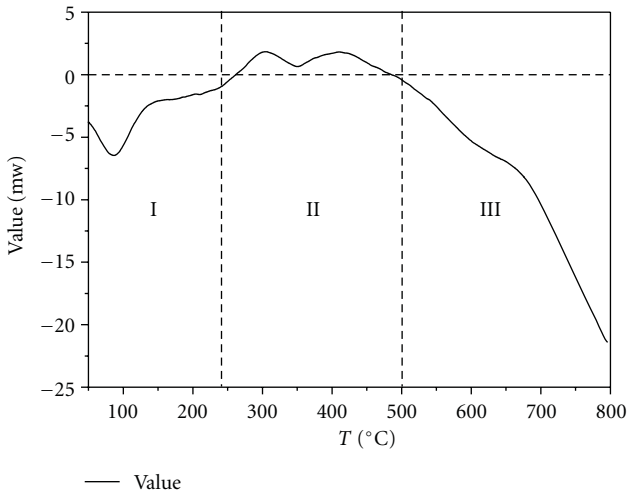

Figure 2: DSC curves of *P. australis*.

The weight losses of *P. australis* during stage I are primarily due to the loss of moisture and are similar to the moisture content values reported in Table 1. The instantaneous maximum reaction rate occurred in zone I of stage II. There was an endothermic peak during stage I that corresponded with the moisture evaporation procedure. As the temperature increased, an exothermic effect appeared during stage II and exothermic peaks were observed at 5–15°C after the maximum weight loss point. These findings indicate that the devolatilization stage (stage II) produced heat. Specifically, there was an endothermic effect during stage III. These findings indicate that the carbonaceous residual may have been decomposed at temperatures above 600°C. A maximum exothermic peak corresponding to the maximum weight loss rate peak appeared on the DSC curve of the samples (stage II). These findings indicate that the main pyrolysis process of the samples is an exothermic process. The exothermic effect was due to the charring process, which is the decomposition of the inorganic materials to metal carbonate (Figures 1, 2, and 3) [21, 22].

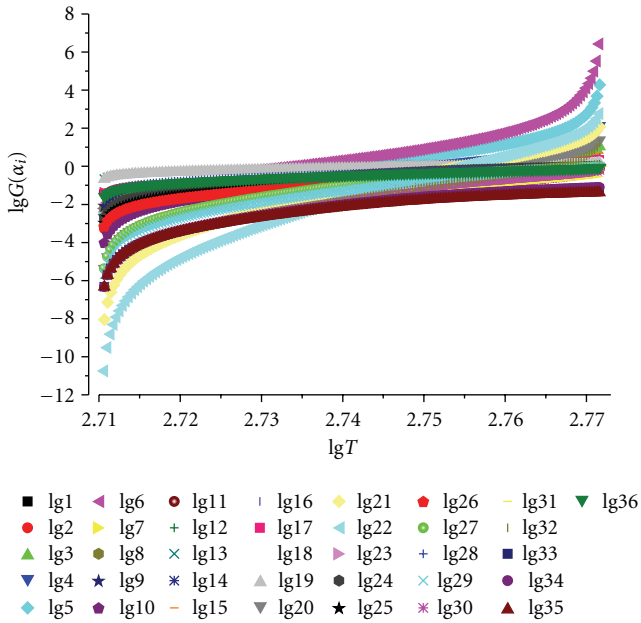

Figure 3: Plot for determination of most probable mechanism functions.

3.3. Kinetic Analysis of the Pyrolysis Process. The most probable mechanism function with integral form can be expressed by $G(\alpha_3) = (1-\alpha)^{1/2} - 1$,

$$m+1 = \frac{n\sum_{i=1}^{n} \lg G(\alpha_i)\lg T_i - \sum_{i=1}^{n} \lg T_i \sum_{i=1}^{n} \lg G(\alpha_i)}{n\sum_{i=1}^{n} T_i^2 - \sum_{i=1}^{n} T_i \sum_{i=1}^{n} T_i},$$
$$\lg B = \frac{\sum_{i=1}^{n} T_i G(\alpha_i) \sum_{i=1}^{n} T_i - \sum_{i=1}^{n} G(\alpha i) \sum_{i=1}^{n} T_i^2}{\sum_{i=1}^{n} T_i \sum_{i=1}^{n} T_i - n\sum_{i=1}^{n} T_i^2}, \quad (10)$$

and the results calculated according to the above equations are as follows: $\lg B = -116.34877$, $m = 41.18814$, and $\lg C = -113.32564$.

The result indicates that the model is in good agreement with the experimental data (Figure 4).

Comparisons of the decomposition temperature and activation energy of several types of biomass are provided in Table 3 [17]. The results indicate that the decomposition temperature of *P. australis* is lower than that of several kinds of plants and single component of biomass.

4. Conclusions

High priority should be given to the development and protection of biomass pyrolysis which is widely recognized as a technically and economically feasible way. This study presents useful information for the design of a pyrolytic processing system using *P. australis* biomass.

(i) There were three stages in the pyrolytic process of the samples. The second stage is the main pyrolysis process and most of the organic materials are decomposed in this stage which is our study focused on.

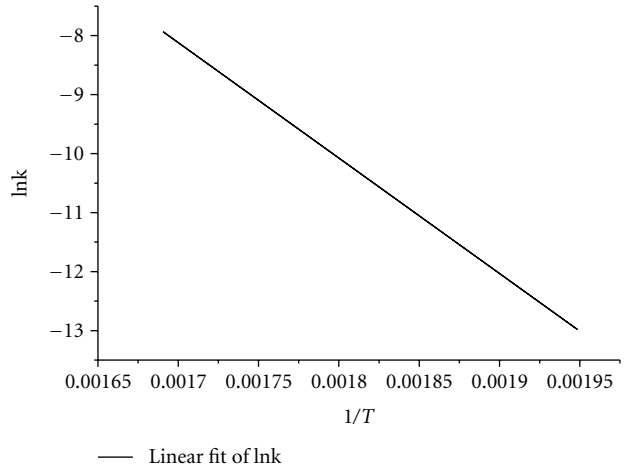

Figure 4: Plot for determination of E and A($\ln A = 25.14\,\text{min}^{-1}$, $E = 162.66\,\text{kJ mol}^{-1}$, $R^2 = 0.9999$).

Table 3: Comparison of various kinetic parameters of pyrolysis for different biomass[17, 25].

Samples	Decomposition temperature (°C)	Activation energy (kJ mol^{-1})
Cellulose	300–430	200
Hemicellulose	250–350	100
Lignin	250–550	80
Chitosan	268–312	95.6–185.7
Enteromorpha prolifera	174–551	228.1
spirulina platensis	190–560	76.2–97
Chlorella protothecoides	150–540	42.2–52.5
Dunaliella tertiolecta	155–299	145.713–146.421
Oak tree	230–400	236.2
Corn stover	250–470	57.95–58.94
Peat	208–334	52.77
P. australis	240–500	163

(ii) Iterative isoconversional procedure has been applied to estimate the values of apparent activation energy. The method of Dollimore combined with 36 mechanism functions is used to define the most probable mechanism $G(\alpha_3) = (1-\alpha)^{-1/2} - 1$; the preexponential factor $A = 8.28 \times 10^{10}\,\text{min}^{-1}$ and $E = 1.63 \times 10^5$ J mol^{-1} are obtained on the basis of $G(\alpha)$.

(iii) Comparisons of various kinetic parameters of pyrolysis for different biomass types show that *P. australis* biomass has a great potential and a good prospect for producing biofuel by fast pyrolysis process.

To learn more about *P. australis* pyrolysis, characterization of liquid and solid products should be more in-depth understood [26, 27].

Acknowledgments

This research was supported by the National Natural Science Foundation of China (21076117), CAS International partnership program "Typical environment processes and their effects on resources", Outstanding young scholar fellowship of Shandong province (Molecular phycology) (JQ200914), projects of Shandong Province Higher Educational Science and Technology Program (J09LC22 and J10LC15), the Open Funding from the Key Laboratory of Experimental Marine Biology, Institute of Oceanology (Kf201016), and Open Project Program of the Key Laboratory of Marine Bio-resources Sustainable Utilization (LMB101004), SCSIO, Chinese Academy of Sciences. Both Hui Zhao and Huaxiao Yan are equally contributed.

References

[1] L. G. Holm, D. L. Plucknett, J. V. Pancho, and J. P. Herberger, *The World's Worst Weeds*, University Press of Hawaii, Honolulu, Hawaii, USA, 1977.

[2] O. A. Clevering and J. Lissner, "Taxonomy, chromosome numbers, clonal diversity and population dynamics of *Phragmites australis*," *Aquatic Botany*, vol. 64, no. 3-4, pp. 185–208, 1999.

[3] R. M. Chambers, L. A. Meyerson, and K. Saltonstall, "Expansion of *Phragmites australis* into tidal wetlands of North America," *Aquatic Botany*, vol. 64, no. 3-4, pp. 261–273, 1999.

[4] L. Windham and L. A. Meyerson, "Effects of common reed (*Phragmites australis*) expansions on nitrogen dynamics of tidal marshes of the northeastern U.S," *Estuaries*, vol. 26, no. 2B, pp. 452–464, 2003.

[5] M. D. Bertness, P. J. Ewanchuk, and B. R. Silliman, "Anthropogenic modification of New England salt marsh landscapes," *Proceedings of the National Academy of Sciences of the United States of America*, vol. 99, no. 3, pp. 1395–1398, 2002.

[6] L. Windham and R. G. Lathrop, "Effects of *Phragmites australis* (common reed) invasion on aboveground biomass and soil properties in brackish tidal marsh of the mullica river, New Jersey," *Estuaries*, vol. 22, no. 4, pp. 927–935, 2002.

[7] D. L. Raichel, K. W. Able, and J. M. Hartman, "The influence of *Phragmites* (common reed) on the distribution, abundance, and potential prey of a resident marsh fish in the Hackensack Meadowlands, New Jersey," *Estuaries*, vol. 26, no. 2B, pp. 511–521, 2003.

[8] S. Güsewell and F. Klötzli, "Assessment of aquatic and terrestrial reed (*Phragmites australis*) stands," *Wetlands Ecology and Management*, vol. 8, no. 6, pp. 367–373, 2000.

[9] H. Cizkova, L. Pechar, S. Husák et al., "Chemical characteristics of soils and pore waters of three wetland sites dominated by *Phragmites australis*: relation to vegetation composition and reed performance," *Aquatic Botany*, vol. 69, no. 2–4, pp. 235–249, 2001.

[10] J. M. Adams and G. Piovesan, "Uncertainties in the role of land vegetation in the carbon cycle," *Chemosphere*, vol. 49, no. 8, pp. 805–819, 2002.

[11] C. Pevida, M. G. Plaza, B. Arias, J. Fermoso, F. Rubiera, and J. J. Pis, "Surface modification of activated carbons for CO_2 capture," *Applied Surface Science*, vol. 254, no. 22, pp. 7165–7172, 2008.

[12] A. L. Chaffee, G. P. Knowles, Z. Liang, J. Zhang, P. Xiao, and P. A. Webley, "CO_2 capture by adsorption: materials and

process development," *International Journal of Greenhouse Gas Control*, vol. 1, no. 1, pp. 11–18, 2007.

[13] J. Parikh, S. A. Channiwala, and G. K. Ghosal, "A correlation for calculating elemental composition from proximate analysis of biomass materials," *Fuel*, vol. 86, no. 12-13, pp. 1710–1719, 2007.

[14] D. Dollimore, T. Ping, and K. S. Alexander, "The kinetic interpretation of the decomposition of calcium carbonate by use of relationships other than the Arrhenius equation," *Thermochimica Acta*, vol. 282-283, pp. 13–27, 1996.

[15] G. Taralas and M. G. Kontominas, "Energetic valorization of solid residues: pyrolysis of olive husks," in *Science in Thermal and Chemical Biomass Conversion*, A. V. Bridgwater, Ed., Victoria, Vancouver Island, Canada, 2004.

[16] S. P. Zou, Y. L. Wu, M. D. Yang, C. Li, and J. M. Tong, "Pyrolysis characteristics and kinetics of the marine microalgae *Dunaliella tertiolecta* using thermogravimetric analyzer," *Bioresource Technology*, vol. 101, no. 1, pp. 359–365, 2010.

[17] D. Li, L. Chen, X. Yi, X. Zhang, and N. Ye, "Pyrolytic characteristics and kinetics of two brown algae and sodium alginate," *Bioresource Technology*, vol. 101, no. 18, pp. 7131–7136, 2010.

[18] J. Jauhiainen, J. A. Conesa, R. Font, and I. Martín-Gullón, "Kinetics of the pyrolysis and combustion of olive oil solid waste," *Journal of Analytical and Applied Pyrolysis*, vol. 72, no. 1, pp. 9–15, 2004.

[19] A. E. Ghaly and A. Ergudenler, "Thermal degradation of cereal straws in air and nitrogen," *Applied Biochemistry and Biotechnology*, vol. 28-29, no. 1, pp. 111–126, 1991.

[20] J. M. Jones, L. I. Darvella, T. G. Bridgemana, M. Pourkashaniana, and A. Williamsa, "An investigation of the thermal and catalytic behavior of potassium in biomass combustion," *Proceedings of the Combustion Institute*, vol. 31, no. 2, pp. 1955–1963, 2007.

[21] A. B. Ross, J. M. Jones, M. L. Kubacki, and T. Bridgeman, "Classification of macroalgae as fuel and its thermochemical behaviour," *Bioresource Technology*, vol. 99, no. 14, pp. 6494–6504, 2008.

[22] M. Jeguirim, S. Dorge, and G. Trouvé, "Thermogravimetric analysis and emission characteristics of two energy crops in air atmosphere: arundo donax and Miscanthus giganthus," *Bioresource Technology*, vol. 101, no. 2, pp. 788–793, 2010.

[23] R. Z. Hu and Q. Z. Shi, *Thermal Analysis Kinetics*, Science Press, Beijing, China, 1st edition, 2001.

[24] R. Ebrahimi-Kahrizsangi and M. H. Abbasi, "Evaluation of reliability of Coats-Redfern method for kinetic analysis of non-isothermal TGA," *Transactions of Nonferrous Metals Society of China*, vol. 18, no. 1, pp. 217–221, 2008.

[25] H. Sutcu, "Pyrolysis by thermogravimetric analysis of blends of peat with coals of different characteristics and biomass," *Journal of the Chinese Institute of Chemical Engineers*, vol. 38, no. 3-4, pp. 245–249, 2007.

[26] H. Sutcu, "Pyrolysis of *Phragmites australis* and characterization of liquid and solid products," *Journal of Industrial and Engineering Chemistry*, vol. 14, no. 5, pp. 573–577, 2008.

[27] H. Sutcu and H. Demiral, "Production of granular activated carbons from loquat stones by chemical activation," *Journal of Analytical and Applied Pyrolysis*, vol. 84, no. 1, pp. 47–52, 2009.

Hindawi Publishing Corporation
Evidence-Based Complementary and Alternative Medicine
Volume 2011, Article ID 292873, 9 pages
doi:10.1155/2011/292873

Research Article

CI431, an Aqueous Compound from *Ciona intestinalis L.*, Induces Apoptosis through a Mitochondria-Mediated Pathway in Human Hepatocellular Carcinoma Cells

Linyou Cheng,[1,2] Ming Liu,[1] Cuicui Wang,[1,2] Haizhou Liu,[1,3] Yuyan Zhang,[1,3] and Xiukun Lin[1]

[1] *Institute of Oceanology, Chinese Academy of Sciences, Qingdao 266071, China*
[2] *Graduate University, Chinese Academy of Sciences, Beijing 100049, China*
[3] *College of Chemical Engineering, Qingdao University of Science and Technology, Qingdao 266042, China*

Correspondence should be addressed to Xiukun Lin, linxiukun@yahoo.com

Received 21 January 2011; Accepted 21 May 2011

In the present studies, a novel compound with potent anti-tumor activity from *Ciona intestinalis L.* was purified by acetone fractionation, ultrafiltration, gel chromatography and High Performance Liquid Chromatography. The molecular weight of the highly purified compound, designated CI431, was 431Da as determined by HPLC-MS analysis. CI431 exhibited significant cytotoxicity to several cancer cell types. However, only a slight inhibitory effect was found when treating the benign human liver cell line BEL-7702 with the compound. To explore its mechanism against hepatocellular carcinoma, BEL-7402 cells were treated with CI431 in vitro. We found that CI431 induced apoptotic death in BEL-7402 cells in a dose- and time-dependent manner. Cell cycle analysis demonstrated that CI431 caused cell cycle arrest at the G2/M phase, and a sub-G1 peak appeared after 24 h. The mitochondrial-mediated pathway was implicated in this CI431-induced apoptosis as evidenced by the disruption of mitochondrial membrane potential. The results suggest that the CI431 induces apoptosis in BEL-7402 human hepatoma cells by intrinsic mitochondrial pathway.

1. Introduction

It is now clear that the oceans are not only home to a tremendous diversity of species but that their inhabitants produce also a wealth of natural products [1]. Since the 1950s, many structurally diverse natural products with astounding bioactivities have been discovered from marine organisms [2]. These compounds are mainly isolated from sessile animals, such as sponges, tunicates, corals, mollusks, and bryozoans [3, 4].

Among sessile animals, tunicates have received the most attention. More commonly known as Ascidiacea, members of the class Ascidiacea (Ascidians) are the most highly investigated tunicates, since they present a benthonic stage in their life, making their collection easier. The chemistry of ascidians has become one of the most active fields of marine natural products; it has been amply demonstrated that these sea creatures are prolific producers of unusual structures with significant bioactivities. Most of these products fall within the area of cancer therapy [5], and a significant number of ascidian-derived compounds have entered into preclinical and clinical trials as antitumor agents [3, 6].

Didemnin B, is perhaps the most studied marine natural product. This cyclic peptide was isolated from the Caribbean tunicate Tridemnum solidum [7]. Early investigation into the bioactivity of this compound revealed its strong antiproliferative effects in vitro against a variety of human tumor cell lines. It was developed by NCI and went through phase II clinical trials but was withdrawn because it proved to be too toxic. Although didemnin B was never carried into Phase III trials, activity focused on developing the compound as a potential cancer treatment helped pave the way for the rest of the marine-derived products following it into the development pipeline. Aplidine [8], Vitilevuamide [9], Diazonamide [10], and ET-743 [11], all of them were compounds with efficient antitumor activity isolated from Ascidians.

Hepatocellular carcinoma (HCC) is the fifth most common cancer [12], with a 5-year survival rate of less than 5% and is the fourth leading cause of cancer death worldwide

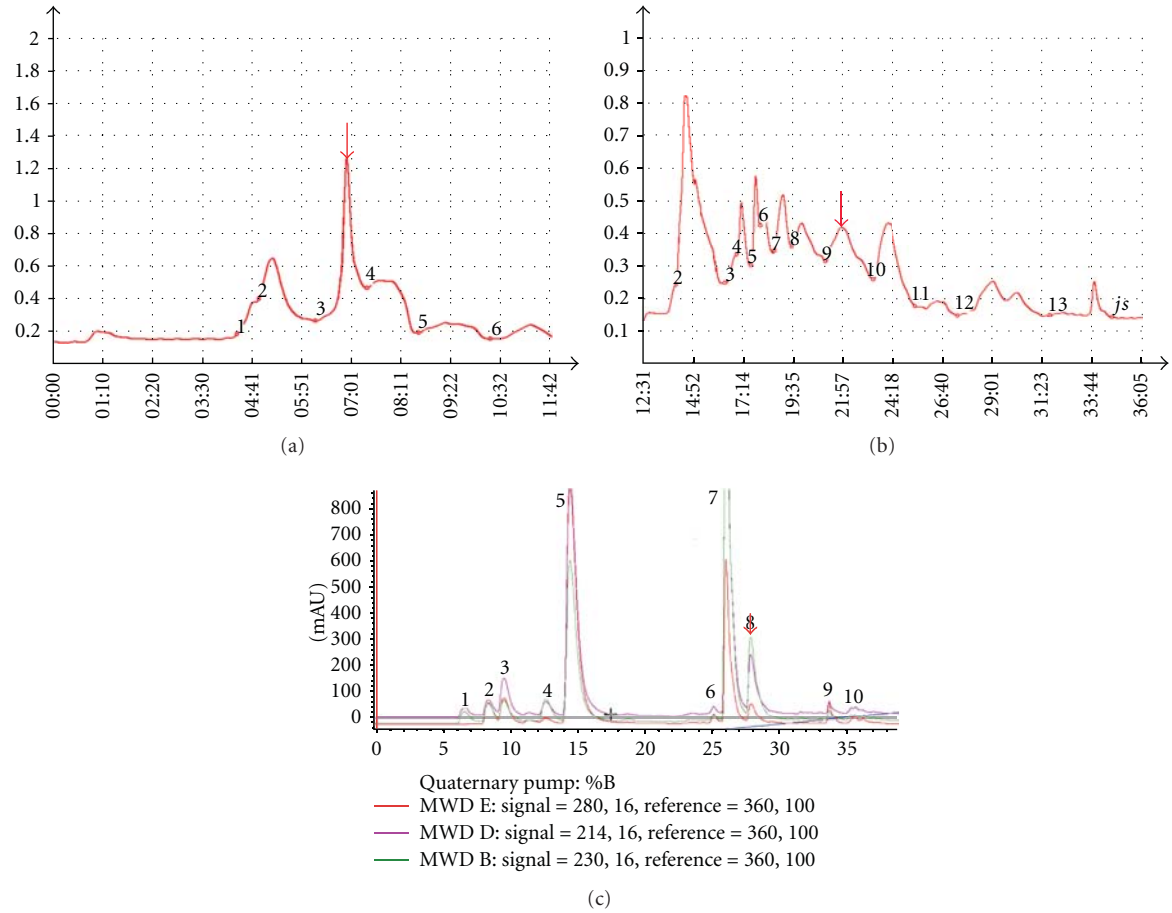

Figure 1: Elution patterns on column chromatography. The fraction of acetone precipitation was applied to Sephadex G25 column (a). The active fraction from Sephadex G25 chromatography was applied to P_2 column (b). The active fraction from P_2 was further purified by high-performance liquid chromatography (c). The arrow indicates the active component during the purification.

[13–15]. Its incidence has been increasing over the past few decades in some areas such as Europe, USA, and East Asia [16, 17]. Despite the high mortality and frequency of this cancer, surgical resection is an available option for only a small proportion of patients because metastases are often present when the cancer is discovered. In addition, because of the inherent chemotherapy-resistant nature of HCC, systemic cytotoxic chemotherapy agents are minimally effective at improving patient survival [18]. Thus, novel strategies and agents, which have greater targeting on HCC but lower toxicity for normal liver cells, are seen as a direction of enormous potential.

Previous studies have shown that several agents derived from Ascidiae can induce the apoptosis of many cancer cells [5]. However, *Ciona intestinalis L.*, a selected species in the present study, has not been studied for its anticancer effects. Therefore, we attempted to investigate the growth-inhibitory and apoptotic effects of components from *Ciona intestinalis L.* against human liver cancer cells. A bioguided isolation was performed to purify the active components from the species. We found that a component, CI431, was a potent inhibitor against human hepatoma Bel-7402 cells and may be developed as a novel class of anticancer agents.

2. Subjects and Methods

2.1. Materials. *Ciona intestinalis L.* was obtained from the Xunshan Fishery Company of Rongcheng, China. The animals were identified by professor Fuhua-li at Institute of Oceanology, Chinese Academy of Sciences. The human hepatocellular cancer BEL-7402, human colorectal cancer HCT116, human cervical cancer Hela cells as well as human lung adenocarcinoma A549, breast cancer MCF-7, and human benign liver cell BEL-7702 cells were obtained from American Type Culture Collection.

2.2. Extraction and Purification of the Compound from Ciona intestinalis L. Briefly, 50 kg fresh *C. intestinalis* were smashed and incubated at 70°C for 30 min and were then centrifuged at 8,000 rpm for 30 min. Next, the supernatants were added to 3 volumes of acetone at 4°C for 12 h and were centrifuged at 10,000 rpm for 30 min once more. The acetone supernatants were collected and then were disposed through a 5 kDa ultrafiltration membrane (Millipore, USA). The residue with size <5 kDa was lyophilized and dissolved in a small amount of distilled water. The prepared extraction

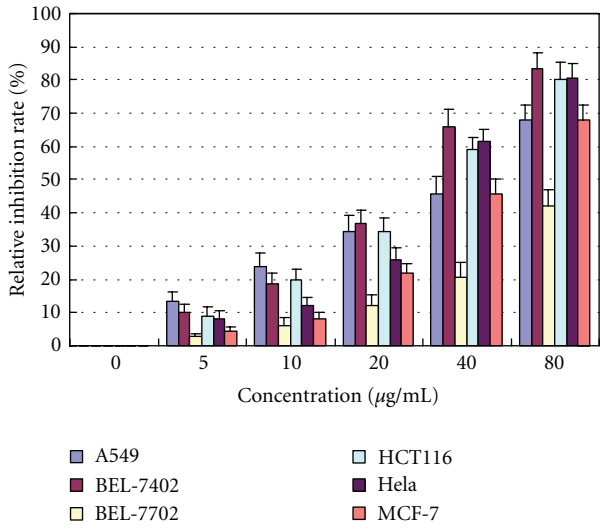

FIGURE 2: CI431 inhibited the growth of several types of cancer cells. Human hepatoma BEL-7402, human colon cancer HCT116, human breast cancer MCF-7, human cervical cancer Hela cells, and human lung adenocarcinoma A549 as well as human benign liver cell BEL-7702 cells were incubated in the absence or presence of certain concentrations of CI431 for 48 h at 37°C. MTT assay was performed to determine the growth inhibition of different cancer cells and benign BEL-7702 cells by CI431. The experiments were performed more than three times.

solution was applied to a Sephadex-G25 column and eluted with distilled water.

All of the fractions were collected and analyzed for cytotoxicity by MTT assay. The active fraction was lyophilized and loaded to a P2 Gel (Bio-Rad Laboratories, Inc) column. The column was eluted with distilled water. The active fraction was pooled and subjected to reverse-phase liquid chromatography on a C18 column (Agilent C18 4.6 × 250 mm) using an Agilent apparatus. The chromatography was performed at a flow rate of 0.5 mL/min, using 0.1% TFA as solvent A and 99.9% acetonitrile containing 0.1% TFA as solvent B. The gradient was 10–60% of solvent B for 50 min. The elution profile was monitored by online measurement of the absorbance at 214 and 280 nm. The fractions were pooled and freeze dried. All of the fractions were collected and analyzed by MTT assay.

2.3. Cell Culture. The carcinoma cells BEL-7402, Hela, HCT116, and benign liver cell BEL-7702 were cultured in RPMI-1640 medium. The MCF-7 cell lines were cultured in DMEM medium. The A549 cell lines were cultured in F12 medium. All cells were incubated in media supplemented with 10% fetal bovine serum in a humidified atmosphere containing 5% CO_2 at 37°C. The media and sera were purchased from Sigma Chemical.

2.4. Assessment of Cytotoxicity. The inhibitory effects of the antitumor agents on the growth of cancer cells as well as benign cells BEL-7702 were assessed in vitro by MTT assay [19]. Four thousand cells per well were seeded into a 96-well microplate. Cells were cultured in 180 μL media of RPMI-1640, 12 K, or DMEM for 24 h. The purified compound with different concentrations was added to the medium. After 48 h, MTT solution (50 μL, 0.5 mg/mL) was added into each well, and the cells were incubated for another 4 h. After adding 150 μL DMSO to each aspirated well, the plate was gently agitated until the color reaction was uniform. The OD590 was determined by a microplate reader (Bio-Tek Instruments, USA) with subtraction of background absorbance [20].

2.5. CI431-Induced Morphological Changes of BEL-7402 Cells. Morphological alterations of BEL-7402 cells after CI431 treatment were investigated using phase contrast microscopy and SEM. The cells were seeded and cultured in 96-well plates, as described above. After incubation with 50 μg/mL CI431, the morphology of cells was observed under the CKX41 phase contrast microscopy (Olympus, Japan) and photographed at 0, 12, and 24 h, respectively. In the SEM experiment, BEL-7402 cells were grown onto poly-L-lysine-coated coverslips in 6-well plates for 24 h to allow firm attachment. Then, they were treated with 50 μg/mL CI431 and incubated for 0, 12, and 24 h. The medium containing CI431 was removed, and subsequently the cells were fixed in glutaraldehyde. After fixation overnight at 4°C, the coverslip was dehydrated in ethanol and dried in a critical point dryer. Cells on coverslip were coated with gold and analyzed by the S-3400N SEM (Hitachi, Japan).

2.6. DAPI (4′-6-diamidino-2-phenylindole) Staining. The cells BEL-7402 were grown onto poly-L-lysine-coated coverslips in 6-well plates and treated with CI431 as described above for the SEM assay. Then the medium containing CI431 was removed, and subsequently the cells were fixed in paraformaldehyde. After fixation overnight at 4°C, the coverslips were stained with DAPI solution followed by observation with a fluorescence microscope [21].

2.7. Flow Cytometric Analysis. The cells BEL-7402 were incubated with 20, 40, and 80 μg/mL of CI431 for 24 h. The cells were harvested and fixed in ice-cold 70% (v/v) ethanol for 24 h at 4°C. After centrifugation, the cell pellet was resuspended in PBS; the cells were subjected to propidium iodide (PI) staining and then analyzed by a flow cytometry (FACSCalibur; BD Biosciences, USA) [22].

2.8. Mitochondrial-Membrane Potential ($\Delta\psi m$). The JC-1 Mitochondrial Apoptosis Detection Kit was used to detect $\Delta\psi m$ disruption. JC-1 is selectively accumulated within intact mitochondria to form multimer J-aggregates emitting fluorescence light at 590 nm (red) at a higher membrane potential, and monomeric JC-1 emits light at 527 nm (green) at a low membrane potential. Thus, the fluorescence color of JC-1 represents mitochondrial-membrane potential, which can be analyzed by FACS system [23]. According to the manufacturer's protocols, cells were seeded in 12-well plates at a density of 3×10^5 cells/mL and treated with CI431 at doses of 20, 40, and 80 μg/mL for 24 h. After treatment with

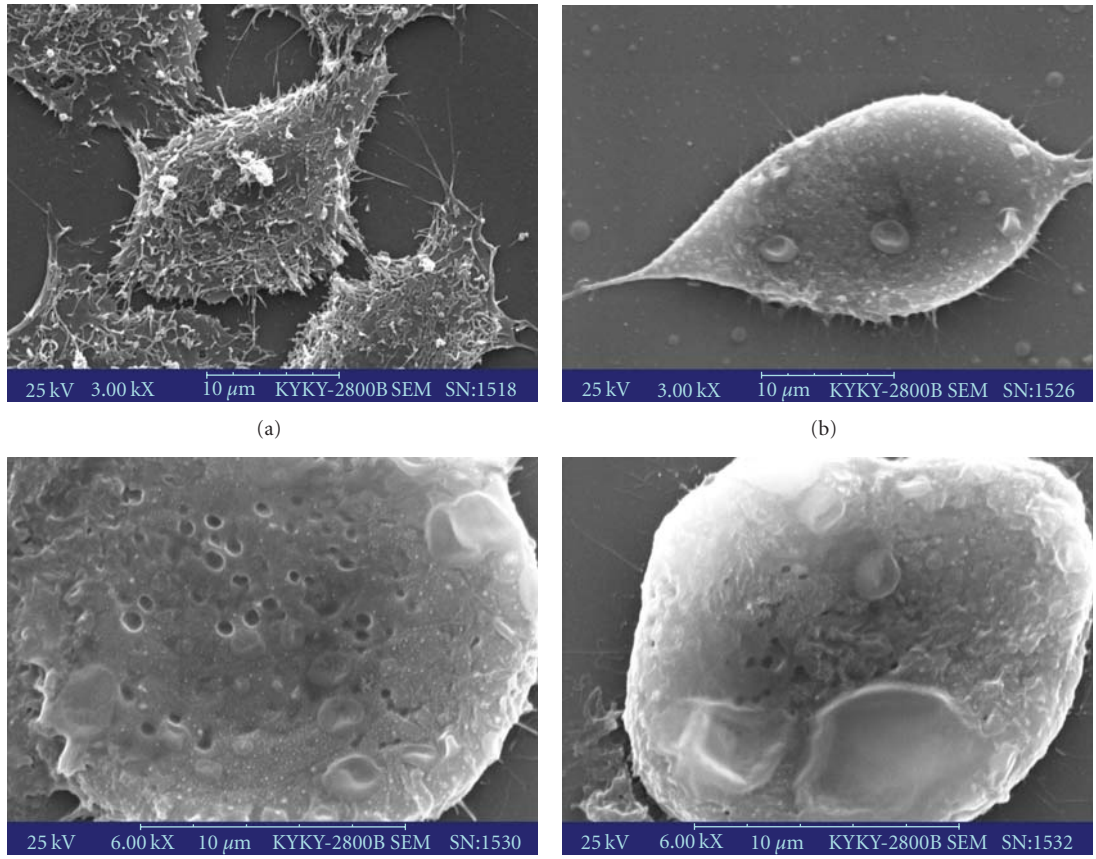

Figure 3: Morphological analysis of BEL-7402 cells induced by CI431. BEL-7402 cells were grown on poly-L-lysine-coated coverslips for 24 h to allow firm attachment and treated with 50 μg/mL CI431 for certain time intervals. Cells were fixed on coverslips coated with gold and analyzed by using the KYKY-2800B SEM. The cells were untreated (a) or treated with CI431 for 12 (b), 18 (c), and 24 h (d). The untreated BEL-7402 cells showed a normal smooth surface. In contrast, the cells treated with CI431 became rounded, and the surface of the cell membrane was markedly disrupted (Scale bar = 10 μm).

CI431 200 μL, prewarmed incubation buffer containing 0.2 μL MitoCapture was added to each well and plates were incubated for 15 min at 37°C in a 5% CO_2 incubator. Then, cells were analyzed by a fluorescence spectrophotometer (F-4500, HITACHI).

2.9. Statistical Analysis. All experiments were done three times in triplicate (n = 9), and the results were expressed as means ± SD (standard deviation). A one-way analysis of variance (ANOVA) and the Duncan test were used for multiple comparisons (SPSS program, ver 10.0).

3. Results

3.1. Extraction and Purification of the Compound from Ciona intestinalis L. In order to isolate novel antitumor agents from *Ciona intestinalis L.*, we developed a purification protocol involving heat-inactivation, acetone precipitation, ultrafiltration concentration, gel filtration, and reverse-phase chromatography HPCL. Briefly, acetone precipitation, and ultrafiltration concentration were carried out to obtain a pool of antitumor agents as previously described. The fraction obtained after acetone precipitation was concentrated through a 5 kDa ultrafiltration membrane. The fraction of acetone precipitation solution, which contained several major compounds below 5 kDa, showed strong inhibitory activity against several tumor cell lines.

The fraction of acetone precipitation compounds was applied to a Sephadex-G25 column and eluted with distilled water (Figure 1(a)). The active fractions were further purified by P2 column (Figure 1(b)). After gel chromatography, the active components were submitted to reverse-phase chromatography using a C18 column, and purified to homogeneity (Figure 1(c)). The purified agent, designated CI431, was revealed as a single MW by MS.

3.2. Assessment of Cytotoxicity. MTT assays were performed to investigate the effects of CI431 on the proliferation of sixcell lines. As shown in Figure 2, CI431 (over 50 μg/mL) had a significant growth-inhibiting effect on the five cancer cell lines and a slight growth-inhibiting effect on the benign liver BEL-7702 cell line. Results indicated that CI431 had

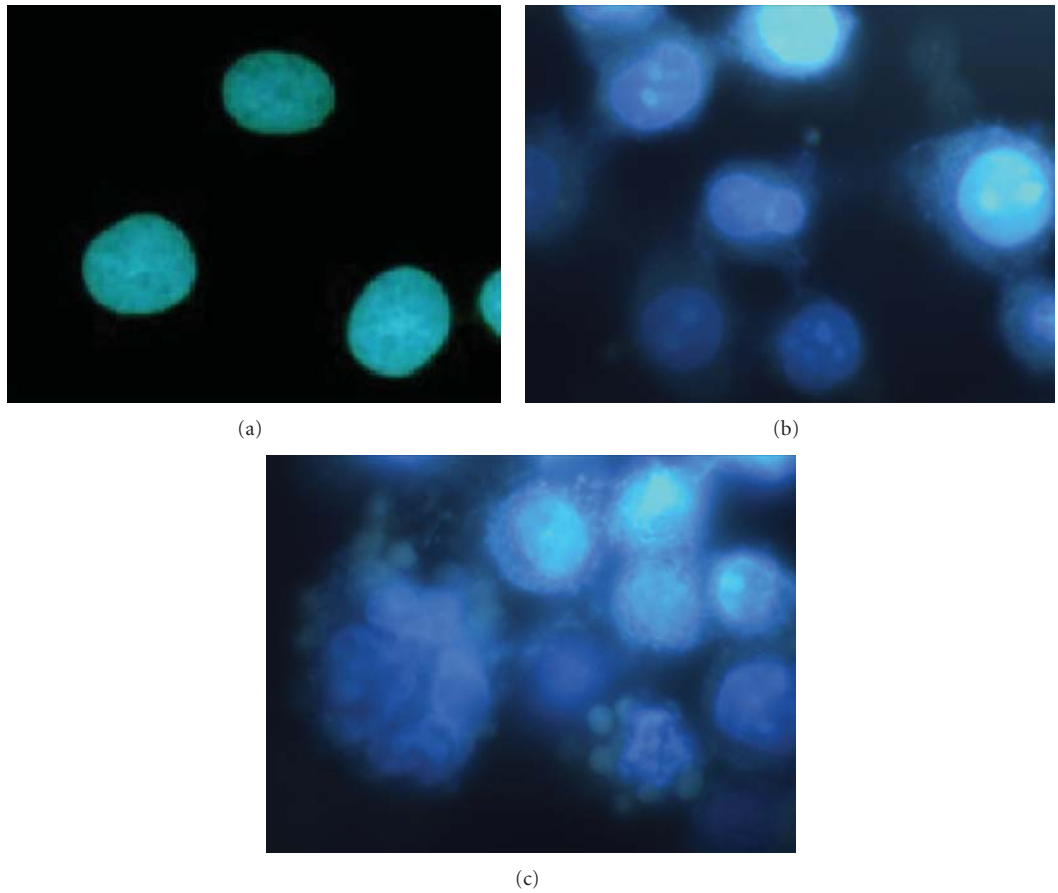

Figure 4: DAPI staining assay. The cells BEL-7402 were grown on poly-L-lysine-coated coverslips in 6-well plates and treated with CI431. After incubation for 24, the cells were stained with DAPI and then observed under the fluorescence microscopy. BEL-7401 cells in the control medium were stained homogeneously with DAPI (a), whereas treatment with CI431 led to marked chromatin condensation and nuclear fragmentation together with the appearance of small structures like apoptotic bodies. These observations indicated that the cells treated with CI431 entered apoptosis (b, c).

a significant grow-inhibiting effect on the five cell lines in a time-dependent manner (data not shown) and in a dose-dependent manner (Figure 2). Among these cell lines, the BEL-7402 cells were much more sensitive than the other cell lines. From this result, BEL-7402 cells were chosen for the subsequent experiments.

3.3. CI431-Induced Morphological Changes of BEL-7402 Cells. The morphologic changes of the cell membrane were clearly visualized by SEM. Remarkable alterations of the cell membrane of BEL-7402 cells were observed after CI431 treatment. The architecture of untreated BEL-7402 cells displayed a typical polygon shape (Figure 3(a)). However, the morphology of the cells started to change after incubation with CI431. The cells detached from the substratum, became spindle shape (Figure 3(b)), and separated from each other after exposure to CI431 for 12 h. Membrane bulge and detachment from cytoplasmic inclusion were observed in 18 h and 24 h after CI431 treatment (Figures 3(c) and 3(d)). The untreated BEL-7402 cells showed a normal smooth surface. In contrast, the cells treated with CI431 became rounded, and the surface of the cell membrane was markedly disrupted.

3.4. DAPI (4′-6-diamidino-2-phenylindole) Staining. We characterized the changes in the nuclear morphology by staining with DAPI. BEL-7401 cells in the control medium were stained homogeneously with DAPI, whereas treatment with CI431 led to marked chromatin condensation and nuclear fragmentation together with the appearance of small structures like apoptotic bodies, a biochemical hallmark of apoptosis. The sizes of CI431-treated BEL-7402 cells increased as compared with those of untreated cells. Double nucleated cells or giant multinucleated cells can be easily found. These observations indicated that the cells treated with CI431 entered apoptosis (Figure 4).

3.5. CI431 Induces Apoptosis and G2/S Phase Arrest in BEL-7402 Cells. To gain an insight into the antiproliferation mechanism of CI431, the cell cycle distribution of CI431-treated cells was determined by flow cytometry analysis. The results showed that CI431 significantly induced

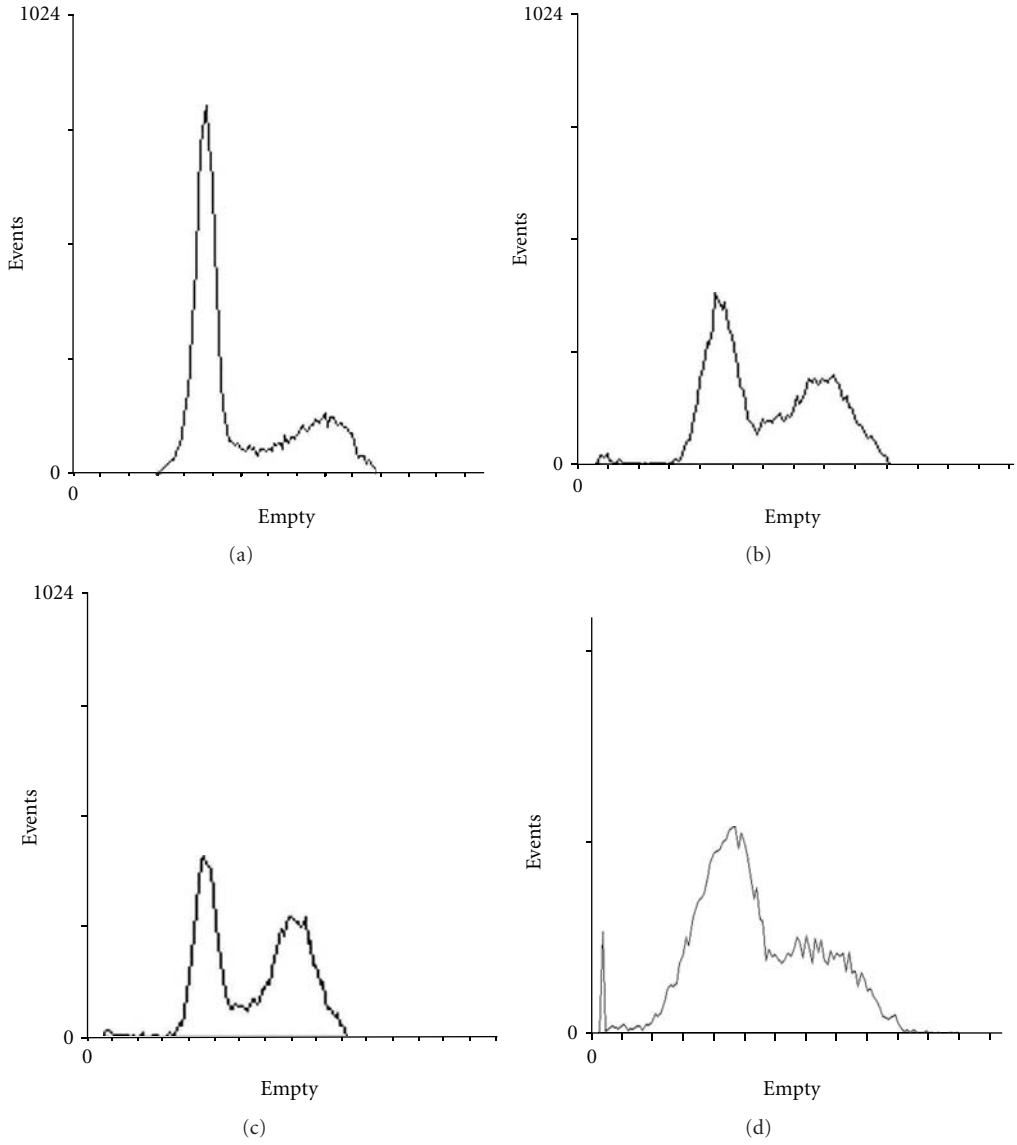

Figure 5: Effect of CI431 on cell cycle distribution. BEL-7402 cells were seeded at 3 x 10^4/cm^2 in 10-cm dishes and treated with CI431 at 20 (b), 40 (c) or 80 μg/mL, respectively or without treatment (a). After incubation for 24 h, cells were collected and the DNAs were stained by PI, while the RNAs were removed by digestion with RNase A. The DNA contents of the cells were determined with the FACSCalibur cytometer. The results showed that CI431 significantly induced a G_2/S phase arrest with a decrease in G_0/G_1 phase population at 20, 40, and 80 μg/mL, while a dramatic increase of sub-G1 phase (hypodiploid cells) was observed at doses higher than 80 μg/mL.

a G_2/S phase arrest with a decrease in G_0/G_1 phase population at 20, 40, and 80 μg/mL, while a dramatic increase of sub-G1 phase (hypodiploid cells) was observed at doses higher than 80 μg/mL (Figure 5).

3.6. Mitochondrial-Membrane Potential ($\Delta\psi m$). To investigate the involvement of the mitochondrial pathway, depolarization of the mitochondrion was analyzed by loading with JC-1. BEL-7402 were exposed to CI431 at doses of 20, 40, and 80 μg/mL for 24 h, and the ratio of green fluorescence intensity to red fluorescence intensity was used for quantitative analysis of the disruption of $\Delta\psi m$. As shown in Figure 6, after treatment with CI431, $\Delta\psi m$ began to decrease, and the ratio is 0.61 ± 0.07 (blank), 1.92 ± 0.19 (20 μg/mL), 5.08 ± 0.45 (40 μg/mL), and 8.28 ± 0.61 (80 μg/mL), respectively, indicating disruption of mitochondrial function.

4. Discussion

Over 17,000 biologically active compounds have been identified from marine sources, mainly isolated from sessile animals, such as sponges, tunicates, corals, mollusks, and bryozoans [3, 4]. Many of these substances are potent cytotoxins that are of great interest for anticancer drug development. The discovery of new marine drug candidates is a highly efficient process due to the availability of sophisticated

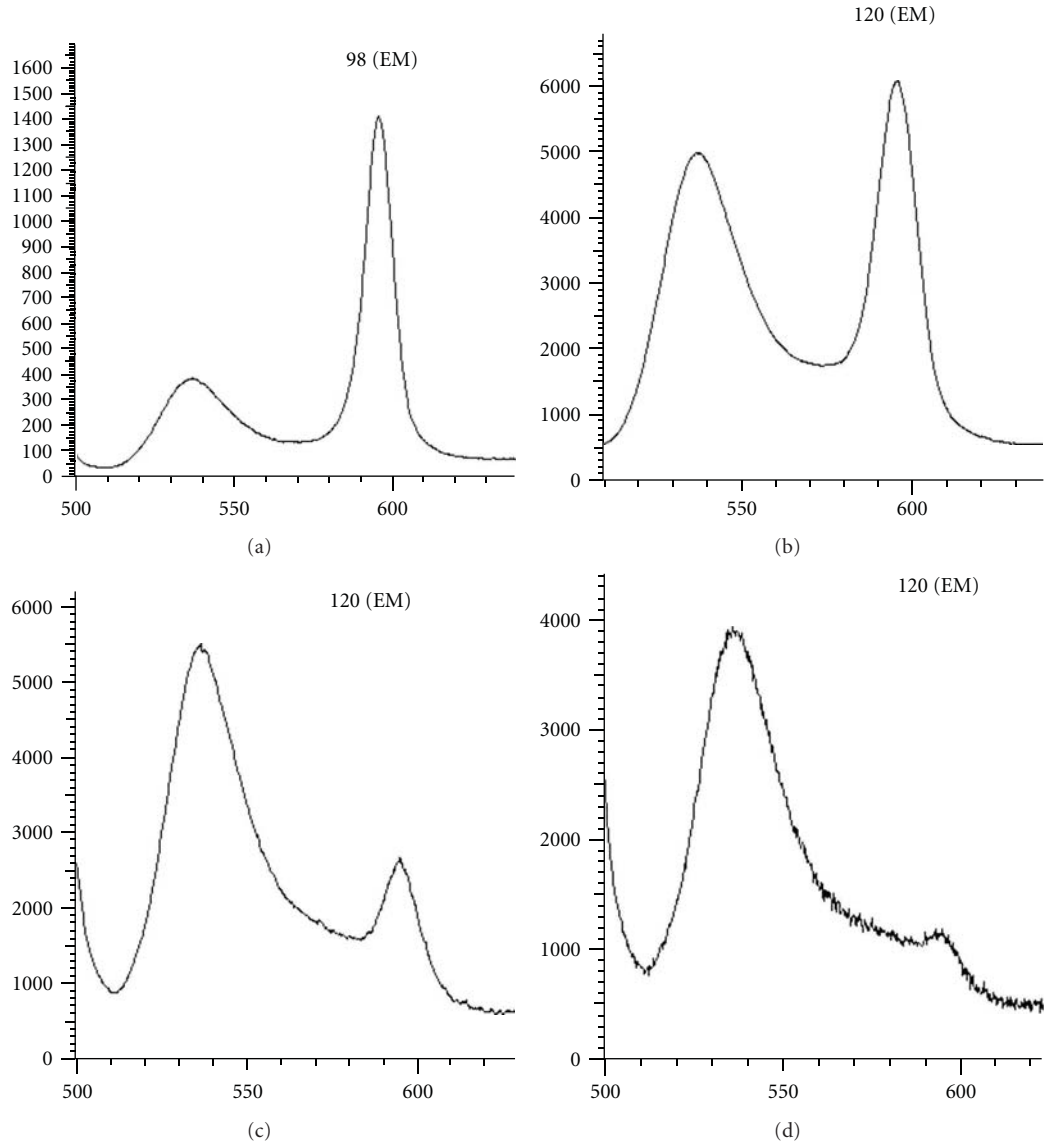

Figure 6: Cytofluorometric analysis of $\Delta\psi m$ BEL-7402 cells were seeded in 12-well plates at a density of 3×10^5 cells/mL and treated with CI431 at doses of 20, 40, and 80 μg/mL for 24 h. After treatment with CI431 200 μL pre-warmed incubation buffer containing 0.2 μL MitoCapture was added to each well and plates were incubated for 15 min at 37°C in a 5% CO_2 incubator. Then, cells were analyzed by a Fluorescence Spectrophotometer (F-4500, HITACHI, Japan). After treatment with CI431, $\Delta\psi m$ began to decrease, and the ratio of green fluorescence intensity to red fluorescence intensity was 0.61 ± 0.07 (blank, a), 1.92 ± 0.19 (20 μg/mL, b), 5.08 ± 0.45 (40 μLgmL, c) and 8.28 ± 0.61 (80 μg/mL, d), respectively, indicating disruption of mitochondrial function.

screening, dereplication, and characterization techniques. In this study, we describe a novel protocol which allows efficient and rapid purification of low-molecular weight marine drug candidates with antitumor activity from *Ciona intestinalis L.* We have utilized for their isolation a combination ofvspace.5pt extraction/purification procedures, including heating, acetone fractionation, gel chromatography and high performance liquid chromatography. The proposed protocol resulted in obtaining homogeneous preparations of one compound from *Ciona intestinalis L.* with MW of 431 Da, which exhibited strong antitumor activity. The MW identity of the purified compound was determined by mass spectrometry.

We used the MTT assay to test the cytotoxic effects of CI431 and found that CI431 exhibited potent cytotoxicity against various types of cancer cell lines in a dose- and time-dependent manner but inhibited the viability of Bel-7702, human benign liver cells, very slightly. That CI431 has opposite effects on tumor cells and normal cells is intriguing. This shows that CI431 may have little toxicity for normal liver cells. When the cells were stained with different concentrations of CI431 for 48 h, marked morphological changes were clearly observed, including chromatin condensation, nuclear and cytoplasmic fragmentation, and apoptotic body appearance. Further studies using PI staining and flow cytometry analysis showed that CI431 significantly induced a G2/S

phase arrest with a decrease in G0/G1 phase population, and 17.3% hypodiploid cells were observed when the dose up to 60 μg/mL. Considering figures of apoptosis bodies obtained from staining with DAPI and 17.3% hypodiploid BEL-7402 cells reserved from flow cytometry, we concluded that CI431 could induce the apoptosis of BEL-7402 cell lines. In addition, marked mitochondrial-membrane-potential changes were clearly observed especially after treatment with 0.1 mg/mL of CI431 for 24 h. Loss of mitochondrial-membrane potential ($\Delta\Psi m$) is an early event in apoptosis. It indicated that maybe CI431 induced BEL-7402 cell apoptosis through a mitochondria-mediated apoptosis pathway.

5. Conclusion

This study describes for the first time an efficient method for the purification of a kind of antitumor compound from *Ciona intestinalis L.* It could effectively induce apoptosis in HCC cell lines, mediated through a disruption of mitochondrial membrane potential. Our results suggest that CI431 is a promising drug candidate for the treatment of HCC. However, the specific mechanism of the apoptosis-inducing effect of CI431 has not yet been elucidated. The effective and powerful components in this extracted compound need to be further characterized. Because some secondary metabolites are generated in organisms just in a very short period of their life cycles, and some target chemicals are in low concntration, how to obtain enough chemicals for structure analyzing and preclinical testing has become a crucial problem in marine medicine research. In this study, the yield rate of CI431 from *Ciona intestinalis L.* was extremely low. In order to elucidate its structural formula, more samples should be collected, isolated, and purified.

Acknowledgments

This study was supported by 863 High Technology Project (no. 2007AA091403 and 2007AA09Z408) from the Chinese Ministry of Science and Innovative Drug Development Projects of China (2009ZX09103-661 and 2009ZX09102). The authors are grateful to Dr. Chunguang Wang at the College of Life Science and Technology, Tongji University for her careful review of the study, and also to all members of the laboratory for their continuous technical advice and helpful discussion. They would also like to thank Dr. Fred Bogott at the Austin Medical Center, Austin of Minnesota, USA, for his excellent English editing of the manuscript.

References

[1] J. W. Blunt, B. R. Copp, W. P. Hu, M. H. G. Munro, P. T. Northcote, and M. R. Prinsep, "Marine natural products," *Natural Product Reports*, vol. 26, no. 2, pp. 170–244, 2009.

[2] J. W. Blunt, B. R. Copp, W. Hu, M. H. G. Munro, P. T. Northcote, and M. R. Prinsep, "Marine natural products," *Natural Product Reports*, vol. 25, no. 1, pp. 35–94, 2008.

[3] D. J. Newman and G. M. Cragg, "Marine natural products and related compounds in clinical and advanced preclinical trials," *Journal of Natural Products*, vol. 67, no. 8, pp. 1216–1238, 2004.

[4] M. D. Lebar, J. L. Heimbegner, and B. J. Baker, "Cold-water marine natural products," *Natural Product Reports*, vol. 24, no. 4, pp. 774–797, 2007.

[5] K. L. Rinehart, "Antitumor compounds from tunicates," *Medicinal Research Reviews*, vol. 20, no. 1, pp. 1–27, 2000.

[6] D. J. Newman and G. M. Cragg, "Advanced preclinical and clinical trials of natural products and related compounds from marine sources," *Current Medicinal Chemistry*, vol. 11, no. 13, pp. 1693–1713, 2004.

[7] K. L. Rinehart, J. B. Gloer, J. C. Carter, S. A. Mizsak, and T. A. Scahill, "Structures of the didemnins, antiviral and cytotoxic depsipeptides from a Caribbean tunicate," *Journal of the American Chemical Society*, vol. 103, no. 7, pp. 1857–1859, 1981.

[8] J. L. Urdiales, P. Morata, I. N. de Castro, and F. Sánchez-Jiménez, "Antiproliferative effect of dehydrodidemnin B (DDB), a depsipeptide isolated from Mediterranean tunicates," *Cancer Letters*, vol. 102, no. 1-2, pp. 31–37, 1996.

[9] M. C. Edler, A. M. Fernandez, P. Lassota, C. M. Ireland, and L. R. Barrows, "Inhibition of tubulin polymerization by vitilevuamide, a bicyclic marine peptide, at a site distinct from colchicine, the vinca alkaloids, and dolastatin 10," *Biochemical Pharmacology*, vol. 63, no. 4, pp. 707–715, 2002.

[10] N. Lindquist, W. Fenical, G. D. Van Duyne, and J. Clardy, "Isolation and structure determination of diazonamides A and B, unusual cytotoxic metabolites from the marine ascidian Diazona chinensis," *Journal of the American Chemical Society*, vol. 113, no. 6, pp. 2303–2304, 1991.

[11] K. Rinehart, T. G. Holt, N. L. Fregeau et al., "Ecyeinascidin 729, 743, 759A, and 770: potent antutumor agents from the Caribbean tunicate Ecteinascidia turbinata," *Journal of Organic Chemistry*, vol. 55, no. 15, pp. 4512–4515, 1990.

[12] M. Zhang, H. Zhang, C. Sun et al., "Targeted constitutive activation of signal transducer and activator of transcription 3 in human hepatocellular carcinoma cells by cucurbitacin B," *Cancer Chemotherapy and Pharmacology*, vol. 63, no. 4, pp. 635–642, 2009.

[13] M. A. Avila, C. Berasain, B. Sangro, and J. Prieto, "New therapies for hepatocellular carcinoma," *Oncogene*, vol. 25, no. 27, pp. 3866–3884, 2006.

[14] J. Martin and J. F. Dufour, "Tumor suppressor and hepatocellular carcinoma," *World Journal of Gastroenterology*, vol. 14, no. 11, pp. 1720–1733, 2008.

[15] N. J. Gusani, Y. Jiang, E. T. Kimchi, K. F. Staveley-O'Carroll, H. Cheng, and J. A. Ajani, "New pharmacological developments in the treatment of hepatocellular cancer," *Drugs*, vol. 69, no. 18, pp. 2533–2540, 2009.

[16] A. I. Gomaa, S. A. Khan, M. B. Toledano, I. Waked, and S. D. Taylor-Robinson, "Hepatocellular carcinoma: epidemiology, risk factors and pathogenesis," *World Journal of Gastroenterology*, vol. 14, no. 27, pp. 4300–4308, 2008.

[17] T. Wang, W. Huang, and T. Chen, "Baclofen, a GABAB receptor agonist, inhibits human hepatocellular carcinoma cell growth in vitro and in vivo," *Life Sciences*, vol. 82, no. 9-10, pp. 536–541, 2008.

[18] M. Thomas, "Molecular targeted therapy for hepatocellular carcinoma," *Journal of Gastroenterology*, vol. 44, no. 19, pp. 136–141, 2009.

[19] Q. J. He, B. Yang, Y. J. Lou, and R. Y. Fang, "Contragestazol (DL111-IT) inhibits proliferation of human androgen-independent prostate cancer cell line PC3 in vitro and in vivo," *Asian Journal of Andrology*, vol. 7, no. 4, pp. 389–393, 2005.

[20] H. L. Xu, Y. Inagaki, F. S. Wang, N. Kokudo, M. Nakata, and W. Tang, "Effect of benzyl-N-acetyl-α-galactosaminide

on KL-6 mucin expression and invasive properties of a human pancreatic carcinoma cell line," *Drug Discoveries & Therapeutics*, vol. 2, pp. 282–285, 2008.

[21] P. N. Chen, S. C. Chu, H. L. Chiou, C. L. Chiang, S. F. Yang, and Y. S. Hsieh, "Cyanidin 3-glucoside and peonidin 3-glucoside inhibit tumor cell growth and induce apoptosis in vitro and suppress tumor growth in vivo," *Nutrition and Cancer*, vol. 53, no. 2, pp. 232–243, 2005.

[22] C. Riccardi and I. Nicoletti, "Analysis of apoptosis by propidium iodide staining and flow cytometry," *Nature Protocols*, vol. 1, no. 3, pp. 1458–1461, 2006.

[23] S. K. Mantena, S. D. Sharma, and S. K. Katiyar, "Berberine, a natural product, induces G1-phase cell cycle arrest and caspase-3-dependent apoptosis in human prostate carcinoma cells," *Molecular Cancer Therapeutics*, vol. 5, no. 2, pp. 296–308, 2006.

Hindawi Publishing Corporation
Evidence-Based Complementary and Alternative Medicine
Volume 2011, Article ID 486845, 13 pages
doi:10.1155/2011/486845

Research Article

Isolation and Characterization of Adhesive Secretion from Cuvierian Tubules of Sea Cucumber *Holothuria forskali* (Echinodermata: Holothuroidea)

Malgorzata Baranowska,[1] Ute Schloßmacher,[1] J. Douglas McKenzie,[2] Werner E. G. Müller,[1] and Heinz C. Schröder[1]

[1] *Institute for Physiological Chemistry, University Medical Center of the Johannes Gutenberg University, Duesbergweg 6, 55128 Mainz, Germany*
[2] *Xanthella Ltd., Marine Resource Centre, Barcaldine, Argyll, Scotland PA37 1SG, UK*

Correspondence should be addressed to Werner E. G. Müller, wmueller@uni-mainz.de and Heinz C. Schröder, hschroed@uni-mainz.de

Received 15 January 2011; Accepted 16 May 2011

The sea cucumber *Holothuria forskåli* possesses a specialized system called Cuvierian tubules. During mechanical stimulation white filaments (tubules) are expelled and become sticky upon contact with any object. We isolated a protein with adhesive properties from protein extracts of Cuvierian tubules from *H. forskåli*. This protein was identified by antibodies against recombinant precollagen D which is located in the byssal threads of the mussel *Mytilus galloprovincialis*. To find out the optimal procedure for extraction and purification, the identified protein was isolated by several methods, including electroelution, binding to glass beads, immunoprecipitation, and gel filtration. Antibodies raised against the isolated protein were used for localization of the adhesive protein in Cuvierian tubules. Immunostaining and immunogold electron microscopical studies revealed the strongest immunoreactivity in the mesothelium; this tissue layer is involved in adhesion. Adhesion of Cuvierian tubule extracts was measured on the surface of various materials. The extracted protein showed the strongest adhesion to Teflon surface. Increased adhesion was observed in the presence of potassium and EDTA, while cadmium caused a decrease in adhesion. Addition of antibodies and trypsin abolished the adhesive properties of the extract.

1. Introduction

Adhesion plays an important role in many invertebrates for a variety of different functions. Some species of holothuroid echinoderms (sea cucumbers) possess a special defence system involving adhesion, based on secretion of highly adhesive filaments that can entangle predators. This system called Cuvierian tubules is mainly activated when animals are mechanically stimulated but may also be stimulated by heat. As a result sea cucumbers release white filaments, tubules, which become sticky upon contact with any object [1–5].

In the search for potential technological applications understanding the chemistry of the adhesive secretion from Cuvierian tubules is important. Applications may include the design of water-resistant adhesives, sealants, and biomedical coatings and the development of new antifouling strategies [6, 7].

The amazing adhesivity of the Cuvierian tubule filaments was investigated by Müller et al. [8], Zahn et al. [9], and Flammang et al. [2], whereby tubules were treated with various substances and adhesion to different surfaces was measured. However, protein extracts from Cuvierian tubules have not yet been investigated for their adhesion properties. Many researchers have studied the histochemistry of Cuvierian tubules, as early as in 1868 (Semper [10], followed by Jourdan [11], Hérouard [12], and later Müller et al. [13]).

The fine structure of Cuvierian tubules was investigated by VandenSpiegel and Jangoux [14]. Quiescent Cuvierian tubules consist of an outer mesothelium, an inner epithelium, and between them, a thick connective tissue layer that includes muscle fibres. Biochemical investigations by DeMoor et al. [5] revealed that Cuvierian tubules are made up of 60% protein and 40% carbohydrates. They are highly insoluble.

Antibodies raised against the material that remained on the substratum after detachment of the tubule have been used to detect and localize tubule protein(s) [5].

Also the adhesion of mussels has been thoroughly investigated. After isolation of the first adhesive protein, Mepf-1, which contains DOPA (3,4-dihydroxy-L-phenylalanine), ten further proteins have been isolated [7]. One of them is precollagen D which possesses a central collagen domain flanked by two fibroin-like domains with sequences similar to spider silk fibroin. This protein is found in spiders' drag line [15] and also in the silkworm *Bomyx mori* [16]. A similar protein has been found in sea urchin [17]. Using antibodies raised against recombinant precollagen D from the mussel *Mytilus galloprovincialis*, we could identify a protein with adhesive properties in sea cucumber Cuvierian tubule extracts.

2. Materials and Methods

2.1. Sea Cucumber. Sea cucumber *Holothuria forskåli* was collected at the coast of the Adriatic Sea near Rovinj (Istria, Croatia) with a dragnet at a depth 20 m in August 2007. Specimens were anaesthetized for 1 h in a saturated solution of urethane (Sigma-Aldrich, Taufkirchen, Germany) and then transported in methanol at 4°C to the laboratory before Cuvierian tubules were removed.

2.2. Extraction of Cuvierian Tubules. Cuvierian tubules were dried by lyophilization and ground in a mortar containing liquid nitrogen. Dried material (2 g) was stirred with 50 mL of buffer (4 M urea, 0.5 M Tris-HCl, pH 7.5) overnight at 4°C. The homogenate was then centrifuged at 14,000 ×g for 15 min. The supernatant was collected, filtered through 2-μm filter (Centrifugal Filter Devices Microcon, Millipore, Schwalbach, Germany) and dialyzed overnight against 5 l of distilled water which was changed every 3 h. To concentrate the sample, the dialysate was centrifuged (4.000 ×g) in a concentration tube (50 mL) using a centrifugal concentrator (Amicon, Millipore, Schwalbach, Germany) until 1 mL of extract was obtained.

2.3. SDS-PAGE and Western Blot Analysis. Extract from Cuverian tubules was concentrated with Ready Prep 2-D Clean-up Kit (Bio-Rad, Munich, Germany). The concentrated protein was dissolved in loading buffer (Roti-Load, Roth, Karlsruhe, Germany), boiled for 5 min and subjected to electrophoresis in a 12% polyacrylamide gel containing 0.1% sodium dodecyl sulfate (SDS-PAGE). After protein separation the gel was washed with distilled water for 15 min and then stained with Gel Code Blue Reagent (Pierce, Bonn, Germany).

For Western blot analysis, proteins were transferred from the gels to PVDF membranes (Millipore, Schwalbach, Germany) using a Trans-Blot SD system (Bio-Rad, Munich, Germany). The membranes were blocked with Blocking reagent (Roche, Mannheim, Germany), then rinsed in TBS-T (20 mM Tris-HCl pH 7.6, 137 mM NaCl, 0.1% Tween-20) and incubated for 1 h with polyclonal antibodies (rabbit) that had been raised against precollagen D from mussel *M. galloprovincialis* (PoAb-pCD). The dilution of the antiserum was 1 : 1000. The membrane was washed three times in TBS-T and then incubated for 1 h with anti-rabbit IgG (whole molecule) alkaline phosphatase (Sigma-Aldrich, Taufkirchen, Germany). After washing, proteins were visualized using 5-bromo-4-chloro-3-indolyl phosphate-*p*-toluidine salt (BCIP) and *p*-nitrotetrazolium blue chloride (NBT) (Roth, Karlsruhe, Germany).

2.4. Isolation of Adhesive Protein by Electroelution. The protein band from the electrophoresis gel which reacted with antibodies against precollagen D was cut from the gel and electroeluted using a Model 422 Electro-Eluter (Bio-Rad, Munich, Germany). The purity of the obtained protein was checked by SDS-PAGE and Western blot analysis and concentration was estimated by 2-D Quant kit (Amersham Biosciences, Freiburg, Germany).

2.5. Antibody Production. Polyclonal antibodies (PoAb) were raised against the protein obtained by electroelution by immunization of female rabbits (White New Zealand) as described [18]. After three boosts the serum was collected and screened in a conventional ELISA assay as well as by Western blotting.

2.6. Collection of Adhesive Proteins. Glass beads (1 g) with a size of 2 mm (Elring-Klinger Kunststofftechnik GmbH Grossostheim-Ringheim, Germany) were washed with 4 M urea buffer (containing 0.5 M Tris-HCl, pH 7.5) and added to each of four tubes containing the same amount of protein (500 μg) but various concentrations of urea (1 M, 2 M, and 3 M). The tubes with the glass beads were incubated under shaking for 2 h and vortexed every 10 min. The supernatants were then discarded and the beads were washed with 0.05 M Tris-HCl pH 7.5 (1 mL) by shaking and vortexing. The washing step was repeated three times. The buffer was then removed and 50 μL of sample buffer (4-times concentrated; 100 mM Tris-HCl, pH 6.8, 2% SDS, 5% ß-mercaptoethanol, 15% glycerol, 0.006% bromophenol blue) was added to each tube. The glass beads were then boiled and shaken for 15 min at 95°C in a thermomixer. Thereafter the supernatants were collected and 40 μL each were taken for loading onto two 12% SDS PAGE gels. One gel was stained with Gel Code Blue Reagent and destained with water, then scanned with an Odyssey Scanner using the Odyssey v.1.2 software to quantify the protein bands. The proteins of the second gel were transferred to PVDF membrane and incubated with antibody against adhesive protein and developed using anti-rabbit IgG (whole molecule) alkaline phosphatase and visualized with NBT and BCIP.

2.7. Immunoprecipitation. For immunoprecipitation of the adhesive protein, the Seize × Immunoprecipitation Kit (Pierce, Bonn, Germany) was used; 50 μL of polyclonal antibody against adhesive protein from Cuvierian tubules (PoAb-Ctub) and 250 μL of Cuvierian tubule extract were

applied. Results were checked by SDS PAGE and Western blotting.

2.8. Gel Filtration. Sephadex G50 (Pharmacia Fine Chemicals, Uppsala, Sweden) was used for preparation of a gel filtration column (1 cm × 15 cm). Calibration of the column was performed using a mixture of bovine serum albumin (BSA), silk fibroin, and carbonic anhydrase. The retention time of each sample was recorded. The presence of the protein in each fraction was checked by the Bradford assay [19].

Before loading the extract, the column was washed with 4 M urea buffer. One milliliter of the 4 M urea extract of the Cuvierian tubules was loaded onto the column. Protein was eluted using 4 M urea. Forty 500-μL fractions were collected. The protein concentration in each fraction was assayed using the Bradford assay. Protein-containing fractions were loaded onto a 12% SDS PAGE gel. The gel was stained with Gel Code Blue Reagent, destained with water, and scanned with an Odyssey scanner.

2.9. Histology

2.9.1. Preparation of Tissue Sections. Cuvierian tubule tissue was fixed in 2% paraformaldehyde in PBS pH 7.4 overnight. After washing in PBS buffer (pH 7.4) containing 6.8% sucrose at 4°C overnight, dehydration was performed in 100% acetone. During the first 5 minutes acetone was renewed several times. The last portion of acetone was left overnight. Infiltration of the samples was done using Technovit 8100 (Heraeus Kulzer, Hanau, Germany) according to the instructions of the manufacturer. After hardening, 3–10 μm thick sections were prepared using a rotary microtome. Slices were mounted on silane-coated slides (Sigma, Taufkirchen, Germany) for histology and immunohistochemistry.

2.9.2. Hematoxylin and Eosin Staining. After washing in PBS and in distilled water, tissue sections on slides were stained in hematoxylin solution for 5 min. After staining slides were washed in tap water for 25 min and in distilled water for 5 min. Sections were stained in eosin for 1 min. After washing in distilled water, sections were dehydrated with increasing concentrations of isopropanol (75–100%) for 1 min each. Before mounting, slides were washed in detergent Roti Clear (Roth, Karlsruhe, Germany). Slides were mounted in DPX (Sigma, Taufkirchen, Germany), covered with cover slips, and sealed with nail polish.

2.9.3. Cason's Trichrome. Sections on slides were washed in PBS for 5 min, then placed in staining solution (1% orange G, 1.5% acid fuchsine, 0.5% aniline blue, and 1% phosphotungstic acid) for 5 min. After staining sections were washed in water for 5 min, dehydrated in solutions containing increasing concentration of ethanol, cleared in detergent (Roti Clear), mounted with DPX, and sealed with nail polish.

2.9.4. Methylene Blue and Azure B. A mixture of 1% azure and 1% methylene blue was used. Before staining sections were warmed up to 70°C. A drop of the stain was put on the sections. After drying (60°C), unbound stain was washed out with distilled water. Slides were then dried, mounted with DPX, and sealed with nail polish.

2.10. Immunohistochemistry. Sections were kept overnight in 4% BSA in PBS. After washing with PBS, samples were incubated with polyclonal antibody against adhesive protein from Cuvierian tubules (PoAb-Ctub; dilution 1 : 100). Sections with antibody were kept in a humid chamber at room temperature for 2 h. After washing in PBS (2 × 10 min), sections were incubated with Cy3-conjugated goat anti-rabbit IgG (Dianova, Hamburg, Germany) (diluted 1 : 100) in the dark at 37°C for 120 min. After additional washing (2 × 10 min) in PBS, staining with DAPI (4′-6-diamidino-2-phenylindole; Sigma-Aldrich, Taufkirchen, Germany) for 30 min was performed to highlight the nuclei. After washing and mounting with the Gel/Mount (Fluorescent mounting medium, Dako, Hamburg, Germany), sections were inspected for immunofluorescence using an Olympus AHBT3 light microscope. Preimmune serum was used as a negative control.

2.11. Transmission Electron Microscopy. Electron immunogold labeling was performed with Cuvierian tubule samples treated with 0.1% glutaraldehyde/3% paraformaldehyde in phosphate buffer, pH 7.4 for 3 h at room temperature. The material was dehydrated in ethanol and embedded in LR-White resin. Sections (60-nm thick) were cut and blocked with bovine serum albumin in PBS and then incubated with the primary antibody against adhesive protein from Cuvierian tubules (PoAb-Ctub; 1 : 1,000 for 12 h at 4°C). In controls, preimmune serum was used. After three washes with PBS, 1% BSA, sections were incubated with a 1 : 100 dilution of the secondary antibody (1.4-nm nanogold anti-rabbit IgG; diluted 1 : 200) for 2 h. Sections were rinsed in PBS, treated with glutaraldehyde in PBS, washed, and dried. Subsequently, enhancement of immunocomplex detection was performed with silver as described by Danscher [20]. The samples were transferred onto coated copper grids and analyzed using a Tecnai 12 microscope (FEI Electron Optics, Eindhoven, Netherlands).

2.12. Measurement of Adhesion. To measure adhesion, the instrument shown in Figure 1 was used. This instrument was based on a laboratory balance, modified by adding two blocks to it (made from either Teflon, iron, gelatine, glass, or silicone). The upper block was attached to one beam of the balance, while the lower block was attached to a movable platform. Adhesion was measured as follows: a drop of measuring liquid (10 μL) was put on the block and stuck to the second block hanging from the beam. In this position, the drop of measuring liquid was incubated for 15 min at room temperature. To determine the adhesion of the liquid, standard masses were added until the two blocks separated when the adhesion of the liquid failed. The amount of

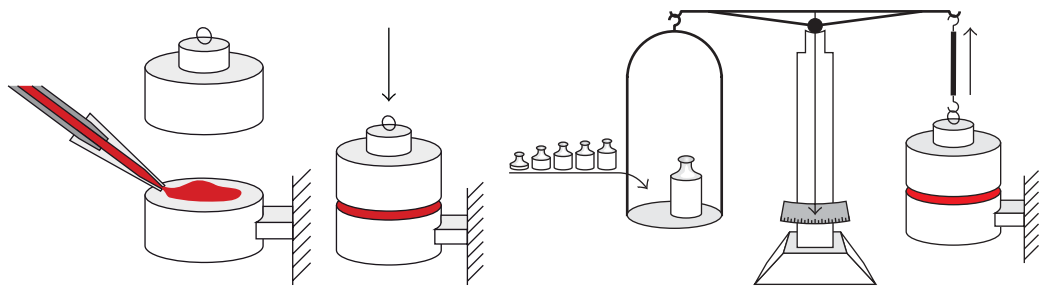

Figure 1: Scheme of equipment used for measurement of adhesion. (a) Application of the sample between two blocks; the upper block is attached to one of the beams of a laboratory balance, while the lower block is fixed. (b) Attachment of both blocks via the adhesive protein containing sample. (c) Addition of standard weights until both blocks become separated to determine the adhesive forces of the sample.

weights put on, to release the block and liquid was equivalent to the adhesion forces between them.

2.13. Statistics. Statistical evaluation of the data was performed as described [21].

3. Results

3.1. Extraction of Cuvierian Tubules. Several buffers were used for the extraction of protein from Cuvierian tubules. Protein solubilization was improved in basic rather than acidic buffers. Urea, SDS, and reducing buffers increased the extraction of tubule adhesive proteins. The amounts of protein extracted using various buffers were compared by SDS PAGE analysis. The best results were obtained using 4 M urea, 0.5 M Tris-HCl pH 7.5 (Figure 2, lane A), and sample loading buffer (100 mM Tris-HCl, pH 6.8, 2% SDS, 5% ß-mercaptoethanol, 15% glycerol, 0.006% bromophenol blue; results not shown). To improve visualization of the protein the extract shown in lane A was purified by the Ready Prep 2-D Clean-up kit. Other buffers like 150 mM NaCl, 1.5% NP_{40}, 0.1% SDS, 0.1% DOC, 50 mM Tris-HCl pH 8 buffer or 0.5 M NaCl, 5 mM Tris-HCl pH 7.5, 7 mM Na_2SO_4, 0.4 mM $NaHCO_3$, 20 mM EDTA buffer solubilized less protein (not shown). The 4 M urea buffer was used for further analysis because the composition of the sample loading buffer (see above) might interfere with further tests.

SDS PAGE analysis of the purified Cuvierian tubule extract showed the presence of a wide size range of proteins (Figure 2, lane A). At this stage it was not possible to recognise which protein could be involved in adhesion. To get information about the conformation and possible dimerization/oligomerization of the proteins, the extract was run on a seminative gel (Figure 2, lane F). This method yielded a lower number of protein bands, indicating that some proteins might have been present as dimers/oligomers.

3.2. Identification of Adhesive Protein in Cuvierian Tubules. An antibody (PoAb-pCD; polyclonal antibody number N374) against a mussel byssus protein (recombinant precollagen D from *M. galloprovincialis*) was used to identify adhesive protein(s) of Cuvierian tubules. Precollagen D is a special collagen, found in the byssal thread, which is involved in tension-bearing. After reaction with the antibody the membrane showed a strong band (Figure 2, lane B) with one of the Cuvierian tubule proteins of a size 18 kDa. In further experiments this protein was recognized as the protein involved in adhesion.

3.3. Isolation of Identified Protein

3.3.1. Electroelution. The next step after the identification of the adhesive protein was its isolation. The band with a molecular mass of 18 kDa was cut out from the gel and electroeluted. The purity of the eluted protein was determined by SDS PAGE and Western blot analysis (Figure 2, lane C). The isolated protein was injected into a rabbit and after 4 weeks, the specific antibody designated PoAb-Ctub was obtained.

3.3.2. Neutralization of Antibody. Western blot analysis of the crude extract of Cuvierian tubules using the PoAb-Ctub antibody revealed a strong reaction with several proteins of the extract even in the presence of optimized concentrations of antibody and extract (not shown).

The antibody was neutralized by incubation with Cuvierian tubule extract for 1-2 hours. After binding, the resulting mixture was applied onto the membrane of the Western blot. If the mixture contained an excess of specific antibodies, they would bind to the antigen on the membrane.

The maximum increase in specificity of the antibody was observed after dilution to 1 : 1000 and addition of extract at a ratio of 1 : 5 (Figure 2, lane E). The Western blot showed two proteins which reacted with the antibody, one with a molecular mass of 18 kDa and the other of 36 kDa. Cuvierian tubule extract incubated with preimmune serum against the adhesive protein gave no reaction (Figure 2, lane D). We hypothesized that the upper protein band in lane E may represent a dimer of the lower protein band. In order to verify this, a native gel was run (Figure 2, lane F). After transfer of the protein, the membrane was incubated with the antibody against the adhesive protein. The results revealed the presence of only one band most likely caused by dimer formation of the adhesive protein (Figure 2, lane G).

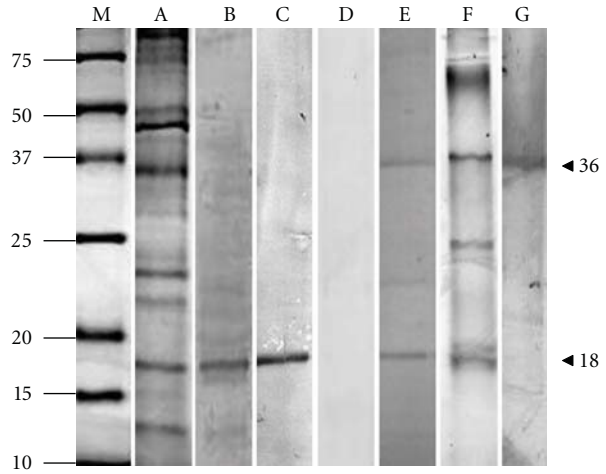

Figure 2: Analysis and identification of adhesive protein in Cuvierian tubule extract from sea cucumber *H. forskåli.* Proteins were analyzed by 12% SDS PAGE and Western blotting. Gels were stained with Gel Code Blue Reagent. (A) Cuvierian tubule extract (4 M urea, 0.5 M Tris-HCl pH 7.5) purified with Ready Prep 2-D Clean up kit. (B) Western blot of Cuvierian tubule extract, incubated with antibody against precollagen D (1 : 1000 dilution) and developed with anti-rabbit IgG alkaline phosphatase. (C) Western blot detection of adhesive protein from *H. forskåli*, isolated by electroelution, using antibody against precollagen D of mussel *M. galloprovincialis* (1 : 1000 dilution) (positive control). (D) Western blot of Cuvierian tubule extract incubated with preimmune serum. (E) Western blot of Cuvierian tubule extract incubated with antibodies against isolated (electroeluted) adhesive protein from *H. forskåli* (dilution 1 : 1000); the serum was purified by treatment with Cuvierian tubule extract (dilution 1 : 10) at a ratio of 1 : 5. (F) Cuvierian tubule extract, separated on seminative gel. (G) Western blot of Cuvierian tubule extract, separated on seminative gel (dilution of antibody, 1 : 1000); the serum was purified by treatment with Cuvierian tubule extract (dilution 1 : 10) at a ratio of 1 : 10. M: Molecular mass markers. *Arrowheads*: adhesive protein (18 kDa) and dimer (36 kDa).

3.3.3. Immunoprecipitation. Because the amount of adhesive protein obtained by electroelution was low and the buffer used for elution of the protein could complicate further analysis, other methods for isolation of the protein were employed. Immunoprecipitation is based on the interaction between a protein and its specific antibody, separation of the formed immune complex with Protein A, and subsequent Western blot analysis (Figure 3, lane (a)).

In a parallel experiment, extract from mussels *M. galloprovincialis* was applied on the immunocolumn with antibody against the adhesive protein from Cuvierian tubules. The result revealed a weak band at 20 kDa (Figure 3, lane (b)).

3.3.4. Gel Filtration. Gel filtration chromatography (Sephadex G-50) was used for separation of the proteins based on their size. The fractions collected were assayed using the Bradford assay to detect the presence of protein. Protein-containing fractions were analyzed by SDS PAGE and measured for adhesion.

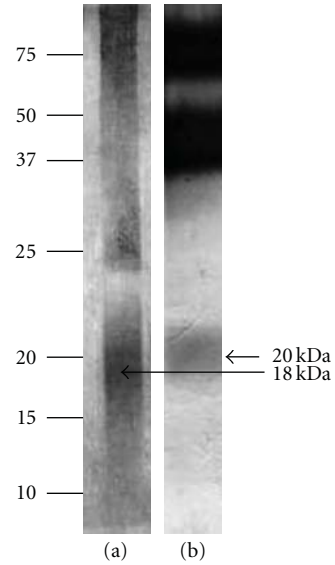

Figure 3: Western blot analysis of adhesive protein from Cuvierian tubule extract, purified by immunoprecipitation. The blot was developed using antibodies against adhesive protein from *H. forskåli* (PoAb-Ctub) and anti-rabbit IgG alkaline phosphatase secondary antibody. (a) Adhesive protein incubated with antibody against adhesive protein from *H. forskåli*. (b) Protein from mussels (precollagen D), incubated with antibody against adhesive protein from Cuvierian tubules. Numbers to the left indicate molecular masses of marker proteins in kDa.

The presence of adhesive protein was observed in fractions 6 to 8 (Figure 4). The strongest adhesion was found in fraction 7 (Figure 4(b)) where the concentration of adhesive protein was the highest (Figure 4(a)). Fractions 7 and 8 contained a higher degree of contamination by high-molecular-mass proteins. Relative molecular masses were determined using the equation: $\log M = M_0 - (6.062 - 5.00 \cdot d)\ (V_e/V_0)$ (M, molecular mass; d, density of the swollen gel; V_e, elution volume; V_0, void volume) [22]. For the column used in the experiment shown in Figure 4, the equation is as follows: $\log M = 5.189 - 0.712\ (V_e/V_0)$ (see also [23]).

3.3.5. Collection of Adhesive Proteins. Adhesive proteins may adhere to various surfaces. In this experiment adhesion to glass surface was used to isolate the *H. forskåli* protein from crude extract. Glass beads were incubated with protein extract containing the adhesive protein. After removing the extract and incubation of the glass beads with nondenaturing buffer, adhesive protein remained bound on the beads. To remove the protein from the glass surface, the beads were boiled with electrophoresis sample buffer and loaded onto 12% SDS PAGE. Relative band intensities corresponding to the adhesive protein were estimated using the Odyssey software. Proteins were transferred to PVDV membrane and analyzed by Western blot using the antibody against adhesive protein from Cuvierian tubules. The Western blots confirmed that the 18-kDa protein was the dominant protein harvested by using the glass beads procedure (not shown). Results after testing adhesion in the presence of

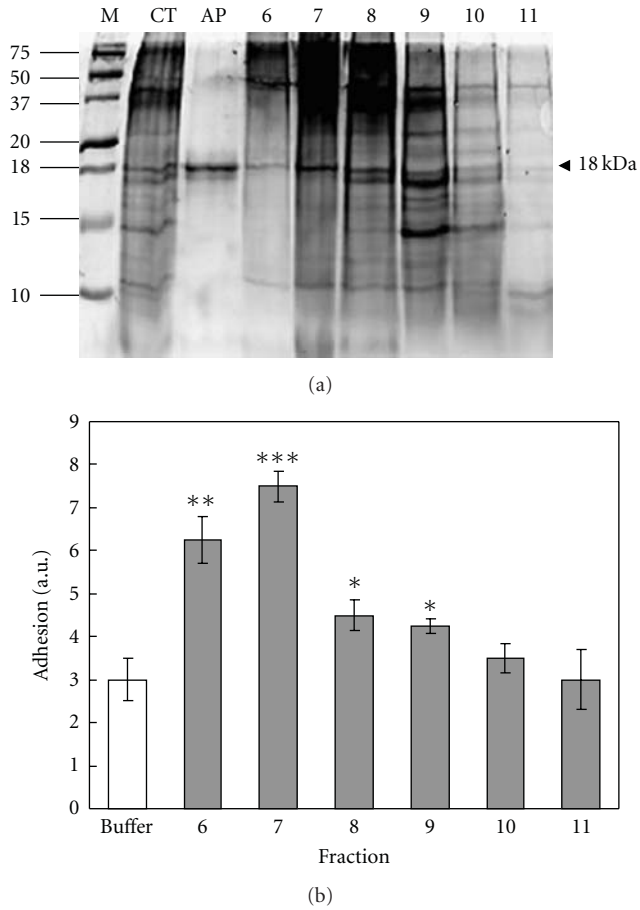

Figure 4: Analysis of fractions of gel filtration chromatography of Cuvierian tubule extract. (a) 15% SDS PAGE. *CT*: extract of Cuvierian tubules in 4 M urea, 0.5 M Tris-HCl buffer pH 7.5. *AP*: adhesive protein obtained by electroelution from Cuvierian tubule extract (positive control). *6–11*: fractions with highest concentration of protein according to Bradford assay. *M*, Molecular mass markers. *Arrowhead*: adhesive protein (18 kDa). (b) Adhesive activity, given in arbitrary units ± SD ($n = 3$), of fractions 6–11 compared to control (0.5 M urea buffer). Numbers to the left indicate molecular masses of marker proteins in kDa. Level of significance: $^{*}P < 0.05$; $^{**}P < 0.01$; $^{***}P < 0.001$.

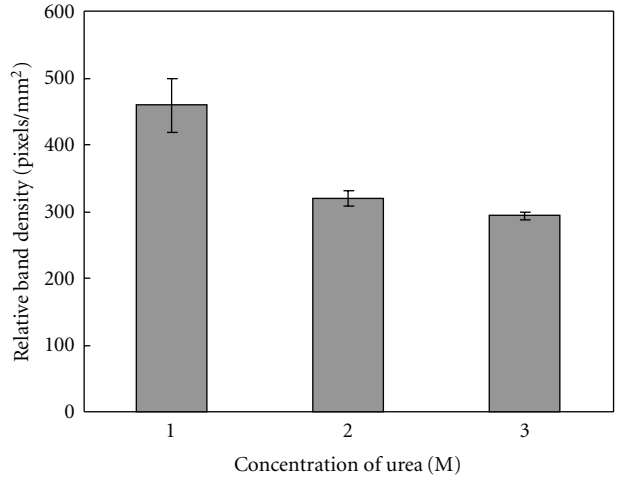

Figure 5: Binding of adhesive protein from Cuvierian tubule extract to glass beads in the presence of various concentrations of urea. Glass beads (size, 2 mm) were incubated with adhesive protein extract in the presence of various concentrations of urea (1 M, 2 M, and 3 M; containing 0.5 M Tris-HCl, pH 7.5), as described in Materials and Methods. After washing, the glass beads were boiled in SDS sample buffer and the released protein was analyzed by 12% SDS PAGE. The gel was stained with Gel Code Blue Reagent. Relative band intensities corresponding to the adhesive protein were determined by scanning of the gel using an Odyssey Scanner and applying the Odyssey v.1.2 software to quantify the protein bands.

various concentrations of urea revealed that a decrease in urea concentration of the extract resulted in an increased adhesion of the protein (Figure 5).

3.4. Histology. Cuvierian tubules were stained with Cason's trichrome, hematoxylin, and eosin, and methylene blue and azure to study their structure. Staining with these dyes showed that the quiescent tubules of *H. forskåli* consist of an outer mesothelium and an inner epithelium encompassing a thick connective tissue layer. The mesothelium is made of two cell layers, an upper layer of adluminal cells and a lower layer of granular cells.

3.4.1. Cason's Trichrome. This stain visualizes various organelles like nuclei (stained red) and collagen (blue). In sections of Cuvierian tubules, mesothelium was stained red, and the inner connective tissue was stained blue (Figures 6(a) and 6(b)).

3.4.2. Hematoxylin and Eosin. Hematoxylin stains nuclei blue-purple. Eosin can be used to stain cytoplasm, collagen, and muscle fibers. In sections stained with hematoxylin and eosin, it was possible to observe the inner connective tissue layer stained red (eosin), while in the mesothelium the granular cells were stained purple (Figures 6(c) and 6(d)).

3.4.3. Methylene Blue and Azure B. Methylene blue is used to visualize intracellular metachromatic granules. Azure, a methylated thiazine dye, is a metachromatic basic dye ranging from green (chromosomes) and blue (nuclei and cytoplasmic ribosomes) to red colour (deposits containing mucopolysaccharides).

Sections stained with methylene blue and azure B showed the presence of blue mesothelium and red inner connective tissue, while granular cells were stained dark (Figures 6(e) and 6(f)).

3.5. Immunostaining. The localization of adhesive protein in Cuvierian tubules of *H. forskåli* was studied by immunofluorescence microscopy. The tubule wall is made up of an outer mesothelium and an inner epithelium encompassing a thick connective tissue sheath [5]. The mesothelium is the tissue layer involved in adhesion. Antibodies raised against the adhesive protein were used to localize the protein in the

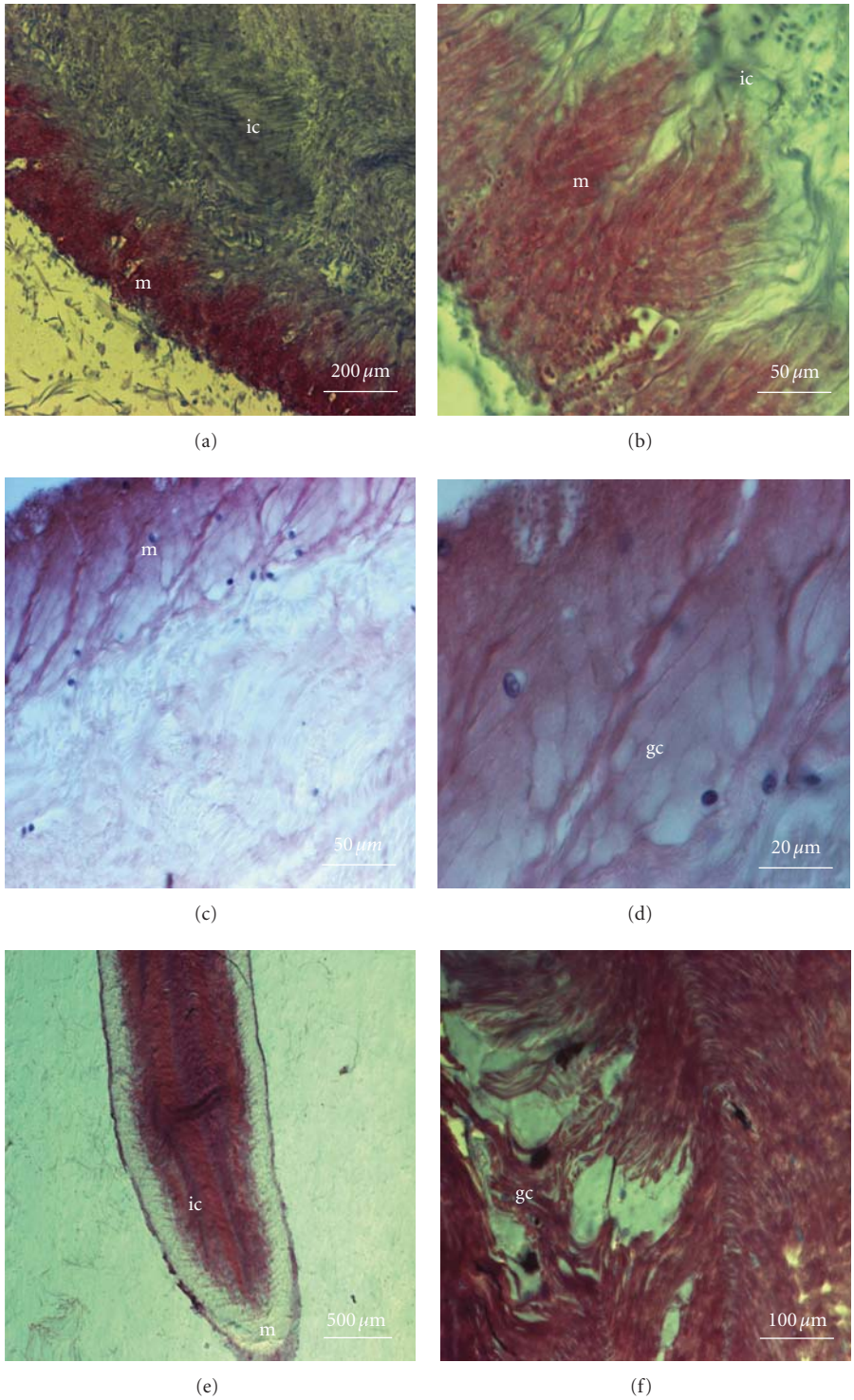

Figure 6: Sections of Cuvierian tubules stained with Cason's trichrome (a, b), hematoxylin and eosin (c, d), and methylene blue and azure B (e, f). *m*: mesothelium; *ic*: inner connective tissue; *gc*: granular cells.

sections. The strongest immunoreactivity was found in the mesothelium, which was extensively labelled (Figure 7(a)). The sections were counterstained with DAPI (Figures 7(b) and 7(d)) which stains the nuclei. Preimmune serum was used as a negative control (Figure 7(c)).

3.6. Immunogold Electron Microscopy. Transmission electron microscopy showed a strong immunoreactivity in the mesothelium layer and in vacuole cells (darker areas indicated by arrows in Figure 8(a)). Preimmune serum did not show any immunoreactivity (Figure 8(b)).

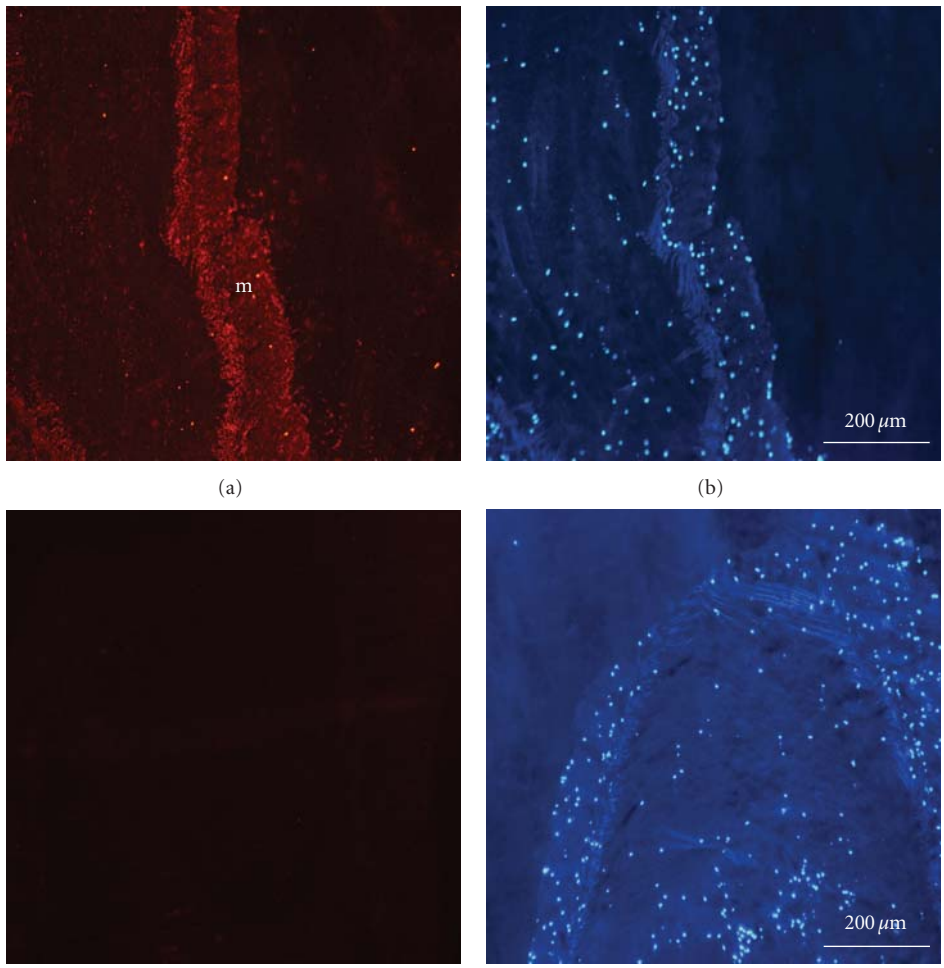

Figure 7: Immunohistological identification of adhesive protein in sections of Cuvierian tubules. (a, b) Sections of Cuvierian tubules stained with antibody against adhesive protein (PoAb-Ctub; 1 : 100 dilution (a) and counterstained with DAPI (b)). (c, d) Sections of Cuvierian tubules stained with preimmune serum (1 : 100; (c)) and counterstained with DAPI (d). Cy3-conjugated goat anti-rabbit IgG was used as secondary antibody. *m*: mesothelium.

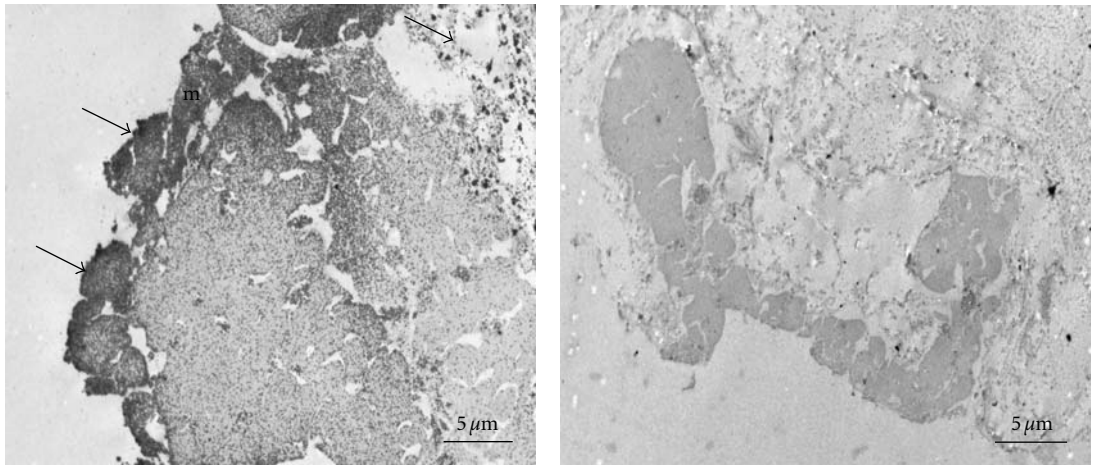

Figure 8: Immunocytochemical localization of adhesive protein in Cuvierian tubules. (a) Sections of Cuvierian tubules incubated with antibody against adhesive protein from Cuvierian tubules (PoAb-Ctub). (b) Sections of Cuvierian tubules incubated with preimmune serum. Nanogold-labeled anti-rabbit IgG was used as secondary antibody. *Arrows*: nanogold particles; *m*: mesothelium.

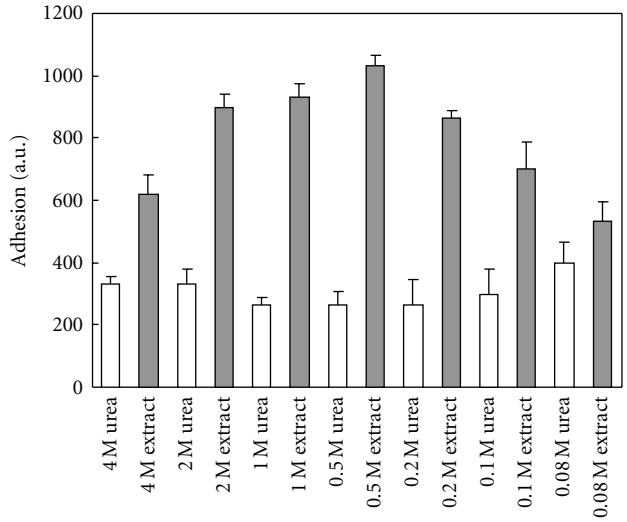

Figure 9: Effect of various concentrations of urea on adhesion to Teflon surface. Results are given in arbitrary units ± SD ($n = 3$).

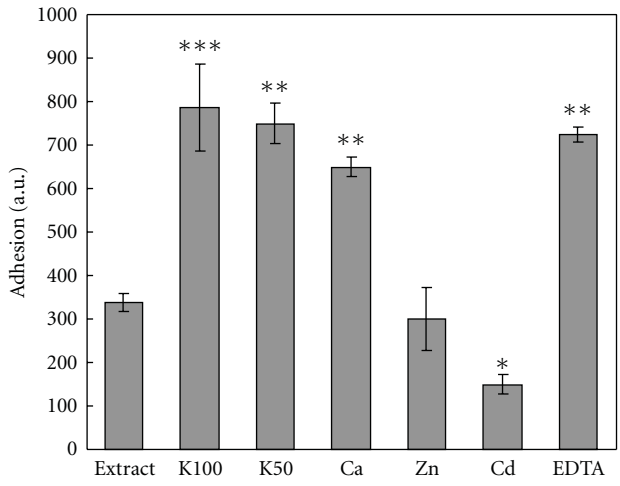

Figure 11: Effect of metal cations and EDTA on adhesion in 0.5 M urea extract. Results are given in arbitrary units ± SD ($n = 3$). Level of significance: $^{*}P < 0.05$; $^{**}P < 0.01$; $^{***}P < 0.001$.

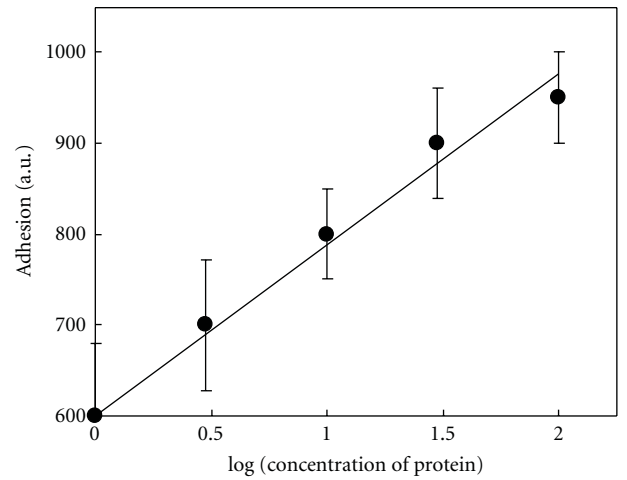

Figure 10: Correlation between various concentrations of protein in logarithmic scale and adhesion (standard curve). The highest concentration measured was 100 μg/mL of protein. Results are given in arbitrary units ± SD ($n = 3$).

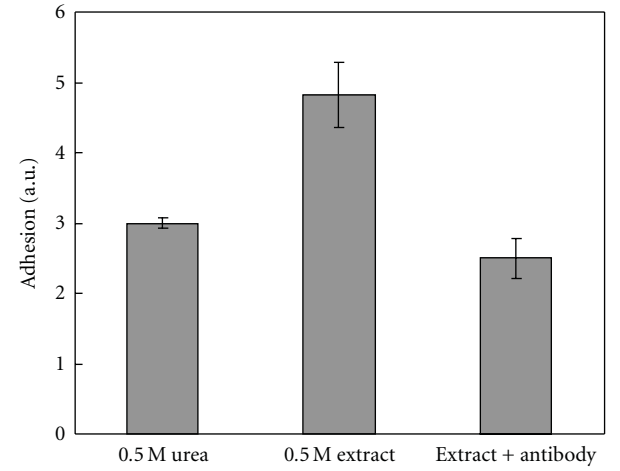

Figure 12: Neutralization of adhesion of *H. forskåli* extract by antibody (PoAb-Ctub). Results are given in arbitrary units ± SD ($n = 3$).

3.7. Adhesion of Cuvierian Tubule Extract to Various Surfaces

3.7.1. Teflon. Cuvierian tubules were extracted with 4 M urea, 0.5 M Tris-HCl pH 7.5. Adhesion was measured after dilution of the extract to various urea concentrations. As a reference, buffers with the same concentration of urea were used. The strongest adhesion to Teflon blocks was obtained at a dilution of extract to 0.5 M urea (767 arbitrary units, after subtraction of adhesion measured with buffer alone [control value]; 0.125 mg/mL of protein) (Figure 9). Higher or lower concentrations of urea resulted in lower adhesion.

In control experiments, no adhesive properties of BSA (1 mg/mL) in various urea solutions were observed.

A standard curve was obtained with a logarithmic dilution of 0.5 M urea extract (the concentration of urea at which the highest adhesion was observed). Dilution of protein caused a decrease in adhesion (Figure 10).

3.7.2. Glass Surface. Cuvierian tubule extract in 4 M urea, 0.5 M Tris-HCl pH 7.5 buffer was diluted to various concentrations and adhesion to glass blocks was measured. The strongest adhesion was observed at 1 M urea concentration of the Cuvierian tubule extract (366 arbitrary units, after subtraction of control value; 0.25 mg/mL of protein).

3.7.3. Iron Surface. Extract of Cuvierian tubules was diluted to various concentrations of urea and adhesion was measured using two iron blocks. Strong interference of the extraction buffer was observed in almost all urea

concentrations. The strongest adhesion was observed with 1 M urea extract (350 arbitrary units, after subtraction of control value; 0.25 mg/mL of protein).

3.7.4. Silicone Surface. Adhesion of various concentrations of Cuvierian tubule extract was measured using two silicone blocks. The strongest adhesion was observed at a concentration of 1 M and 0.5 M urea (316 and 250 arbitrary units, after subtraction of control value; 0.25 mg/mL and 0.125 mg/mL of protein).

3.7.5. Gelatine Surface. Adhesion of various concentrations of Cuvierian tubules extract was measured using blocks covered with gelatine. Measurement was interfered by buffer which also showed strong adhesion. The highest adhesion of the extract was observed with 2 M urea extract (400 arbitrary units, after subtraction of control value; 0.5 mg/mL of protein).

3.8. Effect of Metal Ions and EDTA on Adhesion. The adhesive forces of Cuvierian tubule extract were measured in the presence of K^+ (100 mM and 50 mM), Ca^{2+} (5 mM), Zn^{2+} (5 mM), Cd^{2+}(5 mM), and EDTA (10 mM). The results revealed a positive effect on adhesion by potassium and EDTA and a negative effect by cadmium (Figure 11). Zinc did not cause a significant change of adhesion.

3.9. Effect of Antibody. Adhesion could be neutralized by addition of antibody (PoAb-Ctub). Adhesion of neutralized extract decreased in comparison to the nontreated extract in the absence of antibody (Figure 12). The results indicate that the antibody binds to the adhesive protein and inhibits the adhesion.

Adhesion could also be abolished by treatment of the Cuvierian tubule extract with trypsin solution (not shown).

4. Discussion and Conclusions

Investigation of marine adhesives is a challenging task because of their very poor solubility in water [5, 24]. Studies on adhesive proteins from invertebrates hitherto mainly concerned the characterization of permanent adhesives from organisms like mussels and barnacles (e.g., [25, 26]). Great success has been obtained in mussels, where ten proteins are currently known to be involved in adhesion and nine have been actually isolated [7, 27]. Approaches to their biotechnological and biomedical exploitation have been started [28–31]. One of the ten proteins that have been identified to be involved in mussel adhesion is precollagen D that has been found in the distal thread of mussels, which is flanked by a silk-fibroin domain [32]. The adhesives employed by echinoderms are, in contrast, poorly understood. Studies on the adhesive secretion from Cuvierian tubules mainly focused on histological characterization (e.g., [14]); biochemical studies have been performed by Flammang et al. [2] and DeMoor et al. [5].

In our approach, we combined the wide knowledge on mussel adhesives and the poorly understood model of *H. forskåli*. Using antibodies against recombinant precollagen D, we could identify a protein involved in adhesion in *H. forskåli*.

The first task was homogenization of Cuvierian tubules which are highly insoluble [5]. In order to solubilize the material several buffers were used. Basic, strong denaturing buffers like 4 M urea, 0.5 M Tris-HCl pH 7.5 gave best results, but some nonsolubilized material still remained. We did not use buffers containing SDS like DeMoor et al. [5] because SDS might interfere with further experiments.

After extraction we had to prove the presence of adhesive proteins in the solubilized material. One proof to confirm the presence of adhesive proteins was the use of glass beads to isolate adhesive protein. Only proteins with adhesive properties will remain on the beads after several washing cycles. Second, measurement of adhesion of the extract was used as a test for the presence of adhesive protein as well. From these experiments we obtained convincing evidence that the protein which we identified is indeed an adhesive protein.

The reason why Cuvierian tubules are so poorly soluble was not investigated in this study. Aggregation of proteins may be due to the formation of cross-links between proteins composing the adhesive [5] like di-DOPA in mussels [33, 34] and disulfide bonds in barnacles [26, 35]. However, by using the buffer advised by Kamino et al. [26] for barnacles, solubilization was not improved, which may suggest that other cross-links are involved in tubule adhesive aggregation.

Electrophoretic analysis of tubule print material from Cuvierian tubules done by DeMoor et al. [5] revealed ten different proteins in the range from 17–220 kDa. In our experiments, several proteins in the range from 10–220 kDa were detected in Cuvierian tubule extract. In seminative gels, a reduced number of bands was observed, indicating the presence of conformational oligomers of some of the proteins or the presence of dimers.

After identification, isolation of the protein was a challenging task. Adhesive proteins from Holothuroidea have not been isolated so far. In this work several methods were tested which had previously been applied for isolation of nonadhesive protein [23, 36, 37] to get a high quality and quantity of the adhesive protein. Electroelution was found to produce the highest quantity of the protein, which then allowed its use for the production of antibodies.

The antibody obtained was used in a further isolation method, immunoprecipitation. From all the methods of isolation, electroelution and gel filtration were found the most useful for other applications.

Using various staining methods, the composition of Cuvierian tubules was analyzed. From sections stained with Cason's trichrome it is possible to conclude that Cuvierian tubules mainly contain collagen. In the mesothelium, cytoplasm of adluminal cell was observed. By staining with hematoxylin and eosin, it was possible to observe collagen which is stained red (eosin). Immunostaining of the sections of Cuvierian tubules with antibodies against adhesive protein from Cuvierian tubules confirmed that the mesothelium is the tissue layer responsible for adhesion as reported by DeMoor et al. [5].

To localize more precisely the adhesive protein in the Cuvierian tubules, immunogold labelling and transmission electron microscopy studies were performed. The antisera were strongly immunoreactive in the mesothelium and vacuole, confirming previous studies showing that the adhesive is located in this layer. There was no labelling with the preimmune sera, confirming that the observed immunoreaction is genuinely between a specific antibody and antigen.

Measurement of adhesion of Cuvierian tubules has previously been studied under various conditions [8, 9, 38], but measurement of the adhesive strength of Cuvierian tubules extract and isolated protein has not been done. A protein which can adhere to different surfaces underwater and at low temperature could have a great potential for application in technology and in antifouling. Therefore, various tests on the adhesion properties of the isolated protein/extract were performed.

Dalsin et al. [39] and Lee et al. [40] found that mussels can adhere to any organic or inorganic surfaces. In our experiments with Cuvierian tubule extracts from *H. forskåli* not all surfaces were suitable for adhesion. The best results were obtained with Teflon [poly(tetrafluoroethylene)], a hydrophobic polymer. There was a very low adhesion of the extraction buffer and strong adhesion of the extract. By measuring adhesion in various dilutions of Cuvierian tubule extract it was possible to find the urea concentration with the highest adhesion of the adhesive protein and to develop a standard curve for the extract. The highest adhesion was obtained with 0.5 M urea extract; this result is in line with our previous results [8] showing that urea has an impact on adhesion.

The finding that Teflon shows strong adhesion is thought to be caused by the fact that the adhesive protein is quite hydrophobic (hence its insolubility) and will tend to displace water from the Teflon, resulting in a force (from the water molecules) that will resist water being pulled into the space between the two Teflon blocks and hence producing a "bond" where in consequence water is moving to its lowest possible energy state.

Measurement of adhesion on silicone surface gave similar results to Teflon but adhesion in the presence of buffer alone could be observed. Silicone surface is rougher than Teflon surface, perhaps resulting in a higher bonding energy between the surfaces compared to that of Teflon for both extract and buffer only.

The other tested surfaces (glass, iron, and gelatine) showed strong adhesion in the presence of buffer only, which prevented them from being used as suitable surfaces for measuring adhesion mediated by the Cuvierian tubule extract.

Comparing Teflon and glass it is possible to conclude that adhesion depends on the surface. If the surface is hydrophobic (Teflon) adhesion is strong and there is no interference of buffer; when surface is hydrophilic (glass) [41] interaction between buffer and surface could be observed.

Studies on the effect of cations and EDTA on adhesion revealed that cadmium inhibited adhesion, while EDTA and potassium increased it. Cadmium inhibits formation of disulfide bonds, possibly resulting in the protein losing its structure and adhesive properties [42]. EDTA is a chelating agent which is widely used to sequester di- and trivalent metal ions; it is possible that it chelates some cations which are involved in adhesion. Potassium affects the solubility of amino acids in aqueous electrolyte solutions [43] which could cause better solubilization of the adhesive protein and increase its adhesive properties, or make protein refold and groups responsible for adhesion more suitable for adhesion. Ionic strength could be involved in increasing adhesion as well.

The adhesive properties of Cuvierian tubule extract could be neutralized by addition of the antibodies against the adhesive protein, most likely because of the binding of the antibodies to epitopes on the protein molecule that are involved in adhesion or by sterical interference with the adhesion between the protein and the surface. Neutralization of the adhesive protein by trypsin or antibodies could be useful in designing antifouling compounds. Knowledge about blocking adhesion can be helpful to understand adhesive processes and their inhibition if necessary.

The isolation of the adhesive protein will facilitate the identification of the gene encoding this molecule, which may be used to produce the recombinant protein. This study could help to develop new water-resistant adhesive proteins for (bio)technical and biomedical applications.

Acknowledgments

This work was supported by grants from the European Commission (Marie Curie Research Training Network BIOCAPITAL and project BIO-LITHO) and the Bundesministerium für Bildung und Forschung Germany (Project: Center of Excellence BIOTECmarin).

References

[1] P. Flammang, "Adhesion in echinoderms," in *Echinoderm Studies*, M. Jangoux and J. M. Lawrence, Eds., vol. 5, pp. 1–60, Balkema, Rotterdam, The Netherlands, 1996.

[2] P. Flammang, J. Ribesse, and M. Jangoux, "Biomechanics of adhesion in sea cucumber Cuvierian tubules (Echinodermata, Holothuroidea)," *Integrative and Comparative Biology*, vol. 42, no. 6, pp. 1107–1115, 2002.

[3] D. VandenSpiegel, M. Jangoux, and P. Flammang, "Maintaining the line of defense: regeneration of Cuvierian tubules in the sea cucumber *Holothuria forskali* (Echinodermata, Holothuroidea)," *Biological Bulletin*, vol. 198, no. 1, pp. 34–49, 2000.

[4] J. F. Hamel and A. Mercier, "Cuvierian tubules in tropical holothurians: usefulness and efficiency as a defence mechanism," *Marine and Freshwater Behaviour and Physiology*, vol. 33, no. 2, pp. 115–139, 2000.

[5] S. DeMoor, J. H. Waite, M. Jangoux, and P. Flammang, "Characterization of the adhesive from Cuvierian tubules of the sea cucumber *Holothuria forskali* (Echinodermata, Holothuroidea)," *Marine Biotechnology*, vol. 5, no. 1, pp. 45–57, 2003.

[6] P. Flammang, R. Santos, and D. Haesaerts, "Echinoderm adhesive secretions: from experimental characterization to

biotechnological applications," in *Progress in Molecular and Subcellular Biology, Marine Molecular Biotechnology, Echinodermata*, V. Matranga, Ed., pp. 201–220, Springer, Berlin, Germany, 2005.

[7] H. G. Silverman and F. F. Roberto, "Understanding marine mussel adhesion," *Marine Biotechnology*, vol. 9, no. 6, pp. 661–681, 2007.

[8] W. E. G. Müller, R. K. Zahn, and K. Schmidt, "The adhesive behaviour in Cuvierian tubules of *Holothuria forskåli*: biochemical and biophysical investigations," *Cytobiologie*, vol. 5, pp. 335–351, 1972.

[9] R. K. Zahn, W. E. G. Müller, and M. Michaelis, "Sticking mechanisms in adhesive organs from a Holothuria," *Research in Molecular Biology*, vol. 2, pp. 47–88, 1973.

[10] C. Semper, "1. Holothurien," in *Reisen im Archipel der Philippinen. 2. Wissenschaftliche Resultate*, Wilhelm Engelmann, Leipzig, Germany, 1868.

[11] M. Jourdan, "Recherches sur l'histologie des holothuries," *Annales du Musée d'Histoire Naturelle de Marseille*, vol. 1, pp. 1–64, 1883.

[12] E. Hérouard, "Recherches sur les holothuries des côtes de France," *Archives de Zoologie Expérimentale et Générale*, vol. 7, pp. 535–704, 1889.

[13] W. E. G. Müller, R. K. Zahn, and K. Schmidt, "Morphologie und Funktion der Cuvier'schen Organe von *Holothuria forskåli* delle chiaje (Echinodermata: Holothuriodea: Aspidochirota: Holothuriidae)," *Zeitschrift für Wissenschaftliche Zoologie*, vol. 181, pp. 219–231, 1970.

[14] D. VandenSpiegel and M. Jangoux, "Cuvierian tubules of the holothuroid *Holothuria forskali* (Echinodermata): a morphofunctional study," *Marine Biology*, vol. 96, no. 2, pp. 263–275, 1987.

[15] J. M. Gosline, P. A. Guerette, C. S. Ortlepp, and K. N. Savage, "The mechanical design of spider silks: from fibroin sequence to mechanical function," *Journal of Experimental Biology*, vol. 202, no. 23, pp. 3295–3303, 1999.

[16] T. Chirila, Z. Barnard, Zainuddin, D. G. Harkin, I. R. Schwab, and L. W. Hirst, "*Bombyx mori* silk fibroin membranes as potential substrata for epithelial constructs used in the management of ocular surface disorders," *Tissue Engineering—Part A*, vol. 14, no. 7, pp. 1203–1211, 2008.

[17] W. R. Pearson and J. F. Morrow, "Discrete-length repeated sequences in eukaryotic genomes," *Proceedings of the National Academy of Sciences of the United States of America*, vol. 78, no. 7 I, pp. 4016–4020, 1981.

[18] J. Schütze, A. Skorokhod, I. M. Müller, and W. E. G. Müller, "Molecular evolution of the metazoan extracellular matrix: cloning and expression of structural proteins from the demosponges *Suberites domuncula* and *Geodia cydonium*," *Journal of Molecular Evolution*, vol. 53, no. 4-5, pp. 402–415, 2001.

[19] M. M. Bradford, "A rapid and sensitive method for the quantitation of microgram quantities of protein utilizing the principle of protein dye binding," *Analytical Biochemistry*, vol. 72, no. 1-2, pp. 248–254, 1976.

[20] G. Danscher, "Light and electron microscopic localization of silver in biological tissue," *Histochemistry*, vol. 71, no. 2, pp. 177–186, 1981.

[21] R. E. Welch, "Stepwise multiple comparison procedures," *Journal of the American Statistical Association*, vol. 72, pp. 566–575, 1977.

[22] H. Determann, *Gel Chromatography*, Springer, New York, NY, USA, 1969.

[23] W. E. Müller, W. Hanske, A. Maidhof, and R. K. Zahn, "Influence of apurinic acid on programmed synthesis in different *in vitro* systems," *Cancer Research*, vol. 33, no. 10, pp. 2330–2337, 1973.

[24] J. H. Waite, "Nature's underwater adhesive specialist," *International Journal of Adhesion and Adhesives*, vol. 7, no. 1, pp. 9–14, 1987.

[25] S. W. Taylor and J. H. Waite, "Marine adhesives: from molecular dissection to application," in *Protein-Based Materials*, K. McGrath and D. Kaplan, Eds., pp. 217–248, Birkhäuser, Boston, Mass, USA.

[26] K. Kamino, K. Inoue, T. Maruyama, N. Takamatsu, S. Harayama, and Y. Shizuri, "Barnacle cement proteins. Importance of disulfide bonds in their insolubility," *Journal of Biological Chemistry*, vol. 275, no. 35, pp. 27360–27365, 2000.

[27] J. H. Waite and X. Qin, "Polyphosphoprotein from the adhesive pads of *Mytilus edulis*," *Biochemistry*, vol. 40, no. 9, pp. 2887–2893, 2001.

[28] T. J. Deming, "Mussel byssus and biomolecular materials," *Current Opinion in Chemical Biology*, vol. 3, no. 1, pp. 100–105, 1999.

[29] J. H. Waite, "Reverse engineering of bioadhesion in marine mussels," *Annals of the New York Academy of Sciences*, vol. 875, pp. 301–309, 1999.

[30] A. Nishida, K. Ohkawa, I. Ueda, and H. Yamamoto, "Green mussel *Perna viridis* L.: attachment behaviour and preparation of antifouling surfaces," *Biomolecular Engineering*, vol. 20, no. 4–6, pp. 381–387, 2003.

[31] N. Holten-Andersen and J. H. Waite, "Mussel-designed protective coatings for compliant substrates," *Journal of Dental Research*, vol. 87, no. 8, pp. 701–709, 2008.

[32] J. H. Waite, X. X. Qin, and K. J. Coyne, "The peculiar collagens of mussel byssus," *Matrix Biology*, vol. 17, no. 2, pp. 93–106, 1998.

[33] L. M. McDowell, L. A. Burzio, J. H. Waite, and J. Schaefer, "Rotational echo double resonance detection of cross-links formed in mussel byssus under high-flow stress," *Journal of Biological Chemistry*, vol. 274, no. 29, pp. 20293–20295, 1999.

[34] L. A. Burzio and J. H. Waite, "Cross-linking in adhesive quinoproteins: studies with model decapeptides," *Biochemistry*, vol. 39, no. 36, pp. 11147–11153, 2000.

[35] M. J. Naldrett and D. L. Kaplan, "Characterization of barnacle (*Balanus eburneus* and *B. cenatus*) adhesive proteins," *Marine Biology*, vol. 127, no. 4, pp. 629–635, 1997.

[36] E. Jacobs and A. Clad, "Electroelution of fixed and stained membrane proteins from preparative sodium dodecyl sulfate-polyacrylamide gels into a membrane trap," *Analytical Biochemistry*, vol. 154, no. 2, pp. 583–589, 1986.

[37] C. D. Bavington, R. Lever, B. Mulloy et al., "Anti-adhesive glycoproteins in echinoderm mucus secretions," *Comparative Biochemistry and Physiology Part B*, vol. 139, no. 4, pp. 607–617, 2004.

[38] P. Flammang, "The glue of sea cucumber Cuvierian tubules: a novel marine bioadhesive," *IFREMER Actes de Colloques*, vol. 36, pp. 176–185, 2003.

[39] J. L. Dalsin, B. H. Hu, B. P. Lee, and P. B. Messersmith, "Mussel adhesive protein mimetic polymers for the preparation of nonfouling surfaces," *Journal of the American Chemical Society*, vol. 125, no. 14, pp. 4253–4258, 2003.

[40] H. Lee, B. P. Lee, and P. B. Messersmith, "A reversible wet/dry adhesive inspired by mussels and geckos," *Nature*, vol. 448, no. 7151, pp. 338–341, 2007.

[41] M. Krasowska, M. Krzan, and K. Malysa, "Bubble collisions with hydrophobic and hydrophilic surfaces in α-terpineol solutions," *Physicochemical Problems of Mineral Processing*, vol. 37, pp. 37–50, 2003.

[42] D. N. Weber, C. F. Shaw, and D. H. Petering, "*Euglena gracilis* cadmium-binding protein-II contains sulfide ion," *Journal of Biological Chemistry*, vol. 262, no. 15, pp. 6962–6964, 1987.

[43] M. K. Khoshkbarchi and J. H. Vera, "Effect of NaCl and KCl on the solubility of amino acids in aqueous solutions at 298.2 K: measurements and modeling," *Industrial & Engineering Chemistry Research*, vol. 36, no. 6, pp. 2445–2451, 1997.

Hindawi Publishing Corporation
Evidence-Based Complementary and Alternative Medicine
Volume 2011, Article ID 785831, 7 pages
doi:10.1155/2011/785831

Research Article

Comparative Cytogenetics Analysis of *Chlamys farreri*, *Patinopecten yessoensis*, and *Argopecten irradians* with C_0t-1 DNA by Fluorescence *In Situ* Hybridization

Li-Ping Hu, Wen-Cong Shang, Yan Sun, Shan Wang, Xiao-Liang Ren, Xiao-Ting Huang, and Zhen-Min Bao

Key Laboratory of Marine Genetics and Breeding (MGB), College of Marine Life Sciences, Ocean University of China, Ministry of Education, Qingdao 266003, China

Correspondence should be addressed to Xiao-Ting Huang, xthuang@ouc.edu.cn

Received 12 January 2011; Accepted 16 May 2011

The chromosomes of *Chlamys farreri*, *Patinopecten yessoensis,* and *Argopecten irradians* were studied by FISH using *C. farreri* C_0t-1 DNA probes. The results showed that C_0t-1 DNA signals spread on all chromosomes in the three scallops, whereas signal density and intensity were different strikingly. Clustering brighter signals presented in the centromeric and telomeric regions of most *C. farreri* chromosomes, and in the centromeric or pericentromeric regions of several *P. yessoensis* chromosomes. Comparative analysis of the mapping indicated a relatively higher homology in the repetitive DNA sequences of the genome between *C. farreri* and *P. yessoensis* than that between *C. farreri* and *A. irradians*. In addition, FISH showed that the distribution of C_0t-1 DNA clustering signals in *C. farreri* displayed completely similar signal bands between homologous chromosomes. Based on the C_0t-1 DNA fluorescent bands, a more exact *karyotype* of *C. farreri* has been obtained. In this study, the comparative analysis based on C_0t-1 DNA provides a new insight into the chromosomal reconstructions during the evolution process, and it is helpful for understanding an important source of genomic diversity, species relationships, and genome evolution.

1. Introduction

The scallop family, Pectinidae, including more than 300 living species recognized in worldwide oceans, is one important fauna of bivalve not only at commercial and ecological levels, but also in terms of biological evolution and basic biology research. Given their importance, scallops have been the subject of much research. In the last few decades, a wide range of systematic studies have been conducted in accordance with morphological features [1–3] and molecular phylogeny [4, 5]. In addition, cytogenetic methods also have played important roles in the analysis of karyotype evolution. In recent years, cytogenetic analysis by Fluorescence *in situ* hybridization (FISH) has been effectively carried out in Pectinidae, such as localizing repetitive sequences [6–12], and karyotypic evolution by comparison of rRNA and histone H3 gene loci [13, 14]. The cytogenetic data available has indicated great deviation in chromosome number and morphologies among species, suggesting that significant changes in chromosome number and structure have occurred during the evolution of Pectinidae [13]. However, the current cytogenetic evidences on the scallops evolution most focus on comparison of chromosome numbers by karyotype or the locus of a single gene (rRNA or H3 gene) by FISH. The comparative cytogenetics investigations in the genomewide level have not been reported among Pectinidae species.

Comparative cytogenetics, as a powerful tool to study karyotypic variation, is based on accurate chromosome identification. Chromosome banding and FISH techniques have facilitated cytogenetic research for many animal and plant species, unfortunately, chromosome identification remains a challenge in scallop and other bivalve species. The practice of conventional chromosome banding in scallops and oysters confirms its low reliability to identify individual chromosomes [10, 15, 16]. The current researches on the identification of the chromosomes of scallops are on the basis of localization of repetitive sequences by FISH, such as rRNA genes [6, 9, 13] and histone H3 genes [14]. Furthermore,

fosmid clones have been applied to identification of *C. farreri* chromosomes and identified 8 from 19 chromosome pairs [17]. So far, there has not been a successful example to identify all the chromosome pairs of any scallop species.

The genomes of eukaryotic species contain numerous types of highly or moderately repetitive DNA elements. It has been showen that the variation in genome size is largely caused by differences in the amount of repetitive DNA sequences. The repetitive DNA sequences used as the molecular marker play significant roles in comparative genomics study, especially the research on structure and function of species genomes and the evolution of chromosomes. For example, the satellite repeat sequences were exploited for genetic linkage maps construction [18] and variety identification [19, 20]. The *in situ* investigation of repetitive DNA sequences adds new informative characters useful in comparative genomics at chromosomal level and provides insights into the evolutionary relationships among scallops [13, 14], as well as the hybridization of satellite DNAs has contributed to the relationship among fish species and their karyotypic diversification [21–23].

C_0t-1 DNA is enriched with highly and moderately repetitive DNA sequences, which have been widely used as a blocking agent to inhibit hybridization of repeats present within DNA probes. In some plant species, C_0t-1 DNA has also been used for karyotyping and comparative analysis of genomes by FISH [24, 25]. Zhikong scallop (*Chlamys farreri* Jones et Preston, 1904), Yesso scallop (*Patinopecten yessoensis* Jay, 1857), and Bay scallop (*Argopecten irradians* Lamarck, 1819) are important commercial species in China. *C. farreri* distribute naturally in the northern seacoasts of China. *P. yessoensis* and *A. irradians* were introduced to China from their original distribution areas—Hokkaido, Japan in 1980 [26] and North America in 1982 [27], respectively. To analyze the genome structure and detect chromosome evolution of these three species, we used C_0t-1 DNA of *C. farreri* (called CF C_0t-1 DNA for short) as probes for *in situ* hybridization on mitotic metaphase chromosomes of these scallops and analyzed the signals distribution of the repetitive sequences in the three genomes. In addition, since these DNA sequences dispersed in the whole genome, we tried to identify individual pairs from all the chromosome pairs of *C. farreri* with the hybridization signal bands.

2. Materials and Methods

2.1. Scallop Materials and Chromosome Preparations. Sexually mature scallops (*C. farreri, A. irradians,* and *P. yessoensis*) were obtained from a hatchery in Shandong Province, China. The chromosome preparations were performed following the method of Zhang et al. [14]. Briefly, the larvae were treated with colchicine (0.01%) for 2 h at room temperature and KCl (0.075 M) for 30 min, then fixed in Carnoy's fixative (methanol : glacial acetic acid = 3 : 1 v/v) for three times (15 min each). The fixed larvae were dissociated in 50% acetic acid, and then the cell suspension was dropped onto hot-wet slides and air-dried.

2.2. Genomic DNA Extraction and Preparation of CF C_0t-1 DNA. The total genomic DNA extraction was carried out by the standard phenol-chloroform procedure using adductor muscle [28]. CF C_0t-1 DNA was prepared according to the procedure described by Zwick et al. [29] with slightly modified. In brief, genomic DNA was diluted to a concentration of 600 ng/μl in 0.3 M NaCl and was sonicated to 100–1500 bp DNA fragments. The shearing DNA was denatured in 95°C bath water for 10 min, and then annealed in 65°C bath water for the required time which was calculated according to the formula C_0t-1 = mol/L × Ts. After the tube was put into ice water for 2 min, the appropriate amount of S1 nuclease (1 U/μg DNA) was added, and reaction at 23°C for 30 min. Finally, the reaction was stopped by adding appropriate amount of EDTA (final concentration of 25 mM). Then the DNA was extracted by Tris-equilibrated phenol, deposited by 2.5 volumes of absolute ice-ethanol and washed with prechilled 70% ethano1, then air-dried and resuspended in TE buffer. CF C_0t-1 DNA was stored in −20°C after quantitative analysis.

2.3. Probe Labeling and FISH. CF C_0t-1 DNA was labeled with digoxigenin-11-dUTP by nick translation following the manufacturer's instruction (Roche). The length of the CF C_0t-1 DNA used as the probe for FISH was between 100 bp and 600 bp, which was estimated by 2% gel electrophoresis.

FISH was carried out according to Huang et al. [8]. Firstly, chromosomes spreads were pretreated with 0.005% pepsin in 10 mM HCl for 10 min, and followed by washing in 2 × SSC twice 5 min at room temperature. Chromosome spreads were then denatured in a mixture containing 75% formamide and 2 × SSC at 76°C for 2-3 min, dehydrated with a chilled ethanol series, 70%, 90%, 100%, 5 min each, and air-dried. The hybridization mix (10 ng/ul probes, 10% dextran sulfate, and 50% deionized formamide in 2 × SSC) was denatured at 95°C for 6-7 min and chilled immediately by putting on ice for at least 10 min. Denatured probe was applied onto the slide and DNA-DNA *in situ* hybridization was carried out in a humidity chamber at 37°C for 12–16 h. Following hybridization, the slides were washed in 2 × SSC at 42°C 5 min, 50% formamide in 2 × SSC at 42°C 10 min, 1 × SSC at 42°C three times (5 min each), and 2 × SSC once for 5 min at room temperature. Fluorescent signals were detected with antidigoxigenin rhodamine (Roche). Chromosomes were counterstained with DAPI (Vector). Slides were observed using a Nikon E-600 epifluorescence microscope equipped with a CCD camera (COHU). The signals were collected using appropriate filter sets and LUCIA software. The karyotype was reconstructed according to the karyotype standard of Levan et al. [30], as well as CF C_0t-1 DNA signal bands patterns using Lucia-FISH Image System.

3. Results

The size of the genomic DNA obtained from *C. farreri* was more than 20 kb (data not shown). After being sonicated, the majority of DNA fragments were within the desired size range of 100–1500 bp. Then by reannealing and S1 nuclease

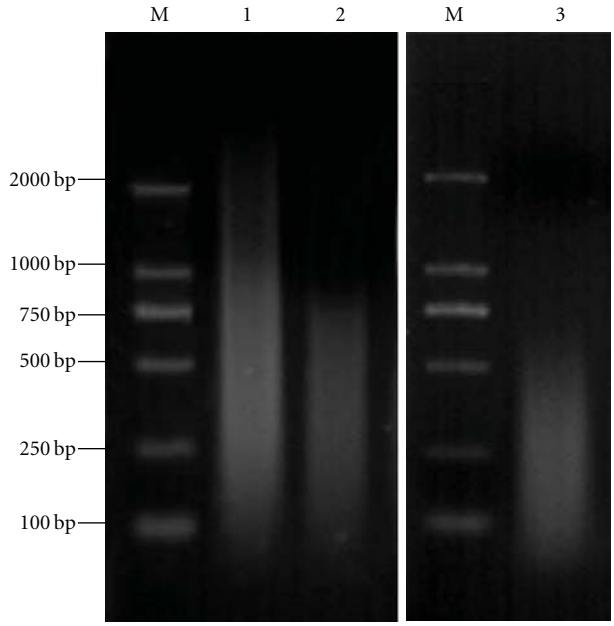

Figure 1: Preparation of C_0t-1 DNA probes of *C. farreri* M DL2000 marker; 1 Shearing genomic DNA; 2 C_0t-1 DNA; 3 Labeled C_0t-1 DNA probes.

digestion, the final size range of CF C_0t-1 DNA is 100–800 bp. The size of CF C_0t-1 DNA probes labeled with digoxigenin-11-dUTP by nick translation was ranged from 100 bp to 600 bp (Figure 1).

The labeled CF C_0t-1 DNA was hybridized to the chromosome spreads of *C. farreri, P. yessoensis,* and *A. irradians*. The results were shown in Figure 2. On the metaphase chromosomes of *C. farreri*, the signals of CF C_0t-1 DNA presented in all chromosomes, and the clustering brighter signals of CF C_0t-1 DNA distributed mainly in areas of centromeres, subcentromeres, and near telomeres, and fewer in the middle regions of chromosome arms (Figures 2(a) and 2(g)). In detail, on three pairs of metacentric chromosomes, two pairs of submetacentric chromosome and one pair of subtelocentric chromosomes, the brighter CF C_0t-1 DNA signals mainly concentrated in areas of centromere; on the other three pairs of submetacentric chromosomes and nine pairs of subtelocentric chromosomes, more intensive CF C_0t-1 DNA distributed in areas of centromeres, subcentromeres, and telomeric regions of the long arms; and on another pair of subtelocentric chromosomes, more intensive CF C_0t-1 DNA distributed in telomeric regions of the long arms. From the characteristics of the signals distribution, the repetitive sequences had specific, strong and steady signal bands on chromosomes, and the homologous chromosomes exhibited similar signal bands, so that karyotype analysis could be conducted based on CF C_0t-1 DNA specific fluorescence bands in *C. farreri*. And the karyotype result was shown in Figure 3. Based on the karyotype picture, the signals were much brighter in centromeres areas of the chromosome pairs 1, 5, 7, 9, 10, 16 and 18, and telomeric regions on the long arms of the chromosome pairs 4, 8, 13, 16, 17, 18 and 19 (Figure 3). On the metaphase chromosomes of *P. yessoensis*, the signals of CF C_0t-1 DNA were also detected in all chromosomes, whereas, the brighter clustering signals of CF C_0t-1 DNA could be seen on several chromosomes at centromeric and pericentromeric regions, or near centromeric regions of the long arms (Figures 2(b) and 2(h)). Furthermore, on one or two pairs of subtelocentric chromosomes, the brighter CF C_0t-1 DNA signals mainly concentrated in areas of centromeric and pericentromeric regions; on another pair of subtelocentric chromosomes, more intensive CF C_0t-1 DNA distributed near centromeric regions of the long arms; on the remaining chromosomes, the signals of CF C_0t-1 DNA were dispersed. In contrast, no obviously clustering brighter signals of CF C_0t-1 DNA regions were shown and the signals were dispersed on chromosomes of *A. irradians* (Figures 2(c) and 2(i)).

Overall, according to the FISH images, the signals of CF C_0t-1 DNA were detected in all chromosomes of the three species, whereas signal density and intensity were different strikingly. The signals of CF C_0t-1 DNA in *C. farreri* appeared the most intensive and brightest, followed by which in *P. yessoensis*, and the signals of CF C_0t-1 DNA in *A. irradians* were the most sparse and weakest. Additionally, CF C_0t-1 DNA showed the clustering brighter signals region on all chromosomes of *C. farreri*, although they displayed different coverage, brightness, and location on different chromosomes, while only several chromosomes in *P. yessoensis* showed the clustering brighter signals regions whose coverage and brightness were smaller and weaker than those in *C. farreri*. Moreover, no obvious clustering signals of CF C_0t-1 DNA regions were found in *A. irradians*.

4. Discussion

In bivalves, most comparative cytogenetic studies using FISH have concentrated on some multicopy genes, such as histone and ribosomal RNA genes (rDNAs). Whereas all these studies were relied on the locus of a single gene, and so far there have been no reports about the comparative analysis of highly and moderately repetitive sequences in the whole genomewide in bivalve species. Among repetitive DNAs, C_0t-1 DNA mainly contains highly and moderately repetitive DNA sequences [29]. And *C. farreri* possesses the mode haploid number for Pectinidae (n = 19) and the highest number of chromosomal arms (38), which is considered the closest representative of the ancestral karyotype of Pectinidae [13]. Thus, in this study, we used C_0t-1 DNA of *C. farreri* (CF C_0t-1 DNA) as probes to compare the repetitive sequences distribution among *C. farreri*, *P. yessoensis,* and *A. irradians*. We localized the CF C_0t-1 DNA on chromosomes of three scallops by FISH. The results showed that the distributions of highly and moderately repetitive sequences from *C. farreri* not only existed in the genome of *C. farreri,* but also in those of *P. yessoensis* and *A. irradians.* These indicated that the repetitive DNA sequences showed a certain degree of conservation in the process of species evolution. The similar comparative study has also been performed in genus Oryza by Lan et al. [25] and indicated that highly and moderately

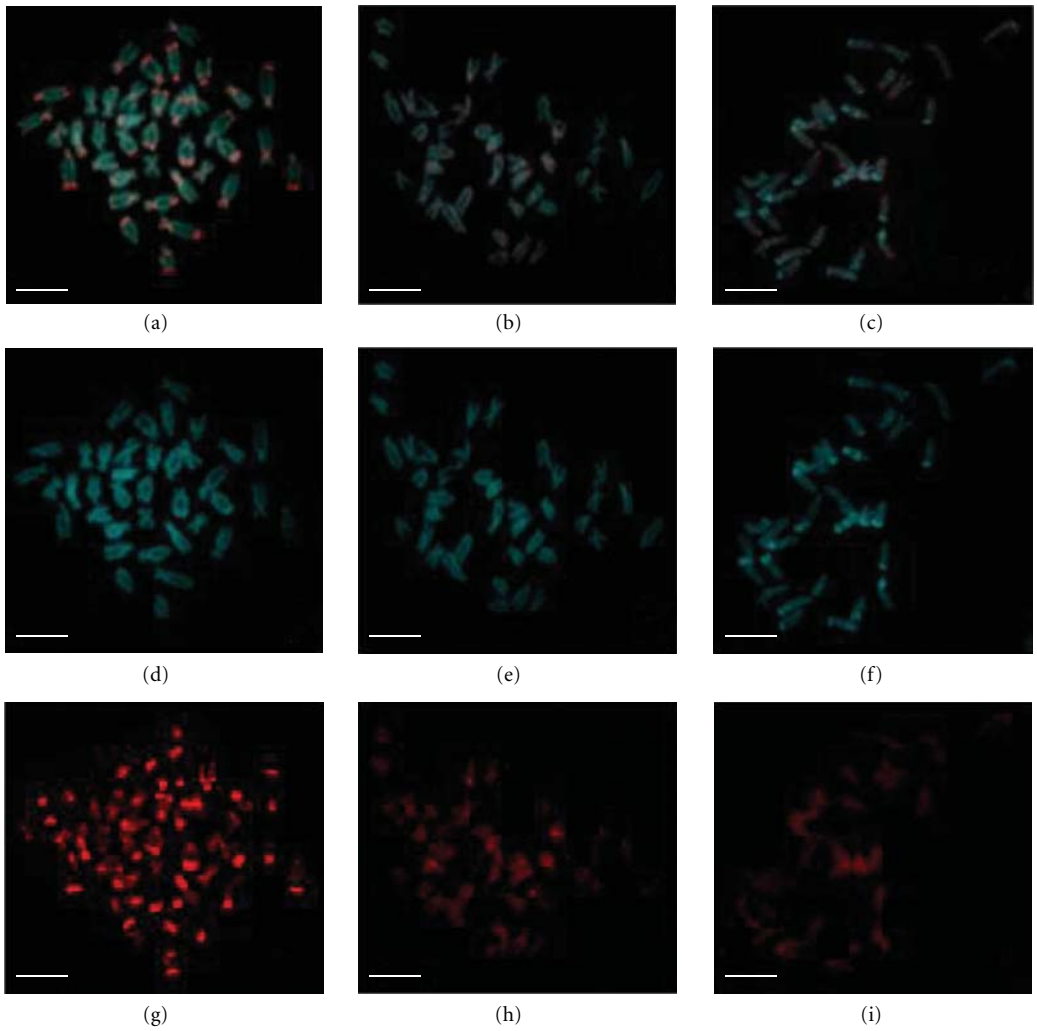

Figure 2: FISH results of C_0t-1 DNA probes to the metaphase chromosomes of *C. farreri*, *P. yessoensis* and *A. irradians.* Bar = 5 μm. (a) and (g), FISH combined image and red hybridization signals image of *C. farreri* probed with its own C_0t-1 DNA; (b) and (h), FISH combined image and red hybridization signals image of *P. yessoensis* probed with C_0t-1 DNA of *C. farreri*; (c) and (i), FISH combined image and red hybridization signals image of *A. irradians* probed with C_0t-1 DNA of *C. farreri*; (d), (e), and (f), DAPI staining images of *C. farreri, P. yessoensis,* and *A. irradians*, respectively.

repetitive sequences in genus Oryza were quite conserved during evolution.

Although highly and moderately repetitive sequences of *C. farreri* existed in the genomes of *C. farreri*, *P. yessoensis,* and *A. irradians*, signal coverage, strength, and area on chromosomes of these three species were different strikingly. We speculated that highly and moderately repetitive sequences are most likely species-specific. Moreover, CF C_0t-1 DNA showed more intensive and brighter signals on the chromosomes in *P. yessoensis* than in *A. irradians,* which may indicate a relatively higher homology in the repetitive DNA sequences between the genome of *P. yessoensis* and *C. farreri*, than that between *A. irradians* and *C. farreri.* The relationship among these three scallops herein are in accordance with the previous molecular studies that used sequences of the mtDNA [4] or internal transcribed spacer region [31], and the classification system based on microsculpture of shell features and morphological characteristics of juveniles [2, 3].

Comparative studies on diverse bivalves have shown that chromosome structures are incredibly dynamic in terms of number and location of rDNAs [32–34]. Moreover, Wang and Guo [13] postulated chromosomal translocation and duplication may play a dominant role in the karyotypic evolution of Pectinidae by detecting the major and minor rDNA patterning in *C. farreri* and *A. irradians*. Huang et al. [7] speculated that the nonreciprocal translocation of chromosome with 18S–28S rDNA loci lead to one 18S–28S rDNA site in *C. farreri* into two in *P. yessoensis*. In addition, the comparative chromosomal localization of histone H3 gene in four scallop species (*C. farreri, C. nobilis, P. yessoensis,* and *A. irradians*) suggested that gene duplication/diminution and chromosome rearrangements may have played important roles during chromosome evolution in Pectinidae [14]. In

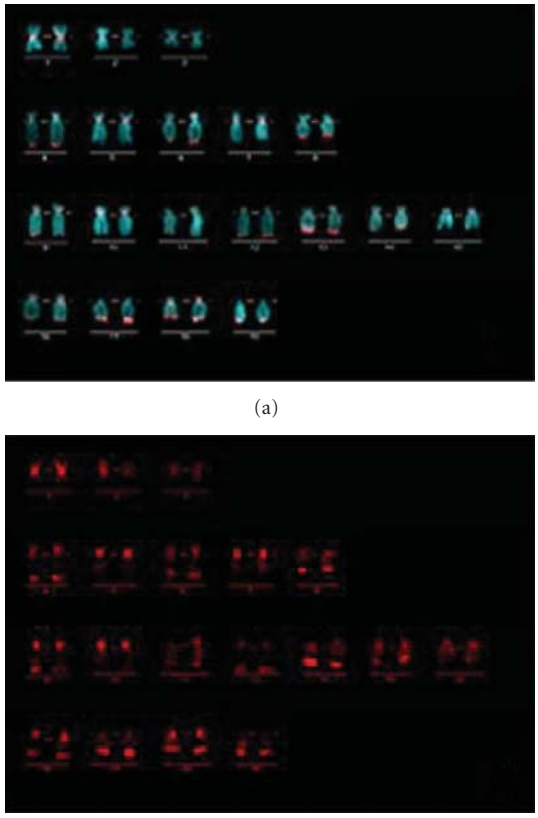

(a)

(b)

Figure 3: Karyotype of *C. farreri* and corresponding C_0t-1 DNA signal bands.

this study, contrasting the similar-dissimilar distribution of CF C_0t-1 DNA on *P. yessoensis* and *C. farreri* chromosomes, we speculate that in the chromosome evolution, highly and moderately repetitive sequences variation, losses, or rearrangement took place in some chromosomes but not all chromosomes. In other words, the evolution of these repetitive sequences was not synchronized between different chromosomes. And the variable distribution patterns of the CF C_0t-1 DNA suggested that repetitive sequences variation, losses, as well as chromosome rearrangements may have played important roles in the genomic evolution of Pectinidae.

In the present study, our results revealed the distribution of these repetitive DNA sequences in the genome of *C. farreri*. FISH demonstrated that CF C_0t-1 DNA not only dispersed on all chromosomes, but also more densely organized in centromeric, pericentromeric, and telomeric regions of the most chromosomes, which showed clearly fluorescent signal banding. Repetitive sequence regions usually correspond to constitutive heterochromatin in the genome. As has been shown by Chang et al. [35], the FISH of C_0t fractions and of various tandem and dispersed repeats in tomato demonstrated that most of the repeats are confined to the clearly distinguishable heterochromatin blocks at the telomeres, in the pericentromeres and in the large nucleolar organizer region (NOR). In the case of *C. farreri*, 18S–28S rDNA, as well as nucleolar organizer region (NOR) has been located on the short arm of subtelecentric chromosome 10 [6]. A tandem repeats satellite DNA *Cf303* has also been hybridized to the centromeric and telomeric region of the long arm of a pair of subtelocentric chromosomes and the telomeric region of the long arm of 13 pairs of submetacentric or subtelocentric chromosomes [17]. Based on our FISH result of C_0t fractions and the former published FISH data of tandem repeats satellite DNA and rDNA, we can basically distinguish the constitutive heterochromatin regions in the genome of *C. farreri*.

Chromosome identification is the first step in understanding the genome organization of one species. The chromosomes of *C. farreri* show a similarity and continuity except for three pairs of metacentric chromosomes. It is difficult to identify homologues and distinguish different chromosomes to generate an accurate karyotype by traditional karyotype analysis. The application of FISH can help in achieving this target, but FISH with satellite DNA or vertebrate telomere sequence has been demonstrated to be unsuitable for the similar and even identical location of signals on chromosomes in bivalve species [36–38]. Repetitive genes such as rRNA and histone H3 genes can be used for chromosome identification [13, 14], yet these specific probes containing repetitive sequences were very limited. Unique sequences like large-insert clones are easy to achieve and fosmid clones of *C. farreri* have been applied to develop chromosome-specific probes, and 8 of the 19 fosmid clones selected were successfully used for chromosome identification [17]. However, there has not been a successful example to realize the identification of all the 19 chromosome pairs of *C. farreri*. In the present study, the mitotic metaphase chromosome pairs of *C. farreri* could be stably banded by CF C_0t-1 DNA, and the specific and analogous banding patterns were exhibited on the two members of the homologous chromosome pairs (Figure 3). This indicated that the homologous chromosomes possessed homologous or similar highly and moderately repetitive DNA sequences, while nonhomologous chromosome pairs did not. These were the foundation of karyotyping with C_0t-1 DNA banding. This karyotyping method based on C_0t-1 DNA fluorescent bands has been successfully practiced in *Brassica napus* L. [39] and *Brassica oleracea* L. [24]. Compared with conventional karyotype analysis, the karyotyping technique reported in this paper was based on the genome constitution, and therefore it was faster and more exact to match the homologous chromosomes and discriminates different chromosomes. Although the majority of chromosomes were identified based on FISH of CF C_0t-1 DNA, and karyotype analysis was carried out in *C. farreri*. It would be difficult to judge the exact location of CF C_0t-1 DNA on the long arm, the short arm, or the centromeric sites of the chromosomes because the emanative fluorescence signals existing on the pericentromeric sites covered the centromeres. Different chromosomes are still difficult to distinguish when they show very similar banding patterns. Therefore, the technology combining the banding patterns of CF C_0t-1 DNA with the FISH location analysis of specific sequence probes (such as BAC-FISH) would increase the veracity and reliability of chromosome identification in *C. farreri*.

Acknowledgments

This research was funded by National Natural Science Foundation of China (30901096), National High Technology Research and Development Program of China (2010AA10A401), National Basic Research Program of China (2010CB126406), the Earmarked Fund for Modern Agroindustry Technology Research System, and The Key Laboratory of Experimental Marine Biology, Institute of Oceanology, Chinese Academy of Sciences (KFN92007NO12).

References

[1] I. A. Korobkov, "Family pectinidae lamarck, 1801," in *Osnovy Paleontologii, Mollusca-Loricata, Bivalvia and Scaphopoda*, U. A. Orlov, Ed., pp. 82–85, Academy Nauk USSR, Moscow, Russia, 1960.

[2] T. R. Waller, "Evolutionary relationship among commercial scallops (Mollusca: Bivalvia: Pectinidae)," in *Scallops: Biology, Ecology & Aquaculture*, S. E. Shumway, Ed., pp. 1–73, Elsevier, Amsterdam, The Netherlands, 1991.

[3] T. R. Waller, "The evolution of "*Chlamys*" (Mollusca:Bivalvia: Pectinidae) in the tropical western Atlantic and eastern Pacific," *American Malacological Bulletin*, vol. 10, no. 2, pp. 195–249, 1993.

[4] M. Barucca, E. Olmo, S. Schiaparelli, and A. Canapa, "Molecular phylogeny of the family Pectinidae (Mollusca: Bivalvia) based on mitochondrial 16S and 12S rRNA genes," *Molecular Phylogenetics and Evolution*, vol. 31, no. 1, pp. 89–95, 2004.

[5] M. Matsumoto and I. Hayami, "Phylogenetic analysis of the family pectinidae (Bivalvia) based on mitochondrial cytochrome C oxidase subunit I," *Journal of Molluscan Studies*, vol. 66, no. 4, pp. 477–488, 2000.

[6] X. Huang, Z. Bao, K. Bi et al., "Chromosomal localization of the major ribosomal RNA genes in scallop *Chlamys farreri*," *Acta Oceanologica Sinica*, vol. 25, no. 3, pp. 108–115, 2006.

[7] X. Huang, X. Hu, J. Hu et al., "Mapping of ribosomal DNA and $(TTAGGG)_n$ telomeric sequence by FISH in the bivalve *Patinopecten yessoensis*," *Journal of Molluscan Studies*, vol. 73, no. 4, pp. 393–398, 2007.

[8] X. Huang, J. Hu, X. Hu et al., "Cytogenetic characterization of the bay scallop, *Argopecten irradians* irradians, by multiple staining techniques and fluorescence *in situ* hybridization," *Genes & Genetic Systems*, vol. 82, no. 3, pp. 257–263, 2007.

[9] A. Insua, M. J. López-Piñón, R. Freire, and J. Méndez, "Karyotype and chromosomal location of 18S-28S and 5S ribosomal DNA in the scallops *Pecten maximus* and *Mimachlamys varia* (Bivalvia: Pectinidae)," *Genetica*, vol. 126, no. 3, pp. 291–301, 2006.

[10] A. Insua, M. J. López-Piñón, and J. Méndez, "Characterization of *Aequipecten opercularis* (Bivalvia: Pectinidae) chromosomes by different staining techniques and fluorescent *in situ* hybridization," *Genes & Genetic Systems*, vol. 73, no. 4, pp. 193–200, 1998.

[11] M. J. López-Piñón, A. Insua, and J. Méndez, "Chromosome analysis and mapping of ribosomal genes by one- and two-color fluorescent *in situ* hybridization in *Hinnites distortus* (bivalvia: Pectinidae)," *Journal of Heredity*, vol. 96, no. 1, pp. 52–58, 2005.

[12] G. Odierna, G. Aprea, M. Barucca, and A. Canapa, "Capriglione, *E. Olmo*, karyotype of the Antarctic scallop *Adamussuim colbecki*, with some comments on the karyological evolution of pectinids," *Genetica*, vol. 127, no. 1–3, pp. 341–349, 2006.

[13] Y. Wang and X. Guo, "Chromosomal rearrangement in pectinidae revealed by rRNA loci and implications for bivalve evolution," *Biological Bulletin*, vol. 207, no. 3, pp. 247–256, 2004.

[14] L. Zhang, Z. Bao, S. Wang, X. Huang, and J. Hu, "Chromosome rearrangements in pectinidae (Bivalvia: Pteriomorphia) implied based on chromosomal localization of histone H3 gene in four scallops," *Genetica*, vol. 130, no. 2, pp. 193–198, 2007.

[15] G. Gajardo, M. Parraguez, and N. Colihueque, "Karyotype analysis and chromosome banding of the Chilean-Peruvian scallop *Argopecten purpuratus* (lamarck, 1819)," *Journal of Shellfish Research*, vol. 21, no. 2, pp. 585–590, 2002.

[16] Y. Wang, Z. Xu, J. C. Pierce, and X. Guo, "Characterization of eastern oyster *(Crassostrea virginica Gmelin)* chromosomes by fluorescence *in situ* hybridization with bacteriophage P1 clones," *Marine Biotechnology*, vol. 7, no. 3, pp. 207–214, 2005.

[17] L. Zhang, Z. Bao, S. Wang, X. Huang, and J. Hu, "FISHmapping and identification of Zhikong scallop *(Chlamys farreri)* chromosomes," *Marine Biotechnology*, vol. 10, no. 2, pp. 151–157, 2008.

[18] A. Zhan, J. Hu, X. Hu et al., "Construction of microsatellite-based linkage maps and identification of size-related quantitative trait loci for Zhikong scallop *(Chlamys farreri)*," *Animal Genetics*, vol. 40, no. 6, pp. 821–831, 2009.

[19] A. Zhan, J. Hu, X. Hu et al., "Fast identification of scallop adductor muscles using species-specific microsatellite markers," *European Food Research & Technology*, vol. 227, no. 2, pp. 353–359, 2008.

[20] A. Zhan, X. Hu, Z. Bao et al., "Molecular identification of scallop planktonic larvae using species-specific microsatellites," *Acta Oceanologica Sinica*, vol. 27, no. 5, pp. 134–146, 2008.

[21] P. M. Galetti Jr, A. C. G. Cesar, and P. C. Venere, "Heterochromatin and NORs variability in Leporinus fish (Anostomidae, Characiformes)," *Caryologia*, vol. 44, pp. 287–292, 1991.

[22] V. P. Margarido and P. M. Galetti Jr, "Heterochromatin patterns and karyotype relationships within and between the genera *Brycon* and *Salminus* (Pisces, Characidae)," *Genetics & Molecular Biology*, vol. 22, no. 3, pp. 357–361, 1999.

[23] W. F. Molina, M. Schmid, and P. M. Galetti Jr, "Heterochromatin and sex chromosomes in the Neotropical fish genus *Leporinus* (Characiformes, Anostomidae)," *Cytobios*, vol. 1998, no. 377, pp. 141–149, 1998.

[24] T. Wang, C. Wu, J. Huang, and W. Wei, "Karyotyping of *Brassica oleracea* L. based on rDNA and C_0t-1 DNA fluorescence in situ hybridization," *Frontiers of Biology in China*, vol. 2, no. 4, pp. 403–407, 2007.

[25] W. Lan, G. He, C. Wang, S. Wu, and R. Qin, "Comparative analysis of genomes in *Oryza* sativa, *O. officinalis*, and *O. meyeriana* with C_0t-1 DNA and genomic DNA of cultivated rice," *Agricultural Sciences in China*, vol. 6, no. 9, pp. 1027–1034, 2007.

[26] Q. Wang and Y. Liu, "The artificial breeding experiment of the Japanese scallop, *Patinopecten yessonensis* (Jay)," *Fisheries Science*, vol. 2, pp. 1–7, 1982.

[27] F. Zhang, Y. He, X. Liu, J. Ma, S. Li, and L. Qi, "A report on the introduction, seed culture and experimental grow-out of the bay scallop, *Argopecten irradiands* larmarck," *Oceanologia et Limnologia Sinica*, vol. 17, no. 5, pp. 367–374, 1986.

[28] J. Sambrook, E. F. Fritsch, and T. Maniatis, *Molecular Cloning: A Laboratory Manual*, Cold Spring Harbor Laboratory, New York, NY, USA, 2nd edition, 1989.

[29] M. S. Zwick, R. E. Hanson, T. D. McKnight et al., "A rapid procedure for the isolation of C_0t-1 DNA from plants," *Genome*, vol. 40, no. 1, pp. 138–142, 1997.

[30] A. Levan, K. Fredga, and A. A. Sandberg, "Nomenclature for centromeric position on chromosomes," *Hereditas*, vol. 52, pp. 201–220, 1964.

[31] X. Huang, K. Bi, J. Hu, X. Hu, and Z. Bao, "Phylogenetic analysis of Pectinidae (Bivalvia) based on the ribosomal DNA internal transcribed spacer region," *Acta Oceanologica Sinica*, vol. 26, no. 6, pp. 83–90, 2007.

[32] A. Insua, R. Freire, J. Ríos, and J. Méndez, "The 5S rDNA of mussels Mytilus galloprovincialis and *M. edulis*: sequence variation and chromosomal location," *Chromosome Research*, vol. 9, no. 6, pp. 495–505, 2001.

[33] A. Insua and J. Méndez, "Physical mapping and activity of ribosomal RNA genes in mussel Mytilus galloprovincialis," *Hereditas*, vol. 128, no. 3, pp. 189–194, 1998.

[34] Y. Wang, Z. Xu, and X. Guo, "Differences in the rDNA-Bearing chromosome divide the asian-pacific and atlantic species of *Crassostrea* (Bivalvia, Mollusca)," *Biological Bulletin*, vol. 206, no. 1, pp. 46–54, 2004.

[35] S. B. Chang, T. J. Yang, E. Datema et al., "FISH mapping and molecular organization of the major repetitive sequences of tomato," *Chromosome Research*, vol. 16, no. 7, pp. 919–933, 2008.

[36] X. Guo and S. K. Allen, "Fluorescence *in situ* hybridization of vertebrate telomere sequence to chromosome ends of the Pacific oyster, *Crassostrea gigas* Thunberg," *Journal of Shellfish Research*, vol. 16, no. 1, pp. 87–89, 1997.

[37] A. González-Tizón, A. Martínez-Lage, L. Mariñas, R. Feire, L. Cornudella, and Y. Méndez, "Cytogenetic characterization of *Donax trunculus* (Mollusca, Bivalvia) 13th International Chromosome Conference," *Cytogenetics & Cell Genetics*, vol. 81, p. 109, 1998.

[38] Y. Wang, Z. Xu, and X. Guo, "A centromeric satellite sequence in the pacific oyster *(Crassostrea gigas Thunberg)* identified by fluorescence *in situ* hybridization," *Marine Biotechnology*, vol. 3, no. 5, pp. 486–492, 2001.

[39] W. H. Wei, W. P. Zhao, L. J. Wang, B. Chen, Y. C. Li, and Y. C. Song, "Karyotyping of *Brassica napus* L. based on C_0t-1 DNA banding by fluorescence *in situ* hybridization," *Journal of Integrative Plant Biology*, vol. 47, no. 12, pp. 1479–1484, 2005.

Hindawi Publishing Corporation
Evidence-Based Complementary and Alternative Medicine
Volume 2011, Article ID 742963, 10 pages
doi:10.1155/2011/742963

Research Article

Characteristics of the Aragonitic Layer in Adult Oyster Shells, *Crassostrea gigas*: Structural Study of Myostracum including the Adductor Muscle Scar

Seung-Woo Lee, Young-Nam Jang, and Jeong-Chan Kim

CO_2 Sequestration Research Department, Korea Institute of Geoscience and Mineral Resources, Gwahangno 92, Yuseonggu, Daejeon 305-350, Republic of Korea

Correspondence should be addressed to Jeong-Chan Kim, jckim@kigam.re.kr

Received 29 December 2010; Accepted 16 April 2011

Myostracum, which is connected from the umbo to the edge of a scar, is not a single layer composed of prismatic layers, but a hierarchically complex multilayered shape composed of minerals and an organic matrix. Through the analysis of the secondary structure, the results revealed that a β-antiparallel structure was predominant in the mineral phase interface between the myostracum (aragonite) and bottom folia (calcite). After the complete decalcification and deproteinization, the membrane obtained from the interface between the myostracum buried in upper folia, and the bottom folia was identified as chitin. The transitional zone in the interface between the adductor muscle scar and folia are verified. The myostracum disappeared at the edge of the scar of the posterior side. From this study, the entire structure of the myostracum from the adult oyster shell of *Crassostrea gigas* could be proposed.

1. Introduction

The mollusk shell has been investigated as a typical biomineralization model for nearly 25 years [1–4], and it has become especially important due to its potential as a novel synthetic route to high-performance composite materials [5–8]. However, the exact understanding and a control technique on organic matrices are needed to develop a novel synthetic route [9–11]. The organic matrix intercalated in a shell is generally assumed to play a role in crystal nucleation, crystal orientation, crystal size regulation, and crystal polymorphism and to contribute to the shell's biomechanical properties [12]. Furthermore, it is reported that the organic matrix of the aragonitic layer differed from that of the calcitic layer. In mollusks with calcitic shells, one protein and one or two mucopolysaccharide bands were present, whereas in species with shells of aragonite or both aragonite and calcite, three or more proteins and three or more mucopolysaccharides were evident [13]. Additionally, the study of the interface between the aragonitic layer and calcitic layer could be a good guideline for the novel material synthesis related to organic-inorganic composites. It is reported that only two small, distinct, well-defined areas of the adult oyster shell are composed of aragonite: the myostracum and the ligament [14]. The myostracum is located in the attachment of the adductor muscle, commonly called the muscle scar or imprint, to the umbo of each valve. The adductor muscle scar (AMS) is the most conspicuous area on bivalves and *Crassostrea gigas*. The adductor muscle functions to close the shell [15, 16]. The studies on the organic matrix and the structural role of the myostracum, however, are few in number. Studies of the myostracum buried in the folia are still far from fully elucidating the structure and matrix by which it controls crystallization. Thus, the structural study of the entire myostracum is required, and the adult oyster shell of *Crassostrea gigas* has been chosen. The myostracum has significant advantages. We can study both the aragonitic layer and calcitic layer simultaneously because the matrix structure and the mechanism can be understood, and we can study the key role of the organic matrix through the physical and the chemical characteristics of the interface of the aragonitic and calcitic layers during shell formation. The information from this study could be used in the field of novel biocomposite

synthesis and marine biomineral formation, such as that of bivalve shells.

2. Materials and Methods

2.1. Sample Preparation. Shells of *Crassostrea gigas* (Namhae and Tongyoung in Korea) were freshly collected, soaked in 5% NaOH, lightly scrubbed, and dried at room temperature. After they had dried completely, the samples were finely separated using a mill, cutting knife and optical microscope. The decalcified samples were prepared by submerging myostracum buried in folia into acetic acid solution. They were partly or completely removed by controlling the treatment time and the concentration of acetic acid. Deproteinization process was carried out as follows: the samples were treated by 20% sodium hydroxide at 65°C for 1 hour and then washed with distilled water. Soluble or insoluble protein obtained from the adductor muscle scar was prepared by the method of Choi and Kim [17].

2.2. Observation Procedure. Analysis is equipment-like as the following equipment is used to analyze a sample separated from myostracum and organic matrix. Crystal structure and crystallinity were characterized by recording a RIGAKU horizontal powder X-ray diffractometer using CuKα radiation via a rotating anode at 30 kV and 20 mA. Microstructures of the specimens were studied by using an Aspex personal scanning electron microscope (PSEM) with EDS capability. During SEM analysis, the features identified as organic matrix were relocated. Residual products of decalcification and deproteination were observed by scanning electron microscopy (SEM) (S-2500C HITACHI, Japan) with an acceleration voltage of 20 kV and a beam current of 5×10^{-10} A.

2.3. Amide I and Secondary Structure Determination of Proteins. The amide I feature, located approximately in the 1680–1597 cm^{-1} region, results primarily from the C=O stretching vibration coupled to the in-plane NH bending and CN stretching modes. The exact frequency of this vibration depends on the nature of hydrogen bonding involving the C=O and NH moieties; this, in turn, is determined by the particular secondary structure adopted by the polypeptide chains. The relationship between the position of the amide I band and the type of secondary structure may be best observed from the infrared spectra of homopolypeptides that adopt well-defined, and often highly homogeneous secondary structures [18, 19].

The spectra were recorded using a Fourier transform infrared spectrometer with a resolution of 2 cm^{-1}. The system was purged with dry N_2 to reduce interfering water vapor IR absorption and verified no water contribution by measuring KBr pellets. For intracrystalline proteins intercalated within either calcite or aragonite, the subtraction was performed [20, 21]. To obtain the undisturbed protein vibration spectra, each synthetic calcite and aragonite reference IR spectrum was subtracted from each mineral-specific layer, respectively. The subtracted spectra were analyzed by second derivatization, resolution-enhanced Fourier self-deconvolution in the amide I region and Gaussian curve-fitting using the origin 6.1. Second-derivative spectra [22] were smoothed by the 9-point FFT filter method. The number of components and their peak positions were determined by second derivatization and used as starting parameters [23]. The secondary structure contents were calculated from the area of each Gaussian band and their fraction of the total area in the amide I spectral region [24]. The assignment of these bands is based on the studies of proteins by vibrational spectroscopy.

3. Results and Discussion

3.1. Overview of the Myostracum of the Adult Oyster Shell of C. gigas. The adductor muscle scar is the surface of the myostracal support for the attachment of the adductor muscle, and it is contained in the shell of most bivalves [15]. Figure 1(a) shows the inner surface of the *C. gigas* shell. Most of the area in the inner surface is composed of folia that appear to be nacreous layers and chalky layers, of which 20~30% have been identified. The folia are composed of foliated laths. The chalky layer is frequently marked by irregularly shaped, chalky-white areas and relatively soft, porous material compared to the folia [4]. The adductor muscle scar (AMS) is the most conspicuous area on the inner surface of the *C. Gigas* shell. It is pigmented, and its color varies in different individuals from light, lavender-white to dark purple. The scar is located slightly in the center toward the posterodorsal side of each valve. Figure 1(b) shows a vertical section of the center of the scar. The myostracum is elongated from the scar to the umbo. As shown in Figure 1(b), the transitional zone (approximately 0.5 mm in thickness) with granule-like material exists around the outside of the scar. Foliated laths have been developed from the anterior to the scar and from the scar to the posterior. The thickness of the myostracum in the hidden area is identified as above, approximately 10 μm, but the thickness decreases to be closer to the transitional zone. Additionally, the myostracum disappears at the transitional zone (Figure 1(c)).

Figure 1(c) shows a scheme of the oyster shell with an enlargement including the myostracum. A specific stratum between the folia and myostracum could exist, but the thickness may be several hundred nanometers. Myostracum with the exception of the adductor muscle scar is buried between the foliated lath and the chalky structure. As shown in this figure, the myostracum has been surrounded by the folia; the polymorph of the myostracum is aragonite, but the folia are calcite. The shape of the myostracum is a prismatic layer (approximately 5~35 μm in thickness), but that of the folia is a laminated layer (approximately 100~200 μm in thickness). This single layer that comprises the myostracum is the myostracal prism, and the layer comprising the folia is the foliated lath. In this study, the interface was defined as the point of interaction between the two layers. As previously mentioned, the polymorph and the shape of the two layers are different. Thus, a buffer zone (organic matrix) could be necessary for the morphological and polymorphic control.

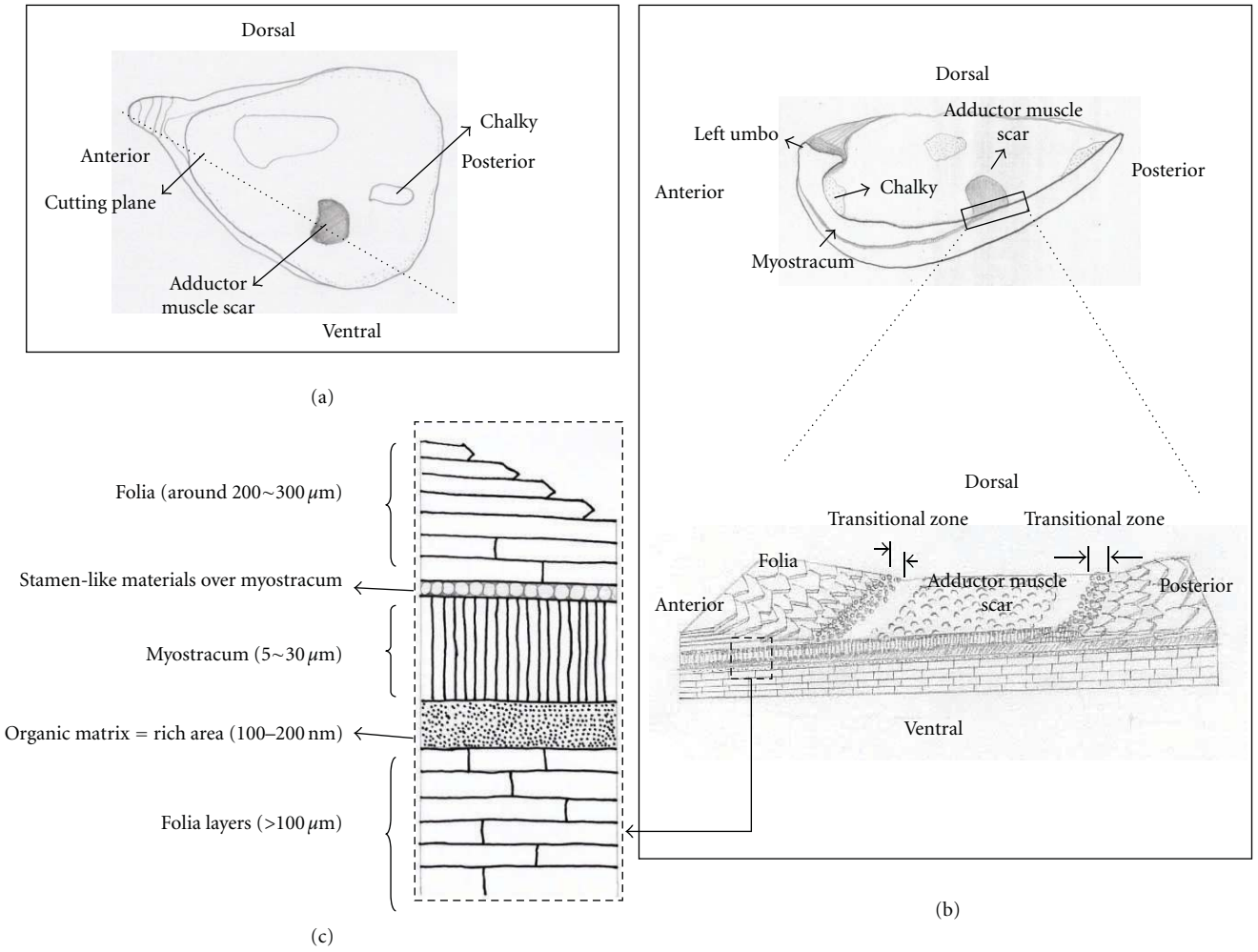

Figure 1: (a) Schematic of the inner surface of the left valve of an oyster shell, *Crassostrea gigas* (black dotted line: cutting plane). (b) Schematic of the vertical section with the cutting plane of the adductor muscle scar. The bottom schematic is an enlargement of the cutting plane including the AMS (adductor muscle scar), myostracum, and folia. (c) An enlargement indicating the thickness of the myostracum buried in the folia on the anterior side. The size of each layer is exaggerated for clarity. Various terms are in common use in the description of the bivalve shell [25].

At the organic layer, the interface between the folia and myostracum is rich at the bottom interface as compared to the upper interface. Consequently, the area including the interface between the folia and myostracum contains well-ordered arrays and structural characteristics of each layer.

3.2. Characteristic Approach of the Myostracum in the Adult Muscle Scar of C. gigas. As previously mentioned, the point of attachment of the adduct muscle scar (AMS) is the most evident area on the interior surface of *C. gigas*. Galtsoff [25] reported that the ratio of the scar area to the shell surface area varies from 8 to 32. Although the adductor muscle is comprised of two distinct parts (approximately two-thirds of which is the anterior, translucent area, and one-third of which is the posterior, milky-white area), no microstructural differences are evident in the scar in these two areas. The study of the AMS is important because it contains

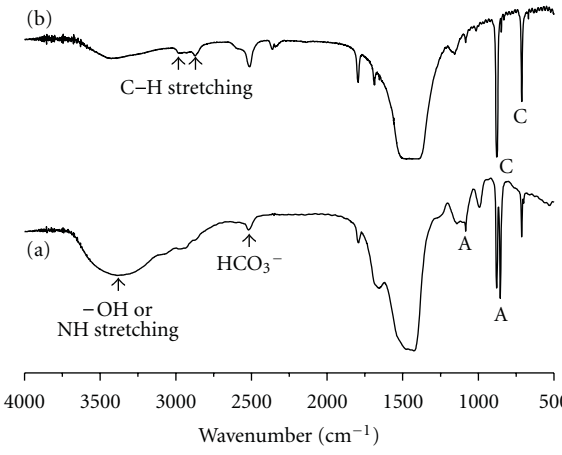

Figure 2: FTIR spectra of the myostracum of the AMS (adductor muscle scar) (a) and folia (b) (A: aragnonitic peak, C: calcitic peak).

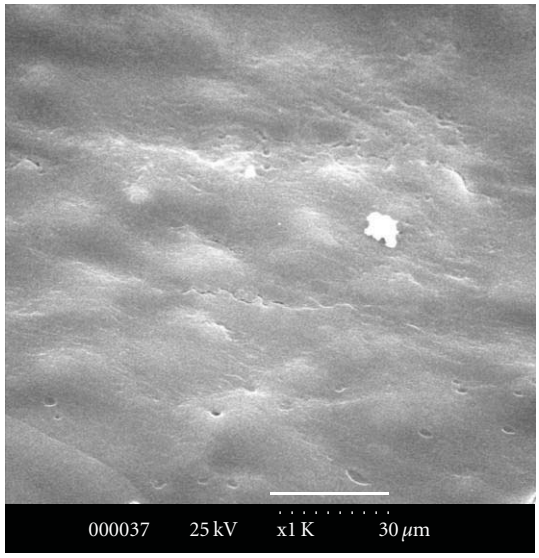

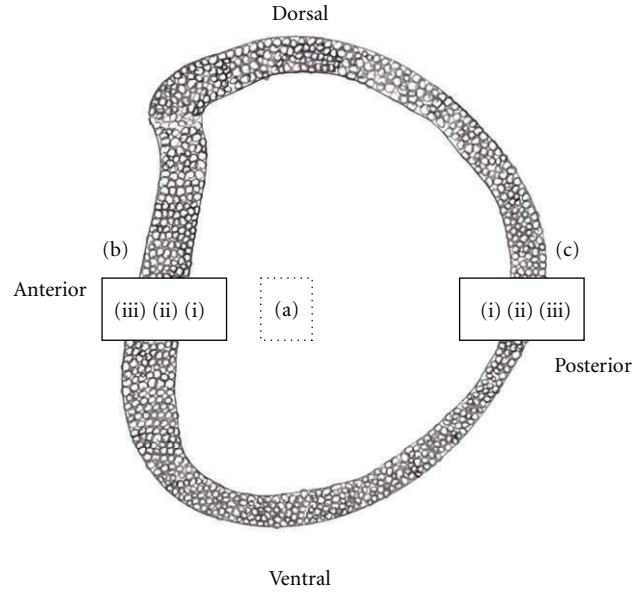

(a) (Scale bar: 30 μm), the area including the transitional zone (refer to Figure 1(b)) from the anterior to the scar side

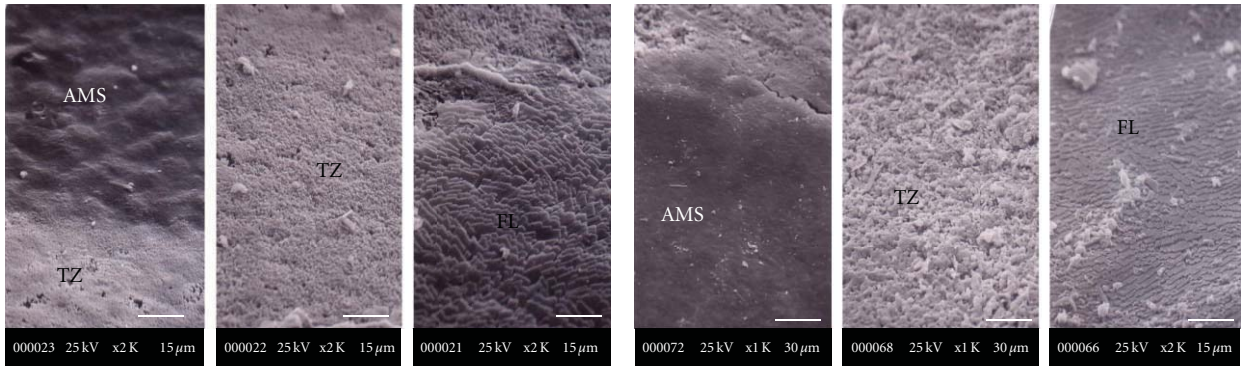

(i) (ii) (iii) (i) (ii) (iii)

(b) (Scale bar: 15 μm) and the area including the transitional zone from the scar to the posterior side

(c) (Scale bar of (i) and (ii) 30 μm; scale bar of (iii) 15 μm). The left valve of *C. gigas* was used (AMS: Adductor Muscle Scar, TZ: Transitional Zone, FL: Folia)

Figure 3: The surface image of the central adductor muscle scar.

the morphological and polymorphic interface. An adult oyster shell is composed of a high concentration of $CaCO_3$ (above 97 wt.%) and a low concentration of organic matrix (approximately 3 wt.%) [3]. $CaCO_3$ has three polymorphs, including aragonite, vaterite, and calcite. Among these, the polymorph of the myostracum is aragonite, and that of the folia is calcite. Even more interesting for this study is the hierarchical structure of the morphological interface.

From the analysis of the FTIR spectrum of the myostracum in the AMS and folia (Figure 2), the polymorph of the folia is identified as calcite, and that of the myostracum is identified as aragonite. The carbonate ions in the mineral were demonstrated by the internal vibration modes of the CO_3^{2-} ions: 696, 713(v_4)–858, 875(v_2)–1082(v_1) and 1490(v_3) cm^{-1}. The strong IR band detected at 1792 cm^{-1} could also be attributed to the C=O groups of the carbonate ions. The splitting of v_4(696), v_2(858), and v_1(1082) is characteristic of the aragonite structure. Moreover, the peak of the –OH or NH stretching (3450 cm^{-1}), the CH stretching (2929 cm^{-1}) as the organic matrix characteristic and the peak of HCO_3^- (2650~2520 cm^{-1}) that plays a role in providing the carbonate ion in Ca^{2+} protein binding in the formation of the shell are confirmed. As shown in Figure 2, organic characteristics are identified in the myostracum of the AMS and folia. Additionally, it is verified that the myostracum in the AMS has a rich organic matrix.

The area between the scar and the folia contains a transitional zone with a granular-like structure, as shown in Figure 3. The surface of the central scar from which the adductor muscle has been removed with acetic acid is extremely smooth and slightly berm-like (Figure 3(a)). In the case of *C. gigas*, the ratio of the scar area in the oyster inner shell surface area is from 8 to 15. Figures 3(b) and 3(c) show the interface, or transitional zone, between the AMS and folia

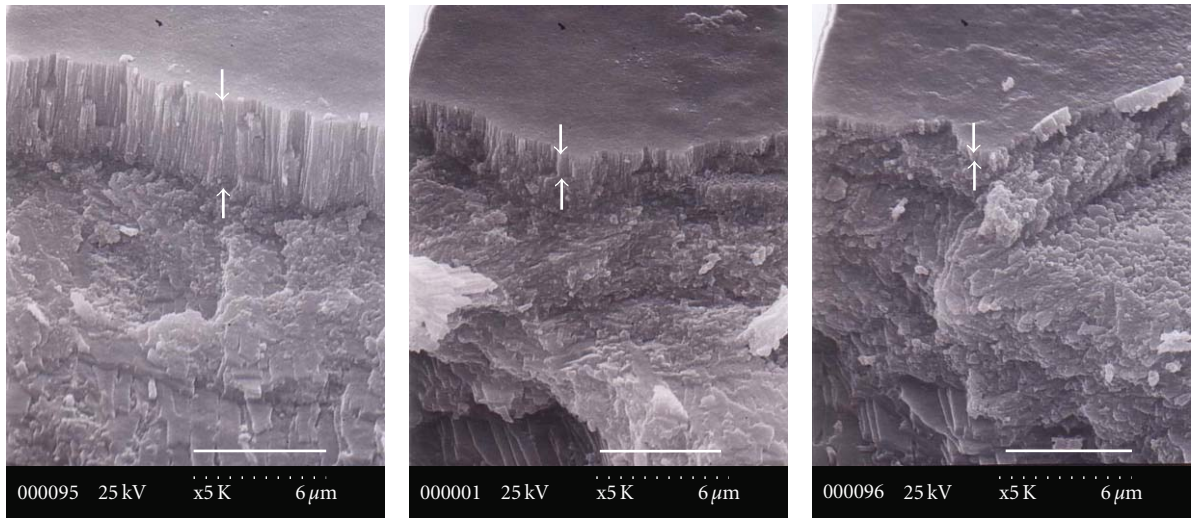

(a) (b) (c)

Figure 4: SEM images of the myostracum. (a) Central AMS (adductor muscle scar) and (b) the area between the central AMS and the edge of the scar on the posterior side (Scale bar of (a), (b), and (c) 6 μm).

in both directions. The first is from the anterior side to the AMS (Figure 3(b)), and the second is from the AMS to the posterior side (Figure 3(c)). The AMS is present at the front of the posterior-advancing edge of the growing adductor muscle and shows a transitional zone of the newly deposited scar approximately 0.5 to 1 mm wide (Figures 3(b) and 3(c)). The surface of the AMS near the transitional zone typically consists of a smooth shape similar to that of the central scar. The granules between the transitional myostracum and the foliated structure on the ventral and dorsal sides of the scar are usually much narrower than that on the posterior side and are finely granular. The granule is approximately 60-μm (ventral and dorsal side) to 100-μm (posterior and anterior side) wide. The distinctly granular nature of this transitional zone is characteristic. The granule-to-transitional surface of *C. virginica* [15] consists of a muffin- or mulberry-like microstructure ranging in complexity from single to multiple granular mounds, in contrast to *C. gigas* in which a muffin- or mulberry-like microstructure does not exist. Moreover, Carriker et al. [15] reported that granules in *C. virginica* adhere closely between the chalky structure and plywood-like calcite. However, in the case of *C. gigas*, the granules also do not exist. From these results, a granule may be a certainly distinctive characteristic to classify the differences between *C. virginica* and *C. gigas*.

Figure 4 shows that the myostracum outlines in the posterior end of the scar are irregular, with reentrant angles. Especially interesting is that the thickness of the myostracal prism was rapidly tapered (indicated by the white arrows in Figure 4). As evident from Figure 4, the thickness of the myostracum decreases toward the posterior direction and then disappears in the region of the granule that exists in the interfacial posterior side. The interesting aspect is how an oyster could control a gradual decrease in the thickness. The organic matrix intercalated in the myostracum or located in the interface between the myostracum and folia could be a key factor to control the system.

Table 1 shows the difference in the amino acid composition of *C. virginica* [26] and *C. gigas* [17]. The amino acid composition of *Crassostrea gigas* was quoted in a previously published paper. As evident in Table 1, *C. gigas* and *C. virginica* have a difference in their amino acid composition according to the position and characteristics of each layer, respectively. Aspartate, serine, and glycine in *C. virginica* are rich, while serine in *C. gigas* is relatively low (Table 1). It is known that the secondary structure [27] of proteins exists mostly as a β structure if Asp, Gly, and Ser are mostly contained in the protein. The proportion of nonpolar residues is 0.52 in *C. virginica* and 0.47 in *C. gigas,* which is similar to Wheeler's result (0.41) [28]. The analysis by Wheeler et al. was performed on the dark and light fractions of the insoluble matrix extracted from the whole shell; therefore, a direct comparison with our data may not be appropriate. However, if their dark or light fractions are assumed to be the foliated lath and adductor muscle scar, respectively, then the data of those two reports agree relatively well (The insoluble matrix of the prismatic layer has a darker color than that of the foliated lath.) Several researchers [29, 30] reported that the amino acid composition of mollusks affected the structure of the shell and differed in the shape of the shell. A comparison between *C. gigas* and *C. virginica* in Table 1 indicates that aspartate, glycine, and serine are rich residues. Wheeler et al. reported the ratio of aspartate, glycine, and serine as 80% of the total residue.

Through chemical treatment (10% acetic acid), the decalcification of myostracum in AMS was carried out (Figure 5). Granules (approximately 3 μm) on the myostracum were identified (Figure 5(b)), and the decalcified myostracal prisms possessed horizontal striations along

Table 1: Amino acid compositions of the soluble and insoluble proteins from *Crassostrea virginica* [26] and *Crassostrea gigas* [17] (Asx: Asp + Asn, Glx: Glu + Gln).

Species	Layer	Asx	Thr	Ser	Glx	Pro	Gly	Ala	Val	Tyr
C. virginica	Folia	29.4	0.8	22.0	5.2	3.5	33.4	1.42	1.2	0
	Whole shell, insoluble only	18.1	1.2	14.2	3.5	6.2	34.1	4.7	3.0	4.9
C. gigas	Folia	24.8	1.9	6.6	4.2	5.5	29.3	10.3	3.0	2.2
	Whole shell, insoluble only	8.7	2.8	5.8	6.3	6.9	27.4	12.4	5.6	2.0
	Myostracum in AMS	20.9	2.7	6.4	7.6	5.1	30.0	6.5	3.2	1.8

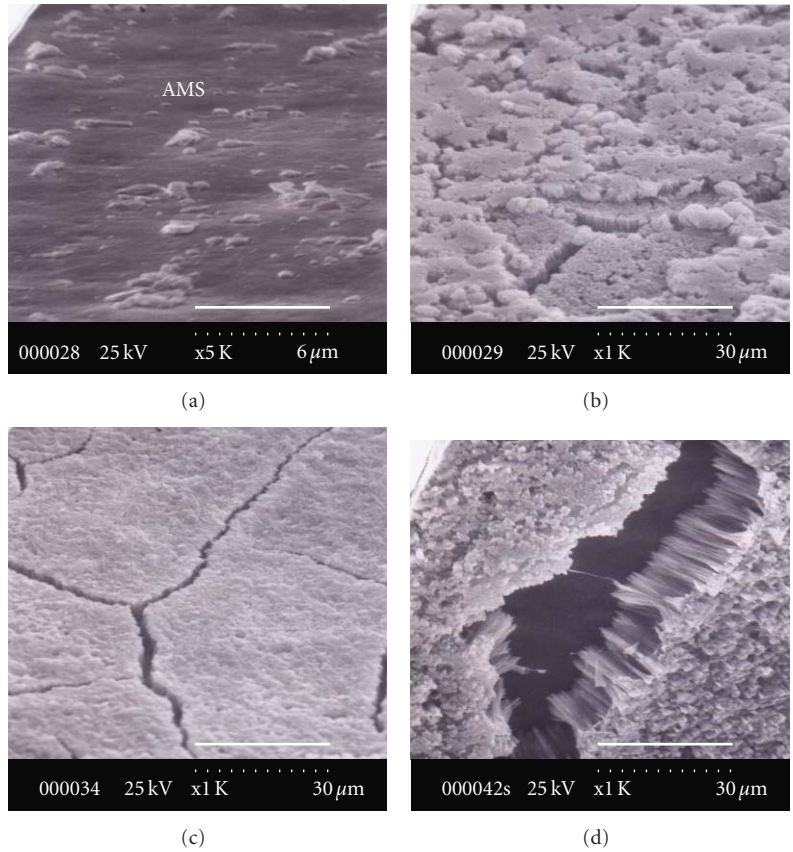

Figure 5: The decalcified AMS including the myostracum by acetic acid (10 wt.%) for 30 min (Scale bar of (a) 6 μm; scale bar of (b), (c), and (d) 30 μm).

the axis (Figure 5(c)). Furthermore, the separation of the myostracum at the interface with the folia was easier to accomplish after an acidic treatment. It is estimated that the removal of the organic matrix allowed the myostracum to adhere to the folia.

3.3. Characteristic Approach of the Myostracum Buried in the Folia of C. gigas. A vertically fractured foliated lath on the anterior side shows that the thickness of the folia is from 500 μm to 800 μm (the white dotted line in Figure 6(a)). The folia structure does not fracture as cleanly as does the scar, but the fractures provide valuable information on the form of the laths. The surface texture ranges form smooth to slightly dimpled, parallel-lined, or chevron-marked, representing the growth halts of the crystal fronts, which point in the direction of the shell margin (Figure 6(b)). Especially in the region between the posterior side and the scar, the laths remain parallel to each other, and the growing front of each lath faces the posterior margin. The formation of the foliated laths with uniform width and length could be attributed to the influence of the mantle tissue of the hidden organic matrix. Wilbur and Saleudin (1983) reported that the shell formation occurs in the secretion by the mantle epithelial cells and in an extrapallial space in which mineral crystals are nucleated and oriented with the secreted organic matrix. The process by which the myostracum is buried in the folia could be dictated by a uniform prismatic structure into the AMS. Any organic matrix would control the structure. The most important factor is a template to control the structure and polymorphism of the myostracum.

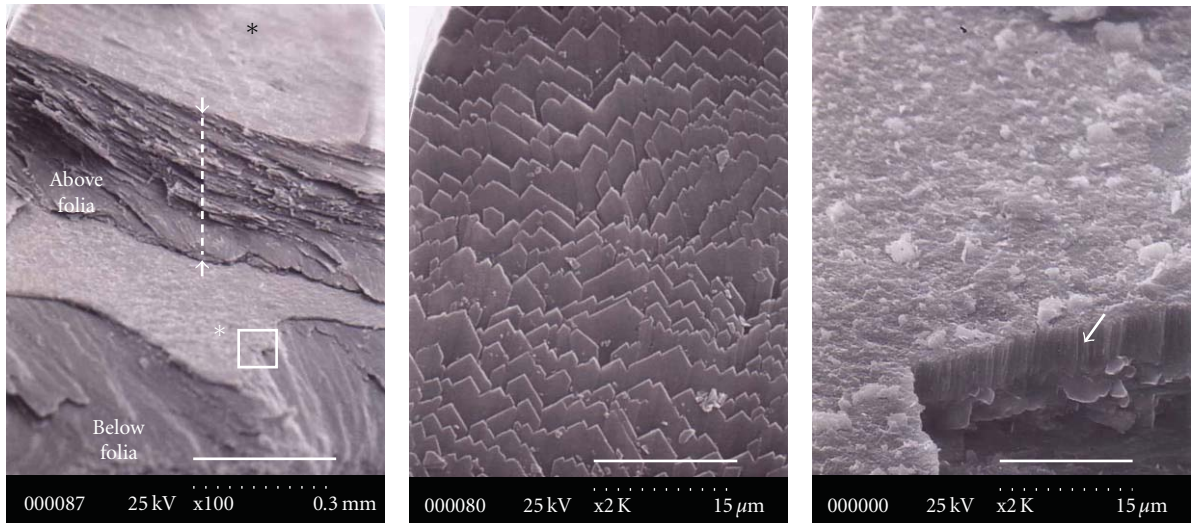

Figure 6: SEM images of the myostracum buried in the folia on the anterior side. (a) the area including the folia, myostracum, and folia; (b) an enlargement of the black star region; (c) an enlargement of the white star region (scale bar of (a) 0.3 mm; scale bar of (b) and (c) 15 μm). The thickness of the upper folia is approximately 300 μm. It appears that the myostracum was inserted in the folia.

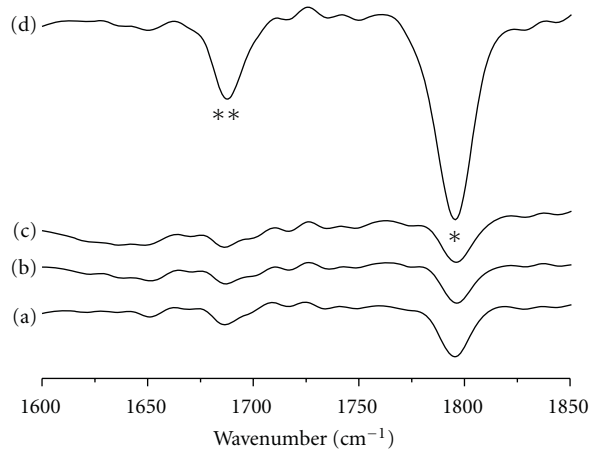

Figure 7: FTIR spectra of the fractured folia and myostracum on the anterior side (black star: amide I, double black stars: C=O bond). (a) Folia by fracturing in first, (b) foliated lath by fracturing in second, (c) foliated lath by fracturing in third, and (d) folia and myostracum buried in folia.

To identify the polymorphism of the myostracum buried in the folia, FTIR analysis was conducted by fracturing: the fractured outside folia (Figure 7(a)), the fractured folia lath in second (Figure 7(b)), fractured folia in third (Figure 7(c)), and the folia (Figure 7(d)) containing the myostracum. As shown in Figure 7, the intensity of the layer containing the myostracum in the amide I is higher than that in the others. The amide I feature, located approximately in the 1680–1597 cm^{-1} region, results primarily from the C=O stretching vibration coupled to the in-plane NH bending and CN stretching modes. From the above result, it may be analogized that the interface between the aragonite and calcite includes a higher content of the organic matrix than the other interfaces.

Table 2 shows that the secondary structures of the intracrystalline protein of the fractured folia (refer to Figures 7(a)–7(c)) and the layer including the myostracum (refer to Figure 7(d)) were determined by FSC and Gaussian curve fitting. When the secondary structure of the protein was analyzed by FTIR, the advantage is that the dimensional structure of the ligand in the shell tissue can be obtained without decalcification of the shell. As shown in the table, a~c (folia) mostly consist of α-helices, while the layer including the myostracum and folia consists mainly of β-antiparallel structures. The β-structure is a major component of the protein that forms the geometric matching needed when controlling the nuclear generation in mineralization; the β structure offers ligands of regular and continuous negative charge to bond with the calcium ion. It is reported that the shape of calcium carbonate that is formed in this way is determined by the protein and especially represents a conformation dependence [31]. The above information explains that the secondary structures of the protein in the folia (calcite) and myostracum (aragonite) have considerable differences. The β-antiparallel structure was composed a large majority in the area, which included an interface between the folia (calcite) and the myostracum (aragonite).

From a previous research [17], it was confirmed that the organic matrix faced the crystal (001) plane of the myostracum of the AMS and folia. The structural or geometric matching at the inorganic-organic interfaces is a key concept in oriented nucleation in biomineralization. Mann [31] explained the specific nucleation of the (001) face of the aragonite on the surface of highly acidic β-anti proteins in the shell nacre. The results show that the a-

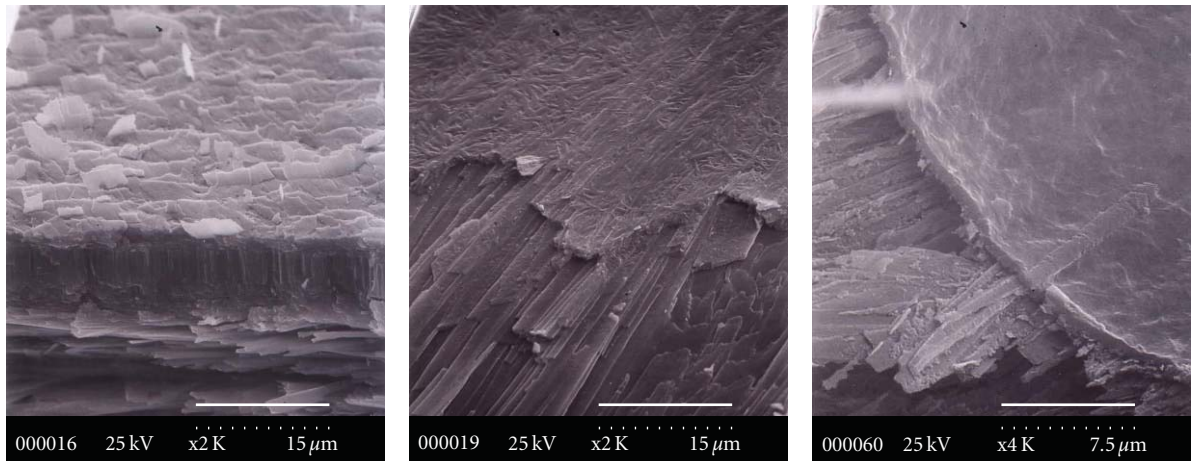

Figure 8: The decalcified myostracum buried in folia by acetic acid (10 wt.%). (a) fractured myostracum including the folia; (b) decalcification for 30 min; (c) decalcification for 1 hr (scale bar of (a) and (b) 15 μm; scale bar of (c) 7.5 μm).

Table 2: Secondary structure of the intracrystalline proteins of each layer *in vivo*: (a) Folia by fracturing in first, (b) Folia by fracturing in second, (c) Folia by fracturing in third, and (d) Folia and myostracum buried in folia.

Assignment	Band position (cm^{-1})	(a)	(b)	(c)	(d)
α-helix	1647–1660	58.0	58.5	66.1	8.6
β-sheet	1615–1640	7.7	9.8	9.0	13.1
Turns	1661–1680	—	—	3.9	3.8
β-anti	1681–1692	34.3	31.7	21.0	74.5

Unit: area %.

and b-axes of the β-anti of the matrix are aligned with the a- and b-crystallographic directions of the aragonite lattice. That is, the crystals are oriented such that the (001) crystal face (the a-b plane) and c axis are parallel and perpendicular to the underlying matrix surface, respectively. Thus, the crystal orientation (001) of the myostracum composed of aragonite could indicate the identity of the β-structure in the myostracum buried in the folia. This result, moreover, incorporates both an ionotropic and an epitaxial formation of the myostracum that could be induced by the β-structure. Of course, only the β-structure is a major factor in accounting for the formation of the myostracum and the control of the interface between the myostracum and folia.

The optical microscope is used to verify the separation of the myostracum at the boundary of the folia after fracturing. Figure 8 shows the results; within 30 min of decalcification, the myostracal prism is verified (Figure 8(a)), and lawn-like material is also verified (Figure 8(b)). After the myostracal prism is eliminated, a membrane is verified (Figure 8(c)). The morphology and shape of the membrane differ from previous minerals. It can be analogized that the organic matrix in contact with the myostracum is mostly soluble, while the membrane to be eliminated from the myostracal prism was occupied by a major portion of insoluble matrix. It is known that proteins extracted from the shell play an important role in biomineralization. Numerous experiments grown *in vitro* in crystals of proteins extracted from the shell have been performed to elucidate their functions during the formation of either aragonite or calcite. From various *in vitro* experiments, some researchers [32] reported that a polyanionic-soluble protein determines the phase of the calcium carbonate, while other researchers have reported that an insoluble protein determines the phase [33]. Belcher et al. [34] also produced an *in vitro* system capable of specifically inducing the formation of aragonite and calcite crystals in the presence of appropriate acidic macromolecules extracted from nacre. This specificity is dependent not only on the acidic macromolecules but also requires the presence of β-chitin, as opposed to α-chitin, and silk fibroin [35]; chitin has an intimate relationship among proteins of the silk-fiber type, rich in Gly and Ala [36]. As shown in Table 1, Gly in *C. gigas* and *C. virginica* is rich (27~35%), and Ala of the insoluble portion of *C. gigas* is approximately three times higher than that of *C. virginica*. The interface between the myostracum, and folia may have a significant effect on the mechanical properties of the overall composites.

After the complete decalcification, the membrane obtained from the interface of the myostracum buried in the folia was deproteinized. After eliminating the insoluble protein, the membrane was identified by XRD analysis (Figure 9); it is verified that the organic membrane from the myostracum buried in the folia possesses chitin-like

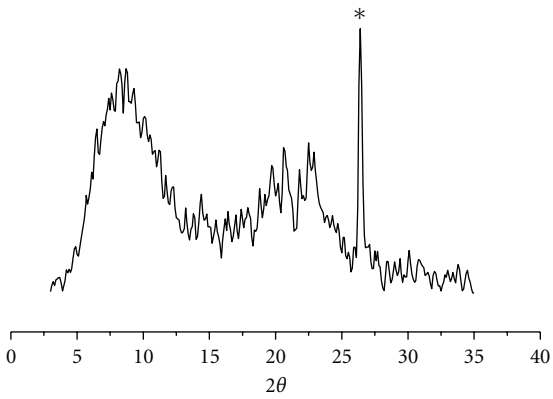

Figure 9: XRD-diffraction profile of the membrane obtained from the myostracum buried in folia (* indicates the main peak of aragonite).

characteristics. It is known that the peaks of β-chitin are 9.2 and 20.3 for the 2θ value. In the case of the mambrane, both peaks, a strong peak at 9.2 and a weak peak at 20.3, were identified. Above all, β-chitin has a good relationship with the β-structure of the protein secondary structure for the nacre formation [37]. Thus, the correlation between the organic matrix including the β-structure and chitin and the formation of the myostracum buried in the folia could be inferred.

The study on the interface with different polymorph and morphology is significant for the synthesis of hierarchical composites with organic-inorganic interactions. The information obtained from this study will be valuable for marine biomineralogists and material scientists.

4. Conclusions

This study presents a comprehensive characterization of the structure, minerals, and organic matrix of the interface between aragonite and calcite in *Crassostrea gigas*.

(i) The myostracum from the umbo to the scar is a hierarchically complex multilayer composed of a myostracal prism and organic matrix. The thickness of the myostracum was rapidly tapered at the end of the posterior side of the scar.

(ii) Although *Crassostrea virginica* and *Crassostrea gigas* belong to the same genus and are similar in shape, there are differences between them, including the Quenstedt muscle scar, granules buried in the foliated lath, and the lack of a muffin-like microstructure.

(iii) The myostracum was identified as a prismatic layer oriented to (001). A β-antiparallel structure was predominant at the interface between the myostracum (aragonite) and the bottom folia (calcite). Thus, the β-antiparallel structure may be attributed to the orientation of the myostracal prism.

(iv) After the complete decalcification and proteinization, the membrane obtained from the interface of the myostracum buried in the folia was identified by XRD analysis; it was verified that the organic matrix is characteristic of chitin.

The myostracum of the oyster shell of *C. gigas* is a hierarchical structure from the cooperation between the organic matrices (protein and polysaccharide). The polymorph and the morphology have been controlled by their close interaction.

Acknowledgment

This research was supported by the General Research Project (Utilization and Sequestration of CO_2 Using Industrial Minerals) of the Korea Institute of Geoscience and Mineral Resources (KIGAM) funded by the Ministry of Knowledge Economy of Korea.

References

[1] S. Albeck, L. Addadi, and S. Weiner, "Regulation of calcite crystal morphology by intracrystalline acidic proteins and glycoproteins," *Connective Tissue Research*, vol. 35, pp. 365–370, 1996.

[2] A. Sellinger, P. M. Weiss, A. Nguyen et al., "Continuous self-assembly of organic-inorganic nanocomposite coatings that mimic nacre," *Nature*, vol. 394, no. 6690, pp. 256–260, 1998.

[3] S. W. Lee and C. S. Choi, "The correlation between organic matrices and biominerals (myostracal prism and folia) of the adult oyster shell, *Crassostrea Gigas*," *Micron*, vol. 38, no. 1, pp. 58–64, 2007.

[4] S. -W. Lee, Y. -N. Jang, K. -W. Ryu, S. -C. Chae, Y. -H. Lee, and C. -W. Jeon, "Mechanical characteristics and morphological effect of complex crossed structure in biomaterials: fracture mechanics and microstructure of chalky layer in oyster shell," *Micron*, vol. 42, no. 1, pp. 60–70, 2011.

[5] S. I. Stupp and P. V. Braun, "Molecular manipulation of microstructures: biomaterials, ceramics, and semiconductors," *Science*, vol. 277, no. 5330, pp. 1242–1248, 1997.

[6] S. Oliver, A. Kuperman, N. Coombs, A. Lough, and G. A. Ozin, "Lamellar aluminophosphates with surface patterns that mimic diatom and radiolarian microskeletons," *Nature*, vol. 378, no. 6552, pp. 47–50, 1995.

[7] C. R. Lowe, "Nanobiotechnology: the fabrication and applications of chemical and biological nanostructures," *Current Opinion in Structural Biology*, vol. 10, no. 4, pp. 428–434, 2000.

[8] H. Colfen, "Biomineralization: a crystal-clear view," *Nature Materials*, vol. 9, pp. 960–961, 2010.

[9] M. Suzuki, K. Saruwatari, T. Kogure et al., "An acidic matrix protein, Pif, is a key macromolecule for nacre formation," *Science*, vol. 325, no. 5946, pp. 1388–1390, 2009.

[10] Y. Yamamoto, T. Nishimura, T. Saito, and T. Kato, "$CaCO_3$/chitin-whisker hybrids: Formation of $CaCO_3$ crystals in chitin-based liquid-crystalline suspension," *Polymer Journal*, vol. 42, no. 7, pp. 583–586, 2010.

[11] I. M. Weiss, "Jewels in the Pearl," *ChemBioChem*, vol. 11, no. 3, pp. 297–300, 2010.

[12] A. Berman, L. Addadi, and S. Weiner, "Interactions of sea-urchin skeleton macromolecules with growing calcite crystals-a study of intracrystalline proteins," *Nature*, vol. 331, no. 6156, pp. 546–548, 1988.

[13] S. Kobayashi, "Calcification in fish and shell-fish I. Tetracycline labelling patterns on scale, centrum and otolith in young goldfish," *Bulletin of the Japanese Society for the Science of Fish*, vol. 30, pp. 893–907, 1964.

[14] H. B. Stenzel, "Aragonite and calcite as constituents of adult oyster shells," *Science*, vol. 142, no. 3589, pp. 232–233, 1963.

[15] M. R. Carriker, "The shell and ligament," in *The Eastern Oyster*, V. S. Kennedy, R. I. E. Newell, and A. F. Eble, Eds., pp. 75–168, Maryland Sea Grant Collage, 1996.

[16] H. A. Lowenstam and S. Weiner, *On Biomineralization*, Oxford University Press, New York, NY, USA, 1989.

[17] C. S. Choi and Y. W. Kim, "A study of the correlation between organic matrices and nanocomposite materials in oyster shell formation," *Biomaterials*, vol. 21, no. 3, pp. 213–222, 2000.

[18] F. N. Fu, D. B. DeOliveira, W. R. Trumble, H. K. Sarkar, and B. R. Singh, "Secondary structure estimation of proteins using the amide III region of fourier transform infrared spectroscopy: application to analyze calcium-binding-induced structural changes in calsequestrin," *Applied Spectroscopy*, vol. 48, no. 11, pp. 1432–1441, 1994.

[19] W. K. Surewicz, M. A. Moscarello, and H. H. Mantsch, "Secondary structure of the hydrophobic myelin protein in a lipid environment as determined by Fourier-transform infrared spectrometry," *Journal of Biological Chemistry*, vol. 262, no. 18, pp. 8598–8602, 1987.

[20] E. Goormaghtigh, V. Cabiaux, and J. M. Ruysschaert, "Secondary structure and dosage of soluble and membrane proteins by attenuated total reflection Fourier-transform infrared spectroscopy on hydrated films," *European Journal of Biochemistry*, vol. 193, no. 2, pp. 409–420, 1990.

[21] S. J. Gadaleta, N. P. Camacho, R. Mendelsohn, and A. L. Boskey, "Fourier transform infrared microscopy of calcified turkey leg tendon," *Calcified Tissue International*, vol. 58, no. 1, pp. 17–23, 1996.

[22] H. Susi and D. Michael Byler, "Protein structure by Fourier transform infrared spectroscopy: Second derivative spectra," *Biochemical and Biophysical Research Communications*, vol. 115, no. 1, pp. 391–397, 1983.

[23] A. Dong, P. Huang, and W. S. Caughey, "Protein secondary structures in water from second-derivative amide i infrared spectra," *Biochemistry*, vol. 29, no. 13, pp. 3303–3308, 1990.

[24] W. K. Surewicz and H. H. Mantsch, "New insight into protein secondary structure from resolution-enhanced infrared spectra," *Biochimica et Biophysica Acta - Protein Structure and Molecular Enzymology*, vol. 952, no. 2, pp. 115–130, 1988.

[25] P. S. Galtsoff, "The American oyster *Crassostrea virginica* (Gmelin)," *Fishery Bulletin*, vol. 64, pp. 1–48, 1964.

[26] T. Kawaguchi, "The organic matrices of the shell of the American oyster Crassostrea virginica Gmelin," *Journal of Experimental Marine Biology and Ecology*, vol. 170, no. 1, pp. 11–28, 1993.

[27] D. L. Nelson and M. M. Cox, *Lehninger Principles of Biochemistry*, Worth Publishers, City, State, USA, 2000.

[28] A. P. Wheeler, K. W. Rusenko, and C. S. Sikes, "Organic matrix from carbonate biomineral as a regulator of mineralization," in *Chemical Aspects of Regulation of Mineralization*, C. S. Sikes and A. P. Wheeler, Eds., pp. 9–13, Unversity South Alabama Publication, Ala, USA, 1988.

[29] H. Kasai and N. Ohta, "Relationship between organic matrices and shell structures in recent bivalves," in *Study of Molluscan Paleobiology*, T. Habe and M. Omori, Eds., chapter 4, pp. 101–106, Niigata University Press, Niigata, Japan, 1981.

[30] T. Samata, "Ca^{2+}-binding glycoproteins in molluscan shells with different types of ultrastructure," *Veliger*, vol. 33, pp. 190–201, 1990.

[31] S. Mann, *Biomineralization Principles and Concepts in Bioinorganic Materials Chemistry*, Oxford University Press, New York, NY, USA, 2001.

[32] G. Falini, S. Albeck, S. Weiner, and L. Addadi, "Control of aragonite or calcite polymorphism by mollusk shell macromolecules," *Science*, vol. 271, no. 5245, pp. 67–69, 1996.

[33] K. M. Wilbur and N. Watabe, "Experimental studies on calcification in molluscs and the alga Cocolithus huxleyi," *Annals of the New York Academy of Sciences*, vol. 109, pp. 82–112, 1963.

[34] A. M. Belcher, X. H. Wu, R. J. Christensen, P. K. Hansma, G. D. Stucky, and D. E. Morse, "Control of crystal phase switching and orientation by soluble mollusc-shell proteins," *Nature*, vol. 381, no. 6577, pp. 56–58, 1996.

[35] Y. Levi-Kalisman, G. Falini, L. Addadi, and S. Weiner, "Structure of the nacreous organic matrix of a bivalve mollusk shell examined in the hydrated state using Cryo-TEM," *Journal of Structural Biology*, vol. 135, no. 1, pp. 8–17, 2001.

[36] N. Kensuke and C. Yoshiki, "Control of crystal nucleation and growth of calcium carbonate by synthetic substrates," *Chemistry of Materials*, vol. 13, no. 10, pp. 3245–3259, 2001.

[37] S. Weiner and W. Traub, "X-ray diffraction study of the insoluble organic matrix of mollusk shells," *FEBS Letters*, vol. 111, no. 2, pp. 311–316, 1980.

Hindawi Publishing Corporation
Evidence-Based Complementary and Alternative Medicine
Volume 2011, Article ID 103425, 6 pages
doi:10.1155/2011/103425

Research Article

Novel 5,6-Dihydropyrrolo[2,1-a]isoquinolines as Scaffolds for Synthesis of Lamellarin Analogues

Shao Han Liao,[1,2] Dai Hua Hu,[3] Ai Ling Wang,[1,2] and De Peng Li[1,2]

[1] *College of Environment and Chemical Engineering, Dalian University, Dalian 116622, China*
[2] *Liaoning Key Laboratory of Bio-Organic Chemistry, Dalian University, Dalian 116622, China*
[3] *College of Agronomy, Northwest A&F University, Yangling 712100, China*

Correspondence should be addressed to Ai Ling Wang, wangailing@dlu.edu.cn

Received 31 December 2010; Accepted 3 June 2011

As core skeletons of lamellarins: 5,6-Dihydropyrrolo[2,1-a]isoquinolines are one of the important alkaloids that exhibit significant biological activities, in this study, an efficient synthetic route was described for two novel compounds, 5,6-dihydropyrrolo[2,1-a]isoquinolines **I** and **II**. Compound **I** was synthesized from isovanillin with 28.3% overall yield by a six-step reaction while **II** from 2-(3,4-dimethoxyphenyl) ethanamine was with 61.6% overall yield by a three-step reaction. And the structures of these two compounds were confirmed by means of IR spectrum, ^{1}H NMR, ^{13}C NMR, MS, HRMS, and melting point measurements.

1. Introduction

Lamellarins are a group of hexacyclic marine alkaloids that were initially isolated from a prosobranch mollusk by Faulkner and coworkers in 1985 [1]. Since then, over 70 compounds belonging to this group have been isolated and identified [2].

Some of these lamellarins and related compounds exhibit interesting biological activities in multidrug resistance (MDR) and their corresponding parental cell lines [3]. As well known [4], Lamellarin D (LMD) exhibits a significant cytotoxicity against a large panel of cancer cell lines and is a potential non-CPT (camptothecin) topoisomerase 1 poison [5, 6]. LMD affects cell cycle and acts on cancer cell mitochondria to induce apoptosia [7].

Due to the fascinating novel structures and biological activities, more and more researchers have devoted into the synthetic studies of lamellarins [8] and related 3,4-diarylpyrrolo derivatives. As one of the important alkaloids, 5,6-Dihydropyrrolo[2,1-a]isoquinolines exhibits pronounced biological activities. The biological activity of 5,6-dihydropyrrolo[2,1-a]isoquinolines **I** and **II** was evaluated by their effects on the proliferation of MDA-MB-231 (breast cancer cell line) by MTT assay. Our results showed that compound **I** could significantly inhibit the proliferation of MDA-MB-231 at the concentration of 40 μg/mL, in contrast, compound **II** could enhance the proliferation of the MDA-MB-231 at the same concentration. In addition, they are also scaffolds for synthesis of lamellarin analogues [9].

Increasingly elegant synthetic routes have been developed. An efficient synthetic route for two compounds, 8-benzyloxy-9-methoxy-2-(2,4,5-trimethoxyphenyl)-5,6-dihydropyrrolo[2,1-a]isoquinoline (**I**) and 8,9-dimethoxy-2-(2,4,5-trimethoxyphenyl)-5,6-dihydro[2,1-a]isoquinoline (**II**), is mainly introduced in this study. The synthetic procedure is very valuable because it employs 5,6-dihydropyrrolo[2, 1-a]isoquinolines as starting materials and represents an easy and direct approach to a wide variety of 3,4-dihydroisoquinolines. The synthetic strategy is outlined in Scheme 1.

Isovanillin was protected with benzyl chloride to get 3-benzyloxy-4-methoxy-benzaldehyde (1) with 84.4% yield [10], which was condensed with nitromethane giving 2-benzyloxy-1-methoxy-4-(2-nitrovinyl)-benzene (2) with 80.5% yield [11]. Compound **2** was then reduced with $LiAlH_4$ to get 2-(3-benzyloxy-4-methoxyphenyl)-vinylamine (3) with 84.9% yield [12]. Treatment of **3a**∼**b** with acetylchloride ($n(\mathbf{3a}\sim\mathbf{b}):n(CH_3COCl):n(Et_3N)=1:1.8:4.0$) afforded acetamide (**4a**∼**b**) with 81.9% and 90.7% yield, respectively, followed by cyclization with phosphorous oxychloride to get 3,4-dihydroisoquinoline (**5a**∼**b**) with 80.0% and 83.6% yield ($n(\mathbf{4a}):n(POCl_3)=1:8$). A solution of

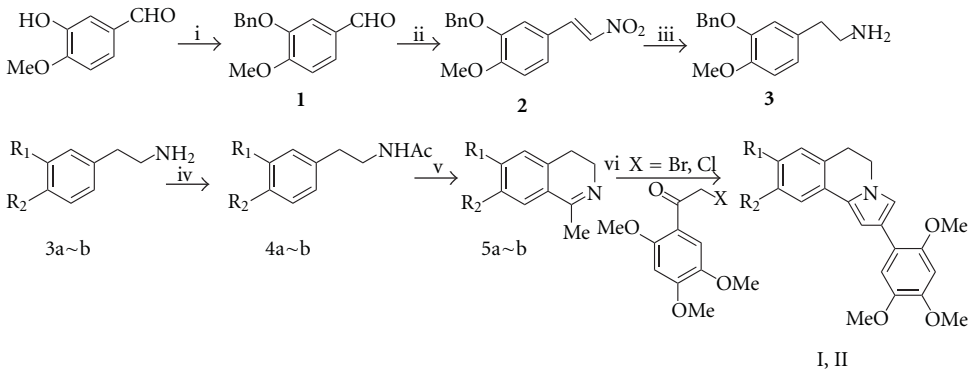

	I	II	a	b
R_1	OBn	OMe	OBn	OMe
R_2	OMe	OMe	OMe	OMe

Scheme 1: Reagents and conditions: (i) BnCl, K_2CO_3, EtOH, reflux, 5 h, 94%; (ii) CH_3NO_2, NH_4OAc, AcOH, reflux, 4 h, 80.5%; (iii) $LiAlH_4$, THF, reflux, 6 h, 84.9%; (iv) CH_3COCl, Et_3N, CH_2Cl_2, 0°C, 2 h, 4a: 81.9%, 4b: 90.7%; (v) $POCl_3$, CH_2Cl_2, reflux, 3 h, 5a: 80.0%, 5b: 83.6%; (vi) 2-halogen-1-(2,4,5-trimethoxyphenyl)ethanone, CH_3CN, K_2CO_3, reflux, 20 h, I: 74.7%, II: 72.6%.

5a~**b**, 2-bromo-1-(2,4,5-trimethoxy-phenyl)-ethanone and anhydrous K_2CO_3 in anhydrous acetonitrile was refluxed for 15 h. After a series of treatment, 5,6-dihydropyrrolo[2,1-a]isoquinoline **I** and **II** were obtained with 28.3% and 61.6% total yield, respectively.

2. Material and Methods

2.1. Analysis Means of Compounds. Melting points (uncorrected) were determined by a Gongyi X-4 apparatus. Infrared spectra(IR) were determined by Nicolet 550 spectrometer. NMR spectra were recorded by Bruker DRX500 or Bruker DRX400 spectrometer. All data were calibrated at δ 0.00 ppm for ^{1}H spectra and ^{13}C spectra from the original spectra (TMS). Low resolution mass spectra (LRMS) were recorded with an HP 6890/5973 GC-MS mass spectrometer. High resolution mass (HRMS) for unreported compounds were recorded with a Micromass GTC Gas Chromatography/TOF Mass spectrometer. All solvent were redistilled prior to use, unless otherwise stated, all other commercially available chemicals were used without further purification.

2.2. Chemical Synthesis

2.2.1. 3-(benzyloxy)-4-methoxybenzaldehyde (1). A mixture of isovanillin (10.0 g, 66 mmol), benzyl chloride (16 mL, 139 mmol), and anhydrous K_2CO_3 (6.5 g, 47 mmol) in EtOH (150 mL) was refluxed for 5 h. After being stirred, the reaction mixture was concentrated to dry and redissolved in 70 mL CH_2Cl_2, and then 5% aqueous NaOH (3 × 100 mL) was added. The organic layer was washed with brine (2 × 50 mL) and H_2O (2 × 50 mL), dried with anhydrous Na_2SO_4, and evaporated to dryness. Needles were obtained after crystallization from MeOH/CH_2Cl_2 corresponding to 3-(benzyloxy)-4-methoxybenzaldehyde (15.0 g, 94%): m.p. 61~62°C (lit.[13] m.p. 61~62°C); ^{1}H NMR (400 MHz, $CDCl_3$) δ 9.82 (s, 1H), 7.45~7.47 (m, 4H), 7.38 (t, 2H, J = 7.34 Hz), 7.32 (t, 1H, J = 7.34 Hz), 6.99 (d, 1H, J = 8.24), 5.19 (s, 2H), 3.96 (s, 3H); MS (EI, 70 ev) m/z: 242(M^+), 92, 91, 79, 77, 65, 63, 51.

2.2.2. (E)-2-(benzyloxy)-1-methoxy-4-(2-nitrovinyl)benzene (2). A solution of compound **1** (10.0 g, 41 mmol), nitromethane (7 mL, 129 mmol) and NH_4OAc (8.0 g, 104 mmol) in AcOH (125 mL) was refluxed for 4 h. After cooling, the mixture was diluted with H_2O (100 mL) and extracted with CH_2Cl_2 (3 × 100 mL). The organic solution was washed with brine (2 × 100 mL) and H_2O (2 × 100 mL), dried with anhydrous Na_2SO_4, and evaporated to dryness. Yellow needles were obtained from EtOH corresponding to (E)-2-(benzyloxy)-1-methoxy-4-(2-nitrovinyl)benzene (2) (9.6 g, 80.5%): m.p. 127~128°C (lit.[14] m.p. 125~126°C)^{1}H NMR (400 MHz, $CDCl_3$) δ 7.91 (d, J = 13.6 Hz, 1H), 7.33~7.46 (m, 6H) 7.18 (dd, J = 2.0, 8.36 Hz, 1H), 7.03 (d, J = 2.0 Hz, 1H), 6.93 (d, J = 8.36 Hz, 1H), 5.17 (s, 2H), 3.95 (s, 3H); MS (EI, 70 ev) m/z: 285 (M^+), 92, 91, 77, 65, 63, 51.

2.2.3. 2-(3-(benzyloxy)-4-methoxyphenyl)ethanamine (3). A solution of compound **2** (4.0 g, 14.0 mmol) in 14 mL of anhydrous THF was added dropwise to a well-stirred suspension of $LiAlH_4$ (2.0 g, 52.8 mmol) in 50 mL of anhydrous THF and was refluxed for 6 h. After the solution was cooled, the excess reagent was destroyed by dropwise addition of EtOAc and 15% aqueous NaOH. After partial evaporation of the filtered portion, the aqueous solution was extracted with CH_2Cl_2 (3 × 30 mL), and the organic solution was washed with brine (2 × 20 mL) and H_2O (2 × 20 mL), dried with anhydrous Na_2SO_4, and evaporated to dryness, and then 2-(3-(benzyloxy)-4-methoxyphenyl)ethanamine (3) (3.0 g, 84.9%) was obtained as an oil. ^{1}H NMR (400 MHz, $CDCl_3$)

δ 6.73∼7.44 (m, 8H), 5.12 (s, 2H), 3.85 (s, 3H), 2.85 (t, J = 6.7 Hz, 2H), 2.62 (t, J = 6.7 Hz, 2H), 2.20 (br s, 2H); MS (EI, 70 ev) m/z: 257 (M^+), 229, 228, 167, 137, 92, 91, 65.

2.2.4. N-(3-(benzyloxy)-4-methoxyphenethy)acetamide (4a). A solution of 0.4 mL of acetyl chloride (5.6 mmol) in 5 mL anhydrous CH_2Cl_2 was added dropwise at 0°C to a solution of compound **3** (1.0 g, 3.88 mmol) and Et_3N (1.7 mL, 12.26 mmol) in 20 mL anhydrous CH_2Cl_2, with stirring at 0°C for 2 h. After the mixture was stirred, 2.5% aqueous HCl was added and the organic solution was washed with brine (2×10 mL) and H_2O (2×10 mL), dried with anhydrous Na_2SO_4, evaporated to dryness, and pale-yellow solid was obtained. Crude product was crystallized with EtOAc to afford *N*-(3-benzyloxy-4-methoxyphenylethyl)acetamide (0.94 g, 81.9%) as white crystals. m.p. 106∼108°C (lit.[15] m.p. 122∼123°C); ^{1}H NMR (400 MHz, $CDCl_3$) δ 7.44 (d, J = 7.2 Hz, 2H), 7.36 (t, J = 7.2 Hz, 2H), 7.30 (d, J = 7.2 Hz, 1H), 6.84 (d, J = 8.8 Hz, 1H), 6.74 (d, J = 6.8 Hz, 2H), 5.14 (s, 2 H), 3.87 (s, 3H), 3.43 (q, J = 6.8, 12.8 Hz, 2H), 2.70 (t, J = 6.8 Hz, 2H), 1.88 (s, 3H).

2.2.5. 6-(benzyloxy)-7-methoxy-1-methyl-3,4-dihydroiso-quinoline (5a). A solution of 0.9 mL of $POCl_3$ (9.8 mmol) in 6 mL anhydrous CH_2Cl_2 was added dropwise at 40°C to a solution of compound **4a** (0.4 g, 1.06 mmol) in 10 mL anhydrous CH_2Cl_2, with stirring at 40°C for 3 h, then was poured into ice-water mixture, 2.5% aqueous NaOH was added to make pH about 12, the aqueous solution was extracted with CH_2Cl_2 (3 × 20 mL), and the organic solution was washed with brine (2×10 mL) and H_2O (2×10 mL), dried with anhydrous Na_2SO_4, evaporated to dryness and solid was obtained. The crude product was purified with a silica gel column (Petroleum : EtOAc(v/v) = 3 : 1, 200∼300 H) to afford 6-(benzyloxy)-7-methoxy-1-methyl-3,4-dihydroisoquinoline (5a) (0.24 g, 80%) as brick red crystals. m.p. 95∼96°C; ^{1}H NMR (500 MHz, $CDCl_3$) δ 7.30∼7.44 (m, 5H), 7.01 (s, 1H), 6.7 (s, 1H), 5.17 (s, 2H), 3.90 (s, 3H), 3.61 (t, J = 7.2 Hz, 2H), 2.57 (m, J = 1.3, 7.5 Hz, 2H), 2.35 (t, J = 1.3 Hz, 3H).

2.2.6. 8-benzyloxy-9-methoxy-2-(2,4,5-trimethoxyphenyl)-5,6-dihydropyrrolo[2,1-a]isoquinoline (I). To a solution of 0.52 g compound 5a (1.85 mmol) in 15 mL anhydrous CH_3CN was added 0.45 g 2-bromo-1-(2,4,5-trimethoxyphenyl)-ethanone (1.85 mmol). The reaction mixture was stirred at 85°C for 10 h, then 0.38 g anhydrous K_2CO_3 (2.75 mmol) was added and continued to stir for another 10 h. After that the mixture was poured into 15 mL brine and extracted with CH_2Cl_2 (3 × 15 mL), the combined organic layers were dried with anhydrous Na_2SO_4, evaporated to dry, and brown oil was obtained. The crude product was purified with a silicagelcolumn (Petroleum : EtOAc(v/v) = 2 : 1, 200∼300 H) to afford 8-benzyl-9-methoxy-2-(2,4,5-trimethoxyphenyl)-5,6-dihydropyrrolo [2,1-a]isoquinoline (I) (0.65 g, 74.7%) as offwhite sheet solid. m.p. 128°C; IR (KBr) ν: 2993, 2934, 2830, 1614, 1568, 1529, 1508, 1453,1427, 1365, 1336, 1274, 1166, 1130, 1035, 848, 810, 784, 738, 695 cm^{-1}; ^{1}H NMR (500MHz, $CDCl_3$) δ 7.29–7.46 (m, 5H), 7.12 (d, J = 1.6 Hz, 1H), 7.11 (s, 1H), 7.10 (s, 1H), 6.73 (s, 1H), 6.69 (d, J = 1.6 Hz, 1H), 6.60 (s, 1H), 5.14 (s, 2H), 4.05 (t, J = 6.6 Hz, 2H), 3.94 (s, 3H), 3.91 (s, 3H), 3.91 (s, 3H), 3.88 (s, 3H), 2.95 (t, J = 6.6 Hz, 2H); ^{13}C NMR (500 MHz, $CDCl_3$) δ: 29.61, 44.91, 56.96, 56.97, 57.14, 57.43, 72.14, 99.34, 102.13, 107.32, 112.83, 115.18, 117.55, 120.83, 121.02, 123.60, 123.78, 128.03, 128.03, 128.50, 129.21, 129.21, 130.31, 137.98, 144.06, 147.25, 148.13, 149.82, 151.07; MS (LC-MS) m/z: 472 $(M+1)^+$, 367, 318, 273; HRMS (ESI-Q-TOF) calcd for $C_{29}H_{29}NO_5$ $[M+1]^+$ 472.4856, found 472.4819.

2.2.7. N-(3,4-dimethoxyphenethyl)acetamide (4b). A solution of 7.6 mL of acetyl chloride (0.11 mol) in 10 mL anhydrous CH_2Cl_2 was added dropwise at 0°C to a solution of compound **3b** (10 mL, 0.059 mol) and Et_3N (32.8 mL, 0.23 mol) in 25 mL anhydrous CH_2Cl_2, with stirring at 0°C for 2 h. After the mixture was stirred, 2.5% aqueous HCl was added and the organic solution was washed with brine (2 × 30 mL) and H_2O (2 × 20 mL), dried with anhydrous Na_2SO_4, evaporated to dryness, and yellow solid was obtained. Crude product was crystallized with EtOAc to afford N-(3,4-dimethoxyphenethyl) acetamide (4b) (11.8 g, 90.7%) as yellow crystals. m.p. 85∼86°C (lit.[16] m.p. 94°C); IR (KBr) ν: 1642.54 cm^{-1} (–C=O), 3301.49 cm^{-1} (–NH–).

2.2.8. 6,7-dimethoxy-1-methyl-3,4-dihydroisoquinoline (5b). A solution of 9.8 mL of $POCl_3$ (0.1 mol) in 40 mL anhydrous CH_2Cl_2 was added dropwise at 40°C to a solution of compound **4b** (3.0 g, 13.4 mmol) in 30 mL anhydrous CH_2Cl_2, with stirring at 40°C for 3 h, then was poured into ice-water mixture; 2.5% aqueous NaOH was added to make pH about 12, the aqueous solution was extracted with CH_2Cl_2 (3 × 60 mL), and the organic solution was washed with brine (2 × 50 mL) and H_2O (2 × 50 mL), dried with anhydrous Na_2SO_4, evaporated to dryness, and solid was obtained. The crude product was purified with a silica gel column (Petroleum : EtOAc(v/v) = 1 : 1, 200∼300 H) to afford 6,7-dimethoxy-1-methyl-3,4-dihydroisoquinoline (5b) (2.3 g, 83.6%) as brick red crystals. m.p. 98∼99°C (lit.[17] m.p. 85∼96°C)^{1}H NMR (500 MHz, $CDCl_3$) δ 6.99 (s, 1H), 6.89 (s, 1H), 3.92 (s, 3H), 3.91 (s, 3H), 3.63 (m, J = 1.4, 7.5 Hz, 2H), 2.63 (t, J = 7.5 Hz, 2H), 2.36 (t, J = 1.4 Hz, 3H).

2.2.9. 8,9-dimethoxy-2-(2,4,5-trimethoxyphenyl)-5,6-dihydro [2,1-a]isoquinoline (II). To a solution of 1.5 g compound 5b (7.32 mmol) in 20 mL anhydrous CH_3CN was added 1.78 g 2-bromo-l-(2,4,5-trimethoxy-phenyl)-ethanone (7.34 mmol). The reaction mixture was stirred at 85°C for 10 h, then 1.52 g anhydrous K_2CO_3 (11.0 mmol) was added and continued to stir for another 10 h. After that the mixture was poured into 30 mL brine and extracted with CH_2Cl_2 (3 × 30 mL), the combined organic layers were dried with anhydrous Na_2SO_4, evaporated to dryness, and brown oil was obtained. The crude product was purified with a silica gel column (Petroleum : EtOAc(v/v) = 2 : 1, 200∼300 H) to afford 8,9-dimethoxy-2-(2,4,5-trimethoxyphenyl)-5,6-dihydro[2,1-a]isoquinoline (II) (0.65 g, 72.6%) as gray solid. m.p. 137∼138°C; IR (KBr) ν: 2993, 2934, 2836, 1608,

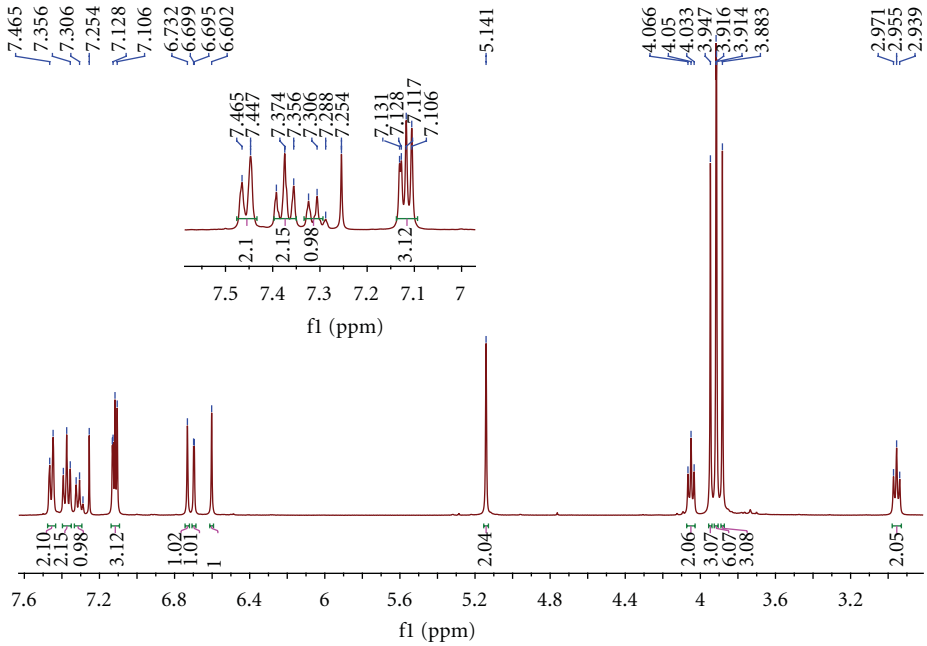

Figure 1: ^{1}H NMR spectrum of the **I**. Inserted figure is the magnification of the part of 7.00–7.50 of chemical shift.

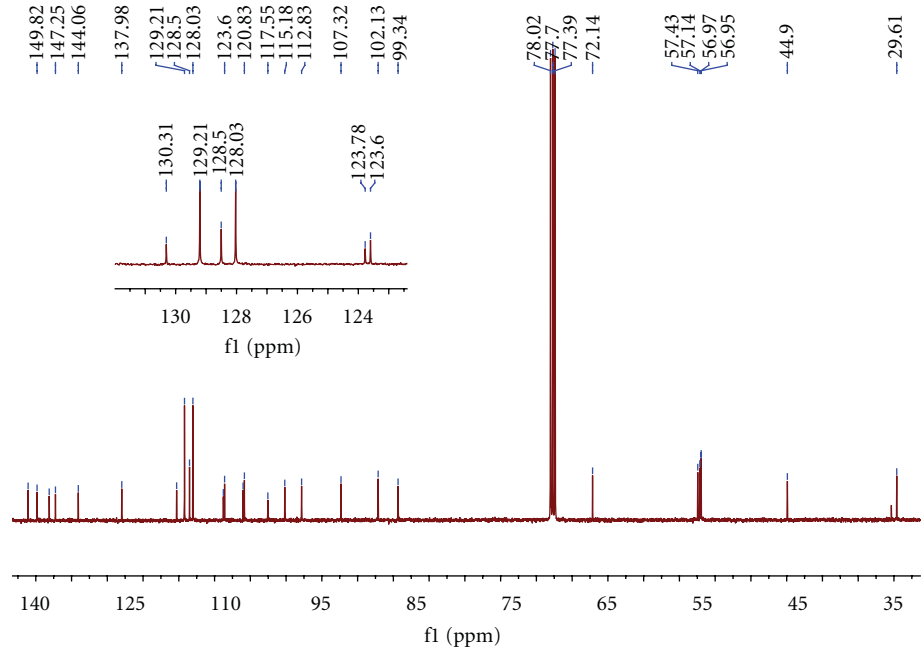

Figure 2: ^{13}C NMR spectrum of the **I**. Inserted figure is the magnification of the part of 120.00–135.00 of chemical shift.

1560, 1530, 1508, 1484, 1397, 1272, 1212, 1126, 1036, 808, 776 cm^{-1}; ^{1}H NMR (500 MHz, $CDCl_3$) δ: 3.01 (t, J = 6.6 Hz, 2H), 3.87 (s, 3H), 3.88 (s, 3H), 3.91 (s, 3H), 3.92 (s, 3H), 3.95 (s, 3H), 4.07 (t, J = 6.6 Hz, 2H), 6.60 (s, 1H), 6.69 (d, J = 1.7 Hz, 1H), 6.70 (s, 1H), 7.08 (s, 1H), 7.12 (s, 1H), 7.13 (d, J = 1.7 Hz, 1H); ^{13}C NMR (500 MHz, $CDCl_3$) δ: 29.07, 44.28, 56.08, 56.15, 56.30, 56.49, 56.78, 98.68, 106.08, 101.36, 111.51, 112.19, 116.90, 120.12, 120.36, 122.43, 122.93, 129.70, 143.40, 147.38, 147.47, 148.38, 150.42; DEPT 135 (500 MHz, $CDCl_3$) δ: two –CH_2 (29.06, 44.28), five –CH_3 (56.07, 56.14, 56.29,56.48,56.76), six –CH (98.62, 101.34, 106.05, 111.47, 112.15, 120.11); MS (LC-MS) m/z: 396 $(M+1)^+$, 371, 276; HRMS (ESI-Q-TOF) calcd for $C_{23}H_{25}NO_5$ $[M+1]^+$ 396.4852, found 396.4884.

3. Results

The target compounds **I** and **II** had been synthesized by our route and their structures were determined by interpretation

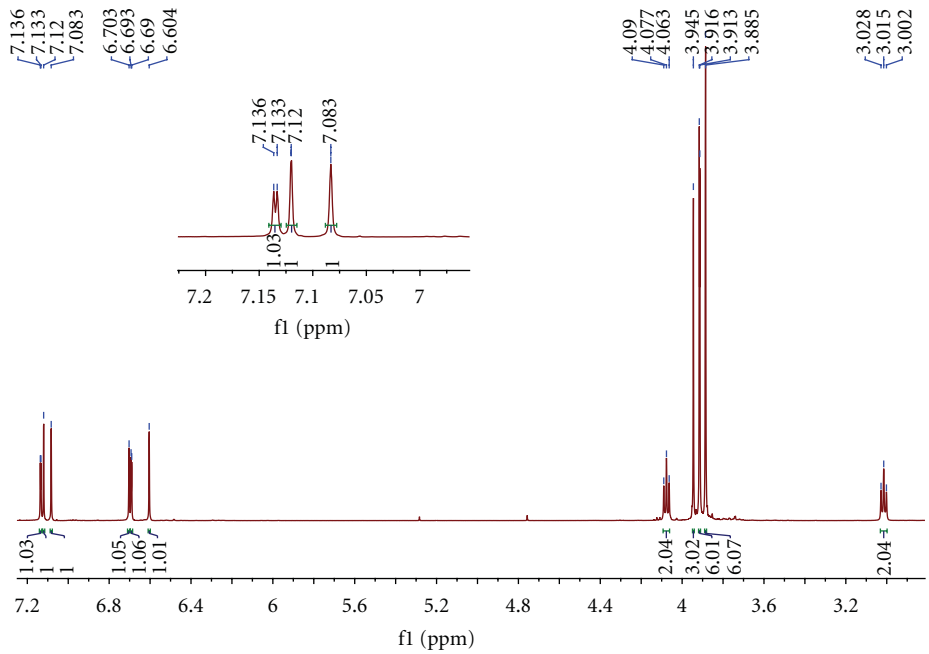

Figure 3: ^{1}H NMR spectrum of the **II**. Inserted figure is the magnification of the part of 7.00–7.20 of chemical shift.

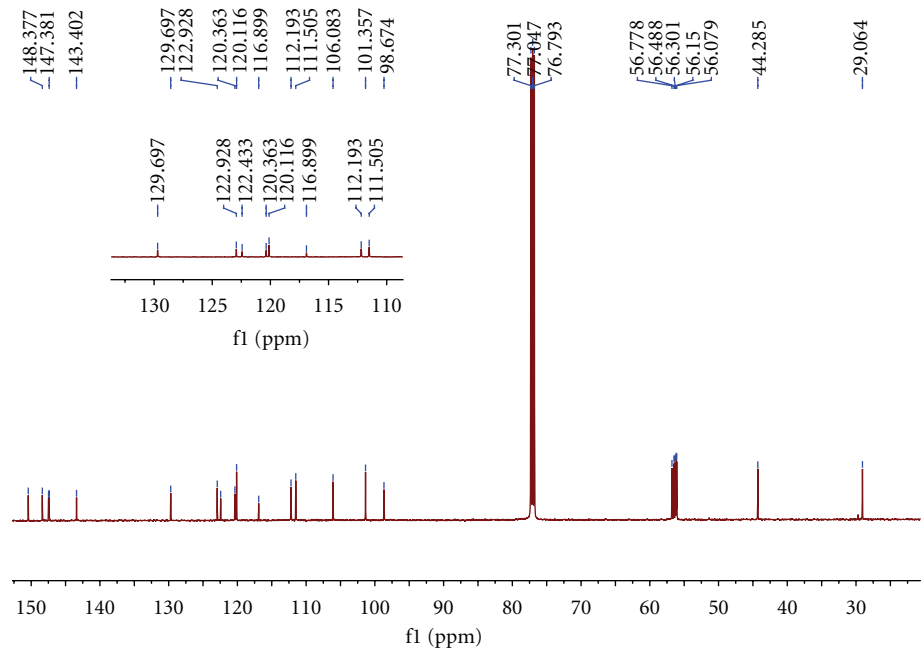

Figure 4: ^{13}C NMR spectrum of the **II**. Inserted figure is the magnification of the part of 110.00–130.00 of chemical shift.

of spectral data. The ^{1}H NMR and ^{13}C NMR spectra of them were assigned as indicated in Figures 1, 2, 3, and 4.

An initial ^{1}H-NMR spectrum of **I** (in $CDCl_3$) revealed four –OMe–H signals at 3.94 (s, 3H), 3.91 (s, 3H), 3.91 (s, 3H), 3.88 (s, 3H). These peaks are the featured signals of the –OMe–. 2.95 and 4.05 *doublets* (J = 6.6 Hz) indicate $–CH_2N–$ and $–CH_2–$ moieties connected with it in the isoquinoline ring. It can be seen that the distinguishing feature of Ar–CH_2O 5.14 (s, 2H) is shown in Figure 1. There are several groups of signals in the aromatic region; they are 7.12 (d, J = 1.6 Hz, 1H), 7.11 (s, 1H), 7.10 (s, 1H), 6.73 (s, 1H), 6.69 (d, J = 1.6 Hz, 1H), and 6.60 (s, 1H), respectively. Among them, 7.12 (d, J = 1.6 Hz, 1H) and 6.69 (d, J = 1.6 Hz, 1H) are the signals in the pyrrole ring; this can be estimated from the peak type. Since Ar–H in the Ar–CH_2O are influenced by other protons more slightly, they will overlap together and show the multiplet in the spectra. So 7.29–7.46 (m, 5H) is the signal of Ar–H in the Ar–CH_2O. A molecular formula

of $C_{29}H_{29}NO_5$, resulted from HR-MS data of **I.** The ^{13}C NMR spectrum of **I** displayed twenty-seven signals, which represented all twenty-nine C-atoms, eighteen of which were assignable to three aromatic-C moieties and accounted for sixteen spectral signals. Of the remaining eleven signals, four were from OMe (56.96, 56.97, 57.14, 57.43 ppm), and seven were from isoquinoline and pyrrole ring C-atoms.

NMR data of **II** (see Figures 3 and 4) indicated a $C_{23}H_{25}$ framework, which HR-MS analysis expanded to a molecular formula of $C_{23}H_{25}NO_5$. The simplest assumed relationship between the two isoquinoline, **I** as an BnO-substituted **II**, was reinforced by characterization of the NMR data, which exhibited many similar signals. Specifically, too many shifts of H and C resonances are very similar to each other which proved the basic framework between **I** and **II**. The NMR signals which distinguished **I** from **II** were those of three aromatic protons appropriate for Ar–H (7.29–7.46 ppm, m, 5H) and $–CH_2–$ in the $Ar–CH_2O$. The remaining distinguishing feature was the number of –OMe– signal in ^{13}C NMR at 56-57 ppm.

4. Discussions

I and **II** from 1-methyl-3,4-dihydroisoquinoline and 2,4,5-trimethoxy-α-halogen-acetophenone were obtained with high yields under mild conditions for the first time. This novel method, as the key reaction step, provides a general and highly efficient method for the preparation of 5,6-dihydropyrrolo[2,1-a]isoquinolines. We envisaged that the 5,6-dihydropyrrolo[2,1-a]isoquinolines could be constructed by the formation of quaternary ammonium salt, and subsequent lactonization in the presence of anhydrous K_2CO_3. The negative carbon ion of 1-methyl-3,4-dihydroisoquinoline is also active in the Knorr reaction. Both 2,4,5-trimethoxy-α-bromoacetophenone and 2,4,5-trimethoxy-α-chloracetophenone were employed. We found that the yield of the former is about 5% higher than the later. Therefore, 2,4,5-trimethoxy-α-bromoacetophenone is used in the synthesis of **I** and **II**.

5. Conclusion

Based on the facile synthetic route depicted in Scheme 1, two novel scaffolds for synthesis of lamellarin analogues 8-benzyloxy-9-methoxy-2-(2,4,5-trimethoxyphenyl)-5,6-dihydropyrrolo[2,1-a] isoquinoline (**I**) and 8,9-dimethoxy-2-(2,4,5-trimethoxyphenyl)-5,6-dihydro[2,1-a]isoquinoline (**II**) were obtained under mild condition. These two compounds are characterized by ^1H NMR, ^{13}C NMR, IR spectrum, and melting points. The products are stable and may be expected to exhibit biological activities to some extend.

Acknowledgments

This work was supported by the National Natural Science Foundation of China (no. 20372013) The outstanding young talent fund from the Dalian science and technology bureau (2009J22DW038). The authors thank Professor Yecheng You Dalian University and Professor John Joule University of Manchester (UK) for helpful suggestion on this paper.

References

[1] R. J. Andersen, D. John Faulkner, H. Cun-heng, G. D. Van Duyne, and J. Clardy, "Metabolites of the marine prosobranch mollusc Lamellaria sp," *Journal of the American Chemical Society*, vol. 107, no. 19, pp. 5492–5495, 1985.

[2] S. M. Reddy, M. Srinivasulu, N. Satyanarayana, A. K. Kondapi, and Y. Venkateswarlu, "New potent cytotoxic lamellarin alkaloids from Indian ascidian Didemnum obscurum," *Tetrahedron*, vol. 61, no. 39, pp. 9242–9247, 2005.

[3] F. Ishibashi, S. Tanabe, T. Oda, and M. Iwao, "Synthesis and structure-activity relationship study of lamellarin derivatives," *Journal of Natural Products*, vol. 65, no. 4, pp. 500–504, 2002.

[4] J. Kluza, M. A. Gallego, A. Loyens et al., "Cancer cell mitochondria are direct proapoptotic targets for the marine antitumor drug lamellarin D," *Cancer Research*, vol. 66, no. 6, pp. 3177–3187, 2006.

[5] M. Facompré, C. Tardy, C. Bal-Mahieu et al., "Lamellarin D: a novel potent inhibitor of topoisomerase I," *Cancer Research*, vol. 63, no. 21, pp. 7392–7399, 2003.

[6] N. Dias, H. Vezin, and A. Lansiaux, "DNA binders and related subjects," *Topics in Current Chemistry*, vol. 253, pp. 89–109, 2005.

[7] M. Vanhuyse, J. Kluza, C. Tardy et al., "Lamellarin D: a novel pro-apoptotic agent from marine origin insensitive to P-glycoprotein-mediated drug efflux," *Cancer Letters*, vol. 221, no. 2, pp. 165–175, 2005.

[8] P. Ploypradith, T. Petchmanee, P. Sahakitpichan, N. D. Litvinas, and S. Ruchirawat, "Total synthesis of natural and unnatural lamellarins with saturated and unsaturated D-rings," *Journal of Organic Chemistry*, vol. 71, no. 25, pp. 9440–9448, 2006.

[9] M. Nyerges and L. Tőke, "1,5-Electrocyclisation of azomethine ylides leading to pyrrolo[2,1-a] isoquinolines - Concise construction of the lamellarin skeleton," *Tetrahedron Letters*, vol. 46, no. 44, pp. 7531–7534, 2005.

[10] A. Bermejo, I. Andreu, F. Suvire et al., "Syntheses and antitumor targeting G1 phase of the cell cycle of benzoyldihydroisoquinolines and related 1-substituted isoquinolines," *Journal of Medicinal Chemistry*, vol. 45, no. 23, pp. 5058–5068, 2002.

[11] N. Cabedo, P. Protais, B. K. Cassels, and D. Cortes, "Synthesis and dopamine receptor selectivity of the benzyltetrahydroisoquinoline, (R)-(+)-nor-roefractine," *Journal of Natural Products*, vol. 61, no. 6, pp. 709–712, 1998.

[12] S. Batra, Y. A. Sabnis, P. J. Rosenthal, and M. A. Avery, "Structure-based approach to falcipain-2 inhibitors: synthesis and biological evaluation of 1,6,7-Trisubstituted dihydroisoquinolines and isoquinolines," *Bioorganic and Medicinal Chemistry*, vol. 11, no. 10, pp. 2293–2299, 2003.

Hindawi Publishing Corporation
Evidence-Based Complementary and Alternative Medicine
Volume 2011, Article ID 730356, 9 pages
doi:10.1155/2011/730356

Research Article

Expression of Pigment Cell-Specific Genes in the Ontogenesis of the Sea Urchin *Strongylocentrotus intermedius*

Natalya V. Ageenko,[1] Konstantin V. Kiselev,[2] and Nelly A. Odintsova[1,3]

[1] *A.V. Zhirmunsky Institute of Marine Biology, Far Eastern Branch of the Russian Academy of Sciences, Palchevsky Street 17, Vladivostok 690041, Russia*
[2] *Institute of Biology and Soil Sciences, FEB RAS, Vladivostok 690022, Russia*
[3] *Far Eastern Federal University, Vladivostok 690950, Russia*

Correspondence should be addressed to Natalya V. Ageenko, natkuprina@mail.ru

Received 12 January 2011; Accepted 16 May 2011

One of the polyketide compounds, the naphthoquinone pigment echinochrome, is synthesized in sea urchin pigment cells. We analyzed polyketide synthase (*pks*) and sulfotransferase (*sult*) gene expression in embryos and larvae of the sea urchin *Strongylocentrotus intermedius* from various stages of development and in specific tissues of the adults. We observed the highest level of expression of the *pks* and *sult* genes at the gastrula stage. In unfertilized eggs, only trace amounts of the *pks* and *sult* transcripts were detected, whereas no transcripts of these genes were observed in spermatozoids. The addition of shikimic acid, a precursor of naphthoquinone pigments, to zygotes and embryos increased the expression of the *pks* and *sult* genes. Our findings, including the development of specific conditions to promote pigment cell differentiation of embryonic sea urchin cells in culture, represent a definitive study on the molecular signaling pathways that are involved in the biosynthesis of pigments during sea urchin development.

1. Introduction

Polyketide compounds are a large group of structurally very diverse multifunctional proteins mainly found in bacteria, fungi, and plants. One of these polyketide compounds, the pigment echinochrome, is synthesized in sea urchin pigment cells in larvae and in adults [1, 2]. These compounds from sea urchins, as well as many marine secondary metabolites, possess highly effective antioxidant, antibacterial, antifungal, antitumor, and psychotropic activities [3–7] and may play a role in immune defense [8].

Although great progress has been made in characterizing sea urchin quinone pigments [1, 2, 9], no definitive information is available on the molecular signaling pathways that are involved in pigment cell specification and the biosynthesis of pigments during sea urchin development. Three basic biosynthetic pathways, the polyketide pathway, the shikimic acid pathway, and the mevalonic acid pathway, are involved in the synthesis of quinones, including benzoquinones, naphthoquinones, anthraquinones, and upper quinones [10]. Different individual compounds are formed by modifications of the basic chemical structure. The bioactive secondary metabolite, echinochrome (2,3,5,6,8-pentahydroxy-7-ethylnaphthoquinone), is in the chemical class of naphthoquinones (Figure 1(a)). It is generated after a series of enzymatic, oxidative, and photochemical reactions from shikimic acid, similar to the formation of chimaphilin through the mevalonic acid biosynthetic pathway, as shown in Figure 1(b).

The drug "histochrome" (registered trademark) was developed from the echinochrome base structure and has unique therapeutic properties [3, 4]. There are three ways to produce echinochrome: aquaculture, chemical synthesis, and the *in vitro* production. The industrial-scale procurement of echinochrome may lead to the extinction of the organisms that produce this substance. Chemically synthesized echinochrome has some toxic effects. Cultured pigment cells of sea urchins could provide a source of pharmacologically important quinone pigments that would help reduce the impact on the adult sea urchin population. The *in vitro* production of biologically active substances is one promising way to solve this problem.

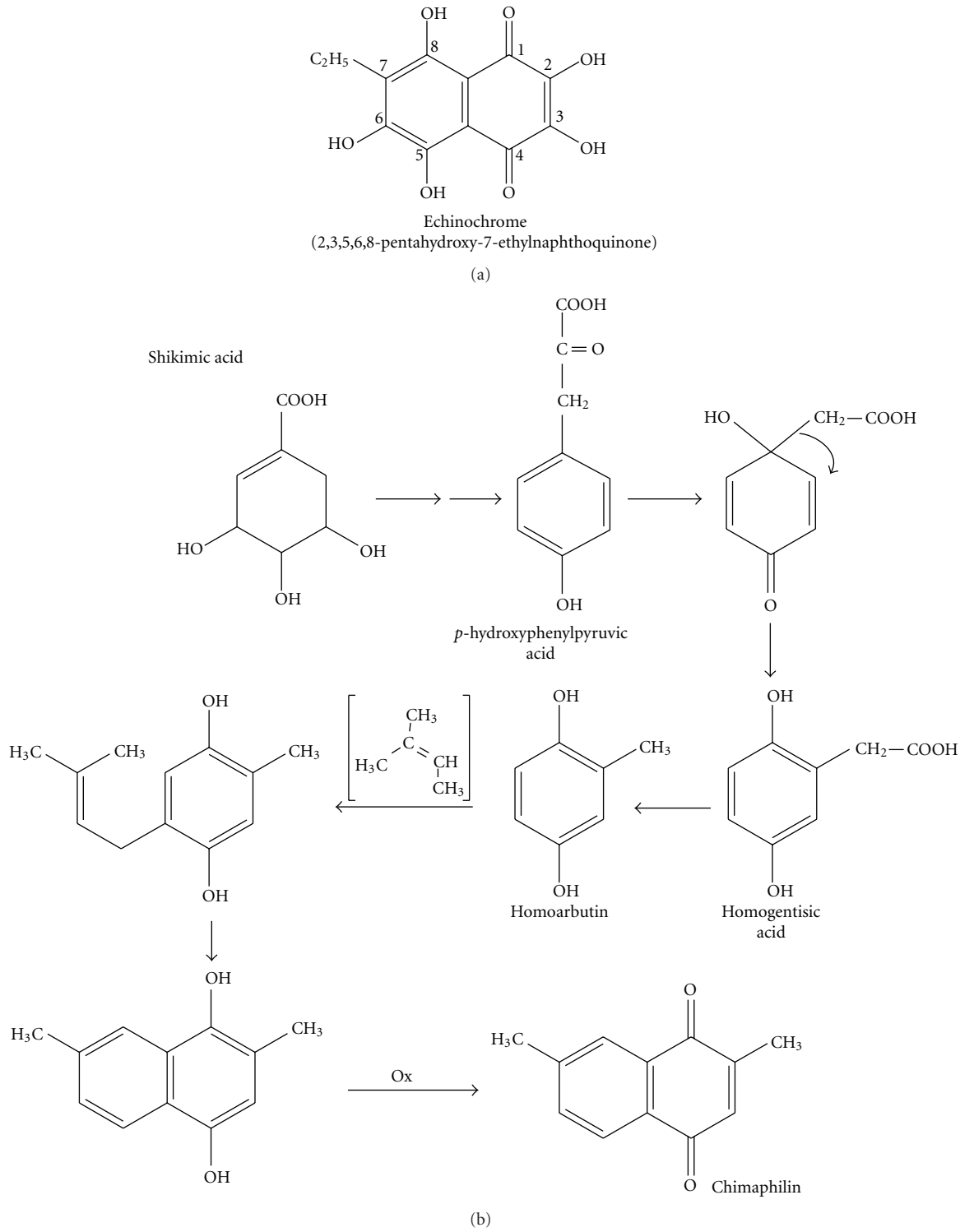

Figure 1: The structure of the naphthoquinone pigment echinochrome (a). One of the quinone biosynthesis pathways (the formation of chimaphilin from a shikimic acid through the mevalonic acid biosynthetic pathway) in accordance with [9] (b).

Pigment cells are the first type of secondary mesenchymal cells (SMCs) to be specified at the mesenchyme blastula stage in sea urchins [11]. These cells accumulate red-brown pigment granules in their cytoplasm [12] and become easily detectable from the late gastrula stage onwards. The cytoplasmic granules store carotenoids and naphthoquinone compounds [2, 12, 13], which have been suggested to function in body coloring and phototropism which aid in the defense of larval ectoderm [14, 15]. Pigment cell precursors are released from the vegetal plate during the initial phase

of gastrulation, and they have the ability to migrate within the ectodermal layer of the larval epithelium [16]. The ability of phagocytosis exhibited by pigment cells suggests their participation in wound healing in larvae [17]. Changes in the normal sequence or rate of sea urchin embryo development affect echinochrome synthesis [18].

Studies have revealed that expression of genes involved in the regulation of embryogenesis and development of sea urchins is mediated by a complex and extended cis-regulatory system [19]. The participation of the sea urchin gene regulatory networks in development has been characterized in detail [20]. The use of the whole mount *in situ* hybridization has revealed that the polyketide synthase (*pks*) gene cluster, three different members of the flavin-containing monooxygenase gene family, and a sulfotransferase gene (*sult*) are specifically expressed in pigment cells, suggesting that they are required for the biosynthesis of the pigment echinochrome [21]. Sea urchin embryos lacking *Sppks* (knock-down) develop pigment cells but appear unpigmented (albino phenotype) [21].

This study is focused on a detailed gene expression profile for two pigment cell-specific genes, *Sipks* and *Sisult*, during sea urchin embryo development and in specific adult tissues. The effect of a precursor of naphthoquinone pigments, shikimic acid, on the expression of pigment cell-specific genes and embryo development was investigated. In addition, specific conditions for promotion of pigment cell differentiation in sea urchin cell culture were developed. The present study is an attempt to increase our understanding of the intracellular mechanisms affecting echinochrome synthesis.

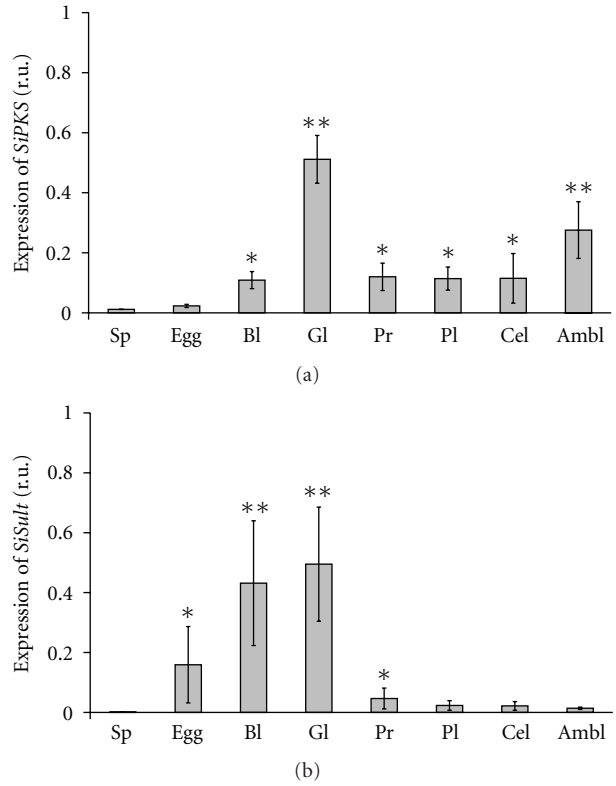

Figure 2: Expression of the *Sipks* (a) and *Sisult* (b) genes in spermatozoids (Sp), unfertilized eggs (Egg), coelomocytes (Cel), ambulacra (Ambl), embryos, and larvae of the sea urchin *S. intermedius* at various stages of development: blastula, 14 hpf (Bl), gastrula, 24 hpf (Gl), prism, 34 hpf (Pr), and pluteus, 72 hpf (Pl). $^{*}P < .05$; $^{**}P < .01$.

2. Materials and Methods

2.1. Animals. Adult sea urchins of *Strongylocentrotus intermedius* were collected in the Sea of Japan (Amursky Bay or Vostok Bay) and kept in tubs filled with running, aerated seawater. The animals were rinsed free of any debris with UV-sterilized, filtered seawater and injected with 2-3 mL of 0.5 M KCl to chemically induce spawning. The embryonic material was obtained by artificial fertilization and then placed in tanks with UV-sterilized seawater (17°C) throughout development until the mesenchymal blastula, gastrula, prism, or pluteus stages (14, 24, 34, and 72 hours after fertilization, hpf, resp.). After 48 hpf, the larvae were fed the microalga *Isochrysis galbana* (100 000 cells/mL) daily. The embryos and cell cultures were examined with an inverted microscope Axiovert 200 M (Carl Zeiss, Goettingen, Germany) with 10× and 20× dry objectives.

2.2. Real-Time Quantitative Polymerase Chain Reaction (Real-Time PCR). Quantitative real-time PCR was used to measure the relative amount of *Sppks* and *Spsult* transcripts during the course of development and in specific tissues of the adults. Using BLAST, we showed a high identity (98-99%) of the central part of the *pks* and *sult* genes in the sea urchin *S. intermedius* with that of the *pks* and *sult* genes in the closely related sea urchin *S. purpuratus* (GeneBank accession numbers XM 788471 and DQ176319 for the *pks* and *sult* genes, resp.). Then, we used the obtained nucleotide sequences from cDNA of *S. intermedius* to design the real-time PCR primers and probes.

Total RNA from spermatozoids, unfertilized eggs, coelomocytes, ambulacra, embryos, and larvae of the sea urchin *S. intermedius* at various stages of development was extracted with Yellow Solve reagent (Clonogen, St. Petersburg, Russia) and treated with DNase. The RNA pellet was washed with 1 mL of 75% ethanol. The sample was then centrifuged at 13,200 g at 4°C for 10 min. Following centrifugation, the supernatant was removed, and the RNA pellet was air-dried and stored at −25°C. For TaqMan real-time RT-PCR, cDNAs were amplified in 20 μL of the reaction mixture containing 1 × TaqMan Buffer B, 2.5 mM $MgCl_2$, 250 μM of each deoxynucleotide, 1 U Taq DNA polymerase, 0.5 μL cDNA sample, and 0.25 μM of each primer and probe (Real-Time PCR Kit, Syntol, Russia). Quantitative real-time PCR was performed using the established protocol [22] in the Instrumental Centre of Biotechnology and Gene Engineering of Institute of Biology and Soil Sciences (FEB RAS) using an ABI 310 and 3130 Genetic Analyzers (Applied Biosystems, Foster City, USA). The amplification conditions consisted of one cycle of 2 min at 95°C followed by 50 cycles of

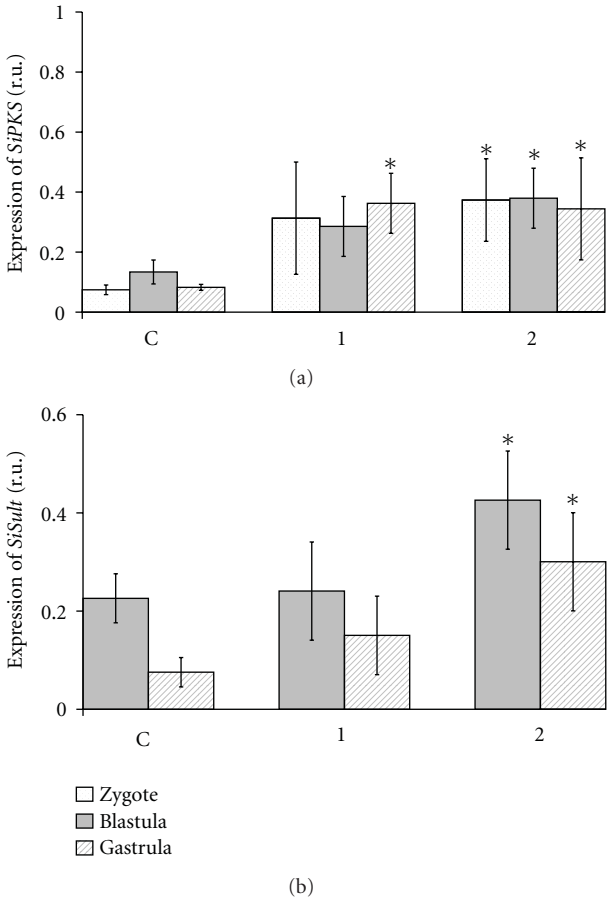

Figure 3: Effect of shikimic acid (ShA) on the expression of the *Sipks* (a) and *Sisult* (b) genes in zygotes, blastula, and gastrula cells of *S. intermedius*. The time of incubation with ShA is 8 days (all embryos of the control group (C) were at the pluteus stage). ShA concentrations tested: 1—0.1 mM, 2— 0.5 mM. $^*P < .05$.

10 s at 95°C and 25 s at 62°C. The TaqMan PCR assays were performed in an iCycler thermocycler supplied with the iQ5 Multicolor Real-Time PCR detection system (Bio-Rad Laboratories, Inc., Hercules, Calif, USA), and data were analyzed with the iQ5 Optical System Software v.2.0 according to the manufacturer's instructions; expression was normalized according to the $2^{-\Delta\Delta CT}$ method, and the highest scaling option was used (the highest expressing sample was assigned the value 1 in the relative mRNA calculation). The *S. intermedius* actin gene (GenBank accession number DQ229162) was used as an endogenous control to normalize variance in the quality and the amount of cDNA used in each real-time RT-PCR experiment. A nontemplate control for each primer set and a non-RT control (DNase-treated RNA as a template) for each developmental stage were included. No-cycle threshold (Ct) values were consistently obtained after 50 cycles of PCR. The TaqMan probe for the actin gene was labeled with an FAM reporter dye at the 5′-end and an RTQ-1 quencher dye at the 3′-end, and TaqMan probes for the *pks* and *sult* genes were labeled with an ROX reporter dye at the 5′-end and a BHQ-2 quencher dye at the 3′-end (Syntol, Russia). The data were summarized from five independent experiments. The primers 5′GAT CTC CGT CAA CCC ATG AT, 5′CTT GCC CAT GTC ACC ATC,and the probe 5′AAC TAC GGT GTC GAC TCC CTC ATG GC were used for the expression analysis of the *pks* gene. The primers 5′AGA AGC GGC GAA ACA GAA, 5′CCA GAG CCA TTG GTT TTT C, and the probe 5′TGG CGA CTG GAA AAA TCA TTT TAC CGT AGC CCA GA were used for the expression analysis of the *sult* gene. For the actin gene, the primers 5′TGT TGC CCC AGA GGA GCA, 5′ATC TTT TCC CTG TTG GCC TT, and the probe 5′TCC TCC TTA CCG AGG CTC CCC TCA A were used.

2.3. Experiments with Shikimic Acid (ShA). Sterile solutions of ShA in seawater at the desired concentrations (0.1, 0.5, and 2 mM) were added to sea urchin zygotes (after 20 min pf) and developing embryos at the blastula (14 hpf) and gastrula (24 hpf) stages. Embryos and larvae were cultivated with ShA for 8 days. The development of the culture was monitored to ensure that the embryos were developing normally. After this period, total RNA was isolated from the larvae for the following quantitative real-time PCR. ShA was obtained from Sigma (St. Louis, USA).

2.4. Cell Culture. Developing sea urchin embryos were cultivated in 5 L tanks at 17°C and collected on a fine 30 μm nylon mesh at the mesenchymal blastula stage, washed in artificial seawater (Ca^{+2} and Mg^{+2}-free salt solution, CMFSS) containing antibiotics (100 IU/mL penicillin and 100 mg/mL streptomycin), and dissociated into single cells with 0.25% collagenase (produced from the hepatopancreas of the red king crab *Paralithodes camtschatica* in the Pacific Institute of Bioorganic Chemistry (PIBOC) of FEB RAS, Vladivostok, Russia) at 17°C (for 20–30 min). The resulting cell suspension containing all cell types was washed several times in seawater with antibiotics, and then sterile seawater supplemented with 2% fetal bovine serum (Sigma) was added. Cell viability was estimated by a trypan blue exclusion test. The cells were seeded at the density of 3×10^6–5×10^6 cells/cm^2 in plastic Petri dishes (Lux Culture Dishes, ICN Biomedicals), and after two to three days of cultivation, a subset of cells (after several strokes of gentle pipetting) was transferred into new Petri dishes on glass coverslips coated preliminarily with fibronectin (Sigma). The solutions of fibronectin (0.01 mg/mL) were left to settle for 12 h at room temperature (RT). After two washings in sterile seawater, the dishes with the coverslips were stored at RT for 12 to 24 h prior to cell seeding. To cultivate transferred cells, we used two types of the cell culture media: the coelomic fluid preparations of control sea urchins and injured sea urchins. Previously, injured sea urchins were obtained by needle pricks in the area of Aristotle's lantern. Then after a day, the coelomic fluids from 5 control and 5 injured sea urchins were collected by puncture in the area of Aristotle's lantern. After 15–20 min, when the coelomic fluid is taken out of the animal, the coelomocytes aggregated (at 4°C). The coelomic fluid preparations were then centrifuged at 2,300 g (4°C) for 20 min to remove coelomocytes, and the supernatant was sterilized by filtration (0.22 μm, Millipore, USA). The

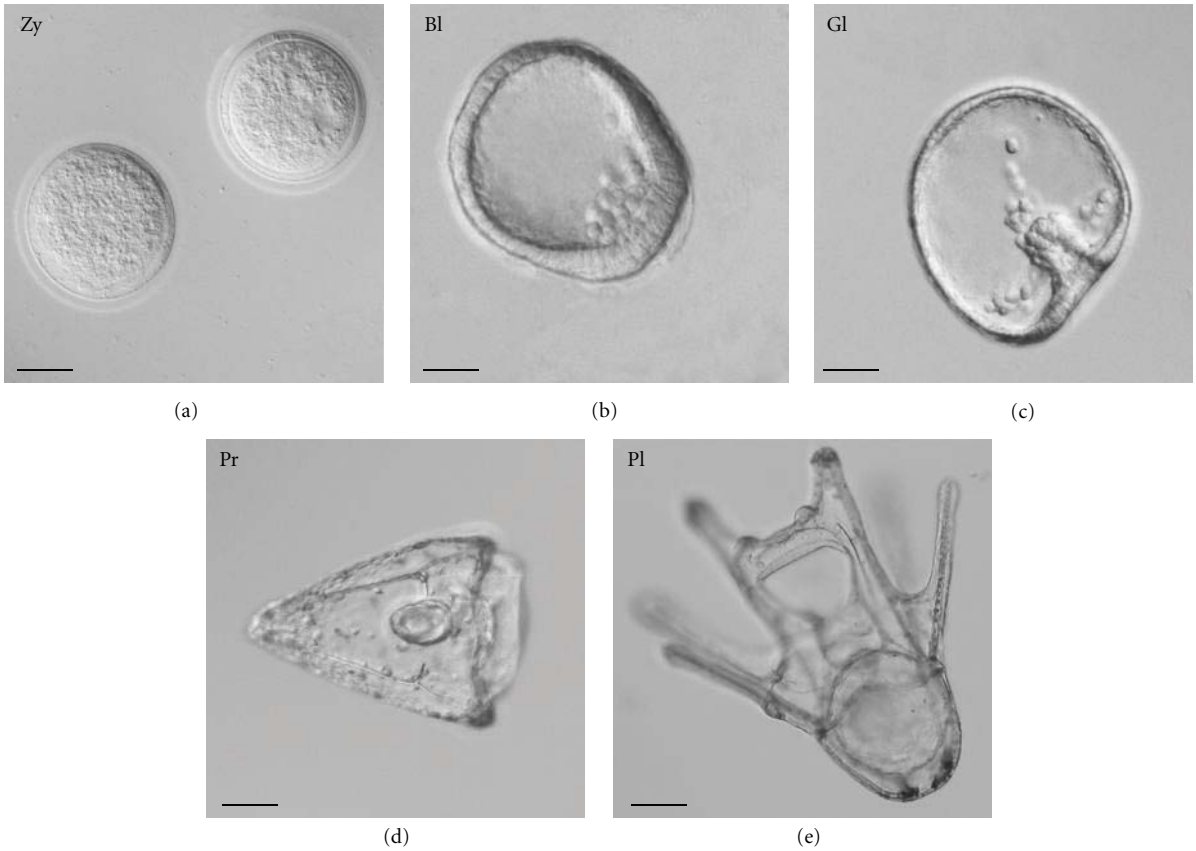

Figure 4: Normal embryo development of the sea urchin *S. intermedius*: zygotes (20 min pf, Zy); blastula stage (14 hpf, Bl); gastrula stage (24 hpf, Gl); (d) prism stage (34 hpf, Pr); (e) pluteus (8 dpf, Pl). Nomarski's optics. *Bar*, 50 μm.

protein content in the supernatants was determined as described previously [23] and averaged 450–475 μg/mL. The cell cultures were maintained by changing the old medium with new medium at 3–5-day intervals for 20 days at 17°C.

2.5. Statistical Analysis. Statistical analysis was carried out using the Statistica 8.0 program. The results are represented as the mean ± standard error and were tested by paired Student's t-test. $P < .05$ was selected as the point of minimal statistical significance in all analyses.

3. Results

3.1. Sipks and Sisult Expression Profiles in Sea Urchin Embryo Development and in Specific Adult Tissues. In unfertilized eggs, only trace amounts of the *pks* and *sult* transcripts were detected, whereas no transcripts of these genes were observed in spermatozoids (Figure 2). We observed the highest level of expression of the *pks* gene at the gastrula stage (Figure 2(a)), which exceeded the expression level of this gene at the blastula, prism, and pluteus stages, and in coelomocytes, and ambulacra by 4.6-, 4.3-, 4.5-, 4.5-, and 1.9-fold, respectively. The gene expression profile for *Sisult* had a similar trend to that of *Sipks*. The onset of transcription for the *sult* gene began at the blastula stage, and then the level of the expression increased drastically through the start of gastrulation (approximately 24 hours) (Figure 2(b)). After that, the level of transcript decreased by more than 10 and 20 times at the prism and pluteus stages, respectively. In addition, *sult* gene expression was detected in coelomocytes and ambulacra, where the level of the *sult* gene expression was lower than that at the gastrula stage by 22.7- and 35.5-fold, respectively.

3.2. Experiments with a Precursor of Naphthoquinone Pigments: Shikimic Acid (ShA). *Sipks* and *Sisult* expression in embryo development was significantly increased after the incubation of sea urchin embryos with 0.1 mM–0.5 mM ShA (Figure 3), but not 2.0 mM ShA, which blocked the expression of the pigment genes (data not shown). No apparent effect on normal development (Figure 4) was detected after the addition of ShA (0.1 mM and 0.5 mM) to sea urchin zygotes, which developed into morphologically almost normal plutei (Figures 5(a)((1), (2))). In contrast, the addition of ShA (0.1 mM and 0.5 mM) to the blastula and gastrula embryos resulted in a marked slowdown of development (Figures 5(b) and 5(c)). In these cases, after 8 days of cultivation with ShA, the development of the sea urchin larvae was retarded in the prism stage, while the control embryos reached the pluteus stage. The addition of 2.0 mM ShA to the zygotes, blastula, and gastrula embryos

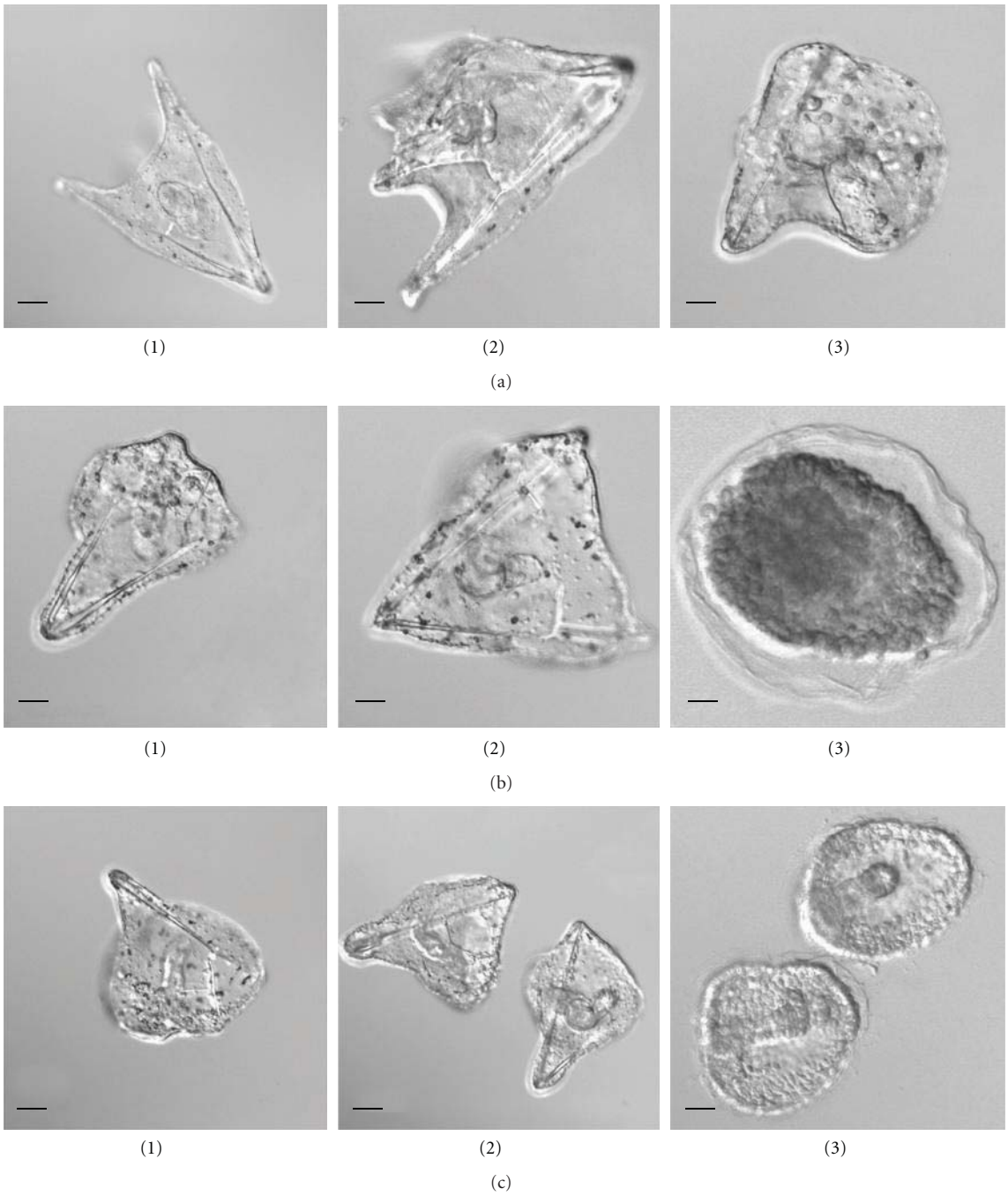

Figure 5: Effect of shikimic acid (ShA) on the larval morphology of the sea urchin *S. intermedius*. Disturbances in embryo development after 8 days of incubation with ShA. ShA was added to (a) zygotes; (b) embryos of the blastula stage; (c) embryos of the gastrula stage. ShA concentrations tested: 1–0.1 mM, 2–0.5 mM, and 3–2.0 mM. Nomarski's optics. *Bar*, 50 μm.

led to significant disturbances in normal development which was clearly delayed or arrested (Figures 5(a)(3), 5(b)(3), and 5(c)(3)). After the incubation with 2.0 mM ShA, the embryos from the blastula and gastrula stages remained spherical in shape for up to 8 days of development.

3.3. Differentiation of Pigment Cells in Cell Culture. Different conditions of cell cultivation may determine the cytodifferentiation patterns of sea urchin embryonic cells. Two days after a blastula-derived cell culture was initiated, two types of substrate-attached cells developed: epithelial and mesenchymal cells, which formed dense multilayer cell sheets (Figure 6(a)). The appearance of pigment cells among the mesenchymal elements indicated that they are derived from the secondary mesenchyme. The transfer of these cells to new dishes with fibronectin-coated coverslips resulted in intensive pigment differentiation during the following two days. It should be noted that the morphological appearance

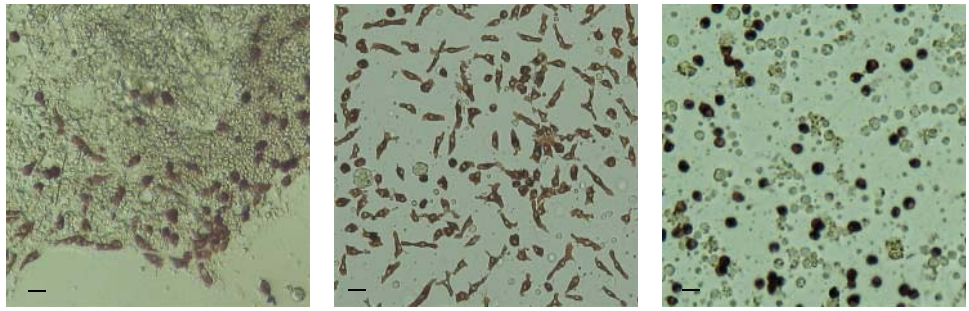

(a) (b) (c)

Figure 6: Embryonic pigment cells in a blastula-derived cell culture of the sea urchin *S. intermedius*. (a) Multilayer cell sheets (2-3 days of cultivation in seawater supplemented with 2% fetal bovine serum); (b) spread pigment cells cultivated in the coelomic fluid of control sea urchins for 3 days; (c) rounded pigment cells cultivated in the coelomic fluid of injured sea urchins for 3 days. *Bar*, 10 μm.

of pigment cells was dependent on the cell culture medium. If the coelomic fluid of control sea urchins was used as the medium, all the pigment cells were well attached and spread (Figure 6(b)). However, if the coelomic fluid of injured sea urchins was used as the culture medium, all the pigment cells were rounded and unspread (Figure 6(c)). Following 20 days in culture, the pigment cells maintained their morphology; however, further cell division was not detected. Cell viability was 90–95% immediately after seeding and declined to 70–75% after 20-day cultivation.

4. Discussion

Marine organisms passed through the long path of evolution and adaptation, and this is reflected in the peculiarities of their biosynthesis and metabolism. It is known that the transcription factor glial cells missing (SpGCM) is required for the activation of transcription for pigment cell-specific differentiation genes; the onset of transcription of these genes occurs a few hours after the activation of *Spgcm* (12 hours) [20]. Phylogenomic studies have suggested that some animal genomes (sea urchins, birds, and fish) possess a previously unidentified group of *pks* genes in addition to *fas* genes used in fatty acid metabolism. These *pks* genes in the chicken, fish, and sea urchin genomes do not appear to be closely related to any other animal or fungal genes and instead are closely related to *pks* genes from the slime mold *Dictyostelium* and eubacteria [24].

Our results agree with the data of Calestani with colleagues that showed that the *pks* genes are expressed in sea urchin pigment cells beginning from the blastula stage and that this expression is maintained throughout the pluteus stage [21]. The level of *pks* transcripts has been found to be highest at the gastrula stage and then gradually decreases. The addition of shikimic acid (0.1 mM and 0.5 mM), a precursor of naphthoquinone pigments, to zygotes and embryos was shown to increase the expression of the *pks* and *sult* genes. The addition of lower concentrations of shikimic acid to sea urchin zygotes did not influence the larval developmental stages. However, the addition of 0.5 mM and 2.0 mM shikimic acid to the blastula and gastrula embryos resulted in a marked slowdown of normal development or in larval growth inhibition, respectively.

As shown by Kominami [25], pigment cells differentiate in embryos treated with aphidicolin, a specific inhibitor of DNA polymerase alpha although gastrulation and successive morphogenesis are blocked due to the absence of cell divisions and DNA synthesis. The number of pigment cells observed in aphidicolin-treated embryos increased as the treatment was initiated at later time points (from 9, 10, 12, 16, and 24 h of development) [25]. Pigment cells can be induced even from animal blastomeres at the 8-cell stage or mesomeres at the 16-cell stage, if the blastomeres are treated with LiCl [26, 27]. These data indicate the possible existence of an inductive signal for the specification of the pigment cell lineage.

Using dissociated sea urchin embryos transfected with the yeast gene *gal4,* we have previously shown that the absorption spectrum of red-brown pigments extracted from the cultured cells coincides with that of echinochrome [28]. The number of cells containing the red-brown pigments in two-month-old cell culture reached 50–60%, while the number of naphthoquinone pigments in these cells, as calculated per one cell [29], increased 9-10-fold [28] compared to the cells of normal plutei *in vivo* [5]. Here, we continued the studies of the differentiation process of sea urchin pigment cells in culture and developed conditions for the promotion of pigment cell differentiation without transfection of sea urchin embryos with foreign genes. Many pigmented cells formed and showed spread morphology similar to pigment cells embedded in the embryonic or larval ectoderm [16, 29]. However, there is no cell division in these cultures. Today, only cells of developmental anomalies in sea urchin embryos transformed by the yeast *gal4* gene [30], and malignant mussel hemocytes [31] have been reported to be involved in active proliferation.

We have found the specific effect of the coelomic fluid of control and injured sea urchins on the morphology of cultivated pigment cells. The origin of this phenomenon is unclear. We failed to develop a potential permanent cell line; however, the results obtained allow us to assert that the culture conditions used promote pigment cell differentiation

and can be useful for studying sea urchin pigment cells. The technology of directed differentiation of marine invertebrate embryonic cells *in vitro* opens the pathway for solution-applied tasks, including the generation of cell cultures that produce complex bioactive compounds with therapeutic potential.

Acknowledgments

This study was supported in part by the Far Eastern Branch of Russian Academy of Sciences (Grants nos. 09-I-P22-04 and 09-II-SB-06-001) and Program at the Far Eastern Federal University (Grant no. 11 G34.31.0010). The authors are grateful to Dr. A. G. Shilov (Institute of Cytology and Genetics, Siberian Branch of RAS, Novosibirsk) and Dr. K. V. Yakovlev (Zhirmunsky Institute of Marine Biology, FEB RAS, Vladivostok) for their help in cultivation of sea urchin embryonic cells. We greatly appreciate their time and effort.

References

[1] D. L. Fox and B. T. Scheer, "Comparative studies of the pigments some Pacific Coast echinoderms," *Biological Bulletin*, vol. 80, pp. 441–455, 1941.

[2] M. Griffiths, "A study of the synthesis of naphthaquinone pigments by the larvae of two species of sea urchins and their reciprocal hybrids," *Developmental Biology*, vol. 11, no. 3, pp. 433–447, 1965.

[3] S. A. Fedoreyev, N. P. Mischenko, E. A. Kol'tsova et al., "Drug, Histochrome, from the sea urchin," in *Abstracts of 5th International Marine Biotechnology Conference*, p. 53, Townsville, Australia, 2000.

[4] N. P. Mishchenko, S. A. Fedoreev, and V. L. Bagirova, "Histochrome: a new original domestic drug," *Pharmaceutical Chemistry Journal*, vol. 37, no. 1, pp. 48–52, 2003.

[5] E. A. Koltsova, L. V. Boguslavskaya, and O. V. Maximov, "On the functions of quinonoid pigment production in sea urchin embryos," *International Journal of Invertebrate Reproduction*, vol. 4, pp. 17–28, 1981.

[6] E. L. Cooper, "Drug discovery, CAM and natural products," *Evidence-Based Complementary and Alternative Medicine*, vol. 1, no. 3, pp. 215–217, 2004.

[7] K. Benkendorff, C. M. McIver, and C. A. Abbott, "Bioactivity of the Murex homeopathic remedy and of extracts from an Australian muricid mollusc against human cancer cells," *Evidence-Based Complementary and Alternative Medicine*, vol. 2011, Article ID 879585, 2011.

[8] M. Service and A. C. Wardlaw, "Echinochrome-A as a bactericidal substance in the coelomic fluid of *Echinus esculentus* (L.)," *Comparative Biochemistry and Physiology Part B*, vol. 79, no. 2, pp. 161–165, 1984.

[9] K. Nishibori, "Studies on pigments of marine animals. III. Echinochrome from the Spine of sand-dollar Echinorachnius mirabilis," *Bulletin of Society of Scientific Fishing*, vol. 22, no. 11, pp. 708–711, 1957.

[10] G. Britton, *The Biochemistry of Natural Pigments*, Cambridge University Press, London, UK, 1983.

[11] S. W. Ruffins and C. A. Ettensohn, "A clonal analysis of secondary mesenchyme cell fates in the sea urchin embryo," *Developmental Biology*, vol. 160, no. 1, pp. 285–288, 1993.

[12] R. R. Chaffee and D. Mazia, "Echinochrome synthesis in hybrid sea urchin embryos," *Developmental Biology*, vol. 7, pp. 502–512, 1963.

[13] E. Ryberg and B. Lundgren, "Some aspects on pigment cell distribution and function in the developing echinopluteus of *Psammechinus miliaris*," *Development Growth and Differentiation*, vol. 21, no. 2, pp. 129–140, 1979.

[14] T. Matsuno and M. Tsushima, "Carotenoids in sea urchins," in *Edible sea Urchins: Biology and Ecology*, J. M. Lawrence, Ed., Elsevier Science, Amsterdam, The Netherlands, 2001.

[15] L. C. Smith, J. P. Rast, V. Brockton et al., "The sea urchin immune system," *Invertebrate Survival Journal*, vol. 3, pp. 25–39, 2006.

[16] A. W. Gibson and R. D. Burke, "The origin of pigment cells in embryos of the sea urchin *Strongylocentrotus purpuratus*," *Developmental Biology*, vol. 107, no. 2, pp. 414–419, 1985.

[17] T. Hibino, M. Loza-Coll, C. Messier et al., "The immune gene repertoire encoded in the purple sea urchin genome," *Developmental Biology*, vol. 300, no. 1, pp. 349–365, 2006.

[18] M. Asashima, "On the tyrosinehydroxylase and tyrosinase activities in developing sea urchin embryos with special reference to the biosynthesis of echinochrome," *Journal of the Faculty of Science, the University of Tokyo. Section IV*, vol. 12, pp. 279–284, 1971.

[19] C. H. Yuh, H. Bolouri, and E. H. Davidson, "Genomic cis-regulatory logic: experimental and computational analysis of a sea urchin gene," *Science*, vol. 279, no. 5358, pp. 1896–1902, 1998.

[20] E. H. Davidson, *The Regulatory Genome: Gene Regulatory Networks in Development and Evolution*, Academic Press, San Diego, Calif, USA, 2006.

[21] C. Calestani, J. P. Rast, and E. H. Davidson, "Isolation of pigment cell specific genes in the sea urchin embryo by differential macroarray screening," *Development*, vol. 130, no. 19, pp. 4587–4596, 2003.

[22] A. Giulietti, L. Overbergh, D. Valckx, B. Decallonne, R. Bouillon, and C. Mathieu, "An overview of real-time quantitative PCR: applications to quantify cytokine gene expression," *Methods*, vol. 25, no. 4, pp. 386–401, 2001.

[23] M. M. Bradford, "A rapid and sensitive method for the quantitation of microgram quantities of protein utilizing the principle of protein dye binding," *Analytical Biochemistry*, vol. 72, no. 1-2, pp. 248–254, 1976.

[24] T. A. Castoe, T. Stephens, B. P. Noonan, and C. Calestani, "A novel group of type I polyketide synthases (PKS) in animals and the complex phylogenomics of PKSs," *Gene*, vol. 392, no. 1-2, pp. 47–58, 2007.

[25] T. Kominami, "Establishment of pigment cell lineage in embryos of the sea urchin, *Hemicentrotus pulcherrimus*," *Development Growth and Differentiation*, vol. 42, no. 1, pp. 41–51, 2000.

[26] B. T. Livingston and F. H. Wilt, "Lithium evokes expression of vegetal-specific molecules in the animal blastomeres of sea urchin embryos," *Proceedings of the National Academy of Sciences of the United States of America*, vol. 86, no. 10, pp. 3669–3673, 1989.

[27] B. T. Livingston and F. H. Wilt, "Range and stability of cell fate determination in isolated sea urchin blastomeres," *Development*, vol. 108, no. 3, pp. 403–410, 1990.

[28] N. A. Odintsova, K. V. Kiselev, V. P. Bulgakov, E. A. Koltsova, and K. V. Yakovlev, "Influence of the activator of transcription gal4 on growth and development of embryos and embryonic cells in primary cultures of sand dollar," *Russian Journal of Developmental Biology*, vol. 34, no. 4, pp. 217–222, 2003.

[29] T. Kominami and H. Takata, "Process of pigment cell specification in the sand dollar, *Scaphechinus mirabilis*," *Development Growth and Differentiation*, vol. 44, no. 2, pp. 113–125, 2002.

[30] V. P. Bulgakov, N. A. Odintsova, S. V. Plotnikov, K. V. Kiselev, E. V. Zacharov, and Y. N. Zhuravlev, "Gal4-gene-dependent alterations of embryo development and cell growth in primary culture of sea urchins," *Marine Biotechnology*, vol. 4, no. 5, pp. 480–486, 2002.

[31] C. Walker, S. A. Böttger, J. Mulkern, E. Jerszyk, M. Litvaitis, and M. Lesser, "Mass culture and characterization of tumor cells from a naturally occurring invertebrate cancer model: applications for human and animal disease and environmental health," *Biological Bulletin*, vol. 216, no. 1, pp. 23–39, 2009.

Hindawi Publishing Corporation
Evidence-Based Complementary and Alternative Medicine
Volume 2011, Article ID 723696, 5 pages
doi:10.1155/2011/723696

Research Article

Distribution and Abundance of Archaea in South China Sea Sponge *Holoxea* sp. and the Presence of Ammonia-Oxidizing Archaea in Sponge Cells

Fang Liu,[1] Minqi Han,[1] Fengli Zhang,[1] Baohua Zhang,[2] and Zhiyong Li[1]

[1] *Marine Biotechnology Laboratory, State Key Laboratory of Microbial Metabolism and School of Life Sciences and Biotechnology, Shanghai Jiao Tong University, 800 Dongchuan Road, Shanghai 200240, China*
[2] *Eastern Hepatobiliary Surgery Hospital, Second Military Medical University, Changhai Road 225, Shanghai 200438, China*

Correspondence should be addressed to Baohua Zhang, zhbh_1@tom.com and Zhiyong Li, zyli@sjtu.edu.cn

Received 14 January 2011; Revised 13 May 2011; Accepted 28 June 2011

Compared with bacterial symbionts, little is known about archaea in sponges especially about their spatial distribution and abundance. Understanding the distribution and abundance of ammonia-oxidizing archaea will help greatly in elucidating the potential function of symbionts in nitrogen cycling in sponges. In this study, gene libraries of 16S rRNA gene and ammonia monooxygenase subunit A (*amoA*) genes and quantitative real-time PCR were used to study the spatial distribution and abundance of archaea in the South China Sea sponge *Holoxea* sp. As a result, *Holoxea* sp. specific AOA, mainly group C1a (marine group I: *Crenarchaeota*) were identified. The presence of ammonia-oxidizing crenarchaea was observed for the first time within sponge cells. This study suggested a close relationship between sponge host and its archaeal symbionts as well as the archaeal potential contribution to sponge host in the ammonia-oxidizing process of nitrification.

1. Introduction

The biodiversity and biogeography of sponge microbial symbionts has received a great deal of attention, and the past 10 years has witnessed huge advances in revealing the phylogenetic diversity of sponge symbionts. Until the beginning of 2011, 30 bacterial phyla and 2 archaeal phyla have been detected in sponges [1]. However, the role of microbial symbionts remains largely unknown [2–4] and the nature of the sponge-microorganism interaction has to date only been inferred from loose correlations [2]. The present information of sponge microbial symbionts is mainly on the microorganisms in sponge mesohyl, that is, extracellular symbionts [5]. The difficulty in identifying and discriminating between intra- and extracellular symbionts has made it hard to determine the true nature of sponge-microorganism interactions. Therefore, investigation of the intracellular symbionts, which are likely "true" and "stable" symbiotic populations and may play a more significant role in the sponge biology and ecology, is very helpful for the understanding of sponge-microorganism interaction and the roles of sponge microbial symbionts.

Up to now, evidence of intracellular symbionts of sponges is mainly derived from transmission electronic microscopy (TEM) visualization analyses. For example, intracellular algal symbionts in sponges were first confirmed by TEM in 1979 [6]. Using a similar approach, intracellular dinoflagellates [7], filamentous unicellular cyanobacteria [8], and yeast [9] have been observed in sponges. Furthermore, a complex bacterial consortium was revealed in *Ectyoplasia ferox* oocytes using fluorescent in situ hybridization (FISH) in 2008 [10]. Because TEM- or FISH-based methods can provide only limited phylogenetic information, the diversity and abundance of intracellular endosymbionts in sponge cells remain poorly understood.

Numbers of studies on archaeal sponge symbionts have emerged since 1996 [11–15]. The recent discovery of genes responsible for ammonia oxidation in sponge-associated crenarchaea and evidence of vertical transmission of these symbionts strongly support the argument that these archaea are essential for the metabolism of the sponge host [16, 17]. Though diverse archaea have been observed in sponges [12–15, 18], little is known about the spatial distribution and abundance of archaea in the sponge host and we do not know

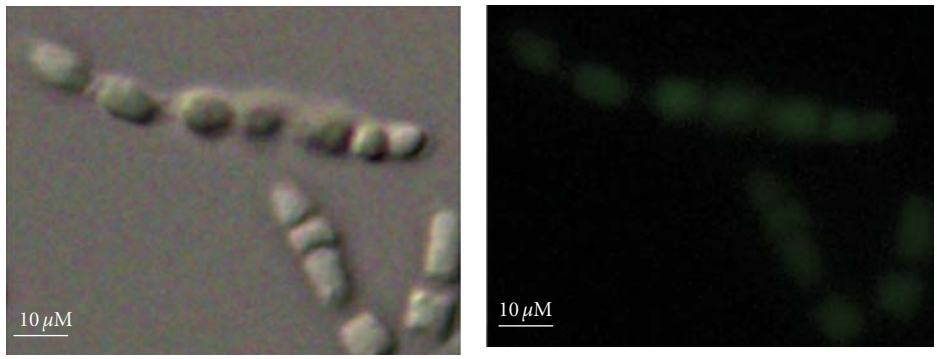

(a) (b)

Figure 1: Sponge cells isolated in this study (a) and their autofluorescence (b) ($\lambda = 480$ nm).

whether there are archaea in sponge cells. Thus, the examination of the spatial distribution, diversity, and abundance of archaea within sponges especially in sponge cells will greatly help in better understanding the role of archaea play in sponge biology and ecology.

In this study, gene library and quantitative real-time quantitative PCR (RT-qPCR) were used to determine the distribution, diversity, and abundance of archaea in the different parts such as cells and mesohyl of South China Sea sponge *Holoxea* sp. The copy number of ammonia-oxidizing genes was also studied to assess the distribution of the AOA community in different parts of sponge *Holoxea* sp. It is the first report of intracellular archaeal symbionts in marine sponges.

2. Materials and Methods

2.1. Sampling and Cell Sorting. Marine sponge *Holoxea* sp. was collected nearby Yongxing Island (112°20′E, 16°50′N) in the South China Sea at depth of *ca*. 20 m and processed as described by Li and Liu [19]. Small cubes of sponge tissues (<0.5 cm^3) were transferred into a 100 mL conical flask and washed using 40 mL sterile artificial seawater (ASW) (1.1 g $CaCl_2$, 10.2 g $MgCl_26H_2O$, 31.6 g NaCl, 0.75 g KCl, 1.0 g Na_2SO_4, 2.4 g Tris-HCl, and 0.02 g $NaHCO_3$, 1L distilled water, pH 8.2) 3 times for 40 min with shaking at 150 rpm and 20°C. The resulting artificial seawater, which contained extracellular ectosymbionts, was collected, filtered using 300-mesh stainless steel sieve, and further centrifuged at 15,000 ×g to gain extracellular ectosymbionts which refers to microbes loosely attached to the sponge surface and canals, choanocyte chambers (sample W).

The resulting tissue cubes were disintegrated in Ca^{2+}- and Mg^{2+}-free ASW and were separated using differential centrifugation method described previously [20]. The tissue cubes washed from the previous step were dissociated in Ca^{2+}- and Mg^{2+}-free ASW at 110 rpm and 20°C for 60 min. The resulting cell suspension was filtered using 300-mesh stainless steel sieve. *Holoxea* sp. has thin outer layer (1-2 mm thick). After 60 min disassociation, outer layer remained intact and was removed through the filtration. Sponge cells, named sample B for analysis of intracellular archaea, were collected by centrifugation at 300 ×g for 10 min, and the supernatant was transferred into a new tube. The resulting pellets were rinsed three times with Ca^{2+}- and Mg^{2+}-free ASW and identified to be free of bacteria from mesohyl by their autofluorescence ($\lambda = 480$ nm) (Figure 1). No bacteria-like particulates were found, which proved that the obtained sponge cells were free of bacteria from mesohyl and, thus, were used for diversity analysis of intracellular prokaryotic symbionts of sponge. Supernatants resulted from the previous step were further centrifuged at 15,000 ×g for 10 min. The resulting pellet was named sample J and used to analyze extracellular archaeal endosymbionts (mesohyl).

Sponge tissues without treatments above, named sample T, were used to extract genomic DNA for the analysis of the total communities of bacteria associated with the sponge *Holoxea* sp.

2.2. DNA Extraction, Gene Library Construction, and RT-qPCR. Genomic DNA was extracted from samples B, J, and W and sponge specimens (sample T) using the QIAGEN genomic tip protocol. To target the diversity of archaeal community, archaea-specific 16S rRNA gene primer set 21F/958R [21] was used for the construction of 16S rRNA gene libraries, named as BArc, JArc, WArc, and TArc for samples B, J, W, T, respectively. The 16S rRNA gene was amplified using the Arch21F/Arch958R primers with the following PCR condition: 95°C for 3 min; 35 cycles of 95°C for 30 s, 55°C for 30 s, 72°C for 1 min; 72°C for 10 min. Ammonia monooxygenases subunit A (*amo*A) gene was amplified with primer pair Arch-*amo*AF/Arch-*amo*AR [22] from sample T's genomic DNA to construct an *amo*A gene library. The PCR condition: 95°C for 3 min; 35 cycles of 95°C for 30 s, 53°C for 45 s, 72°C for 45 s; 72°C for 5 min.

The abundance comparison of archaea *amo*A gene between different samples was made using real-time quantitative PCR (SYBR Premix Ex Taq II, Takara) with primer set *amo*A19F/*amo*A643R [23]. As a control, universal archaea 16S rRNA gene primer set 340F/519R [24] was used to quantify the total archaea in the four samples. Specificity for real-time PCR reactions was tested by electrophoresis through a 1.5% agarose gel and melting curve analyses. Copy numbers of *amo*A and 16S rRNA gene were determined using external standards. A standard curve that describes the relationship

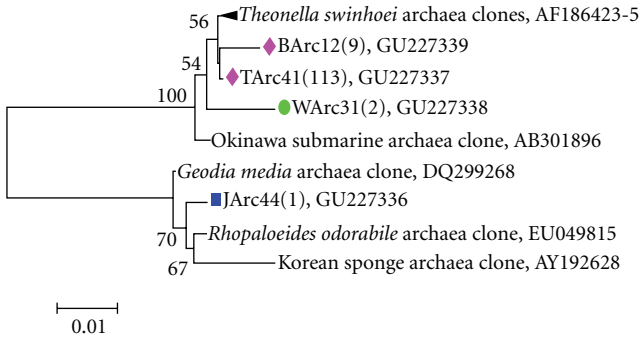

Figure 2: Unrooted 16S rRNA gene-based phylogenetic consensus tree displaying the affiliation of sponge-associated *Crenarchaeota* within group C1a (marine group I: *Crenarchaeota*). Bootstrap values under 50% were cut off after 100 resamplings. Bar: 1 nucleotide substitutions per 100 nucleotides. Numbers in parenthesis stand for the number of clones found in individual library.

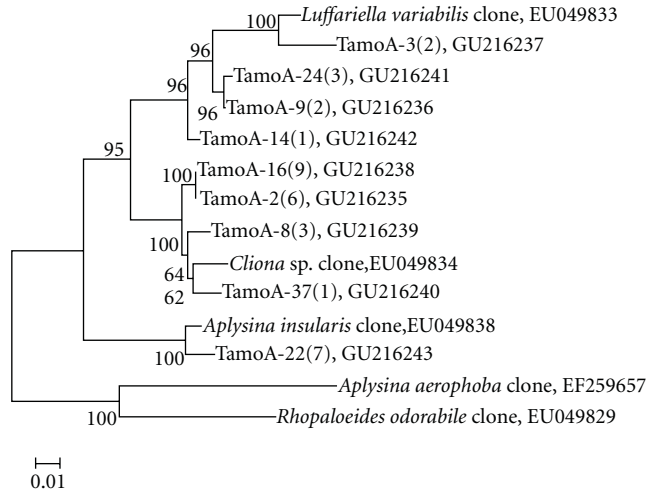

Figure 3: Unrooted *amo*A-based phylogenetic consensus tree of AOA affiliated with the group C1a (marine group I: *Crenarchaeota*). Bootstrap values under 50% were cut off after 100 resamplings. Bar: 1 nucleotide substitutions per 100 nucleotides. Numbers in parenthesis stand for the number of clones found in library.

between archaeal and bacterial *amo*A copy numbers and cycle threshold (CT) values was generated using serial dilutions of a known copy number of the 16S rRNA and *amo*A genes of the plasmid DNA: 16S rRNA, GU227337; *amo*A, GU216235. We calculated the copy numbers directly from the concentration of extracted plasmid DNA by spectrophotometry (Nanodrop Technologies, Rockland, Del, USA). Melting curve analysis was performed from 55°C to 95°C with a reading made every 1°C and the samples held for 1 s between readings.

2.3. Statistical and Phylogenetic Analysis. Operational taxonomic units (OTUs) were defined as sequence groups in which sequences differed by ≤1% (2% for *amo*A). Nonparametric richness estimations were performed using DOTUR [25]. A representative clone of each OTU was selected for further phylogenetic analysis. All the OTUs and their closest neighbors determined by BLAST were imported into MEGA 4 [26] for the construction of neighbor-joining trees. Sequences obtained in this study were deposited in the NCBI Genbank under accession numbers: GU227336-GU227339 (16S rRNA archaea) and GU216235-GU216243 (*amo*A archaea).

3. Results and Discussion

3.1. Distribution and Diversity of Archaeal Symbionts in Holoxea sp. According to this study, the archaea community in *Holoxea* sp. was rather simple; all the representative clones in the four groups were identified as group C1a (marine group I: *Crenarchaeota*) and their closest relatives were sponge-derived sequences. Only four OTUs were observed and the biggest one (TArc41) contained 113 clones, including the sequences from all samples. Based on this study, the spatiospecificity for archaea in *Holoxea* sp. was not significant. JArc44 represented the only one singleton (sequence that only occurs in one sample). In phylogenetic tree (Figure 2), these OTUs were divided into two groups: (1) nonsingleton sequences related to *Theonella swinhoei* associated archaea and (2) JArc44 located in another sponge-specific crenarchaeota clade.

Analysis of *amo*A gene fragments of sponge sample T revealed a relative high diversity of ammonia-oxidizing archaea (AOA) in sponge *Holoxea* sp. Richness analysis (observed phylotypes/predicted S_{ACE} = 0.8974 and observed phylotypes/predicted S_{Chao1} = 0.9827) indicated that the *amo*A gene library was large enough to yield a stable estimate of phylotype richness. According to the phylogenetic tree in Figure 3, three branches of *Holoxea* sp. associated AOA community including 9 OTUs could be identified based on 2% cutoff. All the *amo*A genes detected were affiliated with the marine group C1a clones [16, 27] and the diversity was noticeable: three branches, respectively, related to *Luffariella variabilis*, *Cliona* sp., and *Aplysina insularis* were identified, which highlighted the ubiquitous distribution of AOA in marine sponges. Almost all the *amo*A genes clustered together suggesting *Holoxea* sp. specific AOA. Comparing to the Figures 2 and 3, the phylogenetic affiliation was not coherent, possibly suggesting that horizontal gene transfer has occurred.

3.2. Abundance of AOA Varied in Different Parts of Sponge Holoxea sp. RT-qPCR displayed an interesting picture, as the proportion of AOA in archaea community indicated in Table 1, the proportion of AOA in intracellular archaeal community (sample J and sample B) was greater than that in extracellular archaeal community (sample W); especially the proportion of intracellular AOA (sample B, 11.67%) was nearly 3-fold that of AOA in sponge mesohyl (sample J, 4.24%), which strongly suggested the presence of AOA within sponge cells. Sponge cells would not uptake microbes randomly [28]. The mechanisms of the presence and transfer of AOA in *Holoxea* sp. are unknown. It has been shown

Table 1: Abundance of archaea and AOA in different parts of sponge *Holoxea* sp.

Sample	Copy number[a]		Average proportion of AOA
	*amo*A (AOA)	archaea 16S rRNA	
T	$1.71 \pm 0.33 \times 10^3$	$3.36 \pm 0.48 \times 10^4$	5.10%
W	$1.00 \pm 0.24 \times 10^3$	$4.35 \pm 0.55 \times 10^4$	2.30%
J	$2.33 \pm 0.09 \times 10^3$	$5.50 \pm 0.31 \times 10^4$	4.24%
B	$1.89 \pm 0.21 \times 10^3$	$1.62 \pm 0.29 \times 10^4$	11.67%

[a] Average copy numbers of target gene in one nanogram total genomic DNA. T: whole sponge tissue sample; W: sample of microbes loosely attached to the sponge surface and canals, choanocyte chambers; J: sample of microbes in the sponge mesohyl; B: the intracellular microbes sample.

that the microbial community in sponges could be established by vertical transmission [10]. Similarly, sponges may be able to capture AOA by vertical transmission [16]. Archaea of group C1a probably play an important role in the ammonia detoxification within marine sponges [1, 16]. It is known that ammonia oxidation catalyzed by ammonia monooxygenase is the first and rate-limiting step of chemoautotrophic nitrification, the overall oxidation of ammonia to nitrate. Within the sponge body, the AOA would be directly exposed to ammonia released by sponge, so it was suggested that AOA in sponge cells and mesohyl should play a role in ammonia oxidization within the sponge host to remove the toxic ammonia.

It was the first time to find *Holoxea* sp. specific AOA, mainly group C1a (marine group I: *Crenarchaeota*), especially intracellular ammonia-oxidizing archaea in sponge cells. Although the detailed function of the plentiful rest archaea in sponge *Holoxea* sp. needs to be investigated, the finding of AOA accumulation in sponge cells in this study indicates the potential role of sponge symbiotic archaea, especially the intracellular AOA in ammonia oxidization, and suggests a close relationship between sponge host and its archaeal symbionts. To further advance our understanding of the diversity and function of intracellular endosymbionts in sponges, metagenomics technology and novel culture methods will be productive approaches.

Acknowledgments

Financial supports from the National Natural Science Foundation of China (NSFC) (41076077, 30821005) and the High-Tech Research and Development Program of China (2011AA09070203) are greatly acknowledged.

References

[1] O. O. Lee, Y. Wang, J. Yang, F. F. Lafi, A. Al-Suwailem, and P. Y. Qian, "Pyrosequencing reveals high diverse and species-specific microbial communities in sponges from the Red Sea," *International Society for Microbial Ecology Journal*, vol. 5, pp. 650–664, 2010.

[2] N. S. Webster and L. L. Blackall, "What do we really know about sponge-microbial symbioses," *International Society for Microbial Ecology Journal*, vol. 3, no. 1, pp. 1–3, 2009.

[3] M. W. Taylor, R. T. Hill, J. Piel, R. W. Thacker, and U. Hentschel, "Soaking it up: the complex lives of marine sponges and their microbial associates," *International Society for Microbial Ecology Journal*, vol. 1, no. 3, pp. 187–190, 2007.

[4] G. Vogel, "The inner lives of sponges," *Science*, vol. 320, no. 5879, pp. 1028–1030, 2008.

[5] M. W. Taylor, R. Radax, D. Steger, and M. Wagner, "Sponge-associated microorganisms: evolution, ecology, and biotechnological potential," *Microbiology and Molecular Biology Reviews*, vol. 71, no. 2, pp. 295–347, 2007.

[6] C. E. Williamson, "An ultrastructural investigation of algal symbiosis in white and green *Spongilla lacustris* (L.) (Porifera: Spongillidae)," *Transactions of the American Microscopical Society*, vol. 98, pp. 59–77, 1979.

[7] M. J. Garson, A. E. Flowers, R. I. Webb, R. D. Charan, and E. J. McCaffrey, "A sponge/dinoflagellate association in the haplosclerid sponge *Haliclona* sp.: cellular origin of cytotoxic alkaloids by percoll density gradient fractionation," *Cell and Tissue Research*, vol. 293, no. 2, pp. 365–373, 1998.

[8] A. E. Flowers, M. J. Garson, R. I. Webb, E. J. Dumdei, and R. D. Charan, "Cellular origin of chlorinated diketopiperazines in the dictyoceratid sponge *Dysidea herbacea* (Keller)," *Cell and Tissue Research*, vol. 292, no. 3, pp. 597–607, 1998.

[9] M. Maldonado, N. Cortadellas, M. I. Trillas, and K. Rützler, "Endosymbiotic yeast maternally transmitted in a marine sponge," *Biological Bulletin*, vol. 209, no. 2, pp. 94–106, 2005.

[10] S. Schmitt, H. Angermeier, R. Schiller, N. Lindquist, and U. Hentschel, "Molecular microbial diversity survey of sponge reproductive stages and mechanistic insights into vertical transmission of microbial symbionts," *Applied and Environmental Microbiology*, vol. 74, no. 24, pp. 7694–7708, 2008.

[11] C. M. Preston, K. Y. Wu, T. F. Molinski, and E. F. Delong, "A psychrophilic crenarchaeon inhabits a marine sponge: *Cenarchaeum symbiosum* gen. nov., sp. nov," *Proceedings of the National Academy of Sciences of the United States of America*, vol. 93, no. 13, pp. 6241–6246, 1996.

[12] B. Holmes and H. Blanch, "Genus-specific associations of marine sponges with group I crenarchaeotes," *Marine Biology*, vol. 150, no. 5, pp. 759–772, 2007.

[13] N. S. Webster, J. E. M. Watts, and R. T. Hill, "Detection and phylogenetic analysis of novel crenarchaeote and euryachaeote 16S ribosomal RNA gene sequences from a Great Barrier Reef sponge," *Marine Biotechnology*, vol. 3, no. 6, pp. 600–608, 2001.

[14] H. Margot, C. Acebal, E. Toril, R. Amils, and J. L. Fernandez Puentes, "Consistent association of crenarchaeal archaea with sponges of the genus *Axinella*," *Marine Biology*, vol. 140, no. 4, pp. 739–745, 2002.

[15] T. Pape, F. Hoffmann, N. V. Quéric, K. Von Juterzenka, J. Reitner, and W. Michaelis, "Dense populations of archaea associated with the demosponge *Tentorium semisuberites* Schmidt, 1870 from Arctic deep-waters," *Polar Biology*, vol. 29, no. 8, pp. 662–667, 2006.

[16] D. Steger, P. Ettinger-Epstein, S. Whalan et al., "Diversity and mode of transmission of ammonia-oxidizing archaea in marine sponges," *Environmental Microbiology*, vol. 10, no. 4, pp. 1087–1094, 2008.

[17] S. J. Hallam, K. T. Konstantinidis, N. Putnam et al., "Genomic analysis of the uncultivated marine crenarchaeote *Cenarchaeum symbiosum*," *Proceedings of the National Academy of*

Sciences of the United States of America, vol. 103, no. 48, pp. 18296–18301, 2006.

[18] A. S. Turque, D. Batista, C. B. Silveira et al., "Environmental shaping of sponge associated archaeal communities," *PloS One*, vol. 5, Article ID e15774, 2010.

[19] Z. Y. Li and Y. Liu, "Marine sponge *Craniella austrialiensis*-associated bacterial diversity revelation based on 16S rDNA library and biologically active *Actinomycetes* screening, phylogenetic analysis," *Letters in Applied Microbiology*, vol. 43, no. 4, pp. 410–416, 2006.

[20] S. De Rosa, S. De Caro, G. Tommonaro, K. Slantchev, K. Stefanov, and S. Popov, "Development in a primary cell culture of the marine sponge *Ircinia muscarum* and analysis of the polar compounds," *Marine Biotechnology*, vol. 3, no. 3, pp. 281–286, 2001.

[21] E. F. DeLong, "Archaea in coastal marine environments," *Proceedings of the National Academy of Sciences of the United States of America*, vol. 89, no. 12, pp. 5685–5689, 1992.

[22] C. A. Francis, K. J. Roberts, J. M. Beman, A. E. Santoro, and B. B. Oakley, "Ubiquity and diversity of ammonia-oxidizing archaea in water columns and sediments of the ocean," *Proceedings of the National Academy of Sciences of the United States of America*, vol. 102, no. 41, pp. 14683–14688, 2005.

[23] A. Nakaya, Y. Onodera, T. Nakagawa et al., "Analysis of ammonia monooxygenase and archaeal 16S rRNA gene fragments in nitrifing acid-sulfate soil micocosms," *Microbes and Environments*, vol. 24, no. 2, pp. 168–174, 2009.

[24] L. Ovreas, L. Forney, F. L. Daae, and V. Torsvik, "Distribution of bacterioplankton in meromictic Lake Saelenvannet, as determined by denaturing gradient gel electrophoresis of PCR-amplified gene fragments coding for 16S rRNA," *Applied and Environmental Microbiology*, vol. 63, no. 9, pp. 3367–3373, 1997.

[25] P. D. Schloss and J. Handelsman, "Introducing DOTUR, a computer program for defining operational taxonomic units and estimating species richness," *Applied and Environmental Microbiology*, vol. 71, no. 3, pp. 1501–1506, 2005.

[26] K. Tamura, J. Dudley, M. Nei, and S. Kumar, "MEGA4: molecular evolutionary genetics analysis (MEGA) software version 4.0," *Molecular Biology and Evolution*, vol. 24, no. 8, pp. 1596–1599, 2007.

[27] K. Bayer, S. Schmitt, and U. Hentschel, "Physiology, phylogeny and in situ evidence for bacterial and archaeal nitrifiers in the marine sponge *Aplysina aerophoba*," *Environmental Microbiology*, vol. 10, no. 11, pp. 2942–2955, 2008.

[28] M. Wehrl, M. Steinert, and U. Hentschel, "Bacterial uptake by the marine sponge *Aplysina aerophoba*," *Microbial Ecology*, vol. 53, no. 2, pp. 355–365, 2007.

Hindawi Publishing Corporation
Evidence-Based Complementary and Alternative Medicine
Volume 2011, Article ID 540987, 14 pages
doi:10.1155/2011/540987

Research Article

The Largest Bio-Silica Structure on Earth: The Giant Basal Spicule from the Deep-Sea Glass Sponge *Monorhaphis chuni*

Xiaohong Wang,[1,2] Lu Gan,[1] Klaus P. Jochum,[3] Heinz C. Schröder,[2] and Werner E. G. Müller[2]

[1] *National Research Center for Geoanalysis, Chinese Academy of Geological Sciences, 26 Baiwanzhuang Dajie, 100037 Beijing, China*
[2] *Institute for Physiological Chemistry, University Medical Center of the Johannes Gutenberg University Mainz, Duesbergweg 6, 55128 Mainz, Germany*
[3] *Biogeochemistry Department, Max Planck Institute for Chemistry, P.O. Box 3060, 55020 Mainz, Germany*

Correspondence should be addressed to Xiaohong Wang, wxh0408@hotmail.com and Werner E. G. Müller, wmueller@uni-mainz.de

Received 8 January 2011; Accepted 16 May 2011

The depth of the ocean is plentifully populated with a highly diverse fauna and flora, from where the Challenger expedition (1873–1876) treasured up a rich collection of vitreous sponges [Hexactinellida]. They have been described by Schulze and represent the phylogenetically oldest class of siliceous sponges [phylum Porifera]; they are eye-catching because of their distinct body plan, which relies on a filigree skeleton. It is constructed by an array of morphologically determined elements, the spicules. Later, during the German Deep Sea Expedition "Valdivia" (1898-1899), Schulze could describe the largest siliceous hexactinellid sponge on Earth, the up to 3 m high *Monorhaphis chuni*, which develops the equally largest bio-silica structures, the giant basal spicules (3 m × 10 mm). With such spicules as a model, basic knowledge on the morphology, formation, and development of the skeletal elements could be elaborated. Spicules are formed by a proteinaceous scaffold which mediates the formation of siliceous lamellae in which the proteins are encased. Up to eight hundred 5 to 10 μm thick lamellae can be concentrically arranged around an axial canal. The silica matrix is composed of almost pure silicon and oxygen, providing it with unusual optophysical properties that are superior to those of man-made waveguides. Experiments indicated that the spicules function *in vivo* as a nonocular photoreception system. In addition, the spicules have exceptional mechanical properties, combining mechanical stability with strength and stiffness. Like demosponges the hexactinellids synthesize their silica enzymatically, via the enzyme silicatein. All these basic insights will surely contribute also to a further applied utilization and exploration of bio-silica in material/medical science.

1. Introduction

In the last decade, the phylogenetically oldest metazoan phylum, the Porifera (sponges) gained special interest. Mainly due to the introduction of molecular biological techniques, solid evidence was elaborated which indicated that this phylum harbors a cornucopia of new information for the understanding of the dynamics of evolutionary processes that occurred during the Earth period of Ediacara, the time prior to the Cambrian Explosion which can be dated back to approximately 540 million years ago. Furthermore, the species of this phylum are rich and valuable sources for bioprospecting, the translation of life science discoveries into practical products or processes for the benefit of the society.

Sponges are the simplest multicellular animals which are grouped to the phylum Porifera according to Grant [1]. Grant [1] described these sessile, marine animals to be built just of soft, spongy (amorphously shaped) material. Later, with the discovery of the glass sponges (class Hexactinellida) [2], this view changed drastically; they were then regarded as the "most strongly individualized, radial symmetrical" entities [3]. Since their discovery, the hexactinellids were appraised as "the most characteristic inhabitants of the great depths, which rival" with the second class of Porifera, the demosponges, "in beauty" [4]. Their thin network of living tissues is supported by the characteristic skeleton, a delicate scaffold of siliceous spicules, some of which may be fused together by secondary silica deposition to form a

rigid framework [5]. The Hexactinellida together with the Demospongiae forms a common taxonomic unit comprising the siliceous sponges. Their skeletons are built of silica that is deposited in the form of amorphous opal ($SiO_2 \cdot nH_2O$) and constructs a variety of distinct structures termed spicules. According to molecular data from sponge genes that encode receptors and signal transduction molecules [6–8], the Hexactinellida were established to be the phylogenetically oldest class of the Porifera. Based on the discovery that the Porifera share one common ancestor, the Urmetazoa, with the other metazoans [9, 10], it was deduced that these animals represent the oldest, still extant metazoan taxon. Even more, the emergence of these animals could be calculated back to 650–665 million years ago [Ma], a date that was confirmed by fossils records [11]. Hence the Porifera must have lived already prior to the Ediacaran-Cambrian boundary, 542 Ma, and thus their elucidated genetic toolkit [8] may contribute to the understanding of the Ediacaran soft-bodied biota as well, as sketched by Pilcher [12]. It was the evolutionary novelty, the formation of a hard skeleton, that contributed significantly to the radiation of the animals in the late Proterozoic [13] and the construction of the metazoan body plan [14]. Later in evolution after the Ediacaran period [15] the third class of Porifera appeared, the Calcarea, which comprises a calcium-carbonate skeleton.

The hexactinellid sponges are characterized by siliceous spicules that display hexactinic, triaxonic (cubic) symmetries, or morphologies derived by reduction from the basic building plans of the spicules. Their body shapes are less variable and more structured than those found in Demospongiae. The Hexactinellida have been divided into two main lineages, the Amphidiscophora and the Hexasterophora [16]. They are funnel to cup shaped and achieve the stability of their bodies by pinular pentactines, and rarely by hexactins, while the fixation to the substrate is maintained by basalia (monactines). It is the variation in the basalia that gives the Amphidiscophora their distinguished morphology. The basalia can be bundled or even balled together. The most outstanding species of this order are *Monorhaphis* and *Hyalonema* due to their sizes. The second order of hexactinellids is represented by the Hexasterophora that comprise a rigid dictyonal framework originating from simple hexactins. Their body plans typically feature branching and anastomosing forms with terminal oscular plates. The best known example is *Euplectella aspergillum*.

The siliceous Hexactinellida and Demospongiae as well as the Calcarea, comprise spicules which apparently have the same basic construction plan. It remains enigmatic by which genetic program this complex skeleton is initiated, run and maintained. We adopt the view that the formation of the spicules, their morphology, is the primary origin of the skeleton, while the spongin cement is secondary. We hope that this paper will provide a further basis for a molecular/cell biological understanding of spicule formation in Hexactinellida, taking the giant basal spicules [GBS] from *Monorhaphis* as the model structural element since they represent the largest bio-silica structure on Earth and allow exemplarily investigations on the formation of the sponge spicules on different morphological levels.

1.1. Monorhaphis chuni. The 19th century marks the beginning of the deep sea research, when it became overt how densely populated this region of our planet is (Figure 1(c)) [19]: during the repair of a telegraph cable that was laid across the bed of the Mediterranean, was brought up in 1860 from a depth of 2000 m, and was found to be covered with mollusks, worms, and bryozoa. It then became evident that the deep sea presents a cornucopia of "exotic" species. Already Barboza du Bocage [20] described the first *Hyalonema* species (Figure 2(e)). In the following years, an armada of expeditions was sent off to explore the biotic and abiotic world of the deep sea, with the Challenger Expeditions (1870 and 1872) as the most famous and pioneering ones. The major results were published in the series "Report of the Scientific Results of the Voyage of the H.M.S. Challenger During the Years 1873–76". One complete volume in this series was already devoted to the Hexactinellida; the material collected during this expedition was prepared and analyzed by Schulze [21]. This author was initially and primarily focused on the species *Aspergillum*, but finally also gave a first comprehensive classification of the different hexactinellids known at that time. In this compilation, Schulze [21] did not primarily concentrate on the cytological, structural, and functional aspects of the spicules but on taxonomy. However, with this opus he laid the basis for his intriguing description of the hexactinellids, with *Monorhaphis*, collected during the German Deep Sea Expedition "Valdivia" in the years 1898-1899, in the center [22]. The Chief of the Expedition Chun [17] gave in his first summary a photograph of a *Monorhaphis* specimen collected from a depth of 1644 m off the coast of East Africa (Somalia basin). This specimen had an estimated size of 3 m and surrounded one equally long siliceous spicule (Pfahlnadeln) which became one of the most lionized collected objects of that expedition (Figure 1(a)). The spicule was surrounded by stony corals (Figure 1(a)). Because of their sizes and the depths from which the specimens were collected, no complete spicule was found. Using the giant basal spicules (GBS) from this expedition, Schulze [22] provided a detailed description of their morphology and their development. His data, with their scientific accuracy, are still the reference for present day reviews.

2. Organism

Three species of Monorhaphididae have been described *Monorhaphis chuni* [22], *Monorhaphis dives* [22], and *Monorhaphis intermedia* [18]. These sponges (Figures 1(a) and 1(b)) are distributed in the Indo-West Pacific region and were found in depths between 516 and 1920 m [24]. *Monorhaphis* inhabits muddy substrata and is fixed there by a single GBS. Photographs from the natural environment are only available from Roux et al. (Figures 2(d), 2(f), and 2(g)) [25]. Young specimens have been imagined to comprise a continuous body, as has been sketched by Schulze [22]; one GBS anchors the specimen to the substratum and carries the cylindrical body (Figures 2(a) and 2(b)). The cylindrical/oval body of *Monorhaphis* is interspersed with many atrial openings which are located along one side

(a) (b) (c)

Figure 1: Discovery of *Monorhaphis chuni*. The hexactinellid *M. chuni* has first been described by Schulze [17]. (a) Original GBS which was used by Schulze for his description. (b) Glass slides prepared by Schulze for the description of the spicules. (c) Alegoric view how the scientists at that time advertised the deep sea collection of animals in general and of *M. chuni* (circled in blue) in particular to the public [18].

(Figures 2(b), 2(c), and 2(g)). Through these openings, the regular choanosomal skeleton consisting of 14 different types of siliceous spicules can be observed (Figure 2(h)). The diameter of the body reaches in larger specimens 12 cm. During growth, the specimens elongate together with the extension of their GBSs (Figures 2(a) and 2(b)).

3. Spicule Diversity

Like all other hexactinellids, also *Monorhaphis* possesses microscleres [<0.1 mm] (Figures 2(i) and 2(j)) as well as megascleres [0.2–30 mm to 3 m] (Figure 3(a)). Within the oblong, laterally compressed body (choanosomal body) which is arranged around the single GBS, 14 further types of siliceous spicules with lengths ranging from a few micrometers to 50 mm are found [22–24]. The likewise large comitalia (around 60 mm) support the basal characteristic habitus of this species and stabilize the tissue through which particulate food is filtrated through the aquiferous canal system of the animal. The choanosomal body comprises mainly triactines (tauactines), diactines, and amphidiscs. The hexactin spicules of the choanosome with their six nonbranched rays are arranged perpendicular to one another.

4. GBSs

The spicules are formed from an inorganic silica layer/mantel and an organic scaffold. The silica mantel is constructed of individual lamellae; these have been analyzed mainly by High Resolution Scanning Electron Microscopy (HR-SEM). The description here proceeds from the mm to the nm scale.

A diagonal SEM analysis of a fractured comitalia (large spicules existing in the body around the atrial openings) shows already the lamellar organization of the silica mantel (Figure 4). The lamellae are arranged perfectly concentrically around the central axial cylinder (Figures 4(a) to 4(f)). If the comitalia or the GBSs are broken, the central cylinder remains almost intact, while the peripheral lamellar zone is fractured into concentric piles of chipped lamellae (Figure 4(c)).

Millimeter Scale. The basic microscopic architecture of the GBSs (up to 3 m long) is also identical with that of the large comitalia (~60 mm) that are found in the choanosomal skeleton of the body. The spicules are, due to their composite texture and structure, distinguished from other bio-silica structures by an unusual mechanical stability with respect to strength, flexibility, and toughness.

Micrometer Scale. Recently published studies have been performed by HR-SEM [23, 26]. Cross sections showed a structural division of the spicules into three zones (Figure 5). In the center of the spicules lies the axial canal, which harbors the axial filament; in cross sections the axial canal has a square appearance [27–30] which is more pronounced towards the tips of the spicules. The axial canal is surrounded by a region of electron-dense homogeneous silica constituting the axial cylinder with a diameter of 100–150 μm. The third and major zone of the spicules is composed of 300 to 800 regularly and concentrically arranged lamellae (each 3 to 10 μm thick). The interlamellar space of the spicules is surprisingly not a continuous open slit [23]. It is in average 0.1-0.2 μm wide and displays fusion zones and open spaces;

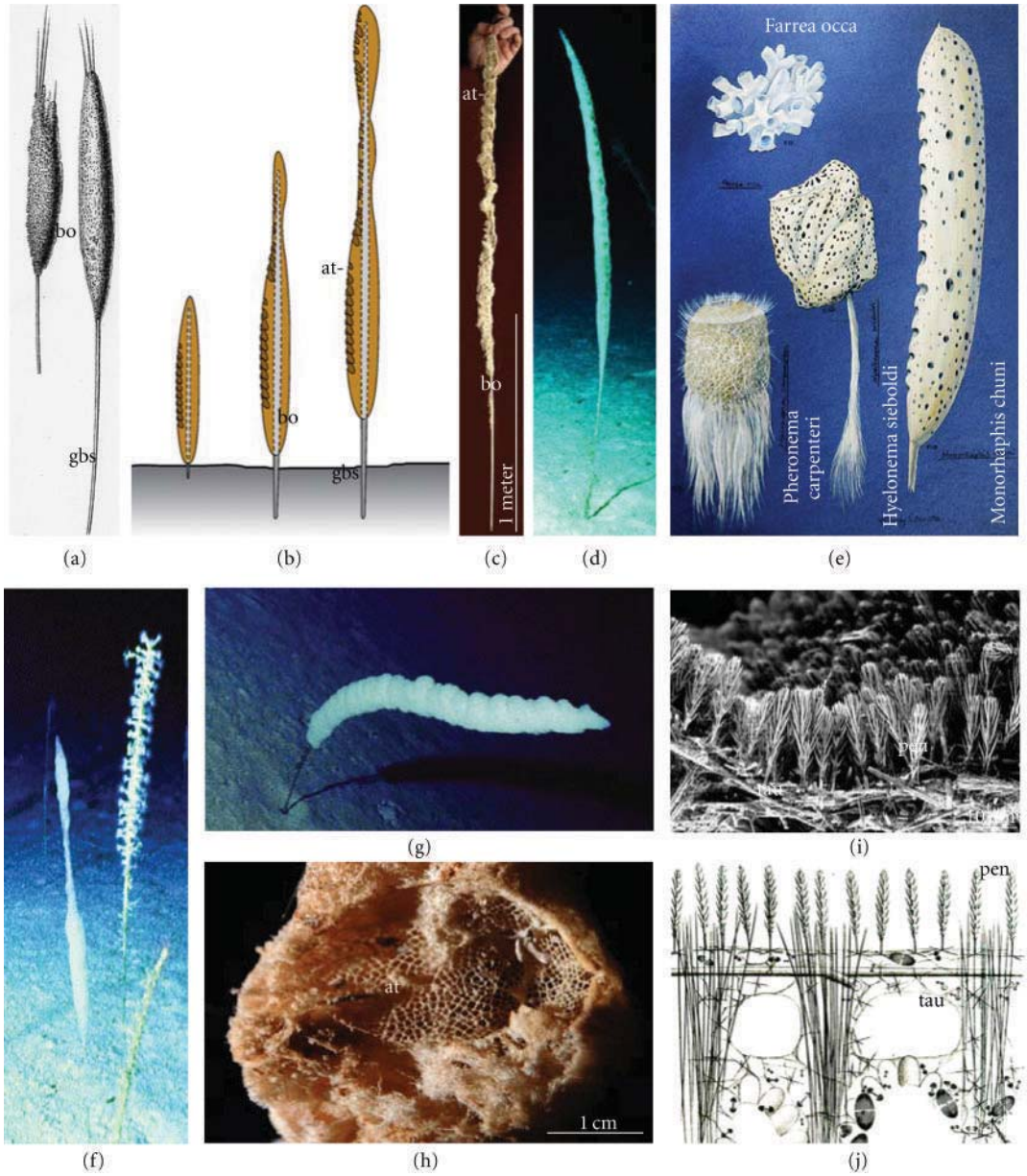

Figure 2: *M. chuni*. (a) Young specimens are anchored to the muddy substratum by one single giant basal spicule (gbs). The body (bo) surrounds the spicule as a continuous, round cylinder. (b) Schematic representation of the growth phases of the sessile animal with its GBS (gbs) which anchors it to the substratum and holds the surrounding soft body (bo). The characteristic habitus displays linearly arranged large atrial openings (at) of approximately 2 cm in diameter. With growth, the soft body dies off in the basal region and exposes the bare GBS (a to c). (c) Part of the body (bo) with its atrial openings (at). The body surface is interspersed with ingestion openings allowing a continuous water flow though canals in the interior which open into oscules that are centralized in atrial openings, the sieve-plates. (d) *M. chuni* in its natural soft bottom habitat of bathyal slopes off New Caledonia (photograph taken by Michel Roux, University of Reims; reproduced with permission). The specimens live at a depth of 800–1,000 m [23]. In this region, the sponge occurs at a population density of 1-2 individuals per m^2. The animals reach sizes of around 1 m in length. (e) Drawing from different hexactinellids. (f and g) Living *M. chuni*. (h) Part of the body with one atrium (at). (i) HR-SEM image of the lattice of a grille. The pentactines (pen) are oriented towards the exterior of the body thus forming a mechanical and relative sealing of the atrial opening. (j) Grilles forming the atrial openings are composed of tauactines (tau), framing of lattices, on which the pentactines (pen) are arranged in a phalanx.

apparently the fusion zones allow a continuum between two silica lamellae.

Nanometer Scale. Insights into the structural organization of the spicules at the nm scale can be obtained by partial and limited dissolution of the silica using hydrofluoric acid (HF) with the limitations described [31]. A rapid dissolution results in the removal of the inorganic scaffold, while gentle exposure of cross breaks of the spicules to

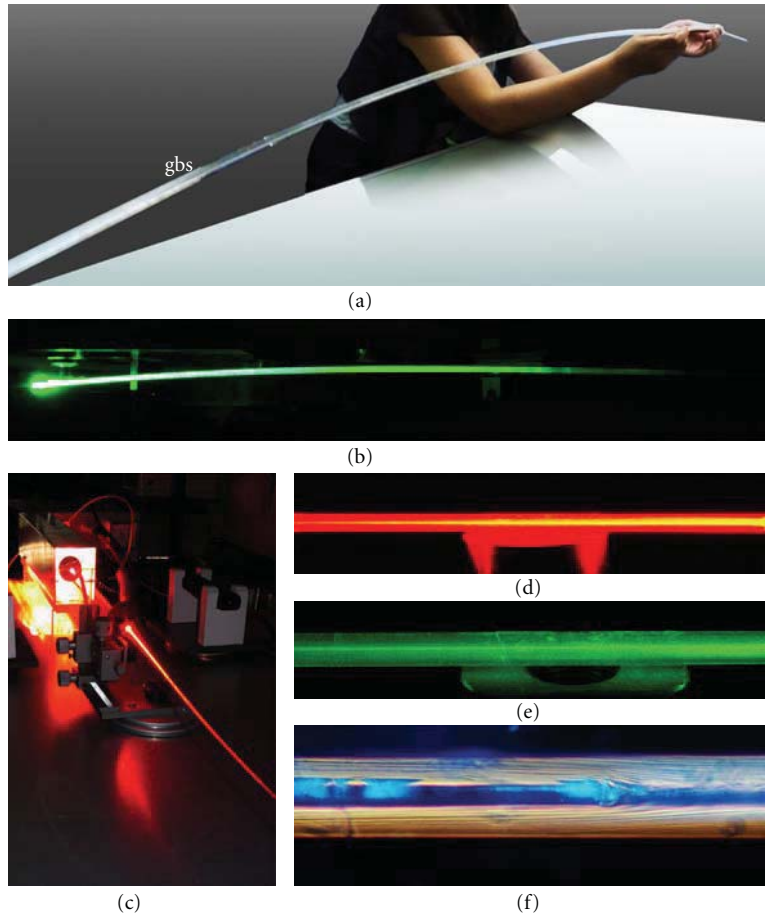

Figure 3: Giant basal spicules (gbs) from *M. chuni*. (a) Largest GBS hitherto found. GBS lighted with different laser light, green and red (b to e). The length of the spicule is 270 cm and the diameter 10 mm. (f) Illumination of a spicule with "daylight" to show the organization of the lamellae.

HF vapor results in the dissolution of the silica material under release of the organic component of the lamellae [32, 33].

5. Chemical Composition

In a first approach to understand the chemical composition of the bio-silica within the GBS, polished thin sections were prepared for electron-probe microanalysis (EPMA or electron microprobe). These analyses showed that besides of Si and O trace amounts of Ca, Fe, and Mn are present in the GBS (Figure 6). The gross chemical composition of sponge spicules has been described for both Demospongiae and Hexactinellida in general [see: [28]] and also for *Monorhaphis* in particular. Already Schulze [22] determined that, other than Si minerals (96%), only trace amounts of Na and K contribute to the inorganic material in measurable amounts (Figure 6(c)). This composition was later confirmed by Sandford [28] and Lévi et al. [34]. Based on microprobe analyses, experimental evidence has been presented indicating that Si is uniformly distributed throughout the silica shell of the spicules, whereas Na and K are not [23, 34]. Higher levels of K (around 1 wt%) have been measured in the central part of the spicules, whereas the amount dropped considerably (≈0.4 wt%) at the surface. The opposite is true for the distribution of Na; this level was almost negligible at the center (≈0.03 wt%) but increased towards the surface to ≈0.4 wt%. However, recent studies using the Laser Ablation-Inductively Coupled Plasma-Mass Spectrometry (LA-ICP-MS; Figure 6), allowing the simultaneous determination of 40 elements at detection limits as low as ng per g and at 120 μm spots, revealed an almost uniform distribution of the elements [32]. For those studies GBSs with a diameter of approximately 7 mm were systematically and completely analyzed [32]. Si was chosen as an internal standard and an SiO_2 content of 86% (wt) was accepted [remaining: 4.6% of protein and 9% of water]. The result that the contribution of the trace elements to the total inorganic components in the spicules is less than 0.005-fold with respect to Si is of prime interest. This implies that the quality of bio-silica in the spicules is in the range of quartz grade with respect to the low concentrations of elements other than silicon and oxygen. These trace elements are split as follows: among the monovalent counterions, Na^+ contributes to 86% (wt) [0.21% (wt) with respect to total inorganic material in the bio-silica] and among the divalent ions, Ca^{2+} to 12% (wt) [0.03% (wt)]. All other 35 remaining

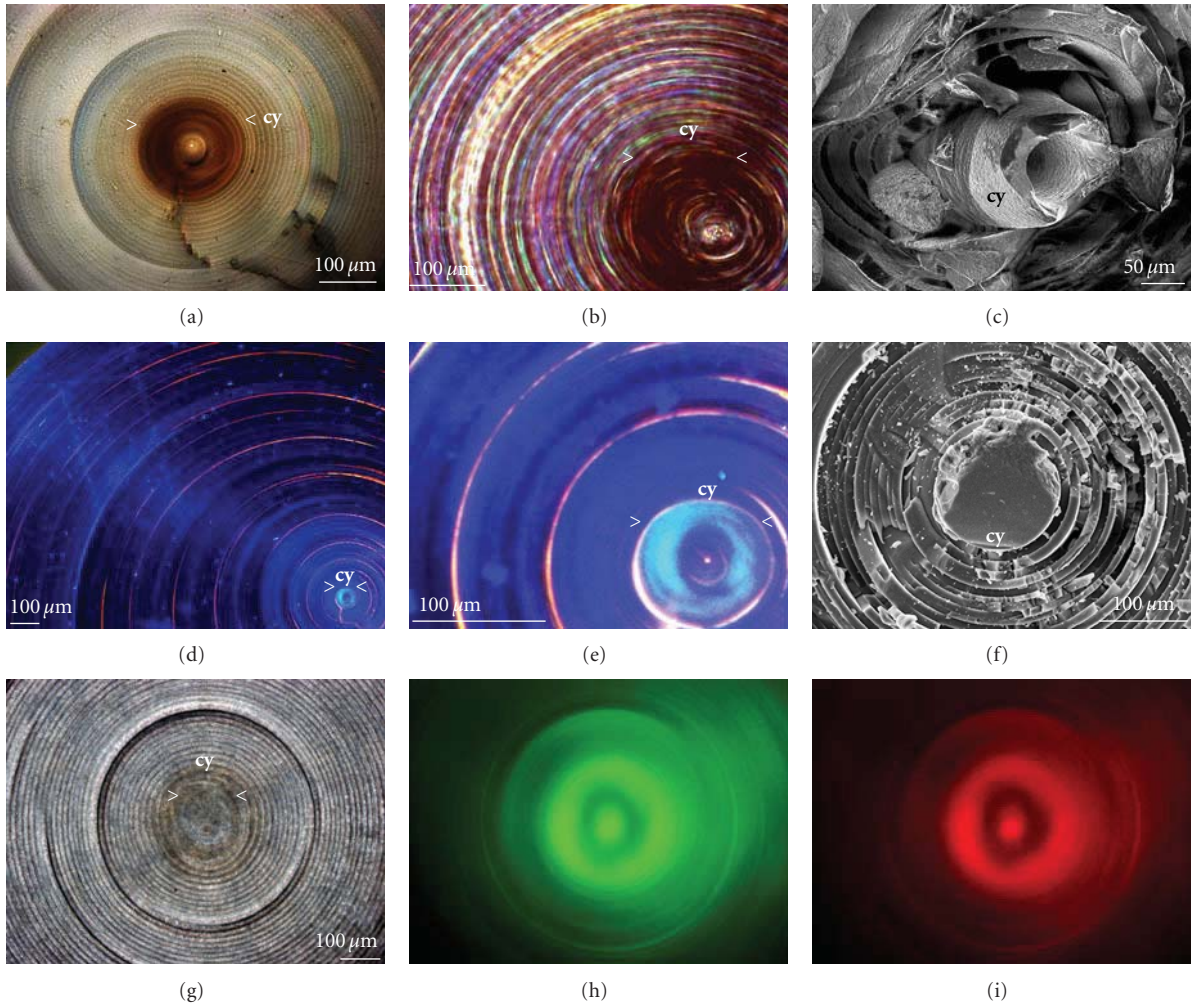

Figure 4: Lamellar composition of the GBS axial cylinder; light microscopic (a, b, d, e, g-i) and SEM images (c and f). The cross sections illuminated with red and green light; overlays from those images were computed. (g) A cross section illuminated with white light; the same section illuminated with green (h) or red laser light (i) to highlight that the axial cylinder is a better/more effective waveguide. The solid axial cylinder (>< cy) is marked.

elements contribute with <2% (wt) only unimportantly to the inorganic composition of the trace elements in bio-silica. The impact of this finding becomes even more meaningful in comparison with the element composition of seawater. Referring to natural seawater, Na and Cl are dominant there with 32.4% and 58.5% [solid material], respectively. Mg contributes 3.9%, Ca 1.2%, and Si only 0.006%.

6. Mechanical Properties

From studies with *Monorhaphis*, Lévi and coworkers [34] suggested that the layered structure of the spicules has a "beneficial" effect on the mechanical properties of the spicules. Inspired by these findings, the concept of natural composite material in rigid biological systems was born and fundamentally outlined by Mayer [35]. The organic phase controls energy dissipation especially in systems that are interspersed by very thin organic layers. In continuation of this topic, Mayer et al. [36] proposed from their load-displacement studies that in *Euplectella* breakage of spicules follows a telescope-like pattern. In more recent studies we could demonstrate that the proteinaceous matrix of the *Monorhaphis* spicules (the GBSs and the comitalia) is not evenly distributed throughout the inorganic shell around the axial canal. In fact, two morphological/structural zones can be distinguished: the axial cylinder and the lamellar zone. After having described the morphology of the GBSs of *Monorhaphis*, applying modern electron microscopic techniques [23], we demonstrated that the layers setting up the lamellar zone contain one major protein (size: ~27 kDa). Based on its binding to labeled E-64, this ~27-kDa molecule could be characterized as a protease, a (silicatein-related) polypeptide.

Considering the morphological construction and the composite nature of the GBSs from *Monorhaphis*, we studied by load-displacement experiments if these properties provide them with an exceptional mechanical stability [33, 37]. The pattern of fractures within the spicules was correlated with the organization of the lamellar zone and the axial cylinder, since both areas are characterized by different bioorganic/inorganic hybrid compositions [23]. The consecutively

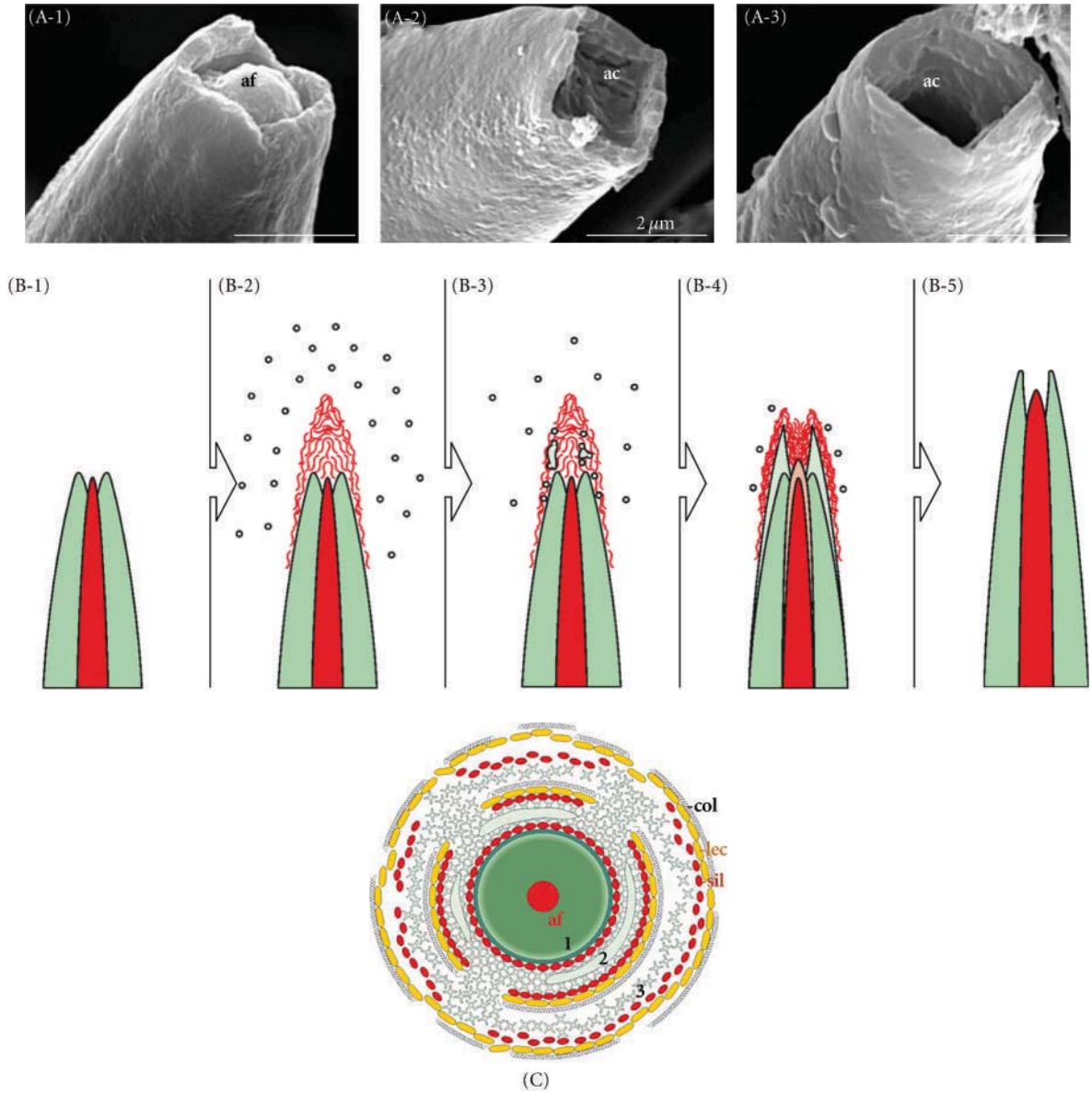

Figure 5: Tauactin spicules with open tips. (A-1–A-3) All spicules in Hexactinellida display a square opening of the axial canal (ac); SEM analysis. The quadrangular axial filament (af) is connected with the outer surface of the spicules and permits longitudinal growth; it also determines the direction of spicule formation. Whereas in most spicules, the opening does not contain any material (A-2, A-3), the axial canal of some spicules contains an axial filament (af; A-1). (B-1–B-5) Scheme of the longitudinal growth of the spicules. (B-1) In the initial stage, the spicule with its silica layers (dark green) has within its axial canal the axial filament (red), which reaches almost to the tip of the spicule. (B-2–B-4) During the growth of the spicule, silicatein-like material mediates the deposition of the polymeric silica (green dots and patches), which is deposited as a new layer on top of the previous silica layer (light green). (B-4-B-5). With progress of the axial growth of the spicules, the organic material becomes internalized into the spicule and contributes to the elongation of the axial filament. (C) Proposed formation of spicules in the hexactinellid *M. chuni* by appositional lamellar growth. The center of the spicule comprises an axial canal filled with an axial filament (af, red); the protein composition includes also the silicatein(-related) protein. Around the axial filament, the first lamella has been formed (1). The formation of the next silica lamella is thought to be mediated by silicatein(-related) proteins (red ellipsoid dots) arranged on both the surface of the first lamella and on a proteinaceous tube/cage stabilized in its outer layer by lectin molecules (yellow dots). The final orientation of the tube is provided by the collagen mat. Within the cage, a solid silica lamella is formed through an association of the silica clusters (left to right). During this growth process of the spicules, a thickening of the spicules takes place by the formation of new silica lamellae (2-3). The organic material of the cage undergoes proteolytic disintegration, as indicated in layer 2. The concentric arrangement of the silicatein(-related) proteins/lectin associates is proposed to be stabilized by collagen (gray fibers).

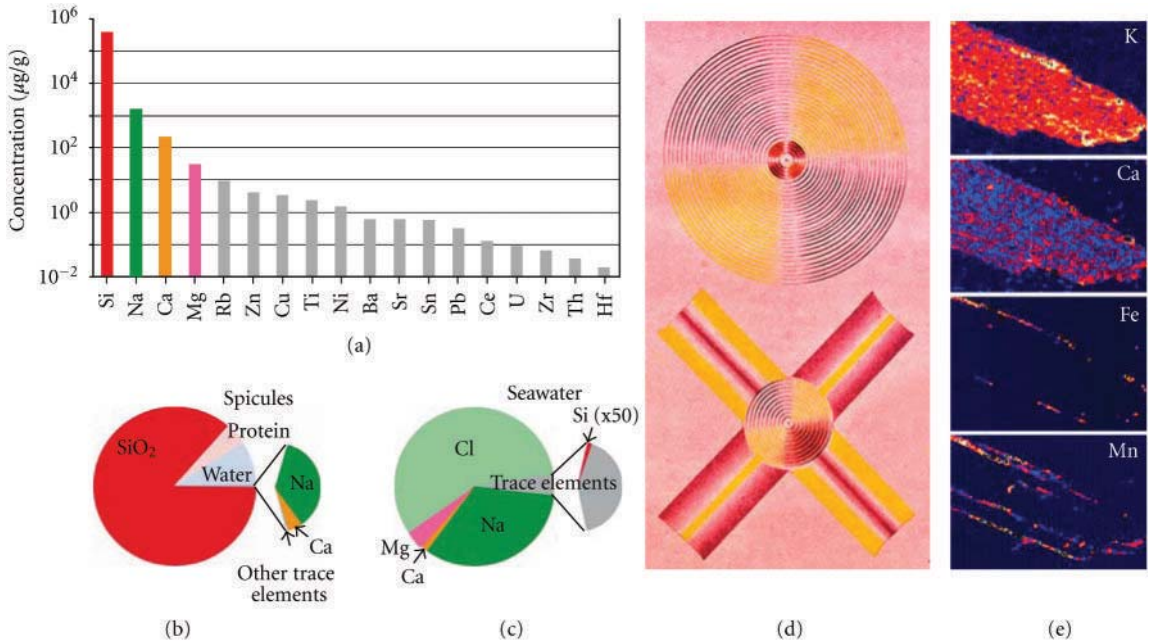

FIGURE 6: LA-ICP-MS and spectral light analyses. (a) Element concentrations (μg/g) within the *Monorhaphis* spicule "Q-B"; the elements are arranged according to their abundance. Note the logarithmic scale of the abscissa. (b) Pie diagram, showing the abundance of SiO_2, protein, and water, in comparison to the low portion of trace elements (sector part), including Na- and Ca-oxides, and further trace components. (c) A comparative diagram showing the distribution of these elements in seawater; there, Si exists as a trace element, as seen in the sector piece, whereas Cl, Na, Mg, and Ca are abundant. (d) Refraction of polarized light by spicules from the hexactinellid *M. chuni* [18]. Spectral light pattern of a cross-sectioned GBS (above) and a stauractine spicule (below) after illumination with two crossed nicol prisms. (e) Electron microprobe analysis of a GBS. The maps for the elements K, Ca, Fe, and Mn are shown.

recordable elastic responses of the spicules which are caused by cracks of distinct lamellar piles could be resolved. By this property, the spicules acquire an unusually high stability. We attribute this property, the combination of mechanical stability with strength and stiffness, to the existence of organic molecules, especially to the ~27-kDa protein existing within the inorganic rigid bio-silica material. The inner organic axial barrel stabilizing the axial cylinder is composed of rope-like filaments and provides the spicules with more mechanical flexibility and less rigidity. It must be stressed that in our studies we could not obtain conclusive results for the existence of any organic layer between the individual lamellae of the spicules. Therefore, we do not attribute the assumed viscoelastic and/or energy dissipation properties to a possible organic interphase between the lamellae but to the proteins within them.

7. Nanosecondary Ion Mass Spectrometry

Nanosecondary ion mass spectrometry (NanoSIMS) has been performed to obtain a further insight into the silica material [38]. The selected GBS used for NanoSIMS comprised 243 concentrically arranged lamellae (Figure 7(a)) with an axial cylinder of 250 μm. The lamellae nearest to the axial cylinder are thicker (10–30 μm) than those which exist more distantly, towards the surface of the spicules (2–10 μm; Figure 8). The larger lamellae (10–30 μm), surrounding the axial cylinder, were analyzed by HR-SEM and found to be separated from each other by 50 and 100 nm wide gaps (Figures 8(a) to 8(e)). Closer inspection by NanoSIMS revealed that those lamellae are composed of substructures that are not delimited by gaps but are closely packed; these were termed sublamellae. Hence, every lamella is formed of three to six stacked solid sublamellae, each measuring 3–6 μm (Figures 8(f) to 8(h)).

The distribution of C, O, S, and Si has been investigated on a $7 \times 7\,\mu m^2$ area, spanning a total of three sublamellae with one complete sublamella in the middle (Figure 7(C-a)). The NanoSIMS 50 ion microprobe, operating in the multicollection detector mode, allowed a simultaneous imaging of C^-, O^-, Si^-, and S^-. C, S, and O were normalized to Si in order to minimize crater effects, which occur towards the edge of the image (Figure 7(C)). Normalization of the signals to silicon (^{28}Si) revealed that the peak signals obtained followed distinct lines which correspond to the borders of the sublamellae (Figure 7(C-c) and 7(C-d)). The borders of the sublamellae are especially highlighted in the scan obtained from the $^{16}O^-/^{28}Si^-$ mapping. The ratio of C and Si (Figure 7(C-b)) and the ratios of these two elements [$^{12}C^-/^{28}Si^-$] indicate a further substructure within the sublamella, [5 μm thick] the 1.6–1.8 μm subsublamellae, which we term here cylindrical slats. It is obvious that this particular sublamella, from which the mappings were derived, is composed of three slats (Figure 7(C-c)). The ratio $^{12}C/^{28}Si$ indicates that the C concentrations within the slats differ from each other (Figure 7(C-b)). It is interesting to note that the highest $^{12}C/^{28}Si$ values were not found at

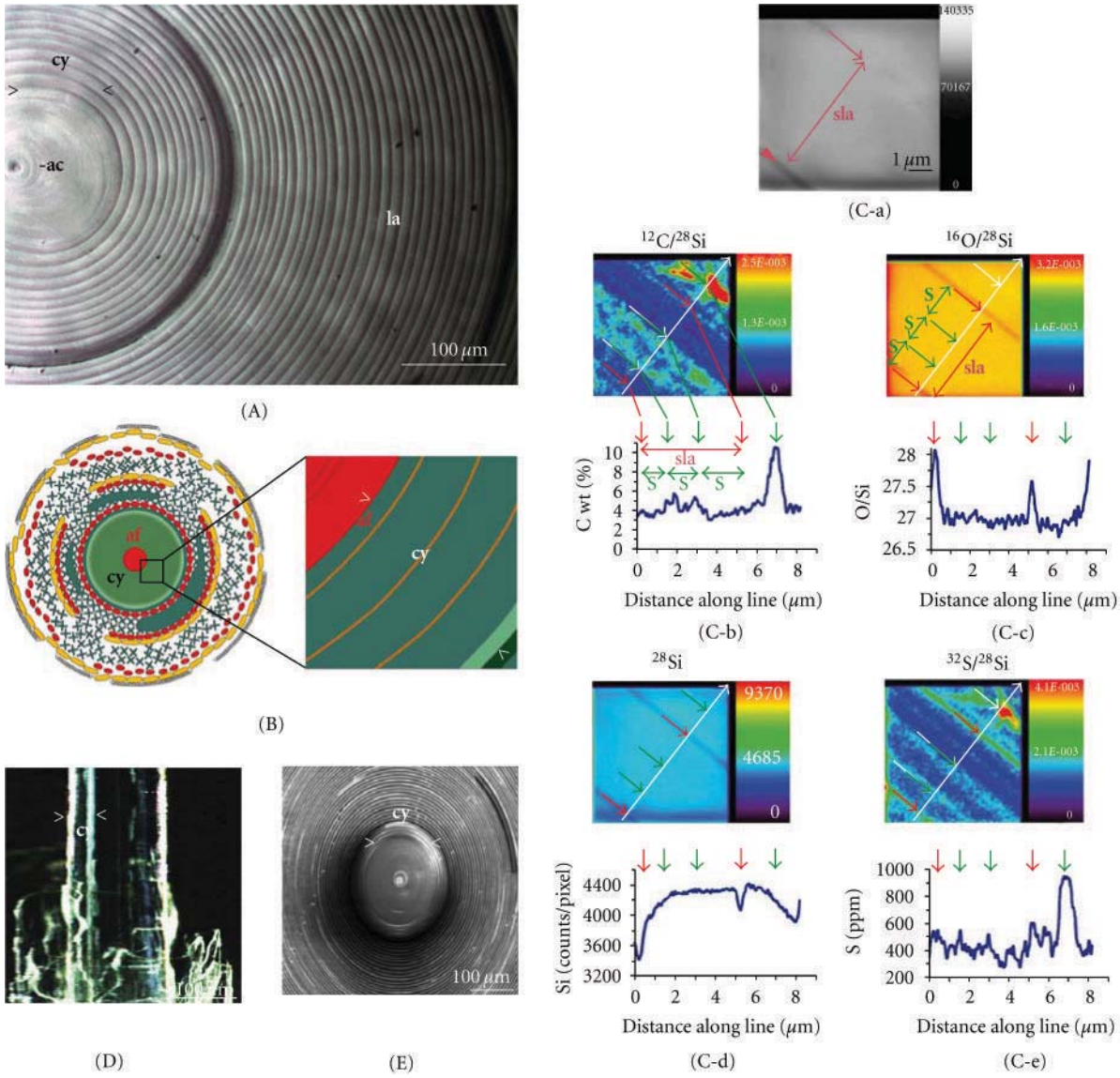

FIGURE 7: NanoSIMS images taken from a sublamella of the GBS. (A) Polished cross section through a GBS showing the three morphological regions within a spicule, the central axial canal (ac), the surrounding axial cylinder (cy), and the lamellar region (la). Light microscopic image. (B) Schematic illustration of the cross section through the GBS outlining the growth of the spicules with emphasis on the outlining the axial cylinder (cy) of which lamellae have been "biosintered". The measurements have been performed in the boxed area. The axial cylinder surrounds the axial filament (af). (C) NanoSIMS analyses. (C-a) Image taken simultaneously with the NanoSIMS by secondary electrons; the sublamella is marked (sla) and has a thickness of 5 μm. (C-b to C-e) NanoSIMS mapping to determine the distributions of ^{12}C, ^{28}Si, ^{18}O, and ^{32}S. (C-b) The pseudocolor image reflects the changes of the $^{12}C/^{28}Si$-ratio along the indicated line field. Below: the ^{12}C concentrations are calculated based on the $^{12}C/^{28}Si$-ratio and applying the relative sensitivity factors. (C-c) $^{16}O/^{28}Si$-ratio shows the homogeneity of the "biological glass" within the lamellae. The absolute ratio is caused by the difference of the ionization probability of silicon and oxygen in this matrix. Mapping of (C-d) silicon; the total counts of ^{28}Si are given, and of (C-e) sulfur and silicon; the $^{32}S/^{28}Si$ ratios are computed. Either (absolute) concentrations or the ratio of concentrations are given as pseudocolor images. Different colors correspond to different intensities of signal or ratio, increasing from black to red. Below the color images the corresponding line-scan data are given. In (C-a), (C-b), and (C-c), the hierarchical composition of one 5 μm sublamella (sla; double-headed arrow; bordered by red arrows) from three slats (s; framed by green arrows), displaying widths of about 1.5 to 1.8 mm each, is indicated. (D) and (E) Light and SEM microscopical images showing the location of the axial cylinder (cy).

the borders of the sublamella but between two slats. The determination of the relative level of Si, given in counts/pixel, revealed the highest level within the sublamellae and showed a distinct decrease at their "borders" (Figure 7(C-d)). Finally, the $^{32}S^-/^{28}Si^-$ ratios were determined along the same lines (Figure 7(C-e)). Based on these mapping data, we can conclude that the lamellae are hierarchically built from three to five sublamellae which are composed of three slats each. This new insight into the highly ordered distribution of protein within lamellae and lamellar substructures confirms

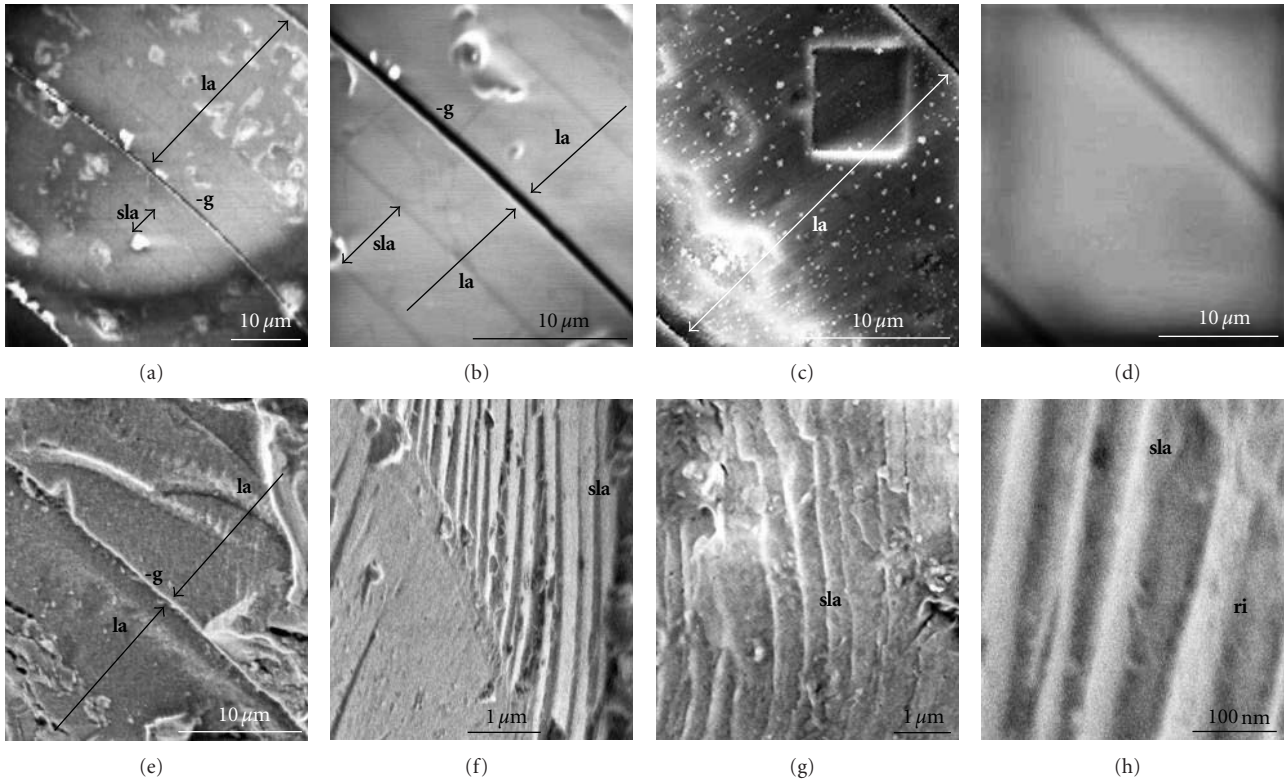

Figure 8: Presence of the three sublamellae within the lamella where the NanoSIMS analysis has been performed. (a) to (e) The 18 μm thick lamella (la) shows a substructuring into three sublamellae (sla). In contrast to the lamellae, the sublamellae are not delimited by visible gaps (g). At higher magnifications, the spacing of the gap (g), separating individual lamellae (la), and the absence of any gap/slit between the sublamellae (sla) is more distinct. (e) The location of the area ([quadratic area]) within a lamella that had been analyzed by NanoSIMS is shown. (f) to (h) View of a GBS cross-fracture, obtained by mechanical breaking, showing a ribbed surface. Magnification at the submicron level reveals that the surface of the fracture is a rib-like corrugated sheet (ri) without gap.

earlier findings, revealing that the silica nanospheres built from 2.8 nm small colloids and reaching sizes of 50–200 nm in diameter are arranged within the GBS in a highly ordered, concentric manner.

8. Optophysical Properties

Sponges can react fast to physical stimulation from the environment with contraction or expansion. Morphological and cellular structures for such responses are conceivable based on the complex cell-cell- and the diverse cell-matrix-interaction systems in sponges that have already been detected [see: [8]]. These observations could imply that the coordinate reactions are governed by a nerve system. However, until now no nerve fibers or synapses could be identified in sponges. Nevertheless, our previous studies showed that the siliceous demosponges *Suberites domuncula* and *Geodia cydonium* contain and express genes coding for neuronal molecules, for example, a metabotropic glutamate/GABA [γ-aminobutyric acid-] like receptor [39].

Especially suitable for optophysical studies are the longer *Monorhaphis* GBSs, as well as the stalk spicules of *Hyalonema sieboldi* [40]. Using those spicules, comparable and more extensive studies have been published [26, 40]. The giant spicules (*Monorhaphis*) were exposed at their end with the wider diameter to a white light source with a spectrum ranging from 400 nm to >1600 nm (Figures 3(b) to 3(f)). Even with the naked eye, the optical waveguide properties of the GBS could be recorded. During the passage of the light, a distinct white-to-red color gradient along the spicules of glass sponges was seen, suggesting a (partial) scattering of the light (Figure 3(c)). In a closer view, it became obvious that the guided light in the paraxial region of the spicule has a bright yellow color in contrast to the light quality at the outer surface. The spectrum of the output of the light source was measured between 400 nm and >1600 nm. A distinct cut-off of the wavelengths below 600 nm and above 1400 nm could be measured, while the light transmission between these borders was only slightly/gradually reduced. Hence, the spicules act as optical fibers [like a high pass filter] cutting off the light of wavelengths below about 600 nm from transmission by more than 2 orders. A similar cut-off of the spicule was observed in the infrared wavelength range above 1400 nm. Here light transmission was blocked like a low pass filter. Three weaker absorption minima were observed on the overall profile at the centre wavelengths at around ~960 nm and ~1150 nm which were attributed to the existing water. Within the visible part of the spectrum transmitted by the fibers, less pronounced absorption wavelength regions were found which matched the molecular

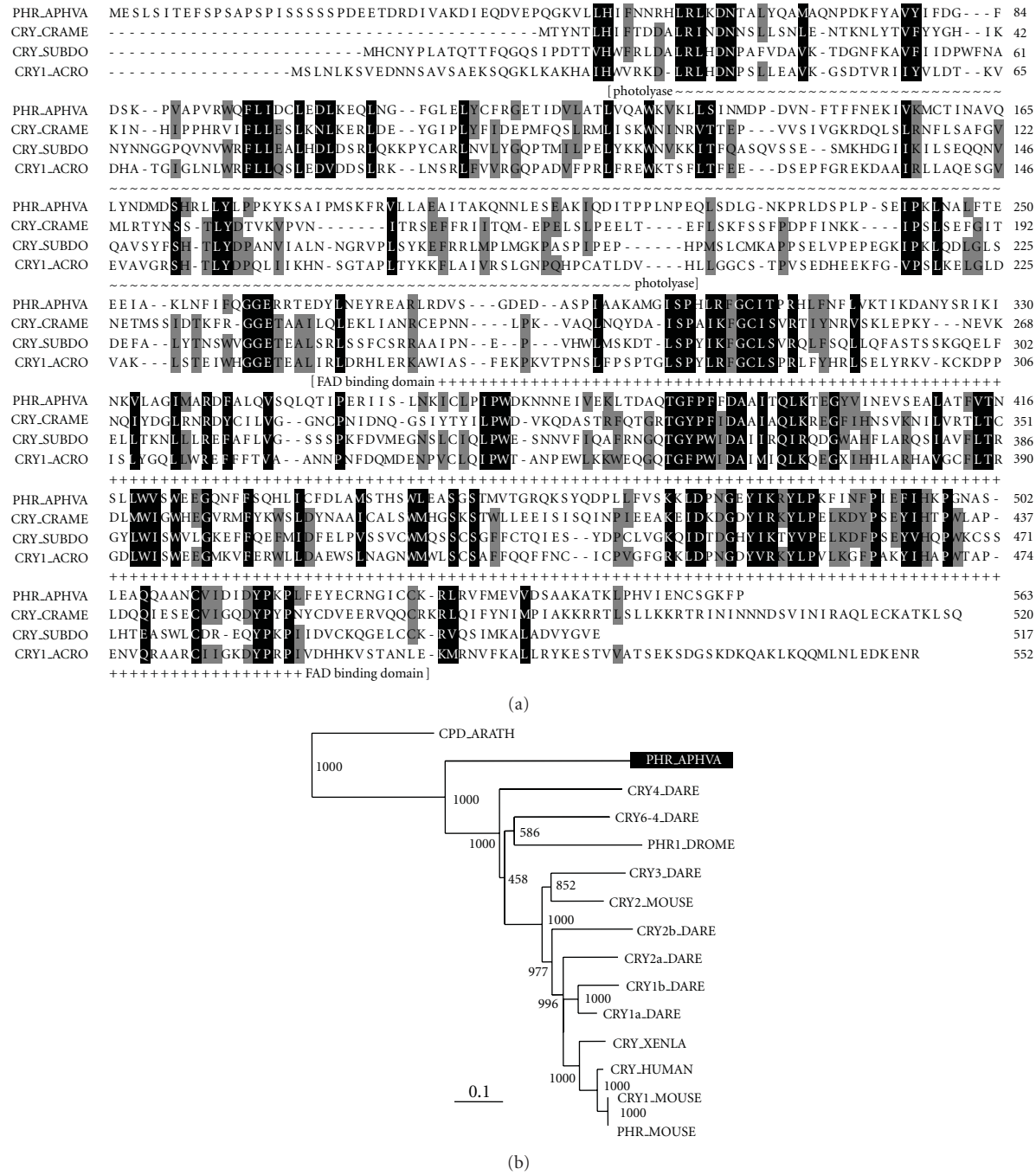

Figure 9: Poriferan cryptochromes. (a) The deduced poriferan cryptochrome protein sequences CRY_SUBDO (*Suberites domuncula* (CRYPTO_SUBDO; accession number FN421335), CRY_CRAME (*Crateromorpha meyeri*; FN421336), and the photolyase-related protein from *Aphrocallistes vastus* (PHR_APHVA; AJ437143.1) were aligned with the coral (*Acropora millepora*) cryptochrome CRY1 (CRY1_ACRO; 145881069). Residues conserved (identical or similar with respect to their physicochemical properties) in all sequences are shown in white on black; those which share similarity in three sequences are shown in black on gray. The characteristic domains the N-terminal photolyase-related region (photolyase), and the FAD-binding domain, are marked. (b) Phylogenetic relationship of the photolyase/cryptochrome polypeptides. The sponge photolyase-related molecule (PHR_APHVA) has been aligned with related sequences; finally a rooted tree has been computed. The numbers at the nodes are an indication of the level of confidence for the branches as determined by bootstrap analysis (1000 bootstrap replicates). The scale bar indicates an evolutionary distance of 0.1 aa substitutions per position in the sequence. The following sequences have been included ["class I photolyases"]. The cryptochrome sequences from *Danio rerio* zcry1a (CRY1a_DARE; AB042248/AB042248), zcry1b (CRY1b_DARE; AB042249/AB042249.1), zcry2a (CRY2a_DARE; AB042250/AB042250.1), zcry2b (CRY2b_DARE; AB042251/AB042251.1), zcry3 (CRY3_DARE; AB042252/AB042252.1), zcry4 (CRY4_DARE; AB042253/AB042253.1), and (6–4) photolyase (CRY6-4_DARE; AB042254), the human photolyase (CRY_HUMAN; D83702), mouse photolyase/blue-light receptor homolog 1 (CRY1_MOUSE; AB000777) and homolog 2 (CRY2_MOUSE; AB003433), frog cryptochrome 1 (CRY_XENLA; AY049033), the photolyase from *D. melanogaster* (PHR1_DROME; BAA12067.1). The *Arabidopsis thaliana* class II photolyases (CPD photolyase; CPD_ARATH; CAA67683.1) were used as outgroup to root the tree.

absorption lines of water (970 nm and 1150/1190 nm, resp.) [41].

In a first approach, a cryptochrome [CRY] sequence from the hexactinellid sponge *Aphrocallistes vastus*, that comprises high sequence similarity to genes encoding (6–4) photolyases and related proteins, has already been identified [26]. Earlier, functional studies showed that this gene codes in *S. domuncula* for a photolyase-related protein [42]. Based on sequence similarities, the DNA photolyase from *A. vastus* has been classified together with the cryptochromes, which include blue-light receptors, into a single DNA photolyase/chryptochrome protein family (Figure 9) [26]. Taking this experimental finding together with the demonstration of the luciferase in *S. domuncula*, we propose that sponges are provided with an unusual, (perhaps) unrecognized photoreception system. We postulate that sponges coordinate their sensory reception systems not through a protein-based nervous network alone, but primarily through a siliceous spicular meshwork and nerve-cell-related sensory molecules at the ends of those spicules. Since sponges are provided with the genetic machinery to express luciferase enzymes and also a photolyase/chryptochrome molecule, the optical fibers [spicules] might guide and convert the light, via a chemical/photoelectric reaction, into electric signals. The subsequent amplification system which translates the electric signals into the nervous transmission system in sponges as well as to other metazoan phyla might be mediated by similar biological amplifiers/receptors.

9. Synthesis of GBS

As outlined earlier [43, 44] the initial phase of spicule formation proceeds intracellularly in sclerocytes, where the spicules elongate up to 8 μm. These cells are loosely embedded in the mesohyl and usually start to synthesize several spicules simultaneously; the lengths of the spicules observed reach values of 0.7–8 μm and diameters of up to 0.9 μm.

Silicatein, the major structural protein in the GBS and also the enzyme that mediates the synthesis of polymeric silica, is present not only in the axial canal, but also in the extra-spicular and extra-cellular space [43, 45]. Recently Ehrlich et al. [46] got some experimental evidence that spicules in hexactinellids contain collagen onto which they deposit silica.

The Intracellular Phase of Spicule Formation in Sclerocytes. Silica is actively taken up by a Na^+/HCO_3^- [$Si(OH)_4$] cotransporter [47]. In the first steps silicatein is synthesized as a proenzyme (signal peptide-propeptide-mature enzyme: 36.3kDa) and processed via the 34.7kDa form (propeptide-mature enzyme) to the 23/25kDa mature enzyme. Very likely during the transport through the endoplasmic reticulum and the Golgi complex, silicatein undergoes phosphorylation and is transported into vesicles where silicatein forms rods, the axial filaments. After assembly to filaments, the first layer(s) of silica is (are) formed. Finally the spicules are released into the extracellular space where they grow in length and diameter by appositional growth. The immature spicules are extruded from the pinacocytes.

Extracellular Phase (Appositional Growth). Silicatein is present also in the extracellular space. As mentioned, the immunogold electron microscopic analysis showed that the silicatein molecules are arranged along strings, which are organized in parallel to the surfaces of the spicules. In the presence of Ca^{2+}, silicatein associates with galectin and allows the appositional growth of the spicules. Since the surface of a newly siliceous spicule is also covered with silicatein, the appositional growth/thickening of a spicule hence proceeds from two directions [axial (Figure 5B) and radial (Figure 5C)].

Extracellular Phase (Shaping). In the next step, the galectin-containing strings are organized by collagen fibers to net-like structures [45]. It is very likely that collagen, which is released by the specialized cells the collencytes, provides the organized platform for the morphogenesis of the spicules. The longitudinal growth of the spicules can be explained by the assumption that at the tips of the spicules, the galectin/silicatein complexes are incorporated into deposited biosilica under formation and elongation of the axial canal.

10. Concluding Remarks

Until 15 years ago, the Porifera [sponges] were an enigmatic animal taxon whose evolutionary origin, its phylogenetic position, and its genetic toolkit were largely unknown. The discovery of one protein, the cell adhesion molecule galectin, clarified those questions almost suddenly [48]. Cloning and functional studies of that molecule solved the question on the evolutionary origin of the multicellular animals by the demonstration that all metazoan phyla including the Porifera originate from one common ancestor, the hypothetical Urmetazoa [48]. After having established the monophyly of animals and having underscored the relevance of the phylum Porifera for the elucidation of the deep phylogeny of animals [9], it could be resolved that among the three classes in the phylum Porifera the evolutionary oldest class is represented by the Hexactinellida [7]. This insight came as a surprise, since the members display the most sophisticated body plan among the sponges. This enlightenment was supported and flanked by the realization that sponges comprise (almost all) basic functional circuits known also from higher metazoan phyla. Regardless of that progress, one main issue remained mysterious, the genetic basis for the construction of the highly complex skeleton built of spicules. Focusing on the siliceous sponges, major progress has been made in the understanding of the formation and the development of the spicules in the last few years. Furthermore, with the availability of the GBSs from *Monorhaphis*, substantial advances in the insight of the construction of the siliceous spicules have been achieved as outlined in this paper.

Acknowledgments

Werner E. G. Müller is a holder of an ERC Advanced Investigator Grant (no. 268476 BIO-SILICA). The authors thank the Chinese Academy of Sciences for providing them with the *Monorhaphis chuni* spicules for their research. They are

indebted to Professors A. Bick and S. Richter (Institut für Biowissenschaften, Allgemeine und Spezielle Zoologie; Universität at Rostock; Germany) for the loan of the original microscopic slides of *M. chuni* GBS that had been used by F. E. Schulze. The examined type specimen originates from the collection of the Zoological Institute in Leipzig and is kept at the Museum für Naturkunde Berlin, Germany (ZMB Por 12700). They acknowledge Emily S. Damstra (Kitchener, Ontario) for providing the drawing of hexactinellids; it is used by permission. This work was supported by grants from the German Bundesministerium für Bildung und Forschung (project "Center of Excellence *BIOTEC*marin"), the Deutsche Forschungsgemeinschaft (Schr 277/10-1), the European Commission/EUREKA (EUROSTARS, no. 4289 - SILIBACTS), the International Human Frontier Science Program, the European Commission (Project no. 244967 -Mem-S Project), the Public Welfare Project of Ministry of Land and Resources of the People's Republic of China (Grant no. 201011005-06), and the International S & T Cooperation Program of China (Grant no. 2008DFA00980).

References

[1] R. E. Grant, "Lectures on comparative anatomy and animal physiology; on the classification of the animals," *The Lancet*, vol. 1, pp. 153–159, 1833.

[2] O. Schmidt, *Grundzüge Einer Spongien-Fauna des Atlantischen Gebietes*, W. Engelmann, Leipzig, Germany, 1870.

[3] L. H. Hyman, *The Invertebrates: Protozoa Through Ctenophora*, McGraw-Hill, New York, NY, USA, 1940.

[4] L. G. Campbell, *Log Letters from "The Challenger"*, MacMillan, London, UK, 1876.

[5] S. P. Leys, G. O. Mackie, and H. M. Reiswig, "The Biology of glass sponges," *Advances in Marine Biology*, vol. 52, pp. 1–145, 2007.

[6] M. Kruse, I. M. Müller, and W. E. G. Müller, "Early evolution of metazoan serine/threonine and tyrosine kinases: identification of selected kinases in marine sponges," *Molecular Biology and Evolution*, vol. 14, no. 12, pp. 1326–1334, 1997.

[7] M. Kruse, S. P. Leys, I. M. Müller, and W. E. G. Müller, "Phylogenetic position of the hexactinellida within the phylum Porifera based on the amino acid sequence of the protein kinase C from *Rhabdocalyptus dawsoni*," *Journal of Molecular Evolution*, vol. 46, no. 6, pp. 721–728, 1998.

[8] W. E. G. Müller, M. Wiens, T. Adell, V. Gamulin, H. C. Schröder, and I. M. Müller, "The bauplan of the urmetazoa: the basis of the genetic complexity of metazoa using the siliceous sponges [Porifera] as living fossils," *International Reviews in Cytology*, vol. 235, pp. 53–92, 2004.

[9] W. E. G. Müller, "Origin of metazoa: sponges as living fossils," *Naturwissenschaften*, vol. 85, no. 1, pp. 11–25, 1998.

[10] W. E. G. Müller, I. M. Müller, B. Rinkevich, and V. Gamulin, "Molecular evolution: evidence for the monophyletic origin of multicellular animals," *Naturwissenschaften*, vol. 82, no. 1, pp. 36–38, 1995.

[11] J. Reitner and G. Wörheide, "Non-lithistid fossil demospongiae—origins of their plaeobiodiversity and highlights in history of preservation," in *Systema Porifera: A Guide to the Classification of Sponges*, J. N. A. Hooper and R. van Soest, Eds., Kluwer Academic, New York, NY, USA, 2002.

[12] H. Pilcher, "back to our roots," *Nature*, vol. 435, no. 7045, pp. 1022–1023, 2005.

[13] A. H. Knoll, "Biomineralization and evolutionary history," *Reviews in Mineralogy and Geochemistry*, vol. 54, pp. 329–356, 2003.

[14] W. E. G. Müller, "Spatial and temporal expression patterns in animals," in *Encyclopedia of Molecular Cell Biology and Molecular Medicine*, R. A. Meyers, Ed., vol. 13, pp. 269–309, WILEY-VCH, Weinheim, Germany, 2005.

[15] J. Schütze, M. R. Custodio, S. M. Efremova, I. M. Müller, and W. E. G. Müller, "Evolutionary relationships of metazoa within the eukaryotes based on molecular data from Porifera," *Proceedings of the Royal Society London B*, vol. 266, no. 1414, pp. 63–73, 1999.

[16] H. M. Reiswig, "Classification and phytogeny of Hexactinellida (Porifera)," *Canadian Journal of Zoology*, vol. 84, no. 2, pp. 195–204, 2006.

[17] C. Chun, *Aus den Tiefen des Weltmeeres*, Fischer, Jena, 1900.

[18] J. Li, "*Monorhaphis intermedia*—a new species of Hexactinellida," *Journal of Oceanology and Limnology*, vol. 18, pp. 135–137, 1987.

[19] J. Murray and J. Hjort, *The Depths of the Ocean*, Macmillan, London, UK, 1912.

[20] J. V. Barboza du Bocage, "Note sur la découverte d'un zoophyte de la famille Hyalochaetides sur la côte du Portugal," *Proceedings Zoological Society London*, vol. 1864, pp. 265–269, 1864.

[21] F. E. Schulze, *Report on the Hexactinellida Collected by H.M.S. "Challenger" During the Years 1873–1876, H.M.S. Challenger Scientific Results in Zoology*, H.M.S. Challenger Reports, Neill, Edinburgh, UK, 1887.

[22] F. E. Schulze, "Wissenschaftliche Ergebnisse der deutschen Tiefsee-Expedition auf dem Dampfer "Valdivia" 1898-1899," in *Hexactinellida*, Fischer, Stuttgart, Germany, 1904.

[23] W. E. G. Müller, C. Eckert, K. Kropf et al., "Formation of giant spicules in the deep-sea hexactinellid *Monorhaphis chuni* (Schulze 1904): electron-microscopic and biochemical studies," *Cell and Tissue Research*, vol. 329, no. 2, pp. 363–378, 2007.

[24] K. R. Tabachnick, "Family monorhaphididae ljima, 1927," in *Systema Porifera: A Guide to the Classification of Sponges*, J. N. A. Hooper and R. van Soest, Eds., pp. 1264–1266, Kluwer Academic, New York, NY, USA, 2002.

[25] M. Roux, P. Bouchet, J. P. Bourseau, C. Gaillard, R. Grandperrin, A. Guille et al., "L'environment bathyal au large de la nouvelle-calédonie: résultats preliminaries de la campagne CALSUB et consequences paléoécologiques," *Bulletin de la Societe Geologique de France*, vol. 162, pp. 675–685, 1991.

[26] X. H. Wang, J. Li, L. Qiao et al., "Structure and characteristics of giant spicules of the deep sea hexactinellid sponges of the genus *Monorhaphis* (Hexactinellida: Amphidiscosida: Monorhaphididae)," *Acta Zoologica Sinica*, vol. 53, pp. 557–569, 2007.

[27] A. Pisera, "Some aspects of silica deposition in lithistid demosponge desmas," *Microscopy Research and Technique*, vol. 62, no. 4, pp. 312–326, 2003.

[28] F. Sandford, "Physical and chemical analysis of the siliceous skeletons in six sponges of two groups (Demospongiae and Hexactinellida)," *Microscopy Research and Technique*, vol. 62, no. 4, pp. 336–355, 2003.

[29] M. J. Uriz, "Mineral skeletogenesis in sponges," *Canadian Journal of Zoology*, vol. 84, no. 2, pp. 322–356, 2006.

[30] M. J. Uriz, X. Turon, M. A. Becerro, and G. Agell, "Siliceous spicules and skeleton frameworks in sponges: origin, diversity, ultrastructural patterns, and biological functions," *Microscopy Research and Technique*, vol. 62, no. 4, pp. 279–299, 2003.

[31] T. L. Simpson, P. F. Langenbruch, and L. Scalera-Liaci, "Silica spicules and axial filaments of the marine sponge *Stelletta grubii* (Porifera, Demospongiae)," *Zoomorphology*, vol. 105, no. 6, pp. 375–382, 1985.

[32] W. E. G. Müller, K. Jochum, B. Stoll, and X. H. Wang, "Formation of giant spicule from quartz glass by the deep sea sponge *Monorhaphis*," *Chemistry of Materials*, vol. 20, no. 14, pp. 4703–4711, 2008.

[33] W. E. G. Müller, X. Wang, K. Kropf et al., "Bioorganic/inorganic hybrid composition of sponge spicules: matrix of the giant spicules and of the comitalia of the deep sea hexactinellid *Monorhaphis*," *Journal of Structural Biology*, vol. 161, no. 2, pp. 188–203, 2008.

[34] C. Lévi, J. L. Barton, C. Guillemet, E. Le Bras, and P. Lehuede, "A remarkably strong natural glassy rod: the anchoring spicule of the *Monorhaphis* sponge," *Journal of Materials Science Letters*, vol. 8, no. 3, pp. 337–339, 1989.

[35] G. Mayer, "Rigid biological systems as models for synthetic composites," *Science*, vol. 310, no. 5751, pp. 1144–1147, 2005.

[36] G. Mayer, R. Trejo, E. Lara-Curzio et al., "Lessons for new classes of inorganic/organic composites from the spicules and skeleton of the sea sponge *Euplectella aspergillum*," in *Materials Research Society Symposium Proceedings*, vol. 844, pp. 79–86, December 2005.

[37] X. Wang, U. Schloßmacher, K. P. Jochum et al., "Silica-protein composite layers of the giant basal spicules from *Monorhaphis* Basis for their mechanical stability," *Pure and Applied Chemistry*, vol. 82, no. 1, pp. 175–192, 2010.

[38] W. E. G. Müller, X. Wang, B. Sinha, M. Wiens, H. C. Schröder, and K. P. Jochum, "NanoSIMS: insights into the organization of the proteinaceous scaffold within hexactinellid sponge spicules," *ChemBioChem*, vol. 11, no. 8, pp. 1077–1082, 2010.

[39] S. Perović, I. Prokić, A. Krasko, I. M. Müller, and W. E. G. Müller, "Origin of neuronal-like receptors in metazoa: cloning of a metabotropic glutamate/GABA-like receptor from the marine sponge *Geodia cydonium*," *Cell and Tissue Research*, vol. 296, no. 2, pp. 395–404, 1999.

[40] W. E. G. Müller, K. Wendt, C. Geppert, M. Wiens, A. Reiber, and H. C. Schröder, "Novel photoreception system in sponges? unique transmission properties of the stalk spicules from the hexactinellid *Hyalonema sieboldi*," *Biosensors and Bioelectronics*, vol. 21, no. 7, pp. 1149–1155, 2006.

[41] C. L. Braun and S. N. Smirnov, "Why is water blue?" *Journal of Chemical Education*, vol. 70, pp. 612–617, 1993.

[42] H. C. Schröder, A. Krasko, D. Gundacker, S. P. Leys, I. M. Müller, and W. E. G. Müller, "Molecular and functional analysis of the (6–4) photolyase from the hexactinellid *Aphrocallistes vastus*," *Biochimica et Biophysica Acta*, vol. 1651, no. 1-2, pp. 41–49, 2003.

[43] W. E. G. Müller, M. Rothenberger, A. Boreiko, W. Tremel, A. Reiber, and H. C. Schröder, "Formation of siliceous spicules in the marine demosponge *Suberites domuncula*," *Cell and Tissue Research*, vol. 321, no. 2, pp. 285–297, 2005.

[44] W. E. G. Müller, S. I. Belikov, W. Tremel et al., "Siliceous spicules in marine demosponges (*example Suberites domuncula*)," *Micron*, vol. 37, no. 2, pp. 107–120, 2006.

[45] H. C. Schröder, A. Boreiko, M. Korzhev et al., "Co-expression and functional interaction of silicatein with galectin:matrix-guided formation of siliceous spicules in the marine demosponge *Suberites domuncula*," *Journal of Biological Chemistry*, vol. 281, no. 17, pp. 12001–12009, 2006.

[46] H. Ehrlich, R. Deutzmann, E. Brunner et al., "Mineralization of the meter-long biosilica structures of glass sponges is templated on hydroxylated collagen," *Nature Chemistry*, vol. 2, pp. 1084–1088, 2010.

[47] H. C. Schröder, S. Perović-Ottstadt, M. Rothenberger et al., "Silica transport in the demosponge *Suberites domuncula* fluorescence emission analysis using the PDMPO probe and cloning of a potential transporter," *Biochemical Journal*, vol. 381, pp. 665–673, 2004.

[48] W. E. G. Müller, "How was metazoan threshold crossed: the hypothetical urmetazoa," *Comparative Biochemistry and Physiology*, vol. 129, pp. 433–460, 2001.

Hindawi Publishing Corporation
Evidence-Based Complementary and Alternative Medicine
Volume 2011, Article ID 824962, 8 pages
doi:10.1155/2011/824962

Research Article

Modulation and Interaction of Immune-Associated Parameters with Antioxidant in the Immunocytes of Crab *Scylla paramamosain* Challenged with Lipopolysaccharides

Singaram Gopalakrishnan, Fang-Yi Chen, Harikrishnan Thilagam, Kun Qiao, Wan-Fang Xu, and Ke-Jian Wang

State Key Laboratory of Marine Environmental Science, College of Oceanography and Environmental Science, Xiamen University, Xiamen, Fujian 361005, China

Correspondence should be addressed to Ke-Jian Wang, wkjian@xmu.edu.cn

Received 14 January 2011; Accepted 16 April 2011

Invertebrates are dependent on cellular and humoral immune defences against microbial infection. *Scylla paramamosain* is an important commercial species, but the fundamental knowledge on its immune defense related to the antioxidant and immune-associated reactions is still lacking. The study was to differentiate the responses of immune-associated parameters of haemolymph components in *S. paramamosain* when challenged with bacterial lipopolysaccharides (LPSs). The immunostimulating effects of LPS in crab by triggering various immune parameters (phagocytosis, lysozyme, antibacterial activity, phenoloxidase, and the generation of superoxide and nitric oxide) were investigated. Results showed that the generation of free radicals, phenoloxidase, lysozyme and antibacterial activities was significantly increased through the exposure periods. Conversely, total hemocyte count and lysosomal membrane stability decreased significantly as the exposure period extended to 96 h. The relationship between the antioxidant enzymes and immune reactions due to LPS was highly significant. In addition, ROS production was positively correlated with antioxidant showing immediate response of antioxidant defense to the oxyradicals generated. Overall, the study indicated that nonspecific immune components in hemocytes of crab showed active response to the LPS stimulation, and their responses suggested that many immune-associated parameters could be modulated and interrelated with the influence of antioxidants in crustaceans.

1. Introduction

Hemocytes play a fundamental role in invertebrate innate immune system [1] and its functional role includes phagocytosis of nonself molecule [2, 3]. NADPH-oxidase driven "respiratory burst" is characteristic of invertebrate phagocytes [4, 5], and the phagocytic defences are highly dependent on generation of superoxide anion and production of other reactive oxyradical species during the respiratory burst. In aerobic organisms, reactive oxygen species (ROS) can be continually generated in response to both external and internal stimuli [6], and the reactive oxygen intermediates produced during the process are highly toxic to microbes and recognized to have an important role in immune defense and could play multiple functions in many biological processes [7]. On the other hand, excess production of ROS could cause deleterious effects on biomolecules, and hence need to be scavenge by the cellular antioxidant defense system.

Previous studies have reported ROS production, antioxidant enzyme defences and oxidative damage in invertebrates [8–10]. Importantly, recent research in crustaceans shows that ROS-dependent immunity is critical for host survival [11–13]; in addition, it has been reported that the antioxidant enzymes such as CAT and SOD could participate in crustaceans innate immune defense against immunostimulant [14–16]. Recently, a few studies have been undertaken on immunomodulation in crustaceans [17, 18]. However, little is known about the responses of these antioxidant enzymes (CAT and SOD) and their interaction with ROS production and other immune reaction in farmed crabs after the challenge of immune stimulant such as LPSs, which is an important component of Gram-negative bacterium.

Our previous studies reported that antioxidant enzyme *Sp*-CAT and *Sp*-SOD gene expression were induced towards LPSs challenge in crab [19, 20], and it has been well documented that these antioxidant activities or their gene expression increased parallelly to immunostimulant challenge or pathogen infections in crustaceans [14, 16]. Following our previous work, the present study was designed to evaluate the hemocyte immune functions when the crab challenged with LPSs. The immune parameters analyzed include total hemocyte counts, membrane stability, phagocytosis, superoxide anion generation, nitric oxide production, phenoloxidase, lysozyme, and antibacterial activity. In addition, the relationship between the immune parameters with the antioxidant enzymes such as SOD and CAT was also analyzed. This investigation will provide general information on the immunomodulation of many immune-associated parameters and their interrelation with the antioxidants generated in *S. paramamosain* due to LPSs challenge.

2. Materials and Methods

2.1. Collection and Maintenance of Mud Crab S. paramamosain. S. paramamosain (300 ± 50 g in weight) purchased from a local commercial crab farm in Xiamen, Fujian Province, China were acclimatized at 25 ± 2°C for one week before the experiments were carried out.

2.2. Lipopolysaccharide (LPSs) Injection. LPSs from *E. coli* (L2880, Sigma, USA) was prepared as described previously [19, 20]. To study the immune parameters, 36 crabs were injected with a dose of 0.1 and 0.5 mg kg^{-1} LPSs, respectively, and the other 18 individuals were injected with an equal volume of sterile saline solution as control treatments. The crabs for each group (3 crabs per group) were separately reared in individual container under the same culture conditions. Meanwhile, three normal crabs were reared in an individual tank as a normal control group. Sampling was performed at different time intervals (3, 6, 12, 24, 48, and 96 h) after LPSs challenge. Haemolymph collection and separation of hemocytes and preparation of serum and hemocyte lysate suspension were described in detail in our earlier study [19, 20].

2.3. Total Hemocyte Count. Total hemocytes in haemolymph were determined by using hemocytometer. A sample of 20 μL of diluted haemolymph was added to a hemocytometer and counted in microscope under 40x magnifications.

2.4. Superoxide Anion Production by Hemocytes. The generation of superoxide anion (O_2^-) by hemocytes of individual crab was quantified by measuring the reduction of nitroblue tetrazolium (NBT) following the procedure of Arumugam et al. [4]. Briefly, hemocyte suspension obtained from individual crab was incubated with 1 mg mL^{-1} of NBT at 22°C for 15 min. At the end of incubation, the reaction was stopped by adding 70% methanol and centrifuged (1500 rpm, 10 min, 4°C). Two mL of extraction fluid (6 mL KOH + 7 mL DMSO) were added to the pellet, to dissolve the insoluble formazan formed from NBT reduction. The samples were further centrifuged (8,000 rpm, 15 min, 4°C), and the O.D. was measured at 625 nm using spectrophotometer, against a reagent blank.

2.5. Nitrite Production. Nitric oxide (NO) production by crab hemocyte lysate was evaluated as described previously [21] by the Griess reaction, which quantifies the nitrite (NO_2^-) content of supernatants. Aliquots of HLS was incubated for 10 min in the dark with 1% (w/v) sulphanilamide in 5% H_3PO_4 and 0.1% (w/v) N-(1-naphthy)-ethylenediamine dihydrochloride. The O.D. of the samples was measured at 540 nm in a spectrophotometer against a suitable reagent blank. The molar concentration of nitrite in the samples was determined from a standard curve generated using known concentrations of sodium nitrite and was represented as μM nitrite.

2.6. Detection of Phenoloxidase (PO). Plasma PO was investigated following the procedure of Asokan et al. [22]. Briefly, plasma samples (100 μL) were preincubated with the same volume of L-dihydroxyphenyl-alanine (L-DOPA) or with TBS for 20 min at 22°C. All incubation experiments were performed in the dark. The O.D. of both control and experimental was measured at 460 nm. Plasma samples were estimated for protein content by Bradford [23].

2.7. In Vitro Phagocytosis. Suspensions of lyophilised *Saccharomyces cerevisia* were prepared in a sterile saline solution (0.15 M NaCl). The cells were washed three times with saline solution and suspended (10^6 cells mL^{-1}) in 0.45 M NaCl. Hemocyte monolayers were prepared on glass slides, allowing the cells to attach for 15–20 min at 20°C. The monolayers were carefully rinsed with TBS and incubated with suspension of *S. cerevisiae* for 1 h at room temperature. After incubation, the monolayers were carefully rinsed with TBS, fixed for 10 min in methanol, stained with Giemsa for 20 min, and rinsed with distilled water [24]. Then, the slides were mounted and examined under the light microscope to record the phagocytosis of the yeast by the hemocytes.

2.8. Lysozyme Assay. Serum lysozyme assay was determined by using modified turbidometric assay developed by Hutchinson and Manning [25]. Briefly, 0.3 mg mL^{-1} suspension of freeze-dried *Micrococcus lysodeikticus* was prepared in 0.05 M Na_2HPO_4 buffer immediately before use and the pH adjusted to 6.0 using 1.0 M NaOH. Ten microlitres of serum were added to 250 μL of the bacterial suspension and allowed to equilibrate at 28°C. Hen egg white lysozyme (HEWL), with a specified activity of 46 200 Units mg^{-1} was used as an external standard. The reduction in O.D. at 450 nm was determined over a 10 min period at 28°C in a microplate reader. The standard curve was constructed by using HEWL. The amount of lysozyme present in the serum was calculated from the standard.

2.9. Lysosomal Membrane Stability. Haemolymph (100 μL) sample pipetted into 0.5 mL centrifuge tube and aliquots

(10 μL) of 0.33% neutral red (Sigma) solution in TBS was added to each tube, and the tube was incubated for 1 h at 10°C. The tubes were then centrifuged for 5 min and washed twice in TBS. Aliquots (100 μL) of 1% acetic acid in 50% ethanol were added to all tubes. The tubes were covered with foil, incubated for 15 min at 20°C, and then read at 550 nm.

2.10. Antibacterial Activity of Haemolymph. Antibacterial activity of the haemolymph was investigated by measurement of growth inhibition by turbidometry [26]. Briefly, 100 μL of serum from both control and experimental groups were added to 96 wells plate. A log phase broth culture of *Aeromonas hydrophilla* suspension (100 μL) in NB was prepared ($\sim 10^8$ bacteria mL^{-1}; OD 600 = 0.509) and added to each of the experimental and control wells. Positive control with broth and bacteria were also maintained. Aliquots of 100 μL sterile TBS and 100 μL sterile broth were added to a well to act as a blank. The plate was incubated at room temperature and absorbance measured after 0, 1, and 24 h, respectively.

2.11. Statistical Analyses. The SPSS software version 11.0 for Windows was used for the statistical analysis. Results are reported as mean ± S.D. of three individuals per group per time point ($n = 3$). The data were processed by two-way analysis of variance (ANOVA) followed by Tukey's multiple-comparison post hoc test to identify statistical differences. Pearson correlation coefficient was used in the correlation matrix. Differences were statistically significant when $P < .05$ and .01.

3. Results and Discussion

3.1. Total Hemocyte Count (THC). THC plays an important role in regulating the physiological functions including haemolymph coagulation, phagocytosis, encapsulation, and confinement of invasive organisms. In addition, it also involves in hardening of exoskeleton, carbohydrate metabolism, and transport or storage of protein and amino acid [27, 28], and more important THC will reflect the health status of the host. There was no significant difference in THC for crabs challenged with LPSs up to 24 h with the respective control groups; however, after 48 h, the THC decreased significantly in both groups challenged with LPSs (Figure 1(A)). Similar decrease in THC due to nonself challenge in crustaceans was described previously, which led to the rapid reduction in the numbers of circulating hemocytes [29–31]. Variations in hemocyte numbers may result in different defense activities including hemocyte migration to the injection site and hemocyte lysis [32]. The loss of hemocytes from the haemolymph might result from degranulation, lysis, and the formation of cell clumps or nodules [30].

3.2. Phagocytosis. Phagocytosis is one of the most important parameter associated with immune reaction in both invertebrates and vertebrates [24, 33], which normally mobilizes lysosomes for the invading phagocytosed materials [34]. The effect of endotoxin on the phagocytic ability of the hemocytes of *S. paramamosain* is shown in Figure 1(B). After LPSs injection, the phagocytic ability of hemocytes of the crab was triggered significantly in both groups. Though increase in phagocytosis was observed after LPSs challenge in both groups, such increase in activity was significant only after 3 h and at 24 h after challenge. The similar result was observed in crustacean hemocytes as described previously, as the phagocytic activity triggered by LPSs was able to accelerate the cellular reactions [35].

3.3. Superoxide Anion Generation. Phagocytosis is also associated with the production of ROS namely superoxide anion generation (O_2^-) which is highly microbicidal [36]. Although ROS play an important role in host defense, over-induced and residual ROS may lead to cellular damage in the host. Consequently, phagocytosis becomes essential for cells exerting proper functions to rapidly eliminate excessive ROS, and thus maintain the homeostasis of organisms. This cellular reaction is immunologically vital and studied in crustaceans [18, 37]. Significant induction of superoxide generation observed following LPSs challenge in both groups indicated that the bacterial endotoxin can stimulate generation of superoxide in *S. paramamosain* even at a low dose (Figure 1(C)). These results were similar to those of Song and Hsieh [38] in which the relative *in vitro* intracellular O_2^- production was enhanced twice for *Penaeus monodon* hemocytes treated by heat killed *Vibrio vulnificus*, β-1,3-1,6-glucan and zymosan. However, whether such induction would help crabs survival for a longer time if the crabs suffered from a pathogen remains to be further elucidated.

3.4. Nitric Oxide Generation. LPSs injection also stimulated an increased level of nitric oxide, a molecule considered as precursor of a variety of reactive nitrogen intermediates. As shown in Figure 1(D), there was up to 3- and 4-fold increase in nitrite generation in the case of hemocytes collected from LPSs-injected crab, and this increase was significant during the exposure period. The maximum nitrite generation was observed after 12 h after injection of 0.5 mg of LPSs to crab. As observed in crayfish *Procambarus clarkii* by Yeh et al. [39], the hemocyte-derived NO increased by two-fold following LPSs challenge.

3.5. Phenoloxidase Activity. Phenoloxidase (PO) is an important humoral defense component in crustaceans, as it can be activated by nonself material. Its activation results in induction of a number of potent bioactive products which assist phagocytosis, cell adhesion, and formation of melanin deposits [40]. In general, PO is present in crab plasma in an inactive proPO state. Modulations in the levels of this important defense enzyme will have positively influence on the survivability of animals upon challenge with infectious pathogens. Earlier studies showed that LPSs induce prophenoloxidase activation and melanisation reactions [31, 41]. Significant induction of plasma PO due to endotoxin was observed when the crab was injected with LPSs, the levels of PO activity in the plasma were altered in both groups

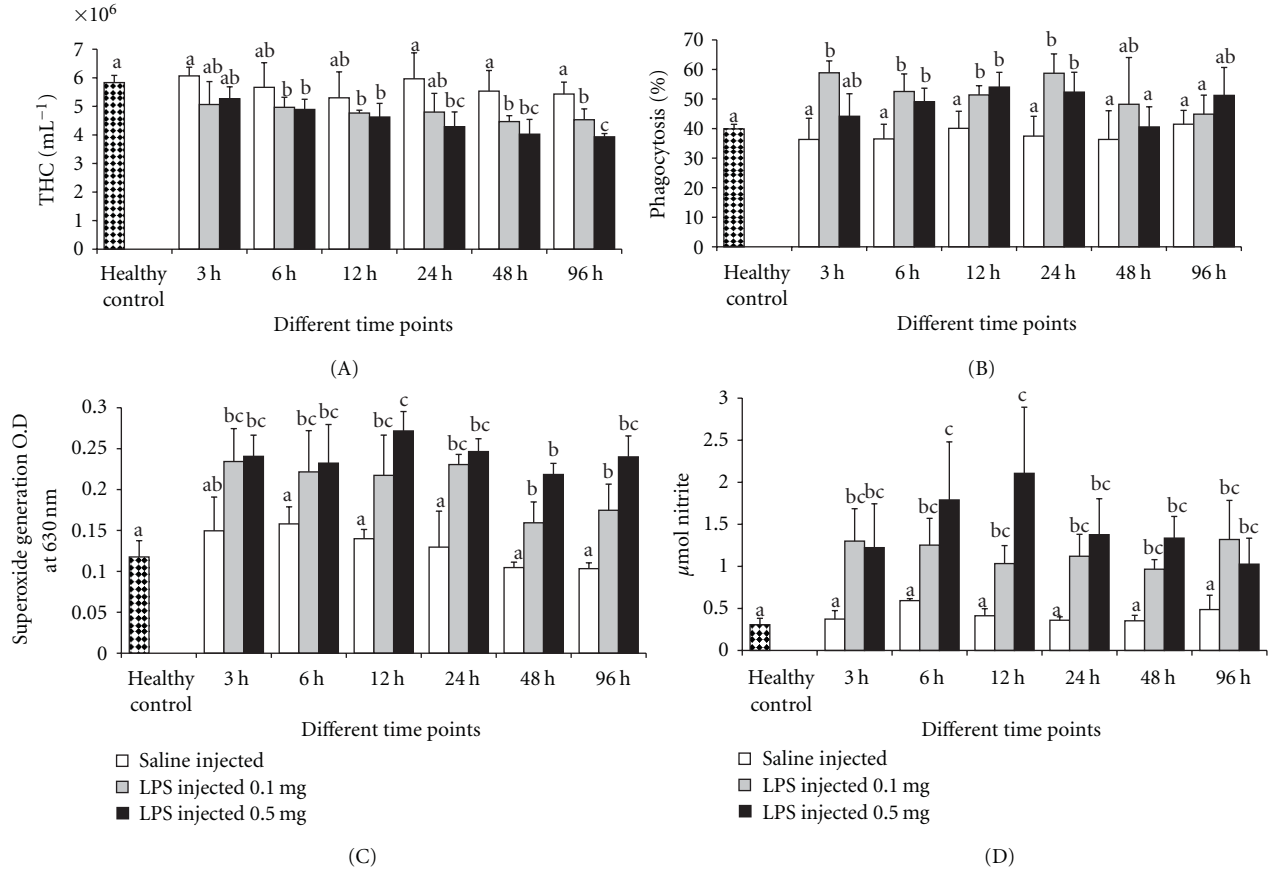

Figure 1: The effect of LPSs on (A) THC, (B) percent phagocytosis, (C) superoxide anion generation, and (D) nitric oxide. Data, representing the mean ± S.D. of 3 determinations using samples from different preparations, were analyzed using ANOVA followed by the Tukey post hoc test. The same letters (a, b, and c) indicate no significant difference between challenge groups at different exposure periods, whereas different letters indicate statistically significant differences ($P \leq .05$) between different exposure periods and groups.

of LPSs-injected crabs, indicating active responses of proPO to a nonself molecule (Figure 2(A)). Earlier research on crustaceans' species demonstrated that PO activation by glucans or other nonself molecules generates a range of immunoactive agents and activities, including peroxinectin and ROS [42].

3.6. Lysosomal Membrane Stability. Stability of lysosomal membranes in hemocytes of *S. paramamosain* following LPSs injection was evaluated by the neutral red retention assay. Membrane stability is a sensitive indicator of lipid membrane integrity in shellfish [43]. Membrane stability can be affected by both chemical and nonchemical stressors, suggesting that hemocyte viability itself is central to the response to both immunological challenge and other stressors [44]. The results of the present study indicated that lysosomal membrane stability was significantly reduced after 24 h of LPSs challenge when compared to respective control groups (Figure 2(B)). With the challenge time increased, the membrane stability became weaker and the figure clearly showed that LPSs affected the lysosomal membrane. The stability of hemocyte lysosomal membranes following LPSs injection decreased and well correlated with the decrease of THCs. The similar phenomenon was founded in other studies [45].

3.7. Lysozyme Activity. Lysozyme is a lysosomal enzyme secreted by the host during phagocytosis and has an important bacteriolytic characteristic in the immune system of crustaceans against pathogenic bacteria. In the study, significant induction of lysozyme activity was only observed after 12 and 24 h post challenge in both groups (Figure 2(C)). An increase in phagocytic activity observed in *S. paramamosain* after LPSs injection reflected the involvement of induced lysozyme activity. In addition, the lysozyme activity began to raise after 12 h LPSs injection, which suggests that the cellular reactions are in the first line of defense followed by an increase in antimicrobial activity [35]. The present results were consistent with previous study in which lysozyme activity in the shrimp *Fenneropenaeus chinensis* increased by nonself molecule [46].

3.8. Antibacterial Activity. Earlier reports revealed that crustacean haemolymph has the ability to inhibit bacterial

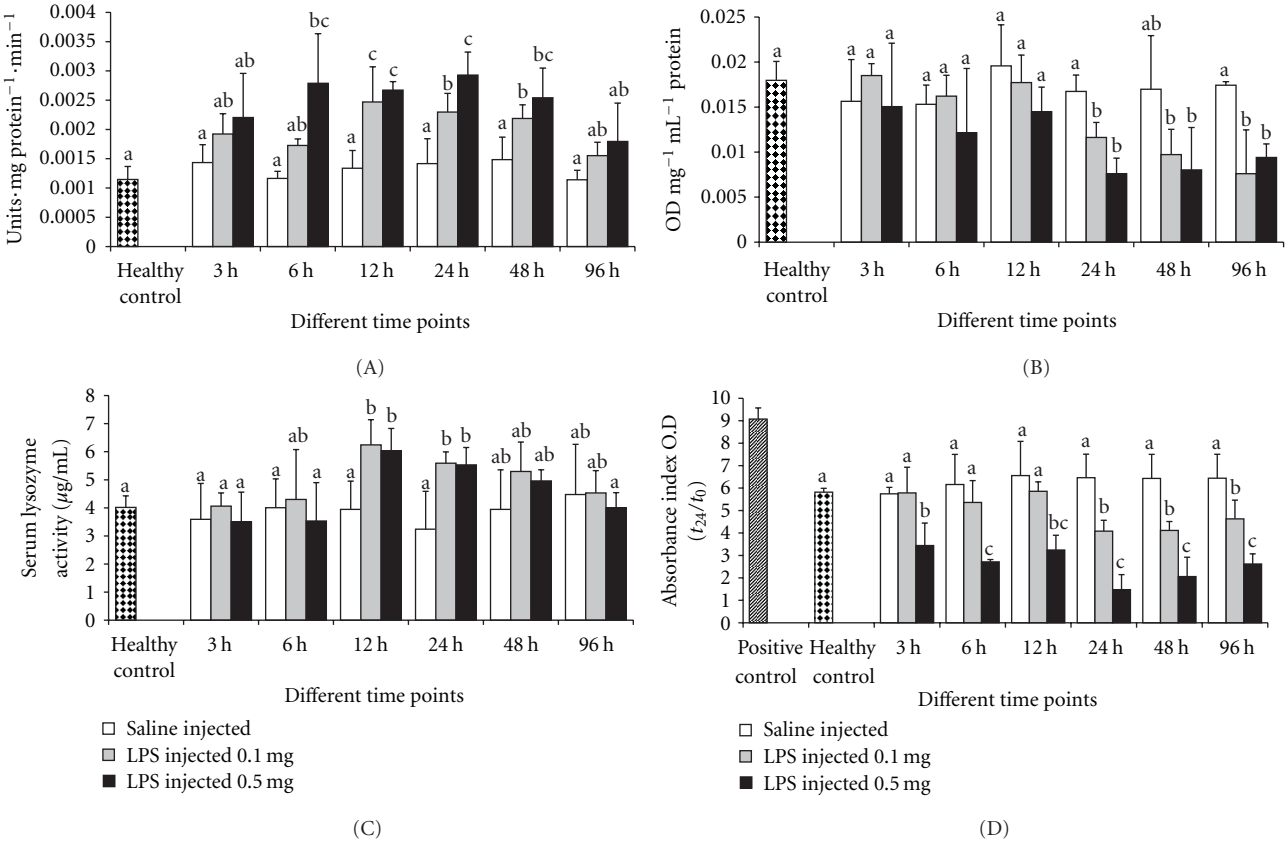

Figure 2: The effect of LPSs on (A) phenoloxidase, (B) membrane stability, (C) lysozyme activity, and (D) antibacterial activity. Data, representing the mean ± S.D. of 3 determinations using samples from different preparations, were analyzed using ANOVA followed by the Tukey post hoc test. The same letters (a, b, and c) indicate no significant difference between challenge groups at different exposure periods, whereas different letters indicate statistically significant differences ($P \leq .05$) between different exposure periods and groups.

growth [39, 47, 48]. Yeh et al. [39] reported that hemocyte-derived NO promotes bacterial adhesion to hemocytes and increase the bactericidal activity of hemocytes. Bacterial growth was significantly slower in serum of LPSs challenged crab, indicating the antibacterial activity in serum was triggered due to endotoxin (Figure 2(D)). It was noted that the results were accompanying to the decrease in lysosomal membrane stability after 24 h LPSs injection in both groups. Similar findings were observed for the Chinese shrimp hemocytes as a response to injection with *Vibrio anguillarum* [49]. However, the high dose of LPSs injection suppresses the bacterial growth in all the exposure periods.

3.9. Correlation Analyses and Summary. In earlier study, we reported that the gene expression of antioxidants such as SOD and CAT and their activities were induced significantly when the crab were challenged with LPSs [19, 20]; correspondingly, it was found in the present study that there was a relationship between the immune associated parameters and the antioxidants (Table 1). The correlation between the antioxidant and immune parameters such as phenoloxidase, antibacterial activity, phagocytosis, superoxide generation, and nitric oxide production was much high. In higher invertebrate species like arthropods and molluscs, NADPH-oxidase and phenoloxidase are two redox-catalyzing systems which play important physiological roles including immunological functions [4, 50, 51]. Though these two enzymes play different roles, the common function is the generation of superoxide radicals (NADPH-oxidase) and by lesser extent in producing phenoloxidase.

Moreover, these two enzymes remain in an inactive state in the cytosol and are activated by various stimulants [5, 52]. Upon stimulation, phenoloxidase is activated, catalyzes the melanin synthesis, and deposits near the pathogen, and this cascade reaction is characterized by numerous redox intermediates which generate the superoxide [53, 54]. On the other hand, during phagocytosis, there will be an increase in production of ROS as a positive immune reaction by the host to invade the pathogen. It has been reported that nonself induced nitric oxide generation involving nitric oxide synthase in crustacean hemocytes and the generation of nitric oxide during phagocytosis as a cellular immune reaction [18]. In the immune system of higher invertebrates like arthropods and molluscs, lysozyme is one of the most important bacteriolytic agents against corresponding species of Gram-positive and Gram-negative bacteria, and during phagocytosis, the hemocytes produce lysozyme which actively participate in the inactivation of invading pathogens. In addition, the breakage of membrane of hemocyte might have increased acid phosphates activity which contributed

Table 1: Correlation matrix for measured parameters in *Scylla paramamosain* challenged with LPSs.

Correlation Matrix												
	LMS	PO	LY	AB	PHA	SO_2^-	NO	THC	HLS-SOD	HLS-CAT	SERUM-SOD	SERUM-CAT
LMS	1.000	−0.483*	−0.293	0.807**	−0.202	−0.374	−0.453	0.684**	−0.326	−0.441	0.192	0.265
PO		1.000	0.565*	−0.799**	0.606**	0.787**	0.799**	−0.601**	0.652**	0.671**	0.249	0.298
LY			1.000	−0.313	0.540*	0.399	0.444	−0.549∗	0.069	0.432	0.000	0.066
AB				1.000	−0.416	−0.733**	−0.724**	0.724**	−0.673**	−0.671**	−0.144	−0.117
PHA					1.000	0.769**	0.693**	−0.520*	0.433	0.661**	0.206	0.381
SO_2^-						1.000	0.863**	−0.559*	0.725**	0.818**	0.394	0.561*
NO							1.000	−0.590**	0.709**	0.726**	0.343	0.304
THC								1.000	−0.446	−0.632**	0.125	−0.006
HLS-SOD									1.000	0.742**	0.690**	0.638**
HLS-CAT										1.000	0.472*	0.639**
SERUM-SOD											1.000	0.772**
SERUM-CAT												1.000

**Correlation is significant at the 0.01 level (2-tailed); *Correlation is significant at the 0.05 level (2-tailed).
LMS: lysosomal membrane stability, PO: phenoloxidase, LY: lysozyme activity, AB: antibacterial activity, PHA: phagocytosis, SO_2^-: superoxide anion generation, NO: nitric oxide, THC: total hemocyte count, HLS: hemocyte lysate solution, SOD: superoxide dismutase, and CAT: catalase.

in lysis and eventual decomposition of pathogens and by the evident of antibacterial activity shown to increase in the present study. All these cellular defense reactions were vital in immune response and have been well characterized in invertebrates.

The correlation between antioxidant enzyme and oxyradicals produced were high in the present study. Increase in these oxyradicals can cause direct or indirect damage to the membrane and DNA. SOD is the first enzyme to deal with oxyradicals by accelerating the dismutation of superoxide generated, and CAT is a peroxisomal haemoprotein which catalyses the removal of H_2O_2 formed during the reaction catalyzed by SOD. ROS, thus, generated may modulate the levels of SOD, which leads to alteration of CAT activity as a chain reaction. In this sense, the antioxidants interact with excess oxyradicals produced in aerobic animals. Hence, the net result of these antioxidant enzymes provides a postphagocytosis self-protection in the host. Correlation between the free radicals generated in hemocytes and the antioxidants produced to counteract the free radicals were significantly high indicating that the antioxidant enzymes (SOD and CAT) detoxify the free radicals generated and these enzymes might act as important acute defense molecules under stress of immunostimulant challenge or microbial infection.

The present study showed that LPSs could modulate the immune parameters of the crab, and the response was quick, time dependent/dose dependent. The immune parameters such as phagocytosis, phenoloxidase, lysozyme, and antibacterial activity were all significantly induced after LPSs after injection indicating that crabs respond positively to LPSs stimulation. The overall results indicated that nonspecific components actively responded to the bacterial endotoxic stimulation and their responses implied that the immune-related parameters were involved in the immunomodulation of crustacean's immune system. Furthermore, the correlation existing between the immune associated parameters and antioxidants strongly supports our previous work that the antioxidant enzymes play an important role in ROS detoxification in host-microbe interactions. Future work will be focus on evaluating whether the induced antioxidant and immune-associated reactions provoked by LPSs will together enhance the capability of *S. paramamosain* resistant to an infection caused by live pathogenic bacteria.

Acknowledgments

This work was supported by a grant (2007AA091406) from the National High Technology Research and Development Program of China (863 Program), by program for Changjiang Scholars and Innovative Research Team in University (PCSIRT, IRT0941), and the Minjiang Scholar Program to K.-J. Wang (2009). S. Gopalakrishnan and F.-Y. Chen contributed equally to this work.

References

[1] T. Koshiba, T. Hashii, and S. Kawabata, "A structural perspective on the interaction between lipopolysaccharide and factor C, a receptor involved in recognition of gram-negative bacteria," *Journal of Biological Chemistry*, vol. 282, no. 6, pp. 3962–3967, 2007.

[2] G. G. Martin, D. Poole, C. Poole et al., "Clearance of bacteria injected into the hemolymph of the penaeid shrimp, *Sicyonia ingentis*," *Journal of Invertebrate Pathology*, vol. 62, no. 3, pp. 308–315, 1993.

[3] S. Iwanaga and B. L. Lee, "Recent advances in the innate immunity of invertebrate animals," *Journal of Biochemistry and Molecular Biology*, vol. 38, no. 2, pp. 128–150, 2005.

[4] M. Arumugam, B. Romestand, J. Torreilles, and P. Roch, "*In vitro* production of superoxide and nitric oxide (as nitrite and nitrate) by *Mytilus galloprovincialis* haemocytes upon incubation with PMA or laminarin or during yeast phagocytosis," *European Journal of Cell Biology*, vol. 79, no. 7, pp. 513–519, 2000.

[5] S. Y. Lee and K. Söderhäll, "Early events in crustacean innate immunity," *Fish and Shellfish Immunology*, vol. 12, no. 5, pp. 421–437, 2002.

[6] J. M. Mates, C. Perez-Gomez, and I. N. de Castro, "Antioxidant enzymes and human diseases," *Clinical Biochemistry*, vol. 32, no. 8, pp. 595–603, 1999.

[7] J. D. Lambeth, "NOX enzymes and the biology of reactive oxygen," *Nature Reviews Immunology*, vol. 4, no. 3, pp. 181–189, 2004.

[8] S. Arun, P. Krishnamoorthy, and P. Subramanian, "Properties of glutathione peroxidase from the hepatopancreas of freshwater prawn *Macrobrachium malcolmsonii*," *International Journal of Biochemistry and Cell Biology*, vol. 31, no. 6, pp. 725–732, 1999.

[9] R. T. Di Giulio, W. H. Benson, B. M. Sanders, and P. A. Van Veld, "Biochemical mechanisms: metabolism, adaptation and toxicity," in *Fundamentals of Aquatic Toxicology, Effects, Environmental Fate, and Risk Assessment*, G. Rand, Ed., pp. 523–561, Taylor and Francis, London, UK, 1995.

[10] A. D. Correia, M. H. Costa, O. J. Luis, and D. R. Livingstone, "Age-related changes in antioxidant enzyme activities, fatty acid composition and lipid peroxidation in whole body *Gammarus locusta* (Crustacea: Amphipoda)," *Journal of Experimental Marine Biology and Ecology*, vol. 289, no. 1, pp. 83–101, 2003.

[11] E. M. Ha, C. T. Oh, Y. S. Bae, and W. J. Lee, "A direct role for dual oxidase in Drosophila gut immunity," *Science*, vol. 310, no. 5749, pp. 847–850, 2005.

[12] E. M. Ha, C. T. Oh, J. H. Ryu et al., "An antioxidant system required for host protection against gut infection in Drosophila," *Developmental Cell*, vol. 8, no. 1, pp. 125–132, 2005.

[13] U. E. Zelck, B. Janje, and O. Schneider, "Superoxide dismutase expression and H_2O_2 production by hemocytes of the trematode intermediate host *Lymnaea stagnalis* (Gastropoda)," *Developmental and Comparative Immunology*, vol. 29, no. 4, pp. 305–314, 2005.

[14] A. I. Campa-Cordova, N. Y. Hernandez-Saavedra, R. De Philippis, and F. Ascencio, "Generation of superoxide anion and SOD activity in haemocytes and muscle of American white shrimp (*Litopenaeus vannamei*) as a response to beta-glucan and sulphated polysaccharide," *Fish and Shellfish Immunology*, vol. 12, no. 4, pp. 353–366, 2002.

[15] S. Mathew, K. A. Kumar, R. Anandan, P. G. Viswanathan Nair, and K. Devadasan, "Changes in tissue defence system in white spot syndrome virus (WSSV) infected Penaeus monodon," *Comparative Biochemistry and Physiology*, vol. 145, no. 3, pp. 315–320, 2007.

[16] P. F. Ji, C. L. Yao, and Z. Y. Wang, "Immune response and gene expression in shrimp (*Litopenaeus vannamei*) hemocytes and hepatopancreas against some pathogen-associated molecular patterns," *Fish and Shellfish Immunology*, vol. 27, no. 4, pp. 563–570, 2009.

[17] V. J. Smith, J. H. Brown, and C. Hauton, "Immunostimulation in crustaceans: does it really protect against infection?" *Fish and Shellfish Immunology*, vol. 15, no. 1, pp. 71–90, 2003.

[18] R. Thiagarajan, M. Arumugam, and P. Mullainadhan, "Agglutinin-mediated phagocytosis-associated generation of superoxide anion and nitric oxide by the hemocytes of the giant freshwater prawn *Macrobrachium rosenbergii*," *Fish and Shellfish Immunology*, vol. 24, no. 3, pp. 337–345, 2008.

[19] F. Y. Chen, H. P. Liu, J. Bo, H. L. Ren, and K. J. Wang, "Identification of genes differentially expressed in hemocytes of *Scylla paramamosain* in response to lipopolysaccharide," *Fish and Shellfish Immunology*, vol. 28, no. 1, pp. 167–177, 2010.

[20] H. P. Liu, F. Y. Chen, S. Gopalakrishnan, K. Qiao, J. Bo, and K. J. Wang, "Antioxidant enzymes from the crab *Scylla paramamosain*: gene cloning and gene/protein expression profiles against LPS challenge," *Fish and Shellfish Immunology*, vol. 28, no. 5-6, pp. 862–871, 2010.

[21] C. L. Green, A. D. Wagner, J. Glogowski, L. P. Skipper, S. J. Wishnok, and S. R. Tannenbaum, "Analysis of nitrate, nitrite and [15N] nitrate in biological fluids," *Analytical Biochemistry*, vol. 126, no. 1, pp. 131–138, 1982.

[22] R. Asokan, M. Arumugam, and P. Mullainadhan, "Activation of prophenoloxidase in the plasma and haemocytes of the marine mussel *Perna viridis* Linnaeus," *Developmental and Comparative Immunology*, vol. 21, no. 1, pp. 1–12, 1997.

[23] M. M. Bradford, "A rapid and sensitive method for the quantitation of microgram quantities of protein utilizing the principle of protein dye binding," *Analytical Biochemistry*, vol. 72, no. 1-2, pp. 248–254, 1976.

[24] R. Thiagarajan, S. Gopalakrishnan, and H. Thilagam, "Immunomodulation the marine green mussel *Perna viridis* exposed to sub-lethal concentrations of Cu and Hg," *Archives of Environmental Contamination and Toxicology*, vol. 51, no. 3, pp. 392–399, 2006.

[25] T. H. Hutchinson and M. J. Manning, "Seasonal trends in serum lysozyme activity and total protein concentration in dab (*Limanda limanda* L.) sampled from Lyme Bay, U.K," *Fish and Shellfish Immunology*, vol. 6, no. 7, pp. 473–482, 1996.

[26] E. C. Wootton, E. A. Dyrynda, R. K. Pipe, and N. A. Ratcliffe, "Comparisons of PAH-induced immunomodulation in three bivalve molluscs," *Aquatic Toxicology*, vol. 65, no. 1, pp. 13–25, 2003.

[27] G. G. Martin, J. E. Hose, S. Omori, C. Chong, T. Hoodbhoy, and N. McKrell, "Localization and roles of coagulogen and transglutaminase in hemolymph coagulation in decapod crustaceans," *Comparative Biochemistry and Physiology* , vol. 100, no. 3, pp. 517–522, 1991.

[28] C. B. T. Van de Braak, M. H. A. Botterblom, W. Liu, N. Taverne, W. P. W. van de Knaap, and J. H. W. M. Rombout, "The role of the haematopoietic tissue in haemocyte production and maturation in the black tiger shrimp (*Penaeus monodon*)," *Fish and Shellfish Immunology*, vol. 12, no. 3, pp. 253–272, 2002.

[29] S. Lorenzon, S. de Guarrini, V. J. Smith, and E. A. Ferrero, "Effects of LPS injection on circulating haemocytes in crustaceans in vivo," *Fish and Shellfish Immunology*, vol. 9, no. 1, pp. 31–50, 1999.

[30] V. J. Smith and K. Söderhäll, "Induction of degranulation and lysis of haemocytes in the freshwater crayfish, *Astacus astacus* by components of the prophenoloxidase activating system in vitro," *Cell and Tissue Research*, vol. 233, no. 2, pp. 295–303, 1983.

[31] V. J. Smith, K. Söderhäll, and M. Hamilton, "β 1,3-Glucan induced cellular defence reactions in the shore crab, Carcinus maenas," *Comparative Biochemistry and Physiology*, vol. 77, no. 4, pp. 635–639, 1984.

[32] S. A. Omori, G. G. Martin, and J. E. Hose, "Morphology of hemocyte lysis and clotting in the ridgeback prawn, *Sicyonia*

ingentis," *Cell And Tissue Research*, vol. 255, no. 1, pp. 117–123, 1989.

[33] W. Cheng, F. M. Juang, and J. C. Chen, "The immune response of Taiwan abalone *Haliotis diversicolor supertexta* and its susceptibility to *Vibrio parahaemolyticus* at different salinity levels," *Fish and Shellfish Immunology*, vol. 16, no. 3, pp. 295–306, 2004.

[34] C. J. Bayne, "Phagocytosis and non-self recognition in invertebrates: phagocytosis appears to be an ancient line of defense," *BioScience*, vol. 40, pp. 723–731, 1990.

[35] D. Wittwer, C. Weise, P. Götz, and A. Wiesner, "LPS (Lipopolysaccharide)-activated immune responses in a hemocyte cell line from *Estigmene acraea* (Lepidoptera)," *Developmental and Comparative Immunology*, vol. 21, no. 4, pp. 323–336, 1997.

[36] A. I. Campa-Córdova, N. Y. Hernández-Saavedra, and F. Ascencio, "Superoxide dismutase as modulator of immune function in American white shrimp (*Litopenaeus vannamei*)," *Comparative Biochemistry and Physiology*, vol. 133, no. 4, pp. 557–565, 2002.

[37] M. H. Lee and S. Y. Shiau, "Dietary vitamin C and its derivatives affect immune responses in grass shrimp, *Penaeus monodon*," *Fish and Shellfish Immunology*, vol. 12, no. 2, pp. 119–129, 2002.

[38] Y. L. Song and Y. T. Hsieh, "Immunostimulation of tiger shrimp (*Penaeus monodon*) hemocytes for generation of microbicidal substances: analysis of reactive oxygen species," *Developmental and Comparative Immunology*, vol. 18, no. 3, pp. 201–209, 1994.

[39] F. C. Yeh, S. H. Wu, C. Y. Lai, and C. Y. Lee, "Demonstration of nitric oxide synthase activity in crustacean hemocytes and anti-microbial activity of hemocyte-derived nitric oxide," *Comparative Biochemistry and Physiology*, vol. 144, no. 1, pp. 11–17, 2006.

[40] K. Söderhäll and L. Cerenius, "Role of the prophenoloxidase-activating system in invertebrate immunity," *Current Opinion in Immunology*, vol. 10, no. 1, pp. 23–28, 1998.

[41] M. Ashida and K. Söderhäll, "The prophenoloxidase activating system in crayfish," *Comparative Biochemistry and Physiology*, vol. 77, no. 1, pp. 21–26, 1984.

[42] T. Holmblad and K. Söderhäll, "Cell adhesion molecules and antioxidative enzymes in a crustacean, possible role in immunity," *Aquaculture*, vol. 172, no. 1-2, pp. 111–123, 1999.

[43] D. M. Lowe, V. U. Fossato, and M. H. Depledge, "Contaminant-induced lysosomal membrane damage in blood cells of mussels *Mytilus galloprovincialis* from the Venice Lagoon: an in vitro study," *Marine Ecology Progress Series*, vol. 129, no. 1–3, pp. 189–196, 1995.

[44] T. S. Galloway and M. H. Depledge, "Immunotoxicity in invertebrates: measurement and ecotoxicological relevance," *Ecotoxicology*, vol. 10, no. 1, pp. 5–23, 2001.

[45] P. K. Sahoo, B. R. Pillai, J. Mohanty, J. Kumari, S. Mohanty, and B. K. Mishra, "In vivo humoral and cellular reactions, and fate of injected bacteria *Aeromonas hydrophila* in freshwater prawn *Macrobrachium rosenbergii*," *Fish and Shellfish Immunology*, vol. 23, no. 2, pp. 327–340, 2007.

[46] C. L. Yao, C. G. Wu, J. H. Xiang, F. Li, Z. Y. Wang, and X. Han, "The lysosome and lysozyme response in Chinese shrimp *Fenneropenaeus chinensis* to Vibrio anguillarum and laminarin stimulation," *Journal of Experimental Marine Biology and Ecology*, vol. 363, no. 1-2, pp. 124–129, 2008.

[47] D. Destoumieux, M. Muñoz, C. Cosseau et al., "Penaeidins, antimicrobial peptides with chitin-binding activity, are produced and stored in shrimp granulocytes and released after microbial challenge," *Journal of Cell Science*, vol. 113, no. 3, pp. 461–469, 2000.

[48] M. Muñoz, F. Vandenbulcke, D. Saulnier, and E. Bachère, "Expression and distribution of penaeidin antimicrobial peptides are regulated by haemocyte reactions in microbial challenged shrimp," *European Journal of Biochemistry*, vol. 269, no. 11, pp. 2678–2689, 2002.

[49] Z. Zhao, Z. Yin, S. Weng et al., "Profiling of differentially expressed genes in hepatopancreas of white spot syndrome virus-resistant shrimp (*Litopenaeus vannamei*) by suppression subtractive hybridisation," *Fish and Shellfish Immunology*, vol. 22, no. 5, pp. 520–534, 2007.

[50] H. Peltroche-Llacsahuanga, N. Schnitzler, S. Schmidt, K. Tintelnot, R. Lütticken, and G. Haase, "Phagocytosis, oxidative burst, and killing of Candida dubliniensis and *Candida albicans* by human neutrophils," *FEMS Microbiology Letters*, vol. 191, no. 1, pp. 151–155, 2000.

[51] E. P. Reeves, H. Lu, H. L. Jacobs et al., "Killing activity of neutrophils is mediated through activation of proteases by K1 flux," *Nature*, vol. 416, no. 6878, pp. 291–297, 2002.

[52] K. Söderhäll and V. J. Smith, "The prophenoloxidase activating cascade as a recognition and defence system in arthropod," in *Hemocytic and Humoral Immunity in Arthropods*, A. P. Gupta, Ed., pp. 251–285, Wiley Interscience Publication, New York, NY, USA, 1986.

[53] A. J. Nappi, E. Vass, F. Frey, and Y. Carton, "Superoxide anion generation in Drosophila during melanotic encapsulation of parasites," *European Journal of Cell Biology*, vol. 68, no. 4, pp. 450–456, 1995.

[54] J. L. Freeman and J. D. Lambeth, "NADPH oxidase activity is independent of $p47^{phox}$ in vitro," *Journal of Biological Chemistry*, vol. 271, no. 37, pp. 22578–22582, 1996.

Hindawi Publishing Corporation
Evidence-Based Complementary and Alternative Medicine
Volume 2011, Article ID 613629, 10 pages
doi:10.1155/2011/613629

Research Article

Polymorphism and Balancing Selection of MHC Class II DAB Gene in 7 Selective Flounder (*Paralichthys olivaceus*) Families

Min Du,[1,2,3] Song-lin Chen,[1] You Liang,[1] Lei Wang,[1] Feng-tao Gao,[1] Yang Liu,[1] and Xiao-Lin Liao[1]

[1] *Key Lab for Sustainable Utilization of Marine Fisheries Resources, Ministry of Agriculture, Yellow Sea Fisheries Research Institute, Chinese Academy of Fishery Sciences, Nanjing Road 106, Qingdao 266071, China*
[2] *College of Aqua-life Science and Technology, Shanghai Ocean University, Shanghai 200090, China*
[3] *Honghe University, Yunnan Province, Mengzi, 661100, China*

Correspondence should be addressed to Song-lin Chen, chensl@ysfri.ac.cn

Received 15 January 2011; Revised 28 April 2011; Accepted 30 May 2011

In order to determine the genetic variation of the MHC class IIB exon2 allele in the offspring, 700 fry from seven families of Japanese flounder challenged with *V. anguillarum* were studied, and different mortality rates were found in those families. Five to ten surviving and dead fry from each of the seven families were selected to study the MHC class II B exon2 gene with PCR and a direct sequencing method. One hundred and sixteen different exon2 sequences were found and 116 different alleles were identified, while a minimum of four loci were revealed in the MHC class II B exon2 gene. The ratio (d_N/d_S) of nonsynonymous substitution (d_N) to synonymous substitutions (d_S) in the peptide-binding region (PBR) of the MHC class IIB gene was 6.234, which indicated that balancing selection is acting on the MHC class IIB genes. The MHC IIB alleles were thus being passed on to their progeny. Some alleles were significantly more frequent in surviving than dead individuals. All together our data suggested that the alleles *Paol-DAB* 4301*, *Paol-DAB* 4601*, *Paol-DAB* 4302*, *Paol-DAB* 3803*, and *Paol-DAB* 4101* were associated with resistance to *V. anguillarum* in flounder.

1. Introduction

Genes of the major histocompatibility complex (MHC) are characterized by extremely high levels of polymorphism in cell surface glycoprotein class I and II molecules. They play a primary role in both innate and adaptive immunity by presenting self- and foreign peptides to T cells ($CD4^+$ T cells or $CD8^+$ T cells) [1] in vertebrate organisms, and subsequently initiate a specific immune response [2].

Unlike the case in mammals, MHC class I and class II regions in teleost fish are situated on different linkage groups and therefore do not form a complex [3–5]. MHC genes in fish have received considerable attention since the first teleost fish MHC gene fragments were isolated from carp (*Cyprinus carpio L.*) by Hashimoto et al. [6]. MHC class I and class II both contain a peptide-binding region (PBR). The exon2 sequence of the MHC class II B gene is known to cover the majority of the polymorphism and has been considered a candidate molecular marker for an association between these alleles and resistance/susceptibility to various diseases [7]. There are reports of polymorphism of exon2 of MHC class II B gene in a number of vertebrates, including mammals [8, 9], reptiles [10, 11], amphibians [12], and fish [13–15].

It is believed that balancing selection maintains this large variation, which includes frequency-dependent selection, over dominant selection, and positive selection across habitats, but the exact nature of the selection process continues to be a topic of debate [16–18].

Japanese flounder (*Paralichthys olivaceus*) is an economically important marine fish in China, and a few studies have been reported on the MHC class II B gene [15, 19, 20]. For example, Srisapoome et al. [19] reported the expression level of MHC II B cDNA. Zhang et al. [20] studied polymorphism in the flounder MHC class II B gene. Xu et al. [15] demonstrated an association between MHC class II B exon2 and resistance to *V. anguillarum* in 60 families of Japanese flounder, and thus the alleles associated with resistance and susceptibility to *V. anguillarum* were discovered.

In order to breed a new flounder strain with enhanced disease resistance and growth rate, selective breeding has

been carrying out, since 2002. Three basic populations (i.e., Japanese (JS), Resistance (RS), and Yellow Sea (YS) populations) were developed in 2002 and 2003 [21]. JS were imported from Japan in 2003; RS were obtained from natural selection and artificial challenge with *Vibrio anguillarum*; YS were captured from the Yellow Sea in 2003. These were called "generation 0" (G_0). A little more than three years later, in March, 2007, the fry of the three basic populations that had become sexually mature were selected to mate and produced 63 full-sib families or half-sib families and were designated "generation 1" (G_1). After artificial challenge with *Vibrio anguillarum*, the survival percentage ratios (Mean ± S.D. (%)) of the families studied (family 0751, family 0768, family 0743, family 0750, and family 0719) were 54.13 ± 1.23, 62.08 ± 22.52, 7.27 ± 3.57, 64.05 ± 0.74, and 30.86 ± 7.22, respectively; the survival ratio of the resistance families was not available. Two years later, in March, 2009, sexually mature fish were selected for mate (generation 2 (G_2)) and artificial challenge were performed, with the result that the survival ratios of the families were different.

The fry of the next generation exhibited clear genetic information within each family. In this study, their offspring were infected with *V. anguillarum* and their survival rate was recorded. We amplified and directly sequenced MHC class II B exon2 in order to estimate the number of MHC class II loci, assess the MHC polymorphism of selected individuals, and test for balancing selection, as well as to discover the pattern of the inheritance of the allele in seven families of Japanese flounder.

2. Materials and Methods

2.1. Experimental Design. According to a previous study [15], the fish from family 0768 and family 0751 had the *Paol-DAB*4301* allele, while the fish from the 0743, R7, 0750, and 0719 families did not. The *Paol-DAB*4301* allele in flounder was associated with resistance to *V. anguillarum*. The survival ratio of families 0768 and 0751 was higher than that of the 0743, R7, 0750, and 0719 families. Males and females from G_1 in these six families were selected as parental fish to propagate the offspring in G_2 (Figure 1). The brood fish in G_0 were involved in our previous study [21]. Families 92, 102, and 5 were offspring of self-cross of families 0751, 0768, and 0750, respectively, (Figure 1). Family 101 had one dam from family 0743 crossed with one sire from family 0751. Family 41 had a dam from family R7 crossed with one sire from family 0768. Family 75 were the offspring of one dam from family 0750 and one sire from family 0743, and family 104 were the offspring of one dam from family 0719 and one sire from family 0768. A total of 7 full-sib families of Japanese flounder were established, as reported by Chen et al. [21] and were reared at the fish farming factory at Haiyang city, Shandong province. The fry were fed a commercial diet and were kept in separate tanks.

2.2. Challenge Experiment. Approximately 100 individuals from each family and a total of 700 offspring from 7 full-sib families were used in the challenge experiment. The body weight of the fish analyzed was 12–17 g. The test fish of each family were kept in a separate tank at the same farming factory under flow-through conditions with a fresh water supply at 20 ± 0.5°C and were fed twice daily. The *V. anguillarum* isolated by our laboratory was used in the challenge test and prechallenge experiment, and the median lethal concentration was determined according to Xu et al. [15]. Dead fish were recorded and collected every day. The challenge experiment was terminated 14 days after infection. The survival ratio (Mean ± S.D. (%)) of families 5, 41, 102, 75, 101, 92, and 104 was 78.3 ± 7.43, 32.2 ± 3.61, 31.9 ± 22.36, 37.9 ± 9.44, 33.4 ± 3.7, 21.8 ± 11.97, and 55.6 ± 1.83, respectively. In addition to the daily recording of the fish that had died, fin clippings were taken from all fish and were stored individually in absolute ethanol.

Table 1: Numbers of the dead/surviving individuals when infected with the *V. anguillarum* were selected from seven families of Japanese flounder.

Family	Individuals per family		Total
	Dead	Surviving	
Family 101	20	20	40
Family 104	20	20	40
Family 5	10	10	20
Family 41	10	10	20
Family 75	10	10	20
Family 92	10	10	20
Family 102	10	10	20
Total	90	90	180

2.3. Sampling and DNA Isolation. Fin samples from the top 10 (families 5, 41, 75, 92, and 102, resp.) or 20 (families 101, 104, resp.) individuals to die and the top 10 (families 5, 41, 75, 92, and 102, resp.) or 20 (families 101 and 104, resp.) surviving individuals from each family were collected from the challenge trials (Table 1). Table 1 shows the number of the dead fish. Surviving individuals were selected from the seven families of Japanese flounder in the study. Genomic DNA was extracted from the dorsal or caudal fin tissue of the dead and surviving fry via a modified phenol-chloroform method [22]. The integrity of the DNA was analyzed on a 1% agarose gel containing 0.5% μg/mL ethidium bromide by electrophoresis and visualized under UV light. The concentrations of DNA were measured using a GENEQUANT Pro (Pharmacia Biotech Ltd.) RNA/DNA spectrophotometer. Finally, DNA was adjusted to 100 ng/μL and stored at −20°C.

2.4. Primer Design and Polymerase Chain Reaction (PCR). Two oligonucleotides of the gene-specific primers: fMPN (5-CTCCCTCTTCTTCATCACGG T-3) and fMPC (5-ACACACTCACCTGACTTCGT-3) were used for amplifying the flounder MHC II B sequences, which were designed according to the flounder cDNA sequences reported [20] and published communications [15]. The forward primer for class II B is based on the end of exon1 sequence,

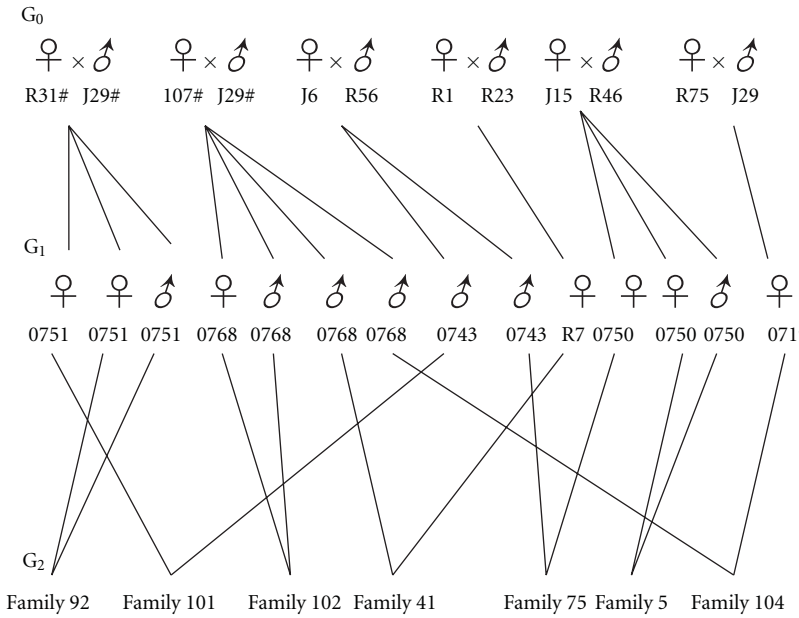

Figure 1: The pedigree denotes the families in generation G_2 with parents in G_1 and grandparents in the G_0.

and the reverse primer for class II B is on the end of exon2 sequence, respectively. Polymerase chain reaction (PCR) was performed in a total volume of 25 μL, which consisted of 100 ng template DNA, 2.5 μL of 10 × *Taq* polymerase buffer (*TransGen Biotech*), 1.5 mM $MgCl_2$, 0.2 mM deoxynucleotide triphosphate, 0.2 μM each of the forward and reverse primers, and 1 unit of *Taq* polymerase (*TransGen Biotech*). The amplification conditions were optimized to reduce the nonspecific amplification [23]. Thermocycling was conducted on a Peltier Thermal Cycler (PTC-200) and the amplification schedule was 94°C for 5 minutes, 30 cycles of 94°C for 40 s, 52°C for 40 seconds, 72°C for 50 seconds, and finally 72°C for 10 minutes. The Molecular Imager Gel Doc XR system (*Bio-rad*) was used to check for integrity and visualize the PCR products by electrophoresis on a 1% agarose gel. The amplified fragments exhibited one distinct band with an approximate length of 500 bp.

2.5. Cloning and Sequencing. PCR products were excised and then purified with the QIAEX II gel extraction kit (*Qiagen*). According to the standard protocol, the purified products were ligated into a PBS-T vector with a TA cloning kit (*Takara*) and then cloned into TOP 10 *Escherichia coli* competent cells (*TransGen Biotech*). Positive clones were screened in PCR reactions with the cloning primers T7 and M13R. The PCR products for appropriately sized clones were cleaned with a Qiaquick PCR purification column (Qiagen) before cycle sequencing with a Big Dye Terminator cycle-sequencing kit following the manufacturer's instructions on an ABI 3730 automated sequencer (Applied Biosystems, Foster City, CA, USA). All of the alleles shown in the present study were confirmed by sequencing a minimum of five times in ten individuals from five of the families, but up to 10 times or more in twenty individuals from two of the families.

2.6. Genotyping, Sequence Analysis, and Statistical Tests. MHC gene sequences were aligned using DNAMAN software. Comparison of these nucleotide sequences and deduced amino acid sequences was performed using the MEGA4.0 program [24]. The relative rates of synonymous (d_S) and non-synonymous (d_N) substitution were determined according to Nei and Gojobori [25] and corrected for multiple hits (Jukes and Cantor) [26] using MEGA4.0. The frequency of polymorphism was analyzed using all of the alleles in the program by means of DnaSP4.0 [27] and DAMBE [28] with Jukes-Cantor distances. Statistical analysis was obtained using SPSS13.0. Allele frequency discrepancies were verified using Fisher's exact test and the significance level [29] was determined for every individual ($n = 180$) and every family ($n = 7$).

3. Results

The average mortality ratio was 66.65 ± 24.31 (the Mean ± S.D. (%)), which was calculated 14 days after the bacterial infection in the 7 families. In this study, we verified 116 distinct MHC class II nucleotide sequences from 180 individuals of the seven flounder families (Table 1). Among these sequences, 72 sequences were present only once, and 17 sequences were the same as in previous reports [15], that is, *Paol-DAB*0101*, *Paol-DAB*0301*, *Paol-DAB*0801*, *Paol-DAB*0901*, *Paol-DAB*2201*, *Paol-DAB*3201*, *Paol-DAB*3501*, *Paol-DAB*3801*, *Paol-DAB*3803*, *Paol-DAB*3804*, *Paol-DAB*3805*, *Paol-DAB*4302*, *Paol-DAB*0102*, *Paol-DAB*2202*, *Paol-DAB*0502*, *Paol-DAB*4101*, and *Paol-DAB*4301*. 99 sequences were newly discovered in the present study and were deposited in GenBank (accession no. HQ634973–HQ635071; Table 2).

Table 2: The alleles and GenBank accession numbers.

Allele	GenBank accession no.	Allele	GenBank accession no.	Allele	GenBank accession no.
*Paol-DAB*0103*	HQ634973	*Paol-DAB*2212*	HQ635006	*Paol-DAB*4901*	HQ635039
*Paol-DAB*0104*	HQ634974	*Paol-DAB*2213*	HQ635007	*Paol-DAB*5001*	HQ635040
*Paol-DAB*0105*	HQ634975	*Paol-DAB*2214*	HQ635008	*Paol-DAB*5101*	HQ635041
*Paol-DAB*0106*	HQ634976	*Paol-DAB*2215*	HQ635009	*Paol-DAB*5102*	HQ635042
*Paol-DAB*0107*	HQ634977	*Paol-DAB*2216*	HQ635010	*Paol-DAB*5201*	HQ635043
*Paol-DAB*0108*	HQ634978	*Paol-DAB*2217*	HQ635011	*Paol-DAB*5202*	HQ635044
*Paol-DAB*0109*	HQ634979	*Paol-DAB*3204*	HQ635012	*Paol-DAB*5203*	HQ635045
*Paol-DAB*0110*	HQ634980	*Paol-DAB*3205*	HQ635013	*Paol-DAB*5301*	HQ635046
*Paol-DAB*0111*	HQ634981	*Paol-DAB*3206*	HQ635014	*Paol-DAB*5401*	HQ635047
*Paol-DAB*0112*	HQ634982	*Paol-DAB*3207*	HQ635015	*Paol-DAB*5402*	HQ635048
*Paol-DAB*0113*	HQ634983	*Paol-DAB*3208*	HQ635016	*Paol-DAB*5501*	HQ635049
*Paol-DAB*0114*	HQ634984	*Paol-DAB*3209*	HQ635017	*Paol-DAB*5601*	HQ635050
*Paol-DAB*0115*	HQ634985	*Paol-DAB*3502*	HQ635018	*Paol-DAB*5701*	HQ635051
*Paol-DAB*0116*	HQ634986	*Paol-DAB*3806*	HQ635019	*Paol-DAB*5801*	HQ635052
*Paol-DAB*0117*	HQ634987	*Paol-DAB*4307*	HQ635020	*Paol-DAB*5802*	HQ635053
*Paol-DAB*0118*	HQ634988	*Paol-DAB*4308*	HQ635021	*Paol-DAB*5803*	HQ635054
*Paol-DAB*0119*	HQ634989	*Paol-DAB*4309*	HQ635022	*Paol-DAB*5804*	HQ635055
*Paol-DAB*0120*	HQ634990	*Paol-DAB*4310*	HQ635023	*Paol-DAB*5901*	HQ635056
*Paol-DAB*0121*	HQ634991	*Paol-DAB*4311*	HQ635024	*Paol-DAB*6001*	HQ635057
*Paol-DAB*0122*	HQ634992	*Paol-DAB*4312*	HQ635025	*Paol-DAB*6101*	HQ635058
*Paol-DAB*0123*	HQ634993	*Paol-DAB*4313*	HQ635026	*Paol-DAB*6201*	HQ635059
*Paol-DAB*0304*	HQ634994	*Paol-DAB*4314*	HQ635027	*Paol-DAB*6301*	HQ635060
*Paol-DAB*0802*	HQ634995	*Paol-DAB*4315*	HQ635028	*Paol-DAB*6401*	HQ635061
*Paol-DAB*0902*	HQ634996	*Paol-DAB*4316*	HQ635029	*Paol-DAB*6402*	HQ635062
*Paol-DAB*0903*	HQ634997	*Paol-DAB*4317*	HQ635030	*Paol-DAB*6501*	HQ635063
*Paol-DAB*2204*	HQ634998	*Paol-DAB*4601*	HQ635031	*Paol-DAB*6601*	HQ635064
*Paol-DAB*2205*	HQ634999	*Paol-DAB*4602*	HQ635032	*Paol-DAB*6801*	HQ635065
*Paol-DAB*2206*	HQ635000	*Paol-DAB*4603*	HQ635033	*Paol-DAB*6901*	HQ635066
*Paol-DAB*2207*	HQ635001	*Paol-DAB*4604*	HQ635034	*Paol-DAB*7001*	HQ635067
*Paol-DAB*2208*	HQ635002	*Paol-DAB*4605*	HQ635035	*Paol-DAB*7101*	HQ635068
*Paol-DAB*2209*	HQ635003	*Paol-DAB*4701*	HQ635036	*Paol-DAB*7201*	HQ635069
*Paol-DAB*2210*	HQ635004	*Paol-DAB*4801*	HQ635037	*Paol-DAB*7301*	HQ635070
*Paol-DAB*2211*	HQ635005	*Paol-DAB*4802*	HQ635038	*Paol-DAB*6701*	HQ635071

The new alleles detected in this study were based on the deduced amino acid sequences and designated based on the rules reported previously [15, 30–32]. For example, in *Paol-DAB*0103, Paol* refers to *Paralichthys olivaceus*, D to class II, A to the family designation, and B to the β chain-encoding genes. In the four digits after the asterisk, the first two digits refer to the major type (i.e., alleles that differ by at least five amino acid substitutions), and the last two digits to the subtype (i.e., alleles that differ by less than five amino acid substitutions within a single major type).

3.1. MHC Class II B Sequence Diversity. The length of the amplified MHC class II sequence was 407 bp. The sequences covered 91 amino acid residues of the MHC class II B exon2 and complete intron1 (84/96 bp, including a 12 bp repeat loci) [15]. There were no frame-shift mutations or stop codons in these alleles. There were 151 polymorphic sites across the 116 different MHC class II exon2 sequences. The average number of nucleotide differences (k) was 20.84, and the nucleotide diversity value (P_i) for these sequences was 0.07634. Among the individuals of the seven families, five (10 individuals from families 5, 41, 75, 92, 102, resp.) or ten (20 individuals from family 101, 104, resp.) clones per individual were sequenced. Only one sequence was present in five clones per individual from 25 individuals of families 102, 92, 75, 41, and 5; two sequences were detected in five or ten clones per individual from 71 individuals; three sequences were found in five or ten clones per individual from 57 individuals; four sequences were present in five or ten clones per individual from 18 individuals; five sequences were only detected in ten clones per individual from 5 individuals from family 101 and family 104; six sequences were only detected in ten clones per individual from 3 individuals from family 101; seven sequences were detected in ten clones per individual from one individual from family 101, indicating that this primer set amplifies at least four loci or copies in this species (Table 3) [6, 33].

Table 3: The number of allele in each of seven flounder families.

Individual no.	Allele no.						
	1 allele	2 alleles	3 alleles	4 alleles	5 alleles	6 alleles	7 alleles
Family 101		6	21	7	2	3	1
Family 104		22	8	6	3		
Family 102	3	11	3	3			
Family 92	5	6	8	1			
Family 75	1	9	9	1			
Family 41	3	9	7	1			
Family 5	9	6	5				
Total	25	71	57	18	5	3	1

```
                  * * *                  * ***     **        *        *    **    * * *   *    * **   ** **
#Paol-DAB*0101 ADGFRHYTVA DCEFNSSKLN DI EYTQSYYY NKLEYVRFSS SVGKYVGYTE YGIKNAERWN NGPEVIARRG EKERYCFHNV GIDVEADLTKS
#Paol-DAB*0301 .....Y.V.T ..........  ..... .. .......... .......... H.................A .......... ...FT.SA....
#Paol-DAB*0801 ........N S.......... .....H.. .. .......... .......... F......K.......T... ........R...N....A....
#Paol-DAB*0901 ....LY.V.T S.......... ...F.E.. .. ....I..... .......... F......S.......T... ........P.......SA....
#Paol-DAB*4601 ....L.. ..T .......... ..... .. ....I..... ....F..... F......S....Q...T... ....V..... .V....A....
#Paol-DAB*2201 .....Y.V.G S.......... ...F.L.. .. .....I.... .......... H.............TS.. ........R...VFT.SA....
#Paol-DAB*3201 .......V.N S.......... .....E.. .. .....I.... .......... H..............S..A ........R...N....A....
#Paol-DAB*3501 .....F.V.T .......... ....IY.H.. .....I.... .......... H.................A ........Y...V....A....
#Paol-DAB*3801 ....L..M D S.......... ....IY.H.. .....I.... ....F..... V.......L.......N..A Q.........VFT..A....
#Paol-DAB*3803 ....L..M D S.......... ....IY.H.. .....I.... ....F..... V.......L.......N..A Q..........FT.SA....
#Paol-DAB*3804 ....L..V.D S.......... ....IY.H.. .....I.... ....F..... V.......L.......N..A Q..........FT.SA....
#Paol-DAB*3805 ....L..M D N.......... ....IY.H.. .....I.... ....F..... V.......L.......T..A Q..V.....VFT.SA....
#Paol-DAB*4101 .....Y.M. E.......... ...F.E.. .. ....FI.... ....F..... H.................. F..S..LN...N...SA....
#Paol-DAB*4301 ....L..V.T .......... .....E.. .. ....II.... ....F..... V.......L.........A Q.S..LS.......SA....
```

Figure 2: Putative amino acid sequences for MHC II B exon2 alleles of Japanese flounder. Dots denote identity with the first sequences; the putative peptide binding region is indicated with asterisks.

The putative amino acid sequences for the MHC II B exon2 alleles of Japanese flounder along with those previously reported are shown in Figure 2. The nucleotide sequence homology in the MHC class II B genes ranged from 87% to 99%. Alleles differed in amino acid composition by one to twenty-eight substitutions out of 91 sites.

3.2. Alleles Distribution in the Seven Flounder Families. Alleles were shared among certain individuals and families in this study. Table 4 summarizes the alleles which were frequently present in individuals of the seven families investigated (one allele *Paol-DAB*4601* was presented only in this study, while the other 16 alleles have been reported previously [15], and these were *Paol-DAB*4301*, *Paol-DAB*4302*, *Paol-DAB*0101*, *Paol-DAB*3201*, *Paol-DAB*2201*, *Paol-DAB*3803*, *Paol-DAB*3804*, *Paol-DAB*0102*, *Paol-DAB*0301*, *Paol-DAB*4101,* *Paol-DAB*0801*, *Paol-DAB*2202*, *Paol-DAB*0901*, *Paol-DAB*3805*, *Paol-DAB*0502*, and *Paol-DAB*3501,* resp.). Thus, four alleles (*Paol-DAB*4301*, *Paol-DAB*0101*, *Paol-DAB*3201*, and *Paol-DAB*2201*) were obtained from three hundred and ninety-seven clones from forty juveniles from family 101, with a frequency of 16%, 22.1%, 20.3%, and 22.6%, respectively. Five alleles (*Paol-DAB*4301*, *Paol-DAB*4601*, *Paol-DAB*3803*, *Paol-DAB*0101*, and *Paol-DAB*0102*) were found to be present in three hundred and ninety-five clones from forty juveniles from family 104, with a frequency of 19.9%, 20.2%, 16.4%, 19.9%, and 7.3%, respectively. Two alleles (*Paol-DAB*0301* and *Paol-DAB*4101*) were obtained from one hundred clones from twenty juveniles from family 5 with a frequency of 6% and 34%. Four alleles (*Paol-DAB*0101*, *Paol-DAB*0801*, *Paol-DAB*3803,* and *Paol-DAB*2202*) were present in one hundred and five clones from twenty juveniles in family 41 with a frequency of 21.9%, 46.7%, and 22.9%, respectively. Four alleles (*Paol-DAB*0901*, *Paol-DAB*2201*, *Paol-DAB*3805* and *Paol-DAB*0502*) were obtained from one hundred and two clones from twenty juveniles in family 75, with a frequency of 25.5%, 22.6%, 20.6%, and 15.7%, respectively. Two alleles (*Paol-DAB*3501* and *Paol-DAB*4301*) were obtained from one hundred and one clones from twenty juveniles family 92 with a frequency of 40.5% and 43.6%, and three alleles (*Paol-DAB*0101*, *Paol-DAB*4301,* and *Paol-DAB*3803*) were presented in ninety-seven clones in twenty juveniles from family 102 with a frequency of 39.2%, 24.7%, and 13.4%, respectively.

3.3. Association between Allele Frequency and Resistance/Susceptibility to V. anguillarum in the Surviving and Dead Individuals within the Seven Families. Most of the 116 alleles were presented only once or twice and therefore they were excluded from the analysis of the association with bacterial resistance. Fourteen alleles were selected

Table 4: The frequency of alleles (>3%) in each of seven families.

Allele	Mode	Number	Frequency	Family	Allele	Mode	Number	Frequency	Family
	S	21	0.21**			S	26	0.26**	
*Paol-DAB*0301*	D	38	0.38	F5	*Paol-DAB*4101*	D	8	0.08	F5
	Total	60	0.6			Total	34	0.34	
	S	12	0.114			S	20	0.19	
*Paol-DAB*0101*	D	11	0.105	F41	*Paol-DAB*0801*	D	29	0.267	F41
	Total	23	0.219			Total	49	0.467	
	S	18	0.171**			S	5	0.05	
*Paol-DAB*3803*	D	6	0.057	F41	*Paol-DAB*2202*	D	1	0.01	F75
	Total	24	0.229			Total	6	0.059	
	S	12	0.118			S	12	0.118	
*Paol-DAB*0901*	D	14	0.138	F75	*Paol-DAB*2201*	D	11	0.108	F75
	Total	26	0.255			Total	23	0.226	
	S	12	0.118			S	7	0.069	
*Paol-DAB*3805*	D	9	0.088	F75	*Paol-DAB*0502*	D	9	0.088	F75
	Total	21	0.206			Total	16	0.157	
	S	16	0.158			S	25	0.248	
*Paol-DAB*3501*	D	25	0.248	F92	*Paol-DAB*4301*	D	19	0.188	F92
	Total	41	0.405			Total	44	0.436	
	S	24	0.061**			S	40	0.102	
*Paol-DAB*3201*	D	56	0.142	F101	*Paol-DAB*0101*	D	47	0.118	F101
	Total	80	0.203			Total	87	0.221	
	S	33	0.084**			S	44	0.112**	
*Paol-DAB*2201*	D	56	0.142	F101	*Paol-DAB*4301*	D	19	0.048	F101
	Total	89	0.226			Total	63	0.16	
	S	8	0.02			S	12	0.03	
*Paol-DAB*0102*	D	9	0.023	F101	*Paol-DAB*4302*	D	2	0.005	F101
	Total	17	0.043			Total	14	0.035	
	S	30	0.076			S	54	0.136**	
*Paol-DAB*4301*	D	49	0.123	F104	*Paol-DAB*4601*	D	26	0.065	F104
	Total	79	0.199			Total	80	0.202	
	S	32	0.081			S	43	0.108	
*Paol-DAB*3803*	D	33	0.083	F104	*Paol-DAB*0101*	D	36	0.091	F104
	Total	65	0.164			Total	79	0.199	
	S	16	0.04			S	5	0.013	
*Paol-DAB*0102*	D	13	0.033	F104	*Paol-DAB*4302*	D	13	0.033	F104
	Total	29	0.073			Total	18	0.045	
	S	7	0.018			S	7	0.072	
*Paol-DAB*3804*	D	5	0.013	F104	*Paol-DAB*3803*	D	6	0.062	F102
	Total	12	0.03			Total	13	0.134	
	S	17	0.175			S	12	0.124	
*Paol-DAB*0101*	D	21	0.217	F102	*Paol-DAB*4301*	D	12	0.124	F102
	Total	38	0.392			Total	24	0.247	

Notes: S denotes survivor individual and D denotes dead individual in the challenge tests. (One allele *Paol-DAB*4601* was first present in this study as well as the other 16 alleles have presented in previous reports [15]). **denotes difference is significant at the 0.05 level ($P < 0.05$).

for further analysis, of which one allele, *Paol-DAB*4601*, was first identified in this study, while the 13 other alleles were identified in previous reports [15]. The latter were *Paol-DAB*0101*, *Paol-DAB*0301*, *Paol-DAB*0801*, *Paol-DAB*0901*, *Paol-DAB*2201*, *Paol-DAB*3201*, *Paol-DAB*3501*, *Paol-DAB*3801*, *Paol-DAB*3803*, *Paol-DAB*3804*, *Paol-DAB*3805*, *Paol-DAB*4101,* and *Paol-DAB*4301*. A sharing of the same alleles, *Paol-DAB*4301* and *Paol-DAB*0101,* were observed in four of the seven families examined (Table 4), with the frequency different in each family. In family 104, there was a 7.6% frequency in the surviving individuals and a 12.3% frequency in dead

individuals for *Paol-DAB*4301*, as well as a 10.8% frequency in the surviving individuals and a 9.1% frequency in dead individuals for *Paol-DAB*0101*. In family 92, there was a 24.8% frequency for *Paol-DAB*4301* in the survivors and an 18.8% frequency in the dead individuals. In family 101, there was an 11.2% frequency for *Paol-DAB*4301* in survivor individuals and a 4.8% frequency in dead individuals, and this difference was significant ($P = 0.0010$); there was a 10.2% frequency found for *Paol-DAB*0101* in the surviving individuals and an 11.8% frequency in the dead. In family 102, there was a 12.4% frequency in the surviving and 12.4% frequency in the dead individuals for *Paol-DAB*4301*, as well as a 17.5% frequency in the survivors and a 21.7% frequency in dead individuals for *Paol-DAB*0101*. In family 41, an 11.4% frequency was found in the surviving individuals while a 10.5% frequency was found in the dead individuals for *Paol-DAB*0101*. Some MHC class II B allele frequencies differed significantly between the surviving and dead individuals within the family. In family 104, the *Paol-DAB*4601* allele, which was newly identified in this study, was significantly more frequent in the surviving (13.6%) individuals than in the dead individuals (6.5%, $P = 0.001$).

In family 101, the *Paol-DAB*2201* frequency in the surviving individuals (8.4%) was significantly lower than in the dead individuals (14.2%, $P = 0.001$), while in family 41, the *Paol-DAB*3803* allele was significantly more frequent in the survivors (17.1%) than the dead (5.7%, $P = 0.009$). In family 5, the *Paol-DAB*4101* allele was significantly more frequent in the surviving (26%) than dead fish (8%, $P = 0.01$), while the *Paol-DAB*0301* allele was significantly more frequent in the dead (38%) than the survivors (21%, $P = 0.008$). In family 75, family 92, and family 102, the difference between the allele frequencies in the surviving and dead individuals was not significant. These results suggested that the *Paol-DAB*4301*, *Paol-DAB*4601*, *Paol-DAB*4302*, *Paol-DAB*3803*, and *Paol-DAB*4101* alleles were associated with resistance to *V. anguillarum,* while *Paol-DAB*2201* and *Paol-DAB*0301* appeared to be associated with susceptibility to this bacteria.

3.4. Evidence for Balancing Selection. The pattern of nucleotide substitution was examined in the putative PBR (peptide-binding region) and other regions. Twenty-three amino acid residues were selected as the putative PBR sites in the human regions [34]. The mean numbers of synonymous substitutions per synonymous site (d_S) and nonsynonymous substitutions per nonsynonymous site (d_N) were based on pairwise comparisons among the whole sequences in seven families (Table 5). In the putative PBR region, the mean d_N (0.231, 0.134, 0.109, 0.180, 0.167, 0.146, 0.147, and 0.177) was significantly higher than the mean d_S (0.037, 0.031, 0.048, 0.060, 0.024, 0.009, 0.024, and 0.004) for all of the pairwise comparisons, respectively. Furthermore the d_N/d_S in the PBR (6.243, 4.323, 2.271, 3.000, 6.96, 16.2, 6.125, 44.25) was greater than that in the non-PBR (1.390, 2.5, 1.109, 1.065, 1.27, 1.410, 1.606, 1.389) in terms of the whole sequence and in each family sequence, respectively. These results indicated that positive selection was at work in the PBR of MHC class II B genes.

3.5. Inheritance of the Allele in the Next Generation. The pedigree of the Japanese flounder was shown in Figure 1. At G_1, both family 0768 and family 0751 had *Paol-DAB*4301* alleles, while family 0768 also had *Paol-DAB*0801* allele. We found that the *Paol-DAB*4301* alleles were presented in families 101, 104, 92, and 102, and *Paol-DAB*0801* in family 41 at G_2, respectively. The sire and dam of family 92 were from family 0751, while the sire and dam of family 101 were from family 0743 and family 0751, respectively. The sire and dam of family 102 were from family 0768. The sire and dam of family 41 were from family 0768 and family R7, respectively, while the sire and dam of family 104 were from family 0768 and family 0719, respectively. This denoted that the MHC II B alleles were passed on to the progeny. Neither *Paol-DAB*4301* nor *Paol-DAB*0801* was present in family 75 and 5. The sire and dam of family 75 were from family 0743 and 0750, respectively, while the sire and dam of family 5 were both from family 0750. The distribution patterns of the alleles in each family were obtained from DNA sequence analysis and are shown in Table 4.

4. Discussion

The major histocompatibility complex (MHC) is a vital portion of the vertebrate immune system, and MHC allele diversity is critical for resistance against parasites [14]. Dixon et al. [35] discovered 57 alleles in 17 individuals with greater polymorphism than is found in most mammals. This region was selected for amplification as a result of it covering the whole of exon2 in the β1 domain, which corresponded to the highly variable region of the PBR. Therefore, in this study, we investigated variations in seven flounder families using MHC class II B exon2 as a gene marker, and the diversity was found to differ significantly (116 sequences in 180 individuals). At least four MHC class II exon2 loci were present in Japanese flounders, which was more than the number previously reported by Xu et al. [15] and Zhang et al. [20]. Homology of these alleles from each individual was from 89% to 100%, and in all the individuals examined was from 87% to 100%, with levels as high as 0.11 in mammals [36].

In a previous study by Xu et al. [15], *Paol-DAB*4301, Paol-DAB*0601, Paol-DAB*0801, Paol-DAB*2001,* and *Paol-DAB*3803* were the alleles which found to be associated with resistance to *V. anguillarum,* while *Paol-DAB*1601, Paol-DAB*2201,* and *Paol-DAB*2701* were the alleles which associate with susceptibility. In the present study, we found that *Paol-DAB*4301*, *Paol-DAB*4601*, *Paol-DAB*3803*, and *Paol-DAB*4101* were associated with resistance to *V. anguillarum,* while *Paol-DAB*3201*, *Paol-DAB*2201,* and *Paol-DAB*0301* alleles were associated with susceptibility. Moreover, the significant difference in the frequency of each allele between the survivors and dead fish was only found in one family.

In addition to the fact that analysis within family was less influenced by the background of the families' genetic variations. The link between the alleles and the bacterial resistance was unpredictable both within and among families, as well as the pooled material. It might be that the alleles are indirectly involved in the resistance to pathogens, or it was possible

Table 5: Synonymous (d_S) and nonsynonymous (d_N) substitution rate in the putative peptides binding region (PBR) and nonpeptides binding region (non-PBR) among Japanese flounder families.

Family	Region	No. of codons	d_N (SE)	d_S (SE)	d_N/d_S
F5	PBR	23	0.134 ± 0.037	0.031 ± 0.022	4.323
	Non-PBR	68	0.04 ± 0.012	0.016 ± 0.009	2.5
	Total	91	0.064 ± 0.014	0.019 ± 0.008	3.368
F41	PBR	23	0.109 ± 0.023	0.048 ± 0.024	2.271
	Non-PBR	68	0.051 ± 0.014	0.046 ± 0.018	1.109
	Total	91	0.066 ± 0.013	0.046 ± 0.014	1.435
F92	PBR	23	0.180 ± 0.034	0.060 ± 0.041	3.000
	Non-PBR	68	0.033 ± 0.010	0.031 ± 0.015	1.065
	Total	91	0.069 ± 0.015	0.037 ± 0.016	1.865
F75	PBR	23	0.167 ± 0.032	0.024 ± 0.013	6.96
	Non-PBR	68	0.047 ± 0.012	0.037 ± 0.018	1.27
	Total	91	0.078 ± 0.013	0.034 ± 0.013	2.294
F102	PBR	23	0.146 ± 0.035	0.009 ± 0.009	16.2
	Non-PBR	68	0.055 ± 0.013	0.039 ± 0.013	1.410
	Total	91	0.079 ± 0.013	0.032 ± 0.013	2.469
F101	PBR	23	0.147 ± 0.030	0.024 ± 0.007	6.125
	Non-PBR	68	0.053 ± 0.013	0.033 ± 0.014	1.606
	Total	91	0.077 ± 0.014	0.031 ± 0.010	2.484
F104	PBR	23	0.177 ± 0.028	0.004 ± 0.004	44.25
	Non-PBR	68	0.050 ± 0.013	0.036 ± 0.014	1.389
	Total	91	0.083 ± 0.014	0.028 ± 0.011	2.964
Whole	PBR	23	0.231 ± 0.051	0.037 ± 0.028	6.243
	Non-PBR	68	0.057 ± 0.020	0.041 ± 0.023	1.390
	Total	91	0.098 ± 0.020	0.038 ± 0.018	2.579

that the families which were challenged displayed different but "functionally similar" alleles by chance.

Xu et al. [15] demonstrated that the MHC II B alleles were passed on to the progeny. In the present study, the allele *Paol-DAB*4301* in family 0768 at G_1 was also discovered in families 101, 104, 92, and 102 at G_2. This stability of inheritance within the families had been shown for two generations. Klein [37] reported that the high levels of allelic diversity and polymorphism in the MHC resulted from the long-term coevolution of parasites and MHC molecules. In this study, no complete sequences (alleles) were shared across all of the families, while certain alleles were shared among individuals and two to three families in the Japanese flounder. The sequences of the MHC alleles were not consistent with the phylogeny relationships of individuals seen as a family. This was in agreement with the result of Ye et al. [38], who reported that the MHC allele sequences were not consistent with the phylogeny relationships of a population in a closely related species. Therefore, to fully understand the polymorphism of the MHC class II genes in Japanese flounder, it was necessary to carry further studies, including an estimation of the number of gene loci, introductions of improved methods, and analysis of a greater number of individuals as well as genes and functions. Genetic polymorphism of MHC was generally thought to be maintained by a balancing selection driven by host-parasite coevolution [39–42]. Evidence for balancing selection operating in the MHC class II B gene was a significantly higher rate of non-synonymous mutation ($d_N/d_S > 1$), which indicated that the rate of non-synonymous substitution per non-synonymous sites exceeds that of synonymous substitution per synonymous sites [43, 44].

We examined the *Paol-DAB* alleles, including both the whole sequences and the sequences in each family discovered in the present study and found that the d_N/d_S ratio (6.234, 4.323, 2.271, 3.000, 6.96, 16.2, 6.125, and 44.25, resp.) in the putative PBR regions was higher than that of d_N/d_S (1.390, 2.5, 1.109, 1.065, 1.27, 1.410, 1.606, and 1.389, resp.) in the non-PBR regions in the MHC class II exon2 domain of Japanese flounder (Table 5), as was also the case for the human, nonhuman primate, and mouse class II genes[44–46]. This was evidence for balancing selection or positive selection at work in the PBR of MHC class II B genes. In this study, certain alleles exhibited a high frequency in individual families (Table 4), while other alleles were found only once or twice in seven families, which indicated frequency-dependent selection [17, 47], that is, one model of balancing selection, acting on the polymorphism of the MHC class II B genes in the Japanese flounder.

In the seven families investigated, the percentage of heterozygosity (two different sequences in one individual) in families 101, 104, 102, 92, 75, 41, and family 5 is 100%, 100%,

85%, 75%, 95%, 85%, and 55%, respectively. All but one of these corresponds to the level of heterozygosity in humans and mice, which was in a range of 80–90% [48]. The sire and dam of family 92 were from family 0751, the sire and dam of family 5 were from family 0750, and sire and dam of family 102 were from family 0768. These exhibited lower heterozygosity (75%, 55%, 85%), especially family 5 with the lowest heteroxygosity (55%), but the survival ratio of family 5 was the highest among the seven families examined in this study. It might indicate that other genes in family 5 or the homozygosity of the MHC class II B gene resulted in the resistance to *V. anguillarum* in the Japanese flounder. Further studies are needed to examine the MHC class II B genes in the offspring of the seven families reported in this study.

Between 5 and 10 clones in each of the individual PCR products had one or seven sequences, and most of these sequences were the same as that of the other clones, indicating that some of these were not the result of PCR amplification "errors" [49] or the mismatch repair of heteroduplex molecules during the course of cloning in *E. coli.* [50]. In this study, ten (20 individuals from family 101 and 104, resp.) or five (10 individuals from family 5, 41, 75, 92 and 102, resp.) clones per individual were sequenced, and we found a significant difference in the allele distribution in the surviving and dead individuals in each of the seven families. It was possible that the results would differ in terms of the clones and samples, so further studies were needed to select a greater number of both for sequencing and analysis.

In summary, the detection of MHC class II B alleles and their polymorphisms as depicted in the present study will be helpful for immunological research in the future. This investigative work has the ultimate aim of developing families or strains of Japanese flounder with bacterial resistance.

Acknowledgments

This work was supported by the National Major Basic Research Program of China (2010CB126303), Special Fund for Agroscientific Research in the Public Interest (200903046), the National Natural Science Foundation of China (30871918), and Taishan scholar project of Shandong province, China.

References

[1] R. Sheng, X. X. Xu, Q. Tang et al., "Polysaccharide of radix pseudostellariae improves chronic fatigue syndrome induced by poly I:C in mice," *Evidence-Based Complementary and Alternative Medicine*. In press.

[2] R. N. Germain, "MHC-dependent antigen processing and peptide presentation: providing ligands for T lymphocyte activation," *Cell*, vol. 76, no. 2, pp. 287–299, 1994.

[3] J. Bingulac-Popovic, F. Figueroa, A. Sato et al., "Mapping of Mhc class I and class II regions to different linkage groups in the zebrafish, *Danio rerio*," *Immunogenetics*, vol. 46, no. 2, pp. 129–134, 1997.

[4] A. Sato, F. Figueroa, B. W. Murray et al., "Nonlinkage of major histocompatibility complex class I and class II loci in bony fishes," *Immunogenetics*, vol. 51, no. 2, pp. 108–116, 2000.

[5] J. D. Hansen, P. Strassburger, G. H. Thorgaard, W. P. Young, and L. Du Pasquier, "Expression, linkage, and polymorphism of MHC-related genes in rainbow trout, Oncorhynchus mykiss," *Journal of Immunology*, vol. 163, no. 2, pp. 774–786, 1999.

[6] K. Hashimoto, T. Nakanishi, and Y. Kurosawa, "Isolation of carp genes encoding major histocompatibility complex antigens," *Proceedings of the National Academy of Sciences of the United States of America*, vol. 87, no. 17, pp. 6863–6867, 1990.

[7] J. Nikolich-Žugich, D. H. Fremont, M. J. Miley, and I. Messaoudi, "The role of mhc polymorphism in anti-microbial resistance," *Microbes and Infection*, vol. 6, no. 5, pp. 501–512, 2004.

[8] N. Otting, N. G. de Groot, G. G. M. Doxiadis, and R. E. Bontrop, "Extensive Mhc-DQB variation in humans and non-human primate species," *Immunogenetics*, vol. 54, no. 4, pp. 230–239, 2002.

[9] K. Musolf, Y. Meyer-Lucht, and S. Sommer, "Evolution of MHC-DRB class II polymorphism in the genus Apodemus and a comparison of DRB sequences within the family Muridae (Mammalia: Rodentia)," *Immunogenetics*, vol. 56, no. 6, pp. 420–426, 2004.

[10] H. C. Miller, K. Belov, and C. H. Daugherty, "Characterization of MHC class II genes from an ancient reptile lineage, Sphenodon (tuatara)," *Immunogenetics*, vol. 57, no. 11, pp. 883–891, 2005.

[11] Y. Shi, W. Xiao-bing, Y. Peng, and C. Bi-hui, "Cloning and sequences analysis of the second exon of MHC class II B genes in Chinese alligator, Alligator sinensis," *Zoological Research*, vol. 25, pp. 415–421, 2004.

[12] D. H. Bos and J. A. DeWoody, "Molecular characterization of major histocompatibility complex class II alleles in wild tiger salamanders (Ambystoma tigrinum)," *Immunogenetics*, vol. 57, no. 10, pp. 775–781, 2005.

[13] S. Consuegra, H. J. Megens, K. Leon, R. J. M. Stet, and W. C. Jordan, "Patterns of variability at the major histocompatibility class II alpha locus in Atlantic salmon contrast with those at the class I locus," *Immunogenetics*, vol. 57, no. 1-2, pp. 16–24, 2005.

[14] K. M. Wegner, M. Kalbe, G. Rauch, J. Kurtz, H. Schaschl, and T. B. H. Reusch, "Genetic variation in MHC class II expression and interactions with MHC sequence polymorphism in three-spined sticklebacks," *Molecular Ecology*, vol. 15, no. 4, pp. 1153–1164, 2006.

[15] T. J. Xu, S. L. Chen, X. S. Ji, and Y. S. Tian, "MHC polymorphism and disease resistance to Vibrio anguillarum in 12 selective Japanese flounder (*Paralichthys olivaceus*) families," *Fish and Shellfish Immunology*, vol. 25, no. 3, pp. 213–221, 2008.

[16] A. L. Hughes and M. Nei, "Models of host-parasite interaction and MHC polymorphism," *Genetics*, vol. 132, no. 3, pp. 863–864, 1992.

[17] R. W. Slade and H. I. McCallum, "Overdominant vs. frequency-dependent selection at MHC loci," *Genetics*, vol. 132, no. 3, pp. 861–862, 1992.

[18] P. W. Hedrick, "Balancing selection and MHC," *Genetica*, vol. 104, no. 3, pp. 207–214, 1998.

[19] P. Srisapoome, T. Ohira, I. Hirono, and T. Aoki, "Cloning, characterization and expression of cDNA containing major histocompatibility complex class I, IIα and IIβ genes of Japanese flounder *Paralichthys olivaceus*," *Fisheries Science*, vol. 70, no. 2, pp. 264–276, 2004.

[20] Y. X. Zhang, S. L. Chen, Y. G. Liu, Z. X. Sha, and Z. J. Liu, "Major histocompatibility complex class IIB allele polymorphism and its association with resistance/susceptibility to Vibrio anguillarum in Japanese flounder (*Paralichthys olivaceus*)," *Marine Biotechnology*, vol. 8, no. 6, pp. 600–610, 2006.

[21] S. L. Chen, Y. S. Tian, T. J. Xu, H. Deng, B. W. Liu, and G. C. Yu, "Development and characterization for growth rate and disease resistance of disease-resistance population and family in Japanese flounder (*Paralichthys olivaceus*)," *Journal of Fisheries of China*, vol. 32, no. 5, pp. 665–673, 2008.

[22] Y. Palti, J. T. Silverstein, H. Wieman, J. G. Phillips, F. T. Barrows, and J. E. Parsons, "Evaluation of family growth response to fishmeal and gluten-based diets in rainbow trout (Oncorhynchus mykiss)," *Aquaculture*, vol. 255, no. 1–4, pp. 548–556, 2006.

[23] P. Zylstra, H. S. Rothenfluh, G. F. Weiller, R. V. Blanden, and E. J. Steele, "PCR amplification of murine immunoglobulin germline V genes: strategies for minimization of recombination artefacts," *Immunology and Cell Biology*, vol. 76, no. 5, pp. 395–405, 1998.

[24] K. Tamura, J. Dudley, M. Nei, and S. Kumar, "MEGA4: Molecular Evolutionary Genetics Analysis (MEGA) software version 4.0," *Molecular Biology and Evolution*, vol. 24, no. 8, pp. 1596–1599, 2007.

[25] M. Nei and T. Gojobori, "Simple methods for estimating the numbers of synonymous and nonsynonymous nucleotide substitutions," *Molecular Biology and Evolution*, vol. 3, no. 5, pp. 418–426, 1986.

[26] T. H. Jukes and C. R. Cantor, "Evolution of protein molecules," in *Mammalian Protein Metabolism*, H. N. Munro, Ed., pp. 21–132, Academic Press, New York, NY, USA, 1969.

[27] P. Librado and J. Rozas, "DnaSP v5: a software for comprehensive analysis of DNA polymorphism data," *Bioinformatics*, vol. 25, no. 11, pp. 1451–1452, 2009.

[28] X. Xia and Z. Xie, "DAMBE: software package for data analysis in molecular biology and evolution," *Journal of Heredity*, vol. 92, no. 4, pp. 371–373, 2001.

[29] W. R. Rice, "Analysis tables of statistical tests," *Evolution*, vol. 43, pp. 223–225, 1989.

[30] R. F. Xu, K. Li, G. H. Chen, Y. Z. Qiang, Y. B. Zhang, and L. Lin, "Genetic variation within exon 2 of the MHC B-LB II gene inTibetan chicken," *Acta Genetica Sinica*, vol. 32, no. 11, pp. 1136–1146, 2005.

[31] S. G. Antunes, N. G. De Groot, H. Brok et al., "The common marmoset: a new world primate species with limited Mhc class II variability," *Proceedings of the National Academy of Sciences of the United States of America*, vol. 95, no. 20, pp. 11745–11750, 1998.

[32] K. Trtková, H. Kupfermann, B. Grahovac et al., "Mhc-DRB genes of platyrrhine primates," *Immunogenetics*, vol. 38, no. 3, pp. 210–222, 1993.

[33] D. Klein, H. Ono, C. O'hUigin, V. Vincek, T. Goldschmidt, and J. Klein, "Extensive MHC variability in cichlid fishes of Lake Malawi," *Nature*, vol. 364, no. 6435, pp. 330–334, 1993.

[34] J. H. Brown, T. S. Jardetzky, J. C. Gorga et al., "Three-dimensional structure of the human class II histocompatibility antigen HLA-DR1," *Nature*, vol. 364, no. 6432, pp. 33–39, 1993.

[35] B. Dixon, L. A. J. Nagelkerke, F. A. Sibbing, E. Egberts, and R. J. M. Stet, "Evolution of MHC class II β chain-encoding genes in the Lake Tana barbel species flock (Barbus intermedius complex)," *Immunogenetics*, vol. 44, no. 6, pp. 419–431, 1996.

[36] M. Nei and A. L. Hughes, "Polymorphism and evolution of the major histocompatibility complex loci in mammals," in *Evolution at the Molecular Level*, R. K. Selander, A. G. Clark, and T. S. Whittam, Eds., pp. 222–247, Sinauer Associates, Sunderland, UK, 1991.

[37] J. Klein, "Of *HLA*, tryps, and selection: an essay on coevolution of MHC and parasites," *Human Immunology*, vol. 30, no. 4, pp. 247–258, 1991.

[38] Y. Ye, J. She, and E. K. Wakeland, "Diversification of class II A within the genus *Mus*," in *Molecular Evolution of the Major Histocompatibility Complex*, J. Klein and D. Klein, Eds., pp. 131–138, Springer, Berlin, Germany, 1991.

[39] J. A. Eimes, J. L. Bollmer, P. O. Dunn, L. A. Whittingham, and C. Wimpee, "Mhc class II diversity and balancing selection in greater prairie-chickens," *Genetica*, vol. 138, no. 2, pp. 265–271, 2010.

[40] S. B. Piertney and M. K. Oliver, "The evolutionary ecology of the major histocompatibility complex," *Heredity*, vol. 96, no. 1, pp. 7–21, 2006.

[41] L. Bernatchez and C. Landry, "MHC studies in nonmodel vertebrates: what have we learned about natural selection in 15 years?" *Journal of Evolutionary Biology*, vol. 16, no. 3, pp. 363–377, 2003.

[42] T. Strand, H. Westerdahl, J. Höglund, R. V. Alatalo, and H. Siitari, "The Mhc class II of the Black grouse (*Tetrao tetrix*) consists of low numbers of B and Y genes with variable diversity and expression," *Immunogenetics*, vol. 59, no. 9, pp. 725–734, 2007.

[43] A. L. Hughes and M. Nei, "Pattern of nucleotide substitution at major histocompatibility complex class I loci reveals overdominant selection," *Nature*, vol. 335, no. 6186, pp. 167–170, 1988.

[44] A. L. Hughes and M. Nei, "Nucleotide substitution at major histocompatibility complex class II loci: evidence for overdominant selection," *Proceedings of the National Academy of Sciences of the United States of America*, vol. 86, no. 3, pp. 958–962, 1989.

[45] T. Bergström and U. Gyllensten, "Evolution of the Mhc class II polymorphism: the rise and fall of class II gene function in primates," *Immunological Reviews*, no. 143, pp. 14–31, 1995.

[46] E. Medina and R. J. North, "Resistance ranking of some common inbred mouse strains to Mycobacterium tuberculosis and relationship to major histocompatibility complex haplotype and Nramp1 genotype," *Immunology*, vol. 93, no. 2, pp. 270–274, 1998.

[47] N. Takahata and M. Nei, "Allelic genealogy under overdominant and frequency-dependent selection and polymorphism of major histocompatibility complex loci," *Genetics*, vol. 124, no. 4, pp. 967–978, 1990.

[48] J. Klein, *Natural History of the Major Histocompatibility Complex*, John Wiley & Sons, New York, NY, USA, 1986.

[49] P. D. Ennis, J. Zemmour, R. D. Salter, and P. Parham, "Rapid cloning of HLA-A,B cDNA by using the polymerase chain reaction: frequency and nature of errors produced in amplification," *Proceedings of the National Academy of Sciences of the United States of America*, vol. 87, no. 7, pp. 2833–2837, 1990.

[50] M. Longeri, M. Zanotti, and G. Damiani, "Recombinant DRB sequences produced by mismatch repair of heteroduplexes during cloning in Escherichia coli," *European Journal of Immunogenetics*, vol. 29, no. 6, pp. 517–523, 2002.

Hindawi Publishing Corporation
Evidence-Based Complementary and Alternative Medicine
Volume 2011, Article ID 965153, 11 pages
doi:10.1155/2011/965153

Research Article

Molecular Characterization and Expression of α-Globin and β-Globin Genes in the Euryhaline Flounder *(Platichthys flesus)*

Weiqun Lu,[1,2] Aurelie Mayolle,[3] Guoqiang Cui,[2] Lei Luo,[2] and Richard J. Balment[3]

[1] *Key Laboratory of Exploration and Utilization of Aquatic Genetic Resources, Shanghai Ocean University, Shanghai 201306, China*
[2] *Laboratory of Adaptive Biology, College of Fisheries and Life Science, Shanghai Ocean University, 999 Huchenghuan Road, Shanghai 201306, China*
[3] *Faculty of Life Sciences, The University of Manchester, Oxford Road, Manchester M13 9PT, UK*

Correspondence should be addressed to Weiqun Lu, wqlv@shou.edu.cn

Received 14 January 2011; Revised 31 March 2011; Accepted 28 June 2011

In order to understand the possible role of globin genes in fish salinity adaptation, we report the molecular characterization and expression of all four subunits of haemoglobin, and their response to salinity challenge in flounder. The entire open reading frames of α1-globin and α2-globin genes were 432 and 435 bp long, respectively, whereas the β1-globin and β2-globin genes were both 447 bp. Although the head kidney (pronephros) is the predicted major site of haematopoiesis, real-time PCR revealed that expression of α-globin and β-globin in kidney (mesonephros) was 1.5 times higher than in head kidney. Notably, the α1-globin and β1-globin mRNA expression was higher than α2-globin and β2-globin in kidney. Expression levels of all four globin subunits were higher in freshwater- (FW-) than in seawater- (SW-) adapted fish kidney. If globins do play a role in salinity adaptation, this is likely to be more important in combating the hemodilution faced by fish in FW than the dehydration and salt loading which occur in SW.

1. Introduction

Haemoglobin (Hb) plays an important role in oxygen transport. In primitive vertebrates such as lamprey, haemoglobin is a monomer. However, in most vertebrate species, including teleost fish, haemoglobin is a tetrameric molecule that consists of two α-globin subunits and two β-globin subunits with one heme group. In human, the haematopoiesis process takes place in bone marrow, but teleost fish do not have bone marrow, and a number of studies have revealed that haemopoietic tissue is found mainly in the head kidney (pronephros) and a smaller amount in the kidney (mesonephros) [1, 2]. However, blood element formation differs among teleost fish [1, 3–5], and while previous studies indicated that head kidney, kidney, and spleen are the main organs forming blood in some species, erythropoiesis is mostly found in kidney [6, 7].

Fish can adequately supply oxygen to all tissues during environmental variations, such as temperature, pH, and oxygen tension changes, by increasing their total haemoglobin content or changing the intrinsic oxygenation characteristics [8, 9]. The haemoglobin-oxygen affinity is higher in hypoxic water than in oxygenated water [10, 11]; as pH decreases, the oxygen affinity of haemoglobin decreases [12, 13]. In order to increase total haemoglobin content, fish usually change globin gene expression at the site of haematopoiesis, which is in turn regulated by adaptive molecular mechanisms [14–16].

Most marine elasmobranchs transferred to lower salinity water exhibit marked changes in plasma and erythrocyte osmolyte composition [17–21]. Plasma dilution and loss of osmolytes can alter the oxygen-carrying capacity and haemoglobin oxygen-binding properties of the blood [22]. In *S. Aurata*, under low-salt concentration, α1 and α2 globin mRNAs levels of the red blood cells (RBCs) increased and decreased, respectively, compared with normal conditions [14]. Unlike marine elasmobranchs, euryhaline flounders are able to survive in both FW and SW but, in common with other euryhaline fish species, maintain a lower blood tonicity in FW. This reflects the long-term adjustments in metabolism and the profile of ion and water transport across gut, kidney, bladder, and gill epithelia that fish require to survive in hypotonic environments. In FW, fish maintain volume regulation by excreting large quantities

of urine through increased renal filtration rate and renal tubule diameter to enhance urine flow [23]. The changing metabolic status and blood tonicity may also cause changes in oxygen consumption. In addition, a number of studies have revealed that nitrite, which is a potent vasodilator in humans, is bioactivated by reaction with deoxyhaemoglobin to preferentially generate nitric oxide (NO) under hypoxic conditions. The physiological function of deoxyhaemoglobin in this process is as an electronically and allosterically regulated nitrite reductase [24–27].

Here, we report the characterization of cDNAs encoding four types of globin in the flounder, along with a preliminary analysis of gene expression and tissue distribution of globins. The kidney was confirmed as the major site of globin expression in this species. Using quantitative real-time PCR measures of the four types of globin mRNA expression, we have examined differences in globin expression along with NO content in kidneys of chronically FW- and SW-adapted fish.

2. Materials and Methods

2.1. Animals. The flounder, *Platichthys flesus*, were collected from Morecambe Bay (Cumbria, UK) and transported to aquarium facilities at the University of Manchester. Flounder were of mixed sex and ranged in weight from 300 to 500 g. The flounder were maintained in recirculating, filtered SW (seawater, Natureland, Skegness, UK) or FW (tap water) tanks at 10–12°C under a 12 h : 12 h/light : dark photoperiod for at least 2 weeks before experimentation. All experiments were performed in accordance with United Kingdom Home Office Regulatory requirements.

2.2. Animal Experiments. To determine the steady-state conditions of fully acclimated animals, fish were studied after being held in SW or FW for 2 weeks in October. Fish were removed from tanks and without anesthetic, blood samples (3–6 mL) were collected within 90 sec into ammonium-heparinized syringes by needle puncture of the caudal blood vessels. Red blood cell count (RBC), hemoglobin (Hb), and hematocrit (Hct) were measured immediately, while plasma obtained by centrifugation of blood was analysed for total NO and electrolytes. The flounder were humanely killed and to reduce RBC contamination of tissue globin content blood was quickly removed from tissues by whole body perfusion via the heart with 50 mL ammonium-heparinized saline solution. Tissues (brain, spinal cord, CNSS, gill, head kidney, kidney, bladder, stomach, intestine, rectum, heart, spleen, liver, gonad, and muscle) were then removed and immediately snap frozen in liquid nitrogen.

2.3. RNA Preparation. Total RNA was extracted from tissues using TRIZOL reagent in accordance with the manufacturer's protocol (Invitrogen, Paisley, UK), and RNA yield was quantified using a NanoDrop spectrophotometer ND-1000 (NanoDrop, Wilmington, DE). At this stage, total RNA from each sample ($n = 8$) was equally pooled for library construction and tissue distribution analysis. Before reverse transcription, total RNA was treated with deoxyribonuclease I (Invitrogen, UK) according to manufacturer's instructions. For the library, mRNA was purified from kidney total RNA using Dynabeads mRNA Direct kit (Dynal, UK).

2.4. cDNA Library Construction and EST Sequence. First strand cDNA synthesis was carried out using the Clontech SMART cDNA Library Kit (Clontech, Basingstoke, UK) as detailed by the manufacturers and amplified by polymerase chain reaction (PCR). The resulting cDNA was purified, cloned to the pDNR-LIB vector (Clontech, Basingstoke, UK), and then transformed into DH5α *Escherichia coli* (Eurogentec). Following cloning, 2,794 colonies (29 plates of 96 wells) were randomly picked from kidney library, sequenced (Macrogen, Seoul, Korea), and aligned with BLAST (basic local alignment search tool) against available databases using Trace2dBest [28]. The sequence alignment and homology analysis was performed using DNAMAN V4.15 software.

2.5. Northern Blot Analysis. 10 μg of total RNA from 15 perfused SW flounder tissues (brain, spinal cord, CNSS, gill, head kidney, kidney, bladder, stomach, intestine, rectum, heart, spleen, liver, gonad, and muscle) were electrophoresed on 1% denaturing agarose formaldehyde gel for 2.5 h at 150 V. The RNA samples were then blotted and subsequently fixed onto Hybond N nylon membranes (Amersham Biosciences, Buckinghamshire, UK) as previously described [29]. The full-length flounder α1-globin and β1-globin were used as cDNA probes for Northern blotting.

2.6. Real-Time Quantitative PCR Analysis. The tissue distribution of α-globin and β-globin mRNAs was analyzed by quantitative PCR of the 15 pooled total RNA tissue samples described above. The effect of salinity on kidney α-globin and β-globin mRNA expression was also examined for individual flounder samples ($n = 7$). All primers and TaqMan probes were designed using Primer Express (ABI) and synthesized commercially (Eurogentec, Seraing, Belgium), and the sequences are given in Table 1.

The optimization and validation of primers and probes were performed using standard ABI protocols. PCRs were performed in triplicate as described by Lu et al. [30]. For the relative quantification of α-globin and β-globin genes expression, the $2^{-\Delta\Delta Ct}$ method as fold changes in the target gene normalized to the reference gene and related to the expression of control was used. The internal control gene used for these analyses was the housekeeping gene 18S, though comparable results were also obtained with β-actin.

2.7. In Situ Hybridisation (ISH). The head kidney and kidney were dissected and fixed in 4% paraformaldehyde [31] and embedded in paraffin wax. Longitudinal 4 μm thick sections were cut, mounted on positive charged slides, and incubated at 60°C for 5 days. *In situ* hybridization was carried out as previously described [29]. The full-length flounder α1-, α2-, β1-, and β2-globin were used to synthesize ^{35}S-labelled RNA probes for *in situ* hybridisation.

Table 1: Gene-specific primers and probes for α-globin, β-globin, β-actin, and 18S rRNA.

Name of primer	Sequence of primer 5′-3′
Hbα1 sense-221F	TCCGCTCCGGTGAGGAA
Hbα1 antisense-323R	GCTCGCTGTATTTGGAGAGGAA
Hbα1 TaqMan probe-273T	6-FAM-CCGTCGGACACATGGATGATCTTCAA-TAMRA
Hbα2 sense-261F	GGGCATGGGCGTGAAAT
Hbα2 antisense-329R	AAGGCGTGCAGCTCACTGA
Hbα2 TaqMan probe-279T	6-FAM-CATCGTTACTCTCACCGAAGCCAT-TAMRA
Hbβ1 sense-F	CATGGTCCAGTGGACAGATAGT
Hbβ1 antisense-R	CTCCCCCACATCGATTTTTC
Hbβ1 TaqMan probe-T	6-FAM-AGCGCAGCGCCATCATTTCCCTTTG-TAMRA
Hbβ2 sense-30F	CATGGTCCAGTGGACAGATAGC
Hbβ2 antisense-100R	TCTCCCCCACATCGATTTTC
Hbβ2 TaqMan probe-53T	6-FAM-AGCGCAGCTCCATCATTGCCCTATG-TAMRA
Actin sense-352F	AAGATGACCCAGATCATGTTCGA
Actin antisense-454R	CGATACCAGTGGTACGACCAGA
Actin TaqMan probe-382T	6-FAM-AACACCCCCGCCATGTACGTTGC- TAMRA
18S sense-625F	TCGTAGTTCCGACCGTAAACG
18S antisense-691R	GCCCGGCGGGTCAT
18S TaqMan probe-649T	6-FAM-CCAACTAGCGATCCGGCGG-TAMRA

2.8. Immunocytochemistry. The α-globin (H80) or β-globin (H-76) antibodies were obtained from Santa Cruz Biotechnology Inc. (Santa Cruz, Calif). These rabbit polyclonal antibodies were raised against amino acid 62–142 of human haemoglobin α and amino acid 62–147 mapping near the C-terminus of human haemoglobin β. Antibody specificity was tested by Western blotting on Wistar rat and flounder blood cell samples. The proliferating cell nuclear antigen (PCNA, C-20; Santa Cruz) antibody is a goat polyclonal IgG mapped at the C-terminus of PCNA of human origin. PCNA is a highly conserved protein in both animal and plant systems and was used as a marker for the heamopoietic stroma of kidney. Immunocytochemistry was carried out based on the method of Lu et al. [30] using goat antirabbit or rabbit antigoat antiserum (DAKO, UK), respectively, as the linking reagent and diaminobenzidine as the chromogen. Control experiments were carried out by omitting the primary antibody.

2.9. Total NO Measurement. To assess the relative nitric oxide status of SW and FW fish kidneys, renal tissue samples from 7 SW- or 7 FW-adapted fish were pooled. NO breakdown products (NO_x) were measured using an enzymatic test (Immundiagnostik, Bensheim, Germany) according to the manufacturer's instructions.

2.10. Statistical Analysis. Plasma and blood analysis data are presented as means ± SE, and comparisons are by t-test. Results for tissue measurements of the mRNA levels of α1-globin, α2-globin, β1-globin, and β2-globin are also expressed as means ± SE. Differences between groups were analysed by ANOVA. Significance levels were set at $^*P < 0.05$.

3. Results

3.1. Isolation and Characterization α-Globin and β-Globin cDNA. Six α1-globin (accession number: HQ843790), three α2-globin (Accession number: HQ843791), six β1-globin (accession number: HQ843792), and two β2-globin (accession number: HQ843793) cDNA clones were obtained following sequence screening of 2,794 randomly picked colonies from the kidney library. They were characterized by nucleotide sequence analysis. The entire open reading frames (including stop codon) of α1 and α2 genes were 432 and 435 bp long, encoding a putative protein of 143 and 144 amino acids, respectively. The α2-globin had a Gly inserted at residue 48 (Figure 1). Comparison of the deduced amino acid sequences of flounder α1-globin and human α-globin polypeptide revealed that 12 of 16 heme interfaces, 9 of 16 $\alpha1\beta1$ interfaces and 11 of 14 $\alpha1\beta2$ interfaces were similar, but 5 of 6 Bohr effect residues were different (Supplementary, see Figure 1(a) in Supplementary Material available online at doi: 10.1155/2011/965153). The homology between α1 and α2 was 58.3% for nucleotides and 65.7% for deduced amino acids. The open reading frames (including stop codon) of β1 and β2 genes were both 447 bp encoding a putative protein of 148 amino acids. The homology between β1 and β2 was 89.9% for nucleotides and 98.6% for deduced amino acids. In the flounder β1-globin, 11 of 16 heme interfaces, 9 of 16 $\alpha1\beta1$ interfaces, and 11 of 13 $\alpha1\beta2$ interfaces were similar to those in human β-globin (Supplementary, see Figure 1(b) in Supplementary Material available online at doi: 10.1155/2011/965153). The deduced amino acid sequences of α-globin and β-globin only shared 15% identity.

```
Flounder α1   ...MSLSGKDKRVVKAIWEKMSSKSDVIGAEALGRMLVS  36
Flounder α2   ...----a---sl-rgl-a-aegrvld--g---------  36
Flounder β1   mvqwtdsersaiislwgkidvgeigpqaltrllivypwtq  40
Flounder β2   mvqwtdserssiialwgkidvgeigpqaltrllivypwtq  40

Flounder α1   YPQTKTYFSHW.ADLSPSSAPVRKHGATIMAAVGDAVGHM  75
Flounder α2   --------ae-gt--t-q-qk-gh--gv--g---mg-kyi  76
Flounder β1   rhfstfgdlstt-ailg-ekvakhgktvmggleravksld  80
Flounder β2   rhfstfgdlstt-ailg-ekvakhgktvmggleravksld  80

Flounder α1   DDLQGFLSKYSELHAFKLRVDPTNFKILAHNMILVMAMYF 115
Flounder α2   vt-team-sl------t-----s-------si--------y 116
Flounder β1   -ikgvysalstmhseklhvdpdnfrllaecisvc-a-kfg 120
Flounder β2   -ikgvysalstmhseklhvdpdnfrllaecisvc-a-kfg 120

Flounder α1   PKDFTAEVHVSVDKFLQCLALALSEKYR              143
Flounder α2   --e--------f----s---w-------              144
Flounder β1   -sv-----qeawq---svvvs--grq-h              148
Flounder β2   -sv-----qeawq---svvvs--grq-h              148
```

Figure 1: Alignment of deduced amino acid sequences of two types of the flounder α-globin cDNAs and two types of the flounder β-globin cDNAs. Dot indicates that the amino acid is absent. Dash indicates the identical amino acid.

3.2. Alignment of α-Globin and β-Globin Amino Acid Se-quences. Cluster analysis of the two types of flounder α-globin cDNAs named α1 and α2 is presented in Figure 2(a). The homology of flounder α1 and α2 was 65.7%, and they were placed in different homology tree clusters. Amino acid homology of the flounder α1-globin gene compared with other reported fish ranged from 62.2% to 79.7%, whereas homology for α2-globin amino acid sequences was between 52.4% and 68.1%. The flounder α1-globin shared 50.0% and α2-globin 43.7% sequence homology with human α1- and α2-globin. Irrespective of the different nomenclature, the flounder α1-globin was closely related to yellowtail α-globin type A, red seabream α-globin type A, and gilthead seabream α-globin type 2, whereas flounder α2-globin was more closely related to yellowtail α-globin type B, Amoy croaker α-globin type 2, large yellow croaker α-globin type 1, red rum α-globin type 2, and gilthead seabream α-globin type 1.

The homology analysis of the flounder β-globin cDNAs is shown in Figure 2(b), both have 148 amino acid residues. β1 and β2 shared 98.6% sequence homology and were placed together in the same homology tree cluster. Comparison of flounder β-globin with orthologous vertebrate β-globin showed that flounder β-globin shared between 59.9% and 85.0% homology with other fish β-globin, and only 50.3% homology with human β-globin. Cluster analysis showed that the β-globin gene in yellowtail was closest to that in flounder.

3.3. Tissue Distribution of Flounder α-Globin and β-Globin mRNA. Northern analysis on a range of flounder tissues showed that α-globin and β-globin transcripts were only present in head kidney, kidney, and spleen RNA samples (Figure 3(a)). The major band size was approximately 650 nucleotides, which was consistent with the predicted length based on the cDNA clones obtained. The relative α-globin and β-globin mRNA expression levels in different tissues were also determined by real-time PCR (Figure 3(b)). The expression levels of α-globin and β-globin mRNA in head kidney and kidney were much greater than in other tissues, while the spleen also appeared to express relatively high levels of α-globin and β-globin transcripts. The expression level of α-globin and β-globin mRNA in the kidney was 1.5 times higher than those in head kidney. In kidney, expression levels of the four individual types of globin mRNA also differed. Figure 3(c) shows that the expression levels of α1-globin and β1-globin mRNAs were higher than those of α2-globin and β2-globin mRNAs.

Table 2: Plasma (a) and blood (b) composition of flounder chronically adapted to SW or FW.

(a) Plasma composition.

	SW	FW
Osmolality (mosmo/kgH_2O)	302.62 ± 3.32	285.2 ± 3.35**
Mg^{2+} (mmol/liter)	4.7 ± 0.18	2.8 ± 0.35**
Cl^- (mmol/liter)	141.4 ± 1.65	124.4 ± 2.21**
Ca^{2+} (free) (mmol/liter)	1.77 ± 0.027	1.8 ± 0.039
Na^+ (mmol/liter)	151.48 ± 2.39	146.92 ± 2.38
K^+ (mmol/liter)	2.7 ± 0.038	2.74 ± 0.13

(b) Blood composition.

	SW	FW
Hematocrit (Hct) %	25.82 ± 1.3	29.78 ± 1.7
RBC × 10^{12}/L	2.258 ± 0.1	2.562 ± 0.2
Hgb g/L	74.4 ± 3.6	84.2 ± 5.4

Independent samples t-test was used to assess differences between chronically adapted FW and SW flounder and between experimental and time matched controls at each time point, $^*P < 0.05$, $^{**}P < 0.005$ ($n = 7$).

3.4. Differential Expression of Globins between SW- and FW-Adapted Fish. Blood composition of chronically FW- and SW-adapted flounder is shown in Table 2. Plasma chloride, magnesium, and osmolality were significantly higher in SW- than in FW-adapted fish. No significant differences were evident for calcium, potassium, and sodium between long-term SW- and FW-adapted fish. There were also no significant differences in blood hematocrit, RBC, and haemoglobin content, which were slightly higher in FW- than in SW-adapted fish. Although there were no statistically significant differences in RBC or haemoglobin content between FW- and SW-adapted flounder, expression levels of α-globin and β-globin mRNAs in the kidney were significantly higher in FW- than in SW-adapted fish (Figure 4(a)). Notably, the pooled kidney NO_x level in FW-adapted fish was double that in SW- adapted fish (Figure 4(b)).

Further study of the kidney as the major site of α-globin and β-globin expression, by *in situ* hybridisation using ^{35}S-labeled α-globin and β-globin RNA probes (antisense) showed that all four types of globin genes were expressed in cells around the renal blood vessels (Figure 5). Abundant expression of both α1 and β globin (both types of β globin)

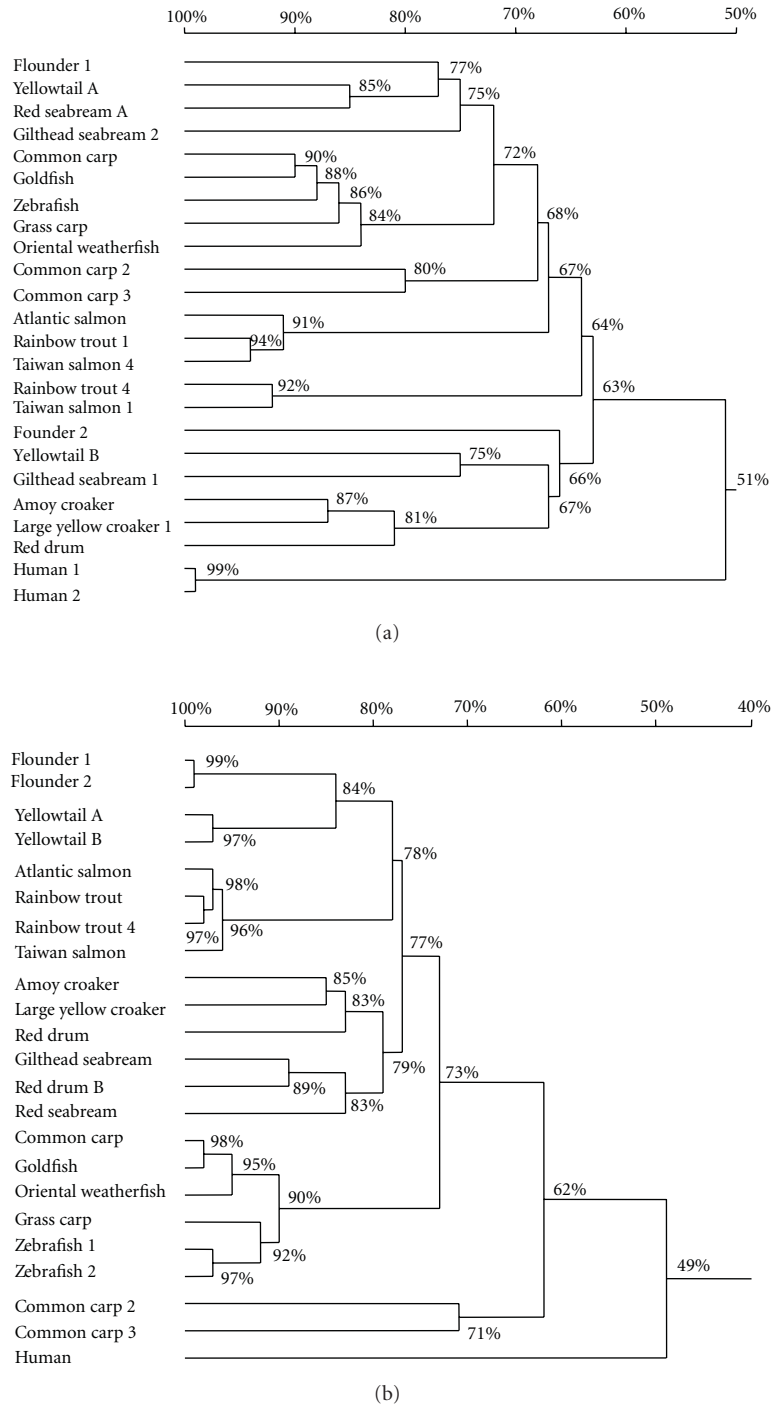

Figure 2: Homology tree of flounder α-globin and β-globin. (a) Comparison of the predicted amino acid sequences of the flounder α-globin with corresponding chains from previously known fish and human α-globin. DDBJ accession numbers: red drum (AAX35759); Amoy croaker (AAZ79649); large yellow croaker 1 (AAV52697); yellowtail A (BAA86218); yellowtail B (BAA86219); gilthead seabream 1 (ABF67512); gilthead seabream 2 (ABF67513); goldfish (CAP69820); grass carp (AAM93257); common carp (BAA20511); common carp 2 (BAB79237); common carp 3 (BAB79240); oriental weatherfish (AAM93258); taiwan salmon 1 (ABY21328); taiwan salmon 4 (ABY21327); red seabream A (AAP20155); atlantic salmon (CAA65949); zebrafish (NP_571332); rainbow trout 1 (NP_001118022); rainbow trout 4 (NP_001118023); human 1 (AAK37554); human 2 (AAN04486). (b) Comparison of the predicted amino acid sequences of the flounder β-globin with corresponding chains from previously known fish and human β-globin. DDBJ Accession Numbers: yellowtail A (BAA86220); yellowtail B (BAA86221); goldfish (CAP69821); grass carp (AAM93253); common carp 1 (BAA13536); common carp 2 (BAB79238); common carp 3 (BAB79239); zebrafish 1 (AAI15159); zebrafish 2 (AAH53176); large yellow croaker (AAV91971); oriental weatherfish (AAM93260); amoy croaker (AAZ79648); taiwan salmon (ABY21329); rainbow trout 1 (ACO07479); rainbow trout 4 (ACO08017); red seabream (AAP20173); atlantic salmon (ACI68343); red drum A (AAW55624); red drum B (AAZ14832); gilthead seabream (ABE2802); human (ACU56984).

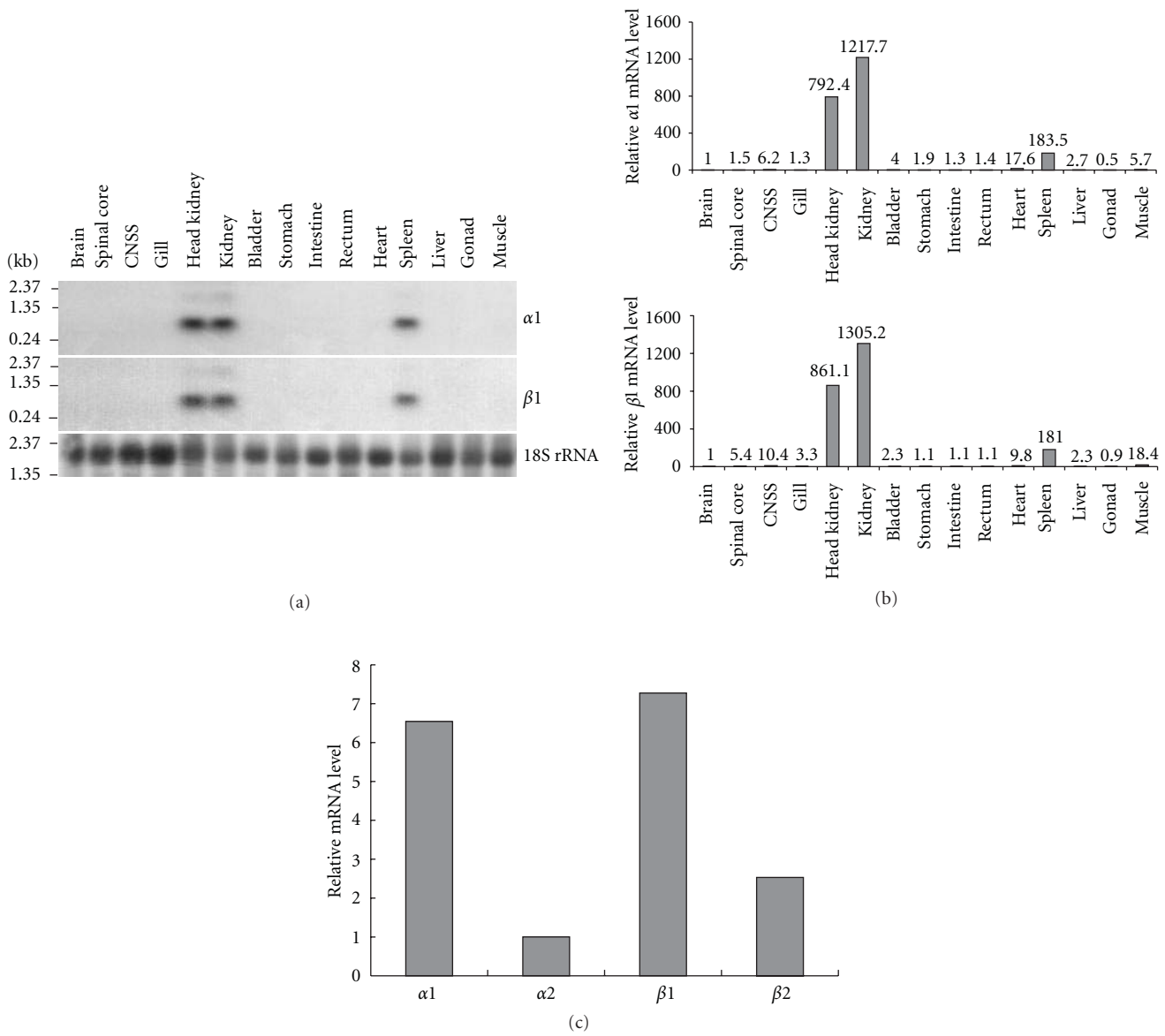

Figure 3: Tissue distribution of α-globin and β-globin mRNA. (a) Northern blot showing tissue distribution and size of the *P. flesus* α1-globin and β1-globin transcripts. (b) Relative mRNA expression levels of α1-globin and β1-globin in different tissues. α-globin and β-globin expressions in different tissues were analyzed by real-time qPCR with 18S rRNA as reference gene. Values are relative fold change with brain as 1 for pooled samples from 8 SW-acclimated adult flounder; (c) expression levels of four types of globin mRNAs in kidney. α-globin and β-globin expressions in kidney were analyzed by real-time qPCR with 18S rRNA as reference gene. Values are relative fold change with α2-globin as 1 for pooled samples from 8 SW-acclimated adult flounder.

genes was evident in the FW-adapted fish kidney, and the incidence and apparent density of signal was much higher for β-globin than α1-globin. There was no precise signal detected in α2-globin-hybridised tissue sections. In SW-adapted fish kidney, the signal obtained was weak, and no cells contained precisely dark dots. The transcriptional activity of both α- and β-globin was clearly higher in FW- than in SW-adapted fish kidney tissue sections. RBCs were void of signal. The negative controls showed few silver grains, indicating the background produced by weak nonspecific binding (Supplementary, see Figure 2 in Supplementary Material available online at doi: 10.1155/2011/965153).

In FW-adapted fish kidney, the immunoreactivity of α1-globin was located in both the haematopoietic stroma and the external contour of renal tubules, whereas β-globins were localised only in the haematopoietic stroma. In SW-adapted fish kidney, α1-globin was localised in the haematopoietic stroma and internal contour of tubules, but there was no detectable signal for β-globin (Figure 6). The protein expression level seemed to be higher in FW- than in SW-adapted kidney tissues. Immunoreactivity for PCNA in kidney appeared limited to the haematopoietic stroma, and again the expression level seemed to be higher in FW- than in SW-adapted kidney tissues (Figure 7). The heterogeneous

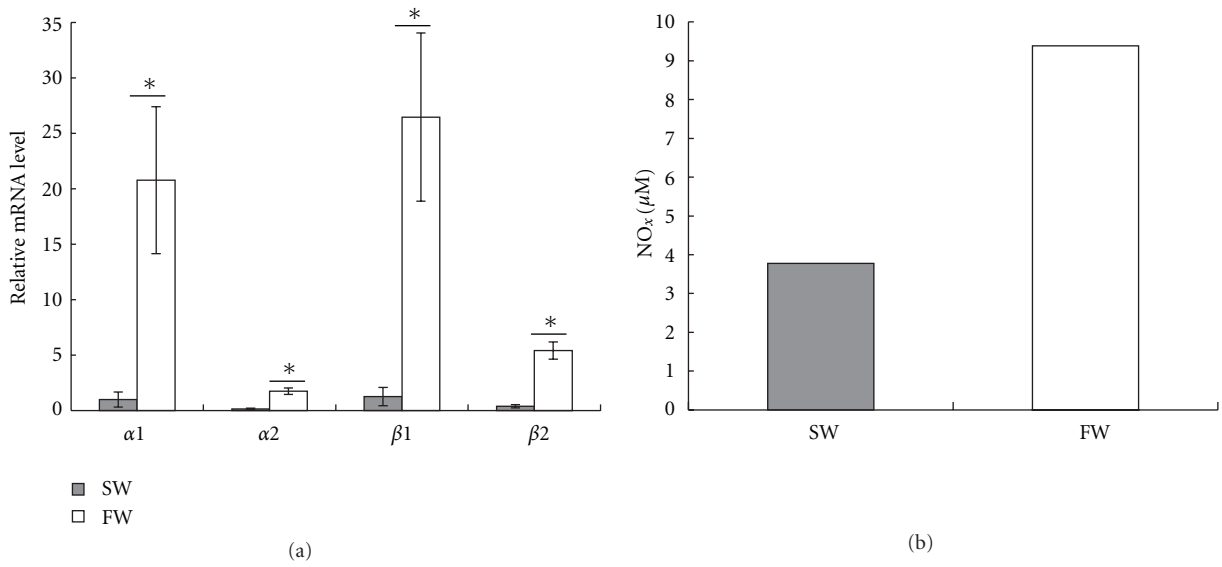

Figure 4: Relative mRNA expression levels of four types of globin and concentration of NO_x in kidney of FW- and SW-adapted flounder. (a) Expressions of four types of globin were analyzed by real-time qPCR with β-actin as reference gene. Values are relative fold change with α2-globin in SW-adapted flounder kidney as 1; the significant difference between FW- and SW-adapted flounder was indicated as $^*P < 0.05$ ($n = 7$). (b) Concentration of total NO in kidney. Values are measurements from 7 pooled kidneys of FW- or SW-adapted flounder.

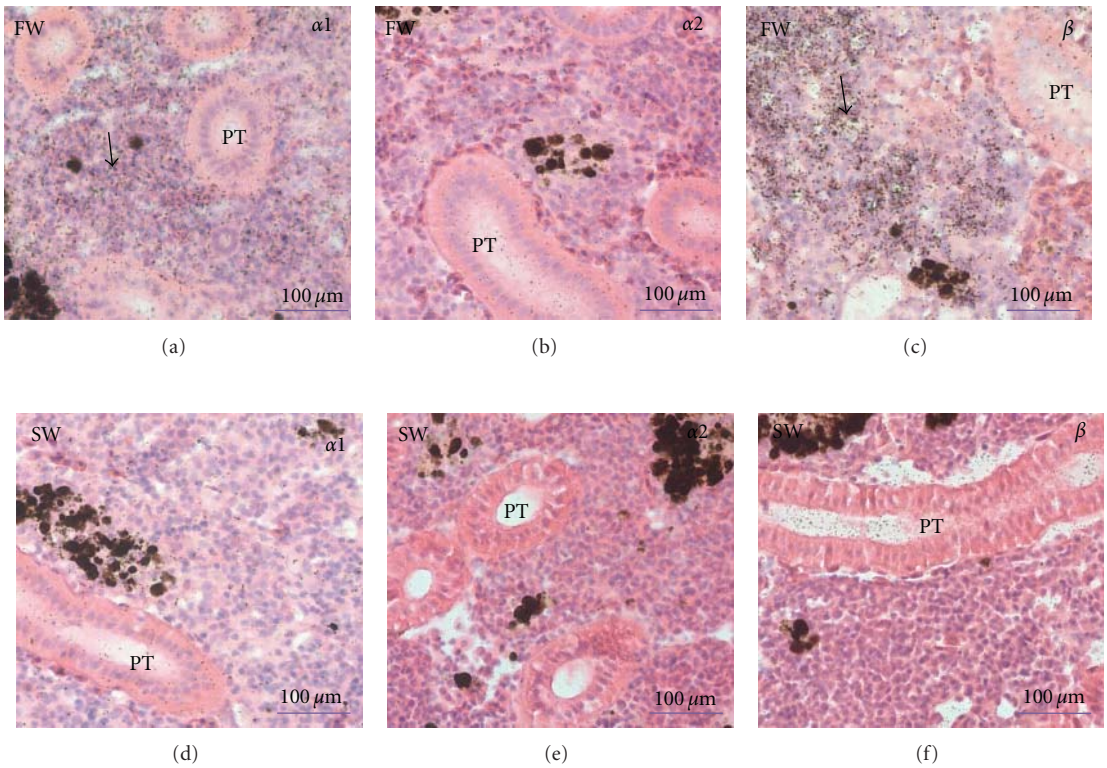

Figure 5: *In situ* hybridization for α1-globin, α2-globin, and β-globin in kidney of FW- and SW-adapted flounder. Abundant α1-globin and β-globin gene expression in haematopoietic stroma of FW-adapted flounder is shown with antisense α1-globin and β-globin ^{35}S RNA probes, and α1-globin and β-globin mRNA was not detected in SW-adapted flounder. α2-globin mRNA was not detected in either of FW- and SW-adapted flounder kidney using an antisense α2-globin ^{35}S RNA probe. The haematopoietic stroma with abundant globins expression are indicated by solid arrows. PT: proximal tubule.

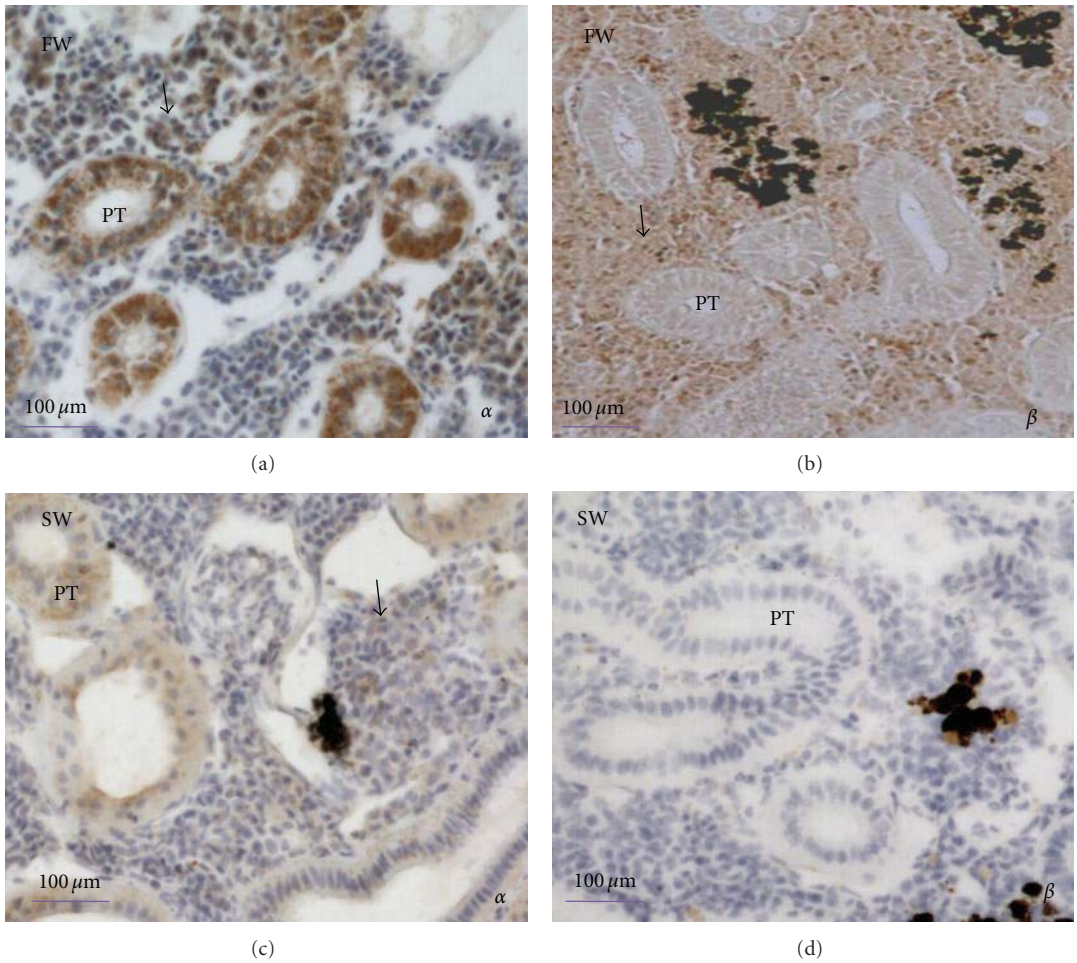

Figure 6: Immunocytochemistry for α-globin and β-globin in kidney of FW- and SW-adapted flounder. The immunoreactivity of α1-globin was located in both of external contour of tubules and haematopoietic stroma, whereas β-globin was localised only in haematopoietic stroma in FW-adapted fish kidney. The haematopoietic stroma with abundant globins is indicated by solid arrows. PT: proximal tubule.

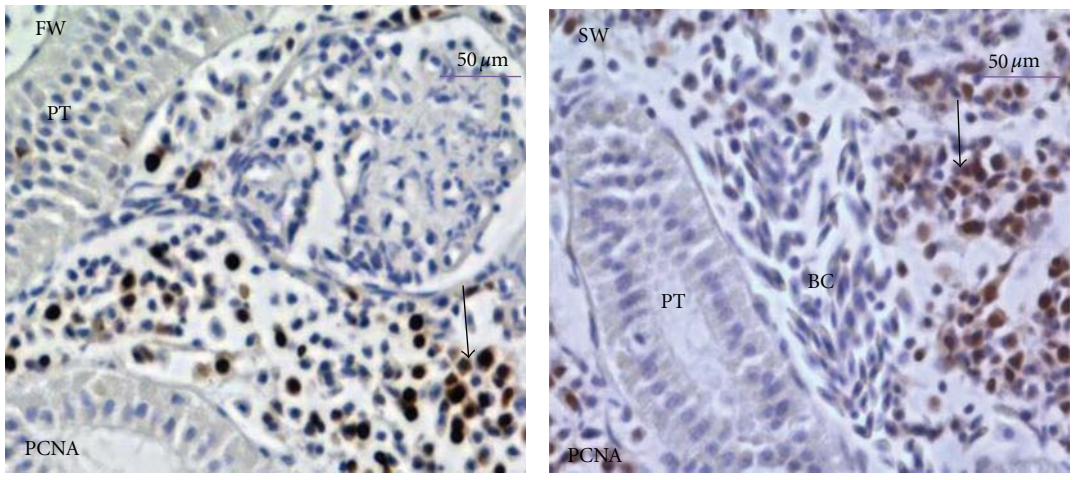

Figure 7: PCNA immunocytochemistry in kidney of FW- and SW-adapted flounder. The immunoreactivity of PCNA was located in haematopoietic stroma. The haematopoietic stroma with abundant PCNA is indicated by solid arrows. PT: proximal tubule; BC: blood cell.

nature of the results regarding the peroxidase precipitates intensity in kidney tissue sections and obviates more precise statements regarding the levels of PCNA, α-globin, and β-globin present.

4. Discussion

This paper is the first to describe the cloning and molecular characterization of flounder α- and β-globin genes, and to examine the effect of altered environmental salinity on α- and β-globin gene expression.

4.1. Molecular Identification and Characterization of α-Globin and β-Globin cDNA. Two α-globin genes were isolated, and the homology of deduced amino acid sequences was 65.7%. The α2-globin had one Gly insertion at position 48. However, Yellowtail α-globin type B has a Gly insertion at position 47 [32, 33]. Miyata et al. [33] suggested that an insertion of Arg or Asp residue at position 47 in carp α-globin produced only inconsequential changes in function and the three-dimensional structure of globin. Despite these structural similarities, a comparison of deduced amino acid sequences of the two types of flounder α-globin placed them in different homology tree clusters, namely, those that are structurally more akin to α1-globin, and those more akin to α2-globin. Flounder α1-globin is most closely related to that of yellowtail α-globin type A, red seabream α-globin type A, and gilthead seabream α-globin type 2 (75–78%), while Salmonidae α1-globin only shares 68% identity with flounder and occupies a separate group. The other two groups consist of the rest of known freshwater teleosts, namely, carp, goldfish, and zebrafish (72–75%), and a separate group which contains human α-globin (Figure 2(a)).

We isolated two β-globin genes in flounder, and the deduced amino acid sequences were 98.6% homologous, and considerably homologous with other vertebrate β-globins. Both types of flounder β-globin had a Phe residue at position 121, in contrast to a Lys residue in yellowtail β-globins, when compared with human β-globin [32]. Yoshizaki et al. [34] suggested that such a residue insertion may affect the function of β-globin. The homology tree was consistent with the phylogeny based on classical taxonomy. The two types of β-globin were placed together and although yellowtail β-globin was the closest β-globin of members of Sciaenidae, Cyprinidae, and Salmonidae were also close to that of flounder. It appears that β-globins are more conserved than α-globin in fishes.

4.2. Tissue Distribution of Flounder Globin mRNAs. Northern blot analysis of total RNA prepared from a range of flounder tissues revealed that the kidney (mesonephros), head kidney (pronephros), and spleen are major sites of expression of the α-globin and β-globin transcripts. Previous histological studies in *Clarias gariepinus* and *Sarotherodon mossambicus* revealed that the kidney, head kidney, and the spleen are the main organs forming blood [6]. Boomker also demonstrated that the cells forming the erythroid and granuloid lineage are mostly found in kidney, while thrombocytes and monocytes are formed in head kidney and spleen in these species [7]. The presence of higher levels of α-globin and β-globin transcripts in kidney, suggests that the kidney may be a more important site of erythropoiesis than head kidney and spleen in flounder.

4.3. Differential Expression of Globins between SW and FW. European flounders are able to survive in both FW and SW but, in common with other euryhaline fish species, maintain a lower blood tonicity, and also increased urine volume and reduced urine osmolality in the FW environment. In terms of blood oxygen transport, we did not see significant differences in blood hematocrit, RBC, or haemoglobin content between FW- and SW-adapted fish. In contrast, the expression levels of all four types of globin mRNAs in the kidney were significantly higher in FW-adapted compared with SW-adapted fish. This is consistent with the observed expression changes of two α-globins following exposure of the elasmobranch, *S. aurata*, to low salinity [14]. These observations suggest that Hb may be involved in some aspects of salinity adaption in fish although exactly the mechanism by which Hb is employed remains unclear.

To clarify these important observations, further investigations were performed using histochemical methods. The apparent increased necessity for globin protein in FW-adapted fish was further supported by the higher globin mRNA expression determined by ISH. This increased mRNA expression in FW kidney was regionalised in the haematopoietic stroma, in a group of cells probably associated with the early stages of erythrocyte generation, but no expression was identified in RBCs themselves. This was coincident with apparently greater immunoreactivity of PCNA, a cell proliferation marker, in the haematopoietic stroma of FW kidney tissue. Importantly, the immunohistochemistry results also showed that both α- and β-globin subunits were located in haematopoietic stroma, confirming the kidney as a major site of production of all four types of globin and of the erythropoietic processes.

In humans, deoxyhaemoglobin is an electronically and allosterically regulated nitrite reductase, and it can convert nitrite to NO preferentially under hypoxic conditions [24–27]. NO may also be controlled by haemoglobin binding properties [35]. Interestingly, kidney tubules dilate and tubule diameter increase in FW flounder [23]. The finding that kidney total NO level in FW-adapted fish was double that in SW-adapted fish, in combination with our previous studies [23], suggests that NO could perhaps play a role in variation of tubule diameter dependent upon haemoglobin binding and reductase activity. The exact mechanisms clearly warrant further investigation.

5. Conclusion

From this study, we conclude that head kidney, kidney, and spleen are erythropoietic tissues in flounder, The kidney is the major site of production of all four types of globin although all four types of globin genes are not expressed equally. Importantly, we also found that α- and β-globin mRNAs are differentially expressed in chronically FW- and

SW-adapted flounder, which raises the possibility that, in fish, these globins may be important in some aspects of salinity adaptation. The newly generated deoxyhaemoglobin may play an important role in combating the hemodilution faced in FW. This may be particularly relevant for migratory fish such as flounder and salmonids as they move between media of different salinities. Similar mechanism may also be of importance in mammals and would be of interest to examine in the future.

Abbreviations

Hb: Haemoglobin
PCR: Polymerase chain reaction
PCNA: Proliferating cell nuclear antigen
CNSS: Caudal neurosecretory system
NO_x: Nitric oxide and nitrogen dioxide
Hct: Hematocrit.

Acknowledgments

This work was supported in part by Shanghai Education Commission Grant (no. 10ZZ102), Shanghai Ocean University (A-2400-09-0140), National Natural Science Foundation of China (31072228), and Science & Technology Committee of Shanghai (09320503500), and Natural Environment Research Council (NER/T/S/2001/00282) also funded the study.

References

[1] C. E. Willett, A. Cortes, A. Zuasti, and A. G. Zapata, "Early hematopoiesis and developing lymphoid organs in the zebrafish," *Developmental Dynamics*, vol. 214, no. 4, pp. 323–336, 1999.

[2] J. H. Rombout, H. B. Huttenhuis, S. Picchietti, and G. Scapigliati, "Phylogeny and ontogeny of fish leucocytes," *Fish and Shellfish Immunology*, vol. 19, no. 5, pp. 441–455, 2005.

[3] J. Meseguer, M. A. Esteban, A. Garcia Ayala, A. Lopez Ruiz, and B. Agulleiro, "Granulopoiesis in the head-kidney of the sea bass (Dicentrarchus labrax l.): an ultrastructural study," *Archives of Histology and Cytology*, vol. 53, no. 3, pp. 287–296, 1990.

[4] M. A. Esteban, J. Munoz, and J. Meseguer, "Blood cells of sea bass (Dicentrarchus labrax L.). Flow cytometric and microscopic studies," *Anatomical Record*, vol. 258, no. 1, pp. 80–89, 2000.

[5] F. J. Stephens, S. R. Raidal, and B. Jones, "Haematopoietic necrosis in a goldfish (Carassius auratus) associated with an agent morphologically similar to herpesvirus," *Australian Veterinary Journal*, vol. 82, no. 3, pp. 167–169, 2004.

[6] J. Boomker, "The haemocytology and histology of the haemopoietic organs of South African fresh water fish. I. The haemopoietic organs of Clarias gariepinus and Sarotherodon mossambicus," *Onderstepoort Journal of Veterinary Research*, vol. 46, no. 4, pp. 217–222, 1979.

[7] J. Boomker, "The haematology and histology of the haemopoietic organs of South African freshwater fish. III. The leucocytes, plasma cells and macrophages of Clarias gariepinus and Sarotherodon mossambicus," *Onderstepoort Journal of Veterinary Research*, vol. 48, no. 4, pp. 185–193, 1981.

[8] P. C. de Souza and G. O. Bonilla-Rodriguez, "Fish hemoglobins," *Brazilian Journal of Medical and Biological Research*, vol. 40, no. 6, pp. 769–778, 2007.

[9] M. E. Favero and F. F. Costa, "Alpha-hemoglobin-stabilizing protein: an erythroid molecular chaperone," *Biochemistry Research International*, vol. 2011, Article ID 373859, 7 pages, 2011.

[10] D. A. Powers, G. S. Greaney, and A. R. Place, "Physiological correlation between lactate dehydrogenase genotype and haemoglobin function in killifish," *Nature*, vol. 277, no. 5693, pp. 240–241, 1979.

[11] M. Nikinmaa, "Haemoglobin function in vertebrates: evolutionary changes in cellular regulation in hypoxia," *Respiration Physiology*, vol. 128, no. 3, pp. 317–329, 2001.

[12] B. Giardina, D. Mosca, and M. C. De Rosa, "The Bohr effect of haemoglobin in vertebrates: an example of molecular adaptation to different physiological requirements," *Acta Physiologica Scandinavica*, vol. 182, no. 3, pp. 229–244, 2004.

[13] F. B. Jensen, "Red blood cell pH, the Bohr effect, and other oxygenation-linked phenomena in blood O_2 and CO_2 transport," *Acta Physiologica Scandinavica*, vol. 182, no. 3, pp. 215–227, 2004.

[14] S. Campo, G. Nastasi, A. D'Ascola et al., "Hemoglobin system of *Sparus aurata* changes in fishes farmed under extreme conditions," *Science of the Total Environment*, vol. 403, no. 1–3, pp. 148–153, 2008.

[15] C. Ton, D. Stamatiou, and C. C. Liew, "Gene expression profile of zebrafish exposed to hypoxia during development," *Physiological Genomics*, vol. 13, no. 2, pp. 97–106, 2003.

[16] D. L. van der Meer, G. E. van den Thillart, F. Witte et al., "Gene expression profiling of the long-term adaptive response to hypoxia in the gills of adult zebrafish," *American Journal of Physiology*, vol. 289, no. 5, pp. R1512–R1519, 2005.

[17] J. A. Sulikowski and L. A. Maginniss, "Effects of environmental dilution on body fluid regulation in the yellow stingray, *Urolophus jamaicensis*," *Comparative Biochemistry and Physiology A*, vol. 128, no. 2, pp. 223–232, 2001.

[18] B. L. Mui, P. R. Cullis, E. A. Evans, and T. D. Madden, "Osmotic properties of large unilamellar vesicles prepared by extrusion," *Biophysical Journal*, vol. 64, no. 2, pp. 443–453, 1993.

[19] P. K. T. Pang, R. W. Griffith, and J. W. Atz, "Osmoregulation in elasmobranchs," *American Zoologist*, vol. 17, no. 2, pp. 365–377, 1977.

[20] T. J. Shuttleworth, "Salt and water balance-extrarenal mechanisms," in *Physiology of Elasmobranch Fishes*, T. J. Shuttleworth, Ed., pp. 171–199, Springer, New York, NY, USA, 1988.

[21] W. N. Holmes and E. M. Donaldson, "Body compartments and distribution of electrolytes," in *Fish Physiology*, W. S. Hoar and D. J. Randall, Eds., vol. 1, pp. 1–89, Academic Press, New York, NY, USA, 1969.

[22] A. R. Cooper and S. Morris, "Haemoglobin function and respiratory status of the Port Jackson shark, *Heterodontus portusjacksoni*, in response to lowered salinity," *Journal of Comparative Physiology B*, vol. 174, no. 3, pp. 223–236, 2004.

[23] E. Weybourne, J. M. Warne, H. Hentschel, M. Elger, and R. J. Balment, "Renal morphology of the euryhaline flounder (*Platichthys flesus*): distribution of arginine vasotocin receptor," *Annals of the New York Academy of Sciences*, vol. 1040, pp. 521–523, 2005.

[24] R. Grubina, Z. Huang, S. Shiva et al., "Concerted nitric oxide formation and release from the simultaneous reactions of nitrite with deoxy—and oxyhemoglobin," *Journal of Biological Chemistry*, vol. 282, no. 17, pp. 12916–12927, 2007.

[25] K. Cosby, K. S. Partovi, J. H. Crawford et al., "Nitrite reduction to nitric oxide by deoxyhemoglobin vasodilates the human circulation," *Nature Medicine*, vol. 9, no. 12, pp. 1498–1505, 2003.

[26] K. T. Huang, A. Keszler, N. Patel et al., "The reaction between nitrite and deoxyhemoglobin: reassessment of reaction kinetics and stoichiometry," *Journal of Biological Chemistry*, vol. 280, no. 35, pp. 31126–31131, 2005.

[27] S. Shiva, Z. Huang, R. Grubina et al., "Deoxymyoglobin is a nitrite reductase that generates nitric oxide and regulates mitochondrial respiration," *Circulation Research*, vol. 100, no. 5, pp. 654–661, 2007.

[28] S. Kalujnaia, I. S. McWilliam, V. A. Zaguinaiko et al., "Transcriptomic approach to the study of osmoregulation in the European eel *Anguilla anguilla*," *Physiological Genomics*, vol. 31, no. 3, pp. 385–401, 2007.

[29] E. Lu, L. Dow, S. Gumusgoz et al., "Coexpression of corticotropin-releasing hormone and urotensin I precursor genes in the caudal neurosecretory system of the euryhaline flounder (*Platichthys flesus*): a possible shared role in peripheral regulation," *Endocrinology*, vol. 145, no. 12, pp. 5786–5797, 2004.

[30] W. Lu, M. Greenwood, L. Dow et al., "Molecular characterization and expression of urotensin II and its receptor in the flounder (*Platichthys flesus*): a hormone system supporting body fluid homeostasis in euryhaline fish," *Endocrinology*, vol. 147, no. 8, pp. 3692–3708, 2006.

[31] A. E. Nikolaev, G. Myszkiewicz, G. Berden, W. L. Meerts, J. F. Pfanstiel, and D. W. Pratt, "Twisted intramolecular charge transfer states: rotationally resolved fluorescence excitation spectra of 4,4'- dimethylaminobenzonitrile in a molecular beam," *Journal of Chemical Physics*, vol. 122, no. 8, Article ID 084309, 10 pages, 2005.

[32] K. Okamoto, M. Sakai, and M. Miyata, "Molecular cloning and sequence analysis of α—and β-globin cDNAs from yellowtail, *Seriola quinqueradiata*," *Comparative Biochemistry and Physiology B*, vol. 130, no. 2, pp. 207–216, 2001.

[33] M. M. Miyata, I. Hirono, and T. Aoki, "Analysis of α-globin gene family of carp α-globin gene structure of no. 3, no. 6 and no. 7," *Nippon Suisan Gakkaishi*, vol. 59, no. 6, pp. 1077–1083, 1983.

[34] G. Yoshizaki, I. Hirono, T. Aoki, and F. Takashima, "Cloning and sequencing of cDNAs of the β-globin gene family in carp," *Journal of Fish Biology*, vol. 51, no. 6, pp. 1125–1136, 1997.

[35] T. L. Stepuro and V. V. Zinchuk, "Nitric oxide effect on the hemoglobin-oxygen affinity," *Journal of Physiology and Pharmacology*, vol. 57, no. 1, pp. 29–38, 2006.

Hindawi Publishing Corporation
Evidence-Based Complementary and Alternative Medicine
Volume 2011, Article ID 978253, 10 pages
doi:10.1155/2011/978253

Research Article

Species Identification of Marine Fishes in China with DNA Barcoding

Junbin Zhang

College of Fisheries and Life Science, Shanghai Ocean University, Shanghai 201306, China

Correspondence should be addressed to Junbin Zhang, jbzhang30@163.com

Received 10 December 2010; Accepted 27 February 2011

DNA barcoding is a molecular method that uses a short standardized DNA sequence as a species identification tool. In this study, the standard 652 base-pair region of the mitochondrial cytochrome oxidase subunit I gene (COI) was sequenced in marine fish specimens captured in China. The average genetic distance was 50-fold higher between species than within species, as Kimura two parameter (K2P) genetic distances averaged 15.742% among congeners and only 0.319% for intraspecific individuals. There are no overlaps of pairwise genetic variations between conspecific and interspecific comparisons apart from the genera *Pampus* in which the introgressive hybridization was detected. High efficiency of species identification was demonstrated in the present study by DNA barcoding. Due to the incidence of cryptic species, an assumed threshold is suggested to expedite discovering of new species and biodiversity, especially involving biotas of few studies.

1. Introduction

Fishes are important animal protein sources for human beings, and they are frequently used in complementary and alternative medicine/traditional medicine (CAM/TM). The delimitation and recognition of fish species is not only of interest for taxonomy and systematics, but also a requirement in management of fisheries, authentication of food products, and identification of CAM/TM materials [1–3].

Due to the complexity and limitations of morphological characters used in traditional taxonomy, several PCR-based methods of genotype analysis have been developed for the identification of fish species, particularly for eggs, larvae, and commercial products. Sequence analysis of species-specific DNA fragments (often mitochondrial or ribosomal genes) and multiplex PCR of species-conserved DNA fragments are efficient for fish species identification [4–10]. However, these molecular methods are limited to particular known species and are not easily applicable to a wide range of taxa. Therefore, Hebert et al. advocated using a standard DNA sequence that is DNA barcoding to identify species and uncover biological diversity [11, 12]. For many animal taxa, sequence divergences within the 5′ region of the mitochondrial cytochrome oxidase subunit I (COI) gene were much greater between species than within them, and this in turn suggests that the approach is widely applicable across phylogenetically distant animal groups [12, 13]. To date, some published papers explicitly address that COI barcodes effectively discriminate different species for a variety of organisms [14–23]. However, several scientists express concerns that species identification based on variations of single mitochondrial gene fragment may remain incorrect or ambiguous assignments, particularly in cases of possible mitochondrial polyphyly or paraphyly [24, 25]. In the current study, we test the efficacy of DNA barcoding in marine fishes of China. The sea area of China is part of the Indo-West Pacific Ocean, which is regarded as the center of the world's marine biodiversity [26]. Highly species-rich biotas are particularly attractive to test the reliability and efficiency of DNA barcoding.

2. Material and Methods

The majority of fish specimens were captured with the drawl net at 20 localities along the coast of China (collection information available at http://www.barcodinglife.org/). A total of 329 specimens from one hundred species of fish were collected. Vouchers were deposited in the South China Sea Institute of Oceanography, Chinese Academy of Sciences, and all specimens were preserved in 70% ethanol. Tissue samples were dissected from the dorsal muscle, and genomic DNA was extracted according to the standard Barcode of Life

protocol [27]. Firstly, fragments of the 5′ region of the mitochondrial COI gene were PCR-amplified using C_FishF1t1/ C_FishR1t1 primer cocktails [28]. The cocktail C_FishF1t1 contained two primers (FishF2_t1/VF2_t1), and C_FishR1t1 also contained two primers (FishR2_t1/ FR1d_t1). All PCR primers were tailed with M13 sequences to facilitate sequencing of products. The nucleotide sequences of the primers were

FishF2_t1: *5′-TGTAAAACGACGGCCAGTCGACTAATCATAAAGATATCGGCAC-3′.

VF2_t1: *5′-TGTAAAACGACGGCCAGTCAACCAACCACAAAGACATTGGCAC-3′.

FishR2_t1: **5′-CAGGAAACAGCTATGACACTTCAGGGTGACCGAAGAATCAGAA-3′.

FR1d_t1: **5′-CAGGAAACAGCTATGACACCTCAGGGTGTCCGAARAAYCARAA-3′.

*The M13F primer sequence is underlined; **the M13R primer sequence is underlined.

PCR reactions were carried out in 96-well plates using Mastercycler Eppendorf gradient thermal cyclers (Brinkmann Instruments, Inc.). The reaction mixture of 825 μl water, 125 μl 10× buffer, 62.5 μl $MgCl_2$ (25 mM), 6.25 μl dNTP (10 mM), 6.25 μl each primer (0.01 mM), and 6.25 μl Taq DNA polymerase (5 U/μl) was prepared for 96 wells of each plate, in which each well contained 10.5 μl mixture and 2 μl genomic DNA. Thermocycling comprised an initial step of 2 min at 95°C and 35 cycles of 30 sec at 94°C, 40 sec at 52°C, and 1 min at 72°C, with a final extension at 72°C for 10 min. Amplicons were visualized on 2% agarose E-Gel 96-well system (Invitrogen). PCR products were amplified again with the primers M13F (5′-TGTAAAACGACGGCCAGT-3′) and M13R (5′-CAGGAAACAGCTATGAC-3′), respectively, using the BigDye Terminator v.3.1 Cycle Sequencing Kit (Applied Biosystems, Inc.). Thermocycling conditions were as follows: an initial step of 2 min at 96°C and 35 cycles of 30 sec at 96°C, 15 sec at 55°C, and 4 min at 60°C. Sequencing was performed on an ABI 3730 capillary sequencer according to manufacturer's instructions.

For specimens that failed to yield sequences using the primer combinations above, a second round of PCR using the alternative C_VF1LFt1/ C_VR1LRt1 primer combination was carried out. C_VF1LFt1 consisted of four primers (VF1_t1/VF1d_t1/LepF1_t1/VFli_t1), and C_VR1LRt1 also comprised four primers (VR1_t1/VR1d_t1/LepR1_t1/VRli_t1) [28].

VF1_t1: *5′-TGTAAAACGACGGCCAGTTCTCAACCAACCACAAAGACATTGG-3′.

VF1d_t1: *5′-TGTAAAACGACGGCCAGTTCTCAACCAACCACAARGAYATYGG-3′.

LepF1_t1: *5′-TGTAAAACGACGGCCAGTATTCAACCAATCATAAAGATATTGG-3′.

VFli_t1: *5′-TGTAAAACGACGGCCAGTTCTCAACCAACCAIAAIGAIATIGG-3′.

VR1_t1: **5′-CAGGAAACAGCTATGACTAGACTTCTGGGTGGCCRAARAAYCA-3′.

VR1d_t1: **5′-CAGGAAACAGCTATGACTAGACTTCTGGGTGGCCAAAGAATCA-3′.

LepR1_t1: **5′-CAGGAAACAGCTATGACTAAACTTCTGGATGTCCAAAAAATCA-3′.

VRli_t1: **5′-CAGGAAACAGCTATGACTAGACTTCTGGGTGICCIAAIAAICA-3′.

*The M13F primer sequence is underlined; **the M13R primer sequence is underlined.

The thermocycling protocol used was 1 min at 95°C and 35 cycles of 30 sec at 94°C, 40 sec at 50°C, and 1 min at 72°C, with a final extension at 72°C for 10 min. Sequecing PCR and sequencing followed above procedure.

DNA sequences were aligned with SEQSCAPE v.2.5 software (Applied Biosystems, Inc.). Sequence divergences were calculated using the Kimura two parameter (K2P) distance model [29], and unrooted NJ trees based on K2P distances were created in MEGA software [30]. In the chosen taxonomic group, phylogenetic analysis was carried out in PAUP 4.010b using the maximum parsimony (MP) method, with 1,000 replications of the full heuristic search.

The following categories of K2P distances were calculated: intraspecific distances (S), interspecies within the congener (G), and interspecies from different genus but within intrafamily (F). These values were plotted using the boxplot representation of R. Boxplots [31] in SPSS 11.5 software (SPSS Inc., Chicago, IL, USA). Only for families containing 2 or more genera, separate boxplot was constructed for the sake of comparisons among taxonomic categories. Boxplots describe median (central bar), interquartile range (IQR: between upper (Q3) and low (Q1) quartile), values lying within 1.5× IQR beneath Q1 or 1.5× above Q3 ("whiskers"), and extreme values (outliers). Mann-Whitney tests were performed between S, G, and F distributions to estimate the overlap among taxonomic ranks.

3. Results

A total of 329 specimens were analyzed, from which 321 sequences (all >500 bp) belonging to 121 species (another species was identified to the genus level) were ultimately obtained (GenBank accession numbers: EF607296-EF607616). These species cover the majority of fishes living in the coastline of the South China Sea. All sequences were aligned with a consensus length of 652 bp, and no insertions, deletions, or stop codons were observed in any sequence. However, multiple haplotypes were detected for some species.

Except for *Acentrogobius caninus, Scomber japonicus, Terapon jarbua, Upeneus sulphureus, Elops hawaiensis, Gymnothorax pseudothyrsoideus, Dendrophysa russelii, and Pennahia anea* (which reached the maximum value of 2.02%), intraspecific genetic distances were generally below 1%, and some decreased to zero (between some intraspecific individuals of *Thryssa setirostris, Parapercis ommatura, Scatophagus argus,* etc.).

The mean intraspecies K2P (Kimura two-parameter) distance was 0.319%; the distance increased sharply to 15.742% among individuals of congeneric species. Overall,

Table 1: Genetic divergences (percentage, K2P distance) within various taxonomic levels. Data are based on 321 sequences (>500 bp) from 122 species.

Comparisons within	Taxa	Number of comparisons	Mean	Median	Minimum	Maximum	s.e.[#]
Species	121	453	0.319	0.150	0	2.021*	0.018
Genus	85	397	15.742	16.490	0.154**	25.189	0.292
Family	55	848	20.199	19.850	11.532	34.333	0.134
Order	15	17881	24.656	—	12.923	39.627	0.024
Class	2	29262	25.225	—	15.730	40.800	0.016

* Pennahia anea; ** Pampus argenteus versus Pampus cinereus.
[#]Standard error.

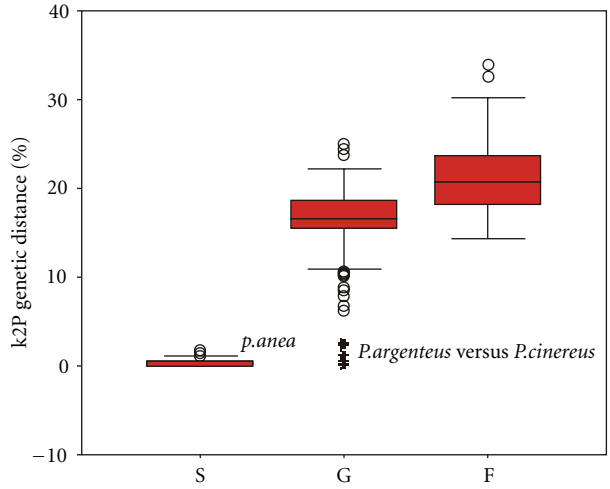

Figure 1: Box plots of K2P distances. IQR: interval into which the "central" 50% of the data fall. Black bar in the box indicates the median. Circle: "mild outlier" and asterisks: "extreme outliers". Extreme outliers are discussed in the text.

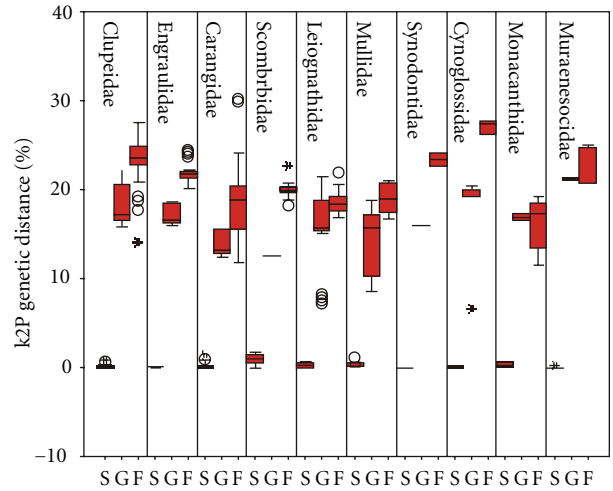

Figure 2: Boxplot distributions of S, G, and F. Intra-species (S), interspecies among congeneric species (G), and intergenera but intrafamily (F) K2P distances for different families.

the average genetic distance among congeneric species is nearly 50-fold higher than that among individuals within species. For the higher taxonomic ranks (family, order, and class), mean pairwise genetic distances increased gradually and reached 20.199%, 24.656%, and 25.225%, respectively (Table 1). Standard errors for K2P genetic distances were small, and values of the mean and median were close within different taxonomic ranks (Table 1). This indicates fluctuations of K2P genetic distances tend to be convergent (Figures 1 and 2).

In the unrooted NJ (neighbour-joining) tree (Figure 3), three specimens of *Pampus argentenus* were grouped together and contained within the cluster of *Pampus cinereus*. These *Pampus argentenus* specimens were collected in the same site off the west coast of the South China Sea, and were difficult to identify because of their complex morphological characteristics (available at http://www.barcodinglife.org/). They possessed combined characteristics of *Pampus cinereus* and *Pampus argentenus*: the asymmetrical tail of *Pampus cinereus* and silver color of *Pampus argentenus*. If the suspicious congeneric K2P distances in the genera *Pampus* are excluded (the extreme outliers in Figure 1), the pairwise genetic divergences among congeneric species are above 10%. There are no overlaps between intraspecific and congeneric K2P distances within the same family (Figure 3).

At the species level, all COI sequences clustered in monophyletic species units. At the family level, there were paraphyletic clusters for three families (Carangidae, Gobiidae, and Ariidae) (Figure 3), though over 98% of specimens fell into the expected division of families. Intrafamily K2P distances (F) were generally higher than congeneric (G) distances, which were definitely higher than intraspecific (S) distances (Table 1, all Mann-Whitney tests were highly significant, P value $<10-6$). However, overlaps between F and G distances were observed in Clupeidae, Carangidae, Mullidae, and Muraenesocidae.

4. Discussion

In morphological taxonomy, characters are delimited usually without any explicit criteria for character selection or coding, and morphological data sets have the potential to be quite arbitrary. For example, morphologists do not generally report their criteria for including or excluding characters,

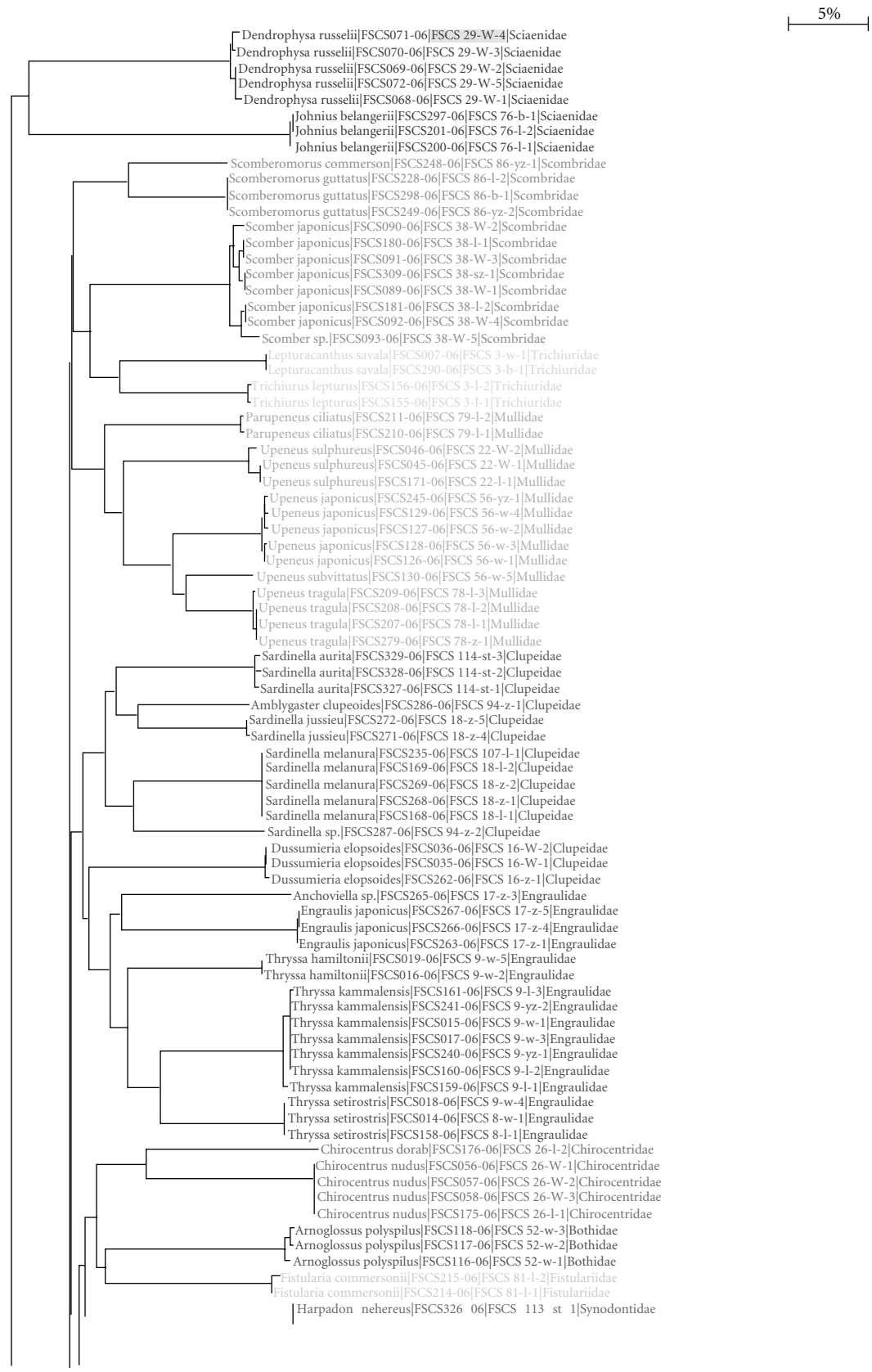

(a)

Figure 3: Continued.

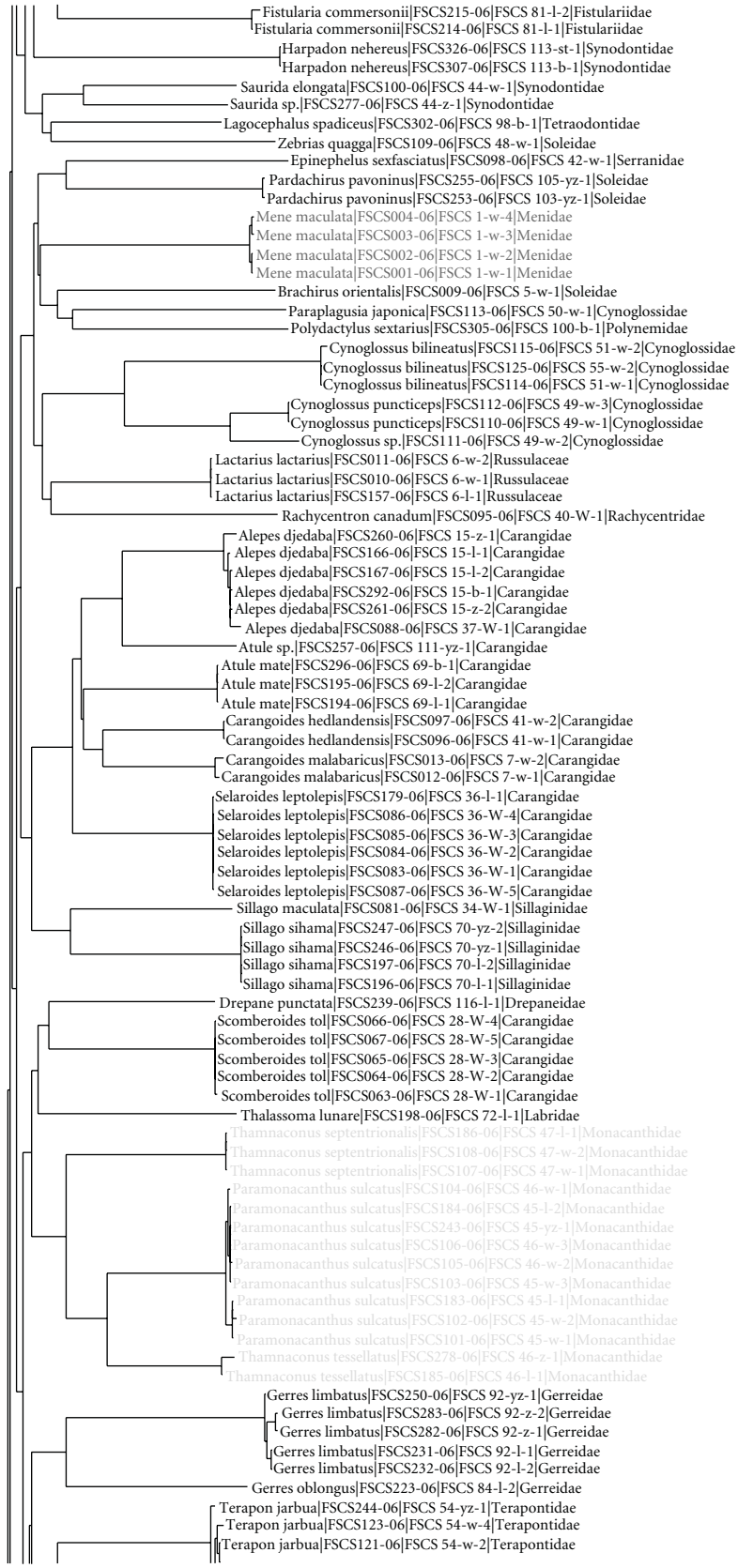

(b)

Figure 3: Continued.

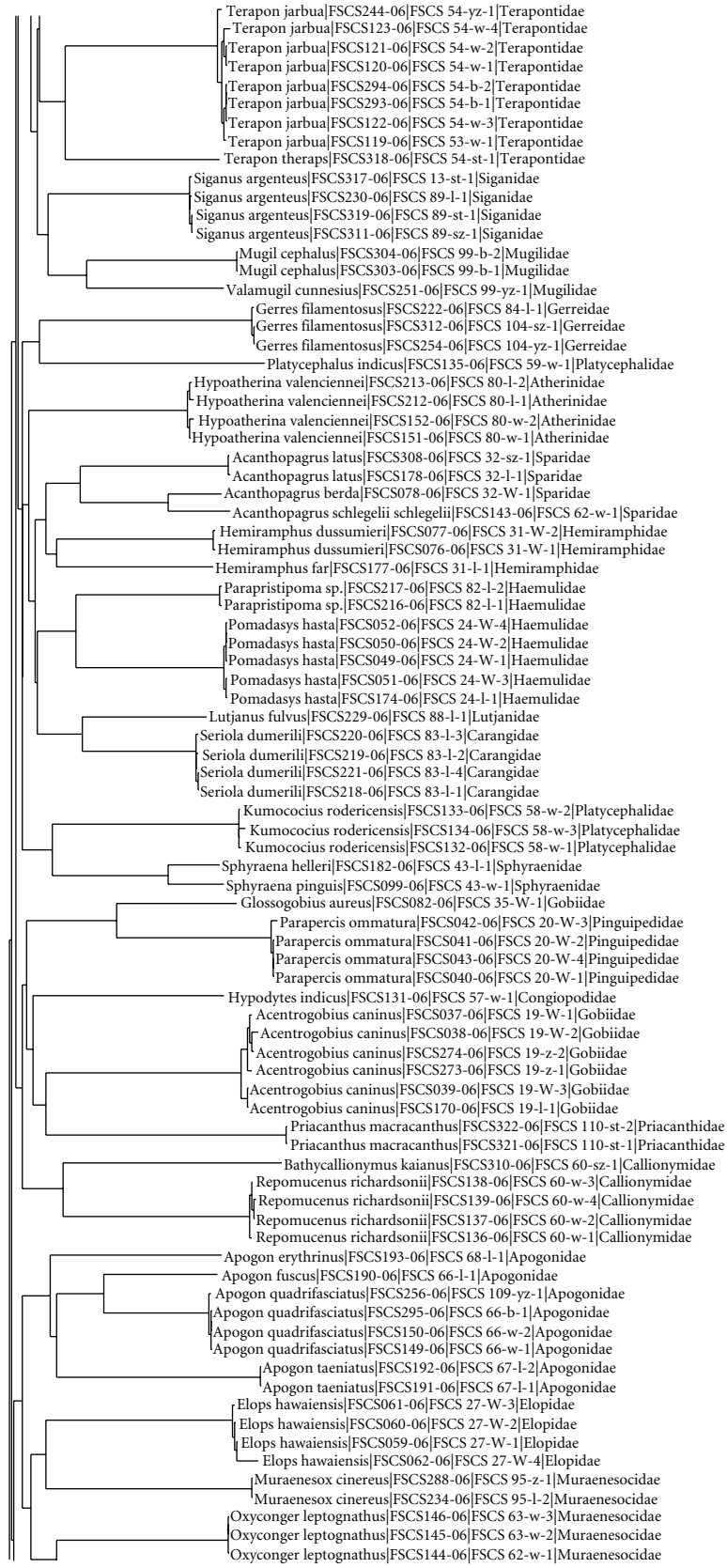

(c)

Figure 3: Continued.

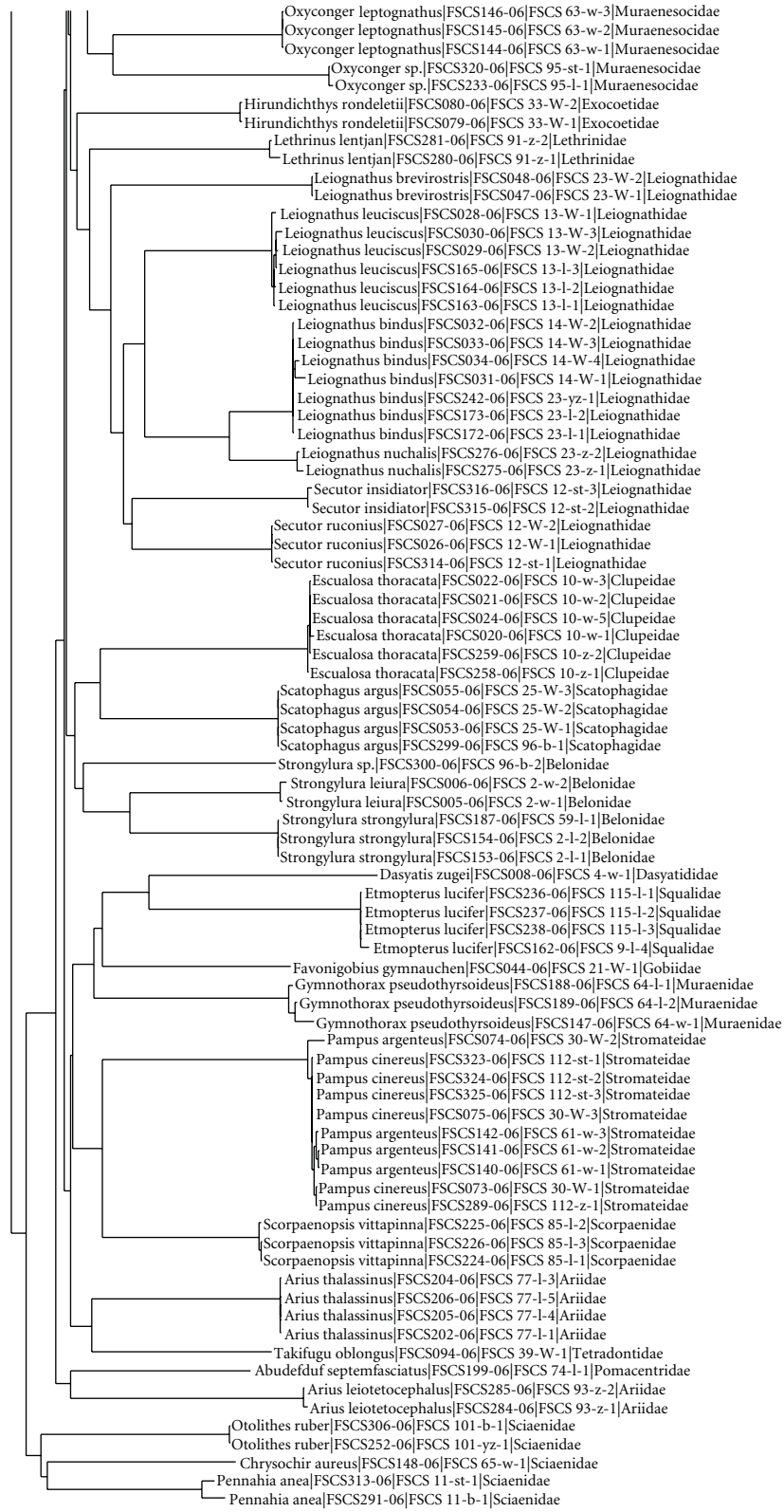

(d)

Figure 3: Neighbor-joining (NJ) tree of COI sequences. Scale: 5% K2P distance. The first numbers following species names are the process IDs, and the latter are the sample IDs.

and when criteria are given, they vary considerably among studies [32]. Thus, it is not surprising that there are so many synonyms for organisms [33], and an objective, rigorous species delimitation according to explicit criteria is therefore necessary for many taxonomic studies [34]. While DNA barcoding provides taxonomic identification for a specimen, the accuracy of such an assignment depends on whether species are monophyletic with respect to sequence variations of the COI gene. That is, individuals of a given species are more closely related to all other conspecifics than to any member of other species. Except for the hybridized specimens in the genus Pampus, there are no overlaps between genetic variations of S and G (Figure 1).

The factors responsible for deviations from taxonomic monophyly may be varied and complex [35]; one potential cause of species-level polyphyly is the occasional mating between distinct species, resulting in hybrid offspring carrying a mixture of genes from both parent species. Furthermore, mitochondrial genes are generally subjected to introgression more frequently than nuclear ones, and introgression also leads to phylogenetic paraphyly [35–38], like the hybridization between *Pampus argentenus* and *Pampus cinereus* in this study. In such cases, combinations of morphological and genotypic data are needed for species assignment of hybrids.

Biological mechanisms, water dynamics, or historical events may cause deep genetic structuring of populations in marine species [26, 39]. Many explanations for genetic population structuring on local and regional scales involve behaviors such as the adoption of pelagic early life stages and movement over broad geographic ranges, and these factors are theoretically associated with gene flow [40–42]. For many marine fishes, there is a lack of phylogeographic structure among populations [43, 44]; in this study, for individuals from long distance localities, some intraspecific genetic variations reduced to zero within families Carangidae, Sciaenidae, and Mullidae. However, some pairwise K2P distances exceeded 1.00% within the coastal species such as *Acentrogobius caninus, Scomber japonicus, Terapon jarbua, Upeneus sulphureus, Elops hawaiensis, Gymnothorax pseudothyrsoideus, and Dendrophysa russelii*. It implied that biological mechanisms were responsible for the fluctuation of intraspecific genetic divergences in marine fishes.

The neighbor-joining method was originally employed in this study for species identification, but some phylogenetic information was also revealed by the dendrogram, and over 98% of specimens were allocated into different families without polyphyly/paraphyly in the NJ tree (Figure 3). However, DNA barcoding is independent of the way the taxonomy has been built, and it cannot be regarded as the "taxonomic" tag [45]. DNA barcoding is no substitute for taxonomy Ebach and Holdrege [46], and a great deal of work is needed to bring about the reconciliation between traditional and molecular taxonomy. It is unfeasible to build the phylogeny of fishes only based on mitochondrial DNA fragments. Polyphyly/paraphyly in the NJ tree probably results from "bad taxonomy" when named species fail to identify the genetic limits of separate evolutionary entities, particularly for perplexing taxa involving cryptic species [47]. If we cannot set a threshold of the genetic variation in species delimitation, we find ourselves sunk in the dilemma facing new or cryptic species. On the one hand, the morphological taxonomy cannot give a definite identification. On the other hand, we cannot claim that it may be a new species based on molecular analysis without the species delimitation. An assumed threshold is helpful to expedite discovery of new species and biodiversity, especially in dealing with little-studied biotas, although a single, uniform threshold for species delimitation seems arbitrary because rates of molecular evolution vary widely within and among lineages [24, 25, 48].

Acknowledgments

Thanks are due to Chinese National Funding U0633007 and 40776089 and CAS Founding KZCX2-YW-213.

References

[1] R. S. Rasmussen, M. T. Morrissey, and P. D. N. Hebert, "DNA barcoding of commercially important salmon and trout species (*oncorhynchus and salmo*) from North America," *Journal of Agricultural and Food Chemistry*, vol. 57, no. 18, pp. 8379–8385, 2009.

[2] B. C. Victor, R. Hanner, M. Shivji, J. Hyde, and C. Caldow, "Identification of the larval and juvenile stages of the Cubera Snapper, *Lutjanus cyanoptems* , using DNA barcoding," *Zootaxa*, no. 2215, pp. 24–36, 2009.

[3] B. Patwardhan, D. Warude, P. Pushpangadan, and N. Bhatt, "Ayurveda and traditional Chinese medicine: a comparative overview," *Evidence-Based Complementary and Alternative Medicine*, vol. 2, no. 4, pp. 465–473, 2005.

[4] S. E. Bartlett and W. S. Davidson, "Identification of *Thunnus tuna* species by the polymerase chain reaction and direct sequence analysis of their mitochondrial cytochrome b genes," *Canadian Journal of Fisheries and Aquatic Sciences*, vol. 48, pp. 309–317, 1991.

[5] A. Rocha-Olivares, "Multiplex haplotype-specific PCR: a new approach for species identification of the early life stages of rockfishes of the species-rich genus Sebastes Cuvier," *Journal of Experimental Marine Biology and Ecology*, vol. 231, no. 2, pp. 279–290, 1998.

[6] A. J. Gharrett, A. K. Gray, and J. Heifetz, "Identification of rockfish (*Sebastes* spp.) by restriction site analysis of the mitochondrial ND-3/ND-4 and 12S/16S rRNA gene regions," *Fishery Bulletin*, vol. 99, no. 1, pp. 49–62, 2001.

[7] B. Horstkotte and H. Rehbein, "Fish species identification by means of restriction fragment length polymorphism and high-performance liquid chromatography," *Journal of Food Science*, vol. 68, no. 9, pp. 2658–2666, 2003.

[8] C. J. Noell, S. Donnellan, R. Foster, and L. Haigh, "Molecular discrimination of garfish *Hyporhamphus* (Beloniformes) larvae in southern Australian waters," *Marine Biotechnology*, vol. 3, no. 6, pp. 509–514, 2001.

[9] J. Zhang, L. Huang, and H. Huo, "Larval identification of *Lutjanus* Bloch in Nansha coral reefs by AFLP molecular method," *Journal of Experimental Marine Biology and Ecology*, vol. 298, no. 1, pp. 3–20, 2004.

[10] G. Comi, L. Iacumin, K. Rantsiou, C. Cantoni, and L. Cocolin, "Molecular methods for the differentiation of species used in

production of cod-fish can detect commercial frauds," *Food Control*, vol. 16, no. 1, pp. 37–42, 2005.

[11] P. D. N. Hebert, A. Cywinska, S. L. Ball, and J. R. DeWaard, "Biological identifications through DNA barcodes," *Proceedings of the Royal Society B: Biological Sciences*, vol. 270, no. 1512, pp. 313–321, 2003.

[12] P. D. N. Hebert, E. H. Penton, J. M. Burns, D. H. Janzen, and W. Hallwachs, "Ten species in one: DNA barcoding reveals cryptic species in the neotropical skipper butterfly *Astraptes fulgerator*," *Proceedings of the National Academy of Sciences of the United States of America*, vol. 101, no. 41, pp. 14812–14817, 2004.

[13] M. Hajibabaei, D. H. Janzen, J. M. Burns, W. Hallwachs, and P. D. N. Hebert, "DNA barcodes distinguish species of tropical Lepidoptera," *Proceedings of the National Academy of Sciences of the United States of America*, vol. 103, no. 4, pp. 968–971, 2006.

[14] D. M. Lambert, A. Baker, L. Huynen, O. Haddrath, P. D. N. Hebert, and C. D. Millar, "Is a large-scale DNA-based inventory of ancient life possible?" *Journal of Heredity*, vol. 96, no. 3, pp. 279–284, 2005.

[15] M. H. Greenstone, D. L. Rowley, U. Heimbach, J. G. Lundgren, R. S. Pfannenstiel, and S. A. Rehner, "Barcoding generalist predators by polymerase chain reaction: carabids and spiders," *Molecular Ecology*, vol. 14, no. 10, pp. 3247–3266, 2005.

[16] R. D. Ward, T. S. Zemlak, B. H. Innes, P. R. Last, and P. D. N. Hebert, "DNA barcoding Australia's fish species," *Philosophical Transactions of the Royal Society B: Biological Sciences*, vol. 360, no. 1462, pp. 1847–1857, 2005.

[17] G. G. Pegg, B. Sinclair, L. Briskey, and W. J. Aspden, "MtDNA barcode identification of fish larvae in the southern Great Barrier Reef, Australia," *Scientia Marina*, vol. 70, no. 2, pp. 7–12, 2006.

[18] N. Hubert, R. Hanner, E. Holm et al., "Identifying Canadian freshwater fishes through DNA barcodes," *PLoS ONE*, vol. 3, no. 6, article e2490, 2008.

[19] M. Vences, M. Thomas, R. M. Bonett, and D. R. Vieites, "Deciphering amphibian diversity through DNA barcoding: chances and challenges," *Philosophical Transactions of the Royal Society B: Biological Sciences*, vol. 360, no. 1462, pp. 1859–1868, 2005.

[20] M. Vences, M. Thomas, A. van der Meijden, Y. Chiari, and D. R. Vieites, "Comparative performance of the 16S rRNA gene in DNA barcoding of amphibians," *Frontiers in Zoology*, vol. 2, article 5, 2005.

[21] M. Aliabadian, M. Kaboli, V. Nijman, and M. Vences, "Molecular identification of birds: performance of distance-based DNA barcoding in three genes to delimit parapatric species," *PLoS ONE*, vol. 4, no. 1, article e4119, 2009.

[22] V. Nijman and M. Aliabadian, "Performance of distance-based DNA barcoding in the molecular identification of Primates," *Comptes Rendus—Biologies*, vol. 333, no. 1, pp. 11–16, 2010.

[23] S. J. Scheffer, M. L. Lewis, and R. C. Joshi, "DNA barcoding applied to invasive leafminers (Diptera: Agromyzidae) in the Philippines," *Annals of the Entomological Society of America*, vol. 99, no. 2, pp. 204–210, 2006.

[24] K. W. Will and D. Rubinoff, "Myth of the molecule: DNA barcodes for species cannot replace morphology for identification and classification," *Cladistics*, vol. 20, no. 1, pp. 47–55, 2004.

[25] R. DeSalle, M. G. Egan, and M. Siddall, "The unholy trinity: taxonomy, species delimitation and DNA barcoding," *Philosophical Transactions of the Royal Society B: Biological Sciences*, vol. 360, no. 1462, pp. 1905–1916, 2005.

[26] P. H. Barber, S. R. Palumbi, M. V. Erdmann, and M. K. Moosa, "Biogeography: a marine Wallace's line?" *Nature*, vol. 406, no. 6797, pp. 692–693, 2000.

[27] N. V. Ivanova, J. R. DeWaard, and P. D. N. Hebert, "An inexpensive, automation-friendly protocol for recovering high-quality DNA," *Molecular Ecology Notes*, vol. 6, no. 4, pp. 998–1002, 2006.

[28] N. V. Ivanova, T. S. Zemlak, R. H. Hanner, and P. D. N. Hebert, "Universal primer cocktails for fish DNA barcoding," *Molecular Ecology Notes*, vol. 7, no. 4, pp. 544–548, 2007.

[29] M. Kimura, "A simple method for estimating evolutionary rates of base substitutions through comparative studies of nucleotide sequences," *Journal of Molecular Evolution*, vol. 16, no. 2, pp. 111–120, 1980.

[30] S. Kumar, K. Tamura, and M. Nei, "MEGA3: integrated software for molecular evolutionary genetics analysis and sequence alignment," *Briefings in Bioinformatics*, vol. 5, no. 2, pp. 150–163, 2004.

[31] J. W. Tuckey, *Exploratory Data Analysis*, Addison–Wesley, Boston, Mass, USA, 1977.

[32] J. J. Wiens, *Phylogenetic Analysis of Morphological Data*, Smithsonian Institution Press, Washington, DC, USA, 2000.

[33] J. Köhler, K. Munn, A. Rüegg, A. Skusa, and B. Smith, "Quality control for terms and definitions in ontologies and taxonomies," *BMC Bioinformatics*, vol. 7, article 212, 2006.

[34] M. Pfenninger, M. Cordellier, and B. Streit, "Comparing the efficacy of morphologic and DNA-based taxonomy in the freshwater gastropod genus Radix (Basommatophora, Pulmonata)," *BMC Evolutionary Biology*, vol. 6, article 100, 2006.

[35] D. J. Funk and K. E. Omland, "Species-level paraphyly and polyphyly: frequency, causes, and consequences, with insights from animal mitochondrial DNA," *Annual Review of Ecology, Evolution, and Systematics*, vol. 34, pp. 397–423, 2003.

[36] J. Arnold, "Cytonuclear disequilibria in hybrid zones," *Annual Review of Ecology and Systematics*, vol. 24, pp. 521–554, 1993.

[37] T. G. Barraclough and S. Nee, "Phylogenetics and speciation," *Trends in Ecology and Evolution*, vol. 16, no. 7, pp. 391–399, 2001.

[38] P. Alexandrino, R. Faria, D. Linhares et al., "Interspecific differentiation and intraspecific substructure in two closely related clupeids with extensive hybridization, *Alosa alosa* and *Alosa fallax*," *Journal of Fish Biology*, vol. 69, pp. 242–259, 2006.

[39] J. S. Nelson, R. J. Hoddell, L. M. Chou, W. K. Chan, and V. P. E. Phang, "Phylogeographic structure of false clownfish, Amphiprion ocellaris, explained by sea level changes on the Sunda shelf," *Marine Biology*, vol. 137, no. 4, pp. 727–736, 2000.

[40] S. F. Chenoweth and J. M. Hughes, "Genetic population structure of the catadromous perciform: *Macquaria novemaculeata* (Percichthyidae)," *Journal of Fish Biology*, vol. 50, no. 4, pp. 721–733, 1997.

[41] C. L. Dudgeon, N. Gust, and D. Blair, "No apparent genetic basis to demographic differences in scarid fishes across continental shelf of the great barrier reef," *Marine Biology*, vol. 137, no. 5-6, pp. 1059–1066, 2000.

[42] G. Bernardi, S. J. Holbrook, and R. J. Schmitt, "Gene flow at three spatial scales in a coral reef fish, the three-spot dascyllus, *Dascyllus trimaculatus*," *Marine Biology*, vol. 138, no. 3, pp. 457–465, 2001.

[43] S. R. Palumbi, "Genetic divergence, reproductive isolation, and marine speciation," *Annual Review of Ecology and Systematics*, vol. 25, pp. 547–572, 1994.

[44] M. E. Hellberg, R. S. Burton, J. E. Neigel, and S. R. Palumbi, "Genetic assessment of connectivity among marine populations," *Bulletin of Marine Science*, vol. 70, no. 1, pp. 273–290, 2002.

[45] T. Lefébure, C. J. Douady, M. Gouy, and J. Gibert, "Relationship between morphological taxonomy and molecular divergence within Crustacea: proposal of a molecular threshold to help species delimitation," *Molecular Phylogenetics and Evolution*, vol. 40, no. 2, pp. 435–447, 2006.

[46] M. C. Ebach and C. Holdrege, "DNA barcoding is no substitute for taxonomy," *Nature*, vol. 434, no. 7034, p. 697, 2005.

[47] C. C. Nice and A. M. Shapiro, "Patterns of morphological, biochemical, and molecular evolution in the *Oeneis chryxus* complex (Lepidoptera: Satyridae): a test of historical biogeographical hypotheses," *Molecular Phylogenetics and Evolution*, vol. 20, no. 1, pp. 111–123, 2001.

[48] E. Zuckerkandl and L. Pauling, "Evolutionary divergence and convergence in proteins," in *Evolving Genes and Proteins*, V. Bryson and H. J. Vogel, Eds., pp. 97–166, Academic Press, New York, NY, USA, 1965.

Hindawi Publishing Corporation
Evidence-Based Complementary and Alternative Medicine
Volume 2011, Article ID 827286, 9 pages
doi:10.1155/2011/827286

Research Article

Treatment of Rheumatoid Arthritis with Marine and Botanical Oils: Influence on Serum Lipids

Barbara C. Olendzki,[1] Katherine Leung,[2] Susan Van Buskirk,[3] George Reed,[2] and Robert B. Zurier[4]

[1] *Center for Integrative Nutrition, Division of Preventive and Behavioral Medicine, University of Massachusetts Medical School, Worcester, MA 01655, USA*
[2] *Division of Preventive and Behavioral Medicine, University of Massachusetts Medical School, Worcester, MA 01655, USA*
[3] *Department of Family Medicine and Community Health, University of Massachusetts Medical School, Worcester, MA 01655, USA*
[4] *Division of Rheumatology, University of Massachusetts Medical School, Worcester, MA 01655, USA*

Correspondence should be addressed to Barbara C. Olendzki, barbara.olendzki@umassmed.edu

Received 31 December 2010; Revised 6 June 2011; Accepted 25 July 2011

The gap in mortality between patients with rheumatoid arthritis (RA) and the general population (1.5–3.0 fold risk) is increasing. This disparity is attributable mainly to cardiovascular disease (CVD), as the CVD risk is comparable to patients with diabetes mellitus. The purpose of this study is to determine whether borage seed oil rich in gamma-linolenic acid, fish oil rich in eicosapentaenoic acid (EPA) and docosahexaenoic acid (DHA), or the combination of both oils are useful treatments for dyslipidemia in patients with RA. We randomized patients into a double blind, 18 month trial. Mixed effects models were used to compare trends over time in serum lipids. No significant differences were observed between the three groups: All three treatment groups exhibited similar meaningful improvement in the lipid profile at 9 and 18 months. When all groups were combined, these treatments significantly reduced total and LDL-cholesterol and triglycerides, increased HDL-cholesterol, and improved the atherogenic index. All improvements observed at 9 months persisted at 18 months ($P < 0.001$ verses baseline). *Conclusion*. Marine and botanical oils may be useful treatment for rheumatoid arthritis patients who are at increased risk for cardiovascular disease compared to the general population.

1. Introduction

Over the past 30 years, substantial progress has been made in the medical and surgical management of patients with rheumatoid arthritis (RA). Despite this progress, there is an increasing gap in mortality between patients with RA (1.5–3.0 fold risk) and the general population. The disparity is mainly attributable to cardiovascular disease (CVD) [1] as the CVD risk is comparable to patients with diabetes mellitus [2, 3]. Although the reasons for this gap are not entirely clear, the traditional risk of abnormalities in lipid profiles [4] appears to be enhanced by a chronic increase in inflammatory cytokines [5], resulting in accelerated atherosclerosis. In fact, the elevated risk of cardiovascular disease for patients with RA indicates that atherosclerosis may in fact begin at lower thresholds of lipid dysfunction and inflammation than those in the general population, making the lipid profile and other risk factors of particular concern for patients with RA [6]. In a prospective study, [7] atherogenic lipid profiles were considerably worse in people who later met criteria for RA (as much as 10 years later) than those in matched controls. Although recent advances in the treatment of RA, especially with agents designed to block the actions of tumor necrosis factor alpha (TNFα), have improved the course of the disease [8] and endothelial function [9], results of studies of their influence on circulating lipids are mixed, and adequate evidence for or against such benefit is not available [10–12]. Due to the lack of supporting data, patients with RA, many of whom are limited in their ability to exercise to improve the lipid profile and the risk of CVD [13], have an urgent need for other treatments to control their dyslipidemia.

It is clear that an increased intake of polyunsaturated fatty acids can improve their lipid profile [14]. Abundant experimental evidence supports the view that prostaglandins, thromboxanes, and leukotrienes (collectively termed eicosanoids), derived from polyunsaturated fatty acids, and

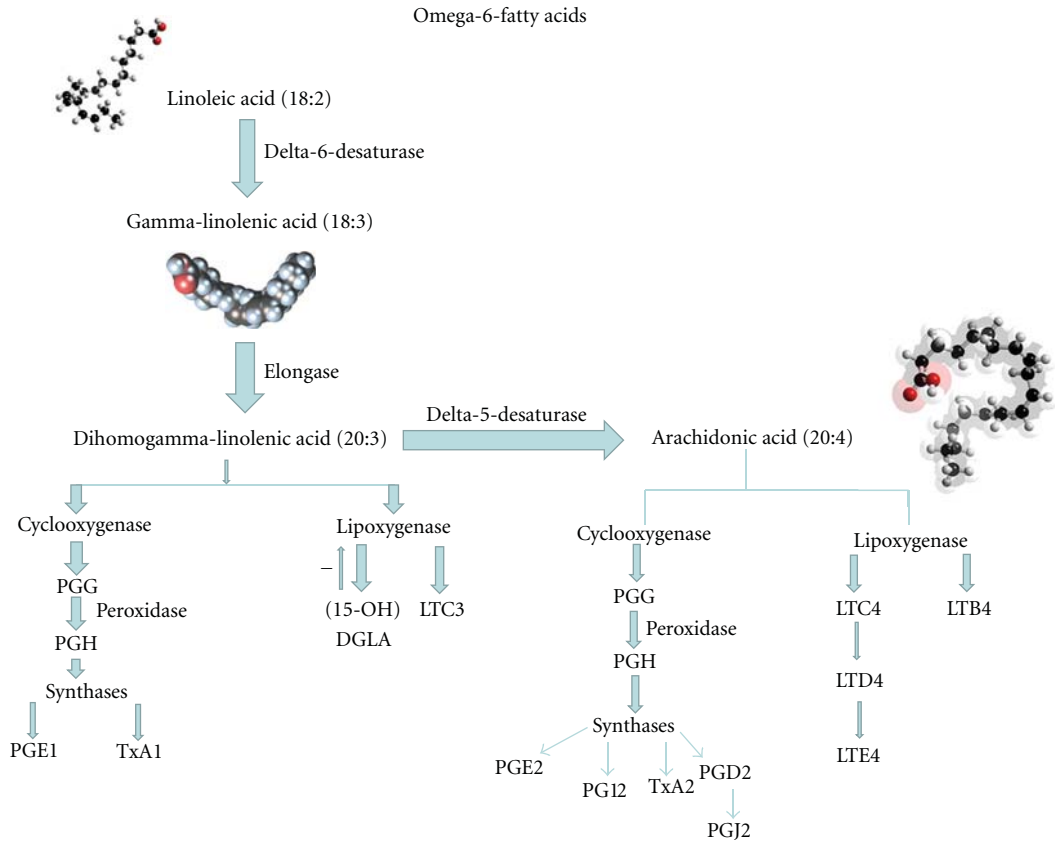

Figure 1

participate in development and regulation of immunological and inflammatory responses [15–18]. The fatty acids themselves, by virtue of their incorporation into cell membranes and signal transduction elements, also have effects on cells involved in inflammation and immune responses that are independent of eicosanoids [18, 19]. A disease such as RA, characterized by abnormal immune responses, persistent inflammation, and joint tissue injury [20], may, therefore, be amenable to control by treatment with oils rich in specific polyunsaturated fatty acids.

Gamma-linolenic acid (GLA: 18:3 omega 6, see Figure 1) is an essential fatty acid found in certain plant seed oils, including borage seed oil. GLA is metabolized to dihomogamma-linolenic acid (DGLA; 20:3 omega 6), the immediate precursor of prostaglandin E_1 (PGE_1), an eicosanoid with anti-inflammatory and immunoregulatory properties [18]. In addition, GLA cannot be converted to inflammatory leucotrienes by 5-lipoxygenase. Instead, it is converted to 15-hydroxy-DGLA which has the additional virtue of suppressing 5-lipoxygenase activity [21]. GLA and DGLA also modulate immune responses in an eicosanoid-independent manner by acting directly on T lymphocytes [18] and GLA suppresses acute and chronic inflammation, including arthritis, in animal models [18]. In addition, fish oil, rich in eicosapentaenoic acid (EPA; 20:5 omega 3, see Figure 2) and docosahexanoic acid (DHA; 22:6 w-3), suppresses formation of the inflammatory eicosanoids PGE_2, thromboxane A_2 (TXA_2), and leucotriene B_4 (LTB_4). Randomized, placebo controlled double blind trials indicated that fish oil treatment of patients with RA result in clinical improvement, and those that monitored NSAID use suggest that fish oil treatment has an NSAID sparing effect [22].

A combination of EPA- and GLA-enriched oils exhibits synergy in reduction of synovitis in animal models [23], and administration of black currant seed oil, which contains the n-3 fatty acid alpha-linolenic acid (which is converted to EPA) and the n-6 GLA, suppresses active synovitis in patients with RA [24]. Taken together, these studies suggest that both EPA and GLA are beneficial therapies for patients with RA. With this knowledge, we carried out an 18-month, multicenter, randomized, double-blind, phase 3 trial of borage seed oil, fish oil, and a combination of both oils in patients with RA and active synovitis, to determine whether the combination of oils is superior to either oil used alone for the treatment of RA. Clinical outcomes of that study will be presented elsewhere. The object of the study presented here is to assess the influence of marine and botanical oils on serum lipids in patients with RA.

2. Methods and Materials

The study was an 18-month randomized double-blind comparison of borage oil, fish oil, or a combination of both oils in RA patients with active joint inflammation.

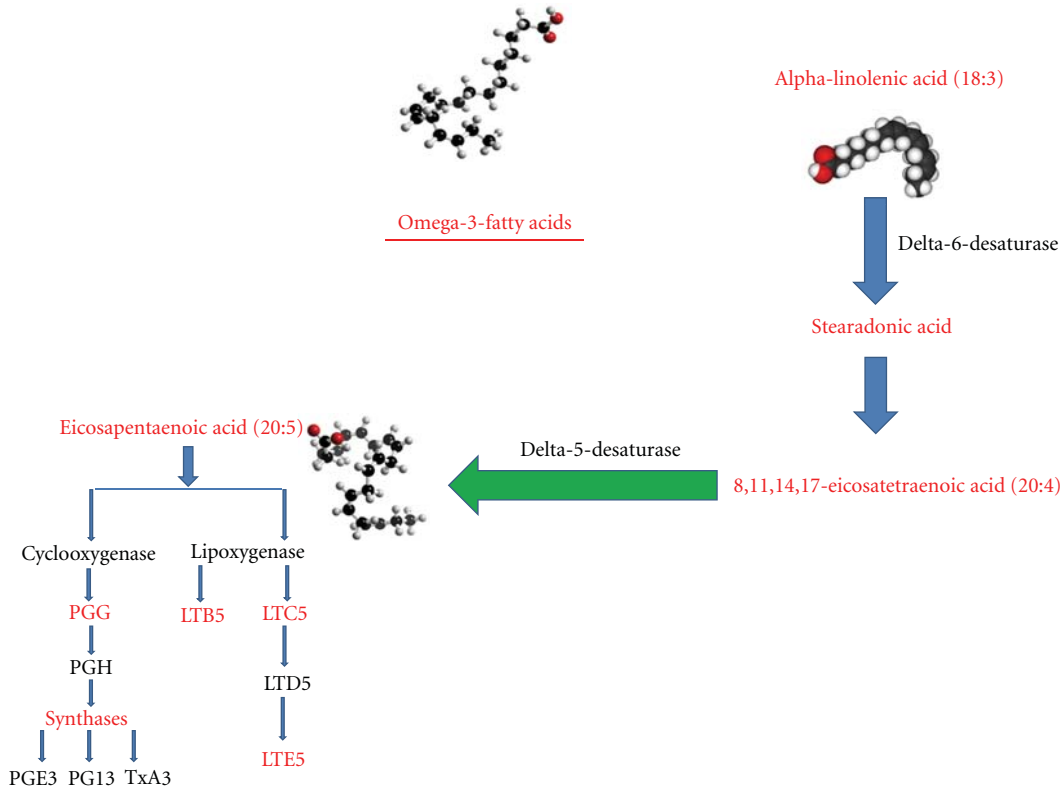

Figure 2

Patients received 3.5 gm omega-3 fatty acids daily in a 2.1 gm EPA/1.4 gm DHA ratio (7 fish oil and 6 sunflower oil capsules daily), 1.8 gm/d GLA (6 borage oil and 7 sunflower oil capsules/d), or 7 fish oil and 6 borage oil capsules daily (combination therapy). All capsules were identical in appearance and color and were purchased from the manufacturer, Bioriginal Food and Service Corp, Saskatoon, Canada, who shipped the capsules in opaque plastic bottles to the University of Massachusetts University Hospital pharmacy, from whence they were distributed to participating centers. Capsules were taken in 2 or 3 divided doses with meals.

The protocol was reviewed and approved initially by the Committee for the Protection of Human Subjects at the University of Massachusetts Medical School and the Food and Drug Administration. Subsequent approvals were obtained from the Review Boards at the University of Alabama, Geisenger Clinic, Fallon Health Care, and the New England IRB. Written informed consent was obtained from each patient.

Patients were eligible to participate in the study if they had RA according to the 1987 criteria of the American Rheumatism Association [25], were in functional class I, II or III according to the revised criteria of the American College of Rheumatology [26], and were between the ages of 18 and 85. Patients were on a stable dose of drugs for RA for at least 2 months before the screening visit and a total duration of therapy of at least 6 months. Doses of nonsteroidal anti-inflammatory drugs (NSAID) and/or prednisone (<10 mg/d) were stable for at least 1 month before screening.

Patients were ineligible for the study if they had been treated with any investigational drug within 1 month of entry. If a patient was taking a fish oil supplement, the dose was stable and ≤2000 mg/d for 2 months before screening. If a patient was taking a borage oil supplement, the dose was stable and ≤2000 mg/d for 2 months before screening. An AST, ALT, or creatinine >1.5 times the upper limit of normal or a total bilirubin >1.8 mg/dL excluded patients from the trial. Patients were instructed to maintain their typical diet.

The lipid profile was assessed at baseline, 9, and 18 months. Diet was assessed by 24-hour dietary assessment calls (24-HR), performed at baseline and 18 months. Both laboratory evaluation and 24-HR were obtained in most patients who dropped out of the study before 18 months and after 3 months. These results are included in the analysis, and were assigned to the closest 9-month interval to the date of patient's termination in the study.

2.1. Dietary Assessment. To measure the effects of supplemental polyunsaturated fats upon lipids, it is necessary to measure the impact, if any, of the background diet. Because a single 24-HR cannot assess day-to-day variation in dietary intake [27], 3 unannounced 24-HRs were conducted on randomly selected days within a 3-week period (two weekdays and one weekend) at baseline and 18 months or time of the final visit. The dietary assessments, including reported intake of supplemental non-study marine and botanical oils or phytosterols, were completed utilizing a computer-assisted telephone interview with a multiple pass

technique [28]. The 24-HR dietary recalls were administered by non-intervention registered dietitians, blinded to the patients' treatment group, and trained to collect dietary data using our interview system. The 24-HR-derived data were analyzed using the University of Minnesota Nutrition Coordinating Center Nutrition Data System for Research software (annually updated, current version: NDS-R 2009). Limitations to 24-HR dietary assessment in this population include factors related to self report, including possible underreporting of nutrient intake which has been observed in several studies [29].

2.2. Laboratory Measurement Methodology. Total cholesterol (TC) and triglyceride (TG) values were measured by conventional enzymatic methods. Briefly, cholesterol esters are converted to a colored quinine imine product. For HDL cholesterol, the lipoprotein particles are solubilized and release HDL cholesterol to react with cholesterol esterase and oxidase in the presence of chromogens to produce a color product. LDL cholesterol is calculated [30] according to the Friedewald Calculation which is TC-HDL − (TG ÷ 5) = LDL. Atherogenic index of plasma (AIP) was used to measure the risk of hypertension, diabetes, and vascular events in this population. The calculation of AIP is log 10 triglyceride/high-density lipoprotein cholesterol [31].

2.3. Statistical Methods. The three treatment arms were characterized at baseline using frequencies for categorical variables and means and standard deviations for continuous variables. Differences in mean values at 18 months or at the final visit were assessed for change in diet by the Student *t*-test [23]. Outcomes that were not normally distributed were log transformed for calculation of *P* values. Nontransformed data are reported for changes from baseline. To assess the effect of the intervention on lipids, lipid values were modeled using linear mixed modeling as a function of time (baseline, 9 month and 18 month, or the final visit treated as a categorical variable to allow for nonlinear trajectories), treatment arm, and their interaction, with adjustment for baseline value. To assess the overall changes over time, outcome measures were modeled using linear mixed modeling as a function of time, treatment arm, and with adjustment for baseline value. All analyses were intention to treat. Analyses included all participants with a baseline lipid measure.

3. Results

One hundred fifty-six patients were randomized, 56 received fish oil, 53 received borage seed oil, and 47 received both fish and borage seed oils. Patients were stratified by site (thus randomized to group within each site), and all sites were combined, resulting in non-significant differences per group. Serum lipids were obtained in 146 patients (93.6%) at baseline, 84 patients (53.8%) at 9 months, and 69 patients (44.2%) at 18 months.

Another 34 patients were screened but not randomized for the following reasons: arthritis medicine dose was not stable, too few tender joints, anticoagulated, high fish oil intake, high borage seed oil intake, medical issues, or abnormal laboratory values. The overall drop-out rate was 51% and was similar across groups: 25 in the borage oil group, 28 in the fish oil group, and 22 in the combination group. Reasons for dropout were mainly gastrointestinal distress (belching, bloating, diarrhea, nausea, cramping) or an inability to swallow the large number of rather sizable capsules.

Table 1: Baseline characteristics in patients with rheumatoid arthritis.

	Total ($N = 146$)*	
	Mean	SD
Age	59.24	11.58
BMI (kg/m^2)	30.55	8.3
	N	%
Gender		
Male	28	19.2%
Female	118	80.8%
Marital status		
Married	100	69.0%
Other	45	31.0%
Race-collapsed		
White	132	90.4%
Minority	14	9.6%
Work status		
Full time	51	34.90%
Part time	14	9.60%
Other	81	55.50%

* None of the demographics are significantly different across the groups at baseline.

Patient characteristics at baseline are presented in Table 1. The mean age of participants was 59 years and the sample predominantly female (80%). Most were white (90%), married (69%), and had a mean body mass index (BMI) of 30.5. An equal number were retired (33%) or working full time (34%), and 16% listed themselves as disabled. There were no significant differences between groups.

3.1. Diet. No significant change in dietary intake of fatty acids was seen (Table 2). However, a significant ($P < 0.001$) reduction in sources of dietary calcium (~200 mg) and a slight increase (1% of total calories) in protein intake were observed.

3.2. Weight. No significant differences in weight between groups were observed. Analysis was done using log-transformed weight; however, results are from the original scale. The mean increase when all groups were combined across the entire study was not significant: 0.5 lb increase at 9 months and 0.4 lb increase at 18 months (Table 4).

3.3. Lipids. There were no significant differences between groups for any lipid measure, with the exception of triglycerides. Therefore, all groups were, combined to evaluate the influence of marine and botanical oils on serum lipids

Table 2: Change in dietary factors from baseline to 18 months.

Change in	Mean	95% CI
Energy	9.01	−121.17 to 139.19
Total dietary fiber	−0.15	−1.75 to 1.45
Soluble dietary fiber	−0.15	−0.64 to 0.33
Insoluble dietary fiber	−0.05	−1.27 to 1.17
Calcium	−204.48	−375.78 to −33.19*
PUFA 18:3 (linolenic acid)	−0.03	−0.22 to 0.16
% calories from fat	−0.31	−2.28 to 1.65
% calories from SFA	0.09	−0.89 to 1.08
% calories from MUFA	−0.13	−0.91 to 0.66
% calories from PUFA	−0.26	−1.21 to 0.69
Omega-3-fatty Acids	0.13	−0.12 to 0.38
% calories from carbohydrate	−1.34	−3.19 to 0.51
% calories from protein	1.17	0.13 to 2.21*

*Values are presented as regression coefficient (95% CI) unless stated otherwise and control from baseline values. $P < 0.001$.

(Table 3(a)). Lipids were done at baseline, 9 months, 18 months, or when the patient terminated the trial.

Total cholesterol reduction from baseline was 3.4 mg/dL ($P = 0.129$) at 9 months and 8.4 mg/dL ($P \leq 0.001$) at 18 months. *LDL* was reduced significantly by 4.4 mg/dL at 9 months ($P = 0.019$) and 9.4 mg/dL at 18 months ($P \leq 0.001$). *HDL* was significant: 4.0 mg/dL increase at 9 months ($P \leq 0.001$) and 5.0 mg/dL increase at 18 months ($P < 0.001$). *TC/HDL ratio* decreased significantly over the time of the trial: a 0.26 reduction at 9 months ($P < 0.001$) and a reduction of 0.43 at 18 months ($P < 0.001$). *Triglycerides* were log transformed for analysis and reporting of P values. However, the coefficients and the differences reported are from the nonlog-transformed scale. Reductions in triglyceride concentrations were observed in all 3 groups (Table 3(a)). The overall decrease across the study period was 22.0 mg/dL at 9 months ($P < 0.001$) and 24.4 mg/dL at 18 months ($P < 0.001$). The TG reduction in the group treated with both oils was significantly greater ($P < 0.031$) than the borage oil or fish oil groups at 9 months, a pattern that persisted at 18 months (Table 3(b)). *Atherogenic index of plasma (AIP)* was reduced in all 3 groups (Table 3(a)). The overall decrease across the study period was 0.22 at 9 months ($P < 0.001$) and 0.26 at 18 months ($P < 0.001$). The reduction in the AIP was significantly greater ($P = 0.011$) at 9 months and 18 months in the group treated with both oils than that in the groups treated with either oil alone (Table 3(b)).

3.4. Sensitivity Analysis of Lipids. A sensitivity analysis was run to detect if missing data might have affected the study results. Missing data were imputed by substituting the baseline value. Since this would be the worst case scenario, in which all missing data return to baseline; analyses were repeated with the imputed data. The intragroup differences seen in triglyceride concentrations were not sustained with the imputed data. However, the intragroup differences seen with the AIP did persist. The significant change seen with all groups combined was also sustained with the imputed data, which indicates that missing data would not have a large impact on results from the all groups combined analyses.

3.5. Blood Pressure. Significant changes in blood pressure within and among groups were not observed. Systolic blood pressure increased 1.8 mm hg at 9 months and decreased 0.2 mm hg at 18 months. Diastolic blood pressure increased 2.3 mm hg at 9 months and 1.9 mm hg at 18 months (Table 4).

3.6. Erythrocyte Sedimentation Rate (ESR) [32] and C-Reactive Protein (CRP). ESR is a common hematology test that is a nonspecific measure of inflammation. CRP is a protein found in the blood, and its levels increase in response to inflammation.

No significant differences in ESR or in CRP were seen among groups. However, when patients from all treatment groups were analyzed together, a modest but significant reduction in ESR was seen at 9 months, and ESR was still reduced from baseline at 18 months. A similar small but significant reduction in CRP was seen at 9 months, but not maintained at 18 months (Table 4).

4. Discussion

Part of the intrigue of research is the often unanticipated findings encountered. The current study was not designed to detect differences in lipids in patients with RA; hence, we lack a control group. Because marine and botanical oils given individually reduce joint inflammation in RA patients [14–18], and because the groups in this study showed improvement in the lipid profile, a trial of these oils with a placebo arm is warranted.

RA is a chronic systemic inflammatory disease. Mediators of inflammation and prothrombotic factors contribute to endothelial dysfunction and development of cardiovascular disease in RA patients [33]. There is little evidence that therapy for inflammation also leads to cardiovascular risk reduction in this group. Marine and botanical oils represent an excellent primary or secondary therapy for improvement of cardiovascular risk management in patients with rheumatoid arthritis.

Results of studies presented in this paper indicate that a GLA-enriched botanical oil (borage seed oil), an EPA/DHA-enriched fish oil, or a combination of these oils are useful for correcting dyslipidemia in patients with RA. Since there were no differences observed between the groups, with the notable exception of triglycerides and the AIP (shown separately in Table 3(b)), all 3 treatment groups were analyzed as a single group. Although lipid profiles of most patients were acceptable at baseline, patients taking these oils exhibit significant additional reductions in total and LDL cholesterol, triglycerides, the TC/HDL ratio, and the atherogenic index, and experience a significant increase in HDL cholesterol. All of these improvements in the lipid profile were seen after 9 months of therapy and increased after 18 months of oils administration. Particularly noteworthy is the group treated with both oils, as they experienced a significantly greater reduction in serum triglyceride concentrations and in the AIP than the groups on either oil alone. Oils enriched in

Table 3

(a) Serum Lipids and Atherogenic Index of Plasma

	Baseline mean (SD) ($N = 145$)	Change from baseline to 9 months ($N = 83$)	Change from baseline to 18 months ($N = 69$)
Total cholesterol	195.77 (37.48)	−3.45 (−7.88 to 0.98)	−8.43* (−12.99 to −3.86)
LDL	114.63 (32.20)	−4.39** (−8.03 to −0.74)	−9.43* (−13.75 to −5.11)
HDL	54.14 (16.21)	3.96* (2.44 to 5.49)	5.02* (3.24 to 6.81)
TC/HDL ratio†	3.83 (1.03)	−0.26* (−0.41 to −0.12)	−0.43* (−0.58 to −0.28)
Triglyceride†	138.05 (79.65)	−21.96* (−30.52 to −13.40)	−24.42* (−33.22 to −15.61)
Atherogenic index of plasma	0.84 (0.67)	−0.22* (−0.29 to −0.16)	−0.26* (−0.33 to −0.19)

Values are presented as regression coefficient (95% CI) unless stated otherwise and control from baseline values. *$P < 0.001$ **$P \leq 0.05$ †P value are from log-transformed data.

(b) Triglycerides and atherogenic index of plasma (AIP) by group

	Combination group	Fish oil group	Borage oil group	P value
Triglyceride**				0.031
9 months	−30.81 (−46.58 to −15.03)	−20.50 (−35.16 to −5.85)	−16.57 (−30.86 to −2.27)	
18 months	−38.24 (−54.28 to −22.19)	−15.27 (−29.81 to −0.74)	−22.10 (−37.32 to −6.89)	
AIP				0.011
9 months	−0.33 (−0.45 to −0.20)	−0.20 (−0.32 to −0.08)	−0.17 (−0.33 to 0.002)	
18 months	−0.45 (−0.57 to −0.32)	−0.16 (−0.28 to −0.05)	−0.21 (−0.33 to −0.09)	

** P value is from log transformation. Changes shown are from the original scale for the group × time interaction and control for baseline values. Values are presented as regression coefficient (95% CI).

Table 4: Change from baseline for anthropometric and inflammatory markers.

	9 months ($N = 88$)	18 months ($N = 71$)
Weight†	0.52 (−1.41 to 2.46)	0.35 (−2.43 to 3.14)
Systolic blood pressure	1.77 (−0.66 to 4.20)	−0.24 (−3.37 to 2.90)
Diastolic blood pressure	2.32* (0.56 to 4.09)	1.88** (−0.003 to 3.79)
ESR†	−5.39* (−9.71 to −1.07)	−4.42** (−9.22 to 0.38)
CRP†	−0.65* (−1.20 to −0.10)	−0.09 (−0.77 to 0.60)

*$P < 0.001$.
**$P \leq 0.05$.
†P values are from log-transformed data.
$N = 90$ at 9 months and $N = 72$ at 18 months for blood pressure measurements.
$N = 81$ at 9 months and $N = 67$ at 18 months for ESR.
$N = 66$ at 9 months and $N = 58$ at 18 months for CRP.

GLA affect inflammation differently than oils enriched in EPA/DHA, and the anti-inflammatory and joint protective effects of the combination of these oils are synergistic in animal models [23]. Thus, it is possible that these different oils influence different aspects of TG synthesis or metabolism. Indeed, fish and botanical oils that provide EPA both reduce hepatic synthesis of TG in rats [34]. In humans the delta-5-desaturase that converts DGLA to arachidonic acid (AA) is sluggish, and we have not seen increases in circulating arachidonic acid after administration of GLA for 24 weeks [17]. Nonetheless, the possibility of increased circulating AA must be considered if treatment is to be long term. When fish oil is administered with borage oil to healthy individuals, bioconversion of GLA to AA is prevented [34], perhaps another reason for administering both GLA- and EPA-rich oils together.

All treatments were safe. Rates and types of adverse events were similar across all treatment groups, and as anticipated, were due entirely to mild to moderate gastrointestinal distress. The main reason for the large drop-out rate (in excess of 45%) was the large size and the number

of capsules ingested each day over the 18-month-study period. It is possible to deliver much larger amounts of the individual polyunsaturated fatty acids (GLA, EPA, and DHA) in far smaller capsules than are needed to accommodate the natural marine and botanical oils, a strategy which should substantially reduce the dropout rate.

Alterations in diet can influence serum lipid concentrations [35]. However, the patients in our study did not change their diets over the course of the trial, suggesting that the improvements in their lipid profiles, including the significant increase in HDL cholesterol, are due to administration of the study oils. Most pharmacological treatments of dyslipidemia address reduction of LDL cholesterol [36, 37]. Since improvement in HDL cholesterol depends to a large extent on an exercise regimen [13, 38], many patients with RA are denied this manner of therapy. Thus, treatment with one or a combination of these oils could aid in the reduction of cardiovascular risk in RA patients whose disability impairs or prevents a prescribed exercise program.

Although LDL-C is the primary target of lipid-lowering therapy, other measures of the lipoprotein lipid profile, as reflected in the AIP and the TC/HDL-C ratios, are also associated with CVD risk. The AIP is a useful monitor of the lipid profile and its subsequent impact on the progression of cardiovascular risk [39]. In the study presented here, the AIP is significantly and beneficially altered at both 9 and 18 months compared to baseline. Patients in this study also exhibit a significant reduction in the TC/HDL ratio at 9 and 18 months, another indication of reduced CVD risk [40]. The safety of marine and botanical oils, and their remarkable impact observed in this study on the lipid profile of RA patients who are at increased risk for dyslipidemia and cardiovascular disease [1], suggest that these oils should have a prominent role in therapy of patients with RA.

Additionally, there is some evidence [41] that these oils can substitute for treatment of RA patients with nonsteroidal anti-inflammatory drugs (NSAIDs). The adverse gastrointestinal and renal events associated with NSAID therapy are well known [42]. In addition, macrophages treated with a cyclooxygenase inhibitor in vitro exhibit greater vulnerability to formation of foam cells, a key element in development of atheromatous plaques [43]. Neither borage oil nor fish oil is associated with serious gastrointestinal events (ulceration, bleeding, perforation). In addition, whereas NSAIDs increase the incidence of myocardial infarction and stroke [44], fish oil reduces the risk of cardiovascular events in patients at risk, including those with RA [45]. The efficacy of omega-3-fatty acids in reducing mortality after a myocardial infarction [46] is further reason to recommend their use in patients with RA. Although studies in humans of the influence of GLA on serum lipids are scant, GLA administration appears to prevent increases in TC and LDL-C [47].

5. Conclusion

Chronic inflammation, experienced by patients with RA, includes development of microthrombi in small vessels and production of inflammatory cytokines and is associated with accelerated atherosclerosis [48]. The capacity of both GLA- and EPA-rich oils to reduce platelet aggregation [49] and production of inflammatory cytokines [18] and the ability of EPA to form resolvins and protectins, compounds that facilitate resolution of inflammation [50], further suggest their potential long-term therapeutic value in patients with RA. The current study suggests their beneficial effect on cardiovascular risk factors in patients with RA. Additional studies of marine and botanical polyunsaturated fatty acids—in isolated form in order to reduce the number and the size of capsules administered—are warranted to further determine their influence on lipid dysfunction in patients with RA and other diseases characterized by chronic inflammation.

Acknowledgments

These studies were supported by the National Institutes of Health Grant RO1-AT000309 from the National Center for Complementary and Alternative Medicine. The authors are grateful for the statistical help of Robert Magner and the efforts of the principal investigators at the 13 sites and their patients, without whom this study would not have been possible.

References

[1] M. Boers, B. Dijkmans, S. Gabriel, H. Maradit-Kremers, J. O'Dell, and T. Pincus, "Making an impact on mortality in rheumatoid arthritis: targeting cardiovascular comorbidity," *Arthritis and Rheumatism*, vol. 50, no. 6, pp. 1734–1739, 2004.

[2] V. P. van Halm, M. J. L. Peters, A. E. Voskuyl et al., "Rheumatoid arthritis versus diabetes as a risk factor for cardiovascular disease: a cross-sectional study, the CARRÉ Investigation," *Annals of the Rheumatic Diseases*, vol. 68, no. 9, pp. 1395–1400, 2009.

[3] V. P. van Halm, M. M. Nielen, M. T. Nurmohamed et al., "Lipids and inflammation: Serial measurements of the lipid profile of blood donors who later developed rheumatoid arthritis," *Annals of the Rheumatic Diseases*, vol. 66, no. 2, pp. 184–188, 2007.

[4] W. H. Yoo, "Dyslipoproteinemia in patients with active rheumatoid arthritis: effects of disease activity, sex, and menopausal status on lipid profiles," *Journal of Rheumatology*, vol. 31, no. 9, pp. 1746–1753, 2004.

[5] G. Kerekes, Z. Szekanecz, H. Dér et al., "Endothelial dysfunction and atherosclerosis in rheumatoid arthritis: a multiparametric analysis using imaging techniques and laboratory markers of inflammation and autoimmunity," *Journal of Rheumatology*, vol. 35, no. 3, pp. 398–406, 2008.

[6] S. van Doornum, G. McColl, and I. P. Wicks, "Accelerated atherosclerosis: an extraarticular feature of rheumatoid arthritis?" *Arthritis and Rheumatism*, vol. 46, no. 4, pp. 862–873, 2002.

[7] V. P. van Halm, M. M. J. Nielen, M. T. Nurmohamed et al., "Lipids and inflammation: serial measurements of the lipid profile of blood donors who later developed rheumatoid arthritis," *Annals of the Rheumatic Diseases*, vol. 66, no. 2, pp. 184–188, 2007.

[8] S. clair, C. L. Wagner, A. A. Fasanmade et al., "The relationship of serum infliximab concentrations to clinical improvement in rheumatoid arthritis: results from ATTRACT, a multicenter,

randomized, double-blind, placebo-controlled trial," *Arthritis and Rheumatism*, vol. 46, no. 6, pp. 1451–1459, 2002.

[9] D. Hürlimann, A. Forster, G. Noll et al., "Anti-tumor necrosis factor-α treatment improves endothelial function in patients with rheumatoid arthritis," *Circulation*, vol. 106, no. 17, pp. 2184–2187, 2002.

[10] E. N. Pollono, M. A. Lopez-Olivo, J. A. M. Lopez, and M. E. Suarez-Almazor, "A systematic review of the effect of TNF-α antagonists on lipid profiles in patients with rheumatoid arthritis," *Clinical Rheumatology*, vol. 29, no. 9, pp. 947–955, 2010.

[11] M. J. L. Peters, M. Vis, V. P. van Halm et al., "Changes in lipid profile during infliximab and corticosteroid treatment in rheumatoid arthritis," *Annals of the Rheumatic Diseases*, vol. 66, no. 7, pp. 958–961, 2007.

[12] C. A. Wijbrandts, S. I. van Leuven, H. D. Boom et al., "Sustained changes in lipid profile and macrophage migration inhibitory factor levels after anti-tumour necrosis factor therapy in rheumatoid arthritis," *Annals of the Rheumatic Diseases*, vol. 68, no. 8, pp. 1316–1321, 2009.

[13] G. Steiner and M. B. Urowitz, "Lipid profiles in patients with rheumatoid arthritis: mechanisms and the impact of treatment," *Seminars in Arthritis and Rheumatism*, vol. 38, no. 5, pp. 372–381, 2009.

[14] G. Zuliani, M. Galvani, E. Leitersdorf, S. Volpato, M. Cavalieri, and R. Fellin, "The role of polyunsaturated fatty acids (PUFA) in the treatment of dyslipidemias," *Current Pharmaceutical Design*, vol. 15, no. 36, pp. 4087–4093, 2009.

[15] P. C. Weber, "Membrane phospholipid modification by dietary n-3 fatty acids: effects on eicosanoid formation and cell function," *Progress in Clinical and Biological Research*, vol. 282, pp. 263–274, 1988.

[16] J. D. Prickett, D. R. Robinson, and A. D. Steinberg, "Dietary enrichment with the polyunsaturated fatty acid eicosapentaenoic acid prevents proteinuria and prolongs survival in NZB x NZW F1 mice," *Journal of Clinical Investigation*, vol. 68, no. 2, pp. 556–559, 1981.

[17] R. B. Zurier, R. G. Rossetti, E. W. Jacobson et al., "Gamma-linolenic acid treatment of rheumatoid arthritis: a randomized, placebo-controlled trial," *Arthritis and Rheumatism*, vol. 39, no. 11, pp. 1808–1817, 1996.

[18] R. B. Zurier, "Prostaglandins, leukotrienes, and related compounds," in *Kelley's Textbook of Rheumatology*, G. S. Firestein, E. D. Harris, I. B. McIness, S. Ruddy, and J. S. Sergent, Eds., pp. 343–358, Saunders, Philadelphia, Pa, USA, 2009.

[19] D. Vassilopoulos, R. B. Zurier, R. G. Rossetti, and G. C. Tsokos, "Gammalinolenic acid and dihomogammalinolenic acid suppress the CD3- mediated signal transduction pathway in human T cells," *Clinical Immunology and Immunopathology*, vol. 83, no. 3, pp. 237–244, 1997.

[20] B. Bartok and G. S. Firestein, "Fibroblast-like synoviocytes: key effector cells in rheumatoid arthritis," *Immunological Reviews*, vol. 233, no. 1, pp. 233–255, 2010.

[21] V. A. Ziboh and R. S. Chapkin, "Biologic significance of polyunsaturated fatty acids in the skin," *Archives of Dermatology*, vol. 123, pp. 1686a–1690, 1987, *Rheumatology*. In press.

[22] P. C. Calder, "n-3 polyunsaturated fatty acids, inflammation, and inflammatory diseases," *The American Journal of Clinical Nutrition*, vol. 83, no. 6, Article ID 986797, pp. 1505S–1519S, 2006.

[23] G. A. Tate, B. F. Mandell, R. A. Karmali et al., "Suppression of monosodium urate crystal-induced acute inflammation by diets enriched with gamma-linolenic acid and eicosapentaenoic acid," *Arthritis and Rheumatism*, vol. 31, no. 12, pp. 1543–1551, 1988.

[24] L. J. Leventhal, E. G. Boyce, and R. B. Zurier, "Treatment of rheumatoid arthritis with blackcurrant seed oil," *British Journal of Rheumatology*, vol. 33, no. 9, pp. 847–852, 1994.

[25] F. C. Arnett, S. M. Edworthy, D. A. Bloch et al., "The American Rheumatism Association 1987 revised criteria for the classification of rheumatoid arthritis," *Arthritis and Rheumatism*, vol. 31, no. 3, pp. 315–324, 1988.

[26] D. T. Felson, J. J. Anderson, M. Boers et al., "The American College of Rheumatology preliminary core set of disease activity measures for rheumatoid arthritis clinical trials," *Arthritis and Rheumatism*, vol. 36, no. 6, pp. 729–740, 1993.

[27] G. H. Beaton, J. Milner, and V. McGuire, "Source of variance in 24-hour dietary recall data: implications for nutrition study design and interpretation. Carbohydrate sources, vitamins, and minerals," *American Journal of Clinical Nutrition*, vol. 37, no. 6, pp. 986–995, 1983.

[28] Y. Ma, B. C. Olendzki, S. L. Pagoto et al., "Number of 24-hour diet recalls needed to estimate energy intake," *Annals of Epidemiology*, vol. 19, no. 8, pp. 553–559, 2009.

[29] B. C. Olendzki, Y. Ma, J. R. Hébert et al., "Underreporting of energy intake and associated factors in a Latino population at risk of developing type 2 diabetes," *Journal of the American Dietetic Association*, vol. 108, no. 6, pp. 1003–1008, 2008.

[30] S. Mora, N. Rifai, J. E. Buring, and P. M. Ridker, "Comparison of LDL cholesterol concentrations by Friedewald calculation and direct measurement in relation to cardiovascular events in 27,331 women," *Clinical Chemistry*, vol. 55, no. 5, pp. 888–894, 2009.

[31] A. Onat, G. Can, H. Kaya, and G. Hergenç, ""Atherogenic index of plasma" (log10 triglyceride/high-density lipoprotein-cholesterol) predicts high blood pressure, diabetes, and vascular events," *Journal of Clinical Lipidology*, vol. 4, no. 2, pp. 89–98, 2010.

[32] D. E. King, B. M. Egan, R. F. Woolson, A. G. Mainous III, Y. Al-Solaiman, and A. Jesri, "Effect of a high-fiber diet vs a fiber-supplemented diet on C-reactive protein level," *Archives of Internal Medicine*, vol. 167, no. 5, pp. 502–506, 2007.

[33] C. Jurcuţ, R. Jurcuţ, and C. Tanasescu, "Cardiovascular risk and rheumatoid arthritis: from mechanisms of atherosclerosis to therapeutic approach," *Romanian Journal of Internal Medicine*, vol. 42, no. 4, pp. 659–669, 2004.

[34] F. H. Chilton, L. L. Rudel, J. S. Parks, J. P. Arm, and M. C. Seeds, "Mechanisms by which botanical lipids affect inflammatory disorders," *American Journal of Clinical Nutrition*, vol. 87, no. 2, pp. 498S–503S, 2008.

[35] C. M. Berg, G. Lappas, E. Strandhagen et al., "Food patterns and cardiovascular disease risk factors: The Swedish INTERGENE research program," *American Journal of Clinical Nutrition*, vol. 88, no. 2, pp. 289–297, 2008.

[36] K. Miyauchi and H. Daida, "Clinical significance of intensive lipid-lowering therapy using statins in patients with coronary artery disease: LDL-cholesterol: the lower, the better; Is it true for Asians? (Pro)," *Circulation Journal*, vol. 74, no. 8, pp. 1718–1730, 2010.

[37] A. L. Catapano, "Perspectives on low-density lipoprotein cholesterol goal achievement," *Current Medical Research and Opinion*, vol. 25, no. 2, pp. 431–447, 2009.

[38] T. R. Thomas, S. O. Warner, K. C. Dellsperger et al., "Exercise and the metabolic syndrome with weight regain," *Journal of Applied Physiology*, vol. 109, no. 1, pp. 3–10, 2010.

[39] M. Dobiášová, "Atherogenic index of plasma [log(triglycerides/HDL-cholesterol)]: theoretical and practical implications," *Clinical Chemistry*, vol. 50, no. 7, pp. 1113–1115, 2004.

[40] B. J. Arsenault, J. S. Rana, E. S. G. Stroes et al., "Beyond low-density lipoprotein cholesterol: respective contributions of non-high-density lipoprotein cholesterol levels, triglycerides, and the total cholesterol/high-density lipoprotein cholesterol ratio to coronary heart disease risk in apparently healthy men and women," *Journal of the American College of Cardiology*, vol. 55, no. 1, pp. 35–41, 2009.

[41] J. J. F. Belch, D. Ansell, R. Madhok, A. O'Dowd, and R. D. Sturrock, "Effects of altering dietary essential fatty acids on requirements for non-steroidal anti-inflammatory drugs in patients with rheumatoid arthritis: a double blind placebo controlled study," *Annals of the Rheumatic Diseases*, vol. 47, no. 2, pp. 96–104, 1988.

[42] N. J. Olsen, "Tailoring arthritis therapy in the wake of the NSAID crisis," *New England Journal of Medicine*, vol. 352, no. 25, pp. 2578–2580, 2005.

[43] E. S. L. Chan, H. Zhang, P. Fernandez et al., "Effect of cyclooxygenase inhibition on cholesterol efflux proteins and atheromatous foam cell transformation in THP-1 human macrophages: a possible mechanism for increased cardiovascular risk," *Arthritis Research and Therapy*, vol. 9, no. 1, article R4, 2007.

[44] M. Amer, V. R. Bead, J. Bathon, R. S. Blumenthal, and D. N. Edwards, "Use of nonsteroidal anti-inflammatory drugs in patients with cardiovascular disease: a cautionary tale," *Cardiology in Review*, vol. 18, no. 4, pp. 204–212, 2010.

[45] L. G. Cleland, G. E. Caughey, M. J. James, and S. M. Proudmam, "Reduction of cardiovascular risk factors with longterm fish oil treatment in early rheumatoid arthritis," *Journal of Rheumatology*, vol. 33, no. 10, pp. 1973–1979, 2006.

[46] P. E. Marik and J. Varon, "Omega-3 dietary supplements and the risk of cardiovascular events: a systematic review," *Clinical Cardiology*, vol. 32, no. 7, pp. 365–372, 2009.

[47] R. L. Tahvonen, U. S. Schwab, K. M. Linderborg, H. M. Mykkänen, and H. P. Kallio, "Black currant seed oil and fish oil supplements differ in their effects on fatty acid profiles of plasma lipids, and concentrations of serum total and lipoprotein lipids, plasma glucose and insulin," *Journal of Nutritional Biochemistry*, vol. 16, no. 6, pp. 353–359, 2005.

[48] A. Sodergren, K. Karp, K. Boman et al., "Atherosclerosis in early rheumatoid arthritis: very early endothelial activation and rapid progression of intima media thickness," *Arthritis Research & Therapy*, vol. 12, no. 4, R158, 2010.

[49] P. C. Calder and R. B. Zurier, "Polyunsaturated fatty acids and rheumatoid arthritis," *Current Opinion in Clinical Nutrition and Metabolic Care*, vol. 4, no. 2, pp. 115–121, 2001.

[50] C. N. Serhan, N. Chiang, and T. E. van Dyke, "Resolving inflammation: dual anti-inflammatory and pro-resolution lipid mediators," *Nature Reviews Immunology*, vol. 8, no. 5, pp. 349–361, 2008.

Hindawi Publishing Corporation
Evidence-Based Complementary and Alternative Medicine
Volume 2011, Article ID 271419, 9 pages
doi:10.1155/2011/271419

Research Article

Novel Lipolytic Enzymes Identified from Metagenomic Library of Deep-Sea Sediment

Jeong Ho Jeon,[1,2] Jun Tae Kim,[1] Hyun Sook Lee,[1,3] Sang-Jin Kim,[1,3] Sung Gyun Kang,[1,3] Sang Ho Choi,[2] and Jung-Hyun Lee[1,3]

[1] *Marine Biotechnology Research Center, Korea Ocean Research & Development Institute, P.O. Box 29, Ansan 425-600, Republic of Korea*
[2] *National Research Laboratory of Molecular Microbiology and Toxicology, Department of Agricultural Biotechnology, Seoul National University, Seoul 151-921, Republic of Korea*
[3] *Department of Marine Biotechnology, University of Science and Technology, Daejeon 305-333, Republic of Korea*

Correspondence should be addressed to Jung-Hyun Lee, jlee@kordi.re.kr

Received 13 January 2011; Accepted 3 June 2011

Metagenomic library was constructed from a deep-sea sediment sample and screened for lipolytic activity. Open-reading frames of six positive clones showed only 33–58% amino acid identities to the known proteins. One of them was assigned to a new group while others were grouped into Families I and V or EstD Family. By employing a combination of approaches such as removing the signal sequence, coexpression of chaperone genes, and low temperature induction, we obtained five soluble recombinant proteins in *Escherichia coli*. The purified enzymes had optimum temperatures of 30–35°C and the cold-activity property. Among them, one enzyme showed lipase activity by preferentially hydrolyzing *p*-nitrophenyl palmitate and *p*-nitrophenyl stearate and high salt resistance with up to 4 M NaCl. Our research demonstrates the feasibility of developing novel lipolytic enzymes from marine environments by the combination of functional metagenomic approach and protein expression technology.

1. Introduction

Lipolytic enzymes such as esterases and lipases belong to the class of carboxylic ester hydrolases that catalyze both the hydrolysis and synthesis of ester bonds. Lipolytic enzymes have been classified into eight families based on the conserved sequence motifs and biological properties [1]. They share a characteristic α/β hydrolase fold in the three-dimensional structure, but show differences in substrate preferences. Esterases (EC 3.1.1.1) hydrolyze water-soluble or emulsified esters with short-chain carboxylic acids ($\leq$10 carbon atoms), while lipases (EC 3.1.1.3) prefer long-chain acylglycerides ($\geq$10 carbon atoms) [2]. Esterases and lipases have a wide range of biotechnological applications, such as organic chemical processing, detergent formulation, synthesis of biosurfactants, the oleochemical industry, the dairy industry, the agrochemical industry, paper manufacturing, nutrition, cosmetics, and pharmaceutical processing [3–6]. Therefore, the identification of novel esterases/lipases will be a useful tactic for finding novel biocatalysts.

The metagenomic approach, direct cloning of genomes of all microorganisms present in a given habitat, can be accessing the potential of nonculturable microorganisms [7–10]. In detail, metagenomic libraries were constructed from DNA of diverse environmental samples in cloning vectors including cosmid, fosmid and bacterial artificial chromosome (BAC) [11–13] and host strains. Two major strategies have been pursued to identify novel biocatalysts or genes with new functions for biotechnological applications. The first approach uses function-based screenings of metagenomic DNA libraries, and the second one includes sequence-based searches [14–16]. Through functional screens of metagenomic libraries, several genes encoding lipolytic enzymes have been previously identified from various environmental samples [17–21].

We have been applying metagenomic approach to search for new lipolytic enzymes from marine environmental samples such as deep-sea and arctic seashore sediments, which possess untouched and potential resources [22–24]. Several novel esterases/lipases have been identified with

unique properties including cold activity. In this study, we used another sediment core sample of deep sea which had been explored in our previous researches and could unveil the existence of novel lipolytic enzymes. Here, we describe the identification of novel lipolytic enzyme-encoding genes from metagenomic library, the enhancement of soluble protein expression, and the biochemical characterization of the purified enzymes.

2. Materials and Methods

2.1. Strains, Library Construction, and Screening Escherichia coli. DH5α (Stratagene, La Jolla, CA, USA), EPI300-T1R (Epicentre, Madison, WI, USA), and BL21(DE3) (Novagen, Madison, WI, USA) were used as host strains for cloning and expression. pBluescript SK- (Stratagene), pET-24a(+) vector (Novagen), and fosmid vector (Epicentre) were used as vectors.

2.2. Metagenomic Library Construction and Screening for Lipolytic Clones. Deep-sea sediment sample was collected from the southern clam beds area around the summit of Edison Seamount in the New Ireland Fore-arc near Papua New Guinea (3°89′S/152°49′E; depth 1,440 m). DNA from the sediment sample was extracted based on a previously described method [25] with minor modifications. After extraction, the DNA was further purified by gel electrophoresis in a 1% low-melting-temperature agarose gel (FMC Bioproducts, Rockland, ME) containing 1% polyvinyl polypyrrolidone (Sigma, St. Louis, MO). Gel electrophoresis was performed at 35 V for 13 h, and DNA fragments of approximately 40 to 50 kb were then isolated from the gel. The isolated DNA was end-repaired with End-It DNA End-Repair kit (Epicentre, Madison, WI), which caused the DNA to be blunt ended and 5′-phosphorylated. The blunt-ended DNA was ligated into a pCC1FOS vector (Epicentre, Madison, WI). Lambda packaging extracts were added to ligations, and infection of phage T1-resistant EPI300-$T1^R$ cells was performed according to the manufacturer's instructions. The *E. coli* transformants were transferred to 96-well microtiter plates and stored at −80°C. To screen for esterase/lipase activity, the transformants were plated on Luria-Bertani (LB) agar plates containing 12.5 μg/mL of chloramphenicol and 1% tributyrin as a substrate. Colonies were incubated for one day at 37°C and subsequently incubated for a week at 4°C. Candidates surrounded by a clear halo on the plate were selected. The positive clones were reconfirmed and subcloned.

Fosmid clones showing lipolytic activity on the tributyrin agar plate were inoculated into 200 mL of LB broth containing 12.5 μg/mL of chloramphenicol. After overnight incubation at 37°C, the cells were harvested by centrifugation at 5,000 ×g for 15 min and washed twice with distilled water. The fosmid DNA was purified using the alkaline lysis method [26] with minor modifications and was randomly sheared by nebulization according to the manufacturer's instruction (Invitrogen, Carlsbad, CA). After nebulization, DNA fragments of 2 to 4 kb were isolated from a 0.6% low-melting-temperature agarose (FMC Bioproducts, Rockland, ME) gel and end-repaired to generate blunt ends. The blunt-ended DNA was ligated into the *Eco*RV site of pBluescript SK(−) (Stratagene, La Jolla, CA), and the ligations were introduced into *E. coli* DH5α cells. The *E. coli* transformants were plated onto LB agar plates containing 100 μg/mL of ampicillin and 1% tributyrin. After incubation at 37°C for 24 h, colonies surrounded by a clear halo were selected. Nucleotide sequencing was performed with the automated sequencer (ABI3100) using the BigDye terminator kit (PE Applied Biosystems, Foster City, CA). The DNA sequence was determined by primer walking in both directions and assembled using the ContigExpress program of the Vector NTI suite 7 software package (InforMax, North Bethesda, Md.). The open reading frame (ORF) was detected using the ORF search tool provided by the National Center for Biotechnology Information (NCBI). Sequence homology searches were performed with the basic local alignment search tool (BLAST) program [27]. Signal sequence search was performed with the SignalP 3.0 program [28]. Multiple alignments between protein sequences were performed with the ClustalW program [29]. The phylogenetic tree was constructed by the neighbor-joining method [30] using the Molecular Evolutionary Genetics Analysis 4.1 software (MEGA, version 4.1) [31].

2.3. Overexpression and Purification of the Lipolytic Enzyme-Encoding Genes. The lipolytic enzyme genes were amplified by PCR with primer pairs, and the amplified DNA fragments were inserted into the pET-24a(+) expression vector (Table 1). Three recombinant plasmids including genes of EM3L1, EM3L2, and EM3L3 were transformed into *E. coli* BL21 (DE3) cells while three recombinant plasmids including genes of EM3L4, EM3L6, and EM3L7 were transformed into *E. coli* BL21 (DE3) expressing molecular chaperones GroEL-GroES with pGro7 (Takara, Kyoto, Japan) and the transformants were inoculated into LB medium containing 20 μg/mL of chloramphenicol and 50 μg/mL of kanamycin for plasmid selection and 0.5 mg/mL L-arabinose for induction of chaperone expression. A transformants were cultivated at 37°C, and 1 mM isopropyl-β-D-thiogalactopyranoside (IPTG) was added to induce gene expression when the optical density at 600 nm reached 0.4. After incubation for 16 h at 16°C, the cells were harvested by centrifugation (6,000 ×g, 20 min, 4°C) and resuspended in 50 mM Tris-HCl buffer (pH 8.0) containing 0.1 M KCl and 10% glycerol. The cells were disrupted by sonication and centrifuged (20,000 ×g, 1 h, 4°C). The resulting supernatants were applied to a column of TALON metal-affinity resin (BD Biosciences Clontech, Palo Alto, CA) and washed with 10 mM imidazole (Sigma, St. Louis, MO) in 50 mM Tris-HCl buffer (pH 8.0) containing 0.1 M KCl and 10% glycerol, and the enzymes were eluted with 300 mM imidazole in the buffer. The protein concentration was measured by the Bradford method using the Bio-Rad protein assay kit (Bio-Rad, Hercules, CA) with bovine serum albumin as a standard [32]. The purity of the protein was examined by sodium

Table 1: Primers used in the cloning of lipolytic enzyme-encoding genes.

Gene	Primer*
EM3L1	5′-TTTGGAGGCATATGCTTATCCCTTCCGATGGTCTGGAAC-3′
	5′-CTGGTGTCCTCGAGGTTTGCCAAAAAACGGCCGTATATC-3′
EM3L2	5′-TGATAAATCATATGAACAGAATGACAATAGGCTTCTC-3′
	5′-CCTTTTAGCTCGAGATTATTGTCTTGCAACCAGGATT- 3′
EM3L3	5′-TAGCTGCACATATGATCCTTTTTAGCTTGGTCGGTGTC-3′
	5′-AAAGTTGGCTCGAGTGTCTTAATCCCAAGAAAATTCAAG-3′
EM3L4	5′-GAGAAGTGAACCGGGGGACATATGACTGGTAGAATTG-3′
	5′-CAAAAGCGCCCCTCGAGCGGCTGCTCCTCC-3′
EM3L6	5′-AGGAGAAGCATATGAAATGCATCCCATCAGACGGCC-3′
	5′-GTTGCAGACTCGAGATCATTATTCGAGCCTAATTCCTC-3′
EM3L7	5′-CGGAGTGAAAGCATATGACTTATCCGATTGTGCTC-3′
	5′-GTATTACCTCTCGAGGTTAAGGTAGTTGTTCCGCGATTC-3′

* Underlined bases in the primers indicate the restriction enzyme recognition site (NdeI/XhoI).

dodecyl sulfate-polyacrylamide gel electrophoresis (SDS-PAGE) under denaturing conditions as described method [33].

2.4. Characterization of Lipolytic Enzymes. Esterase and lipase activities were measured by a spectrophotometric method using *p*-nitrophenyl butyrate and *p*-nitrophenyl palmitate (Sigma, St. Louis, MO) as the substrate, respectively. The reaction mixture contained *p*-nitrophenyl butyrate in acetonitrile, Tris-HCl buffer, and the enzyme solution. *p*-nitrophenyl palmitate solutions were mixed with Tris-HCl buffer containing Triton X-100 as emulsifying agent. After incubation at each optimum temperature for 5 min, the absorbance at 405 nm was measured to detect the released *p*-nitrophenol. One unit of esterase and lipase activity was defined as the amount of enzyme required to release 1 μmol of *p*-nitrophenol from *p*-nitrophenyl butyrate or *p*-nitrophenyl palmitate per min.

The optimum temperature of the enzymes was determined at various temperatures of 5 to 65°C. The optimum pH was determined over a pH range of 4.0 to 10.0, using the following buffer systems: 50 mM sodium acetate (pH 4.0 to 6.0), 50 mM sodium phosphate (pH 6.0 to 7.5), 50 mM Tris-HCl (pH 7.5 to 8.5), and 50 mM CHES (pH 8.5 to 10.0). The substrate specificity was determined with different aliphatic side chain, C2 (acetate), C4 (butyrate), C6 (hexanoate), C8 (octanoate), C10 (decanoate), C12 (laurate), C14 (myristate), C16 (palmitate), and C18 (stearate) as substrates.

Various metal ions ($MnCl_2$, $MgCl_2$, $CaCl_2$, $CuCl_2$, $ZnSO_4$, $FeSO_4$, $CoSO_4$, and $NiSO_4$) and enzyme inhibitors, Phenylmethylsulfonyl fluoride (PMSF) and Ethylenediaminetetraacetic acid (EDTA), at a final concentration of 1 mM were added to the enzyme in 50 mM Tris-HCl buffer (pH 7.5) then assayed for enzyme activity after preincubation at 35°C for 1 hr. The effects of detergents on enzyme activity were determined by incubating the enzyme in 50 mM Tris-HCl buffer (pH 7.5) containing 1% (w/v) of the detergents SDS, Triton X-100, and Tween-20, -40, -60, -80 at 35°C for 1 hr.

The effect of NaCl concentration on enzyme activity was measured using *p*-nitrophenyl hexanoate as the substrate. The reaction mixture contained enzyme solution in 50 mM Tris-HCl (pH 7.5) containing different final NaCl concentrations ranging from 0.5 to 4 M. The mixture was preincubated at 35°C for 30 min, and then the enzyme activity was detected by adding *p*-nitrophenyl hexanoate.

2.5. Nucleotide Sequence Accession Numbers. The obtained nucleotide sequences have been deposited in the GenBank database under the accession numbers EM3L1 (GQ340923), EM3L2 (GQ340924), EM3L3 (GQ340925), EM3L4 (GQ340926), EM3L6 (GQ340927), and EM3L7 (GQ340928).

3. Results

3.1. Screening and Primary Sequence Analysis of Lipolytic Enzyme-Encoding Genes. To explore the untapped esterases/lipases in marine environment, metagenomic approach was applied to the samples from deep-sea sediment, located near a small volcanic cone named the Edison Seamount at a depth of 1440 m where there are extensive clam beds associated with the low-temperature vents [34]. Deep-sea sample was chosen to represent the psychrophilic environment with average temperature below 4°C. A metagenomic library consisting of 81,100 fosmid clones was constructed in a fosmid vector, pCC1FOS. Each clone contained an insert of approximately 15 to 33 kb. Fosmid clones having lipolytic activity were identified by activity screening on agar plates containing 1% tributyrin (TBN). As a result, 6 positive clones (designated as pFosEM3L1, pFosEM3L2, pFosEM3L3, pFosEM3L4, pFosEM3L6, and pFosEM3L7) were obtained by zones of clearance around the colonies.

The 6 fosmid clones were subjected to further subcloning into the pBluescript SK(−) plasmid. The subclones with lipolytic activity were selected on TBN plates again. Sequence analyses of the 2-3 kb DNA inserts in the subclones revealed

the presence of ORFs encoding putative α/β hydrolases with G + C contents of 46.5–66.6%. A BLAST search of the amino acid sequences of six ORFs indicated that they yielded identities of less than 60% to proteins in the database. The deduced amino acid sequences of EM3L1, EM3L2, EM3L3, EM3L4, EM3L6, and EM3L7 showed the highest similarity to α/β hydrolase fold protein (YP_003395264) from *Conexibacter woesei* DSM 14684 (39% identity), hypothetical protein (ZP_01915829) from *Limnobacter* sp. MED105 (49% identity), triacylglycerol acyl hydrolase (AAK07450) from *Moritella marina* (49% identity), LpqC (ZP_01463024) from *Stigmatella aurantiaca* DW4/3-1 (39% identity), α/β hydrolase fold protein (ZP_01697334) from *Bacillus coagulans* 36D1 (33% identity), and lipase (ACJ13070) from uncultured bacterium (58% identity), respectively.

To see how the ORFs were related to known esterases/lipases, the phylogenetic relationship was analyzed based on the esterase/lipase classification (family I–VIII) by Arpigny and Jaeger [1] including recently reported families such as LipG [35], EstA [36], LipEH166 [20], FLS18 [18], and EstD2 [17] (Figure 1). EM3L1, EM3L3, and EM3L6 were grouped into family V in Figure 1, *retaining* the G-X-S-M-G pentapeptide motif and the HG sequence for the oxyanion hole (Figures 2(a) and 2(b)). The His residue consisting of the catalytic triad could not be predicted in EM3L1 and EM3L6 by the sequence alignment (Figure 2(a)). EM3L2 was clustered together with EstD2 reported from metagenomic library of plant rhizosphere soil recently [17]. Multiple alignment analysis of EM3L2 revealed that the active site serine was encompassed by the conserved pentapeptide G-H-S-Q-G in EstD2 family (Figure 2(c)).

On the other hand, it was found that EM3L4 did not show significant similarity to any member in the eight families and branched out to a group together with close homologous genes. It is noteworthy that the comparative analysis of the deduced amino acid sequence revealed that EM3L4 displayed low similarity to poly(3-hydroxyalkanoate) depolymerase (ZP_07602911) from *Streptomyces violaceusniger* (34% identity), and both the active site serines in the two proteins were encompassed by G-X-S-N-G pentapeptide in common (Figure 2(d)). From the sequence analysis, it seems likely that EM3L4 could be a novel enzyme (Figure 1). Lastly, EM3L7 was clustered together with family I bacterial lipolytic enzymes, and the active site serine was encompassed by the characteristic A-X-S-X-G motif (Figure 2(e)). The motif was usually found in *Bacillus* lipases belonging to Subfamily I.4 even if no significant homology (less than 14% identity) was found between them. Taken together, the metagenomic study applied to marine sediment sample of deep sea has the potential to yield novel molecular entities unrelated to the known sequences.

3.2. Expression and Characterization of the Lipolytic Enzyme-Encoding Genes. To express six genes, EM3L1, EM3L2, EM3L3, EM3L4, EM3L6, and EM3L7, we investigated the presence of signal sequences using the SignalP 3.0 program and found that EM3L2, EM3L3, and EM3L4 retained a putative signal sequence 18–25 amino acids long. All the genes with signal sequence removed were amplified, and the resulting expression constructs were expressed in *E. coli* BL21 strain. Total cell lysates, soluble fractions, and insoluble fractions were analyzed by 12% SDS-PAGE, and we found that some portion of the proteins encoded by three of the genes (EM3L1, EM3L2, and EM3L3) were detected in the soluble fraction (Figure 3(a)), whereas the proteins encoded by the three genes (EM3L4, EM3L6, and EM3L7) were expressed as insoluble forms.

Based on the fact that expression at low temperature increases the stability and proper folding of proteins, possibly due to the fact that the hydrophobic interactions that determine inclusion body formation are temperature dependent [37–39], we made three proteins (EM3L4, EM3L6, and EM3L7) being induced at the low temperature of 16°C. However, the induction of expression at low temperature alone was not successful in enhancing the solubility of the expressed proteins (data not shown). Since it has been reported that GroEL-GroES is effective in facilitating their correct folding by minimizing aggregation and misfolding [40], we employed GroEL-GroES co-expression in solubilizing the proteins. It turns out that EM3L4 and EM3L6 proteins were solubly expressed by coexpressing GroEL-GroES at 16°C. In contrast to the other proteins, the majority of the expressed EM3L7 remained in the insoluble fraction regardless of the experimental conditions we tried in this study (Figure 3(b)). The expressed proteins were purified as described in Section 2, and SDS-PAGE analysis of purified EM3L1, EM3L2, EM3L3, EM3L4, and EM3L6 showed a protein band which correlated well to the predicted molecular weight (Figure 3(c)). This result demonstrated that the combination of co-expression of chaperones and induction at low temperature may be effective in achieving soluble expression of lipolytic enzyme-encoding genes.

The purified enzymes showed an optimum activity in the temperature range of 30–35°C and at a neural or slightly alkaline pH (pH 7.5–8.5) (Table 2 and see Figures S1 and S2 in Supplementry Material available on line at doi:10.1155/2011/271419). It is noteworthy that they could be classified as cold-active enzymes based on the temperature profiles and activation energy values. As the source of the genes was a deep-sea sediment sample, we predicted that they are cold-adapted enzymes. A similar phenomenon has been reported in other studies; for example, two cold-adapted esterase from Arctic sediment metagenome showed an optimum temperature at 30°C [23] and thermostable esterase from hot spring metagenome showed enzyme activity above 30°C up to 95°C [41]. This result suggested that the property of lipolytic enzymes derived from metagenomic library might be reflected by their environmental characters.

EM3L1, EM3L2, EM3L3, and EM3L6 could hydrolyze short chain substrates (C_2 to C_{12}) and showed the highest activity toward *p*-Nitrophenyl hexanoate (C_6) (Table 2 and Figure S3). On the other hand, EM3L4 showed enzymatic activity toward long-chain substrates (C_{16}–C_{18}), which can be classified as a lipase. The specific activities of the enzymes were determined to be in the range of 1.7–558.2 U/mg at the optimal conditions (Table 2).

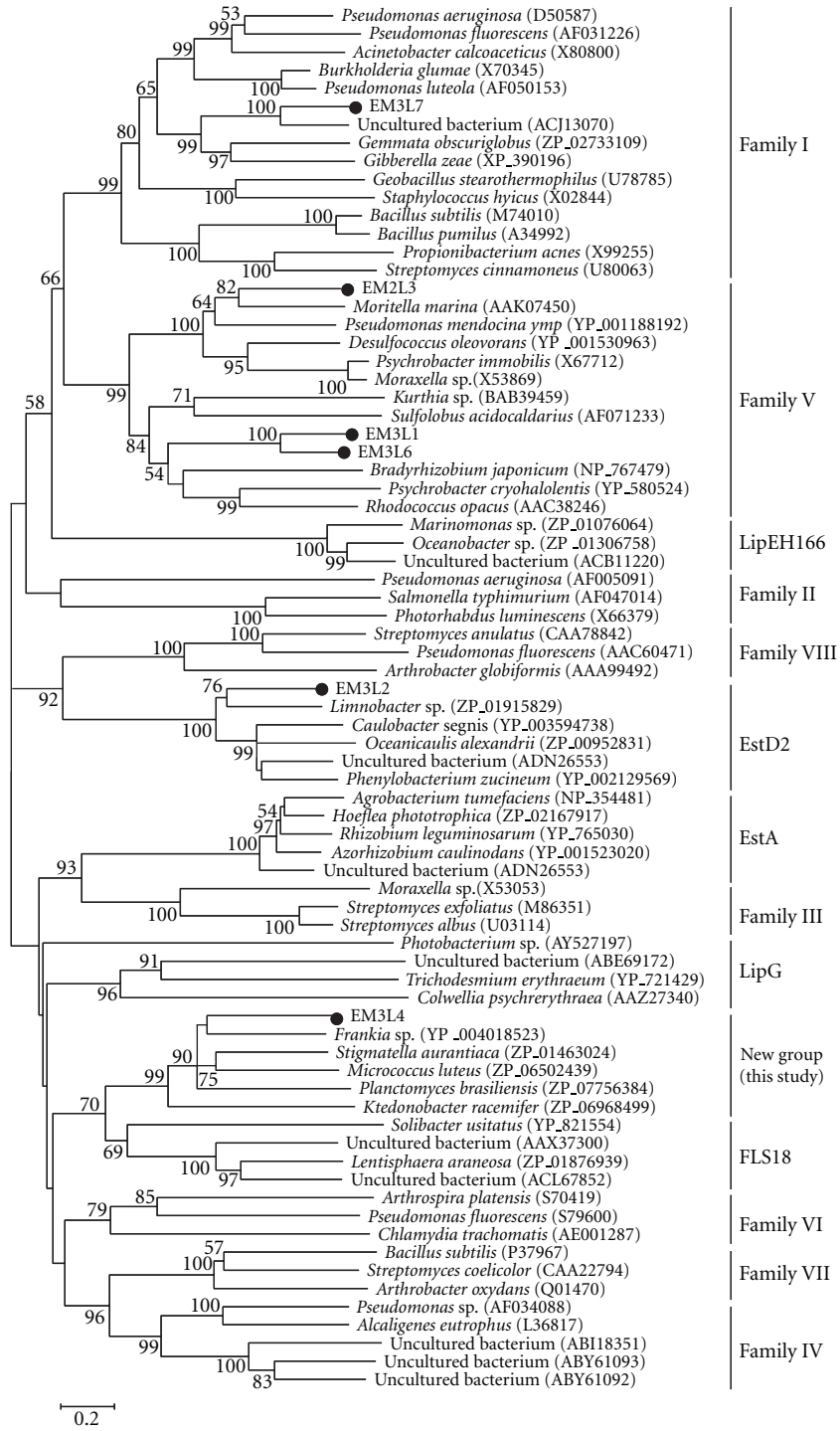

Figure 1: Phylogenetic tree of the lipolytic enzymes. The tree was constructed using the MEGA 4.1 program with the neighbor-joining algorithm. Only bootstrap values greater than 50% are shown. Bar: 0.2 substitutions per amino acid site.

Since EM3L4 belonged to a new group and the homologous proteins have never been characterized, the biochemical property of EM3L4 was further analyzed. To determine the resistance to various chemical agents, the purified EM3L4 was incubated with chemical agents, and the remaining activity was measured with *p*-nitrophenyl palmitate or *p*-nitrophenyl hexanoate as substrate at 35°C. The activity of EM3L4 was increased by the presence of Mn^{2+}, Mg^{2+}, Ca^{2+}, Cu^{2+}, and Ni^{2+}(Table 3). It was inhibited by Zn^{2+}, Fe^{2+}, and Co^{2+} and was completely inhibited by PMSF (Table 3). Besides, it was also inhibited by various nonionic detergents such as Tween-20, -40, -60, -80 and Triton X-100 and ionic detergent, SDS (Table 3). The enzyme activity of EM3L4 was significantly affected by salinity. As shown in Figure 4,

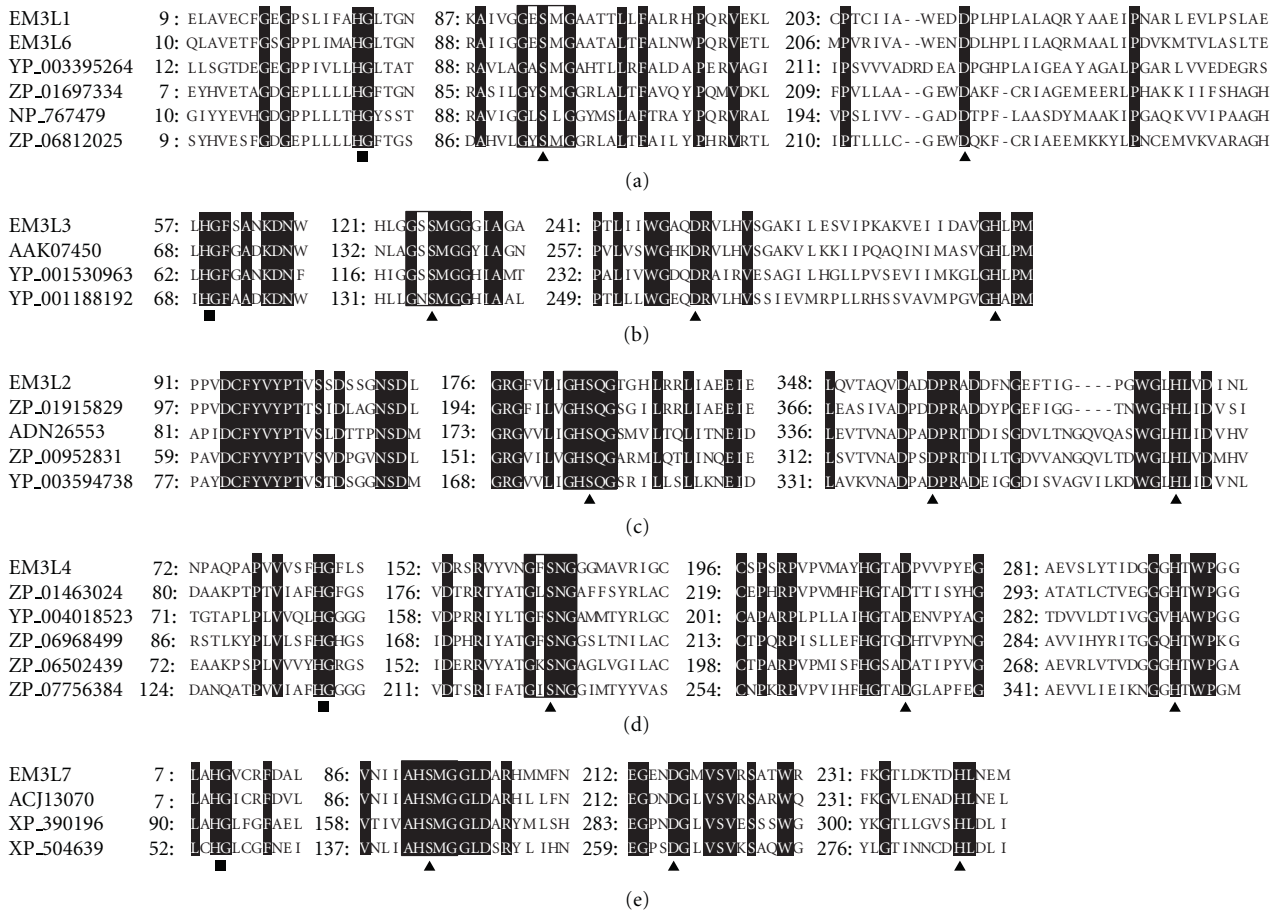

Figure 2: Multiple alignments of the conserved motifs of the ORFs isolated from metagenomic library with the homologs of each family or group. (a) Family V including EM3L1 and EM3L6: YP_003395264, an α/β hydrolase fold protein from *Conexibacter woesei* DSM 14684; ZP_01697334, an α/β hydrolase fold from *Bacillus coagulans* 36D1; NP_767479, a hypothetical protein bll0839 from *Bradyrhizobium japonicum* USDA 110; ZP_06812025, an α/β hydrolase fold protein from *Geobacillus thermoglucosidasius* C56-YS93. (b) Family V including EM3L3: AAK07450, a triacylglycerol acyl hydrolase from *Moritella marina*; YP_001530963, an α/β hydrolase fold from *Desulfococcus oleovorans* Hxd3; YP_001188192, an α/β hydrolase fold from *Pseudomonas mendocina* ymp (YP_001188192). (c) EstD2 family including EM3L2: ZP_01915829, a hypothetical protein from *Limnobacter* sp. MED105; ADN26553, an EstD2 from uncultured bacterium; ZP_00952831, a hypothetical protein from *Oceanicaulis alexandrii* HTCC2633; YP_003594738, a hypothetical protein from *Caulobacter segnis* ATCC 21756. (d) New group including EM3L4: ZP_01463024, an LpqC from *Stigmatella aurantiaca* DW4/3-1; YP_004018523, a lipoprotein from *Frankia* sp. EuI1c; ZP_06968499, a putative lipoprotein from *Ktedonobacter racemifer* DSM 44963; ZP_06502439, a conserved hypothetical protein from *Micrococcus luteus* SK58. (e) Family I including EM3L7: ACJ13070, a lipase from uncultured bacterium; (ACJ13070); XP_390196, a hypothetical protein from *Gibberella zeae* PH-1; XP_504639, a YALI0E31515p from *Yarrowia lipolytica*. Triangles and squares represent the residues involved in the formation of the catalytic triad and the oxyanion hole, respectively, and the conserved pentapeptide motifs are boxed.

Table 2: Characteristics of the purified lipolytic enzymes.

Enzyme	Temperature[a] (optimum) (°C)	Activation energy (kcal/mol)	pH[b] (optimum)	Substrate[c] (optimum)	Specific activity (U/mg)
EM3L1	15–50 (35)	3.6	7.5–9.5 (8.5)	C_2–C_{10} (C_6)	558.2
EM3L2	15–40 (30)	8.6	7.0–10.0 (8.5)	C_6 (C_6)	1.7
EM3L3	15–40 (35)	3.5	7.0–10.0 (8.5)	C_2–C_{10} (C_6)	29.7
EM3L4	20–50 (35)	10.6	7.0–10.0 (7.5)	C_{16}–C_{18} (C_{16})	5.3
EM3L6	15–40 (35)	4.1	7.5–9.0 (8.5)	C_2–C_{10} (C_6)	23.3

[a]The temperature range is the temperatures at which the activities are greater than 50% of the highest value (Figure S1). [b]pH range is the pHs at which the activities are greater than 50% of the highest value (Figure S2). [c]Substrates are the *p*-nitrophenyl esters for which the enzyme shows an activity greater than 20% of the highest value (Figure S3).

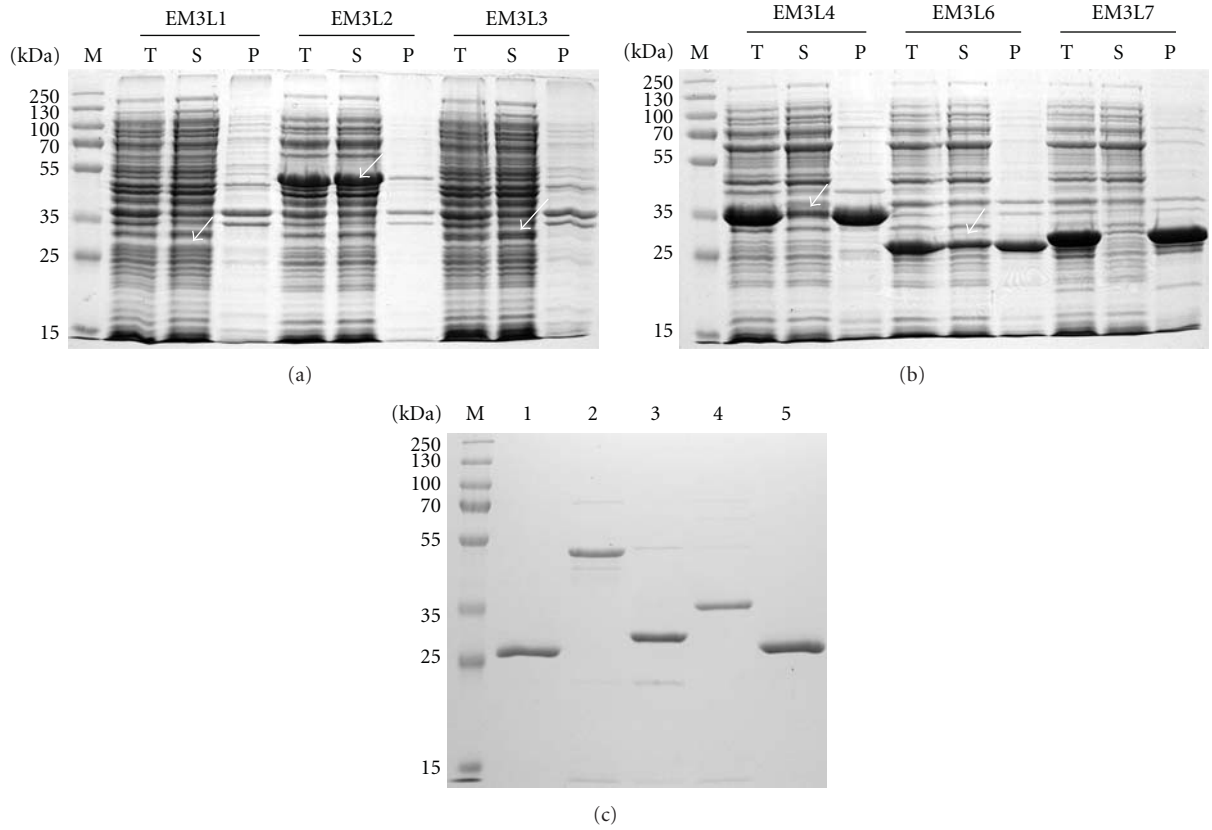

Figure 3: Expression of esterase/lipase genes. (a) Expression analysis of EM3L1, EM3L2, and EM3L3; (b) expression analysis of EM3L4, EM3L6, and EM3L7 with co-expression of the GroEL-GroES chaperone genes at 16°C; (c) purified enzymes. The bands corresponding to the proteins are indicated by arrows. Lane M: molecular mass standards, lane T: total cell lysate, lane S: soluble fraction, lane P: insoluble fraction, lane 1: purified EM3L1, lane 2: purified EM3L2, lane3: purified EM3L3, lane 4: purified EM3L4, and lane 5: purified EM3L6.

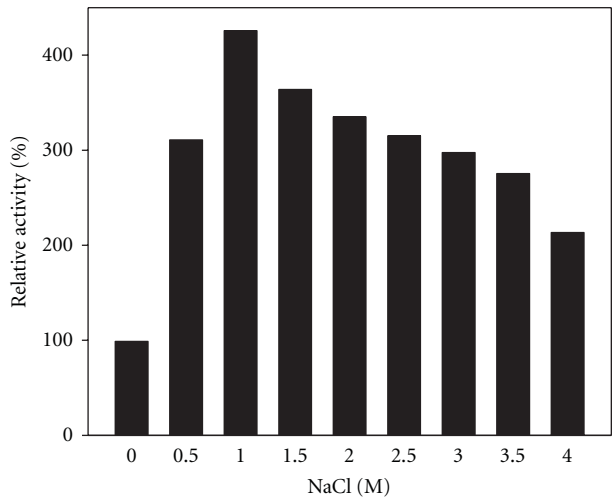

Figure 4: Effect of NaCl on *p*-nitrophenyl hexanoate hydrolysis activity of EM3L4. The activity of the enzyme preparation in the absence of NaCl before incubation was defined as the 100% level.

EM3L4 displayed the highest enzyme activity in the presence of 1 M NaCl. Moreover, the activity was maintained with up to 4 M NaCl (Figure 4).

Table 3: Effect of metal ions and detergents on EM3L4.

Metal ions (1 mM)	Relative activity (%)	Detergent (1%)	Relative activity (%)
None	100	None	100
$MnCl_2$	147	Tween 20	74
$MgCl_2$	175	Tween 40	70
$CaCl_2$	175	Tween 60	54
$CuCl_2$	165	Tween 80	69
$ZnSO_4$	52	Triton X-100	92
$FeSO_4$	0	SDS	0
$CoSO_4$	35		
$NiSO_4$	112		
PMSF	42		
EDTA	107		

4. Discussion

Our approach to search for novel lipolytic enzymes started with the construction of metagenomic library from deep sea sediment. As a result, we could discover six lipolytic enzyme-encoding genes with low sequence similarity (33–58% identity) to the known proteins. By removing signal

sequence in the N-terminus and co-expression of chaperone gene at low temperature, we could obtain soluble recombinant proteins encoded by 5 genes from *E. coli*. The biochemical characterization of them revealed being cold-adapted, reflecting the environmental feature of the origin of metagenome.

Particularly, EM3L4 branched out to a new group in the phylogenetic tree, and any of homologous proteins to EM3L4 has never been characterized. The purified EM3L4 preferred to hydrolyze longer fatty acids, and highly active at high NaCl concentration. Recently, some esterases whose activities were increased in the presence of NaCl have been identified using metagenomic libraries of various marine environments such as deep-sea water [42], sea water [36], and sea sediment [18]. We suggest that EM3L4 is a novel lipase retaining salt-resistance property. Then, a question arises whether homologous proteins belonging to the same group with EM3L4 show similar properties, and it will need further investigation.

Conclusively, this study demonstrated that novel lipolytic enzymes in terms of primary sequence, activity profile, and substrate specificity could be obtained by metagenomic approach using deep-sea sediment sample. They could be potentially used as a biocatalyst in pharmaceutical and fine chemical industries.

Acknowledgments

This work was supported by the KORDI in-house program (PE98513) and the Marine and Extreme Genome Research Center Program and the Development of Biohydrogen Production Technology Using Hyperthermophilic Archaea Program of the Ministry of Land, Transport, and Maritime Affairs, Republic of Korea.

References

[1] J. L. Arpigny and K. E. Jaeger, "Bacterial lipolytic enzymes: classification and properties," *Biochemical Journal*, vol. 343, no. 1, pp. 177–183, 1999.

[2] M. Nardini and B. W. Dijkstra, "α/β hydrolase fold enzymes: the family keeps growing," *Current Opinion in Structural Biology*, vol. 9, no. 6, pp. 732–737, 1999.

[3] K. E. Jaeger, B. W. Dijkstra, and M. T. Reetz, "Bacterial biocatalysts: molecular biology, three-dimensional structures, and biotechnological applications of lipases," *Annual Review of Microbiology*, vol. 53, pp. 315–351, 1999.

[4] K. E. Jaeger and T. Eggert, "Lipases for biotechnology," *Current Opinion in Biotechnology*, vol. 13, no. 4, pp. 390–397, 2002.

[5] A. Pandey, S. Benjamin, C. R. Soccol, P. Nigam, N. Krieger, and V. T. Soccol, "The realm of microbial lipases in biotechnology," *Biotechnology and Applied Biochemistry*, vol. 29, no. 2, pp. 119–131, 1999.

[6] R. Sharma, Y. Chisti, and U. C. Banerjee, "Production, purification, characterization, and applications of lipases," *Biotechnology Advances*, vol. 19, no. 8, pp. 627–662, 2001.

[7] J. Handelsman, M. R. Rondon, S. F. Brady, J. Clardy, and R. M. Goodman, "Molecular biological access to the chemistry of unknown soil microbes: a new frontier for natural products," *Chemistry & Biology*, vol. 5, no. 10, pp. R245–R249, 1998.

[8] P. D. Schloss and J. Handelsman, "Biotechnological prospects from metagenomics," *Current Opinion in Biotechnology*, vol. 14, no. 3, pp. 303–310, 2003.

[9] H. L. Steele and W. R. Streit, "Metagenomics: advances in ecology and biotechnology," *FEMS Microbiology Letters*, vol. 247, no. 2, pp. 105–111, 2005.

[10] J. C. Venter, K. Remington, J. F. Heidelberg et al., "Environmental genome shotgun sequencing of the Sargasso Sea," *Science*, vol. 304, no. 5667, pp. 66–74, 2004.

[11] M. R. Rondon, P. R. August, A. D. Bettermann et al., "Cloning the soil metagenome: a strategy for accessing the genetic and functional diversity of uncultured microorganisms," *Applied and Environmental Microbiology*, vol. 66, no. 6, pp. 2541–2547, 2000.

[12] P. Entcheva, W. Liebl, A. Johann, T. Hartsch, and W. R. Streit, "Direct cloning from enrichment cultures, a reliable strategy for isolation of complete operons and genes from microbial consortia," *Applied and Environmental Microbiology*, vol. 67, no. 1, pp. 89–99, 2001.

[13] O. Béjà, E. V. Koonin, L. Aravind et al., "Comparative genomic analysis of archaeal genotypic variants in a single population and in two different oceanic provinces," *Applied and Environmental Microbiology*, vol. 68, no. 1, pp. 335–345, 2002.

[14] J. Handelsman, "Metagenomics: application of genomics to uncultured microorganisms," *Microbiology and Molecular Biology Reviews*, vol. 68, no. 4, pp. 669–685, 2004.

[15] W. R. Streit, R. Daniel, and K. E. Jaeger, "Prospecting for biocatalysts and drugs in the genomes of non-cultured microorganisms," *Current Opinion in Biotechnology*, vol. 15, no. 4, pp. 285–290, 2004.

[16] W. R. Streit and R. A. Schmitz, "Metagenomics—the key to the uncultured microbes," *Current Opinion in Microbiology*, vol. 7, no. 5, pp. 492–498, 2004.

[17] M. H. Lee, K. S. Hong, S. Malhotra et al., "A new esterase EstD2 isolated from plant rhizosphere soil metagenome," *Applied Microbiology and Biotechnology*, vol. 88, no. 5, pp. 1125–1134, 2010.

[18] Y. Hu, C. Fu, Y. Huang et al., "Novel lipolytic genes from the microbial metagenomic library of the South China Sea marine sediment," *FEMS Microbiology Ecology*, vol. 72, no. 2, pp. 228–237, 2010.

[19] P. Wei, L. Bai, W. Song, and G. Hao, "Characterization of two soil metagenome-derived lipases with high specificity for *p*-nitrophenyl palmitate," *Archives of Microbiology*, vol. 191, no. 3, pp. 233–240, 2009.

[20] E. Y. Kim, K. H. Oh, M. H. Lee, C. H. Kang, T. K. Oh, and J. H. Yoon, "Novel cold-adapted alkaline lipase from an intertidal flat metagenome and proposal for a new family of bacterial lipases," *Applied and Environmental Microbiology*, vol. 75, no. 1, pp. 257–260, 2009.

[21] P. Tirawongsaroj, R. Sriprang, P. Harnpicharnchai et al., "Novel thermophilic and thermostable lipolytic enzymes from a Thailand hot spring metagenomic library," *Journal of Biotechnology*, vol. 133, no. 1, pp. 42–49, 2008.

[22] J. H. Jeon, J. T. Kim, Y. J. Kim et al., "Cloning and characterization of a new cold-active lipase from a deep-sea sediment metagenome," *Applied Microbiology and Biotechnology*, vol. 81, no. 5, pp. 865–874, 2009.

[23] J. H. Jeon, J. T. Kim, S. G. Kang, J. H. Lee, and S. J. Kim, "Characterization and its potential application of two esterases derived from the arctic sediment metagenome," *Marine Biotechnology*, vol. 11, no. 3, pp. 307–316, 2009.

[24] H. J. Park, J. H. Jeon, S. G. Kang, J. H. Lee, S. A. Lee, and H. K. Kim, "Functional expression and refolding of new alkaline esterase, EM2L8 from deep-sea sediment metagenome," *Protein Expression and Purification*, vol. 52, no. 2, pp. 340–347, 2007.

[25] R. A. Hurt, X. Qiu, L. Wu et al., "Simultaneous recovery of RNA and DNA from soils and sediments," *Applied and Environmental Microbiology*, vol. 67, no. 10, pp. 4495–4503, 2001.

[26] H. C. Bimboim and J. Doly, "A rapid alkaline extraction procedure for screening recombinant plasmid DNA," *Nucleic Acids Research*, vol. 7, no. 6, pp. 1513–1523, 1979.

[27] S. F. Altschul, T. L. Madden, A. A. Schäffer et al., "Gapped BLAST and PSI-BLAST: a new generation of protein database search programs," *Nucleic Acids Research*, vol. 25, no. 17, pp. 3389–3402, 1997.

[28] O. Emanuelsson, S. Brunak, G. von Heijne, and H. Nielsen, "Locating proteins in the cell using TargetP, SignalP and related tools," *Nature Protocols*, vol. 2, no. 4, pp. 953–971, 2007.

[29] J. D. Thompson, D. G. Higgins, and T. J. Gibson, "CLUSTAL W: improving the sensitivity of progressive multiple sequence alignment through sequence weighting, position-specific gap penalties and weight matrix choice," *Nucleic Acids Research*, vol. 22, no. 22, pp. 4673–4680, 1994.

[30] N. Saitou and M. Nei, "The neighbor-joining method: a new method for reconstructing phylogenetic trees," *Molecular biology and evolution*, vol. 4, no. 4, pp. 406–425, 1987.

[31] K. Tamura, J. Dudley, M. Nei, and S. Kumar, "MEGA4: Molecular Evolutionary Genetics Analysis (MEGA) software version 4.0," *Molecular Biology and Evolution*, vol. 24, no. 8, pp. 1596–1599, 2007.

[32] M. M. Bradford, "A rapid and sensitive method for the quantitation of microgram quantities of protein utilizing the principle of protein dye binding," *Analytical Biochemistry*, vol. 72, no. 1-2, pp. 248–254, 1976.

[33] U. K. Laemmli, "Cleavage of structural proteins during the assembly of the head of bacteriophage T4," *Nature*, vol. 227, no. 5259, pp. 680–685, 1970.

[34] P. Herzig, M. Hannington, B. McInnes et al., "Submarine volcanism and hydrothermal venting Studied in Papua, New Guinea," *EOS*, vol. 75, no. 44, pp. 513–520, 1994.

[35] M. H. Lee, C. H. Lee, T. K. Oh, J. K. Song, and J. H. Yoon, "Isolation and characterization of a novel lipase from a metagenomic library of tidal flat sediments: evidence for a new family of bacterial lipases," *Applied and Environmental Microbiology*, vol. 72, no. 11, pp. 7406–7409, 2006.

[36] X. Chu, H. He, C. Guo, and B. Sun, "Identification of two novel esterases from a marine metagenomic library derived from South China Sea," *Applied Microbiology and Biotechnology*, vol. 80, no. 4, pp. 615–625, 2008.

[37] L. Niiranen, S. Espelid, C. R. Karlsen et al., "Comparative expression study to increase the solubility of cold adapted Vibrio proteins in *Escherichia coli*," *Protein Expression and Purification*, vol. 52, no. 1, pp. 210–218, 2007.

[38] A. Vera, N. González-Montalbán, A. Arís, and A. Villaverde, "The conformational quality of insoluble recombinant proteins is enhanced at low growth temperatures," *Biotechnology and Bioengineering*, vol. 96, no. 6, pp. 1101–1106, 2007.

[39] J. A. Chesshyre and A. R. Hipkiss, "Low temperatures stabilize interferon α-2 against proteolysis in *Methylophilus methylotrophus and Escherichia coli*," *Applied Microbiology and Biotechnology*, vol. 31, no. 2, pp. 158–162, 1989.

[40] K. Braig, "Chaperonins," *Current Opinion in Structural Biology*, vol. 8, no. 2, pp. 159–165, 1998.

[41] J. K. Rhee, D. G. Ahn, Y. G. Kim, and J. W. Oh, "New thermophilic and thermostable esterase with sequence similarity to the hormone-sensitive lipase family, cloned from a metagenomic library," *Applied and Environmental Microbiology*, vol. 71, no. 2, pp. 817–825, 2005.

[42] M. Ferrer, O. V. Golyshina, T. N. Chernikova et al., "Microbial enzymes mined from the Urania deep-sea hypersaline anoxic basin," *Chemistry & Biology*, vol. 12, no. 8, pp. 895–904, 2005.